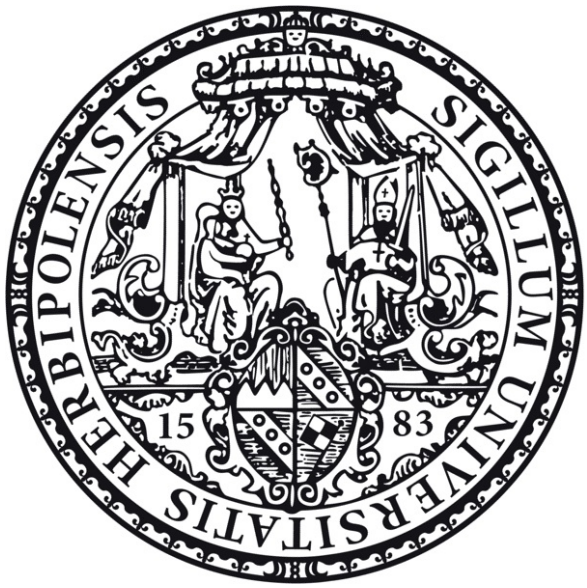
Discrete Holography: Through the Quantum Information Looking-Glass



Dissertation zur Erlangung des naturwissenschaftlichen Doktorgrades
an der Fakultät für Physik und Astronomie
der Julius–Maximilians-Universität Würzburg

vorgelegt von

Pablo Basteiro
aus Ciudad Autónoma de Buenos Aires, Argentinien

Würzburg, im Juli 2024

This document is licensed under the Creative Commons Attribution-ShareAlike 4.0 International License (CC BY-SA 4.0):
http://creativecommons.org/licenses/by-sa/4.0 This CC license does not apply to third party material (attributed to another source) in this publication.

Eingereicht bei der Fakultät für Physik und Astronomie am

Gutachter der Dissertation

1. Gutachter: Prof. Dr. Johanna Erdmenger

2. Gutachter: Prof. Dr. Giorgio Sangiovanni

3. Gutachter:

Prüfer des öffentlichen Promotionskolloquiums

1. Prüfer: Prof. Dr. Johanna Erdmenger

2. Prüfer: Prof. Dr. Giorgio Sangiovanni

3. Prüfer:

4. Prüfer:

5. Prüfer:

Tag des öffentlichen Promotionskolloquiums

Doktorurkunde ausgehändigt am

Supervisor: Prof. Dr. Johanna Erdmenger
Co-Supervisor: Dr. Giuseppe Di Giulio

To my dear sister Laura, and her newborn daughter, Hanna

Acknowledgments

I am deeply grateful for everyone that has supported me throughout my PhD journey. I apologize in advance for any accidental omissions as I try to name you all.
First, I would like to express a sincere thank you to my PhD supervisor, Johanna Erdmenger, for her guidance and support, both on the academic and the personal level. The mere existence of this thesis is due to her backing and encouragement.
A further heartfelt thank you goes to Giorgio Sangiovanni for agreeing to be a second supervisor of this thesis, as well as for the chance of working with him as a teaching assistant. Special thanks go to René Meyer and Ronny Thomale for their steady guidance as part of my mentoring committee.
Moreover, I would like to thank everyone at the Chair of Theoretical Physics 3 for making the work place feel like a second home, as well as for countless memories and experiences as a team.
I would like to thank Nicolas Bauer, Florian Goth, and Philipp Heilmann for their help in all things IT, and Nelia Meyer for her immensely patient help when dealing with German bureaucracy.
I am extremely grateful for all my collaborators and the people I have had the pleasure to discuss with. A non-exhaustive list include Coraline Bacq, Souvik Banerjee, Igor Boettcher, Anffany Chen, Rathindra Nath Das, Santanu Dey, Haye Hinrichsen, Sven Höfling, Jonathan Karl, Jani Kastikainen, Arnab Kundu, Joseph Maciejko, Moritz Meinecke, Sara Murciano, Dominik Neuenfeld, Lizzy Rieth, Henri Scheppach, Björn Trauzettel, and Zhuo-Yu Xian. I candidly thank them for their dedication, guidance, and insightful discussions.
My PhD journey was heavily influenced by attending various conferences and workshops which helped me develop my skills and understanding. I extend my appreciation to all the institutes, universities, and hosting venues for their hospitality and scientifically invigorating atmosphere. I am extremely thankful to the ct-qmat Cluster of Excellence between Würzburg and Dresden for financial support throughout my PhD, which has been crucial for my research.
I would like to extend my deep gratitude to the kind people at the Disharmonie in Schweinfurt, which supported the scientific communication efforts initiated by my good colleague Moritz Dorband in the series called “Physik für Alle”. I had the great honor and pleasure to participate in these efforts to make physics accessible to everyone, regardless of their background. I also thank the other participants of this series for

their camaraderie through the years, namely Manuel Graf, Tobias Kehrer, Valentin Seinige, Yvonne Wagenhäuser, and Anna-Lena Weigel. Beyond creating this series, Moritz Dorband has been a great friend throughout my entire physics career, and our often different approaches to physics have only enriched my understanding countless times. My gratitude goes out to him both as a colleague and as a friend.
I would like to thank my parents, Alejandra and Pablo, my sister Laura, and her partner Tomas for their unconditional and unwavering support at a distance. A further thank you goes out to all my friends in Argentina; the Dino Mix was always present. Special thanks go to Josefina Lita and Francisco Wortmann, who always had an open ear when things got stressful. Another huge thank you goes to Ivaylo Angelov, Felix Brust, and Victoria Costa Ferrero for their invaluable friendship throughout the years. Many of my bad days were instantly made better by the support and patience of my partner, Francine Selms, whose presence in my life has been invaluable throughout my journey. I am indebted to her.
I cannot really put into words how grateful I am for the support, guidance, and wisdom I have received from Giuseppe Di Giulio, initially a colleague who turned into a great friend. This thesis would have been extremely different if it was not for him, and I am deeply grateful to have had the pleasure to work with him these past years. Finally, I am extremely grateful to everyone that spent valuable time reading parts of this thesis and providing constructive comments: Ivaylo Angelov, Victoria Costa Ferrero, Giuseppe Di Giulio, Moritz Dorband, Haye Hinrichsen, Jonathan Karl, Amelie Mierau, Francine Selms and Henri Scheppach.

Abstract

Perhaps the deepest unanswered question in theoretical physics is how to consistently combine the theory of general relativity with the principles of quantum mechanics. In parallel, the holographic principle is expected to be a fundamental property of quantum gravity that allows the latter to be described by a theory in one dimension lower which does not contain gravity. As an explicit realization of the holographic principle, the Anti-de Sitter/Conformal Field Theory (AdS/CFT) correspondence has established itself as our best non-perturbative approach to quantum gravity. Moreover, it has become clear that concepts of quantum information theory play a fundamental role in this duality. Nonetheless, the extent of validity of the holographic principle has not been fully explored yet. In parallel, the AdS/CFT correspondence is still primarily a conjecture rooted in theoretical arguments and, while awaiting a mathematical proof, it would immensely benefit from experimental tests validating its predictions. Motivated by these aspects, in this thesis I advance the field of *discrete holography* by establishing explicit holographic models on both bulk and boundary of discretizations of hyperbolic space. These models assess the wide range of validity of the holographic principle beyond the continuum formulation of AdS/CFT while also enabling the experimental realization of holographic predictions. Furthermore, I investigate quantum information quantities such as circuit complexity, quantum discord, and the operator algebra description of entanglement, and elucidate their roles in describing certain properties of black holes.

In the first part of this thesis I consider regular tilings of hyperbolic space as a discretization of constant-time slices of AdS_3. From the perspective of the bulk, I show that they provide a sensible description of the continuum by establishing how the Breitenlohner-Freedman stability bound for a free scalar field is realized on these tilings. I follow up on this result by considering an interacting scalar field on hyperbolic tilings and showing how a discrete lattice model can emulate CFT correlation functions at both zero and finite temperature. The latter are obtained from a discretization of a constant-time slice of an AdS black hole. Additionally, I present a universal experimental platform based on electric circuits on which the aforementioned results can be measured. My results show that these architectures bear tremendous untapped potential to realize further holographic predictions in the laboratory, beyond those appraised in this thesis.

From a boundary perspective, I establish a large class of explicit Hamiltonians defined at the asymptotic boundary of hyperbolic tilings. These are prime candidates for boundary theories in discrete holographic dualities and consist of aperiodically disordered quantum spin chains with nearest-neighbor interactions. The aperiodic disorder encodes information about the systematic construction of the bulk tiling based on substitution rules. Using real-space renormalization group techniques, I study the ground state of these models in view of their factorized form into two-spin states, their correlation functions, and their entanglement structure. I show how the latter is exactly captured by a tensor network which extends into the bulk, thus providing a geometric bulk dual to the boundary theory. The high degree of analytic tractability of these models enables discrete manifestations of the holographic principle. These are realized by the standard prescription for computing entanglement entropy in tensor networks.

In the second part of this thesis I focus on three quantum information-theoretic quantities and study them in view of describing properties of quantum black holes via the AdS/CFT correspondence. Starting from quantum circuit complexity as a conjectured probe for the emergence of space behind the horizon, I study a novel definition of Nielsen operator complexity for finite- and infinite-dimensional systems. My construction relates complexity with the theory of classical ideal hydrodynamics while still exhibiting the features desired for a holographic complexity measure. Then, I study geometric quantum discord as an efficient tool for diagnosing non-factorization. This quantity is easier to calculate than its NP-hard cousin (quantum discord), and I show how the geometric quantum discord for pure states vanishes if and only if the modular partition function factorizes. I apply this to the explicit example of an eternal wormhole in AdS and discuss the results in view of holography. Moreover, I establish a relation between geometric quantum discord and wormhole contributions to the gravitational path integral, thus shedding light on the mechanisms behind the factorization puzzle of AdS/CFT. Finally, I study local operator algebras as a rigorous approach to entanglement entropy which has been recently employed in AdS/CFT to explain the emergence of time behind the black hole horizon. In particular, I consider operator algebras in an interacting but exactly solvable quantum many-body system of Majorana fermions. I find transitions between different types of operator algebras throughout the phase diagram of the model, which contains a quantum phase transition. This model provides an explicit instance where such operator algebra transitions can be studied in a tractable many-body system.
The results presented in this thesis are published in my works listed in App. A.

Zusammenfassung

Die wahrscheinlich grundlegendste unbeantwortete Frage der theoretischen Physik betrifft die Vereinigung der allgemeinen Relativitätstheorie mit den Prinzipien der Quantenmechanik. Einer der vielversprechendsten Zugänge beruht auf dem holographischen Prinzip, das eine fundamentale Eigenschaft der Quantengravitation zu sein scheint. Es besagt, dass sich eine Gravitationstheorie alternativ durch eine Theorie ohne Gravitation in einer Dimension niedriger beschreiben lässt. Als explizite Realisierung des holographischen Prinzips hat sich die Anti-de Sitter/Konforme Feldtheorie (AdS/CFT) Korrespondenz als führender Ansatz zur Theorie der Quantengravitation etabliert. Darüber hinaus haben sich Konzepte aus der Quanteninformationstheorie als elementare Bestandteile dieser Dualität herauskristallisiert. Dennoch ist der Geltungbereich des holographischen Prinzips bisher nicht vollständig erforscht. Zudem ist die AdS/CFT Korrespondenz weitestgehend noch eine Vermutung. Solange ein mathematischer Beweis nicht zur Verfügung steht, kann sie von experimentellen Tests ihrer Vorhersagen extrem profitieren.
Diese Aspekte motivieren die aktuelle Dissertation, in der ich Fortschritte im Forschungsfeld der *diskreten Holographie* präsentiere. Dazu etabliere ich explizite holographische Modelle auf Diskretisierungen des hyperbolischen Raums. Diese Modelle zeigen einen erweiterten Gültigkeitsbereich des holographischen Prinzips auf, jenseits der kontinuierlichen Formulierung von AdS/CFT. Zudem ermöglichen sie die experimentelle Realisierung holograpischer Vorhersagen. Weiterhin präsentiere ich meine Ergebnisse zu Quanteninformationsmaßen wie der Komplexität von Quantenschaltkreisen, dem Quantendiskord und der Beschreibung von Verschränkungsentropie mittels Operatoralgebren. Ebenso erörtere ich die Signifikanz dieser Maße für die holographische Beschreibung ausgewählter Eigenschaften von Schwarzen Löchern.

Im ersten Teil dieser Dissertation beschäftige ich mich mit regulären Tessellierungen des hyperbolischen Raums als Diskretisierungen von AdS_3-Hyperflächen bei konstanter Zeit. Für den AdS Raum zeige ich, dass diese Tessellierungen das Kontinuum sinvoll nähern, indem ich die Breitenlohner-Freedman-Stabilitätsgrenze eines freien Skalarfeldes auf solchen Diskretisierungen realisiere. Anknüpfend an dieses Ergebnis betrachte ich ein wechselwirkendes Skalarfeld auf hyperbolischen Tessellierungen und zeige, wie ein diskretes Gittermodell Korrelationsfunktionen der CFT sowohl bei verschwindender als auch bei endlicher Temperatur emulieren kann. Die Korrela-

tionsfunktionen bei endlicher Temperatur erhalte ich aus der Diskretisierung einer Hyperfläche eines Schwarzen Lochs im AdS-Raum bei konstanter Zeit. Darüber hinaus stelle ich eine universelle experimentelle Plattform vor, die auf elektrischen Schaltkreisen basiert und auf der die oben genannten Ergebnisse gemessen werden können. Meine Ergebnisse zeigen, dass diese Architekturen ein enormes ungenutztes Potenzial aufweisen, um weitere holographische Vorhersagen im Labor zu realisieren, welche über die in dieser Arbeit getesteten hinausgehen.
Für die Quantentheorie am Rand des AdS-Raums stelle ich eine große Klasse expliziter Hamilton-Operatoren auf, die am asymptotischen Rand hyperbolischer Tessellierungen definiert sind. Diese sind geeignete Kandidaten für Randtheorien in diskreten holographischen Dualitäten und bestehen aus aperiodisch ungeordneten Quantenspinketten mit Wechselwirkungen zwischen nächsten Nachbarn. Die aperiodische Unordnung speichert Informationen über den systematischen Aufbau der Tessellierung. Mit Hilfe von Realraum-Renormierungsgruppen-Techniken untersuche ich den Grundzustand dieser Modelle im Hinblick auf ihre faktorisierte Form in Zwei-Spin-Zustände, ihre Korrelationsfunktionen und ihre Verschränkungsstruktur. Ich zeige, dass diese Struktur exakt durch ein Tensornetzwerk erfasst wird, das sich zurück in den AdS-Raum erstreckt und somit ein geometrisches Dual zur Randtheorie liefert. Die analytische Nachvollziehbarkeit dieser Modelle ermöglicht es aufzuzeigen, wie diese das holographische Prinzip für diskrete Systeme realisieren. Dies erziele ich durch die Standardvorschrift zur Berechnung der Verschränkungsentropie in Tensornetzwerken.

Im zweiten Teil dieser Arbeit konzentriere ich mich auf drei quanteninformationstheoretische Größen und untersuche sie im Hinblick auf die Beschreibung von Schwarzen Löchern mittels der AdS/CFT-Korrespondenz. Ausgehend von der Komplexität von Quantenschaltkreisen, die als Maß für den Raum hinter dem Horizont vorgeschlagen wird, untersuche ich eine neuartige Definition der Nielsen-Operator-Komplexität für endlich- und unendlich-dimensionale Systeme. Mein Ansatz verbindet die Komplexität mit der Theorie der klassischen idealen Hydrodynamik und weist gleichzeitig die Eigenschaften auf, die man sich von einem holographischen Komplexitätsmaß wünscht. Anschließend untersuche ich den geometrischen Quantendiskord als effizientes Werkzeug zur Diagnose von Nicht-Faktorisierung. Diese Größe ist einfacher zu berechnen als ihr NP-schwerer Verwandter, der (nicht-geometrische) Quantendiskord. Darüber hinaus zeige ich, dass der geometrische Quantendiskord für reine Zustände genau dann verschwindet, wenn die modulare Zustandssumme faktorisiert. Ich wende dies auf das explizite Beispiel eines zeitunabhängigen Wurmlochs im AdS-Raum an und diskutiere die holographischen Eigenschaften der Ergebnisse. Daraufhin stelle ich eine

Beziehung zwischen geometrischem Quantendiskord und Wurmloch-Beiträgen zum Gravitationspfadintegral her und beleuchte damit die möglichen Mechanismen hinter dem AdS/CFT-Faktorisierungsproblem. Schließlich untersuche ich lokale Operatoralgebren als mathematischen Ansatz für die Verschränkungsentropie. Diese wurden kürzlich in AdS/CFT verwendet, um die Zeitentwicklung im Inneren des Schwarzen Lochs zu erklären. Insbesondere betrachte ich Operatoralgebren in einem wechselwirkenden, aber dennoch exakt lösbaren Quanten-Vielkörpersystem von Majorana-Fermionen. Im gesamten Phasendiagramm des Modells, das einen Quantenphasenübergang enthält, finde ich Übergänge zwischen verschiedenen Typen von Operatoralgebren. Somit stelle ich ein explizites und nachvollziehbares Vielteilchenmodell dar, in dem solche Algebra-Übergänge realisiert werden.
Die in dieser Dissertation präsentierten Ergebnisse sind in meinen in Anhang A aufgelisteten Originalveröffentlichungen publiziert.

Contents

1. Introduction **1**

2. Foundations **21**

2.1. The Holographic Principle 22

2.2. The AdS/CFT Correspondence 25

2.2.1. Anti-de Sitter Spacetimes 25

2.2.2. Conformal Field Theories 29

2.2.3. The Statement of the Correspondence 32

2.2.4. AdS/CFT at Finite Temperature 37

2.3. Quantum Information Theory 47

2.3.1. Entanglement Entropy 47

2.3.2. Quantum Complexity 60

2.3.3. Quantum Discord 66

2.3.4. Tensor Networks 71

3. Discrete Approaches to Holography **77**

3.1. The Discrete Holography Landscape 79

3.2. Regular Hyperbolic Tilings 83

3.2.1. Poincaré Slices of AdS_{2+1} 83

3.2.2. The Tiler's Dream: Hyperbolic $\{p, q\}$ Tilings 87

3.2.3. Fuchsian Symmetries 98

3.2.4. Constructing Hyperbolic Tilings 111

3.3. The Breitenlohner-Freedman Bound on Hyperbolic Tilings 123

3.3.1. A Scalar Field on AdS 124

3.3.2. Energy Functional of AdS 128

3.3.3. The Klein-Gordon Equation on Hyperbolic Tilings 130

3.3.4. Hyperbolic Electric Circuits 134

3.4. Simulating Conformal Field Theories on Hyperbolic Tilings 140

3.4.1. Holographic Lattice Model 141

3.4.2. Discretizing the BTZ Black Hole 145

3.4.3. Boundary Correlation Functions 148

3.4.4. Measurement Protocol on Electric Circuits 155

3.5. Aperiodic Quantum Spin Chains 158

3.5.1. The Jeweler's Dream: Constructing Aperiodic Chains 159

3.5.2. The Strong-Disorder Renormalization Group and Aperiodic Singlet Phases . . . 163
3.5.3. Correlation Functions in Aperiodic Singlet Phases . . . 172
3.5.4. Entanglement Entropy in Aperiodic Singlet Phases . . . 184
3.5.5. Mutual Information in Aperiodic Singlet Phases . . . 192
3.5.6. Explicit Models . . . 198
3.5.7. Tensor Networks for Aperiodic Spin Chains . . . 217
3.6. Discussion . . . 239

4. Quantum Information and Holography **243**
4.1. Quantum Complexity: When Entanglement is not Enough . . . 245
4.1.1. The Euler-Arnold Approach to Nielsen Complexity . . . 246
4.1.2. An Algebra of N-level Qudits . . . 249
4.1.3. A Cost Function from Hydrodynamics . . . 255
4.1.4. Complexity Geometry at Large N . . . 262
4.2. Geometric Quantum Discord: When Entanglement Connects Universes 269
4.2.1. Geometric Quantum Discord for Pure States . . . 271
4.2.2. Geometric Quantum Discord for the Thermofield Double State . 276
4.2.3. Black Hole Microstates from Geometric Quantum Discord . . . 281
4.3. Local Operator Algebras: When Entanglement is Infinite . . . 287
4.3.1. Local Operator Algebras and Holography . . . 288
4.3.2. Large-N Interacting Majorana Models . . . 298
4.3.3. Thermodynamics and Phase Diagram . . . 302
4.3.4. Transitions of von Neumann Algebras . . . 323
4.3.5. Closed Periodic Chains . . . 332
4.4. Discussion . . . 337

5. Conclusions and Outlook **341**

A. Publications **351**

Bibliography **353**

Introduction 1

"I have approximate answers and possible beliefs and different degrees of certainty about many things, but I am not absolutely sure of anything, and there are many things I don't know anything about."

Richard Feynman

The Pleasure of Finding Things Out

In our everyday lives, we encounter uncountable examples of phenomena which are intuitively clear to us, but whose detailed description in physical terms is surprisingly complex. Although we usually skim over these occurrences due to their familiarity, there are always instances where we stop to wonder "*Why is the sky blue of all colors?*" or "*How do magnets work?*". As famously put by Richard Feynman [1], this is because we are hard-wired to feel pleasure in discovering how the world around us works. Sometimes, our curiosity may drive us to bigger questions like "*How big is the Universe really*?" or "*What else is there out there that we do not know about?*". Such deep inquiries, together with our current understanding of the Universe, even allow us to contemplate fundamentally mysterious questions such as "*What happens if I fall into a black hole?*" or "*How did the Universe even begin?*". It is clear that as curiosity-driven creatures we have an unbounded amount of questions, ranging from the seemingly basic to the exceedingly profound ones. Making progress in answering such questions brings us the pleasure of finding things out, which is the very essence of scientific research.

How do we go about answering all these questions? Throughout the centuries, we have developed an empirical approach to describing Nature, known as the *scientific method*. Using logic and reason, we aim to devise models of reality which not only manage to describe old phenomena, but they also have verifiable predictive power regarding events that have not yet been observed. The currently accepted paradigm we have for describing the Universe is based on two such models: Einstein's theory of general relativity [2–4], and the theory of quantum mechanics [5–10]. These are our best understood description of physical phenomena at cosmological and microscopic scales, respectively. Individually, both these theories have enjoyed a never-before-seen success in terms of predictive power, and they have withstood an uncountable number of experimental scrutiny. However, as we will see in what follows, there exist physical

scenarios in which our current paradigm breaks down, suggesting the need for an over-encompassing theory which combines general relativity with quantum mechanics: a theory of *quantum gravity* [11]. The quest for such a theory has permeated fundamental physics research for almost a century now, and this thesis duly follows this trend. The investigations and results reported herein are motivated by this search for quantum gravity, and we detail the nature of these contributions after providing a pedagogical and historical contextualization.

Atoms, Galaxies & Everywhere in Between

Modern scientific understanding of gravity began with Newton's study of the motion of bodies, summarized in his pivotal work *Principia Mathematica* [12]. The underlying mathematical description required the development of the calculus of continuous variables, in parallel with Leibniz, which explicitly assumes a continuous nature to all physical motion. Newton's theory of gravity, which we presently refer to as classical gravity, presented a very successful paradigm at the time. However, certain observations such as the precession of Mercury's perihelion or the deflection of light by extremely massive objects could not be fully explained in Newtonian gravity. At the break of the 20th century, the paradigm shifting insights of Einstein's theory of general relativity (GR) [2–4] provided satisfactory explanations to these phenomena [13] and predicted other ones such as the gravitational red-shift of light [4, 14]. GR considers space and time to be a unique continuous entity, *spacetime*, in which the gravitational force arises as a consequence of curvature or the presence of matter. As was elegantly summarized by Wheeler: "*Spacetime tells matter how to move; matter tells spacetime how to curve.*" Any solution to Einstein's field equations, given in terms of a *metric tensor* $g_{\mu\nu}$, describes a possible gravitational configuration compatible with GR, which in general has non-vanishing curvature. Further predictions of Einstein's GR include gravitational lensing and gravitational waves [15, 16], all of which have been verified with an immense amount of experimental evidence throughout the last century [17–26], thus cementing its place as our best understood theory of gravity.

One of the most interesting and mysterious predictions of Einstein's GR are spacetime geometries originating from an extremely dense massive object, whose curvature leads to a highly non-trivial causal structure. In particular, these geometries are such that any particle, being massive or simply an electromagnetic wave, cannot escape the gravitational pull caused by the curved spacetime at a finite distance. These intriguing gravitational configurations, which are completely legitimate solutions to Einstein's field equations, came to be known as *black holes*, a term usually attributed

to John Wheeler. The first exact black hole solution was found by Schwarzschild [27, 28] and it described the gravitational field outside a spherically symmetric mass in an otherwise empty flat spacetime. The Schwarzschild black hole exhibits two so-called *singularities* at different values of the radial coordinate r. These are values at which some components of the metric tensor $g_{\mu\nu} = g_{\mu\nu}(r)$ diverge. The first one is at $r = r_{\rm h}$, where $r_{\rm h}$ denotes the position of the *event horizon*. This surface determines the distance at which spacelike and timelike coordinates switch roles, thus imposing a causal boundary such that no observer inside the horizon can affect any events outside of the black hole. The event horizon, however, is merely a coordinate singularity, meaning that nothing drastic actually happens at this position. An observer falling into a black hole will not feel anything in particular when crossing this surface. Rather, it indicates that the causal structure of the spacetime changes, in a way that can only really be perceived when considering the difference in events experienced by two or more observers relative to each other. The second singularity lies at the origin $r = 0$, where $g_{\mu\nu} \to \infty$ as well. However, crucially, the singularity at the origin cannot be removed by coordinate transformations; it is a true *gravitational singularity*. At this point, the spacetime curvature becomes infinite, the metric cannot be smoothly extended, and the actual notion of spacetime is not well-defined. From our observations of the Universe, we do not believe that infinite quantities are part of Nature. Therefore, we interpret the gravitational singularities predicted by GR as an indicator of the breakdown of the theory, an instance where the model ceases to have predictive power. The causal structure of black holes is such that the entire *light cone* of an in-falling observer, i.e. the set of events that can be causally affected by her in view of the finiteness of the speed of light, lies completely within the black hole once she crosses the horizon. As a consequence, she will move spatially towards the singularity in the same way that we "move" towards tomorrow. This means that our observer is guaranteed, no matter what she does, to land at the singularity in a finite amount of time. Thus, the singularity is not a position in space, but rather a moment in time. The predictions of singularities from GR were later formalized by Penrose and Hawking in their famous singularity theorems [29–31]. These results provide a smoking-gun evidence that our current paradigm of physics at the largest scales, namely Einstein's theory of gravity, cannot possibly be a complete theory of Nature.

Almost contemporary to the beginnings of GR, another groundbreaking theory was being developed which aimed to describe our Universe at the smallest scales. After the discovery of the electron by Thomson in 1897 [32], and that of the atomic nucleus by Rutherford in 1911 [33], the Rutherford model provided a primitive description for

the structure of the atom. Electrons in this model were thought to orbit around the nucleus, akin to the orbits of planets around the sun. However, inconsistencies of the model were quickly pointed out, such as a spiraling trajectory of an electron towards the nucleus, expected as a consequence of the electron radiating energy according to classical electromagnetism of accelerated charges. Evidently, this type of unstable atoms due to such a collapse of electrons are not observed in experiment, indicating a fault in the model. Later refinements of the model were proposed by Bohr [6], who postulated the existence of *quantized* orbits, based on previous ideas introduced by Planck [5] in his studies of thermal radiation of bodies at a finite temperature, i.e. black-body radiation. In Bohr's model, the electron may only move on stable orbits around the nucleus without radiating, and there is only a *discrete* amount of such orbits. These quantized orbits correspond to angular momenta which are given as multiples of a fundamental *quantum* determined by Planck's constant $\hbar$. Electrons can only transition between these orbits upon gaining or losing a discrete number of energy quanta equal to the energy difference between them. Though initially successful, providing impressively accurate predictions for hydrogen's spectral emission lines, Bohr's model still presented shortcomings when it came to describing larger atoms. The correct description was finally obtained upon the advent of the theory of *quantum mechanics* [5–10], which provided an encompassing model for the electronic structure of atoms in terms of *electron orbitals*. To this day, quantum mechanics remains as our widely accepted paradigm for the description of Nature at the smallest scales, having survived every experimental test thrown at it. Moreover, a crucial ingredient in the adoption of quantum mechanics is that it is completely consistent with classical mechanics, as can be shown by carefully considering the limit $\hbar \to 0$. Thus, not only can quantum mechanics reproduce any prediction of classical mechanics, but it has an even more extensive predictive power, indicating that the fundamental structures of Nature are inherently quantum.

Though immensely successful, the theory of quantum mechanics was not immediately embraced without skepticism, partly due to some of the extremely counterintuitive phenomena that it contains. One of them is its purely probabilistic nature according to which physical systems are not inherently deterministic, but rather enjoy an intrinsic description in terms of odds and chances. Another one, slightly less philosophical in nature, is the quantum mechanical phenomenon of *entanglement*. Initially disregarded by Einstein himself as some "*spooky action at a distance*" [34], this intrinsic property of quantum mechanics, by which two particles share correlations so fundamental that they effectively act as a single system, has fully permeated the

development of quantum mechanics in the last century. In a highly counterintuitive way, entanglement describes correlations between quantum systems which seemingly disregard any causal restrictions on whether two events can affect each other. As per Einstein's theory of *special relativity* [35, 36], nothing can propagate faster than light in our Universe. Nonetheless, the effects of entanglement can be shown to be fundamentally non-local, as encapsulated by Bell in his famous entanglement inequalities [37], motivated by thought experiments suggested by Einstein, Podolski, and Rosen [38]. Bell's inequalities show how quantum mechanics predicts certain correlations between measurements that cannot be derived by any theory obeying *local realism*. The latter refers to the assumptions that special relativity holds, and that objects have definite intrinsic properties regardless of whether these are measured or not. Since then, countless experiments were devised in order to test whether Nature obeys Bell's inequalities, so-called *Bell tests*, or whether quantum mechanics leads to inconsistent predictions [39–41]. The simplest Bell test, ignoring loopholes for simplicity, consists of the simultaneous measurement of two entangled particles in laboratories that are sufficiently far apart. Quantum mechanics predicts that the measurement of particle A *instantaneously* fixes the measurement outcome on particle B, and it does so 100% of the time. To this day, every single Bell test ever performed has shown that Nature behaves in a way that is incompatible with local realism, indicating that quantum entanglement really is a deep property of physical systems. These efforts culminated in the Nobel Prize in Physics 2022, awarded to Aspect, Clauser, and Zeilinger for hallmark experiments providing definitive evidence for the violation of Bell's inequalities. This, together with innumerable other experimental verifications, has consolidated the place of quantum mechanics as our best model of physics at small scales. As a consequence, we are highly interested in measures that can quantify the amount of entanglement present in a quantum system. The prime example of such a quantity is the *entanglement entropy* of a subregion with respect to its complement, defined as $S(\rho_A) = -\operatorname{Tr}(\rho_A \log \rho_A)$, where ρ_A is the reduced density matrix of the subregion A, obtained by tracing out the degrees of freedom of the complementary region. Entanglement entropy plays a major role in the description of quantum systems, and we will see explicit examples of this below.

In the remaining part of the 20th century, the framework of *quantum field theory* (QFT) [9, 42, 43] arose from the imminent combination of special relativity and quantum mechanics. In this description, spacetime is permeated by fluctuating quantum fields whose values depend on the spacetime coordinates, and individual particles are regarded as excitations of these fields [44]. In particular, the first quantum field theory

devised by Dirac [9] provided such a description for electrically charged particles, e.g. the electron. Later key developments made by Feynman lead to what we currently know as *quantum electrodynamics* (QED) [43, 45], which is our best description of electromagnetically interacting particles. QED is the simplest example of a *gauge theory*, i.e. a theory with an internal redundant symmetry, which in the case of QED is described by the Abelian group U(1). Subsequent explorations in the latter half of the 20th century gave rise to QFT descriptions of two other fundamental forces in Nature, the weak force [46–51], and the strong force [52–56]. Both of these are examples of non-Abelian gauge theories, with gauge groups SU(2) and SU(3), respectively. The unification of these three quantum field theories under a single framework gave birth to the *standard model* of particle physics [57], which correspondingly has a gauge group $\mathrm{SU}(3)\times\mathrm{SU}(2)\times\mathrm{U}(1)$. Enhanced with the discovery of the Higgs boson in 2012 [58, 59], the standard model is the epitome of our understanding of subatomic particles and non-gravitational forces in the Universe, boasting unprecedented predictive power and matching experimental observations to outstanding accuracy.

For most phenomena that we encounter in our daily lives, and even most of the phenomena that are subject of cutting-edge physics research today, general relativity and quantum mechanics can be considered separately from one another to a very good approximation, each providing superb descriptions and predictions of physical systems in their respective regimes of validity. There are two main reasons for this. The first one is that we must view quantum field theory as an effective low-energy theory which is reliable only up to a certain energy scale Λ, and in this regime, gravitational effects are negligible. The energy scale Λ arises in the regularization of momentum integrals. It subsequently enters in the *renormalization* of the theory, which yields predictions for actually measurable values of observables in terms of the otherwise artificial parameters in our Lagrangian. New physics awaits us above the energy scale Λ, but occurrences of such high energies are extremely scarce and we can typically live with our ignorance. The second reason is the enormous hierarchy between the coupling constants of the four fundamental forces. More precisely, the relative interaction strengths of the strong, electromagnetic, and weak forces are $\alpha_{\mathrm{S}} = 1$, $\alpha_{\mathrm{EM}} \approx 1/137$, and $\alpha_{\mathrm{W}} = 10^{-6}$, respectively, and all of them are *dimensionless* couplings [60]. This is an absolutely crucial fact which ensures the renormalizability of these theories [61]. Meanwhile, the gravitational interaction is governed by Newton's constant G_N, and the relative strength of the gravitational forces with respect to the strong force is $\alpha_{\mathrm{G}} = 10^{-41}$, i.e. absurdly small. Thus, we can typically neglect gravitational effects when dealing with quantum mechanical systems, just as we can neglect quantum me-

chanical effects when considering planetary motions.

However, there exist two scenarios where such approximations break down, indicating the need for a more complete description. The first one is the black hole singularity, close to which the energy density diverges while being constrained to an infinitesimally small region of spacetime. Quantum effects at such short distances, typically heralded by the Planck length $l_{\rm P} \sim 10^{-35}$m, are not negligible anymore, and the interaction between gravity and the other fundamental forces needs to be taken into account. The second scenario arises from the theory of cosmic inflation [62], which implies that for time-scales of the order of the Planck time $t_{\rm P} \sim 10^{-44}$s after the Big Bang, the size of the Universe was $\mathscr{O}(l_{\rm P})$ and the energy scales where comparable to the Planck energy (or Planck mass) $E_{\rm P} = M_{\rm P} \sim 10^{28}$eV. Both QFT and GR are incapable of describing physics at these Planck scales on their own, indicating the need of a more complete unified theory of quantum gravity (QG) at high energies.
"Quantize GR then, just so" you might say, just as we quantized the other fundamental forces. Unfortunately, this is not possible. The problem is that Newton's constant is not only *dimensionful*, in contrast to the other three coupling constants, but it also has a negative mass-dimension $[G_N] = [M_{\rm P}^{2-D}]$ (with D the dimension of the spacetime), making GR a perturbatively non-renormalizable theory [61, 63, 64]. The non-renormalizability of GR implies that we cannot straightforwardly quantize the metric tensor $g_{\mu\nu}$, not even when considering perturbatively small fluctuations around flat spacetime $g_{\mu\nu} = \eta_{\mu\nu} + \frac{1}{M_{\rm P}} h_{\mu\nu}$. Though we can still quantize general relativity by treating it as an effective field theory at low energies [65–70], we must bear in mind that this description breaks down at the Planck scale, and a UV complete theory of gravity is thus still needed. The search for a consistent theory of quantum gravity is one of the most significant open questions in current-day theoretical physics. Nonetheless, black holes offer a part of low-energy gravitational physics via which we can learn about UV properties of gravity, as we discuss in what follows.

The challenge of finding a UV complete theory of quantum gravity which reduces to GR at low-energies made a huge step forward via the introduction of *string theory* [71–73]. Though born from early approaches to describe the strong force [74–77], string theory saw a surge in interest as a standalone theory since it automatically contained a massless particle with spin 2 in its spectrum, i.e. a *graviton* [78, 79]. The late part of the 20th century experienced a vast amount of work put into studying string theory as a natural candidate for quantum gravity, with many different versions of it being developed to include predictions on the particle content of our Universe [80–

82]. These were later shown to be part of a larger theory, called "M-theory" [83, 84]. Though it is the currently best candidate we have for a theory of everything unifying general relativity, gauge theories, and strings, many aspects of M-theory remain forbiddingly ***M***ysterious, and the extraction of meaningful verifiable predictions to test it is extremely difficult. Fortunately, ground-breaking progress was made in 1997 as Maldacena [85] provided a specific string-theoretic construction which allowed for completely controllable analyses down to low-energy effective descriptions, thus facilitating the study of potential UV completions of gravity. This so-called AdS/CFT correspondence [85] presents a concrete duality between string theory in negatively curved Anti-de Sitter (AdS) spacetime in $(d+1)$-dimensions and quantum field theories with conformal symmetry (CFTs) in d dimensions [86, 87]. Importantly, the two theories are completely independent of each other, and can be seen as two entirely equivalent descriptions of the same physics, albeit expressed in terms of different quantities. This is the great benefit of AdS/CFT, since it enables the translation of problems from one theory to the other in a consistent way, such that different techniques can be used to tackle them. The formulation of AdS/CFT at low energies states that weakly coupled classical gravity on AdS is dual to strongly coupled CFTs with a large number of degrees of freedom, with quantities on both sides of the duality being mapped to each other via the *holographic dictionary* [86, 87]. Since its inception, it has lead to an abundance of progress in several fields of physics beyond high-energy, including condensed matter [88–95] and particle physics [96–101].

Due to the difference in dimensionalities of both theories, the AdS/CFT correspondence is the best understood realization of the *holographic principle* [102–104]. The latter is believed to be a fundamental property of any theory of quantum gravity, and it was born from considerations on the entropy carried by black holes [105–107]. A universal bound found by Bekenstein states that the entropy S of a spacetime region is upper-bounded by its area A rather than its volume, indicating that entropy in gravity is not a merely extensive quantity. More precisely,

$$S \leq \frac{c^3 k_{\mathrm{B}} A_{\mathrm{horizon}}}{4 G_N \hbar}\,, \tag{1.1}$$

where the bound is only saturated by black holes. We have reinstated the natural constants to make manifest that black hole entropy is really a quantum gravitational effect, as heralded by the presence of both $\hbar$ and G_N in (1.1). The investigations on black hole entropy initiated by Bekenstein were quickly followed by Hawking, who attempted to give a semi-classical description of these gravitational objects [108–111].

Famously, Hawking showed that black holes emit thermal radiation throughout their lifetime [110, 111], allowing for the consideration of black holes as thermal objects with finite temperature. Taking into account the entropy carried by this radiation is key to derive consistent laws for *black hole thermodynamics* and provides a consistent merging of gravity with thermodynamics. In fact, a similar consistency with the statistical interpretation of the entropy would be achieved later as the Bekenstein bound (1.1) was derived directly from the counting of certain black hole microstates in string theory [112, 113]. This key result by Strominger and Vafa undermines our belief that the holographic principle is an indispensable property of quantum gravity.
As an explicit realization of the holographic principle, we should expect to be able to derive the Bekenstein-Hawking bound within the AdS/CFT correspondence. This is indeed possible thanks to the seminal work by Ryu and Takayanagi [114, 115], which provides a geometrization of the entanglement entropy $S(\rho_A)$ of subregions of the boundary CFT in terms of certain hypersurfaces in the bulk. Concretely in the case of $\mathrm{AdS}_3/\mathrm{CFT}_2$, the so-called Ryu-Takayanagi (RT) prescription relates the entanglement entropy of a subregion A in a CFT to the length of a minimal geodesic in the bulk spacetime which is anchored at the entangling points of A. The RT prescription famously reproduces the logarithmic dependence of entanglement entropy on the subsystem size known from two-dimensional CFTs [116–118]. In the case where the AdS spacetime contains a black hole, the dual CFT is in a thermal equilibrium state at temperature equal to the Hawking temperature. When the entangling region is taken to be the entire boundary, the RT formula retrieves the Bekenstein-Hawking black hole entropy (1.1) as the thermal entropy of the CFT. The corresponding RT surface is a geodesic which hugs around the black hole horizon, whose length is precisely the area A_{horizon} of the black hole horizon. The RT prescription can thus be thought of as a generalization of the Bekenstein-Hawking bound. This ground-breaking result of Ryu and Takayanagi not only provided a further manifestation of the holographic principle in AdS/CFT, but it also cemented a first entry in the holographic dictionary with origins in quantum information theory.

The emission of Hawking radiation hinted at a potential problem: although a black hole starts as a pure state (e.g. the one resulting from gravitational collapse), the radiation is purely thermal in nature, such that the final configuration after the evaporation is described by a mixed state. This is a blatant violation of unitary time evolution, which is a pillar of the theory of quantum mechanics, and it implies that information is being lost by black hole evaporation. This contradiction arising when we try to merge predictions from quantum mechanics and general relativity is known

as the *black hole information paradox* [119]. More precisely, the entanglement entropy $S(\rho_R)$ of the density matrix ρ_R describing the Hawking radiation is predicted to be mixed by Hawking's calculation, implying that $S(\rho_R)$ grows monotonically as the black hole evaporates. In contrast, we expect the Bekenstein-Hawking entropy to decrease to zero since $A_{\text{horizon}} \to 0$, hence the paradox.
The unitarity of holographic CFTs strongly suggests that the semi-classical computation of Hawking is incomplete, and that AdS/CFT may provide insights into a resolution to the information paradox. In fact, the RT prescription was used in [120–124] to make great progress towards resolving the paradox by considering a black hole in AdS coupled to a non-gravitating bath which collects radiation. It was shown that as the black hole evaporates, the outgoing Hawking radiation is entangled with modes located in a certain region behind the horizon known as an *island*, which is bounded by a so-called *quantum extremal surface* [125]. This indicates that the black hole interior is in fact encoded in the thermal radiation. From these results obtained from these constructions on the entanglement entropy of Hawking radiation, it was possible to derive a *Page curve* [126] for black hole evaporation, a vital signature of unitary evolution. In essence, the Page curve describes the behavior of entanglement entropy of the Hawking radiation (or the black hole) during evaporation. Unitarity dictates that this should increase monotonically until a given time scale known as the Page time, at which the entanglement entropy of the radiation is equal to the Bekenstein-Hawking entropy of the remaining black hole. After the Page time, the entanglement entropy should decrease back to zero when the black hole fully evaporates. The existence of islands can be traced back to certain wormhole solutions to the gravitational path integral, which experiences a dynamical transition between saddle-points at times of the order of the Page time. Although this provides a preliminary resolution to the paradox, it needs to be stressed that these constructions were obtained in fine-tuned and lower-dimensional quantum gravity settings. For instance, it was pointed out in [127] that these heat-bath constructions allow for massive gravitons, particles that we do not typically expect in standard gravity theories. A generic argument solving the paradox is not yet known, but the AdS/CFT correspondence is manifestly one of the best approaches we have to study this aspect of quantum gravity.

The AdS/CFT correspondence has proven to be an extremely useful framework to also address other issues related to our lack of knowledge about quantum gravity. In particular, it has helped answer questions about black holes via observables in CFTs. A central example for this is the duality proposed by Maldacena in [129] between an eternal black hole in AdS and two copies of a CFT in a specific entangled state known

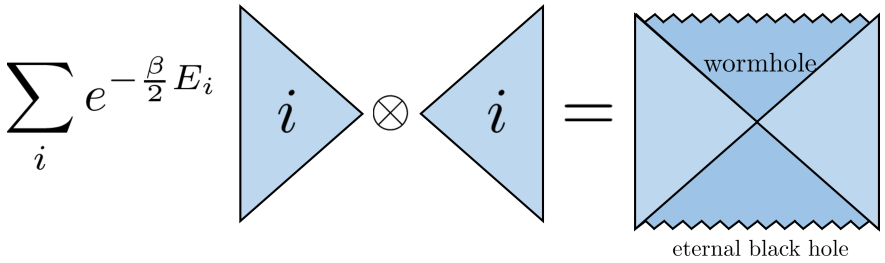


Figure 1.1: Entanglement between two copies of a holographic CFT in the TFD state, each dual to a single sided AdS black hole (blue patches), builds a connected wormhole spacetime represented by the Penrose diagram of the eternal AdS wormhole. Adapted from [128].

as the *thermofield double* (TFD) state [130]. The TFD state is a pure state consisting of a weighted superposition of the energy eigenstates $|E_i\rangle$ of both CFTs, in such a way that the reduced density matrix of a single CFT appears thermal with temperature β^{-1}. The duality between these two systems is one of the main workhorses of AdS/CFT, and it is a manifestation of the dogma that "entanglement builds spacetime" [131–133], also known as the ER=EPR conjecture [134]. The essence of this is that a single CFT at finite temperature should be dual to a black hole geometry in an asymptotically AdS spacetime, such that one may naively expect two copies of a CFT to be dual to two disconnected black hole spacetimes. Crucially, the entanglement between both CFTs, i.e. shared Einstein-Podolski-Rosen (EPR) pairs, creates a smooth interior geometry behind the horizon which connects these two Universes, the *wormhole* or Einstein-Rosen (ER) bridge [129, 134]. A schematic depiction of the TFD state and its geometric interpretation is shown in Fig. 1.1.

The ER=EPR conjecture, and in particular its realization within the eternal black hole to TFD state duality, does however lead to an immediate conundrum: Since the two copies of the CFT do not explicitly interact, the boundary Hilbert space can be assumed to have a factorized tensor product structure $\mathcal{H}_{\text{bdry}} = \mathcal{H}_L \otimes \mathcal{H}_{\mathcal{R}}$. Yet, the wormhole is a completely smooth geometry which cannot be divided into left and right contributions, indicating that the bulk Hilbert $\mathcal{H}_{\text{bulk}}$ space does not allow for such a factorized structure. Since one of the fundamental claims of the AdS/CFT correspondence is that $\mathcal{H}_{\text{bulk}} \overset{!}{=} \mathcal{H}_{\text{bdry}}$, this leads to a contradiction known as the *factorization puzzle* [135, 136]. It is believed that this puzzle simply arises from our incomplete semi-classical description of gravity, and the true Hilbert space of a UV complete theory of gravity should factorize. A resolution to the puzzle has recently been suggested in [137], where it is claimed that the factorization of the bulk Hilbert space is a consequence of non-perturbative wormhole contributions to the gravitational path integral. Although this analysis was only done for two-dimensional JT dilaton gravity, it is a first step towards a full resolution of the factorization puzzle, which would imply a

deep understanding of the Hilbert space of quantum gravity.

A final important open question within holography concerns the emergence of space and time in the black hole interior. There have been conjectures [138–141] that the origin of space, more precisely the size of the wormhole, is related to the *quantum complexity* of time-evolution on the boundary when seen as a quantum circuit. The introduction of quantum complexity into the holographic dictionary represents yet another instance of quantum information quantities in the AdS/CFT correspondence. Meanwhile, the origin of the arrow of time behind the horizon has been recently studied via a novel take on an old paradigm, namely the theory of local operator algebras [142–145]. This rigorous description of infinite-dimensional Hilbert spaces constructed from fundamental local observables is tightly linked to the structure of entanglement in quantum field theories. Recent investigations [146–148] have applied operator algebra techniques to holographic systems, a prime example being the Hawking-Page phase transition [149] between empty thermal AdS and large AdS black holes. Transitions between different types of operator algebras were held accountable for the definition of a time coordinate behind the horizon. More generally, operator algebras are related to entanglement entropy on a very fundamental level, and they offer an excellent tool to inspect the fine structure of entanglement in quantum gravity.

Scope, Structure, and Main Results

Given the historical context given above, let us position the current thesis within the broad landscape of open questions. Our investigations will be set within the context of the AdS/CFT correspondence as an approach to quantum gravity (QG). As we saw above, there are three main fields which play a role, namely general relativity (GR), quantum field theory (QFT), and recently also quantum information (QI). Within holography, it has become manifest that these three fields share significant overlaps, and a description of QG will very likely be based on all of them, as we depict in Fig. 1.2. The goals of this thesis are to explore the validity and extent to which the AdS/CFT correspondence can be realized in discrete settings, as well as to expand our knowledge on the role of quantum information quantities within holography. For this reason, the entire Venn diagram is placed on top of a *regular hyperbolic tiling* [150], our structure of choice for discretizing the AdS/CFT correspondence.

Our motivation for exploring discrete realizations of holographic dualities is twofold: On the one hand, discrete examples of the AdS/CFT correspondence highlight the extreme versatility of the holographic principle, providing evidence for its validity well

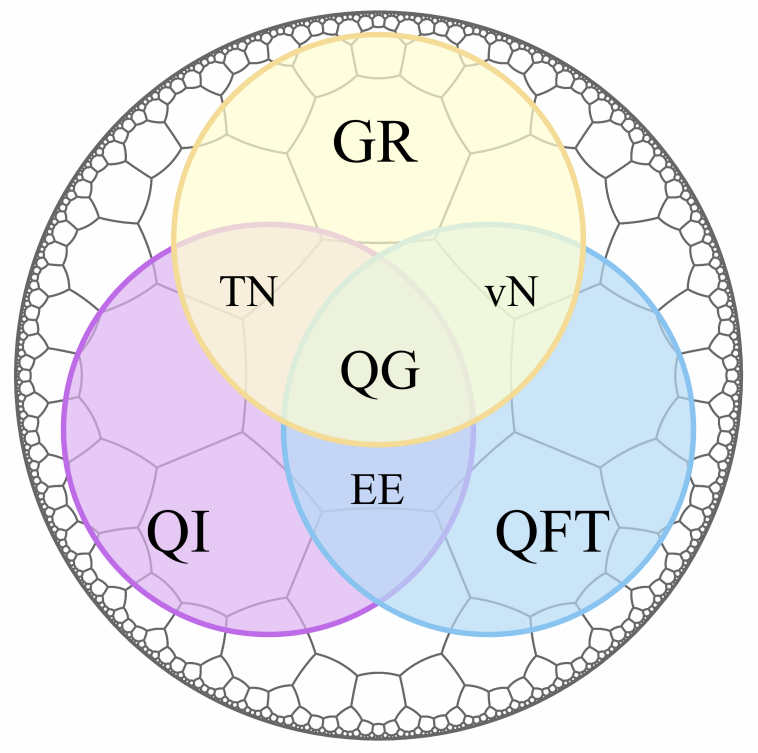


Figure 1.2: Venn diagram summarizing the main fields of physics, namely general relativity (GR), quantum field theory (QFT), and quantum information (QI), which enter the quest for a theory of quantum gravity (QG). The larger framework of the AdS/CFT correspondence, our best known non-perturbative approach to QG, benefits and covers methods and techniques from all aforementioned fields. The overlapping regimes of the diagram denote some of these methods, in particular the ones that will be thoroughly exploited in this thesis, namely tensor networks (TN), entanglement entropy (EE), and von Neumann (vN) operator algebras. The entire picture is set on top of a regular hyperbolic tiling as a visualization of the main goal of this thesis, which is to explore discrete instances of holographic dualities.

beyond the standard string-theoretic or even semi-classical regimes of the correspondence. On the other hand, suitable discretizations of holographic dualities bear the potential of accessing realistic experimental demonstrations of the AdS/CFT correspondence. Empirical laboratory setups are necessarily discrete in their nature, highlighting the necessity of a discrete description of any prediction from the duality. We propose such a realization in terms of electric circuits whose connectivity mirrors that of hyperbolic tilings. This design of suitable experimental architectures leads to real-life tests of otherwise merely conjectured phenomena. All in all, the discrete holography program, reviewed and extended in this thesis, provides a novel approach to investigate quantum gravity aspects from a pragmatic point of view.

Throughout the years, it has proven practical to address different aspects of QG by working at the overlaps of GR, QFT, and QI, and this thesis will follow suit in this

respect. Although each of these overlaps contains an immense amount of literature, techniques, and results, in Fig. 1.2 we highlight those which we actively exploit in this thesis. More precisely, the connection between GR and QI is best realized in the context of tensor networks (TNs) [151–153], which provide a spatially extended description of how spatial geometries can emerge from entanglement patterns in quantum states. These objects are naturally discrete and thus manifestly good candidates for discrete realizations of the holographic principle. We will utilize them to provide geometric descriptions of the entanglement structure of quantum states at the boundary of hyperbolic tilings. Meanwhile, the concept of entanglement entropy (EE), though it could very well be represented on the entire diagram in Fig. 1.2, has its roots in the overlap between QFT and QI. Universal behaviors of EE for QFTs and CFTs have been obtained [116–118], manifesting the fundamental nature of this quantity as a tool to understand the structure of field theories. In parallel, EE in discrete lattice systems has been studied extensively [154–156], and many similarities with holographic computations have been observed. It is thus natural to use entanglement as a fundamental quantity to benchmark any discrete holographic setup. We indeed employ EE in our characterization of potential discrete holographic boundary theories, as well as discrete analogues of the RT formula. Finally, while the overlap between GR and QFT has many facets, we will be particularly interested in the recent developments of von Neumann (vN) operator algebras as a mean to elucidate the complexion of entanglement and observables in a theory of quantum gravity. We will provide an explicit classification of von Neumann algebras in a controlled quantum many-body setting consisting of a general class of interacting Majorana lattice models. This is a first step towards the up-and-coming study of operator algebras in discrete holographic dualities.

Furthermore, this thesis aims to enhance our general knowledge of quantum information quantities within the AdS/CFT correspondence, even beyond any possible interpretations in discrete settings. We present novel results on holographic complexity measures via a definition of complexity that is well-defined for both finite- and infinite dimensional Hilbert spaces and provides a surprising connection to the theory of classical hydrodynamics. Additionally, we provide a diagnosis of factorization of partition functions based on the nature of the correlations within a quantum system. This yields novel interpretations of certain holographic states related to the TFD state, as well as insights into the origin of the factorization puzzle. In particular, we show how such states can be derived entirely from quantum information theory.

The remainder of this thesis consists of a review of background material in Chapter 2,

followed by an exposition of results regarding the discrete holography program in Chapter 3, and a collection of results on quantum information quantities and their implications for holography in Chapter 4. A more comprehensive outline of the thesis is the following:

- In Chapter 2, I introduce and review the relevant background material on which the rest of the thesis is based. More precisely, Sec. 2.1 provides a thorough introduction to the holographic principle following Bekenstein's original arguments for black hole entropy. This section makes clear why the holographic principle is the backbone of the AdS/CFT correspondence, which I individually review in Sec. 2.2. I cover the necessary concepts and definitions of AdS spaces (Sec. 2.2.1), CFTs (Sec. 2.2.2), the holographic dictionary (Sec. 2.2.3), and the AdS/CFT correspondence at finite temperature (Sec. 2.2.4). Then, in Sec. 2.3, I provide an extensive review of the quantum information quantities studied in this thesis, starting from entanglement entropy in quantum mechanics, quantum field theory, and holography (Sec. 2.3.1), through quantum complexity (Sec. 2.3.2) and quantum discord (Sec. 2.3.3). Finally, I review the framework of tensor networks with special emphasis on its implications for AdS/CFT in Sec. 2.3.4.

- Chapter 3 is devoted to the report of novel results within the discrete holography program obtained in [157–160]. Specifically, I give an overview of the state-of-the-art of this field in Sec. 3.1, before going into the detailed description of regular hyperbolic tilings in Sec. 3.2. Since these objects are our primary tool for discretizing hyperbolic spaces, I go into great detail about their isometry groups and geometric properties (Sec. 3.2.3), as well as their systematic construction in terms of substitution rules (Sec. 3.2.4) which results in so-called aperiodic sequences on their asymptotic boundary. Then, in Sec. 3.3, I present proof-of-principle results on the capability of hyperbolic tilings to reproduce predictions from continuous AdS/CFT. More specifically, I consider the Breitenlohner-Freedman stability bound for a massive scalar field on a fixed Euclidean AdS_2 background, which I then discretize using regular hyperbolic tilings (Sec. 3.3.1 and Sec. 3.3.2). I solve the Klein-Gordon equation with a UV cutoff in the continuum and compare the solutions to those obtained from a suitable discretization of the Laplace-Beltrami operator on the tiling (Sec. 3.3.3). This analysis is accompanied by numerical simulations showcasing the feasibility of realizing our setup in hyperbolic electric circuits, presented in Sec. 3.3.4. Following this benchmarking of hyperbolic tilings as appropriate discretizations of hyperbolic space, Sec. 3.4 presents novel results on the emulation of CFT-like correlation functions at zero and finite

temperature from a discrete bulk model on hyperbolic lattices. In Sec. 3.4.1, I consider a lattice model for an interacting massive scalar field defined on discretizations of Euclidean AdS_2 and of a time-slice of a three-dimensional black hole (Sec. 3.4.2). In Sec. 3.4.3, I show how correlation functions of operators on boundary sites of truncated tilings can be computed from the lattice model exploiting a discrete version of the holographic dictionary. The results are compared both to predictions from continuum AdS/CFT and simulations on electric circuits, the latter being accompanied in Sec. 3.4.4 by an explicit measurement protocol for experimental implementations. Then, I report novel results on explicit Hamiltonians at the boundary of regular hyperbolic tilings in Sec. 3.5, as candidates for discrete holographic boundary theories. I explain how aperiodic quantum spin chains, a type of disordered chains, can be constructed from the aperiodic sequence associated to hyperbolic tilings (Sec. 3.5.1). I study the ground state of these disordered chains via a real-space renormalization group technique known as strong-disorder renormalization group, which I review in Sec. 3.5.2. Exploiting this method, I compute expressions for several observables in these ground states, such as correlation functions (Sec. 3.5.3), entanglement entropy (Sec. 3.5.4), and mutual information (Sec. 3.5.5). These general results are then showcased in three specific examples of such aperiodic models in Sec. 3.5.6. Finally, I provide a tensor network description for these ground states in Sec. 3.5.7, which furnishes a potential discrete bulk dual for aperiodic spin chains. I conclude with a general discussion of all these results in Sec. 3.6.

- In Chapter 4, I focus on the study of black hole properties via holographic interpretations of several quantum information theory quantities. The results reported in this chapter were obtained in [161–163]. I start in Sec. 4.1 by reporting results on holographic quantum complexity, in particular a definition of a general complexity measure for both finite- and infinite-dimensional Hilbert spaces. The mathematical framework for this geometric description of complexity, known as the Euler-Arnold approach, is reviewed in Sec. 4.1.1. I explain the construction of a suitable basis for the $\mathfrak{su}(N)$ algebra of unitary gates in Sec. 4.1.2, and show how it gains an interpretation as a theory of hydrodynamics in the limit $N \to \infty$. I specify the details of the chosen complexity measure in terms of a cost function in Sec. 4.1.3, comparing also to other suggested measures in the literature. Sec. 4.1.4 discusses the properties of the complexity geometry at large N and its compatibility with desired features for holographic complexity measures. In Sec. 4.2, I discuss novel progress regarding the factorization

puzzle and report on a new method for diagnosing the factorization properties of partition functions based on a quantity known as geometric quantum discord. I first discuss this method for generic pure states in Sec. 4.2.1, before transitioning to the holographically relevant example of the thermofield double state in Sec. 4.2.2. Then, in Sec. 4.2.3, I explain the relation between geometric quantum discord and the overlaps of microstates of astrophysically relevant black holes. Finally, in Sec. 4.3, I study models of interacting Majorana fermions via the mathematical framework of von Neumann operator algebras. I begin by providing a brief historical context of this field in Sec. 4.3.1, together with the essential definitions and concepts that will be used thereafter. Section 4.3.2 is devoted to the definition of an interacting lattice model with N Majorana fermions at each site, followed by the exact solution at large N using Schwinger-Dyson equations. Then, in Sec. 4.3.3, I present a thorough analysis on the thermodynamics of this model in the case of two- and four-site chains, including computations of the Green's function, the free energy, and the entanglement entropy. I exploit these results to fully characterize the phase diagram of the theory, which I subsequently investigate in Sec. 4.3.4 in view of different types of von Neumann operator algebras underlying it. A comprehensive discussion of the results for the entire chapter can be found in Sec. 4.4.

- I conclude this thesis in Chapter 5 where I provide an encompassing but succinct review of the main results, focusing on their relative significance within the broader body of work in the current literature. I then move on to discuss several future avenues for investigation that are enabled by the outcomes of this thesis, before concluding with some final words.

According to the structure highlighted above, the main results of this thesis can be grouped into two broad categories, namely those pertaining the discrete holography program, and those concerning quantum information quantities in holography.
On the one hand, the main results of this thesis in view of discrete holography can be summarized as follows:

- We establish that the Breitenlohner-Freedman (BF) stability bound, a hallmark result from continuous AdS/CFT, can be reliably implemented on regular hyperbolic tilings seen as a discretization of two-dimensional Euclidean Anti-de Sitter space. We confirm, both analytically and through simulations on electric circuits, that the BF bound of a free scalar field on discrete tilings approaches its continuum value as the tilings are taken to cover the entire hyperbolic space.

This is a proof-of-principle that regular hyperbolic tilings are an excellent platform to study discrete realizations of the AdS/CFT correspondence. Moreover, our results show how the BF bound can be straightforwardly measured via hyperbolic electric circuit experiments. These results are published in [157].

- We expand the platform of hyperbolic lattices as discrete setups for holography by considering an interacting scalar field on hyperbolic tilings and showing how boundary CFT correlation functions can be retrieved from this model. Our concrete and widely implementable framework allows for the emulation of CFT correlation functions both at zero and finite temperature via a lattice discretization of an AdS black hole. We retrieve CFT data such as scaling dimensions and three-point function structure constants of a broad class of CFTs. We again exploit the platform of electric circuits, now enhanced by the introduction of diode elements, to provide an experimentally realizable measurement protocol of these correlation functions. These results are published in [160].

- We establish a large class of aperiodic quantum spin chains at the boundary of hyperbolic tilings as promising candidates for boundary theories in discrete holography. Explicit Hamiltonians are constructed based on a systematic construction of regular hyperbolic tilings via substitution rules, and their ground state properties are analyzed via real-space renormalization group techniques. We study and characterize observables such as correlation functions, entanglement entropy, and mutual information. We retrieve power-law decays of correlation functions, as well as logarithmic growth of the entanglement entropy, whose coefficient we identify as an effective central charge. The latter encodes information about the specific tiling used to construct the bulk tiling. We provide a discrete analogue of the RT formula based on the length of discrete paths through the tilings. Although we do not exactly retrieve results from continuum AdS/CFT, this is to be seen as an extension of the duality and hints at new physics that may be uncovered in discrete settings, and we include thorough discussions on this point. Furthermore, we provide a discrete holographic bulk dual for our aperiodic spin chains in terms of a tensor network construction. These results are published in [158] and [159].

On the other hand, the main results of this thesis regarding quantum information in holography can be summarized as follows:

- We provide an explicit construction for quantum complexity of SU(N) unitary gates which is well-defined even in the limit $N \to \infty$, thus offering a prime start-

ing point for complexity definitions in infinite-dimensional Hilbert spaces. We establish a connection between quantum complexity and the theory of classical ideal hydrodynamics, which we exploit to characterize the Riemannian geometry associated to our definition of complexity. We deliver a thorough curvature analysis on this geometry, showing that it exhibits all desired properties of a holographic complexity measure. Our uncomplicated construction offers novel interpretations of these features based on the geometric properties of the hydrodynamical phase space, as well as an alternative way of computing complexity of large SU(N) unitaries. These results are published in [161].

- We establish a novel diagnostic for the non-factorization properties of modular partition functions of pure states based on the information-theoretic quantity known as geometric quantum discord (GQD). We derive an explicit expression for GQD of arbitrary pure states, which shows that GQD vanishes if and only if the partition function factorizes. We apply our results to the example of a TFD state of holographic CFTs dual to an eternal black hole in AdS. Our results offer a derivation of the thermo-mixed double (TMD) state of [164] from a pure quantum information point of view, as well as a novel interpretation of the TMD state as the closest approximation of the TFD state containing solely classical correlations. We relate GQD and generalizations thereof to black hole microstates and discuss how these may be the origin of the non-factorization of the gravitational path integral, thus advancing our understanding of the factorization puzzle. These results are published in [162].

- We present an exactly solvable lattice model of interacting Majorana fermions with a non-trivial phase diagram exhibiting a quantum phase transition. We analytically compute the entanglement entropy of a two-site subregion in a four-site chain, and show that this entanglement entropy exhibits a discontinuity at the critical point, detecting the phase transition. Following the surging interest on operator algebras in AdS/CFT and quantum gravity, we fully characterize the type of von Neumann algebras underlying the model throughout the entire phase diagram. We observe several transitions between these types of algebra, including a transition which coincides with the phase transition in the limit of strong coupling. Our findings establish a controllable and exactly solvable quantum many-body setting which provides insight into operator algebras without the limiting computational aspects of working with quantum gravity. These results are published in [163].

Conventions and Notation

Throughout this thesis, and unless stated otherwise, I will use natural units where $\hbar = c = k_B = 1$ such that dimensionful quantities are measured in some power of length. The gravitational Newton's constant G_N will be kept explicit throughout most of this thesis, since it provides a natural and useful scale for comparisons. Whenever I use Lorentzian metrics, I will always give them in the mostly plus convention, and the time direction will always be included in the total dimensionality, such that a d-dimensional theory has $d-1$ spatial dimensions and one time direction.

2 Foundations

"When it comes to the world around us, is there any choice but to explore?"

Lisa Randall

In this chapter, I introduce all necessary background concepts which lay the technical foundations for this thesis, focusing on the AdS/CFT correspondence as well as selected topics from condensed matter and quantum information theory. The guiding principle for all investigations in this thesis is to make progress towards a theory of quantum gravity. Such a theory, though elusive, is expected to have several features which can be investigated in a more controlled way when working within the framework of the AdS/CFT correspondence [85–87]. The latter provides connections and equivalence relations between quantities in two seemingly very different theories: On the one hand, we consider gravity in a $(d+1)$-dimensional spacetime exhibiting uniform negative curvature. On the other hand, we have a quantum field theory in d-dimensions equipped with conformal symmetry and is defined on a flat background. These two theories could not be more dissimilar. Yet, there are several features which tell us how they are actually related on a very fundamental level. This manifests itself in the fact that both theories describe the same physical quantities, albeit using different languages. To translate between these languages, we use the *AdS/CFT dictionary*, which contains entries with precise relations between objects on both sides of the correspondence. In its more general form, this duality thus provides a bridge between general relativity and quantum field theory.

In the last 20 years, a third component has entered the holographic paradigm, namely information theory [165–167]. Both in its classical and quantum formulations, information theory has been essential to unveiling the fundamental properties of black holes, which are a key player in practical applications of AdS/CFT, as well as in more fundamentally abstract deliberations on holography and quantum gravity. Time and time again, measures and objects from quantum information theory have found their way into the holographic dictionary. Quantum information seems so inextricably linked to holography that some have even argued that spacetime itself is a consequence of entanglement [132]. Beyond entanglement, other measures such as mutual information, quantum complexity, quantum discord, relative entropy, quantum error-correction and

tensor networks have lead to immense progress towards understanding the many facets of quantum gravity. Thus, quantum information has cemented itself as the third pillar of the holographic paradigm towards quantum gravity, cf. Fig. 1.2.
This Chapter is structured as follows: I start by introducing the holographic principle in Sec. 2.1, following Bekenstein's original argument on black hole entropy. This argument is quite natural and it underpins why the holographic principle is believed to be such a fundamental property of any theory of quantum gravity. Sec. 2.2 then introduces the best understood realization of the holographic principle, namely the AdS/CFT correspondence, also known as holography. I first cover the general spirit of the duality and to some extent its origins in string theory. Then, I go into the individual ingredients of the correspondence in greater detail, such as AdS spacetimes, conformal field theories, the field-operator map and the equivalence of generating functionals. I lay special focus on the symmetry groups on both sides of the duality, since these will play a major role in Chapter 3. For later reference, I also discuss AdS/CFT at finite temperature and introduce the black hole geometries relevant for this thesis, together with the celebrated Hawking-Page phase transition. Finally, in Sec. 2.3, I give an overview of all relevant concepts from quantum information theory that play a role in this thesis. Starting from entanglement entropy and mutual information, concepts like quantum complexity, quantum discord and tensor networks are presented. Along with their definitions, I highlight their relevance in the context of holography by summarizing celebrated results and problems found in previous literature on AdS/CFT, such as the Ryu-Takayanagi formula and the factorization puzzle.
For the exposition of this background material, I largely follow the content of the following references [91, 168–172].

2.1. The Holographic Principle

No introduction to the AdS/CFT correspondence is complete without a mention of the so-called *holographic principle* [102, 103]. When listing some of the properties that a full-fledged theory of quantum gravity ought to have, the holographic principle arises as a seemingly fundamental entry to this list. Though somewhat counterintuitive at first, we have plenty of evidence that indicates to the validity of the holographic principle, as we will shortly review. In its simplest formulation, the principle states the following: In a theory of quantum gravity, the degrees of freedom within a spacetime region of volume V can actually be encoded on its boundary ∂V and the physics within V can be fully described by the degrees of freedom defined on ∂V. As many other conjectures, the holographic principle was born form the identification of cer-

tain pattern in nature, which ultimately lead to its current, very general formulation. Such a principle, in the words of Bousso, "stands by itself, both uncontradicted and unexplained by existing theories, [...] and it declares a given pattern to be at the core of a new theory altogether" [104]. One of the patterns that lead 't Hooft to conjecture the holographic principle was the previous work of Bekenstein [105–107, 173] and Hawking [108–111, 119, 174, 175] on the role of entropy in gravitational systems and the maximal amount of entropy that a given spacetime region can contain.

Bekenstein's argument goes as follows: The area theorem proved by Hawking [109] states that the surface area A of a black hole never decreases in time.[1] Not only does this hold for a single black hole, but also to the merging of several black holes, where the resulting surface area will be necessarily larger than the sum of the individual black hole areas. This behavior is of course intriguingly similar to that of thermodynamic entropy, and one is readily drawn to the idea that the surface area of a black hole may be related to a notion of entropy. More generally, Bekenstein argued that this suggestive relation should be analyzed by considering black holes altogether as thermodynamic objects, thus initiating the field of *black hole thermodynamics* [105, 106]. However, it is important to note that this black hole entropy is not really the thermodynamic entropy of the matter inside the black hole, but rather, it is a measure of the size of equivalent matter configurations which would all lead to the same black hole state. In this sense, the black hole entropy is a measure of the *inaccessibility* to the information about the matter that created the black hole, and is thus very similar to the notion of entropy in information theory [106]. From these arguments, it becomes apparent that a well-founded ansatz is to consider black hole entropy S_{BH} to be given by some monotonically increasing function of the black hole's area

$$S = f(A)\,. \tag{2.1}$$

By means of several physical arguments and Gedanken experiments, Bekenstein argued for the features and flaws of several choices of the function $f(A)$. A particularly promising choice was $f(A) = \gamma A$, with γ being an $\mathcal{O}(1)$ numerical factor. This choice obeys Hawking's area theorem in the case of merging black holes, something that other choices like $f(A) \propto A^{1/2}$ did not. By dimensional analysis, Bekenstein argued that the numerical prefactor should have dimensions of inverse length squared, since the entropy itself should be dimensionless. In particular, this prefactor should further contain a resolution scale, which is naturally provided by considering $\hbar^{-1}$ (in

[1] At least classically. Of course, semi-classical effects would later lead to the concept of black hole evaporation through Hawking radiation, but this plays no role in the current heuristic argument.

natural units). Note that this is not a quantum mechanical computation, rather, Planck's constant arises in a similar manner as for the quantization of the phase space familiar from statistical mechanics. Thus, the role of $\hbar$ is to keep count of the possible configurations. Later, Hawking showed that the correct prefactor should be $\gamma = 1/4\hbar$, which is remarkably close to Bekenstein's original guess of $\gamma = \log 2/2\hbar$. Based on these arguments, and on some consistency checks using the thermodynamic laws for black holes [174], the entropy of a black hole was found to be given by

$$S_{\text{BH}} = \frac{k_B c^3 A}{4\hbar G_N} \propto \frac{A}{4G_N}\,, \tag{2.2}$$

where we have briefly reinstated natural constants for completeness. Given the joint contributions of both authors involved in its derivation, the formula (2.2) is known as the *Bekenstein-Hawking entropy*. Fittingly enough, the subscript "BH" can stand for both black hole or Bekenstein-Hawking. Remarkably, the entropy of a black hole is given by its surface area measured in Planck units, since $G_N \propto l_{\text{P}}^2$. This implies that each Planck area l_{P}^2 carries an amount of information equal to $1/4$ of a bit. In other words, every bit of information that is thrown into a black hole increases its surface area by exactly 4 Plank areas. In particular, notice how the entropy of a black hole is *not* given by it's volume! This is exactly the behavior predicted by the holographic principle, and it is only suitable that it arises in the context of black holes, since the fundamental description of these objects is necessarily in a theory of quantum gravity. In fact, although the equilibrium state of a black hole is classically unique, the Bekenstein-Hawking formula (2.2) suggests that this classical configuration is compatible with an absurdly large number $e^{S_{\text{BH}}}$ of quantum mechanical microstates [104]. However, the precise nature of these quantum states remains one of the most intriguing questions in physics. A promising and celebrated result was the confirmation of the Bekenstein-Hawking formula via a microstate counting of certain classes of black holes arising in string theory [112]. In fact, it is worth mentioning that certain features that nowadays are collectively associated to the validity of the holographic principle were historically encountered within string theory [104, 176–181]. This is really to be expected since string theory *is* a theory of quantum gravity, and therefore these investigations can be seen as further evidence on the validity of this conjecture.

Later on, Bekenstein proposed the so-called *generalized second law* of black-hole thermodynamics [106, 107], which states that only the total entropy of a system consisting of a black hole and matter on its exterior should be constrained to only increase in time. In other words, for $S_{\text{tot}} = S_{\text{BH}} + S_{\text{matter}}$, we have $dS_{\text{tot}} \geq 0$. As a consequence of this law, Bekenstein derived that the value in (2.2) is indeed a universal bound for

the maximal amount of entropy of any matter system contained in a given spacetime region [107]. The fact that this is saturated by black holes shows that these objects are the most efficient encoders of information in the Universe, storing the most amount of information in the smallest area possible. To date, this is one of the strongest hints for the validity of the holographic principle.

2.2. The AdS/CFT Correspondence

Many areas of physics have seen unprecedented progress due to the discovery of *dualities*. A duality implies that there are two or more equivalent descriptions of the same physical phenomenon, where each description has its own independent set of degrees of freedom. The duality at the core of the present thesis is the AdS/CFT correspondence [85–87]. This is a conjectured duality between gravitational and quantum field theories, and it stands as the best understood explicit realization of the holographic principle. The holographic nature of the correspondence is due to the fact that the conformal field theory is defined at the conformal boundary of the bulk AdS spacetime. Although it originated from arguments in string theory, in this thesis we will deal mostly with predictions derived from the low-energy version of the duality, also known as the *weakest form* of the AdS/CFT correspondence [168]. In this regime, AdS/CFT is also an instance of a strong/weak duality, in which the strongly coupled CFT is dual to a weakly coupled gravity theory in the bulk. In the following sections, we will cover the individual ingredients of the correspondence that we will need later in the thesis.

2.2.1. Anti-de Sitter Spacetimes

We begin by defining Anti-de Sitter spacetimes in arbitrary dimensions, following [168] closely. Consider the theory of general relativity in a $(d+1)$-dimensional spacetime, governed by the Einstein-Hilbert action

$$S_{\text{EH}} = \frac{1}{16\pi G_N}\int_{\mathcal{M}} d^{d+1}x\sqrt{-g}\,(R-2\Lambda) - \frac{1}{8\pi G_N}\int_{\partial\mathcal{M}} d^{d}x\sqrt{\gamma}K\,, \tag{2.3}$$

This action can be occasionally enhanced by adding matter fields governed by an action S_{matter}. The EH action in (2.3) is defined over a smooth manifold $\mathcal{M}$, with G_N being Newton's constant, $g \equiv \det(g_{\mu\nu})$ is the determinant of the Riemannian metric tensor, R is its associated Ricci scalar, and Λ is the cosmological constant. The second term is the so-called *Gibbons-Hawking-York* boundary term [182, 183], and it is necessary in order to have a well-defined variational principle in case that $\mathcal{M}$ is

not closed. It contains γ, which is the induced metric at the boundary $\partial\mathcal{M}$ of the manifold, and K is the trace of the extrinsic curvature. The latter is defined in terms of the induced metric, the covariant derivative ∇, and an outward-pointing unit vector n_μ as $K = \gamma^{\mu\nu}\nabla_\mu n_\nu$. Imposing that the variation $\frac{\delta S_{\text{EH}}}{\delta g^{\mu\nu}}$ of the Einstein-Hilbert action (2.3) with respect to the metric tensor $g_{\mu\nu}$ vanishes yields *Einstein's field equations*

$$R_{\mu\nu} - \frac{1}{2}g_{\mu\nu}R + \Lambda g_{\mu\nu} = 8\pi G_N T_{\mu\nu}\,, \tag{2.4}$$

where $R_{\mu\nu}$ is the Ricci tensor, and $T_{\mu\nu} = -\frac{2}{\sqrt{-g}}\frac{\delta S_{\text{matter}}}{\delta g^{\mu\nu}}$ is the stress-energy tensor associated to the matter in the spacetime. Solutions to Einstein's equations (2.4) take the form of admissible Riemannian metrics $g^*_{\mu\nu}$.

Anti-de Sitter (AdS) spacetime is the unique, maximally symmetric solution to Einstein's equations in the vacuum, i.e. $T_{\mu\nu} = 0$, with a negative cosmological constant $\Lambda < 0$ and constant negative curvature. It enjoys the maximal number $(d+1)(d+2)/2$ of independent Killing vector fields. It can be defined as the set of loci obeying an embedding equation of the spacetime into a $(d+2)$-dimensional flat Minkowski ambient space. Coordinates in this ambient space are denoted by $\{X^0, X^1, \ldots, X^{d+1}\} \in \mathbb{R}^{d,2}$, where there are two time-like coordinates and d space-like coordinates, hence the metric signature $\eta = (-,+,\ldots,+,-)$. The invariant line element reads

$$ds^2 = \eta_{MN}dX^M dX^N = -(X^0)^2 + \sum_{i=1}^{d}(X^i)^2 - (X^{d+1})^2\,, \tag{2.5}$$

where we use Latin letters $M, N = \{0, \ldots, d+1\}$ to label the ambient space coordinates. AdS_{d+1} spacetime can then be defined as the hypersurface given by solutions to the embedding equation

$$-(X^0)^2 + \sum_{i=1}^{d}(X^i)^2 - (X^{d+1})^2 = -\ell^2\,, \tag{2.6}$$

where ℓ is the AdS radius of curvature, which sets the constant negative curvature of the spacetime as $R = -\frac{d(d+1)}{\ell^2}$. Crucially for the AdS/CFT correspondence, AdS spacetime enjoys a *conformal boundary* denoted by ∂AdS_{d+1}. This means that even though AdS itself is a non-compact space, it can be conformally compactified to a closed manifold with a boundary. From the perspective of the embedding (2.6), this conformal boundary consists of all points of the AdS hyperboloid which coincide with the light-cone of the ambient space $\mathbb{R}^{d,2}$, i.e. those points which obey $\eta_{MN}X^M X^N = 0$.

More precisely, the conformal boundary is defined as [168]

$$\partial \mathrm{AdS}_{d+1} = \left\{ [X] \,|\, X \in \mathbb{R}^{d,2}, X \neq 0, \eta_{MN} X^M X^N = 0 \right\} , \tag{2.7}$$

where $[X]$ denotes the equivalence class of coordinates up to a global rescaling, i.e. $\{X^M\} \sim \{\lambda \tilde{X}^M\}$, for $\lambda \in \mathbb{R}$. The topology of the conformal boundary in general dimensions is given by $(\mathbb{R} \times S^{d-1})/\mathbb{Z}_2$, where we already assume to have unwrapped the time coordinate such that we deal with the universal covering space of AdS_{d+1}, which does not contain closed time-like curves. The metric on the boundary of AdS is conformally equivalent to the flat Minkowski metric, a key fact which enables the relation between theories with and without gravity within holography.
The definition (2.6) makes manifest that the group of isometries of AdS_{d+1} is the group $\mathrm{SO}(d,2)$ of rotations under which the hypersurface (2.6) remains invariant with respect to the ambient space $\mathbb{R}^{d,2}$. In fact, given that AdS is a maximally symmetric space, it admits an alternative construction as a coset space [168], i.e. the quotient space of the isometry group of a manifold by its stabilizer group. This construction is in fact quite natural to understand in the more familiar example of a sphere S^2, whose isometry group is the group of rotations in three dimensions $\mathrm{SO}(3)$. Any point on the sphere is however also fixed by rotations around the axis connecting it to the center of the sphere. These rotations generate the group $\mathrm{SO}(2)$, and thus the sphere is given by the coset $S^2 = \mathrm{SO}(3)/\mathrm{SO}(2)$. In the case of AdS_{d+1}, the stabilizer group is given by $\mathrm{SO}(d,1)$, and therefore AdS_{d+1} can be defined as the quotient $\mathrm{AdS}_{d+1} = \mathrm{SO}(d,2)/\mathrm{SO}(d,1)$. A crucial fact for the AdS/CFT correspondence is that the isometry group $\mathrm{SO}(d,2)$ of AdS_{d+1} turns out to be precisely the global conformal group of Minkowksi spacetime in d dimensions [168]. This fundamental relation between symmetry groups will be a key motivation for our later discretization approaches investigated in Chapter 3.

It is useful to introduce several sets of coordinates for AdS_{d+1}, which we will often use in the rest of this thesis. The first set of coordinates is known as *global* coordinates and is given by $\{\rho, \tau, \Omega_i\} \in (\mathbb{R}_+, \mathbb{R}_+, [-1,1))$, where Ω_i denotes a set of general angular coordinates obeying $\sum_i \Omega_i^2 = 1$, for example $\cos\phi$ with $\phi \in [0, 2\pi)$. The global coordinates are defined by the hyperboloid parametrization

$$\begin{aligned} X^0 &= \ell \cosh\rho \cos\tau \,, \\ X^i &= \ell \sinh\rho \, \Omega_i \,, \\ X^{d+1} &= \ell \cosh\rho \sin\tau \,. \end{aligned} \tag{2.8}$$

The line element, or metric, of AdS in global coordinates reads

$$ds^2 = \ell^2(-\cosh^2\rho\, d\tau^2 + d\rho^2 + \sinh^2\rho\, d\Omega_{d-1}^2)\,, \tag{2.9}$$

where $d\Omega_{d-1}^2$ denotes the line element of a unit sphere S^{d-1}. The conformal boundary lies at $\rho \to \infty$, while the deep bulk of the geometry is at $\rho \to 0$. There exists an equivalent version of global coordinates, which we will denote as $\{\tilde{\rho}, \tilde{\tau}, \tilde{\Omega}_i\} \in (\mathbb{R}_+, \mathbb{R}_+, [-1, 1))$. They are defined by the following parametrization of the embedded AdS hyperboloid

$$\begin{aligned} X^0 &= \sqrt{\ell^2 + \tilde{\rho}^2}\cos\frac{\tilde{\tau}}{\ell}\,, \\ X^i &= \tilde{\rho}\,\Omega_i\,, \\ X^d &= \sqrt{\ell^2 + \tilde{\rho}^2}\sin\frac{\tilde{\tau}}{\ell}\,. \end{aligned} \tag{2.10}$$

We will later use these coordinates when discussing black hole solutions in AdS_3. These coordinates are related to the first version introduced above in (2.8) via the following transformation,

$$\tilde{\rho} = \ell\sinh\rho\,, \quad \tilde{\tau} = \ell\tau\,, \quad \tilde{\Omega}_i = \Omega_i\,. \tag{2.11}$$

The metric in these coordinates takes on the form

$$ds^2 = -\left(1 + \frac{\tilde{\rho}^2}{\ell^2}\right)d\tilde{\tau}^2 + \frac{1}{\left(1 + \frac{\tilde{\rho}^2}{\ell^2}\right)}d\tilde{\rho}^2 + \tilde{\rho}^2\, d\tilde{\Omega}^2\,, \tag{2.12}$$

where it is standard to define $f(\tilde{\rho}) = 1 + \frac{\tilde{\rho}^2}{\ell^2}$ for simplicity. This function resembles the blackening factor for black hole metrics, although it does not have any real roots. In these coordinates, the conformal boundary is located at $\tilde{\rho} \to \infty$ and the IR region is at $\tilde{\rho} \to 0$. Finally, a third useful coordinate system is given by the so-called *Poincaré patch*, given by $(z, t, \vec{x}) = (\mathbb{R}_+, \mathbb{R}, \mathbb{R}^{d-1})$, with $\vec{x} = (x_1, \ldots, x_{d-1})$. In contrast to the two previous global coordinate systems, which covered the entirety of the hyperboloid defined in (2.6), the Poincaré patch coordinates only cover one half of the entire AdS_{d+1}

spacetime. The hyperboloid parametrization is given by

$$\begin{aligned} X^0 &= \frac{z^2}{2}\left(1+\frac{1}{z^2}(\vec{x}^2-t^2+L^2)\right), \\ X^i &= \frac{Lx_i}{z}, \quad \text{for } i\in\{1,\dots,d-1\}, \\ X^d &= \frac{z^2}{2}\left(1+\frac{1}{z^2}(\vec{x}^2-t^2-L^2)\right), \\ X^{d+1} &= \frac{Lt}{z}, \end{aligned} \tag{2.13}$$

and the metric reads

$$ds^2 = \frac{\ell^2}{z^2}\left(dz^2+\eta_{\mu\nu}dx^\mu dx^\nu\right), \tag{2.14}$$

where $\eta_{\mu\nu}$ denotes the flat Minkowski metric along the boundary directions. The Poincaré patch is particularly useful for computations which focus on the asymptotic region close to the conformal boundary, which now lies at $z\to 0$, while the IR region is at $z\to\infty$. Another beneficial aspect of the Poincaré patch is the fact that it makes explicit the structure of AdS spacetime as a flat spacetime with an additional and orthogonal holographic coordinate, such that at every constant value of z, the transverse d-dimensional plane is flat Minkowski spacetime. This further manifests our previous statement that the metric at the boundary of AdS is conformally flat, as can be seen by rescaling the metric (2.14) by the factor z^2/ℓ^2.

Finally, let us mention that we can obtain the Euclidean version of AdS space by performing a Wick rotation $X^0\to \mathrm{i}X^0$ in the embedding equation (2.6), which has the effect of changing the isometry group from $\mathrm{SO}(d,2)$ to $\mathrm{SO}(d+1,1)$ for EAdS_{d+1}. For the global coordinate systems in (3.2) and (2.12), this amounts to a change in sign in front of the $d\tau^2$ and $d\tilde{\tau}^2$, respectively. In the Poincaré coordinates (2.14), it simply effects the change of $\eta_{\mu\nu}\to\delta_{\mu\nu}$. While the Lorentzian version of AdS_{d+1} admits spatial foliations in terms of hyperbolic spaces as $\mathrm{AdS}_{d+1}=\mathbb{R}\times\mathbb{H}^d$, the Euclidean versions of AdS are themselves entirely isomorphic to higher-dimensional hyperbolic spaces, i.e. $\mathrm{EAdS}_{d+1}\cong\mathbb{H}^{d+1}\cong\mathrm{SO}(d+1,1)/\mathrm{SO}(d+1)$, where the latter denotes the still valid coset construction. We will particularly make use of this connection to hyperbolic spaces in the case of EAdS_2 in Chapter 3.

2.2.2. Conformal Field Theories

Given the level of relevance enjoyed by conformal field theories (CFTs) within holography, it is only justified to dedicate a section to their most relevant features. We will only focus on aspects of CFTs which are pertinent for later arguments and discussions in this thesis. We delegate any further details and context to the standard references

[71, 168, 172].

Conformal field theories are quantum field theories which enjoy a further spacetime symmetry denoted as *conformal invariance*, which describes the invariance of the theory under local scale transformations. Given a generic line element $ds^2 = g_{\mu\nu}(x)dx^\mu dx^\nu$, conformal transformations are local coordinate transformations $x \mapsto \tilde{x} = f(x)$ which leave the metric invariant up to a Weyl rescaling $\Omega^{-2}(x)$, i.e.

$$g_{\mu\nu}(x) \mapsto \Omega^{-2} g_{\mu\nu}(x) = e^{2\sigma(x)} g_{\mu\nu}(x)\,. \tag{2.15}$$

Such transformations can effect local rescalings by changing the infinitesimal line-element, but they leave angles invariant and also preserve the overall causal structure of the spacetime [168]. For a CFT in d spacetime dimensions, the conformal group is given by $\mathrm{SO}(d+1,1)$ or $\mathrm{SO}(d,2)$ in Euclidean and Lorentzian signature, respectively. Crucially, note how this is precisely the isometry group of AdS_{d+1}, as discussed in Sec. 2.2.1. This matching of the symmetries is a key reason for the success of the AdS/CFT correspondence.

Let us focus on the case of Lorentzian signature for concreteness. The generators of the $\mathfrak{so}(d,2)$ conformal are the momentum P_μ, the dilatation D, the Lorentz transformations $L_{\mu\nu}$, and the special conformal transformations K_μ. The generators P_μ and $L_{\mu\nu}$ span the Poincaré algebra $\mathfrak{so}(d-1,1)$ which is a subalgebra of the conformal one. The commutation relations of the conformal algebra are given by [168]

$$\begin{aligned} [D, P_\mu] &= \mathrm{i}P_\mu\,, \quad [D, K_\mu] = -\mathrm{i}K_\mu\,, \quad [D, L_{\mu\nu}] = 0\,, \quad [K_\mu, K_\nu] = 0\,, \\ [K_\mu, P_\nu] &= -2\mathrm{i}(\eta_{\mu\nu} - L_{\mu\nu})\,, \quad [L_{\mu\nu}, K_\rho] = \mathrm{i}(\eta_{\mu\rho}K_\nu - \eta_{\mu\rho}K_\nu - \eta_{\nu\rho}K_\mu)\,. \end{aligned} \tag{2.16}$$

In the special case of $d = 2$, the conformal algebra is infinite-dimensional, highlighting the special character of two-dimensional CFTs. This is because the Killing equation, defining the form of possible conformal transformations, is solved by any holomorphic or anti-holomorphic function. The stress-energy tensor T admits a decomposition into holomorphic and anti-holomorphic modes

$$L_n = \frac{1}{2\pi\mathrm{i}} \oint dz\, z^{n+1} T(z)\,, \quad \bar{L}_n = \frac{1}{2\pi\mathrm{i}} \oint d\bar{z}\, \bar{z}^{n+1} \bar{T}(\bar{z})\,, \tag{2.17}$$

which can be identified with the generators of local conformal transformations. It can be shown that the generators L_n obey the unique central extension of the Witt algebra, known as the *Virasoro algebra*

$$[L_n, L_m] = (n-m)L_{n+m} + \frac{c}{12} n(n^2-1)\delta_{n+m,0}\,. \tag{2.18}$$

An analogous algebra is obeyed by the anti-holomorphic generators $\bar{L}_n$, and we have $[L_n, \bar{L}_m] = 0$. The coefficient $c > 0$ appearing in the Virasoro algebra (2.18) is called the *central charge* of the CFT. We will encounter the central charge again when we discuss entanglement entropy in CFTs. The generators $\{L_{-1}, L_0, L_1, \bar{L}_{-1}, \bar{L}_0, \bar{L}_1\}$ close among themselves and describe the *global conformal subalgebra* in two dimensions, spanning two copies of an $\mathfrak{sl}(2, \mathbb{R})$ algebra. As an algebra, we have the decomposition $\mathfrak{so}(2, 2) = \mathfrak{sl}(2, \mathbb{R}) \oplus \mathfrak{sl}(2, \mathbb{R})$, which is the same decomposition obeyed by the Killing vectors generating the isometries of AdS_{2+1}. This splitting is a special feature of two-dimensional CFTs and AdS_{2+1}. The general group $\mathrm{SO}(d, 2)$ does not admit such a splitting.

The spectrum of a CFT consists of local operators $\{\mathcal{O}\}$ which can be classified into irreducible representations of the conformal group via the method of induced representations [168]. The starting point for this classification are *primary operators* $\mathcal{O}(x)$, which are defined to obey

$$[D, \mathcal{O}(0)] = -\mathrm{i}\Delta\mathcal{O}(0)\,, \quad [K_\mu, \mathcal{O}(0)] = 0\,. \tag{2.19}$$

The first condition in (2.19) contains the so-called *scaling dimension* Δ of the operator, which describes how the operator transforms under scaling transformations $x \mapsto x' = \lambda x$, namely

$$\mathcal{O}(\lambda x) = \lambda^{-\Delta}\mathcal{O}(x)\,. \tag{2.20}$$

The second condition in (2.19) can be seen as the proper definition of a conformal primary operator, and it may be interpreted as the statement that a primary operator is the lowest weight state of the irreducible representation of the conformal group labeled by the dilatation eigenvalue Δ. This is because, given an eigenstate of the dilatation operator D, the operators P_μ and K_μ act on it by increasing and decreasing the scaling dimension, respectively. A primary operator $\mathcal{O}$ is annihilated by the generator K_μ of special conformal transformations, and all other operators obtained by applying other conformal generators onto $\mathcal{O}$ are called the *descendants* of $\mathcal{O}$. A given primary operator with scaling dimension Δ, together with all its descendants, constitutes an irreducible multiplet of the conformal algebra.

The large amount of symmetries enjoyed by CFTs heavily constrains the functional form of correlation functions of primary operators. Particularly the two- and three-point correlation functions are determined by conformal symmetry up to a small number of free parameters. For the two-point function of two primary operators $\mathcal{O}_1(x_1), \mathcal{O}_2(x_2)$ with respective scaling dimensions Δ_1, Δ_2, conformal symmetry con-

strains it to be of the form

$$\langle \mathcal{O}_1(x_1)\mathcal{O}_2(x_2)\rangle = \begin{cases} \dfrac{c_{12}}{|x_1-x_2|^{2\Delta}}\,, & \text{if } \Delta_1 = \Delta_2 \equiv \Delta\,, \\ 0\,, & \text{if } \Delta_1 \neq \Delta_2\,. \end{cases} \tag{2.21}$$

The coefficient can actually be set to $c_{ij} = \delta_{ij}$ upon a suitable normalization for the basis of primary operators [172]. In a similar fashion, the three-point function is constrained to have the form

$$\langle \mathcal{O}_1(x_1)\mathcal{O}_2(x_2)\mathcal{O}_3(x_3)\rangle = \frac{C_{123}}{|x_1-x_2|^{\Delta_1+\Delta_2-\Delta_3}|x_2-x_3|^{\Delta_2+\Delta_3-\Delta_1}|x_3-x_1|^{\Delta_3+\Delta_1-\Delta_2}}\,. \tag{2.22}$$

Given that the operator normalizations have been fixed by the two-point function, the coefficient C_{ijk} of the three-point function contains true information about the theory, and indeed it belongs, together with the scaling dimensions and the central charge, to the *CFT data* characterizing the theory.

2.2.3. The Statement of the Correspondence

Having reviewed its basic components, we now come to the explicit statements of the AdS/CFT correspondence. This thesis will not make use of explicit string theory computations, and therefore I only briefly review the stringy origins of the correspondence. I then turn to the holographic dictionary, which provides a practical equivalence of partition functions for holographic computations and will be a key ingredient in many discussions in Chapter 3.

Stringy Origins

The AdS/CFT correspondence was born from string theory constructions [85] in which both sides of the correspondence could be characterized explicitly, such as in the seminal duality between type IIB superstring theory on $\mathrm{AdS}_5 \times S^5$ and four-dimensional $\mathcal{N} = 4$ Super-Yang-Mills (SYM) theory with $\mathrm{SU}(N)$ gauge group. This is regarded as the *strongest form* of the AdS/CFT correspondence [168]. More broadly, the correspondence conjectures an equivalence between certain interacting QFTs in d-dimensional flat spacetime and quantum string theory on negatively curved backgrounds in $(d+1)$-dimensions. The different dimensionalities of the theories involved makes evident why the AdS/CFT correspondence is the best understood realization of the holographic principle reviewed in Sec. 2.1. Broadly speaking, there are two relevant parameters that enter the correspondence. The first one is a coupling constant λ governing the strength of interactions in the QFT. The second one is an effective

measure of the number of local degrees of freedom in the theory, which we generically denote here by $\#_{\text{dof}}$. In our specific example this is provided by the rank N of the gauge group of SYM, but we keep it generic for the following discussion. The counterparts to these parameters on the gravity theory are certain combinations of the dimensionless ratio ℓ/l_s between curvature radius ℓ and string length l_s and the string coupling g_s governing stringy interactions. For generic values of these parameters, the original duality proposed in [85], though extremely interesting and non-trivial, is not particularly practical given the technical difficulties involved in quantum string theory on curved backgrounds. Fortunately, later developments [86, 87] revealed that many statements could be carried over to more pragmatic versions of the duality in certain limits. The first one is the simplification associated to the limit of $\#_{\text{dof}} \to \infty$, which is commonly referred to as the *planar limit*. In this limit, stringy interactions are weak $g_s \to 0$, leading to classical string theory at tree level in $1/g_s$, while the QFT path integral localizes around saddle points and can be treated perturbatively in a $1/\#_{\text{dof}} \sim \hbar$ expansion [169], following ideas of [184, 185]. This gives rise to the *strong form* of the AdS/CFT correspondence [168], equating classical string theory $(l_s/\ell \neq 0)$ in $(d+1)$-dimensions with an interacting QFT in d-dimensions with large $\#_{\text{dof}}$. Although it provides a great simplification over the strongest form of the correspondence, the planar limit still presents formidable technical challenges for any practical computations. Further simplifications can be obtained by taking the strong coupling limit $\lambda \to \infty$, which on the gravity side has the effect of truncating the string dynamics to classical supergravity. In other words, the curvature radius is much larger than the string length $l_s/\ell \to 0$, yielding the point-particle limit of string theory. Thus, combining both limiting regimes of $\#_{\text{dof}} \to \infty$ and $\lambda \to \infty$, we obtain a duality between strongly coupled QFTs with a large number of degrees of freedom and semi-classical gravity dynamics on weakly curved AdS spacetime, which is known as the *weak form* of the AdS/CFT correspondence [168]. For the original example of the correspondence studied in [85], we have that the coupling strength is given by the so-called 't Hooft coupling $\lambda = g_{\text{YM}} N^2$, where g_{YM} is the Yang-Mills coupling constant, and $\#_{\text{dof}} \propto N^2 - 1$, with N the rank of the SU(N) gauge group [169]. In principle, the strongest form of the duality conjectures an isomorphism between the gravity and QFT Hilbert spaces, where each state on the QFT state can be mapped to a state the string theory Hilbert space. However, by taking the weak form of the correspondence, we are focusing on a corner of the Hilbert space with $\lambda, \#_{\text{dof}} \gg 1$, which denotes a subspace of theories with *geometric duals* [169]. This means we only consider field theory states whose holographic description involves explicit manifolds which are solutions to Einstein's field equations. Examples of this are the ground state

of holographic CFTs, dual to empty AdS, and excited thermal CFT states which are dual to black hole geometries in AdS [168].

Top-Down vs. Bottom-Up

The AdS/CFT correspondence is believed to be general, meaning that any theory of quantum gravity in AdS_{d+1} is holographically dual to a CFT in d dimensions.[2] Nonetheless, having explicit examples of dual theories is important to understand the inner workings of the correspondence. Such constructions typically originate from string theory and consider microscopic definitions of the models involved, e.g. the above-mentioned duality between type IIB string theory on $\mathrm{AdS}_5 \times S^5$ and $\mathcal{N} = 4$ SU(N) SYM in four dimensions. Other string theory constructions of holographic duals were given in [186–192]. These instances are known as *top-down* approaches to holography, and they offer clear settings where results on both sides of the duality can be quantitatively compared. They are therefore vital for trusting the correspondence on general grounds.

However, they are also very complex and technically challenging to handle, not to mention that the involved theories might not always be of physical relevance to real-world systems. An alternative avenue is then to start by assuming the existence of certain CFTs which obey the minimal assumptions of the weak form of the correspondence, without specifying any microscopic details of the theory such as its operator content. This effective description then constructs desired setups on the field theory by adding suitable entries of the holographic dictionary, such as bulk fields, symmetries, or conserved charges. An explicit Lagrangian for the CFT is however not needed and we only require access to knowledge about low-dimension operators in the spectrum. Additionally, one may or may not try to embed this setup into a UV completion of the theory in terms of string theory. This is known as the *bottom-up* approach to AdS/CFT. Even without the desire to include UV completions, the bottom-up approach lends itself quite nicely to construct CFTs which are reasonably good approximations of physically interesting systems. Simpler bottom-up models are thus highly relevant for direct applications of AdS/CFT such as AdS/QCD [97–100], fluid/gravity duality [193–195], and condensed matter (AdS/CMT) [88–93, 95].

In this thesis, all of our discussions and analyses will follow the spirit of the bottom-up paradigm to AdS/CFT. Our goal is to construct *discrete* models of holography from the bottom up, in order to not only investigate the regime of validity of the holographic principle, but also move predictions of AdS/CFT closer to experimental realizations.

[2] The safe statement would be any UV complete theory of gravity which behaves as Einstein gravity plus QFT at low energies.

The Holographic Dictionary

The weak form of the correspondence is of particular interest for explicit applications of the AdS/CFT duality, since it covers a large, albeit specific, class of interesting theories and it allows to derive statements valid on a more general level, regardless of the explicit choice of dual theories. That is, we are able to derive predictions relying only on the $\lambda, \#_{\text{dof}} \gg 1$ limiting regimes via which we can relate objects on both sides of the duality. The collection of such mapping relations between CFT objects and AdS quantities is known as the *holographic dictionary*. Originally, the entries of this dictionary relate fields ϕ in the gravity theory, also denoted as the *bulk*, and gauge-invariant local operators $\mathcal{O}$ in the CFT. Since the latter is considered to be defined on the conformal boundary of the AdS spacetime (cf. (2.7)), the CFT is also referred to as the *boundary theory*. The most general version of the dictionary is known as the Gubser-Klebanov-Polyakov-Witten (GKPW) dictionary [86, 87] which poses an equality between partition functions (or, equivalently, generating functionals) of bulk and boundary theories, i.e. $Z_{\text{AdS}} = Z_{\text{CFT}}$, where $Z = e^{-W}$ denotes the partition function, and W is the generating functional for connected correlators. This is conjectured to hold even for the strong form of the correspondence, in which case Z_{AdS} is the partition function of quantum string theory, an object which we do not know explicitly. A more precise version of the GKPW relation can be given in the semi-classical limit stipulated by the weak form of the correspondence, in which case the bulk path integral is governed by a saddle-point approximation. Explicitly, the GKPW reads

$$e^{-W[\phi_0]} = \left\langle \exp\left(\int d^d x\, \mathcal{O}(x)\phi_0(x) \right) \right\rangle_{\text{CFT}} = e^{-S_{\text{grav}}[\phi(z,x)]}\Big|_{\lim_{z\to 0}(\phi(z,x)z^{\Delta-d})=\phi_0(x)} . \quad (2.23)$$

On the left hand side of (2.23) we have the generating functional $W[\phi_0]$ of connected correlation functions of operators $\mathcal{O}$ in the CFT, which are inserted into the path integral via *sources* $\phi_0(x)$. Here, we use x as an overall index for the d dimensions on the boundary, and we work in Euclidean signature. Following standard techniques from QFT [44, 61], connected n-point correlation functions can be obtained from the generating functional by taking functional derivatives with respect to the sources

$$\langle \mathcal{O}_1(x_1)\mathcal{O}_2(x_2)\cdots\mathcal{O}_n(x_n)\rangle_{\text{CFT}} = -\frac{\delta^n W}{\delta\phi_0^{(1)}(x_1)\delta\phi_0^{(2)}(x_2)\cdots\delta\phi_0^{(n)}(x_n)}\Big|_{\phi_0^{(i)}=0} . \quad (2.24)$$

On the right hand side of the GKPW relation (2.23) we have the saddle-point approximation to the gravitational path integral, which consists of the bulk effective action S_{grav} evaluated on-shell on solutions to the equations of motion with specific boundary conditions. These boundary conditions are a crucial ingredient of the AdS/CFT

correspondence, and they impose a certain asymptotic behavior for the bulk fields, such as to obtain a mapping between bulk fields and boundary operators. This is known as the *field-operator map* of the AdS/CFT correspondence [168]. For instance, a bulk scalar field $\phi(z,x)$, where z denotes here the holographic coordinate, will behave asymptotically towards the AdS boundary as

$$\phi(z,x) \sim z^{d-\Delta}\phi_0(x) + z^{\Delta}\langle\mathcal{O}\rangle\,, \tag{2.25}$$

where the coefficient of the leading term, also called the *normalizable mode*, is identified with the source $\phi_0(x)$ for the dual operator. Meanwhile, the coefficient of the subleading, or *non-normalizable*, mode is identified with the vacuum expectation value of $\mathcal{O}$. The boundary conditions entering the right hand side of the GKPW relation (2.23) precisely impose that the boundary value of the bulk field, after a suitable rescaling, is exactly the source term for the CFT operator insertion, i.e.

$$\lim_{z\to 0}(\phi(z,x)z^{\Delta-d}) = \phi_0(x)\,. \tag{2.26}$$

In this sense, we say that the bulk field $\phi(z,x)$ is holographically dual to the operator $\mathcal{O}$ on the boundary. Notice how this is a key and unique feature of AdS/CFT: we are solving equations of motion in such a way that the *boundary conditions* themselves are quantum fields which fluctuate according to their own theory! Furthermore, a crucial consequence of the GKPW relation (2.23) and the boundary condition (2.26) is an explicit relation between the mass m of the scalar bulk field and the scaling dimension Δ of the dual operator [87], namely

$$m^2\ell^2 = \Delta(\Delta - d)\,. \tag{2.27}$$

The positive root of this formula is given by

$$\Delta = \frac{d}{2} + \sqrt{\frac{d^2}{4} + m^2\ell^2}\,, \tag{2.28}$$

which also determines the exponent appearing in the asymptotic behavior for the bulk scalar field given in (2.25). Surprisingly, notice that negative values $m^2\ell^2 \geq -\frac{d^2}{4}$ of the mass-squared are allowed by the relation (2.28) following the reality of scaling dimensions for unitary CFTs. This is the celebrated Breitenlohner-Freedman bound [196, 197], which arises from contributions of the negatively curved spacetime to the total energy of the system. This indicates that solutions to the equations of motion with slightly negative mass-squared are still stable, albeit tachyonic. In fact, the core

of our discussions in Sec. 3.3 will regard the consequences of spatial discretizations of the bulk on the Breitenlohner-Freedman bound. Furthermore, part of our analysis in Sec. 3.4 will consider a similar question regarding the bulk on the mass-dimension formula (2.27). As a concluding remark, it is worth mentioning that similar relations to those above hold for all bulk fields, and each of them realizes an entry in the holographic dictionary. For instance, vector fields A_μ in the bulk are dual to spin-1 operators J^μ on the boundary (which are conserved currents if A_μ is massless), while fluctuations of the metric tensor $g_{\mu\nu}$ acts as sources for the boundary stress-energy tensor $T^{\mu\nu}$ [168]. Relations analogous to (2.27) can be derived in these cases as well, up to slight modifications depending on the spin of the fields, see [168] for more details.

Let us conclude our review of the AdS/CFT correspondence with a word of caution. Recall the special conditions $\lambda \gg 1$ and $\#_{\text{dof}} \gg 1$ we mentioned in the beginning of this section, which allowed us to restrict to CFT with a holographic geometric dual. The strongly coupled limit implies a large gap in the spectrum of operators of the CFT, separating the low and high-dimension operators (otherwise also denoted as "light" and "heavy" operators by virtue of (2.27). This is to guarantee that bulk fields in our low-energy description only couple to low-lying operators and not the "stringy" operators with large scaling dimension which we specifically removed when going to the weak form of the duality. Moreover, the limit of large number of degrees of freedom was taken to suppress the string theory interactions, leading us to a tree level description of classical strings.
It is one of the goals of this thesis to explore the extent to which these standard requirements for AdS/CFT dualities may be stretched. In view of finding discrete instances of holographic dualities, a goal we pursue in Chapter 3, we will have working assumptions on the validity of application of certain holographic predictions, even though the presented models might not always comply with the strongly coupled or planar regimes elucidated above. Nonetheless, it is our belief that the holographic principle is fundamental enough that these assumptions can be made as a starting point, and we will thoroughly discuss the compliance (or lack thereof) of our results with these assumptions. In this way, we aim to survey the broad range of validity of the AdS/CFT correspondence beyond its archetypal assumptions.

2.2.4. AdS/CFT at Finite Temperature

The AdS/CFT correspondence goes beyond a duality between ground states, and the next immediate entry to the dictionary is the consideration of holographically dual systems at finite temperature. Not surprisingly, from the point of view of the bulk theory,

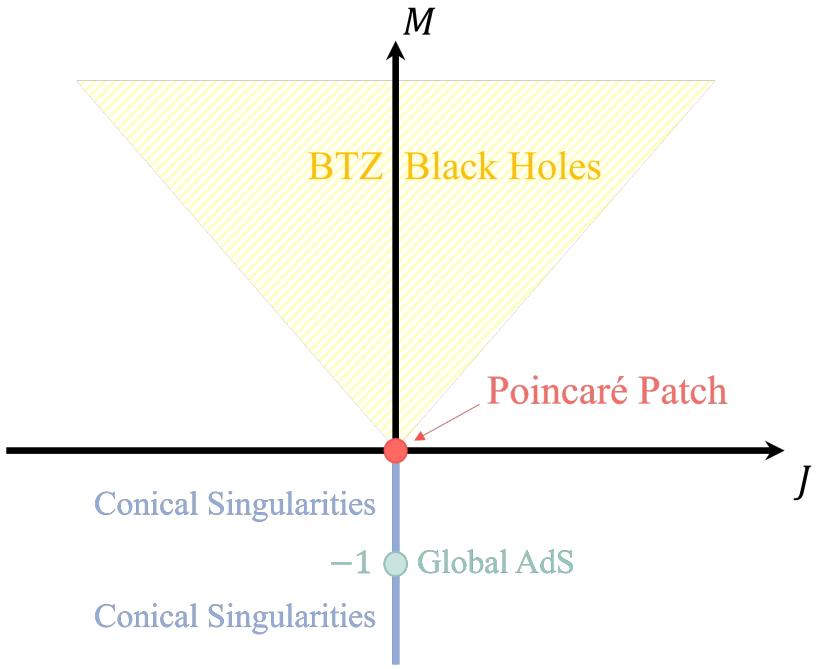


Figure 2.1: Phase diagram of asymptotically AdS solutions to (2+1)-dimensional Einstein-Hilbert gravity, parametrized by the general solution (2.33).

this involves the introduction of black hole geometries, since they naturally carry a notion of temperature given by their Hawking temperature T_{H}. On the boundary side of such a duality, we consider CFTs in a thermal state with temperature precisely given by T_{H}. For concreteness, we will focus on the case of the $\mathrm{AdS}_3/\mathrm{CFT}_2$ correspondence at finite temperature, which is particularly well-studied. In fact, a celebrated duality was formulated in this case between an eternal black hole in AdS and a particular state known as the *thermofield double* (TFD) state [130] constructed from two copies of a CFT [129].[3]

The BTZ Black Hole

In $(2+1)$ dimensions, Einstein-Hilbert gravity without matter is a topological field theory which does not contain any propagating degrees of freedom [201–203]. In particular, its apparent simplicity allows for a completely equivalent description in terms of a Chern-Simons gauge theory [204–206]. Moreover, when the cosmological constant is zero, it can be shown that the theory does not admit any black hole solutions [207]. It is therefore rather surprising that the phase diagram of asymptotically AdS_{2+1} solutions to the vacuum Einstein's equations exhibits such a rich structure, as summarized in Fig. 2.1. In particular, it contains the celebrated Bañados-Teitelboim-Zanelli (BTZ) black hole solution [208, 209], as well as conical singularities and empty AdS space-

[3] See also [198–200] for previous hints at similar ideas.

time at finite temperature, known as *thermal* AdS. The latter is simply an empty AdS spacetime with a periodic identification of its time coordinate, akin to the philosophy of statistical mechanics [149]. It can be thought of as a bath of thermal radiation in an otherwise empty AdS spacetime. In fact, it turns out that the BTZ black hole and thermal AdS exchange dominance at a finite temperature in the canonical ensemble partition function, which leads to the celebrated Hawking-Page phase transition [31], which we review in Box 2.1.

Box 2.1 The Hawking-Page Phase Transition

Following the first arguments that black holes have a temperature [109], studies into the thermodynamical properties of these objects were rampant. A general consideration from this perspective is whether known ideas from classical thermodynamics and statistical mechanics, such as the canonical ensemble, were well-defined for solutions to general relativity. For Schwarzschild black holes in asymptotically flat spacetime, this turns out not to be possible, given that the black hole configurations are only in an unstable thermal equilibrium with surrounding radiation due to their negative specific heat [149]. In 1983, Hawking and Page showed that considering pure gravity in AdS spacetimes not only allows for proper definition of black hole thermodynamics, but it even leads to interesting phase transitions between gravitational configurations [149]. In particular, semi-classically, the contributions to the path integral coming from empty AdS at a finite temperature and a black hole in AdS exchange dominance at a finite critical temperature. This came to be known as the Hawking-Page phase transition, and we sketch its relevant features in the following.

For simplicity, we will not consider any matter fields but rather focus on pure gravity and work in $(4+1)$ dimensions. The Einstein-Hilbert action given by

$$S_{\text{EH}} = -\frac{1}{16\pi G_N}\int d^5x\sqrt{g}\left(R+\frac{12}{\ell^2}\right). \tag{2.29}$$

We define the canonical ensemble via the gravitational path integral over all metrics $Z = \int \mathcal{D}g\, e^{-S_{\text{EH}}[g]}$, subject to the boundary conditions that they are asymptotically AdS with a periodically identified Euclidean time $\tau_E \sim \tau_E + \beta$, where β denotes the inverse temperature. We work in the semi-classical approximation and consider only small fluctuations around classical solutions to the equations of motion. In other words, we look for saddle-points of the gravitational path integral subject to the aforementioned boundary conditions at fixed β, of which there turn

out to be three possible ones: large black holes, small black holes, and thermal AdS [149]. Evaluating the action (2.29) on-shell on these solutions, the dominant contribution to the partition function $Z \approx e^{-S_{\rm EH}^{(\rm large)}} + e^{-S_{\rm EH}^{(\rm small)}} + e^{-S_{\rm EH}^{(\rm thermal)}} + \cdots$ will come from the configuration with the largest on-shell action, since all of them are already large and $\mathcal{O}(1/G_N)$. By carefully taking boundary and counterterms into account [149], one can derive the following expressions for these on-shell actions,

$$S_{\rm EH}^{(\pm)}(\beta) = \frac{\pi^2\beta}{8G_N\ell^2}\left(r_\pm^2(\beta)\ell^2 - r_\pm^4(\beta) + \frac{3\ell^4}{4}\right), \quad S_{\rm EH}^{(\rm thermal)}(\beta) = \frac{\pi^2\beta}{8G_N\ell^2}\left(\frac{3\ell^4}{4}\right), \tag{2.30}$$

where $r_\pm(\beta)$ denotes the radii of the two possible black hole solutions

$$r_\pm^2(\beta) = \frac{\pi\ell^2}{2\beta}\left(1 \pm \sqrt{1 - \frac{2\beta^2}{\pi^2\ell^2}}\right). \tag{2.31}$$

Notice how there exists a minimal temperature for both black holes, given by $\beta_{\rm max} = \frac{\pi\ell}{\sqrt{2}}$. Plotting the on-shell actions (2.30) of all three solutions, as shown in Fig. 2.2, we find that they exchange dominance at a critical temperature, known as the Hawking-Page temperature and given by $\beta_{\rm crit} \equiv \beta_{\rm HP} = \frac{2\pi\ell}{3}$.

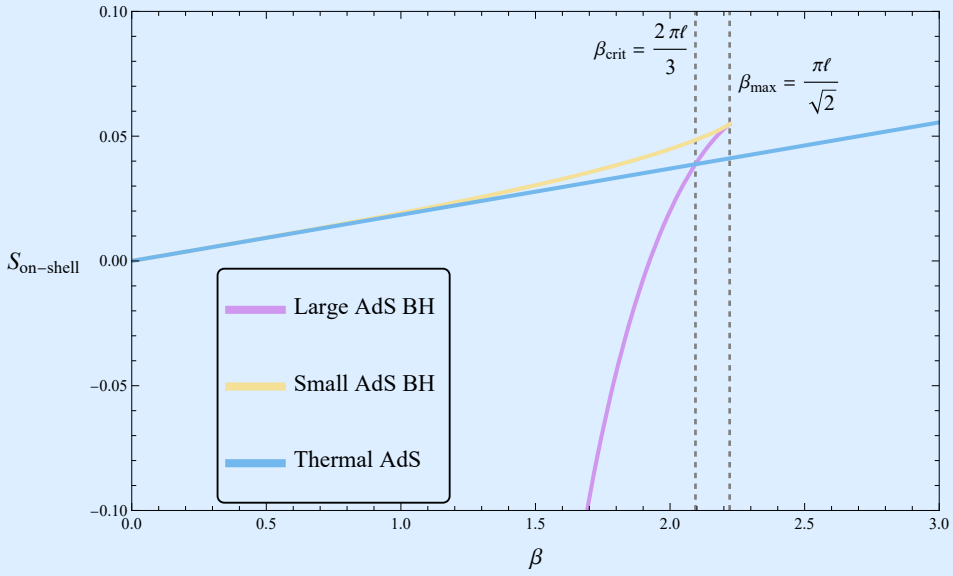


Figure 2.2: Dominance exchange between on-shell actions of the saddle-points of the gravitational path integral, indicating the Hawking-Page phase transition.

At this temperature, the system undergoes a first order phase transition between the low-temperature phase dominated by thermal AdS and the high-temperature phase dominated by large AdS black holes [149]. Moreover we see that the small

AdS black holes never dominate the path integral. One can further show that large black holes have a positive specific heat and are thus thermodynamically stable configurations [149]. Though we have discussed the original example of AdS_{4+1}, the results are qualitatively the same for any dimension up to small technical differences. For example, in AdS_{2+1}, there are no large and small black hole solutions, only the BTZ black hole.
In the context of holography, the Hawking-Page phase transition was shown [210] to be dual to a deconfinement transition in strongly coupled SU(N) gauge theories at large N, where the latter plays the role of the semi-classical regime since $N^2 \sim 1/G_N$. The black hole phase in the bulk corresponds to the deconfined phase, while thermal AdS corresponds to the confined phase.

The phase space of asymptotically AdS solutions shown in Fig. 2.1 is spanned by the gravitational mass M and the angular momentum J of the configuration. Note that the mass M need not always be the physical mass of a particle or a black hole. Rather, it is defined as the conserved charge corresponding to asymptotic time-translation symmetry, but for our purposes we will indeed take it to denote the black hole mass. We can think of it as the mass that an asymptotic observer would assign to the given spacetime configuration based on her knowledge of how the spacetime transforms under time translations [211, 212]. The phase diagram can be derived by using the following general ansatz for a metric solving the $(2+1)$-dimensional Einstein field equations,[4] assuming time independence and spherical symmetry

$$ds^2 = -F^2(r)dt^2 + \frac{dr^2}{F^2(r)} + r^2(G(r)dt + d\phi)^2\,, \tag{2.32}$$

with two, *a priori* unknown, functions $F(r)$ and $G(r)$. Plugging this ansatz into Einstein's equations (2.4), and imposing that the solutions asymptotically approach the metric of empty AdS, explicit expressions for the functions $F(r)$, $G(r)$ can be found. This yields the most general form of the BTZ solutions,[5] given by

$$ds^2 = -\left(-\frac{2M}{k} + r^2 + \frac{J^2}{k^2 r^2}\right)dt^2 + \frac{dr^2}{-\frac{2M}{k} + r^2 + \frac{J^2}{k^2 r^2}} + r^2\left(\frac{J}{kr^2}dt + d\phi\right)^2\,. \tag{2.33}$$

We can see that the solutions are fully specified by M, J and an integer parameter $k = 1/G_N$ (we have set $\ell = 1$). The latter gains a further interpretation of the level of the gauge theory in the Chern-Simons formulation of $(2+1)$-dimensional Einstein-

[4] I am very thankful to Moritz Dorband for explaining this to me.
[5] Units are such that $8G_N = 1$, as is standard in the literature, cf. [209].

Hilbert gravity [206]. For our current purposes, this parameter can be mostly ignored, since it can easily be absorbed in an appropriate rescaling of the gravitational mass M and the angular momentum J. Given our conventions for the units, we will set it to $k = 2$ for the remainder of the discussion. From the general solution (2.33), we can construct the points of interest in the phase diagram in Fig. 2.1. First, when $M > 0$, the condition that $F(r)$ only has real roots (and thus there exist only real horizons) imposes $M > |J|$. This defines the yellow area in the phase diagram, where the solutions describe BTZ black holes with mass M and angular momentum J. The origin, corresponding to $M = J = 0$, retrieves the metric of empty AdS in Poincaré patch coordinates (cf. (2.14)), namely

$$ds^2 = -r^2 dt^2 + \frac{dr^2}{r^2} + r^2 d\phi^2 \,. \tag{2.34}$$

For $J = 0$, the mass can indeed be negative and still describe physical configurations of the spacetime geometry. In fact, there is an exceptional point where the gravitational mass is $M = -1$, where the general BTZ solution (2.33) reduces to the metric of empty AdS in global coordinates (cf. (2.12) with $\ell = 1$),

$$ds^2 = -\left(1 + r^2\right) dt^2 + \frac{dr^2}{(1 + r^2)} + r^2 d\phi^2 \,. \tag{2.35}$$

Upon performing a Wick rotation $t \to \mathrm{i}\tau$ and a subsequent periodic identification $\tau \sim \tau + \beta$ of this Euclidean time coordinate, we see that the metric above describes thermal AdS space at a finite temperature β^{-1} [149]. It was shown in [201] that the rest of the points of the diagram with $J = 0$ and $M < 0$ and $M \neq -1$ correspond to geometries with naked conical singularities. These also have a CFT dual, with operators whose scaling dimension is related to the deficit angle, but we will not be further interested in them in this thesis. Rather, we will concern ourselves with the general BTZ solutions without angular momentum $J = 0$ and with a positive mass $M > 0$, for which the metric (2.33) reads

$$ds^2 = -\left(r^2 - M\right) dt^2 + \frac{dr^2}{r^2 - M} + r^2 d\phi^2 \,. \tag{2.36}$$

Interestingly, the BTZ geometry has negative constant curvature $R = -2$ everywhere, implying that it is locally isometric to empty AdS_{2+1}. In particular, it does not have a curvature singularity at $r = 0$, but rather a causal singularity due to the angular coordinate becoming time-like in this orbifold construction [211, 213]. Nevertheless,

it is most certainly a black hole since it exhibits an event horizon at $r_h = \sqrt{M}$.[6] The Hawking temperature of the BTZ black hole is then given by

$$T_{\mathrm{BTZ}} = \frac{r_h}{2\pi} \,. \tag{2.37}$$

Importantly, the BTZ black hole obeys the generalized laws of black hole thermodynamics [106, 149, 183], and its entropy is given by

$$S_{\mathrm{BTZ}} = 4\pi r_h \equiv \frac{A}{4G_N} \,, \tag{2.38}$$

where we have restored the units $8G_N$ in the last step to highlight the connection to the Bekenstein-Hawking entropy (2.2). This result for the entropy is remarkably robust and has been derived through several different approaches [208, 209, 211, 214–219].
For our later considerations in Chapter 3, it is instructive to consider an alternative construction for the BTZ black hole geometries, namely as quotient spaces of empty AdS_{2+1} by a discrete subgroup of the isometry group of AdS_{2+1}. Details on this construction can be found in [220–226], which we follow closely. More precisely, the (2+1)-dimensional BTZ black hole can be constructed as a quotient space $\mathrm{BTZ} = \mathrm{AdS}_{2+1}/\Gamma$ of empty AdS_{2+1} by a discrete subgroup Γ of the full isometry group of AdS_{2+1}, which is $SO(2,2) \cong SL(2,\mathbb{R}) \times SL(2,\mathbb{R})$. The quotienting procedure is performed on the full AdS_{2+1} geometry by imposing a periodic identification of geodesics with respect to an element of the discrete subgroup Γ. We visualize this construction in the left and center panels of Fig. 2.3. Notice how this procedure breaks down the global isometry group from $SL(2,\mathbb{R}) \times SL(2,\mathbb{R})$ to $\mathbb{R} \times SO(2)$. In its maximally analytically extended form, the BTZ black hole constructed in this way exhibits two event horizons with two causally disconnected asymptotically AdS_{2+1} regions [227]. This geometry is also known as a double-sided BTZ black hole or also *eternal* AdS black hole [129] since it describes a time-reversal invariant geometry that does not rely on a creation from gravitational collapse. It is a black hole that does not evaporate and is in thermodynamical equilibrium with its own Hawking radiation at the temperature T_{BTZ} given in (2.37). We show the Penrose diagram of the eternal black hole in the central panel of Fig. 2.3, where there is an S^1 attached to every point of the diagram corresponding to the compact angular direction. Of particular interest in upcoming section will be the constant-time slice at $t = 0$ of the double-sided BTZ geometry. At this point, the black hole interior is only one-dimensional, in contrast to generic times $t \neq 0$ for

[6] The general BTZ geometry exhibits two event horizons, but in this thesis we will only consider the cases where the inner horizon lies at the origin [211].

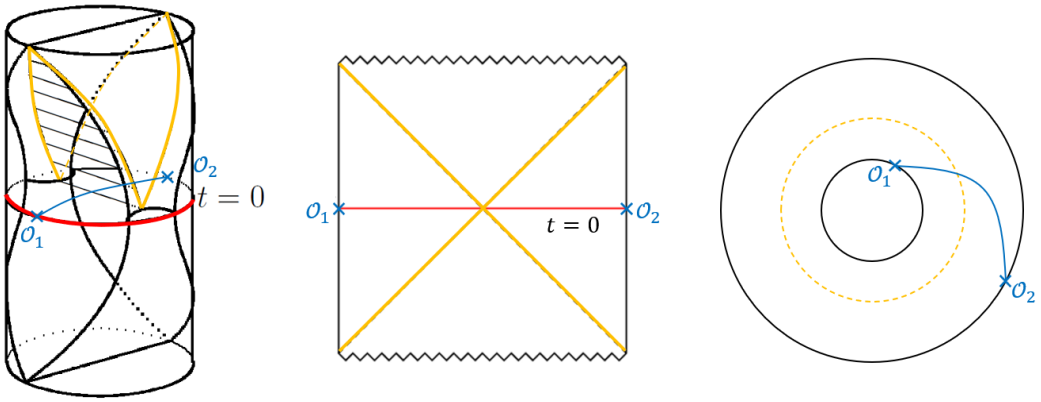


Figure 2.3: Left: The double-sided BTZ black hole embedded into the AdS_{2+1} cylinder as identified hypersurfaces. The red circle denotes the constant-time slice at $t = 0$, while the yellow lines highlight the branching of the black hole horizon into two null hypersurfaces which enclose the black hole interior. Center: Corresponding Penrose diagram of the full double-sided BTZ black hole with the same relevant surfaces highlighted. Each point of the diagram has an S^1 attached to it describing the compact angular direction. The $t = 0$ time-slice (red) is the mirror surface which remains invariant under time-reflection symmetry, manifesting the eternal nature of the wormhole. Right: Full $t = 0$ slice of the Penrose diagram with annular topology with inner and outer boundaries. The black hole horizon, which at $t = 0$ is a single point plus the angular extent, is denoted in yellow. On every panel, we show the insertion of two boundary operators $\mathcal{O}_1, \mathcal{O}_2$ (blue) on opposite asymptotic boundaries of the double-sided geometry for visualization purposes in our discussion of correlation functions in the TFD state (2.39). Figures adapted from [206, 225].

which the wormhole is of finite extent, cf. central panel of Fig. 2.3. Reinstating the angular coordinate, the geometry of this time-slice of the eternal black hole exhibits the topology of an annulus, as shown in the right panel of Fig. 2.3. Let us mention *en passant* that similar constructions are possible in higher dimensions, where the geometry of a one-sided Schwarzschild black holes in AdS_{d+1} with $d \geq 3$ can always be maximally extended to their double-sided counterpart [129] (see also [213] for an excellent overview).

The TFD State

In [129], it was conjectured that the eternal black hole introduced above is holographically dual to two copies of a strongly coupled CFT entangled in a specific state, the so-called *thermofield double* (TFD) state [130]. The TFD state is defined as

$$|\Psi\rangle = \frac{1}{\sqrt{Z(\beta)}} \sum_n e^{-\beta E_n/2} |E_n\rangle_L \otimes |E_n\rangle_R \,, \tag{2.39}$$

where $Z(\beta) = \sum_n e^{-\beta E_n}$ is the partition function of a single copy of the CFT at inverse temperature β, while E_n denotes the energy spectrum of the CFT, with $|E_n\rangle$

the corresponding energy eigenstates. The sum runs over all energy eigenstates of the system and the indices L, R denote the copy of the CFT. The TFD state is defined on a Hilbert space $\mathcal{H} = \mathcal{H}_L \otimes \mathcal{H}_R$ consisting of two copies of the Hilbert space of a CFT. Each of the CFTs is defined on one of the asymptotic boundaries in the double-sided BTZ geometry introduced above, cf. the vertical lines in the Penrose diagram shown in Fig. 2.3. Let us mention that the TFD state can be defined for two copies of any quantum mechanical system, not necessarily a CFT. It is a canonical way of treating a thermal state $\rho = e^{-\beta H}$ by *purifying* it into a bigger system, namely that obtained by simply taking two copies of the original one. It is straightforward to check that $\rho_{\text{TFD}}^2 = \rho_{\text{TFD}}$, with $\rho_{\text{TFD}} = |\text{TFD}\rangle \langle \text{TFD}|$, indicating that it is a pure state. It can be seen as a canonical purification of a subsystem at finite temperature β^{-1}, as can be observed by tracing out the degrees of freedom on either side of the state, e.g.

$$\rho_L = \text{Tr}_R(\rho_{\text{TFD}}) = \frac{1}{Z(\beta)} \sum_n e^{-\beta E_n} |E_n\rangle_L \, {}_L\langle E_n| = \frac{e^{-\beta H_L}}{Z(\beta)} \,, \tag{2.40}$$

where H_L is the Hamiltonian of the left CFT. The resulting reduced density matrix is evidently a mixed thermal density matrix at inverse temperature β. The tracing procedure amounts to an erasure of the second copy of the CFT, such that only a single-sided black hole remains in the bulk, hence the thermal behavior. Moreover, the fact that the TFD state (2.39) is manifestly not a product state indicates that the two CFTs are entangled. Indeed, it can be thought of as a generalization of the EPR or Bell state. From the point of view of either one of the CFTs, a local observer can only see a single black hole at a finite temperature, therefore describing the quantum field theory at a finite temperature. The thermal entropy measured by an observer on one boundary is precisely the Bekenstein-Hawking entropy of the black hole, which at the same time is the entanglement entropy between the two copies of the CFT in the TFD state [129, 228].

In fact, single-insertion expectation values for operators $\mathcal{O}$ on either boundary can be computed in the usual way as $\langle \Psi | \, \mathcal{O}_{L,R} \, | \Psi \rangle = 1/Z(\beta) \, \text{Tr}_{L,R}(\mathcal{O}\rho_{L,R})$ [129]. However, the entanglement between the two CFTs in the TFD has the crucial consequence that correlation functions of operators inserted on different boundaries, such as $\langle \Psi | \, \mathcal{O}_L \mathcal{O}_R \, | \Psi \rangle$, may be non-zero, even though the CFTs do not explicitly interact in the Lagrangian of the full theory. This can be seen as a blatant signature of the entanglement contained in the TFD state, which gives rise to correlations between the boundaries. From the perspective of the bulk, correlators of the form $\langle \Psi | \, \mathcal{O}_L \mathcal{O}_R \, | \Psi \rangle$ are non-zero because of the existence of the black hole interior, providing a smooth geometry connecting both outside regions and thus allowing us to evaluate Witten diagrams with support

in this interior region. Crucially, if we were to take two copies of a CFT in a non-entangled product state $|\psi\rangle = |\psi\rangle_L \otimes |\psi\rangle_R$, the black hole interior would not arise, and the dual geometry would simply be a tensor product of two disconnected AdS patches, cf. Fig.1.1. As a consequence, correlators of the form $\langle\Psi|\,\mathcal{O}_L\mathcal{O}_R\,|\Psi\rangle$ would necessarily vanish. We can therefore regard such correlators as a fundamental probe of the holographic nature of the setup, as well as a concrete realization of the ER=EPR conjecture [134].

Given that we will utilize these different-boundary correlation functions as a diagnostic for the holographic properties of later setups in Chapter 3, we provide some details on these objects here. For a one-sided BTZ black hole and its corresponding dual boundary CFT at finite temperature (given by the Hawking temperature of the black hole), the two-point function of boundary operators was originally computed in [229]. The computation exploits the quotient structure of the BTZ black hole and implements a method of images to obtain the two-point function on the BTZ geometry by summing over the two-point functions obtained in empty AdS_{2+1}. For two operators on the same boundary of the BTZ black hole, the two point function evaluated in the TFD state (2.39) reads [229]

$$\langle\Psi|T(\mathcal{O}_L(t,\phi)\mathcal{O}_L(0,0))|\Psi\rangle \sim \sum_{n\in\mathbb{Z}} \frac{1}{\left[\cosh\left(\frac{2\pi t}{\beta}\right) - \cosh\left(\frac{2\pi(\phi+2\pi n)}{\beta}\right) - \mathrm{i}\epsilon\right]^{2\Delta}}\,. \tag{2.41}$$

Here, Δ is the scaling dimension of the operators, which is related to the mass of the dual scalar field in the bulk via (2.27). The sum in (2.41) runs over all the images generated by the quotienting procedure, which in the case of the discrete subgroup $\Gamma = \mathbb{Z}$ is precisely all integer numbers. The above result does not change when considering the double-sided geometry [129]. However, as explained above, the entanglement between the two copies of the CFT in the TFD state does indeed affect the two-point correlation functions of operators inserted on different boundaries, which we depict on Fig. 2.3. The two-point function in this case was given in [129] based on [229] and reads

$$\langle\Psi|T(\mathcal{O}_L(t_L,\phi_L)\mathcal{O}_R(t_R,\phi_R))|\Psi\rangle \sim \sum_{n\in\mathbb{Z}} \frac{1}{\left[\cosh\left(\frac{2\pi(t_L+t_R)}{\beta}\right) + \cosh\left(\frac{2\pi(\phi_L-\phi_R+2\pi n)}{\beta}\right)\right]^{2\Delta}}\,. \tag{2.42}$$

Notice how the correlations decay exponentially instead of like a power law. This is a consequence of the fact that we do not have the full conformal symmetry after the quotienting procedure, since the isometry group is broken down during the orbifold construction. Note that this result is valid for all times t_L, t_R, in particular also

the case of simultaneous operator insertion $t_L = t_R = 0$ which we will return to in Sec. 3.4. The result (2.42) is an explicit manifestation of the consequences of the entanglement between the two copies of the CFT in the TFD state, leading to non-vanishing correlations between operators that are inserted at causally disconnected points on different boundaries.

2.3. Quantum Information Theory

As foreshadowed in Fig. 1.2, about ten years into the existence of AdS/CFT it became clear that quantities from quantum information (QI) theory play a pivotal part in understanding many features of holographic dualities. Starting from the geometrization of entanglement entropy by Ryu and Takayanagi [114, 115], similar studies have since expanded the holographic dictionary by including bulk descriptions of QI objects. This progress made manifest that there is a variety of QI quantities that, under the umbrella of holography, can help us shed light into certain intriguing properties of black holes, such as the nature of their entropy, their microstates, and the evolution of their interior geometry. We thus find it pertinent to provide a brief review of some of the most relevant quantities from QI theory that will play a role in the remaining of this thesis. Since our explorations are motivated by AdS/CFT, we will also comment on the different interpretations of each of these quantities through the lens of holography.

2.3.1. Entanglement Entropy

We begin with perhaps the most ubiquitous of all measures in quantum information, namely the von Neumann entanglement entropy. The relevance of entanglement in both condensed matter and high-energy physics cannot be overstated, yet a full contextualization of this quantity in the broader landscape of theoretical physics is outside the scope of this thesis. We refer the reader to the reviews [117, 118, 154–156, 165, 169, 230–233] for such an overview. Here, we will only focus on the definitions and properties of entanglement entropy as they will be needed in the later chapters of this thesis, following the aforementioned references, in quantum mechanics, quantum field theory, and holography.

In Quantum Mechanics

Consider a quantum mechanical system described by a pure state $|\psi\rangle$ in a Hilbert space $\mathcal{H}$. Given the vector space structure of a Hilbert space, we can always find a basis $\tilde{\mathcal{B}}$ to span it, and in particular one can always construct an orthonormal basis

$\mathcal{B} = \{|i\rangle\}$ via the Gram-Schmidt procedure [165]. In this basis, any pure state can be written as

$$|\psi\rangle = \sum_{i=1}^{D} c_i \, |i\rangle \ , \tag{2.43}$$

where D denotes the Hilbert space dimension, and the c_i are complex valued coefficients obeying $\sum_i |c_i|^2 = 1$ for normalization purposes. The consideration of a pure state is a natural one if we define our system to not be part of any larger subsystem, which is usually a justifiable assumption. However, even when starting with a pure state, we are typically interested in characterizing the correlations between different subsystems within our system. As we will see, when focusing on a given subsystem, the notion of a *density operator* ρ generally arises, describing an ensemble of pure states in the form of a linear operator acting on $\mathcal{H}$. To see this, we start by defining the density operator associated to our pure state (2.43), which is given by $\rho = |\psi\rangle \langle\psi|$. The normalization condition for the coefficients c_i in (2.43) ensures that $\mathrm{tr}(\rho) = 1$. Equivalently, it is straightforward to check that $\rho^2 = \rho$, readily suggesting the introduction of the so-called *purity* defined as $\mathrm{Tr}(\rho^2)$. States obeying $\mathrm{Tr}(\rho^2) = 1$ are called *pure*, while states with $\mathrm{Tr}(\rho^2) < 1$ are called *mixed* [165]. More general density operators exhibiting this latter property describe a mixture, or ensemble, of pure density operators. The notion of this ensemble is borrowed from statistical mechanics, and it indicates that the exact state of the quantum system is not entirely known, but it is rather given by a superposition of many possible pure states $|\psi_i\rangle$. More precisely, a general density operator is given by

$$\rho = \sum_i p_i \, \rho_i = \sum_i p_i \, |\psi_i\rangle \langle\psi_i| \ , \tag{2.44}$$

where the now real coefficients p_i are interpreted as the classical probabilities of finding the quantum system in state $|\psi_i\rangle$. Normalization of ρ imposes $\sum_i p_i = 1$.

Following the main postulates of quantum mechanics [165, 234, 235], the collection of N quantum mechanical systems, each with their respective Hilbert space $\mathcal{H}_i$ with $i = 1, \ldots, N$, is described by a total Hilbert space constructed as the tensor product of all the individual ones,

$$\mathcal{H} = \bigotimes_{i=1}^{N} \mathcal{H}_i \, . \tag{2.45}$$

Such a Hilbert space is called *composite* [165]. A typical example for this are the Hilbert spaces associated to quantum many-body systems, such as quantum lattice models with N total sites, where each site i carries its own local Hilbert space. The factorized structure (2.45) readily allows us to concentrate on a given subsystem A,

which on a lattice would simply consist of a connected region of sites. This is known as a *bipartition*, via which the Hilbert space can be written as $\mathcal{H} = \mathcal{H}_A \otimes \mathcal{H}_B$, with B being the complementary region to A and $H_{A,B} = \bigotimes_{i \in A,B} H_i$ are the respective Hilbert spaces of the subregions.[7] One of the most fundamental consequences of the purely quantum mechanical phenomenon of entanglement is that even though the Hilbert space factorizes after the bipartition, the same is not guaranteed for the total state $|\psi\rangle$, i.e. $|\psi\rangle \neq |\psi_A\rangle \otimes |\psi_B\rangle$ in general. More generally, states which indeed admit a factorization of the form

$$|\psi\rangle = |\psi_A\rangle \otimes |\psi_B\rangle \ , \tag{2.46}$$

upon performing a bipartition are called *separable* [236]. Let us stress that showing whether a given quantum state is separable or not, known as the separability problem, is an extremely challenging question in general. While separability can be easily diagnosed via entanglement entropy for pure states, it is much more difficult for mixed states. In fact, the separability problem for general mixed states has been shown to be an NP-hard problem [237, 238]. In some instances, separability criteria have been derived, such as the Peres-Horodecki criterion [239, 240] for low-dimensional quantum systems. Yet, a general criterion for separability still eludes us, even after many attempts to tackle the problem, see [241]. Any state which is not separable and therefore does not admit the factorized structure (2.46) is called an *entangled* state. Such entangled states cannot be written as a single tensor product of states in the respective subregions, but rather as a general linear combination of the form

$$|\psi\rangle = \sum_{i,j=1}^{N} a_{ij} \, |A_i\rangle \otimes |B_j\rangle \equiv \sum_{i,j=1}^{N} a_{ij} \, |A_i, B_j\rangle \ , \tag{2.47}$$

with respect to the product basis, with the normalization condition for the coefficient matrix reading $\sum_i^n |a_{ii}|^2 = 1$. States of the form (2.47) are separable if and only if the coefficients obey $a_{ij} = a_i^{(A)} a_j^{(B)}$ for all $i, j = 1, \cdots, N$. There exists an extremely valuable result, known as the *Schmidt decomposition* [165, 242], which greatly simplifies the decomposition (2.47) by effectively diagonalizing the coefficient matrix a via its singular value decomposition [165, 243]. As a result, any pure state $|\psi\rangle$ in a composite bipartite Hilbert space $\mathcal{H} = \mathcal{H}_A \otimes \mathcal{H}_B$ can be written as

$$|\psi\rangle = \sum_i \lambda_i \, |i_A\rangle \, |i_B\rangle \ , \tag{2.48}$$

[7] There are instances where the assumption of a factorized Hilbert space breaks down, such as in quantum field theories or lattice gauge theories. We will discuss these caveats in later sections.

where $\{|i_A\rangle\}$ and $\{|i_B\rangle\}$ are orthonormal bases for subsystem A and B, respectively, and the real, non-negative numbers λ_i are known as the *Schmidt coefficients* of $|\psi\rangle$ [165]. They satisfy the normalization condition $\sum_i \lambda_i^2 = 1$. Notice that the range of the sum in (2.48), denoting the number of non-zero Schmidt coefficients, depends on the particular state and it is known as the *Schmidt number* or *Schmidt rank* of $|\psi\rangle$. It is upper bounded by the dimensionality of the local Hilbert space d, while being lower-bounded by 1, in which case the state is separable. The Schmidt decomposition (2.48) will prove to be immensely useful when considering the entanglement properties of quantum states in bipartite Hilbert spaces, as we will elucidate shortly. For completeness, let us mention that, in terms of density operators, a general mixed state on a bipartite Hilbert space is separable if it can be written as

$$\rho = \sum_i p_i \, \rho_A^{(i)} \otimes \rho_B^{(i)} \,, \tag{2.49}$$

where the p_i again describe some probability distribution, and $\rho_A^{(i)}, \rho_B^{(i)}$ are density operators in the respective subsystems A and B.

While separable states only contain correlations between the subsystems which can be fully described in a classical way, the correlations between A and B subsystems in entangled pure states are exclusively of quantum nature. We can quantify them better by considering what it means to restrict our attention to a subsystem, say A, of a larger pure state $|\psi\rangle$. Mathematically, the restriction to subsystem A amounts to tracing out any degrees of freedom in the complement B of A, which we do via the operation known as the *partial trace* applied on the entire density operator $\rho = |\psi\rangle \langle\psi|$ of the system. This defines the *reduced density operator* for subsystem A as

$$\rho_A \equiv \mathrm{Tr}_B(\rho) \,, \tag{2.50}$$

where the partial trace is given by

$$\mathrm{Tr}_B(|A_1\rangle \langle A_2| \otimes |B_1\rangle \langle B_2|) = |A_1\rangle \langle A_2| \, \mathrm{Tr}(|B_1\rangle \langle B_2|) = |A_1\rangle \langle A_2| \, \langle B_1|B_2\rangle \,, \tag{2.51}$$

with $|A_i\rangle, |B_i\rangle$, $i = 1, 2$ basis vectors in $\mathcal{H}_A$ and $\mathcal{H}_B$, respectively [165]. It is here where the Schmidt decomposition (2.48) showcases its value. For a pure state $|\psi\rangle$ in its Schmidt decomposition, taking the partial trace with respect to subsystem B or A yields the reduced density operators

$$\rho_A = \sum_i \lambda_i^2 \, |i_A\rangle \langle i_A| \,, \qquad \rho_B = \sum_i \lambda_i^2 \, |i_B\rangle \langle i_B| \,, \tag{2.52}$$

respectively. As we can see, the eigenvalues of both ρ_A and ρ_B are identical and are given by the squares of the Schmidt coefficients. Notice how this automatically guarantees also the normalization of ρ_A and ρ_B as density operators. If the state $|\psi\rangle$ had a Schmidt number of 1, then it is a product state with a single non-vanishing Schmidt coefficient $\lambda = 1$, and the reduced density operators are then pure states themselves.

Based on the above considerations, the main object used to quantify the correlations within a pure quantum state is the so-called *von Neumann entropy*, also known as *entanglement entropy*. We will use both terminologies interchangeably. Given a quantum state ρ, its von Neumann entanglement entropy is defined as

$$S(\rho) = -\operatorname{Tr}(\rho \log \rho) \ . \tag{2.53}$$

The entanglement entropy vanishes if ρ itself describes a pure state. The more interesting situation for us is the evaluation of (2.53) on reduced density operators corresponding to subsystems of larger pure states, since in this case the entanglement entropy quantifies the quantum correlations between the degrees of freedom in that subregion and those in its complement. It can be shown that this quantity obeys all the necessary requirements to be a proper measure of entanglement [244, 245], at least for the cases of bipartitions of pure quantum states. For mixed states, entanglement entropy is no longer a reliable quantifier for entanglement, since both classical and quantum correlations contribute to the overall von Neumann entropy. A plethora of other quantities have been suggested in the literature as alternative descriptions of entanglement in general mixed states, such as entanglement negativity [246–249], entanglement of formation [250, 251], relative entanglement entropy [252, 253], distillable entanglement [254] (see [154–156, 255] for a more complete overview). Moreover, quantum discord [256–258] was also suggested as one such measure, and we will review this quantity in detail in a later section, since it will play a key role in our analysis in Sec. 4.2. Still, a definitive consensus on which of these quantities offers the most complete description of the correlations within general mixed states remains elusive.
Let us give some more details on entanglement entropy (2.53), focusing on bipartite pure states. Consider a pure state $|\psi\rangle$ written in its Schmidt decomposition (2.48) in a bipartite Hilbert space $\mathcal{H} = \mathcal{H}_A \otimes \mathcal{H}_B$. The reduced density operator corresponding to subsystem A is given by (2.52) and its eigenvalues are given by λ_i^2. Plugging these into (2.53) we find the following simplified expression for the entanglement entropy

$$S(\rho_A) = -\sum_i \lambda_i^2 \log\left(\lambda_i^2\right) . \tag{2.54}$$

We can immediately see that the entanglement entropy is non-negative, since all Schmidt coefficients are smaller or at most equal to one. Moreover, we saw that the reduced density operators for subsystem A and B share the same eigenvalues, meaning that their entanglement entropy is also equal, i.e. $S(\rho_A) = S(\rho_B)$. Thus, notice how the entanglement entropy is elegantly described in terms of the Schmidt coefficients of the state $|\psi\rangle$. This is because the Schmidt number of $|\psi\rangle$ is precisely the rank of the reduced density operators ρ_A and ρ_B, which in turn is equal to the dimension of the vector space on which they are supported. More precisely, if the state has Schmidt number 1, it is separable and the entanglement entropy vanishes. The reduced density operator has rank one and is thus simply a projector, i.e. a pure state. In fact, the entanglement entropy vanishes if and only if ρ_A is pure. In contrast, if the Schmidt number is maximal and equal to the local Hilbert space dimension d, the Schmidt coefficients are necessarily given by $\lambda_i = 1/d$ and the state is maximally entangled with entanglement entropy equal to $\log d$. This corresponds to the reduced density operator being the maximally mixed state $\rho_A = \mathbb{1}_d/d$. Importantly, given that the Schmidt number of a state is left invariant by any local unitaries $U = U_A \otimes U_B$ acting separately on either system A or B, the entanglement entropy of the state is also preserved [154, 165]. This has a key consequence in quantum communication theory, since it implies that the entanglement shared between two parties cannot be changed by any local measurement or operation.

The interpretation given above of density operators describing ensembles of states in quantum mechanics highlights the deep connection between this theory and the fields of statistical mechanics and thermodynamics. In fact, entanglement entropy got its name precisely for its resemblance to thermodynamic entropy in the sense that it also provides a quantitative measure for the space of microstates of a system. Yet, there are many differences as well. For example, thermodynamic entropy is known to be an extensive quantity and grow according to a volume law. This is actually still true for many states in a bipartite Hilbert space, where the entanglement entropy can be shown to be close to maximal for randomly chosen states if the subregion A can be taken small compared to the entire system. This is known as Page's theorem [259] (see also [260]). However, we are not typically very interested in completely random states, but rather specific ones with a particular physical significance, such as ground states. Here, one finds that entanglement entropy often violates the aforementioned volume law and is rather described by an *area law* [156, 261]. In fact, this particular scaling is generically found in ground states of gapped Hamiltonians in many-body quantum systems. This is because, broadly speaking, the entanglement entropy quantifies the

number of entangled pairs of degrees of freedom that are shared between two subsystems, meaning that the larger the entangling (or bipartition) surface, the more such entangled pairs are included. However, the actual size of the subsystem does not affect this consideration, since correlations between degrees of freedom within the same subsystem do not contribute to the entanglement entropy. Moreover, given that correlations in ground states of gapped Hamiltonians are spatially suppressed as $e^{-E_{\text{gap}}}$, where E_{gap} denotes the energy gap, it is clear that entanglement entropy will be largely dominated by the number of degrees of freedom in close vicinity to the entangling region, again indicating a scaling with area rather than volume. For $(1+1)$-dimensional systems, the conditions for area law entanglement have been proven rigorously in [262]. However, let us stress that violations to the area law also exist, and in many cases these present an even more interesting playground for investigations. These typically arise when quantum systems approach critical points, where the energy gaps close and the correlations exhibit a power-law decay rather than an exponential suppression. This means that degrees of freedom contributing to the entanglement no longer need to be close to the entangling region, but their contribution can be long-ranged, leading to logarithmic corrections to entanglement entropy [116, 263, 264]. This feature makes entanglement a useful tool to detect phase transitions [155], as we will discuss explicitly in Sec. 4.3. We will return to violations of the area law when discussing entanglement entropy in CFTs.

While the volume-vs-area law arguments highlight one of the main differences between the correlations in quantum theory and those in thermodynamics and statistical mechanics, we may find some similarities as well. This is particularly evident from the interpretation of general mixed states as quantum states at a finite temperature, at least formally. With this in mind, since a reduced density operator of the form (2.52) has no negative eigenvalues, it can be shown that ρ_A can always be written in the form

$$\rho_A = \frac{e^{-K_A}}{Z}\,, \tag{2.55}$$

with the normalization $Z = \text{Tr}\left(e^{-K_A}\right)$, and where the object K_A is known as the *entanglement Hamiltonian* or also *modular Hamiltonian*.[8] This terminology has its roots in the manifest resemblance between the operator (2.55) and the thermal density operator $\rho = e^{-\beta H}$ of a quantum system at a finite temperature β^{-1} and governed by a Hamiltonian H. However, let us stress that the entanglement Hamiltonian can be defined even at zero temperature, and the thermal interpretation is simply an analogy.

[8] The former terminology is common in the condensed matter and quantum information communities, while the latter is more widely used in quantum field theory, see e.g. [265].

If one nevertheless wishes to pursue this interpretation, the entanglement Hamiltonian can be seen as the Hamiltonian of a system at "temperature" $\beta^{-1} = 1$, with eigenenergies given by its eigenvalues. As a consequence, entanglement entropy can be equivalently seen as the thermodynamic entropy of this system. In other words, the claim is that the reduced density operator of a pure state, even at zero temperature, will *look* thermal with respect to the entanglement Hamiltonian in (2.55), which is however not necessarily related to any physical Hamiltonian. The entanglement Hamiltonian will be a key object in our later analysis of operator algebras in Sec. 4.3. The entanglement Hamiltonian contains useful information about the entanglement structure of a state. In particular, we can retrieve the entanglement entropy (2.53) as the expectation value of the entanglement Hamiltonian in the given state, since $K_A = -\log(\rho_A)$ by construction. In other words, we have

$$S(\rho_A) = \mathrm{Tr}(\rho_A K)\,. \tag{2.56}$$

In fact, we can say even more. It was pointed out in [266] that the reduced density operator ρ_A of a system contains more information than that which can be accessed via the single number of entanglement entropy alone. This information is contained in the so-called *entanglement spectrum*, i.e. the eigenvalues, of the corresponding entanglement Hamiltonian. This entanglement spectrum was originally introduced to detect topological order [266–268] (see also [269] for a more recent study), but it has since been shown to be of utmost importance for the study of relative entropies also in the context of holography [270–272], as well as in the general characterization of entanglement in quantum-many body systems and quantum field theories [273–275]. In particular, the entanglement spectrum further provides access to the so-called α-Rényi (or simply, Rényi) entropies [276], which are defined as

$$S^{(\alpha)}(\rho_A) = \frac{1}{1-\alpha}\log\left(\mathrm{Tr}(\rho_A^\alpha)\right) = \frac{1}{1-\alpha}\log\left(\mathrm{Tr}(e^{-\alpha K_A})\right)\,. \tag{2.57}$$

The limit $\alpha \to 1$ retrieves the standard von Neumann entropy of ρ_A. If ρ_A is pure, all Rényi entropies vanish. Notice how the Rényi entropies (2.57) are computationally easier to access than the standard entanglement entropy given that we no longer have to deal with the logarithm of an operator. This is particularly useful when a direct diagonalization is out of reach. In fact, as we will see below, the Rényi entropies are also a key tool in the computation of entanglement entropy in quantum field theories.

In Quantum Field Theory and Conformal Field Theory

While the notions of the previous section apply for quantum mechanical systems with finite-dimensional Hilbert spaces, many subtleties come to light when attempting to define entanglement entropy for quantum field theories, or any infinite-dimensional Hilbert space for that matter. These are a direct consequence of the infinitely many degrees of freedom described by such theories, which immediately obscures the notion of a bipartite Hilbert space, i.e. we have that $\mathcal{H} \neq \mathcal{H}_A \otimes \mathcal{H}_B$. The presence of quantum modes at arbitrarily small scales inherently obstructs the proper definition of an entangling surface, necessary to properly specify a spatial bipartition. As mentioned before, the main consequence of this is that entanglement entropy exhibits a universal UV divergence [116, 261, 277, 278], a starkly different behavior not encountered in finite-dimensional systems. Taming these divergences requires a regularization, typically done by introducing a UV cutoff ϵ_{UV} [116, 274, 277, 279]. This renders the Hilbert space finite-dimensional, allowing for the carry-over of many of the properties and results on entanglement entropy we reviewed above to the QFT case. Of course, when removing this cutoff, entanglement entropy is still infinite, but we can learn quite a lot about QFT by studying the *structure* of how the entanglement entropy diverges. For instance, it was shown in [261, 278] that the entanglement entropy in ground states of QFTs in d dimensions also obeys an area law of the form

$$S(\rho_A) = c\frac{\text{Area}(\partial A)}{\epsilon_{\text{UV}}^{d-2}} + \mathscr{O}\left(\epsilon_{\text{UV}}^{d-1}\right) , \tag{2.58}$$

where c is a numerical factor and ∂A denotes the boundary of the subregion A, i.e. the entangling surface. Even more can be said if we consider scale-invariant QFTs. There, the structure of divergences of the entanglement entropy can be arranged into powers of the dimensionless ratio L_A/ϵ_{UV}, where L_A denotes the size of subregion A. By dimensional analysis, the generalized area of the entangling region in (2.58) will be described by $(L_A/\epsilon_{\text{UV}})^{d-2}$. For odd dimensions d, the expansion reads

$$S(\rho_A) = c_{d-2}\left(\frac{L_A}{\epsilon_{\text{UV}}}\right)^{d-2} + c_{d-4}\left(\frac{L_A}{\epsilon_{\text{UV}}}\right)^{d-4} + \cdots + (-1)^{\frac{d-1}{2}} c_{\text{odd}} + \mathscr{O}\left(\epsilon_{\text{UV}}\right) , \tag{2.59}$$

while for even dimensions d, we have

$$S(\rho_A) = c_{d-2}\left(\frac{L_A}{\epsilon_{\text{UV}}}\right)^{d-2} + c_{d-4}\left(\frac{L_A}{\epsilon_{\text{UV}}}\right)^{d-4} + \cdots + (-1)^{\frac{d-2}{2}} c_{\text{even}} \log\left(\frac{L_A}{\epsilon_{\text{UV}}}\right) + \mathscr{O}\left(\epsilon_{\text{UV}}\right) . \tag{2.60}$$

Notice the appearance of a finite term for odd d and a logarithmic term for even d. The coefficients $c_{\text{odd}}, c_{\text{even}}$ of these terms are known as the *central charges* of the theory, and, in contrast to all other coefficients in the expansion, they are *universal*. This means that they do not depend on the details of the regularization scheme and they carry true information about the theory.

The case of $d = 2$ is of particular importance for the later discussions in this thesis. When $d = 2$, scale invariance enhances the Lorentz symmetries of a QFT to full conformal invariance [280, 281].[9] Thus, according to the expansion in (2.60), we find that the area-law is violated in two-dimensional CFTs, and the entanglement entropy instead exhibits a universal logarithmic divergence. In fact, due to the large amount of symmetry enjoyed by two-dimensional CFTs, the entanglement entropy can be computed exactly, at least for the vacuum state. This was first done in [116] and later refined into a systematic framework in [117, 118]. The latter works introduced a tool known as the *replica trick*, via which the higher moments $\text{Tr}(\rho_A^\alpha)$ of the reduced density matrix, needed for the computation of the Rényi entropies (2.57), can be equivalently evaluated as a partition function on an α-sheeted Riemann surface [117, 118] (see also [283]). Since the evaluation of this partition function may not always be straightforward, other techniques have been developed to tackle it. One of these is a rephrasing using the twist field approach [117, 118, 284, 285], whereby the problem is translated to the computation of correlation functions of twist fields. In any case, the replica trick made the evaluation of Rényi entropies for two-dimensional CFTs accessible, yielding the result [116–118, 277, 286, 287]

$$S^{(\alpha)}(\rho_A) = \frac{c}{6}\frac{\alpha+1}{\alpha}\log\left(\frac{L_A}{\epsilon_{\text{UV}}}\right) . \tag{2.61}$$

Moreover, whenever it can be shown that a unique analytic continuation to complex α exists, the replica trick allows to compute the entanglement entropy in two-dimensional CFTs, yielding [116–118, 277, 286, 287]

$$S(\rho_A) = \frac{c}{3}\log\left(\frac{L_A}{\epsilon_{\text{UV}}}\right) . \tag{2.62}$$

This universal behavior will play a key role in many of the discussions of Chapters 3 and 4. Let us mention that since its inception, the replica trick has been generalized to compute also other quantities in field theory, such as entanglement negativity [247, 248] and relative entropies [288, 289]. Moreover, results for the entanglement

[9] This is suspected to be the case also for higher-dimensions, but it has not yet been proven, see [282] for a review.

entropy have since been obtained also for multiple disjoint intervals [290–296], excited states [297, 298], and inhomogeneous systems [299–301]. As we will see below, some of these results also play a key role in holography, perhaps providing an *a posteriori* justification for the amount of effort put into computing entanglement entropy in quantum field theories. Still, even without any intentions to perform holographic computations, entanglement has proven to yield foundational insights into the general structure of QFTs themselves in ways that no other method can. A paramount example of this was the proof of the irreversibility of the renormalization group in $d = 3$ dimensions. While this was proven for $d = 2$ in [280, 281], a statement famously encapsulated in Zamolodchikov's c-theorem that the central charge decreases monotonically under RG flows, the proof is not particularly simple. However, an alternative yet much more elegant proof of the c-theorem was found by Casini and Huerta in [302, 303] exploiting the strong subadditivity property of entanglement entropy [304, 305]. Moreover, this derivation crucially generalizes to $d = 3$ dimensions [306, 307], unlike Zamolodchikov's original one, where the statement is known as the F-theorem. Extensions of these studies for higher-dimensions using entanglement seem promising, see e.g. [308].
On an orthogonal vein, one may wonder whether all of the considerations above may be obviated by attempting to define entanglement entropy without the need for a UV cut-off. In very special cases, such an access to the entanglement properties of relativistic QFTs has been gained by the computation of entanglement Hamiltonians and their associated entanglement spectra. One of the first instances of this was the entanglement Hamiltonian for half-space subregions of ground states of QFTs in generic dimensions in flat Minkowski spacetime. This result, due to Bisognano, Wichmann, and Unruh [309–311] plays a key role in axiomatic approaches to QFT, and it relates the entanglement Hamiltonian to a suitably weighted integral over the stress-energy tensor of the theory. Later extensions of these findings were obtained for free QFTs [312–317], as well as d-dimensional CFTs in the cases where the entangling region is not half-space but a ball-like region [318, 319]. More general scenarios have also been considered in [319–323], as well as in [274, 324–327] for the specific case of two-dimensional CFTs. However, in spite of all this progress, analytic access to entanglement Hamiltonians in generic interacting QFTs remains a highly difficult challenge.

In Holography

The eminent role played by entanglement both in quantum mechanics, quantum field theory, and specially in conformal field theories should be evident by now. The fact that universal features of entanglement entropy can be computed for generic CFT's begs the question of whether this quantity may have a holographic dual when consid-

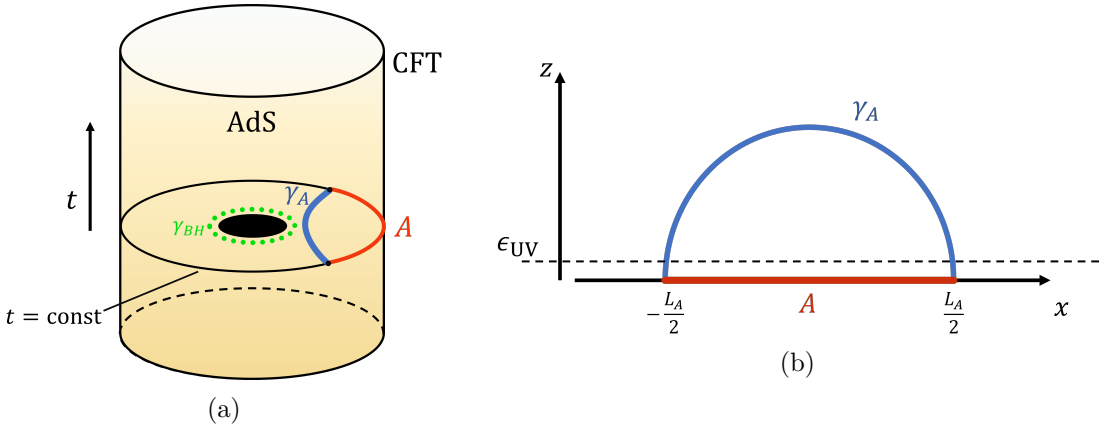


Figure 2.4: Left: Visualization of the RT prescription for the computation of holographic entanglement entropy via (2.63) for the case of AdS_3/CFT_2, potentially with a black hole in the bulk. We have chosen a static metric such that the RT surface γ_A (blue) lies on a constant-time slice of AdS, while the entangling region A (red) is a connected interval of the CFT defined on the boundary circle. In the case of a black hole and an entangling region $A = S^1$, the minimal RT surface γ_{BH} (dotted green) hugs the horizon and reproduces the Bekenstein-Hawking black hole entropy (2.2). Right: Sketch for the computation of the RT formula for empty AdS_3 using Poincaré patch coordinates and a UV regulator ϵ_{UV}. The entangling region A is defined by the interval $x \in [-\frac{L_A}{2}, \frac{L_A}{2}]$, and the RT surface (geodesic) γ_A stretches into the bulk along the holographic coordinate z. This computation leads to the holographic entanglement entropy (2.65) which coincides with (2.62).

ered in the subset of CFTs which can potentially admit such an interpretation. These holographic CFTs ought to have a large number of degrees of freedom, manifested in a large central charge, or equivalently in a large rank N of the gauge group of the theory. Moreover, we should assume that the CFT under consideration is in a state ρ which actually has a geometric dual, since even for holographic CFTs not every state in their spectrum necessarily enjoys a holographic bulk interpretation.

In this respect, a highly celebrated hallmark within the AdS/CFT correspondence was the prescription found by Ryu and Takayanagi to compute the entanglement entropy of a holographic CFT in terms of a geometric quantity in the bulk. In particular, they found that the entanglement entropy of a subregion A in a d-dimensional CFT is given by the *Ryu-Takayanagi* (RT) formula [114, 115]

$$S(\rho_A) = \frac{\text{Area}(\gamma_A)}{4G_N^{(d+1)}}, \tag{2.63}$$

where $G_N^{(d+1)}$ is Newton's constant in $(d+1)$-dimensions, and γ_A is a spacelike, codimension-2 extremal surface in the bulk, which is anchored at the entangling surface such that $\partial\gamma_A = \partial A$. In cases where multiple candidates for such an extremal surface are found, the prescription is to take that with the minimal area. The entanglement entropy

computed from the RT prescription in (2.63) is known as *holographic entanglement entropy* [115, 169, 328, 329], and it was the first entry in the holographic dictionary containing a quantum-information theoretic quantity. We visualize the general setup for the computation of (2.63) in Fig. 2.4a. Importantly, the RT prescription requires the extremal surface γ_A to be *homologous* to the entangling region A on the conformal boundary. This means that it should be continuously retractable onto the portion A of the conformal boundary containing the entangling region. Since the RT surface extends into the bulk spacetime, its area computed via the AdS metric diverges towards the boundary. This is precisely the geometric analog to the universal divergence of entanglement entropy in CFT. In fact, taking as an example the case of $\text{AdS}_3/\text{CFT}_2$, a codimension-2 surface is simply a one-dimensional object in the bulk, i.e. a geodesic. For static spacetimes (like empty AdS), time-translation invariance implies that the extremal surface must lie on a constant-time slice of the AdS geometry. The entangling region A is given by an interval $x \in [-\frac{L_A}{2}, \frac{L_A}{2}]$ of the CFT defined on the conformal boundary, which in this case is the circle S^1 parametrized by the coordinate x. The RT surface stretches in the holographic direction z (in the Poincaré patch coordinates (2.14)) and is given by the bulk geodesic γ_A anchored at the entangling points $\partial A = \left\{\pm\frac{L_A}{2}\right\}$, cf. Fig. 2.4b. Its area is simply given by its geodesic length, i.e. $\text{Area}(\gamma_A) = |\gamma_A|$. As previously mentioned, this length is divergent and thus we regularize it via the UV cutoff $\epsilon_{\text{UV}} \ll 1$. Using the metric for AdS_{2+1} in Poincaré coordinates (2.14) restricted to a constant-time slice $ds^2 = \frac{\ell^2}{z^2}(dx^2 + dz^2)$, it is a straightforward computation to parametrize the curve $\gamma_A \equiv (x(\lambda), z(\lambda))$ with some parameter λ and obtain its geodesic length as $|\gamma_A| = \int ds = 2\ell \log(L_A/\epsilon_{\text{UV}})$. Plugging the result into (2.63) yields the holographic entanglement entropy

$$S(\rho_A) = \frac{\ell}{2G_N^{(3)}} \log\left(\frac{L_A}{\epsilon_{\text{UV}}}\right) . \tag{2.64}$$

Finally, we utilize the relation $c = \frac{3\ell}{2G_N^3}$ found by Brown and Henneaux [330] between the central charge c and the AdS_{2+1} parameters $\ell, G_N^{(3)}$ to obtain

$$S(\rho_A) = \frac{c}{3} \log\left(\frac{L_A}{\epsilon_{\text{UV}}}\right) . \tag{2.65}$$

Remarkably, we see that the RT prescription retrieves *exactly* the result (2.62) for the entanglement entropy of two-dimensional CFTs, including the dependence on the UV regulator. However, notice how the RT formula obtained the correct result while doing so in an immensely simpler fashion, highlighting the practical significance of the geometrization of quantum-information quantities in holographic dualities. Further-

more, the holographic entanglement entropy as derived through the RT prescription can be thought of as a generalization of the Bekenstein-Hawking black hole entropy given in (2.2). This can be argued by applying the RT formula (2.63) to a constant-time slice of a black hole geometry, and choosing the entangling region A to be the entire boundary. This scenario can be broadly visualized as shown in Fig. 2.4. The boundary condition for any RT surface should be $\partial\gamma_A = \partial A = \emptyset$. However, notice how the empty set, seen as a "surface", does not obey the homology condition for the RT prescription, since it cannot be deformed into A. The correct RT surface in this case is the geodesic which hugs the black hole along its horizon, since this will minimize the length. This length is exactly the area of the black hole horizon, thus retrieving the Bekenstein-Hawking entropy.

The derivation of holographic entanglement entropy was a key development in the AdS/CFT correspondence, showing that such quantities do indeed possess geometric interpretations in terms of bulk quantities. Since its introduction in [114, 115] for static geometries, it has been generalized to a covariant formalism for time-dependent geometries, known as the Hubeny-Rangamani-Takayanagi (HRT) formula, in [331, 332]. Further aspects of holographic entanglement entropy were refined in [319, 333–335]. A derivation of holographic entanglement entropy directly from the holographic dictionary was obtained by Lewkowycz and Maldacena in [336], later leading to the computation of $1/N$ corrections to the RT formula in [337]. For bulk geometries containing black holes, transitions in the minimal surfaces were found due to the non-trivial topology, a phenomenon which is a direct consequence of the aforementioned homology and minimality conditions for the RT surface [270, 272, 333, 338–340]. A particular consequence of this exchange of RT surfaces is the prediction of a sharp transition for the holographic mutual information between two intervals as a functions of their separation. We will discuss this aspect in more detail in suggested boundary models for discrete holography in Sec. 3.5.5.

2.3.2. Quantum Complexity

Although entanglement entropy was the go-to information theoretic quantity to study within the AdS/CFT correspondence for several years, it became clear that further additions to the holographic dictionary would be necessary to really encompass all the interesting aspects of black holes. In fact, it was pointed out in [138] that entanglement entropy is not sufficient to capture specific properties of black hole interiors, in particular the continued growth of the ER bridge for times longer than exponential in the systems entropy. The latter signifies the time scale after which the boundary CFT ought to thermalize, leading to a plateau in the growth of entanglement entropy.

Further investigations into entwinement and entanglement shadows [228, 341–344] indeed supported this apparent hurdle of probing the black hole geometry behind its horizon, in particular at very late times. The main culprit for these shortcomings is the aforementioned transition between extremal surfaces in the RT prescription, such that even though some RT surfaces do probe the black hole interior extending through the wormhole at early times, a topological phase transition at times of order $t \sim \beta$ leads to an expulsion of the RT surface from the interior [228]. The immediate course of action, guided by the expectations from AdS/CFT and the paradigm of ER=EPR, was to look for other field theory quantities with suitable geometric interpretations which could potentially access this regime.

Following the ideas of [138–141], attention then turned to the investigation of *quantum circuit complexity* [345–347]. This is a concept borrowed from quantum computer science which aims to quantify the difficulty of implementing a given operation. For example, say we want to implement a unitary transformation U which maps an initial state $|\psi_\mathrm{i}\rangle$ of some quantum mechanical system to a final state $|\psi_\mathrm{f}\rangle$ as $|\psi_\mathrm{f}\rangle = U\,|\psi_\mathrm{i}\rangle$. For a generic U, it is not immediately clear how exactly to implement this transformation. We therefore assume that it can be constructed from a pre-defined set of quantum gates $\{g_i\}$ whose functionality is well-known and are therefore deemed to simple to implement, i.e.

$$U_\mathrm{circuit} = g_1 g_2 \cdots g_n \,. \tag{2.66}$$

These are called *primitive gates*, and it can be shown, at least for qubit systems, that any unitary operation can be decomposed into single- and two-qubit gates [165, 348]. Imposing that a quantum circuit uses only a finite number of such primitive gates, we can approximately emulate the action of U via a quantum circuit representing the unitary U_circuit in (2.66), up to a tolerance ϵ, i.e.[165]

$$1 - \left|\mathrm{Tr}\left(U^\dagger_\mathrm{circuit} U\right)\right| < \epsilon \,. \tag{2.67}$$

An analogous definition can be written down for the states, imposing that $U_\mathrm{circuit}\,|\psi_\mathrm{i}\rangle$ is close in terms of a certain norm $\|\cdot\|$ to the final state $|\psi_\mathrm{f}\rangle$ up to some other tolerance $\delta \ll 1$. The minimum number of primitive gates needed to construct this circuit is then defined as the quantum circuit complexity $\mathcal{C}$ of the unitary U. Notwithstanding, properly quantifying complexity is an inherently subjective goal, since the arduousness of an operation might depend on several factors, like the size and current state of the system, and the fundamental operations at our disposal. Plenty of different choices for all these ingredients can be made. More practically, experimentally addressing any physical realization of a qubit may predisposition some operations to be hard to

implement even though they are theoretically simple to describe. This ambiguity is a double-edged sword for complexity and it can be regarded as both a bug and a feature. Moreover, while the definition given above appears at least somewhat canonical for finite-dimensional quantum mechanical systems, the situation is much more complicated in infinite-dimensional systems such as quantum field theories.

These ambivalent aspects may be overcome, at least partially, by considering a geometric description of quantum complexity as put forward in [349–351]. This continuous approach is commonly referred to as *Nielsen complexity* and we review its essential aspects in Box 2.2.

Box 2.2 Nielsen Complexity

Nielsen's approach to quantum circuit complexity is a geometric one [349–352] and it was devised by applying previous ideas from optimal control theory [353–356] to quantum computing. Rather than considering quantum gates as discrete operations being subsequently implemented on a state, each unitary gate is described as being continuously generated by a geodesic trajectory on the smooth manifold of unitaries. This rephrases the problem into a purely geometric one, enabling the use of tools from differential geometry in its consideration. More precisely, primitive gates are viewed as being of the form $e^{\varepsilon h}$,[a] with h being an element of the Lie algebra, such that when $\varepsilon \to 0$ these infinitesimal gates explore the manifold of unitaries in a continuous manner. This continuous trajectory from the identity to a given point $U(T)$ on the unitary manifold is parametrized by a so-called *control Hamiltonian* $\mathcal{H}(s)$ as

$$U(T) = \overleftarrow{\mathcal{P}} \exp\left(\int_0^T ds\, \mathcal{H}(s)\right) , \tag{2.68}$$

where the path-ordering $\overleftarrow{\mathcal{P}}$ is required to construct the circuit with Hamiltonians at earlier *circuit times* s being applied first. The parameter T simply determines the position along the given trajectory, and it is used to impose the boundary conditions on the path integral, namely $U(T = T_\mathrm{i}) = e$ and $U(T = T_\mathrm{f}) = U$, where $T_\mathrm{i}, T_\mathrm{f}$ are some initial and final positions, e is the identity operator, and U is the target unitary we wish to synthesize. Typically in high-energy physics, the target unitary is taken to be the time-evolution operator under some physical Hamiltonian, i.e. $U = e^{Ht}$. Neither T nor s are necessarily related to the physical time t. Notice how the expression (2.68) is simply the formal solution to an infinitesimal Schrödinger equation $\frac{dU}{ds} = \mathcal{H}(s)U$. The control Hamiltonian can be expanded in terms of a basis $\{\mathcal{O}_K\}$ for the tangent space, which is equivalent to

a basis for the Lie algebra, as

$$\mathcal{H}(s) = \sum_K Y^K(s)\mathcal{O}_K\,. \tag{2.69}$$

This introduces the time-dependent coefficients $Y^K(s)$, thought of as velocity vectors $Y \sim \dot{U}$ for the corresponding trajectory. Importantly, control and physical Hamiltonians should not be confused, with the boundary condition $U(T = T_\mathrm{f}) = U$ relating these objects by imposing constraints on the velocities $Y^K(s)$.
In this geometric description, the choice of any curved Riemannian metric on the manifold defines a landscape for geodesics, pointing out favorable directions for them to evolve in. In other words, it assigns a certain cost to each of the directions in the tangent space of the unitary manifold, and thus a choice of metric is denoted as a *cost function* F in Nielsen's approach. This is a local functional of the position and velocity of a trajectory, i.e. $F \equiv F[U(t), \dot{U}(t)]$, and it was argued in [349, 352, 357] that suitable cost functions should obey the following criteria:

1. **Continuity**: $F \in C^0\ \forall U(t), \dot{U}(t)$.
2. **Positivity**: $F[U(t), \dot{U}(t)] \geq 0$, with equality if and only if $\dot{U}(t) = 0$.
3. **Positive Homogeneity**: $F[U(t), \lambda\dot{U}(t)] = \lambda F[U(t), \dot{U}(t)]\ \forall \lambda \in \mathbb{R}^+$.
4. **Triangle inequality**: $F[U, \dot{U} + \dot{V}] \leq F[U, \dot{U}] + F[U, \dot{V}]$.

At the level of the tangent bundle of the manifold of unitaries, whose individual tangents spaces are each isomorphic to the Lie algebras $\mathfrak{su}(2^n)$ or $\mathfrak{su}(N)$, the choice of a cost function amounts to defining an inner product on the algebra, which imposes so-called *penalty factors* $p_K > 0$ on each direction. These are weights defining the cost associated to every infinitesimal gate in the tangent space, and they can be seen as a unique characterization of the complexity geometry associated to a given cost function. With these ingredients, the complexity of a given unitary U is then identified with its minimal geodesic distance from the identity operation, which is naturally deemed to have vanishing complexity. More precisely, we have

$$\mathcal{C}[U] = \min_{\{U(T)\}} \int_0^{T_\mathrm{f}} ds\, F[U(s), \dot{U}(s)]\,, \tag{2.70}$$

where the minimization is performed over all geodesic trajectories connecting the identity with U at $T = T_{\mathrm{f}}$. The associated minimal geodesic is then interpreted as the optimal quantum circuit which implements the given unitary. It was shown in [352] that this continuous notion of complexity is indeed equivalent to the discrete gate-counting definition introduced before. In Sec. 4.1.3, we will consider an explicit choice of cost function akin to $F[U,Y] = \sqrt{\sum_K p_K |Y^K|^2}$ with polynomial penalty factors $p_K \sim K^2$ which leads to particularly interesting consequences for Nielsen complexity in the limit of infinite-dimensional Hilbert spaces.

[a] We work with anti-Hermitian operators for consistency with conventions used in Sec. 4.1.

This geometric picture of complexity has proven to be highly useful in finite quantum systems, particularly those consisting of large arrays of n qubits, which are a model for quantum computer registries [358–363]. In these setups, physically justified choices for the definition of complexity can be clearly stated. However, for applications in AdS/CFT, we would like to have a definition of complexity for quantum field theories, in particular CFTs. Although some progress has been done in this direction [357, 364–371], there is still a high level of arbitrariness, mostly due to the infinite dimensionality of the Hilbert space. Even when complexity can be defined, its computation can only be carried out explicitly in certain simple cases, such as free field theories.

Nonetheless, many qualitative features of complexity can be estimated in simple toy models, in particular the expected behavior of complexity as time evolves. Such arguments are specially relevant since they support the idea of complexity as an entry into the holographic dictionary, namely as *holographic complexity*, being able to capture signatures of the wormhole growth at times where entropy has long saturated. Based on very simple assumptions, the authors in [139–141] suggested a typical behavior for the complexity of the time-evolution operator under a generic Hamiltonian, which is typically chaotic. This behavior for complexity is sketched in Fig. 2.5. The main characteristics are i) an initial linear growth up to times which are exponential in the system size, typically estimated as e^S where S denotes the entropy of the system counting the number of possible configurations, ii) a saturation to a maximal value at $t^* \sim \mathcal{O}\left(e^S\right)$, and iii) a drop in complexity at doubly-exponential times $t^\star \sim \mathcal{O}\left(e^{e^S}\right)$ due to quantum recurrences [139–141, 359]. The latter corresponds to the unitary circuit having explored the entirety of the unitary manifold, eventually returning to a point very close to the identity [372], which has very low complexity. The general behavior of complexity should then commence once again. In the same Fig. 2.5, we have also included the typical behavior of entanglement entropy to highlight the stark

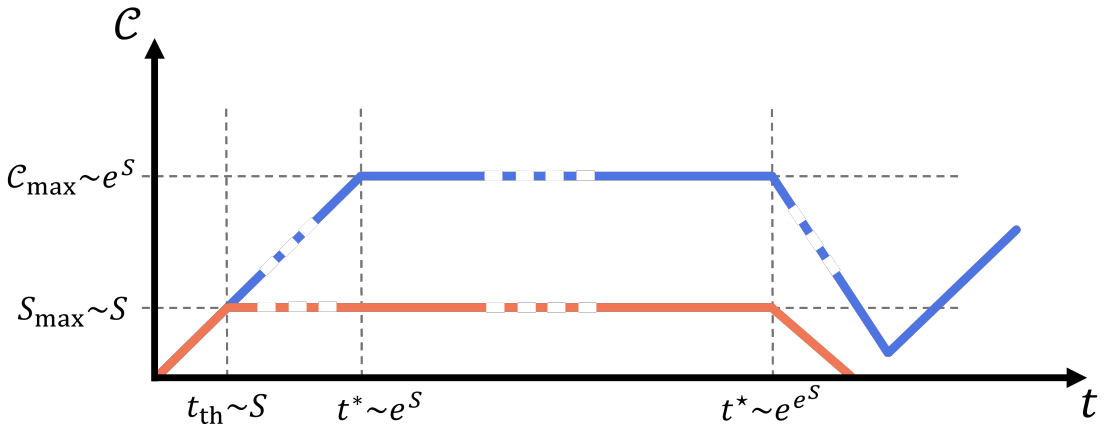


Figure 2.5: Qualitative behavior of complexity of time-evolution under chaotic Hamiltonians conjectured in [139, 140]. The complexity (blue) exhibits a linear growth up to times t^* exponential in the system size, after which it plateaus and fluctuates around a maximal value $\mathcal{C}_{\max} \sim e^S$. After times $t^\star$ doubly-exponential in the system size, quantum Poincaré recurrences imply that a highly unlikely fluctuation will drive the system close to its original configuration, such that complexity drops to near zero [359]. As a comparison, we sketch the temporal evolution of the entanglement entropy, which reaches its maximum value $S_{\max} \ll \mathcal{C}_{\max}$ at the thermalization time scale $t_{\text{th}} \ll t^*$. Figure adapted from [359].

differences between these two quantities.[10] The fact that entanglement reaches its maximum within a thermalization time-scale t_{th} much smaller than the saturation time t^* of complexity is the main desired characteristic supporting the consideration of complexity as a quantity probing the black hole interior at late times. In fact, it was argued in [141] that the volume of the ER bridge indeed reaches a constant value for infinite boundary times.[11] This feature is reflected in the plateau of complexity at exponentially late times. Moreover, it was also conjectured in [141] that for finite boundary times the volume of the ER bridge grows linearly with time, a behavior also expected to be captured by the complexity of the boundary time-evolution.[12] It is thus clear that this quantity presents itself as a good candidate to describe the growth of black hole interiors in a holographic fashion.

Besides the qualitative features of holographic complexity discussed above, much effort was put into finding precise geometric objects in the bulk which act as holographic duals for complexity. There were two main candidates considered in the early stages of complexity, namely the "complexity=volume" [138, 139, 141, 374, 375] and

[10] Notice however, that the complexity of a system of size S effectively behaves as the entropy of a system of size e^S [359].

[11] To the best of my knowledge, the Poincaré recurrence of complexity shown in Fig. 2.5 is never discussed from the point of view of the wormhole. Standard discussions only focus on the linear growth and the plateau of complexity, and we will do so as well here.

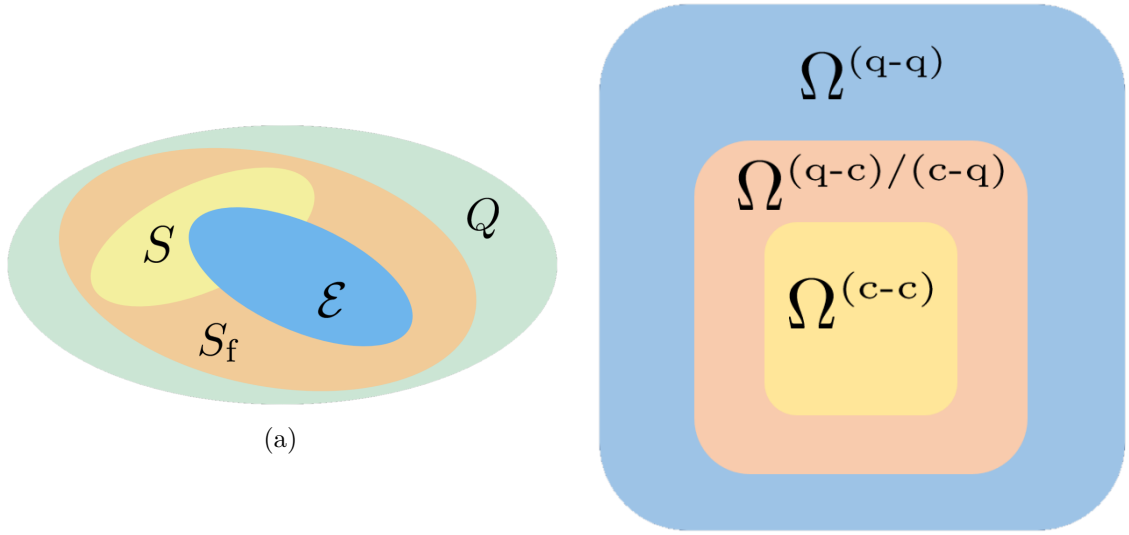
[12] See [373], where a proof of this linear growth of complexity for Haar-random circuits was provided.

"complexity=action" [376, 377] proposals. The former advocated for the volume of the wormhole as the holographic dual to complexity, while the latter suggested that the on-shell gravitational action evaluated on a specific bulk region known as the Wheeler-DeWitt patch is a better-suited candidate. The study and comparison of these two proposals lead to many later works [369, 378–389] (see [346, 347] for extensive reviews), which deepened our understanding of holographic complexity overall. However, due to the innate ambiguities that complexity has, opinions on the exact holographic dual of quantum complexity are still far from unanimous. The situation has even come to the extreme claim that complexity might be *too* arbitrary a quantity, such that it may be dual to an effectively infinite class of quantities in the bulk [390–393]. Nonetheless, the absence of a unique notion of holographic complexity may also be regarded as a blessing in disguise, which allows us to study many geometric features of black holes via different takes on an overarching quantity. Therefore, the study of complexity measures within holography remains to be an intriguing line of research.

From a geometric point of view, the growth of complexity and its saturation can be formulated in terms of specific requirements on Nielsen's approach to complexity, cf. Box 2.2. In particular, these features translate into requirements on the chosen cost function on the unitary manifold, such as ergodic geodesic flow and the existence of conjugate points [349]. Not every cost function exhibits these qualities, and finding a natural choice which still allows for the computation of complexity would be very valuable. Moreover, given that complexity in finite-dimensional systems is relatively better understood, one may hope to define cost functions in these settings which then provide canonical definitions of complexity upon extrapolation in the thermodynamic limit. We will discuss these ideas in detail in Sec. 4.1 when we explicitly construct such a cost function exhibiting these features.

2.3.3. Quantum Discord

We now turn our attention to a quantity from quantum information theory whose potential role within holography is not yet fully understood. Recall from our previous discussions in Sec. 2.3.1 that entanglement entropy, though excellent for quantifying correlations within pure states, falls short when it comes to mixed states. In such cases, classical correlations also enter the picture, whose contribution to the overall correlations between a subsystem and its complement cannot be fully resolved by entanglement entropy. For this reason, the quantity known as *quantum discord* was introduced in [256, 257] and [258]. Though we have previously mentioned other alternative measures of correlations for mixed states (negativity, entanglement of formation, etc.), quantum discord was constructed to be an overarching quantifier for



(a) (b)

Figure 2.6: Left: Illustrative comparison of the different measures of quantum correlations in a generic mixed quantum state ρ mentioned in the main text. Quantum discord $Q(\rho)$ (2.78) is the most general one, capturing non-zero correlations of pure quantum mechanical nature which are out reach for other measures such as entanglement negativity $\mathcal{E}(\rho)$ and entanglement of formation $S_f(\rho)$. The von Neumann entanglement entropy $S(\rho)$ (2.53), while powerful for pure states, it is not well suited to capture correlations in mixed states and it only covers a small portion of them. Right: Set hierarchy $\Omega^{(q\text{-}q)} \subset \Omega^{(q\text{-}c)/(c\text{-}q)} \subset \Omega^{(c\text{-}c)}$ for bipartite states in view of their entanglement properties. Arbitrary quantum states will be (q-q) states of the form (2.81), while a subset of those are such that one of the subsystems can be described classically, namely the (q-c)/(c-q) states (2.80). The smallest set is that of completely classical bipartite systems, denoted by (c-c) (2.79), which do not support any quantum correlations. These figures were adapted from [394] with the consent of the author.

all the purely quantum correlations in a system, thus acting as the most general such measure which reduces to the other suggested quantities in specific instances. This hierarchy between different correlation measures can be visualized as in Fig. 2.6a. Given that quantum discord will play an important role in our later discussions in Sec. 4.2, we review its definition and main properties in the following.

The definition of quantum discord arises from two equivalent yet different ways of writing a quantum version for the classical mutual information. In classical information theory [395, 396], if we consider two random variables A and B, the amount of information shared by both of them is quantified by the mutual information $I(A:B)$. Classically, this quantity can be defined via the Shannon entropy H in two different ways, namely as

$$I(A:B) = H(A) + H(B) - H(A,B)\,, \tag{2.71}$$

or, equivalently, as

$$I(A:B) = H(A) - H(A|B)\,, \tag{2.72}$$

where $H(A|B) = H(A,B) - H(B)$ denotes the so-called conditional entropy. The latter quantifies how much information we could potential retrieve from the variable A given that we know the outcome of variable B. In other words, the conditional entropy quantifies our uncertainty about variable A in the case of having priori knowledge about variable B. For example, two random variables associated to two separate classical and ideal coins would have maximal conditional entropy, since these two events are completely independent. Even if we know the outcome of coin B, the possible outcomes of coin A are still 50% each. In contrast, if we have variable B describe the possible face value $i = 1, 2, 3, 4, 5, 6$ of a die, while variable A describes the parity (even or odd), the conditional entropy $H(A|B)$ would vanish since the knowledge of B completely determines the parity.

If we now wish to describe a quantum system in a general state ρ_{AB}, the typical replacements are to consider the reduced density matrix ρ_A as a quantum mechanical version of the random variable A, and analogously for B. The classical Shannon entropies H are then substituted by von Neumann entropies S given in (2.53). The quantum mutual information as given in (2.71) is then simply given by

$$I(A:B) = S(\rho_A) + S(\rho_B) - S(\rho_{AB})\,, \tag{2.73}$$

where ρ_{AB} denotes the density matrix of the full system. Let us mention that mutual information is a particularly useful quantifier of correlations in the case of multi-partite systems, where entanglement entropy *per se* is no longer a good measure. Indeed, mutual information will play a key role in our analysis in Sec. 3.5.5 for precisely this reason. Returning to the expression (2.73), notice how the simple replacement $H \to S$ does not lead to a positive-definite quantity when applied to (2.72) [397–400]. The culprit for this is the conditional entropy $H(A|B)$, whose quantum mechanical interpretation is subtle and requires more care as to what exactly is meant by having prior knowledge about subsystem B. This necessarily involves a set of measurement outcomes, whose exact form and possible values are *a priori* unclear. To overcome this, a possible definition for quantum conditional entropy, denoted by $S(A|B)$, was given in [257] as

$$S(A|B) = \min_{\Pi_k^B \in \mathcal{M}^B} \sum_k q_k S(\rho_k^A)\,, \tag{2.74}$$

where the operators Π_k^B describe projective measurements performed on subsystem B, the outcomes of which are labeled by the index k. We denote the set of all such measurements by $\mathcal{M}^B$. The minimization over all such measurements represents the fact that we want to find the most efficient way to gain knowledge about system B without unnecessarily perturbing it. Moreover, we have introduced *conditioned* reduced density matrices ρ_k^A, as well as outcome probabilities q_k, which read

$$\rho_k^A = \frac{1}{q_k} \operatorname{Tr}_B \left[\left(\mathbb{1}_2 \otimes \Pi_k^B \right) \rho_{AB} \left(\mathbb{1}_2 \otimes \Pi_k^{B\,\dagger} \right) \right] , \tag{2.75}$$

$$\text{where} \quad q_k = \operatorname{Tr} \left[\left(\mathbb{1}_2 \otimes \Pi_k^B \right) \rho_{AB} \left(\mathbb{1}_2 \otimes \Pi_k^{B\,\dagger} \right) \right] . \tag{2.76}$$

In other words, a given conditioned reduced density matrix ρ_k^A describes the state of subsystem A after a measurement has been made on subsystem B, which yields the outcome k with probability q_k. Let us mention that the definition of other quantities known as *localizable entanglement* [401, 402] and *measurement induced entanglement* [403] is quite similar in spirit to that of quantum conditional entropy given in (2.74). These quantities also consider entanglement measures evaluated on conditioned reduced density matrices and even some extremization procedure over these.[13] However, these quantities are specifically constructed to study bipartite entanglement between two subsystems in a larger *multi-partite* system, while the quantum conditional entropy given in (2.74) is only defined for bipartite quantum systems. It may nevertheless be possible to relate localizable entanglement and quantum conditional entropy in the case of bipartite systems upon replacing the minimization in (2.74) by a maximization, cf. the discussion in [404]. The reason for the minimization in (2.74) is that quantum discord is such that it quantifies the smallest difference between the two equivalent ways of quantizing mutual information. Notice how using (2.74), the mutual information (2.72) takes the form

$$J(A:B) = S(\rho_A) - S(A|B) . \tag{2.77}$$

This quantity, also known as asymmetric mutual information, is exclusively sensitive to classical correlations [258] by construction. It is asymmetric due to the presence of the second term, which does not remain invariant under the exchange $A \leftrightarrow B$. Given that the quantum version of mutual information given in (2.73) is such that it captures all the possible correlations between A and B, and given that the asymmetric mutual information (2.77) captures only classical correlations, it is natural to define quantum

[13] I am very thankful to Sara Murciano for pointing these quantities out to me.

discord as the difference of these quantities

$$Q(A:B) = I(A:B) - J(A:B)\,. \tag{2.78}$$

By construction, this quantity only captures correlations which are purely quantum mechanical in nature, and it does not vanish in general. Moreover, it is also asymmetric due to the presence of $J(A:B)$, although symmetric versions of quantum discord can also be constructed [405, 406]. For pure states, one can readily check that quantum discord reduces exactly to the von Neumann entanglement entropy since in that case $S(A|B) = 0$ because $S(\rho_k^A) = 0$, and also $S(\rho_{AB}) = 0$. For general mixed states, discord captures all the quantum correlations shared between two subsystems. Quantum discord is positive-definite $Q(A:B) \geq 0$ and vanishes if there entirety of the correlations are purely classical, in which case $I = J$. This is the case for the set of states known as classical-classical (c-c) states which are of the form

$$\chi^{(\text{c-c})} = \sum_{m,n} \lambda_{mn} |\phi_m^A\rangle\langle\phi_m^A| \otimes |\phi_n^B\rangle\langle\phi_n^B|\,, \tag{2.79}$$

where $\left|\phi_m^A\right\rangle$ and $\left|\phi_m^B\right\rangle$ denote complete bases for the subsystems A and B, respectively. We denote this set of (c-c) states by $\Omega^{(\text{c-c})}$. However, there is an even larger class of states, denoted by $\Omega^{(\text{q-c})/(\text{c-q})}$, which also have vanishing discord due to the existence of measurements on subsystem B which do not affect the system at all. These are called quantum-classical (q-c) states,[14] and have the form

$$\chi^{(\text{q-c})/(\text{c-q})} = \sum_{m} \lambda_m \rho_m^A \otimes |\phi_m^B\rangle\langle\phi_m^B|\,. \tag{2.80}$$

Finally, the most general set of states in a bipartite quantum system are the quantum-quantum (q-q) states of the form

$$\chi^{(\text{q-q})} = \sum_{m} \lambda_{mn} \rho_m^B \otimes \rho_n^A\,, \tag{2.81}$$

belonging to the set $\Omega^{(\text{q-q})}$. These are the most generic types of states and they will have non-vanishing discord in general. The hierarchy between these three sets of quantum states in a bipartite system is visualized in Fig. 2.6b.

[14] The exact same construction can be done by interchanging the subsystems, such that we obtain classical-quantum (c-q) states. These are equivalent.

2.3.4. Tensor Networks

We conclude this chapter by briefly reviewing one of the frameworks which most vividly highlighted the deep connection between spacetime and quantum information, namely tensor networks. These objects provide a technical arsenal to efficiently emulate certain classes of states in quantum many-body systems, in particular when it comes to reproducing specific entanglement structures therein. From a purists point of view, the highly successful implementation of tensor networks and holographic quantum error-correcting codes within the AdS/CFT correspondence represents one of the first instances of inherently discrete holography. In fact, we will later present our own tensor network construction in Sec. 3.5.7 in the context of explicit boundary models within discrete holographic dualities. This discussion will be accompanied by plenty of technical details regarding the functional structure and evaluation of tensor networks. Therefore, we restrict our review in this section to a qualitative description of this framework, its main benefits, and its current status within the landscape of holographic dualities. For detailed reviews on the technical aspects of tensor networks, we refer the reader to [151, 153, 169, 407–409].

Tensor networks are a tool for the efficient numerical simulation of quantum states based on their entanglement structure. Generically, a state of a quantum many-body system like a collection of N M-level qudits will have a form similar to that in (2.43), which in a more explicit but still completely general notation reads

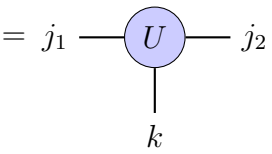
$$|\psi\rangle = \sum_{k_1,k_2,\ldots,k_N}^{M} T_{k_1,k_2,\ldots,k_N} \, |k_1, k_2, \ldots, k_N\rangle \ , \tag{2.82}$$

where the product basis is given by $|k_1, k_2, \ldots, k_N\rangle \equiv |k_1\rangle \otimes |k_2\rangle \otimes \cdots \otimes |k_N\rangle$. For instance, a system of 5 spins would be described by (2.82) with $N = 5$ and two-level systems $M = 2$. Notice how the state is purely characterized by the set of M^N amplitudes contained in the object $T_{k_1,k_2,\ldots,k_N} \in \mathbb{C}$, which can be seen as a complex-valued tensor of rank N [153]. The dimension of the space spanned by each index in this tensor is also called the *bond dimension*, denoted by $\chi = M$. For a generic state of the form (2.82), we manifestly require an exponential amount of resources and memory to store and manipulate the entire information about the state encoded in its amplitudes. However, certain states of particular physical interest may enjoy properties that allow us to focus on the corners of the Hilbert space containing them. In fact, we have already encountered such a class of states, namely the ground states of local gapped Hamiltonians, which obey an area-law for entanglement. These states live in a much more (exponentially) constrained region of the extremely large many-body Hilbert

space. Given this restriction, tensor networks offer an efficient ansatz to obtain the corresponding amplitudes $T_{k_1,k_2,\ldots,k_N}$ via the contraction of particular tensors according to a graphical network. The specific properties of these tensors, together with the given graph pattern dictating their connections, encode the entanglement structure of the resulting state $|\psi\rangle$. In this sense, tensor networks provide a sort of *entanglement representation* or basis for the wave functions of quantum systems [151]. An example of such a tensor contraction for the case of $N = 3$ reads

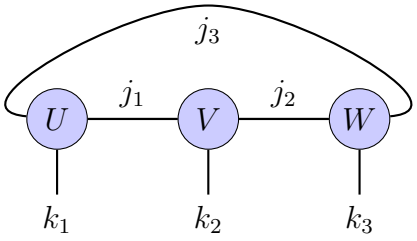
$$T_{k_1,k_2,k_3} = \sum_{j_1,j_2,j_3}^{\chi_j} U_{k_1,j_3,j_1} V_{k_2,j_1,j_2} W_{k_3,j_2,j_3} \,, \tag{2.83}$$

with U, V, W three rank-3 tensors and where χ_j denotes the bond dimension of each of the indices j, which is not necessarily the same for all. Tensor contractions can be thought of as a generalization of Einstein's summation convention, albeit without the notions of co- or contravariant indices associated to indexed objects in relativistic theories. Each index of a tensor is interpreted as a leg, and contractions between two indices amount to gluing the corresponding edges. This provides the graphical aspect associated to tensor networks, since the gluing or contraction pattern of different tensors can be represented by a graph network. For example, by visualizing an individual tensor as

$U_{k,j_1,j_2} =$ 

(2.84)

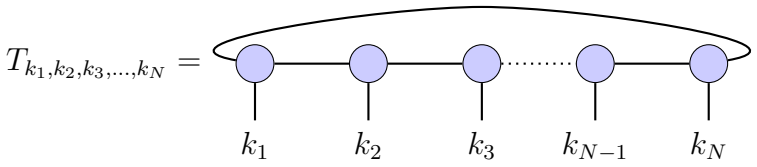
the contraction operation in (2.83) can be graphically represented as [153]

$T_{k_1,k_2,k_3} =$ 

(2.85)

where the leg contractions are explicit, while k_1, k_2, k_3 denote the free or dangling legs. The generalization of this construction to the N qudit state in (2.82) is known as a

matrix product state (MPS) [410–415], and looks like



(2.86)

where we have removed the labels for internal contracted legs and the tensors for clarity. The main benefit of this construction is that we have re-written a large tensor T into the product of smaller tensors with smaller rank. Each of the dangling legs of the MPS represents a local Hilbert space of dimension χ_k, which is associated to a site in a one-dimensional quantum many-body system. In essence, if we write the tensors in the suggestive form $(U_{k_1})_{j_1,j_2}$, the MPS ansatz boils down to the relation

$$T_{k_1,k_2,k_3,\ldots,k_N} = \mathrm{Tr}\left(U_{k_1} U_{k_2} U_{k_3} \cdots U_{k_N}\right) , \tag{2.87}$$

which is to be read element-wise, i.e. for every configuration of $\{k_1, k_2, k_3, \ldots, k_N\}$. The contractions between tensors within the trace determine the diagrammatic form of the network. Finally, the coefficients of the ansatz, i.e. the actual entries of the tensors, are the only parameters that need to be determined, usually through a variational method trying to minimize the expectation value of the energy [153, 169]. The benefit is that, though not unique, the MPS provides an exponentially more efficient way of writing the original χ_k^N amplitudes in terms of only $N\chi_k\chi_j^2$ free coefficients. It is clear that this will however not densely reproduce every state in the large many-body Hilbert space unless the bond dimensions χ_j themselves have an exponential dependence on N. However, for the restricted class of ground states of one-dimensional gapped and local Hamiltonians, the MPS description is indeed enough to efficiently reproduce the area-law entanglement structure [153].

Generalizations of the MPS states to higher-dimensions are provided by so-called *projected entangled pair states* (PEPS) [416], and they also provide an efficient way of reproducing area-law scaling of entanglement [151]. More complex entanglement structures, such as logarithmic violations to the area law present in CFT ground states of two-dimensional CFTs (cf. (2.62)), a more elaborated tensor network known as *multi-scale entanglement renormalization ansatz* (MERA) was introduced in [417, 418]. The MERA consists of two types of tensors, called *isometries* and *disentanglers*, which obey very special properties, allowing for MERA to efficiently reproduce states with long-ranged entanglement. The tensor network of MERA has the structure of a tree, and it performs so-called entanglement renormalization, meaning that the tensors act

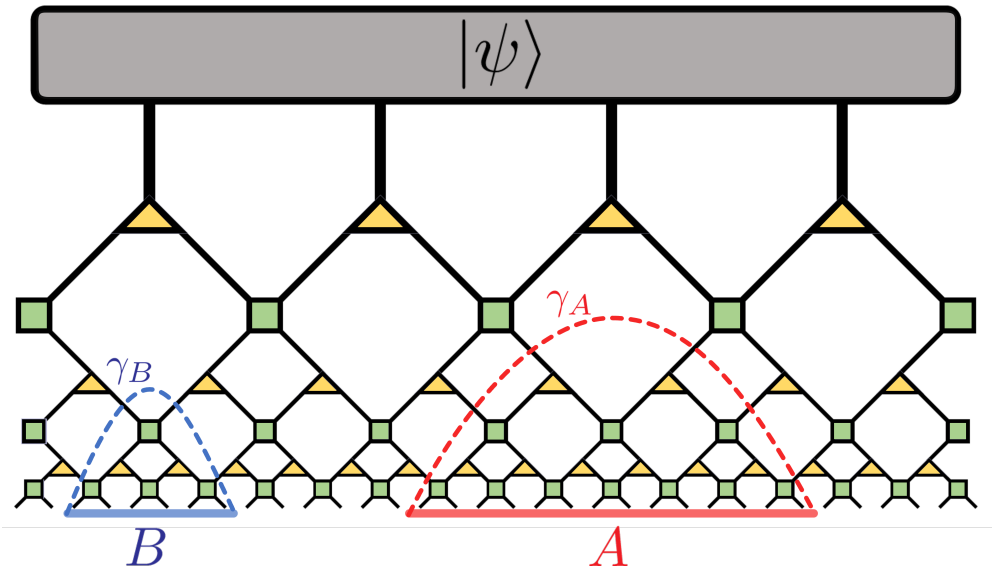


Figure 2.7: Visual depiction of a MERA tensor network consisting of disentanglers (green squares) and isometries (yellow triangles), whose effect is to coarse-grain the short-range entanglement present in the original wave function such as to efficiently reproduce the long-range entanglement structure in ground states of $(1+1)$-dimensional gapless systems. Two exemplary subregions A and B consisting of consecutive uncontracted tensor legs are shown in red and blue, respectively. Their entanglement entropy is obtained from a minimal cut prescription, with their respective minimal cuts γ_A and γ_B shown to extend into the bulk of the network. Each internal tensor leg which is cut by these minimal curves contributes $\log(\chi)$ to the entanglement entropy, with χ the bond dimension. Figure adapted from [153].

as coarse- or fine-graining transformations which break down the structure of the entanglement, cf. Fig. 2.7. As the name suggests, the disentangler tensors remove short-ranged entanglement from the wave function, renormalizing it into entanglement at a larger scale. More precisely, they are local unitary transformations acting on neighboring spin blocks which reduce the amount of entanglement between them, thus ensuring that the next layer of coarse-grained spins do not carry such short-ranged entanglement [169]. Meanwhile, the isometries perform the actual coarse-graining operation reducing the number of sites while preserving the ground state properties [419]. They are maps between Hilbert spaces of not necessarily the same dimension, but which preserve the norm. The geometry of the MERA tensor network is such that it geometrically reproduces desired entanglement entropy bounds via a *minimal cut* argument. Broadly speaking, each contracted leg in the tensor network hosts two Hilbert spaces with dimension equal to the bond dimension. Any cut γ through the network which ends on the boundary of the network (i.e. at the bottom of Fig. 2.7) will necessarily divide the full tensor network into two smaller ones which are only connected via a finite number of legs intersected by γ. When performing the

contraction of these two smaller networks along the cut legs, we effectively generate entanglement at a rate of one $\log \chi$-contribution per internal leg cut. The properties of the tensors within the MERA tree are such that the entanglement entropy of a subregion A of the boundary layer is bounded from above by the length $|\gamma_A|$ of the *minimal* cut γ_A which ends at the entangling points of A, i.e. the curve which cuts the minimal number of legs in the network. If we assume a constant bond dimension χ throughout the MERA tensor network, the entanglement entropy is bounded by

$$S_A \leq |\gamma_A| \log \chi \,. \tag{2.88}$$

Examples of minimal cuts are shown in Fig. 2.7, where $|\gamma_A| = 6$ and $|\gamma_B| = 4$. Note that the bound (2.88) is also valid for MPS and PEPS networks. However, in those cases, $|\gamma_A|$ is constant and the vale of the entanglement entropy can only grow by increasing the bond dimension, irrespective of the size of the subregion. In contrast, the key feature of the MERA tensor network is that is geometry is very similar to hyperbolic geometry, with the presence of the isometries providing an increasing number of free legs towards the boundary. Crucially, it is this geometry which ensures that $|\gamma| \propto \log L$, with $L = |A|$ being the size of the boundary subregion [153]. This allows the MERA to efficiently reproduce the logarithmic scaling of entanglement entropy for gapless systems.

As mentioned above, these properties of the MERA tensor network are strongly reminiscent of features present in the AdS/CFT correspondence, in particular when it comes to the hyperbolic geometry of the network and the minimal cut bound on entanglement entropy, the latter bearing a striking resemblance the RT prescription for holographic entanglement entropy. The fact that the tensor network extends in a direction whose coordinate is associated to a certain RG flow is also very similar to the role of the holographic coordinate in standard AdS/CFT. Many of these ideas were put on a stronger footing in a series of papers [133, 420–422], where the consequences of the hyperbolic geometry of the MERA tensor network were studied in detail. However, it was readily understood that the geometry of MERA is not compatible with that of a constant-time slice of AdS (i.e. the hyperbolic Poincaré disk), but rather with a null-like surface which can be interpreted as a light-cone [423, 424]. Nonetheless, later investigations showed that by choosing the correct properties for the tensors, a network amenable with the Poincaré disk is indeed possible. In particular by choosing so-called *perfect tensors*, and by performing an index contraction scheme following the geometry of regular hyperbolic tilings of the Poincaré disk, the authors of [152] managed to construct a tensor network which saturates the entropy bound (2.88) for

single intervals. Their construction was based on imposing constraints on these networks based on quantum information quantities beyond entanglement entropy like Rényi entropies and the notion of quantum error-correction codes [425–428]. Motivated by this, the authors of [429–431] built a different class of tensor networks using random tensors, which saturate the entropy bound (2.88) even in the case of multiple intervals. Many other holographic properties were shown to be reproduced by these tensor networks in the limit of large bond dimension, which is interpreted as a semi-classical limit from the holographic point of view [153]. In fact, we will make heavy use of the construction put forward in [430] in our analysis on Sec. 3.5.7. After the initial studies on tensor networks and holography mentioned above, a great amount of effort was put into further understanding this fascinating intersection between high-energy physics and quantum information theory, as well as understanding how helpful this framework can be in unveiling fundamental aspects of entanglement in the AdS/CFT correspondence, see e.g. [432–443].

It is evident that tensor networks play an important role within holography as systematic tools to geometrize the entanglement structure of quantum systems. Vitally for this thesis, tensor networks are inherently discrete, thus providing a promising platform to study discrete realizations of the holographic principle. Yet, although they are incredibly efficient in reproducing quantum states, perhaps one of the most evident shortcomings of tensor networks is that they are completely agnostic to the physical origin of these states. In other words, though holographic tensor networks do reproduce several properties of the AdS/CFT correspondence in an arguably discrete way, they do not provide explicit sets of dual theories. In Sec. 3.5.7, we will report on progress made in this direction by constructing a large class of tensor networks with explicitly known parent Hamiltonians, and which still preserve many desired holographic properties.

Discrete Approaches to Holography | 3

"There is nothing wrong with crazy as long as it's right."

Roger Penrose

In the last couple of decades, an immense amount of effort has been put into understanding holographic dualities in their continuous versions. Seeing this undeniable success of theoretical frameworks based on the holographic principle for continuous variables, one is immediately lead to the question of whether this can be achieved in discrete settings as well. Such discrete systems offer a plethora of attractive features, such as computational tractability, well-established methods for numerical manipulation, but perhaps most interestingly, the connection to experimental realizations. The lack of the latter is a common point raised by critics of the AdS/CFT correspondence, who argue that this brain-child of string theory does not lead to any measurable predictions. Although one of the arguably most celebrated results of AdS/CFT, namely the Kovtun-Son-Starinets (KSS) bound [444–446] (see Box 3.1) is indeed in agreement with experimental results [447], some may argue that the list of further confirmed predictions made by holography does not particularly impress with its length. It is therefore an exciting prospect to explore different way of discretizing holographic dualities such as to make them and their predictions accessible to different experimental platforms, which are discrete by construction.

From a different point of view, the motivation for exploring discretizations of the AdS/CFT correspondence, a program that we will often refer to as *discrete holography*, is curiosity-driven. More precisely, we would like to understand the range of validity of such dualities, and how, if at all, holographic correspondences are to be adjusted when defined on discrete systems. One can expect that discrete models of AdS/CFT may shed new light into open questions of continuous AdS/CFT by enabling the usage of new computational methods. Similarly, we may also expect that discrete dualities will expand the holographic dictionary with new entries that are purely discrete in nature. Such an expectation is backed by instances in quantum matter theory where a restriction to discrete lattices leads to new types of excitations that are not present in their continuum counterparts [448]. Thus, there are strong arguments that discrete holography will advance our understanding of the holographic principle.

Box 3.1 The Kovtun-Son-Starinets Bound

One of the main strengths of the AdS/CFT correspondence is that it provides a framework for computing transport coefficients in strongly coupled gauge theories [168, 194, 449], which are otherwise not accessible even in perturbation theory. An example of such a strongly coupled system is the *quark-gluon plasma*, a state of matter which emerges at temperatures beyond the deconfinement regime of quantum-chromodynamics (QCD), and which is well described by a strongly interacting relativistic fluid [168, 450]. There is compelling evidence that the quark-gluon plasma has indeed been experimentally observed in heavy-ion collision events at the Large Hadron Collider (LHC) at CERN in Geneva [447], as well as in the Relativistic Heavy Ion Collider (RHIC) at Brookhaven National Laboratory in Long Island [451–455]. One key property of the quark-gluon plasma is the ratio of two transport coefficients, namely the shear viscosity η and the entropy density s. Broadly speaking, this quantity describes the capability of the system to relax into its equilibrium state [456]. Exploiting AdS/CFT, Kovtun, Son and Starinets, and Policastro [444–446] famously derived the value of this ratio to be

$$\frac{\eta}{s} = \frac{1}{4\pi} \,. \tag{3.1}$$

In fact, the authors further conjectured (3.1) to be a universal lower bound for any relativistic fluid, a claim that was later supported by a perturbative calculation in string theory of the leading corrections to the ratio η/s [457, 458]. In particular, it was shown that these corrections are positive and saturate the KSS bound only in the limit of infinite coupling. Indeed, we have yet to find experimental evidence of a fluid with a lower shear viscosity to entropy density ratio in nature.

In this Chapter, I first give an overview of previous works whose main motivation falls under the umbrella of the discrete holography program, which I do in Sec. 3.1. In Sec. 3.2, I introduce the main tool I will use to investigate discrete holography, namely discretizations of hyperbolic space via regular polygons. This section will cover the mathematical properties and characteristics of these objects, as well as their rich symmetry structure in terms of Fuchsian groups and their systematic construction through so-called inflation rules, leading to the concept of aperiodic sequences. In Sec. 3.3, I present proof-of-principle results on the realization of the celebrated Breitenlohner-Freedman stability bound on these hyperbolic tilings. This contains an analysis of the energy functional to characterize the instability, as well as the discretization and numerical implementation of the Klein-Gordon equation on hyperbolic tilings. An

experimental implementation on electrical circuits is also discussed. In fact, as an extension of these results, Sec. 3.4 is devoted to the implementation of interaction terms in the bulk via a holographic toy model. The latter is defined in terms of the adjacency matrix of the underlying hyperbolic tiling, and I show how correlation functions from putative boundary CFTs can be simulated via this model. This is further backed with a proposal for a measurement protocol on hyperbolic electric circuits. Sec. 3.5 poses a slight change of perspective, and I report results on the definition and characterization of aperiodic spin chain models at the boundary of hyperbolic tilings. After explaining the general construction of spin chains with aperiodic disorder, I explain how to exploit real-space renormalization group methods in the limit of strong disorder to gain insights into the correlation functions and entanglement entropy of the ground state. I present three explicit examples to showcase the applicability of these techniques, before culminating in a tensor network description of such aperiodic spin chains. In particular, our tensor network construction elevates itself from previous ones by introducing an explicit parent Hamiltonian for the ground state that is being reproduced. This allows for boundary dynamics in terms of time-evolution, a feature missing in previous literature. Our construction thus extends the state of the art of tensor networks within AdS/CFT by providing a first step towards including true dynamics into discrete holographic dualities.

3.1. The Discrete Holography Landscape

The idea of discrete holography can be approached in a variety of different ways. This is to be expected, since there are many ways of discretizing a theory, be it at the level of the underlying geometry, or its time-evolution, or perhaps its fundamental degrees of freedom. There is however, no canonical way to do this, and indeed there is extensive literature into different possible ways of defining discrete holographic dualities. It is thus pedagogical to give an overview of the main aspects of the most relevant approaches, in order to set the stage for our own contributions to the field.

Originating from string theory considerations [459–462], so-called *p-adic AdS/CFT* [463–474] attempts to develop the duality by replacing real-valued variables by variables over the discrete number field $\mathbb{Q}_p$ of p-adic numbers. The latter can be thought of as a number system in base p, where p is some prime number. They arise as the completion of the rational numbers with respect to the so-called p-adic norm, which turns out to be the only other non-trivial norm besides the usual Euclidean one according to Ostrowski's theorem [464, 475]. The p-adic numbers have a geometric representation

in terms of the so-called Bruhat-Tits tree [476], which is a discrete infinite tree graph with uniform coordination number $p+1$. The Bruhat-Tits tree plays the role of a discretized space in p-adic AdS/CFT, and indeed it enjoys a conformal boundary on which CFTs can be defined over the p-adic number line. The goal of this program has been to exploit the arsenal of tools of number theory, together with special properties of the p-adic numbers, to compute observables like higher-point functions and scattering amplitudes, which are typically very challenging in usual AdS/CFT. Ultimately, one hopes that these results from the p-adic numbers can be translated into results over the real numbers by means of so-called *Adelic formulas* [477], which relate quantities in the p-adic norm to their counterparts in the Euclidean norm. This is still an open line of research.

As a by-product of p-adic AdS/CFT, and as an attempt to introduce a notion of bulk dynamics and metric fluctuations in the discrete Bruhat-Tits tree, the concept of *edge length dynamics* was introduced in [478] by extending previous ideas of [479, 480] on curvature measures on graphs. As the name implies, the edges of the Bruhat-Tits tree are given length variables which are allowed to fluctuate, playing the role of metric fluctuations around a given background configuration. The main technical insight of the construction is to define localized probability distributions as weights on the vertices of the graph, while leaving the edge-lengths free to vary. By means of so-called Wasserstein distance functions [481], the authors show how to derive a discrete counterpart of the Ricci tensor on the graph [478–480]. This is then used to define a discretized Einstein-Hilbert action functional. The background edge-length configuration is that which minimizes this functional, much in the spirit of a statistical mechanics model. Moreover, a graph-theoretic variational principle is used to derive linearized equations of motion for the edge-length degrees of freedom, although finding solutions to these equations in general graphs has proven to be a formidable task.

From the aforementioned investigations, it became clear that non-Archimedean spaces, i.e. those where distances obey a stronger version of the triangle inequality, offer a rich playground to generalize features of holographic dualities relying on the hyperbolic nature of AdS space. The p-adic numbers and their geometric representation in terms of the Bruhat-Tits tree both exhibit this non-Archimedean property. Inspired by this, the authors of [482] proposed the even more abstract framework of *hyperbolic buildings* [483–485], where hints of holography can be explored. These are geometric constructions that cannot be embedded in Euclidean nor hyperbolic space of any dimension, but which are nevertheless hyperbolic in the sense of Gromov [486].

This means that they are metric spaces that which can still be given a sense of negative curvature by the specific properties of their metric, but they do not have admit a Riemannian description. Such buildings have a plethora of geometric, algebraic, and combinatorial properties, one of the most intriguing ones is the fractal nature of their Gromov boundary [482]. For a particular type of hyperbolic buildings, the so-called *Bourdon's buildings* [487, 488], their Gromov boundary is known to be homeomorphic to the fractal structure denoted as the Menger sponge. More precisely, denoted by $I_{p,q}$, with $p \geq 5$ and $q \geq 3$, Bourdon buildings consist of regular p-gonal *chambers* such that each edge is shared by q such chambers. Moreover, all q neighboring chambers intersect at right angles to each other. Given two chambers, one can consider them to lie on a unique plane, called an *apartment*, which can be thought of as a simple two-dimensional hyperbolic space. The notably counterintuitive characteristic of hyperbolic buildings is their *branching*, a feature which is described locally by the so-called *link* of the building [482]. The link is associated to a vertex and contains the information about all the edges that end on that vertex, together with the precise way these edges are connected by chambers. For Bourdon's buildings, the link at each vertex is given by the complete bipartite graph of $2q$ elements, denoted by $K(q,q)$. This is a graph where two subsets A, B of q elements each can be identified, such that every element $a \in A$ is connected to every element $b \in B$ of the other set, but there are no connections between elements of the same set [489]. The authors of [482] explain how a tensor network constructed on Bourdon's buildings can reproduce an entanglement entropy in agreement with expectations from the Ryu-Takayanagi formula, thus hinting at their holographic properties. Interestingly, the fractal nature of the boundary is indeed resolved by the entanglement entropy, and it manifests itself in the dependence of the area of Ryu-Takayanagi surfaces on the fractal dimension. However, further holographic properties of such constructions on hyperbolic buildings are yet to be explored.

On another formal avenue, the approach of *modular discretization* [490–494] attempts to restrict the symmetry groups on both sides of the AdS/CFT correspondence by means of coset constructions with respect to the discrete modular sets $\mathbb{Z}_n$, $n \in \mathbb{N}$. These spaces provide discrete approximations to the original manifolds denoted as finite arithmetic geometries given by the coset $\mathrm{AdS}_2[n] = \mathrm{SL}(2,\mathbb{Z}_n)/\mathrm{SO}(1,1,\mathbb{Z}_n)$. On these geometries, a discrete time evolution in terms of unitary dynamics of particles is described via isometric maps called *Arnold cat maps* [495–497], which are elements of the $\mathrm{SL}(2,\mathbb{Z}_n)$ group. The action of such maps on coset representatives $s \in \mathrm{AdS}_2[n]$, describing the position of the particle probe on the finite arithmetic geometry, gives

rise to dynamics in these spaces. The boundary is obtained by a similar coset construction as $\mathrm{SL}(2,\mathbb{Z}_n)/\mathfrak{B}_n$, where $\mathfrak{B}_n$ is the Borel subgroup [498, 499] of $\mathrm{SL}(2,\mathbb{Z}_n)$. The latter is the conformal group of the $\mathrm{CFT}_1[n]$ on the boundary, as well as the isometry group of the discretized AdS geometry. This approach contains an elegant construction of Hilbert spaces based on irreducible representations of modular groups, but how to generalize it to higher dimensions or add interactions is unclear.

Finally, we find it relevant to mention an approach which is discrete in nature, but has not yet been explored in the context of holographic dualities. It goes by the name of *causal dynamical triangulations* (CDT) [500–506], and its main goal is to provide a background independent, non-perturbative approach to quantum gravity by discretizing spacetime via fluctuating triangulations. More precisely, it provides a method to evaluate the non-perturbative 4D path integral on certain lattice discretizations consisting of piece-wise flat, simplicial 4d manifolds, and where the sum over different discretizations is referred to as "sum over histories". Let us note that CDT presents a more refined version of an old idea by Regge of considering general relativity without introducing explicit coordinates [507]. The main object of interest within CDT is the partition function $Z = \lim_{a\to 0} \sum_{T\in\mathcal{T}} \frac{1}{C(T)} \mathrm{e}^{\mathrm{i}S_{\mathrm{EH}}[T]}$, where $\mathcal{T}$ denotes the set of all such triangulations, or "histories", for a given spacetime manifold. Each term in the sum is weighted by the evaluation of a lattice discretization of the Einstein-Hilbert action S_{EH} on the corresponding triangulation. The factor $C(T)$ denotes the order of the automorphism group of the triangulation. The goal is to take a suitable continuum scaling limit $a \to 0$ of this path integral in order to obtain a candidate for a partition function of quantum gravity. While conceptually simple, this approach requires rather involved mathematics which later lead to advanced numerical techniques for any practical computations, like Quantum Monte Carlo simulations [508]. Analytical calculations are scarce and usually restrict to simpler toy models in lower-dimensions. Interestingly, although progress has been made while focusing mostly on flat Minkowksi or positively curved de Sitter spacetimes, a proper exploration of causal dynamical triangulations for Anti-de Sitter spacetimes, and a potential connection to AdS/CFT, is still mostly uncharted territory, although see [509–511] for interesting progress in this direction.

This brief review of the most relevant approaches to discrete holography shows that this is a highly active field of research, with still plenty of potential to uncover. In the remaining sections of this chapter, I report on my contributions to this field by expanding on the contents of [157–160].

3.2. Regular Hyperbolic Tilings

After this general overview on discrete approaches to holography, let us now focus on the main mathematical object that we exploit in this chapter. We use a discretization of hyperbolic space based on so-called *regular hyperbolic tessellations*.[1] There are several reasons why these constructions are promising for establishing a discrete holographic duality. First, we can argue that they are canonical in the sense that they naturally generalize the typical notions of lattices from the spherical and Euclidean cases to hyperbolic spaces. From the perspective of negatively curved space, these tilings are as canonical as a square lattice is canonical for the flat Euclidean plane. They arise from the deceivingly simple task of taking a single tile and cover with it an entire space without any gaps or overlaps. Second, regular hyperbolic tilings have an extremely rich symmetry structure [150] which can be exploited to adapt the usual constructions of continuum AdS/CFT to the discrete case. Their mathematical description has connections to many fields of mathematics, like the theory of Riemann surfaces, group theory, number theory, topology, and algebraic geometry [513–523]. Both on truncated and fully extended hyperbolic tessellations, the underlying symmetry groups have interesting representation-theoretic properties, which, in principle, naturally provide a definition of fields on such lattices. However, we will see to which extent this can actually be done in practice. Finally, it turns out that regular hyperbolic tilings also have very interesting construction properties. By this we mean that one can gain meaningful information from a systematic way of constructing such tilings, and this information can be stored at each step in the construction process by employing "aperiodic sequences" [524, 525]. One can broadly think of this as an innate holographic encoding from the information about the bulk tiling into its boundary, a property making them very attractive for the goals of the discrete holography program.

3.2.1. Poincaré Slices of AdS_{2+1}

To set the stage for introducing regular hyperbolic tilings, which we will often simply refer to as hyperbolic tilings, let us begin by considering Anti-de Sitter spacetime in (2+1)-dimensions. For our purposes, the global coordinate system with $\{\rho, t, \phi\} \in$

[1] I will be using the terms "tessellation" and "tiling" interchangeably. In some communities, a tessellation automatically implies the use of congruent tiles, while a tiling could use several different forms in principle, like the Penrose tiling [512]. This distinction will not be necessary in this work.

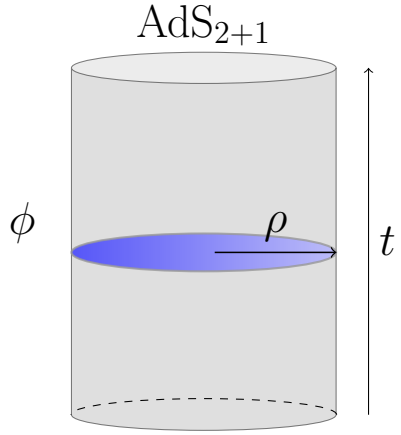


Figure 3.1: Schematic depiction of AdS_{2+1} spacetime, parametrized by global coordinates as in (3.2). Even though the spacetime is not globally hyperbolic, a $t = \text{const}$ Cauchy slice (blue disk) is isomorphic to two-dimensional hyperbolic space $\mathbb{H}^2$, which we model by the Poincaré disk $\mathbb{D}^2$.

$\{[0,1), \mathbb{R}, [0,2\pi)\}$ is a suitable choice, in which the invariant line element is given by

$$ds^2 = \ell^2 \frac{-(1+\rho^2)^2 dt^2 + 4\, d\rho^2 + 4\rho^2\, d\phi^2}{(1-\rho^2)^2}\,. \tag{3.2}$$

Recall that ℓ denotes the AdS radius and sets the constant negative curvature of the spacetime to be $R = -1/\ell^2$, where R is the Ricci scalar. In these compact coordinates, the conformal boundary lies at $\rho \to 1$. This boundary has the topology of a circle, which is also visible from the range of the angular coordinate ϕ in (3.2). The entire AdS_{2+1} spacetime thus exhibits a cylinder topology $\mathbb{R}^2 \times S^1$, as shown in Fig. 3.1. The global coordinates we used in (3.2) make manifest that AdS_{2+1} can be seen as being foliated by constant-time Cauchy slices with an induced metric which reads

$$ds^2 = (2\ell)^2 \frac{d\rho^2 + \rho^2\, d\phi^2}{(1-\rho^2)^2}\,. \tag{3.3}$$

This is precisely the expression of the metric for the *Poincaré disk* $\mathbb{D}^2$ model of two-dimensional hyperbolic geometry [526, 527]. It is defined as the set

$$\mathbb{D}^2 = \{z \in \mathbb{C}\,|\,|z| < 1\} = \{x{+}\mathrm{i}y,\, x, y \in \mathbb{R}\,|\,x^2{+}y^2 < 1\} = \{\rho \in \mathbb{R} \wedge \phi \in [0,2\pi)\,|\,\rho < 1\}\,, \tag{3.4}$$

equipped with the Poincaré hyperbolic metric

$$ds^2 = \frac{(2\ell)^2}{(1-|z|^2)^2} dz d\bar{z} = (2\ell)^2 \frac{dx^2 + dy^2}{(1-x^2-y^2)^2} = (2\ell)^2 \frac{d\rho^2 + \rho^2 d\phi^2}{(1-\rho^2)^2}\,, \tag{3.5}$$

where we have given its expression in Cartesian and polar coordinates for completeness. It is worth mentioning that the high-energy physics community often refers to this space as the Euclidean version of two-dimensional AdS space (obtained from the defining locus equation in (2.6) with Euclidean signature), and we will also make use of this equivalence, i.e. $\mathrm{EAdS}_2 \cong \mathbb{D}^2$.

Two-dimensional hyperbolic space is a non-compact space with infinite area. Equipped with the Riemannian metric given in (3.5), the Poincaré disk $\mathbb{D}^2$ becomes a smooth manifold which is locally conformally equivalent to the flat plane. This can be seen from the fact that (3.5) is the flat Euclidean metric up to a conformal factor. Furthermore, the Poincaré metric on $\mathbb{D}^2$ is also conformally invariant under the so-called *Möbius group*, i.e. the projective general linear group $\mathrm{PGL}(2,\mathbb{C})$. Möbius transformations $f : \mathbb{C} \to \mathbb{C}$ act generally on the complex plane via *fractional linear transformations*,

$$f(z) = \frac{az+b}{cz+d}\,; \quad a,b,c,d \in \mathbb{C}\,; \quad ad-bc \neq 0\,. \tag{3.6}$$

The subset of the complex plane given by the complex unit disk on which the Poincaré model is defined is further left invariant by a subgroup of Möbius transformations, namely those which obey $ad - bc = 1$. This subgroup is the so-called *isometry group* $\mathrm{Iso}(\mathbb{D}^2)$ of the Poincaré disk. In particular, $\mathrm{Iso}(\mathbb{D}^2)$ admits a representation as a matrix group $\mathrm{Iso}(\mathbb{D}^2) = \mathrm{SU}(1,1) \cong \mathrm{SL}(2,\mathbb{R})$ [526, 527]. This can be seen as follows: general isometries on $\mathbb{D}^2$ can be both orientation-preserving or orientation-reversing. Such transformations can be identified with the matrix representation of elements of the special unitary group $M \in \mathrm{SU}(1,1)$ of the form

$$M = \begin{pmatrix} A & B \\ B^* & A^* \end{pmatrix}\,, \tag{3.7}$$

with $A, B \in \mathbb{C}$ subject to the constraint $|A|^2 - |B|^2 = 1$. In this work, however, we restrict our attention to only the orientation-preserving isometries, which effectively means that we have to quotient $\mathrm{SU}(1,1)$ by the mirroring transformations, i.e. the positive and negative identity operators. Thus, we define the group of orientation-preserving isometries of $\mathbb{D}^2$ as

$$\mathrm{Iso}^+(\mathbb{D}^2) = \frac{\mathrm{SU}(1,1)}{\pm\mathbb{1}} = \mathrm{PSU}(1,1)\,. \tag{3.8}$$

The effect of the quotienting procedure is that the identity operation associated to $\mathrm{PSU}(1,1)$ has two different but equivalent representations in the form of (3.7), namely $\mathbb{1}$ and $-\mathbb{1}$. For the so-called *upper half-plane* model $\mathbb{H}^2$ of hyperbolic geometry [526,

527], also known as the *Bolyai-Lobachevskii plane* [528, 529], where the underlying manifold is

$$\mathbb{H}^2 = \{w = x + \mathrm{i}y \in \mathbb{C} | \, \mathrm{Im}(w) > 0\} \,, \tag{3.9}$$

equipped with the Poincaré hyperbolic metric

$$ds^2 = \frac{4\ell^2}{y^2}(dx^2 + dy^2) \,, \tag{3.10}$$

the isometry group is the projective special linear group $\mathrm{PSL}(2,\mathbb{R})$. We can show that this group is isomorphic to $\mathrm{PSU}(1,1)$ by choosing $A = \alpha + \mathrm{i}\beta - \mathrm{i}\gamma + \delta$ and $B = \alpha - \mathrm{i}\beta - \mathrm{i}\gamma - \delta$ in (3.7), with $\alpha, \beta, \gamma, \delta \in \mathbb{R}$. Then, the isomorphism between the groups reads

$$T^{-1}MT = \begin{pmatrix} \alpha & \beta \\ \gamma & \delta \end{pmatrix} \,, \quad \text{with} \quad T = \begin{pmatrix} 1 & -\mathrm{i} \\ 1 & \mathrm{i} \end{pmatrix} \,, \tag{3.11}$$

where $\alpha\delta - \gamma\beta = 1$, and thus we have the matrix representation of elements of $\mathrm{PSL}(2,\mathbb{R})$. The isomorphism T, which in particular is a Möbius transformation itself, is sometimes called the *Cayley transform* [530, 531]. As we will mostly work on the Poincaré disk $\mathbb{D}^2$, we will predominantly utilize the notation of $\mathrm{PSU}(1,1)$, while some specific arguments may be carried out in terms of $\mathrm{PSL}(2,\mathbb{R})$ for simplicity, keeping the isomorphism (3.11) in mind.

As a subgroup of the Möbius group, elements of $\mathrm{PSU}(1,1)$ also act on the Poincaré disk $\mathbb{D}^2$ via fractional linear transformations,

$$z \mapsto z' = M(z) = \frac{Az + B}{B^* z + A^*} \,,$$

and, as isometries, leave the Poincaré metric (3.5) on $\mathbb{D}^2$ invariant. This invariance can be exploited to derive the hyperbolic distance function $d_{\mathbb{D}^2}(z_1, z_2)$ between any two points on the Poincaré disk. Namely, one can derive the geodesic equation for the Poincaré metric (3.5) and find that geodesics on $\mathbb{D}^2$ are given by circular arcs which are perpendicular to the disk's boundary, as well as straight lines through the origin (diameters) [526]. The latter have a rather simple structure which can be used as a parametrized path to integrate the invariant line-element from, say, the origin $z_1 = 0$, and a further radially separated point on the disk, which we can take to lie on the real line $z_2 = r$ without the loss of generality. The hyperbolic distance obtained in this way reads $d_{\mathbb{D}^2}(0, r) = \ell \, \mathrm{arctanh}(r)$. We can now exploit the invariance of the metric under isometries to transform this expression to that of two arbitrary points on the Poincaré disk, upon exploiting some trigonometric formulas. We thus obtain

the hyperbolic distance function on the Poincaré disk [526], which we give in the two equivalent forms most common in the literature

$$d_{\mathbb{D}^2}(z_1, z_2) = \ell \operatorname{arcosh}\left(1 + \frac{2|z_1 - z_2|^2}{(1-|z_1|^2)(1-|z_2|^2)}\right) = 2\ell \operatorname{arctanh}\left(\frac{|z_1 - z_2|}{|1 - z_1\bar{z}_2|}\right) . \quad (3.12)$$

For completeness, in polar coordinates, the distance between two points $z_1 = \rho_1 e^{\mathrm{i}\phi_1}, z_2 = \rho_2 e^{\mathrm{i}\phi_2} \in \mathbb{D}^2$ is given by

$$d_{\mathbb{D}^2}(z_1, z_2) = \ell \operatorname{arcosh}\left(1 + \frac{2(\rho_1^2 + \rho_2^2 - 2\rho_2\rho_1 \cos(\phi_1 - \phi_2))}{(1-\rho_1^2)(1-\rho_2^2)}\right) . \quad (3.13)$$

The invariance of the metric (3.5) under isometries $M \in \mathrm{PSU}(1,1)$ therefore implies that $d_{\mathbb{D}^2}(z_1, z_2) = d_{\mathbb{D}^2}(M(z_1), M(z_2))$.

3.2.2. The Tiler's Dream: Hyperbolic $\{p, q\}$ Tilings

As explained above, there are canonical ways of discretizing two-dimensional spaces, namely by using regular or uniform tilings [150, 532–536]. These are tessellations constructed by attaching congruent copies of a given regular polygon such that we cover the entire underlying space without any gaps or overlaps. These polygons are called *tiles*. Indeed, this concept is nothing new, and the tiles of your kitchen are likely laid out in such a regular pattern. Yet, let us put ourselves in the shoes of a tiler, a person whose profession it is to lay out tiles for rooms like bathrooms, kitchens, patios, and the like. The tiler has spent her whole life tiling other people's floors and walls, in particular using the typical regular patterns we are most familiar with, like a square, triangular, or a hexagonal pattern. However, she now wants to tile her new bathroom, but she is bored of all these typical tilings. In her mind, she feels too restricted, and she would like to do something more exciting. The idea of using different polygons comes to her mind, but she is not particularly fond of it since she is mesmerized by the high amount of symmetries exhibited by the usual tilings she works with. Our tiler starts thinking of using heptagons, octagons, or even decagons. She also starts imagining taking the regular squares or triangles, but now perhaps joining eight or nine of these polygons on a single vertex. Her curiosity runs wild and she comes to the conclusions that there is an infinite number of such combinations that she can come up with! Filled with joy, she starts getting her tools ready, until suddenly she wakes up. After a brief look at her current kitchen tiles, she realizes that the tilings she dreamed of cannot possibly work. She would need to bend her floor to make them not overlap. Unbeknownst to our tiler, the tilings she dreamed of are indeed possible, if

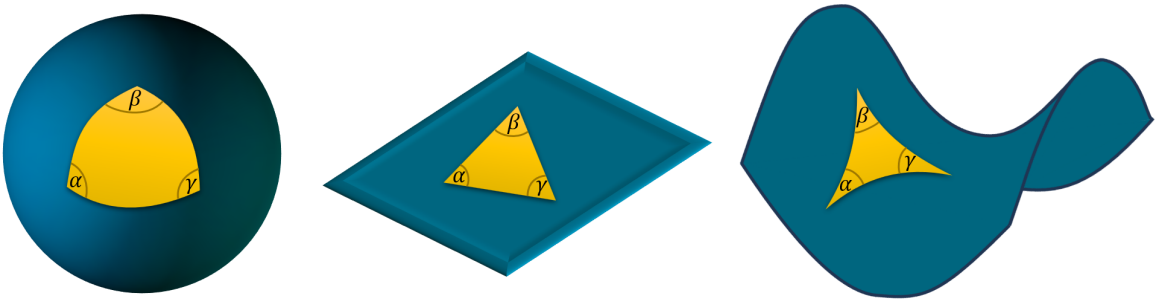


Figure 3.2: Visualization of the three types of geometries: spherical (left), Euclidean or flat (center), and hyperbolic (right). These geometries correspond to spaces of constant positive, zero, and negative curvature, respectively. The influence of the global curvature on geometric objects is portrayed schematically by a triangle on each manifold.

only she lived in not a flat space, but *hyperbolic space*. These so-called regular hyperbolic tessellations, of which there indeed exist infinitely many examples, will be our main subject of study for the following sections. We will see that even though they may not be a viable way to tile our bathroom, they do in fact enjoy a huge number of intriguing properties, making them attractive objects in their own right.

In Sec. 3.2.3, we will give a more rigorous description of these tessellations based on their symmetry groups. For now, we focus on their geometric and trigonometric properties. The edges and vertices of regular tessellations form a lattice with constant coordination number. Their existence is not exclusive to hyperbolic space. In fact, we can give a general description of such regular tilings for spherical, Euclidean (flat) and hyperbolic spaces alike by means of their so-called *Schläfli symbol* $\{p, q\}$ [537]. This symbol describes tessellations by a regular polygon with p sides, denoted as a p-gon, and where the copies are arranged in such a way that q of these p-gons meet at each vertex. In other words, the coordination number of each vertex in the underlying graph of the tiling is q. Depending on the values of the Schläfli parameters p and q, these tessellations can cover spaces with positive (spherical geometry), zero (Euclidean geometry) and negative (hyperbolic geometry) curvature. These three geometries, together with a schematic representation of how triangles appear in each on of them, are shown in Fig. 3.2.

Consider, say, spherical geometry. There, the sum for the triangle is strictly larger than π, due to the underlying positive curvature. This is the reason why, on a sphere, we can have a triangle with only right-angles. The standard example of this is a traveler walking along the equator of the Earth, who then takes a 90 degree turn to the right towards, say, the South pole. At the South pole, the traveler takes another

90 degree right turn. Eventually, she will return to her starting point at the equator. In hyperbolic geometry, one can intuitively expect that the now negative curvature of the space will lead to the opposite case where the sum of inner angles of hyperbolic triangles is strictly *smaller* than π.

Box 3.2 The Gauss-Bonnet Theorem

The Gauss-Bonnet theorem [538] is a beautiful result which connects the global, topological properties of a curved surface to its local, geometric structure. Let $\mathcal{M}$ be a Riemannian surface (i.e. two-dimensional) equipped with a Riemannian metric g. This metric can be exploited to derive an invariant area element dA, which upon integration assigns a surface area to any connected region of $\mathcal{M}$. Moreover, g also fixes the Gaussian curvature K of the surface. In the general case, the surface $\mathcal{M}$ need not be compact and it may further have a boundary, which we denote as $\partial\mathcal{M}$. The Gauss-Bonnet theorem then states that

$$\int\int_{\mathcal{M}} K dA + \int_{\partial\mathcal{M}} k_g ds = 2\pi\chi(\mathcal{M})\,, \tag{3.14}$$

where k_g is the so-called geodesic curvature, to be integrated along the invariant line element on the boundary of $\mathcal{M}$. The quantity k_g broadly describes how close the boundary (or any path for that matter) is close to be a geodesic. On the right-hand side, we have the topological invariant known as the *Euler characteristic* $\chi(\mathcal{M})$ associated to the underlying Riemann surface. The Euler characteristic is further related to the genus g of closed (i.e. without a boundary) oriented Riemann surfaces as $\chi = 2 - 2g$. Moreover, it has also a geometric relation to the number of edges, vertices and faces of a polyhedron as $\chi = V - E + F$ [539]. For the case of two-dimensional polygons, we have $V = E$ and $F = 1$, such that $\chi = 1$.
Let us now consider the case of $\mathcal{M} = \mathbb{D}^2$, with metric g given by (3.5). In particular, let us take a connected subregion of $\mathbb{D}^2$ given by a geodesic triangle $\mathcal{T}$, i.e. a triangle whose edges are geodesics of $\mathbb{D}^2$, with internal angles given by π/p, π/q and π/r, for integers $p, q, r \geq 2$. As mentioned above, the Euler characteristic of this geodesic triangle is $\chi(\mathcal{T}) = 1$, and thus the right-hand side of (3.14) is simply 2π. As for the left-hand side, the Gaussian curvature of the Poincaré disk is simply $K = -1/\ell^2$, which is in particular constant, and therefore $\int\int_{\mathcal{T}} K dA = KA$, with A the (to be determined) area of the hyperbolic triangle $\mathcal{T}$. Finally, let us break down the integral over the geodesic curvature. We parametrize the edges of the triangle counter-clockwise by curves γ_j, and split the integral intro the contributions from the main geodesic segments of each edge and those coming

from the vertices. However, since we are assuming the edges to be geodesics, their geodesic curvature vanishes, leaving only the contribution at the vertices,

$$\int_{\partial\mathcal{T}} k_g ds = \sum_{i=1}^{3} \int_{\gamma_j} k_{g,\gamma_j} ds_j = \sum_{i=1}^{3} \vartheta_j \,. \tag{3.15}$$

Here, the angles ϑ_j are the angles between normal vectors of subsequent edges, or, in other words, they denote the outer angle of our triangle at vertex j, which in our case are related to the interior angles of $\mathcal{T}$. Putting all together, we obtain a formula for the area of a hyperbolic triangle as a function of its inner angles

$$A(\mathcal{T}) = \ell^2(\pi - \frac{\pi}{p} - \frac{\pi}{q} - \frac{\pi}{r}) \,. \tag{3.16}$$

Interestingly, we see that the sum of inner angles of a triangle in hyperbolic space is always *less* than π, in contrast to the Euclidean case where it *equals* π. This difference is given by the total angle defect of the triangle. The relation (3.16) dates back to Lambert [540], who actually derived it in an attempt to disprove hyperbolic geometry as a sensible theory. His work pioneered the concept of hyperbolic space well before the likes of Bolyai, Lobachevskii, and Gauss [541].

Indeed, this expectation is correct. On the most fundamental level, this is a consequence of the application of the *Gauss-Bonnet theorem* [538] to manifolds with constant curvature. We review this theorem in Box 3.2, showing how it relates the area of geodesic triangles on a curved manifold to the sum of its internal angles, summarized in (3.16). This area formula can be used to derive a condition for a regular tiling, specified by its Schläfli symbol $\{p, q\}$, to be an admissible tiling of hyperbolic space. This is because we can divide a regular p-gon into $2p$ hyperbolic triangles with inner angles given by π/p, π/q and a right angle $\pi/2$. These are also known as *Schwarzian* or *fundamental* triangles, and they will play an important role in the next subsection. Based on (3.16), the area of a regular hyperbolic polygon in a $\{p, q\}$ tiling is given by

$$A(p, q) = 2p\, A(\mathcal{T}(p, q, 2)) = \pi\ell^2 \left(p - 2 - 2\frac{p}{q}\right) \,. \tag{3.17}$$

Imposing that this area is positive, we obtain the following inequality condition for the Schläfli parameters of a regular hyperbolic tiling,

$$(p - 2)(q - 2) > 4 \,. \tag{3.18}$$

Each pair of integers p and q obeying the inequality (3.18) thus describes a distinct

regular tiling of the hyperbolic plane. We also see that the Schläfli parameters are related to the curvature of the underlying space being tiled. Not surprisingly, the conditions for regular tilings of flat and spherical spaces are analogous to (3.18), but with an equality $(p-2)(q-2)=4$ and an inverted inequality $(p-2)(q-2)<4$, respectively.[2] Notably, the latter two cases have a finite number of solutions. More precisely, the only regular spherical tilings are given by the Schläfli symbols $\{3,3\}$, $\{3,4\}$, $\{4,3\}$, $\{5,3\}$ and $\{3,5\}$, while only regular tilings of the flat plane are the familiar hexagonal, square and triangular tessellations, with respective Schläfli symbols $\{6,3\}$, $\{4,4\}$ and $\{3,6\}$. In contrast, for tilings of hyperbolic space, the inequality (3.18) remarkably has an infinite number of different solutions! Some examples of hyperbolic $\{p,q\}$ tilings are shown in Fig. 3.3.

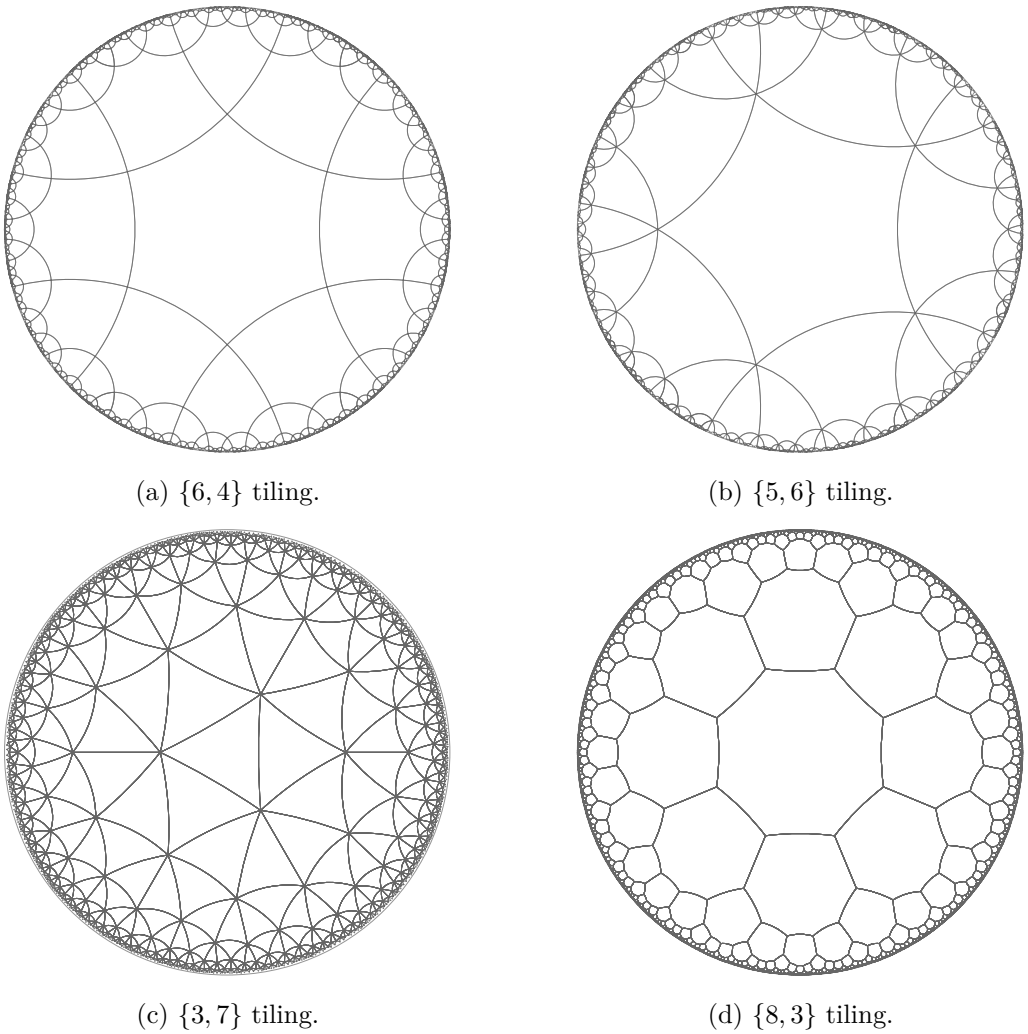
Given that the Poincaré disk $\mathbb{D}^2$ is conformally flat, even though distances are quite different to those in Euclidean space, local angles behave the same way as in flat space. Therefore, we can derive a hyperbolic version of the usual formulas utilized in standard, flat trigonometry. This is known as hyperbolic trigonometry [542, 543]. A key aspect to keep in mind is that hyperbolic space has a fixed length scale, the curvature radius ℓ, with respect to which all other lengths ought to be measured. The sizes and characteristic lengths of tiles in a hyperbolic $\{p,q\}$ tiling are therefore fixed by the underlying geometry, as we derive in the following. However, one can equivalently exploit the projection of hyperbolic space onto the complex unit disk on which $\mathbb{D}^2$ is defined, which has a natural length scale of unity, given by the disk's radius. Distances and positions are then computed based on the complex coordinates of points within the unit disk.

To start our discussion on hyperbolic trigonometry, let us consider a p-gonal tile centered at the origin of the Poincaré disk. An important characteristic length is given by the so-called *circumradius* r_0 of the tile, i.e. the distance between its center and any one of its vertices. We will often denote this quantity simply as the radius of the polygon. In units if the disk's radius, the circumradius is entirely fixed by the Schläfli parameters to be

$$r_0(p,q)=\sqrt{\frac{\cos\left(\frac{\pi}{p}+\frac{\pi}{q}\right)}{\cos\left(\frac{\pi}{p}-\frac{\pi}{q}\right)}}\,. \tag{3.19}$$

First, notice that we may interpret r_0 as a "length", but technically it is a dimensionless quantity. We will often suppress the (p,q) arguments for clarity. Furthermore, note that the formula (3.19) is invariant under the exchange $p\leftrightarrow q$, meaning that the

[2] The spherical counterpart to condition (3.18) is also known as Girard's theorem, named after french mathematician Albert Girard.



(a) $\{6, 4\}$ tiling.

(b) $\{5, 6\}$ tiling.

(c) $\{3, 7\}$ tiling.

(d) $\{8, 3\}$ tiling.

Figure 3.3: Some examples of regular hyperbolic $\{p, q\}$ tilings chosen to showcase all possible parity combinations of the Schläfli parameters. Though some might seem straight, all polygon edges are segments of geodesic arcs in the Poincaré disk $\mathbb{D}^2$.

circumradius of a $\{p, q\}$ tiling is the same as the one for its so-called *dual* tiling with Schläfli symbol $\{q, p\}$. This is to be expected, since the dual tiling is precisely obtained by placing a vertex in the center of each original polygon, and a new, q-gonal tile on each vertex of the original tiling. Moreover, it is clear from (3.19) that $r_0 \in [0, 1)$, which is again natural as it is measured in units of the unity radius of the complex unit disk. In fact, the aforementioned range can be saturated towards $r_0 \to 1$ by taking either $p \to \infty$ or $q \to \infty$. However, there is a minimal possible value for r_0, which corresponds to the $\{3, 7\}$ tiling, with $r_0 \approx 0.300743$. To obtain the actual geodesic distance from the origin to one of the vertices of our tile, we can plug (3.19) into the hyperbolic distance function (3.12). Without the loss of generality, we can orient our tile such that one of the vertices lies on the real line of the complex unit disk. Then,

the *geodesic hyperbolic radius* of the tile, denoted by r, is given by

$$r(p,q) \equiv d_{\mathbb{D}^2}(r_0(p,q),0) = \ell \operatorname{arcosh}\left(1+\frac{2r_0^2}{1-r_0^2}\right) = \ell \log\left(\frac{1+r_0}{1-r_0}\right). \tag{3.20}$$

The hyperbolic radius r is now a proper dimensionful quantity with the units of length inherited from the AdS radius. Based on the hyperbolic radius, we can derive expression for the two other relevant lengths within a p-gonal tile, namely the hyperbolic inradius ρ and the hyperbolic edge length s, both of which are also fixed by the Schläfli parameters. The inradius ρ is the shortest distance from the center of a tile to any of its edges, and, together with the circumradii, it can be used to divide the tile into its fundamental Schwarzian triangles with angles $\pi/p, \pi/q, \pi/2$, cf. Fig. 3.4a. The relationship between these inner angles and the aforementioned characteristic lengths s, ρ are summarized in the *hyperbolic laws of sine and cosine* [542], namely

$$\cos\left(\frac{\pi}{p}\right) = \frac{\tanh(\rho/\ell)}{\tanh(r/\ell)}, \qquad \sin\left(\frac{\pi}{p}\right) = \frac{\sinh(s/2\ell)}{\sinh(r/\ell)}. \tag{3.21}$$

The factor of $1/2$ in the argument of the second term is due to the fact that the side of such a fundamental triangle is half the total edge length s of the polygon. We have further made the arguments dimensionless by dividing them by the AdS radius ℓ. From the relations (3.21) we can derive rather cumbersome yet explicit expressions for the characteristic hyperbolic lengths

$$\begin{aligned}\rho(p,q) &= \ell \operatorname{arctanh}\left(\cos\left(\frac{\pi}{p}\right)\tanh\left(r(p,q)/\ell\right)\right),\\ s(p,q) &= 2\ell \operatorname{arcsinh}\left(\sin\left(\frac{\pi}{p}\right)\sinh\left(r(p,q)/\ell\right)\right).\end{aligned} \tag{3.22}$$

It is also possible to relate these geodesic lengths to their counterparts on the complex unit disk s_0, ρ_0 as $s = d_{\mathbb{D}^2}(s_0,0)$ and $\rho = d_{\mathbb{D}^2}(\rho_0,0)$.[3] For this, it is useful to parametrize any p-gonal tiles as a path on the complex unit disk, consisting of several geodesic arcs [517]. We orient our tile such that the inradius lies parallel to the real line, meaning that the edge of the tile will perpendicularly intersect the real line. The real coordinate at which this intersection happens is precisely the value ρ_0. This coordinate can then be implicitly computed from the first relation in (3.21) as

$$\cos\left(\frac{\pi}{p}\right) = \frac{\tanh\left(2\operatorname{arctanh}(\rho_0)\right)}{\tanh\left(2\operatorname{arctanh}(r_0)\right)}, \tag{3.23}$$

[3] We will always use the subscript "$_0$" for referring to quantities on the complex unit disk, while geodesic quantities are denoted without the subscript.

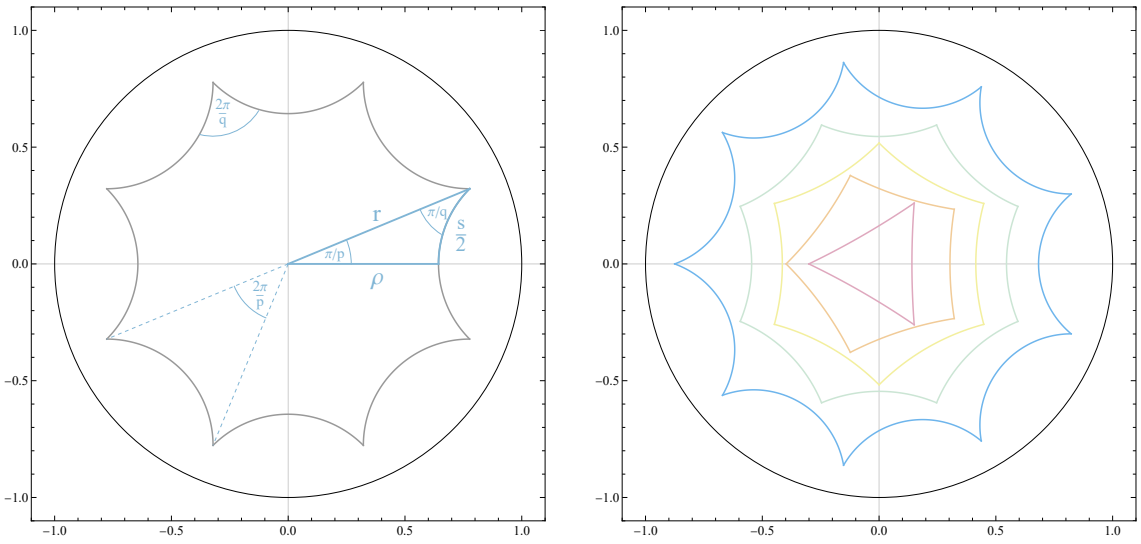


Figure 3.4: (a) Central regular polygon of the $\{8,8\}$ lattice, constructed using the parametrization given in (3.25), together with all its characteristic lengths and angles as specified in (3.20) and (3.22). (b) Several examples of central polygons of different sizes constructed via (3.25), corresponding to the tilings $\{3,7\}$, $\{5,4\}$, $\{6,4\}$, $\{8,4\}$, and $\{9,9\}$. Notice how the area of the polygons changes as a function of the Schläfli parameters p and q, as a consequence of the formula (3.17).

which can be solved for ρ_0 yielding,[4]

$$\rho_0(p,q) = \frac{1 + r_0^2 - \sqrt{1 + r_0^4 - 2\, r_0^2 \cos\left(\frac{2\pi}{p}\right)}}{2\, r_0 \cos\left(\frac{\pi}{p}\right)} \,. \tag{3.24}$$

With these quantities, we can now parametrize edges of our regular centered p-gonal tile by its arcs on the complex unit disk, as done in [517]. More precisely, let $\mu \in 0, \ldots, p-1$ number the edges of the p-gon, such that the arcs are given by

$$\mathcal{C}_\mu = \left\{ (\gamma - \delta\, e^{\mathrm{i}\theta}) e^{2\pi \mathrm{i} \frac{\mu - 1}{p}},\ \theta \in [-\theta_0, \theta_0] \right\} , \tag{3.25}$$

with a set of parameters γ, δ, θ_0 which are obtained as solutions to the following relations $\gamma - \delta = \rho_0$ and $\gamma - \delta e^{-\mathrm{i}\theta_0} = r_0 e^{\mathrm{i}\pi/p}$. The latter condition comes from the fact that, given the way we have oriented our polygon, the first vertex, starting from the real line and going anti-clockwise, is going to lie at a radius r_0 and a polar angle of

[4] There exist two solutions to (3.23), we only consider the solution where $\rho_0 < 1$ and thus lies inside the unit disk.

π/p, cf. Fig. 3.4a. The aforementioned relations are solved [517] by

$$\begin{aligned} \delta &= \frac{\rho_0^2 - 2\,\rho_0\, r_0 \cos\left(\frac{\pi}{p}\right) + r_0^2}{2\, r_0 \cos\left(\frac{\pi}{p}\right) - 2\rho_0}\,, \\ \gamma &= \rho_0 + \delta\,, \quad \sin\theta_0 = \frac{r_0}{\delta}\sin\left(\frac{\pi}{p}\right). \end{aligned} \tag{3.26}$$

Using this parametrization, we show some examples of central hyperbolic polygons constructed this way in Fig. 3.4b. It is interesting to note how the size of the polygons changes with respect to the unit disk, with higher p and q yielding larger central polygons in terms of their hyperbolic area.

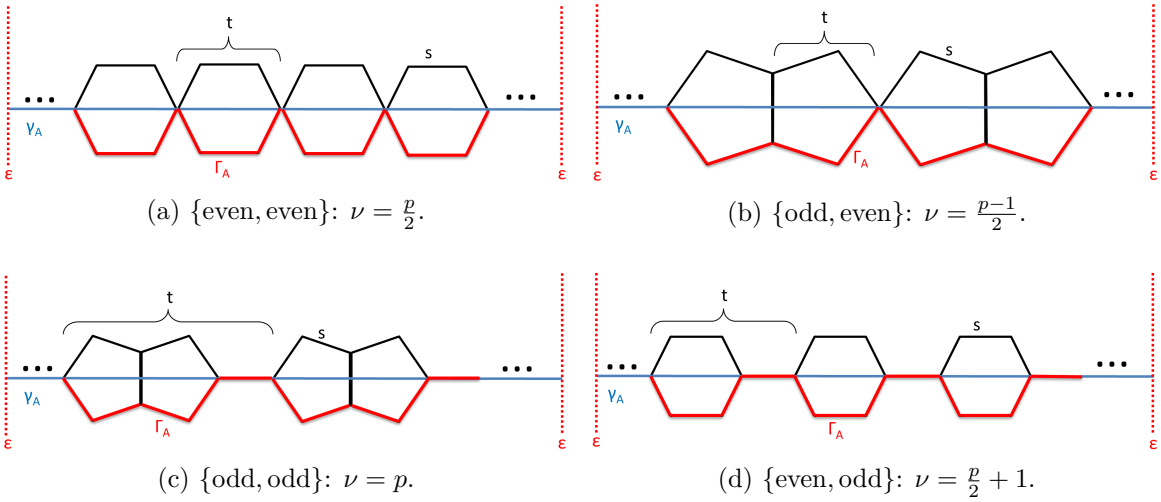
Discrete Geodesics on Hyperbolic Tilings

The discretization provided by hyperbolic $\{p, q\}$ tilings induces discrete counterparts to several geometric objects, a prime example of which are geodesics on the Poincaré disk $\mathbb{D}^2$. These are a vital ingredient in the RT prescription for holographic entanglement entropy, as reviewed in Sec. 2.3.1. Their discrete analogues on hyperbolic tilings are graph geodesics consisting of a collection of consecutive polygon edges. Given that we will later be interested in computing entanglement entropy on discrete models defined on the boundary of hyperbolic tilings, our explorations into a discrete holographic duality would greatly benefit from an analysis of discrete geodesics on $\{p, q\}$ tilings and their dependence on the Schläfli parameters. These considerations were originally motivated by computations in [544] and later refined in [159].

Consider a subregion A of the boundary circle of the Poincaré disk. We denote the continuous geodesic anchored at the end points of A by γ_A. On a hyperbolic tiling, the closest approximation to γ_A will be given by the discrete geodesic Γ_A which is likewise anchored at the end points of A but runs exclusively along polygon edges of the tiling. Since the tiling inherits a notion of distance from the continuous Poincaré disk, the total length $|\Gamma_A|$ of our discrete geodesic Γ_A will be given by the total number of edges $\mathcal{N}$, multiplied by the individual geodesic length s of a polygon edge, given in (3.22). Thus, we have

$$|\Gamma_A| = \mathcal{N}(p, q)\, s(p, q)\,. \tag{3.27}$$

A particular property of the discrete space determined by hyperbolic tilings is that *minimal* discrete geodesics, i.e. those with minimal length, may no longer be unique. For our current argument, we may obviate this peculiarity, but we will come back to it in Sec. 3.5.3 and Sec. 3.5.7. In any case, it turns out the total number $\mathcal{N}$ also depends on the Schläfli parameters, and we derive its expression by a case-by-



(a) $\{\text{even}, \text{even}\}$: $\nu = \frac{p}{2}$.

(b) $\{\text{odd}, \text{even}\}$: $\nu = \frac{p-1}{2}$.

(c) $\{\text{odd}, \text{odd}\}$: $\nu = p$.

(d) $\{\text{even}, \text{odd}\}$: $\nu = \frac{p}{2} + 1$.

Figure 3.5: Pictorial representation of the possible hyperbolic patterns which encompass recurrent segments of length $t(p, q)$ of a continuous geodesic γ_A (blue line) for all different parities of $\{p, q\}$. The continuous geodesic is taken to run diametrically through $\mathbb{D}^2$ for simplicity. The cutoff ϵ is chosen such as to guarantee compatibility between the endpoints of γ_A and the vertices of the tiling. Each individual pattern contributes a number $\nu(p, q)$ of polygon edges to the discrete geodesic trajectory Γ_A (red line) that approximates γ_A. The values of ν for each parity are shown below the corresponding pattern.

case analysis for different parities of p and q. To see this, we must first properly orient any given tiling in a particularly symmetric manner, such that the continuous geodesic γ_A runs diametrically through $\mathbb{D}^2$. This can always be achieved by first transforming any curved geodesic to a diametric one via an isometric transformation, followed by a rotation to fix the orientation. The benefit of this is that now γ_A will cut through the polygons in the tiling in a more tractable way, enabling the identification of discrete paths Γ_A which closely follow the same trajectory as γ_A. Of course, we assume that both Γ_A and γ_A share the same end points. In particular, our choice of orientation introduces the notion of a *pattern*.[5] A pattern is a local and finite geometric substructure of the tiling which repeats exactly along the continuous geodesic. Some examples of these patterns, for all the different parity choices of the Schläfli parameters, are shown in Fig. 3.5.

Due to our chosen orientation, the continuous geodesic γ_A can be split into a collection of n copies of a given pattern, where each pattern will have a specific geodesic length $t(p, q)$, i.e. $|\gamma_A| = n\, t(p, q)$. The quantity $t(p, q)$ can be obtained from a combination of the polygon characteristic lengths given in Fig. 3.4a by using (3.20) and (3.22). As depicted in Fig. 3.5, the discrete geodesics Γ_A approximating γ_A run through the

[5] The concept of a pattern on hyperbolic tilings as used here should not be confused with the notion of patterns on higher-genus Riemann surfaces introduced in [514], which may often arise in similar contexts related to hyperbolic tilings, such as in [517].

edges of all those polygons cut by γ_A in a given pattern. The total number of edges contributing to Γ_A for each pattern depends on the parity of p and q and we denote it by $\nu(p,q)$. In this way, (3.27) becomes

$$|\Gamma_A| = n\, s(p,q)\, \nu(p,q)\,. \tag{3.28}$$

Let us remark that the number n, which is in principle infinite, cannot be directly retrieved from inherent tiling properties. Nevertheless, it can be related to the original length of γ_A after introducing a radial cutoff. More precisely, using Poincaré patch coordinates (2.13), we can derive the length of the continuous geodesic γ_A by integrating the metric (2.14) along a geodesic trajectory up to a radial cutoff $z = \epsilon \ll 1$ near the boundary of $\mathbb{D}^2$, yielding

$$|\gamma_A| = 2\ell \log\left(\frac{L}{\epsilon}\right) + \mathscr{O}\left(\epsilon^2\right)\,, \tag{3.29}$$

where L denotes the size of subregion A, consisting of the set of boundary points $x \in (-\frac{L}{2}, \frac{L}{2})$ in the Poincaré coordinates of (2.13). Using (3.29) and recalling that $|\gamma_A| = n\, t(p,q)$, we obtain the leading divergent behavior of the number n as

$$n = \frac{2\ell}{t(p,q)} \log\left(\frac{L}{\epsilon}\right)\,. \tag{3.30}$$

Plugging this into (3.28), the expression for the length of a discrete geodesic Γ_A on a given $\{p,q\}$ tiling as a function of the Schläfli parameters reads

$$|\Gamma_A| = \frac{2\ell\, s(p,q)\, \nu(p,q)}{t(p,q)} \log\left(\frac{L}{\epsilon}\right)\,. \tag{3.31}$$

This result can stand by itself as a geometric characterization of discrete paths on any regular hyperbolic tiling. Later, we will be interested in a more refined version of (3.31), in which the scaling relation between lengths in the bulk of $\mathbb{D}^2$ and on its boundary is taken into account. This is an implicit step in continuous AdS/CFT where it seems clear that the distance of two boundary points is measured with respect to boundary lengths, and not with respect to the bulk metric where such distances would invariably diverge. We will present an analogous relation for the case of hyperbolic tilings in Sec. 3.5.7, after we introduce a systematic way of constructing such tilings in Sec. 3.2.4.

3.2.3. Fuchsian Symmetries

The tessellations of hyperbolic space introduced in the previous section have an extremely rich mathematical structure, the majority of which is related to their underlying symmetries. The symmetry groups of hyperbolic tessellations are discrete subgroups of the larger isometry group of $\mathbb{D}^2$, and these have fascinating connections to the theory of Riemann surfaces and algebraic geometry. In this section, I will give an exposition of these mathematical details and derive some key statements which will be of later use in this work.

Fuchsian Groups

It is natural to expect that the discretizations of $\mathbb{D}^2$ provided by hyperbolic $\{p, q\}$ tilings will enjoy a smaller group of symmetries which is however contained within the isometry group of $\mathbb{D}^2$. In other words, the symmetries of hyperbolic tilings are going to be described by discrete subgroups of $\mathrm{PSU}(1,1) \cong \mathrm{PSL}(2,\mathbb{R})$. These groups are known as *Fuchsian groups* [515, 545], and we will now review their general mathematical properties, closely following the exposition in [515].
We start with a definition

Definition 1 (Fuchsian Group)**:** *A Fuchsian group $\mathscr{F}$ is any discrete subgroup of PSL$(2,\mathbb{R})$. Alternatively, a subgroup $\mathscr{F} \in$ PSL$(2,\mathbb{R})$ is Fuchsian if and only if it acts properly discontinuously on $\mathbb{D}^2$, i.e. all orbits $\mathscr{F} \cdot z$ are discrete subsets of $\overline{\mathbb{D}^2}$.*

Both definitions allude to the discrete nature of these subgroups, in the sense that the action of its elements on the Poincaré disk can be kept track of in a discrete way. To understand what it means for a subgroups to be discrete, we consider so-called *group orbits* and *group stabilizers*.

Definition 2 (Orbit)**:** *The orbit $\mathscr{F} \cdot z$ of a point $z \in \mathbb{D}^2$ under the action of $\mathscr{F}$ is the set of all points that can be reached from z by applying elements of the group, i.e.*

$$\mathscr{F} \cdot z = \{y \in \overline{\mathbb{D}^2} \,|\, y = f \cdot z,\ f \in \mathscr{F}\}\,,$$

with $\overline{\mathbb{D}^2} = \mathbb{D}^2 \cup \partial\mathbb{D}^2$ being the closure of the Poincaré disk.

Definition 3 (Stabilizer)**:** *The stabilizer $\mathscr{F}_z \subset \mathscr{F}$ of a point $z \in \mathbb{D}^2$ under the action of $\mathscr{F}$ is the set of all group elements $f \in \mathscr{F}$ which leave z invariant, i.e.*

$$\mathscr{F}_z = \{f \in \mathscr{F} \,|\, f \cdot z = z\}\,.$$

Note that the orbit is an object on the underlying space, and not on the group, while the stabilizer is a subgroup of $\mathscr{F}$ defined anew for any given point. In both definitions, the operation "$\cdot$" denotes the group action of an element of the Fuchsian group via linear fractional transformations, as in (3.6). Moreover, we have defined the closure $\overline{\mathbb{D}^2}$ of the Poincaré disk as the union of the set of points in $\mathbb{D}^2$ and the asymptotic conformal boundary of the space $\partial\mathbb{D}^2 \cong S^1$. A properly discontinuous action of a group means that the orbits generated by the group never generate a dense continuous subset of the Poincaré disk. Rather, every point belonging to the orbit is isolated, meaning there exists a neighborhood of finite radius $\varepsilon > 0$ which only contains that point. In fact, a group is discrete if its identity element e is such an isolated point [515]. However, orbits may have so-called *accumulation points* which can only be reached after an infinite number of group element actions, see Def. 4.

Definition 4 (Limit Set)**:** *The limit set $\Lambda(\mathscr{F})$ of $\mathscr{F}$ is the set of all accumulation points of orbits $\mathscr{F} \cdot z$ of $\mathscr{F}$ on $\overline{\mathbb{D}^2}$.*

It turns out that the limit set is independent on the starting point [515]. The importance of the limit set lies in its role for characterizing different types of Fuchsian groups. More precisely, all Fuchsian groups can be classified into two types depending on the precise nature of their limit set. This is the content of Theorem 1 [515].

Theorem 1 (Classification of Fuchsian Groups)**:** *If the limit set $\Lambda(\mathscr{F})$ of a Fuchsian group $\mathscr{F}$ contains more than two points, then $\mathscr{F}$ is either*

1. *of the first kind, meaning that $\Lambda(\mathscr{F}) \cong S^1$,*
2. *or of the second kind, meaning that $\Lambda(\mathscr{F}) \subset S^1$, namely it is a perfect, nowhere-dense proper subset of S^1.*

The natural question arises as to how to determine the precise contents of the limit set for a given Fuchsian group $\mathscr{F}$. This can be traced back to some fundamental geometric properties of the lattices which are associated to the action of said groups on the Poincaré disk, and we will now give a chain of logical statements which answer this question. First, the limit set $\Lambda(\mathscr{F})$ of a Fuchsian group $\mathscr{F}$ consists of more than two points *if and only if* it is *non-elementary*. The property of elementarity refers to the existence of finite orbits [515]. More precisely, a subgroup $\mathscr{F} \subset \mathrm{PSL}(2,\mathbb{R})$ is elementary if there exists at least one finite $\mathscr{F}$-orbit $\mathscr{F} \cdot z$ with $z \in \overline{\mathbb{D}^2}$, i.e. the action of $\mathscr{F}$ has a fixed point z_0 such that $f \cdot z_0 = z_0 \; \forall f \in \mathscr{F}$. In other words, a Fuchsian group $\mathscr{F}$ is elementary if it preserves some point $z \in \mathbb{D}^2$. Conversely, any non-elementary Fuchsian group must contain a hyperbolic element, i.e. an element with no fixed points

in $\mathbb{D}^2$ [515]. Such elements can be associated with translation transformations as we will see in a later part of this subsection. Second, Theorem 1 requires that $\mathscr{F}$ has a so-called *compact fundamental region* $\mathscr{R}$. As we have mentioned above, Fuchsian groups are associated with lattices on the Poincaré disk. As such, these can be generated by acting with all group elements on a minimal fundamental region, over which the action of the group cannot be further simplified. Even though not all such lattices will be related to regular hyperbolic tilings, we can make general statements on the properties of $\mathscr{F}$ based on the geometry of such fundamental regions.

Definition 5 (Fundamental Region)**:** *Given the space* $\mathbb{D}^2$ *and a Fuchsian group* $\mathscr{F}$ *acting properly discontinuously on* $\mathbb{D}^2$*, a fundamental region* $\mathscr{R} = (\mathring{\mathscr{R}} \cup \partial\mathscr{R}) \subset \mathbb{D}^2$ *for the action of* $\mathscr{F}$ *is a closed region in* $\mathbb{D}^2$ *such that:*

1. $\bigcup_{f\in\mathscr{F}} f(\mathscr{R}) = \mathbb{D}^2$*, i.e. the application of all elements of the group onto the fundamental region yields the entire set* $\mathbb{D}^2$*.*
2. $\mathring{\mathscr{R}} \bigcap f(\mathring{\mathscr{R}}) = \{\emptyset\}, \forall\, T \in \mathscr{F} \setminus \{e\}$*, i.e. the regions obtained through the action of* $\mathscr{F}$ *do not overlap with the fundamental region.*

Def. 5 is the more mathematical version of our statement that tilings should cover the space entirely without any gaps or overlaps. The requirement of compactness on $\mathscr{R}$ means that it needs to be connected and have finite hyperbolic area. A Fuchsian group $\mathscr{F}$ with such a finite fundamental region $\mathscr{R}$ is called *geometrically finite* [515].

Definition 6 (Geometrically Finite Groups)**:** *A Fuchsian group* $\mathscr{F}$ *is called geometrically finite if there exists a convex fundamental region* $\mathscr{R}$ *with finitely many sides.*

Whether a given Fuchsian group is actually geometrically finite, or equivalently, whether it has a compact fundamental region, can be related to the generators of the group itself [515]. Although Fuchsian groups are not Lie groups, they still have generator elements which can construct all elements of the group upon their combination. For discrete groups, the notation to define a group $\mathscr{F}$ consists of a set S of generators, and a set R of relations among them, written as $\mathscr{F} = \langle S|R\rangle$. This is called the *presentation* of the group $\mathscr{F}$. The set of relations is such that $R = w(S) = e$, with e the group identity element, and $w(S)$ a *word* describing a specific concatenation of different generators $s \in S$. For example, the cyclic rotation group of order n can be given the presentation $\mathbb{Z}_n = \langle a|a^n = e\rangle$, where a is an abstract generator of the group whose explicit expression can take many forms. In this case, the unique relation identifying the group is the cyclicity relation. For relations of this kind, the order at

which a given generator returns to the identity is called the *period* of that element. If $|S| < \infty$, as is the case for $\mathbb{Z}_n$, we say that the group is *finitely generated*, since it has a finite number of generators. Importantly, a group can have several distinct yet equivalent presentations. For our purposes, a generic Fuchsian group can be given the following presentation:

$$\mathscr{F} = \langle x_1, \ldots, x_r \,|\, x_1^{m_1}, \ldots, x_r^{m_r} = e\,;\, x_1 \ldots x_r [a_1, b_1] \ldots [a_g, b_g] = e \rangle\,, \tag{3.32}$$

with $\{x_i\}$ a set of $r \geq 0$ generators with periods $m_i \geq 2$, and $\{a_k, b_k\}$ a set of edge identifications of the fundamental region. A concise way of specifying a Fuchsian group with a presentation of the form (3.32) is by its so-called *signature* $(g; m_1, \ldots, m_r)$. The set of identifications in (3.32) need not always be defined, but when they are, they dictate a possible way of compactifying the fundamental region to a Riemann surface of genus g.[6] Such compactifications arise from a quotienting procedure of the Poincaré disk by the action of the given Fuchsian group. The resulting quotient space is denoted by $\mathbb{D}^2/\mathscr{F}$. There exists a powerful theorem due to Poincaré himself, cf. Theorem 2, that allows us to specify the existence of a Fuchsian group with presentation (3.32) by imposing a relation between the parameters g, r and m_i of its signature [515].

Theorem 2 (Poincaré's Theorem)**:** *If a set of integer parameters $g \geq 0$, $r \geq 0$, $m_i \geq 2$, with $1 \leq i \leq r$ fulfills the relation*

$$2g - 2 + \sum_{i=1}^{r} \left(1 - \frac{1}{m_i}\right) > 0\,, \tag{3.33}$$

then, there exists a Fuchsian group $\mathscr{F}$ with signature $(g; m_1, \ldots, m_r)$. If this is the case, the fundamental region $\mathscr{R}$ of $\mathscr{F}$ has hyperbolic area given by the above relation

$$A(\mathscr{R})/\pi = 2g - 2 + \sum_{i=1}^{r} \left(1 - \frac{1}{m_i}\right)\,. \tag{3.34}$$

Interestingly, two Fuchsian groups $\mathscr{F}_1, \mathscr{F}_2$ can be shown to be isomorphic if $g_1 = g_2$, $r_1 = r_2$ and $\exists\, \phi \in \mathrm{Perm}(r)$ of the set $\{1, \ldots, r\}$ such that $m_{2,i} = m_{1,\phi(i)}$ [515]. This means that we can find a one-to-one mapping between the generators of both groups, i.e. $S_1 \sim S_2$, as well as between their defining relations $R_1 \sim R_2$.

[6] For now, we will focus solely on Riemann surfaces which have only one face, i.e. where the single fundamental region covers the entire Riemann surface upon edge identification. There are more general constructions based on hyperbolic *patterns* [514, 517], which are of interest when considering periodic boundary conditions [516] in hyperbolic space.

Let us briefly summarize the main statements obtained from the arguments above.

- A Fuchsian group is a subgroup of $\mathrm{PSL}(2,\mathbb{R})$ which acts properly discontinuously on the Poincaré disk $\mathbb{D}^2$.
- A properly discontinuous action is such that all orbits are discrete subsets of $\mathbb{D}^2$.
- A Fuchsian group $\mathscr{F}$ is of the first kind if its limit set is homeomorphic to the circle, i.e. $\Lambda(\mathscr{F}) \cong S^1$, and of the second kind otherwise.
- $\mathscr{F}$ is of the first kind if and only if it is non-elementary, meaning it has no fixed points in $\mathbb{D}^2$, and it is geometrically finite, i.e. it is finitely generated and its fundamental region $\mathscr{R}$ is compact.
- Fuchsian groups obeying the above relations can be obtained via Poincaré's Theorem 2 given their signature $(g; m_1, \ldots, m_r)$.
- The quotient space $\mathbb{D}^2/\mathcal{F}$ is a compact space if and only if the fundamental region of $\mathcal{F}$ is compact.

In the following sections, we will often refer to the definitions and general results from this section when considering specific instances of Fuchsian groups related to hyperbolic $\{p, q\}$ tilings.

Hyperbolic Triangle Groups

Returning to our Poincaré disk, we wish to discretize $\mathbb{D}^2$ by means of regular hyperbolic tessellations. These are characterized by their Schläfli symbol $\{p, q\}$. It seems reasonable to expect that these tessellations will be invariant under only a discrete subgroup of $\mathrm{PSU}(1,1) \cong \mathrm{PSL}(2,\mathbb{R})$. As we have seen above, every $\{p, q\}$ tiling can be further divided into a tessellation with right-angled hyperbolic triangles, i.e. Schwarzian triangles. We will denote these as *hyperbolic triangulations*. The set of all hyperbolic triangulations of $\mathbb{D}^2$ is indeed larger than the set of $\{p, q\}$ tilings, since we can in principle also allow for the third inner angle to be arbitrary, given by π/r. The largest group of isometries of such general hyperbolic triangulations is known as the *triangle group*, denoted by $\Delta(p, q, r)$ [513, 515], and it admits the presentation

$$\Delta(p,q,r) = \langle x, y, z | x^2 = y^2 = z^2 = (xy)^p = (yz)^q = (zx)^r = e \rangle \,. \tag{3.35}$$

The triangle group is generated by reflections on the sides of Schwarzian triangle with inner angles $\frac{\pi}{p}$, $\frac{\pi}{q}$, and $\frac{\pi}{r}$, which simultaneously acts as the fundamental region of the group. Reflections, however, are orientation-reversing transformations, and

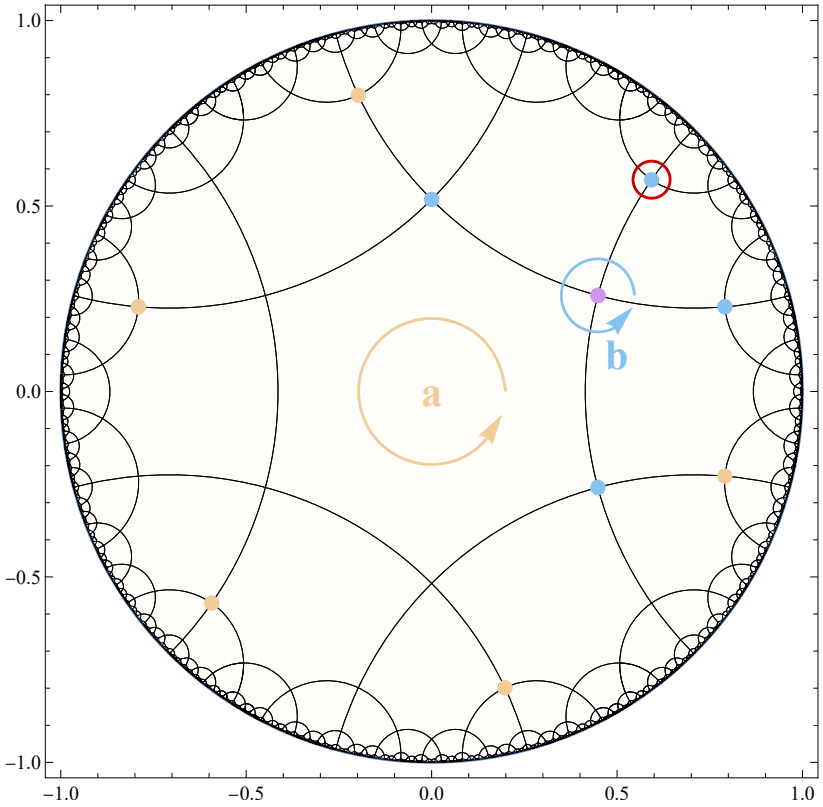


Figure 3.6: Visualization of the action of the generators a and b of the von Dyck group (3.36). Starting from the vertex on the top of the polygon (purple), repeated application of the b generator effects rotations about the purple vertex by $2\pi/q$, producing all the blue vertices. Similarly, the action of a amounts to a global rotation with respect to the origin by $2\pi/p$, which starting from the vertex circled in red, produces all the orange vertices. The set of all vertices of the central polygon (not highlighted here) could alternatively be obtained by applying a^k with $k \in \{1, \ldots, 5\}$ to the purple vertex. Thus, there exist several elements of the von Dyck group than map to the same vertex.

the triangle group $\Delta(p, q, r)$ is therefore not a Fuchsian group. In order to obtain a Fuchsian group and be able to exploit all the results of the previous sections, we consider another class of isometry groups called *von Dyck* groups [513, 546, 547]. These are denoted by $D(p, q, r)$ and are subgroups of index 2 in $\Delta(p, q, r)$ which consist of words $w(x, y, z)$ of even length. Their presentation reads

$$D(p, q, r) = \langle a, b \,|\, a^p = b^q = (ab)^r = e \rangle \,, \tag{3.36}$$

where $a = xy$, $b = zx$, $ba = zy$ are rotations by $\frac{2\pi}{p}$, $\frac{2\pi}{q}$, $\frac{2\pi}{q}$, respectively. The actions of these generators on exemplary points are visualized in Fig. 3.6. The index of this subgroup is due to the fact that the fundamental region of $D(p, q, r)$ is the union of a Schwarzian triangle and its reflection on one of its sides. This implies that we have quotiented the triangle group by a reflection group $D(p, q, r) = \Delta(p, q, r)/\mathbb{Z}_2$, meaning

that every element of $D(p,q,r)$ can be associated to two elements in $\Delta(p,q,r)$, hence index 2. In fact, because this quotient is itself a subgroup of $\Delta(p,q,r)$, we can write the semi-direct product decomposition

$$\Delta(p,q,2) = D(p,q,2) \ltimes \mathbb{Z}_2 \,. \tag{3.37}$$

The von Dyck group is also sometimes denoted as the "proper" triangle group [517]. Importantly, $D(p,q,r)$ only contains orientation-preserving elements by construction, and therefore it is a Fuchsian group. Moreover, for the case of $r = 2$, the von Dyck groups $D(p,q,2)$ are the largest groups of orientation-preserving isometries of a hyperbolic $\{p,q\}$ tiling. A consequence of this is that any vertex $z_i \in \{p,q\}$ of the tiling can be labeled by the word w of generators required to reach it from a given, arbitrary starting point z_0, i.e. $z_i = w(z_0)$. In this way, we can generate the entire tiling.

An interesting question to ask is whether $\Delta^+(p,q,2)$ is a Fuchsian group of the first or second kind. Intuitively, one may expect the latter. The logic behind it is that the geodesic length between two neighboring vertices is constant and always given by the edge length $s_{\{p,q\}}$ in (3.22). Therefore, even for points close to the boundary, we may expect that these are still separated by a finite length, and they thus represent only a subset of the circle S^1 at the boundary. However, it turns out that this intuition is not correct, as we can logically deduce from the results of the previous section on Fuchsian groups. First, the fundamental region of $D(p,q,2)$ is compact and finite as long as p and q are finite, since it consists of two copies of a Schwarzian triangle, which is finite. Therefore, according to Def. 6, $D(p,q,2)$ is geometrically finite. Moreover, it is clearly finitely generated, as can be seen from its presentation given in (3.36). Simultaneously, $D(p,q,2)$ is non-elementary, since there is at least one hyperbolic element built from the generators a, b, namely ab. One can check that this element is hyperbolic and thus has no fixed-points in $\mathbb{D}^2$. Thus, collecting these features, and together with Theorem 1, we can conclude that the limit set of von Dyck groups is the entire circle at the boundary, i.e. $\Lambda(D(p,q,2)) = S^1$. We refer the reader to [515] for a more rigorous proof of this result.

We have seen how the largest isometry groups of $\{p,q\}$ tilings allow us to derive the counterintuitive nature of the boundary. An interesting avenue to pursue at this point would be to utilize these isometry groups to define the field content of putative bulk theories living of such hyperbolic tilings, by imposing that said fields transform covariantly under irreducible representations of the isometry group. Given their non-Abelian and infinite nature, however, von Dyck groups have higher-dimensional irreducible representations for which no explicit parametrization is known. A direct implementation

of this idea thus seems out of reach at the time of writing of this thesis. Nevertheless, some progress can be made by considering further specific subgroups of $D(p,q,2)$ which allow for a connection to the rich theory of compact Riemann surfaces. As we will see in more detail in the next section, this connection works whenever $D(p,q,2)$ is *symmorphic* [517], i.e. it admits a semi-direct product decomposition in the spirit of crystallography, where the overall space group of a lattice is decomposed into a translation and a point group for the unit cell. In general, von Dyck groups $D(p,q,2)$ (and also triangle groups $\Delta(p,q,2)$) are not symmorphic [517] and cannot be written as

$$D(p,q,2) = \mathrm{Aut}(\Sigma_g) \ltimes \Gamma\,, \tag{3.38}$$

where $\mathrm{Aut}(\Sigma_g)$ denotes the group of automorphisms of a compact Riemann surface Σ_g associated with the compactification of the fundamental region of $D(p,q,2)$. This plays the role of a generalized point group, while Γ describes a generalized translation group. The reason why such a decomposition is not always possible is because the quotient group $\mathrm{Aut}(\Sigma_g) = D(p,q,2)/\Gamma$ is not necessarily a subgroup of $D(p,q,2)$ [517–519]. Nonetheless, we will later discuss instances when this is the case. The next section will give an overview on the state of the art of group and representation theory methods to extract meaningful predictions from these rather non-trivial symmetry groups of hyperbolic tilings.

Hyperbolic Translation Groups and Bloch's Theorem

The considerations of the previous subsections shed light on the complex properties of isometry groups of regular hyperbolic tessellations. Let us recall why we would like to have a better understanding of these isometries. From the point of view of defining boundary field theories which are holographically dual to a discretized AdS space, we would like the fields of such theories to covariantly transform under irreducible representations (irreps) of the isometry group of the bulk. However, there exist alternative motivations, which stem from the fields of condensed matter theory and crystallography. Here, the goal is to understand the spectrum of eigenvalues and eigenstates of quantum systems defined on hyperbolic tilings, where the latter are seen as novel alternatives to the usual Bravais lattices known from solid state physics [548]. Recent investigations into such quantum systems on hyperbolic tilings have actually opened a new field of research which goes under the name of *hyperbolic quantum matter* [549]. It turns out that such systems exhibit a plethora of interesting phenomena, ranging from unconventional energy and Hofstadter spectra [521, 550–555], to topological phases and edge states [556–562], not to mention the actual experimental realization on different platforms [448, 563–566] which has only boosted the overall interest. Progress

in this novel field of research, and in particular access to analytic results, relies heavily on the understanding of how the spectrum of tight-binding Hamiltonians is described by the underlying spatial symmetries of the hyperbolic tilings they are defined on. This has been made possible by breakthroughs in so-called *hyperbolic crystallography* [517] and *hyperbolic band theory* [518, 519], at the core of which lies a generalization of the familiar Bloch theorem for Euclidean lattices [548]. It turns out that such an extension is highly non-trivial due to the non-commutative nature of translations in hyperbolic space. In the following, we will review these advancements and elucidate their connection to an extremely rich mathematical structure. Our exposition follows that of [523, 549], and further details can be found in [517–519].

Let us first take a step back and consider Euclidean lattices, examples of which are the Bravais lattices known from solid states physics. In the Euclidean case, we know that the entire band structure of a solid can be computed by only analyzing its form restricted to a certain finite portion of the crystal, namely the *Brillouin zone* (BZ). Restricting our attention to the two-dimensional case, we know that Euclidean lattices are translationally invariant, and, as a consequence, we may apply Bloch's theorem [548] in order to describe the entire wave function ψ of the system. This is the usual notion of identifying a Bravais unit cell and then using translations along a corresponding Bravais lattice to generate the entire underlying lattice. Importantly, the latter need not coincide with the actual Bravais lattice, and so an apparent naive cell of the underlying lattice might not be enough to generate that lattice in its entirety. In any case, Bloch's theorem tells us how this wave function will transform if we act on it with a generator of the group of two-dimensional Euclidean translations $\mathcal{T}(2) = \{T_x, T_y\}$. These transformations are simply shifts in either the x or the y direction. Perhaps misleadingly, we are very familiar with the fact that the translations T_x, T_y commute, i.e. $\mathcal{T}(2)$ is an *Abelian* group. This means that the order in which we apply two different translations does not matter, see the left part of Fig. 3.7. As a consequence of this commutativity, the group $\mathcal{T}(2)$ only admits one-dimensional irreps, which are labeled by the familiar crystal momentum or wave vector $k = (k_x, k_y)$. More precisely, we write

$$\psi_{\vec{k}}(T_{\vec{n}}(\vec{x})) = e^{\mathrm{i}\vec{k}\cdot\vec{n}}\psi_{\vec{k}}(\vec{x})\,, \tag{3.39}$$

where the phase factor $T_j \mapsto e^{ik_j}$, $j = \{x, y\}$ is the explicit form of the one-dimensional unitary irrep of $\mathcal{T}(2)$. In other words, the phase factor is an element of the group U(1). This transformation law indicates that the BZ can be periodically identified in the x and y directions, yielding a compactified BZ described by a torus $\mathbb{T}^2$, as shown on the left side of Fig. 3.7. Importantly, the wave vector has as many components as there

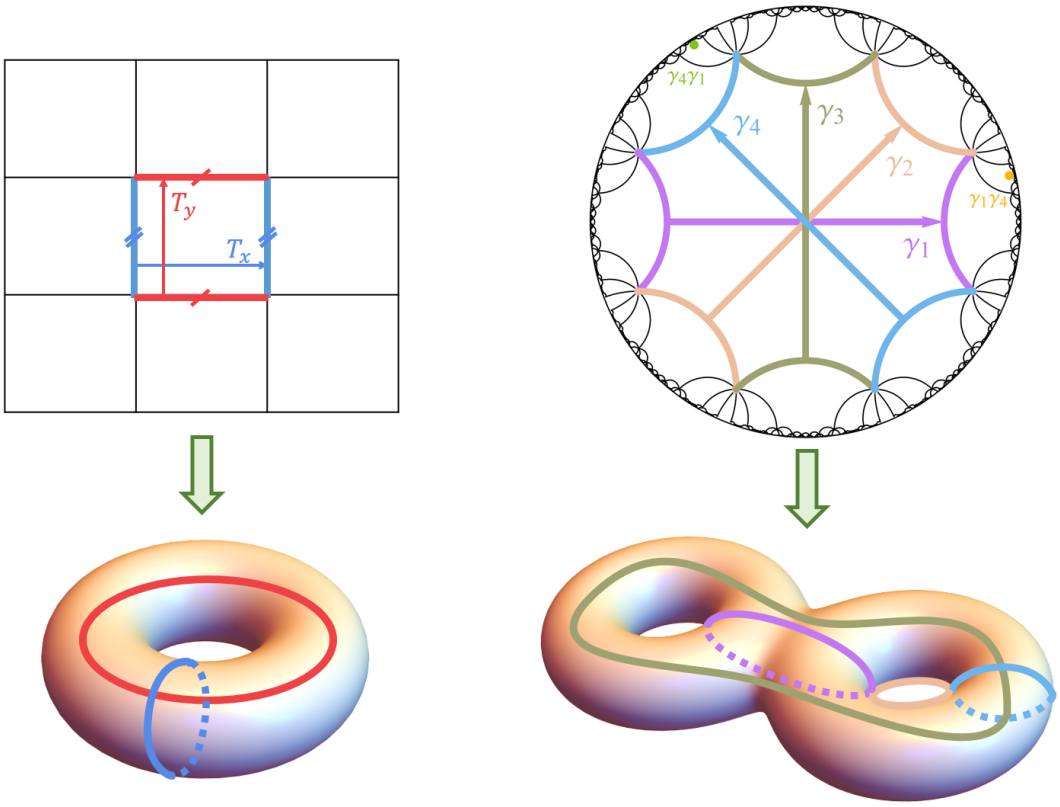


Figure 3.7: Left: Depiction of the Euclidean translation group in two dimensions $\mathcal{T}(2) = \{T_x, T_y\}$, together with the compactification of its fundamental region into a toroidal Brillouin zone. Right: Action of the generators of the hyperbolic translation group Γ (3.41) for the $\{8,8\}$ lattice, and its corresponding compactification via edge identification into a genus-2 Riemann surface as per the Uniformization Theorem 3. The points reached by acting with $\gamma_1\gamma_4 \in \Gamma$ and $\gamma_4\gamma_1 \in \Gamma$ on the origin, which are manifestly different, showcasing the non-commutativity of Γ.

are independent translation generators in $\mathcal{T}(2)$.

Now we turn to hyperbolic lattices, and we may ask if the eigenstates of typical tight-binding Hamiltonians defined on such lattices obey a similar transformation law as that in (3.39). In the hyperbolic case, the transformation law analogous to (3.39) is given by

$$\psi_{k_\mu}(\gamma_\mu(z)) = e^{\mathrm{i}k_\mu}\psi_{k_\mu}(z)\,, \tag{3.40}$$

where now γ_μ is a generator of the group of two-dimensional *hyperbolic translations* $\Gamma = \{\gamma_1, \ldots, \gamma_{2g}\}$, and the wave vector has now a $2g$ components [518]. Later we will provide more insights into this property, but for now, let us introduce some properties of the very special Fuchsian group Γ. First of all, it is a translation group, which means that it is freely acting on $\mathbb{D}^2$, implying that Γ has no fixed-points. In particular, Γ is a so-called *torsion-free* group, i.e. $\gamma^n \neq e$ for any $n < \infty$ [514, 515]. Such torsion-free

groups play a special role in the theory of Riemann surfaces, most prominently via the *Uniformization Theorem* 3 which provides a topological classification of Riemann surfaces according to their construction as quotients of three specific covering spaces.

Theorem 3 (Uniformization Theorem)**:** *Every Riemann surface* Σ_g *is conformally equivalent to the quotient space* $\mathcal{K}/\Gamma$*, with* $\mathcal{K}$ *one of the three canonical spaces: the Riemann sphere* $\mathbb{C}\cup\infty$*, the complex plane* $\mathbb{C}$ *or the open unit disk* $\mathbb{D}^2$*, and* Γ *a torsion-free Fuchsian group of transformations that preserve* $\mathcal{K}$*. Compact Riemann surfaces may be thus classified with respect to their uniformizations (covering spaces):*

- *if* $\mathcal{K} = \mathbb{C} \cup \infty$*, then* $g = 0$*;*
- *if* $\mathcal{K} = \mathbb{C}$*, then* $g = 1$*;*
- *and if* $\mathcal{K} = \mathbb{D}^2$*, then* $g \geq 2$*.*

We will particularly be interested in quotient spaces $\Sigma_g = \mathbb{D}^2/\Gamma$ of the Poincaré disk by the action of hyperbolic translation groups Γ. As a Fuchsian group, Γ can be given the general presentation, cf.(3.32),

$$\Gamma = \langle \gamma_1, \ldots, \gamma_{2g} | R(\gamma_i) = e \rangle \,, \tag{3.41}$$

which makes it isomorphic to the *fundamental group* $\pi_1(\Sigma_g)$ of the Riemann surface Σ_g [515]. The relation $R(\gamma_i)$ fixes a set of edge identifications of the Bravais unit cell. In more general terms, for a given $\{p, q\}$ hyperbolic tiling, Γ is the largest torsion-free normal subgroup of $D(p, q, 2)$ [549]. A subgroup H of some group K is called normal if it is invariant under conjugation by elements of K, i.e.

$$H = \{h \in K \,|\, khk^{-1} \in H \,\forall k \in K\} \subset K \,. \tag{3.42}$$

The fact that Γ is a subgroup of $D(p, q, 2)$ implies that $\Gamma \equiv \Gamma_{(p,q)}$, but we will suppress this notation for clarity, keeping in mind that different tilings will have different associated translation groups. However, remarkably, note that Γ can always be found for *any* $\{p, q\}$ tiling [523]. In fact, it is non-unique, and there infinitely many normal torsion-free subgroups of the triangle group. This subgroup is guaranteed to be of finite index in $D(p, q, 2)$ by Fenchel's conjecture [567–571], meaning that the order of the automorphism group (i.e. the point group), $|\mathrm{Aut}(\Sigma_g)| \equiv \left|\frac{D(p,q,2)}{\Gamma}\right| = n$ is finite [523].[7] However, as discussed around (3.38), this does not automatically imply that

[7] In fact, $|\mathrm{Aut}(\Sigma_g)| \leq 84(g-1)$ and is bounded from above. This is a version of the so-called *Riemann-Hurwitz formula* [572].

$D(p,q,2)$ can be written as a semi-direct product, since $\mathrm{Aut}(\Sigma_g)$ is not necessarily a subgroup of $D(p,q,2)$. A list of $\{p,q\}$ tilings that do indeed admit such a decomposition, and are thus symmorphic, was provided in [517]. Nevertheless, these hyperbolic translation groups Γ are discrete, infinite, and non-Abelian. The latter is the key difference with respect to the Euclidean translation group $\mathcal{T}(2)$. Given that Γ is no longer Abelian the order of the translations matters, as shown in the right part of Fig. 3.7, where we can see that acting with $\gamma_1\gamma_4$ and $\gamma_4\gamma_1$ on the origin leads to completely different points. Moreover, this non-commutativity implies that Γ also admits higher-dimensional irreps, meaning that the one-dimensional irreps given in (3.40) are not enough to characterize the full spectrum of eigenstates of hyperbolic tight-binding models.

The above considerations fall under the overarching theory known as hyperbolic band theory (HBT) [518, 519]. Given a hyperbolic Fuchsian translation group Γ, which is non-Abelian, HBT provides a generalized version of Bloch's theorem in which the eigenstates of tight-binding Hamiltonians on hyperbolic lattices will acquire a Bloch factor representing a higher-dimensional unitary irrep of Γ [523]. These Bloch factors will thus be elements of the $\mathrm{U}(N)$ group, and the band theory of such systems can be broken down into the consideration of particular values of N. As mentioned above, the fact that higher-dimensional irreps can arise as such Bloch factors is a consequence of the hyperbolic translation group being non-Abelian. However, even in the case of one-dimensional irreps, known as U(1) HBT [523], there are stunning differences with the Euclidean case. In particular, the BZ of U(1) HBT is described by a space known as a *character variety*. In particular, it is the so-called *Jacobian variety* $\mathrm{Jac}(\Sigma_g)$ of the Riemann surface Σ_g with genus $g \geq 2$ obtained by identifying opposite edges of the Bravais unit cell on which Γ acts. This is exemplified in Fig. 3.7 with the double torus of $g = 2$ obtained from the compactification of the fundamental region of the $\{8,8\}$ hyperbolic translation group, which happens to coincide with the central octagon. The Jacobian is itself a complex manifold just like the Riemann surface is a complex manifold and they both have complex structures that they inherit from the covering space, i.e. the hyperbolic disk $\mathbb{D}^2$. However, the Jacobian need not be two-dimensional (or one complex dimension). In fact, it is $2g$-dimensional, and in the context of algebraic geometry one can show [518] that this complex manifold is isomorphic to the higher-genus torus $\mathbb{T}^{2g}$, i.e. we have $\mathrm{Jac}(\Sigma_g) \cong \mathbb{T}^{2g}$. Thus, we see how the U(1) BZ is still toroidal as in the Euclidean case, but the corresponding wave vector $k = (k_1, \ldots, k_{2g})$ labeling these one-dimensional irreps has $2g$ components, even though the underlying hyperbolic space is still only two-dimensional. This is a consequence of the larger number of independent generators in the hyperbolic translation group Γ.

Although one may sometimes neglect the contributions of higher-dimensional irreps, it was argued in [523] that they are indeed necessary for an exact agreement between the real-space numerical diagonalization of finite lattices and the predictions from HBT. The corresponding eigenstates which transform under higher-dimensional $N \geq 2$ irreps are called non-Abelian states, and their transformation law reads

$$\psi_a^{(\lambda)}(x) \mapsto \sum_{b=1}^{N} \left(\rho^{(\lambda)}(\gamma)\right)_{ab} \psi_b^{(\lambda)}(\gamma^{-1}(x))\,, \tag{3.43}$$

where the general index λ labels the irrep, and the $N \times N$ matrices $\rho^{(\lambda)}(\gamma)$ are elements of $\mathrm{U}(N)$, with indices $a, b = 1, \ldots, N$. These states are indeed required to have a complete understanding of the spectrum of infinite hyperbolic lattices. It is here where the connection to more advanced fields of mathematics is required. Namely, the corresponding BZ for these non-Abelian states is no longer a simple generalization of the original toroidal BZ. Rather, since Γ is also an infinite group, these higher-dimensional irreps are actually labeled by a continuous set of parameters. The non-Abelian BZ containing these irreps is a mathematical object known as a *moduli space* $\mathfrak{M}(\Sigma_g, U(N))$ of rank-N holomorphic vector bundles [519, 520, 523]. For context, a moduli space $(\mathfrak{M}, \star)$ is a geometric parameter space $\mathfrak{M}$ whose points represent equivalence classes of a specific type of algebro-geometric object with respect to a given operation $\star$. Different points in $\mathfrak{M}$ then describe instances of the same object which cannot be related via the action of $\star$. These moduli spaces, where "modulus" in this context is synonym with parameter, can come in several different flavors and may be associated to many distinct mathematical structures. Very broadly speaking, moduli spaces are the structures lurking in the back of statements like "these two object are equivalent up to isomorphism". Two instances of a mathematical object correspond to the same point on moduli space if and only if they are equivalent or isomorphic with respect to the equivalence relation $\star$ that is associated to $\mathfrak{M}$. If the instances correspond to two different points on moduli space, they cannot be related by this isomorphism and are thus inequivalent. A way of thinking about the dimensionality of a moduli space is asking "How many real parameters do I need to specify in order to uniquely characterize all objects belonging to the same equivalence class?". An illustrative example is the moduli space of homeomorphic tori, which is two-dimensional, meaning that we need to specify 2 real parameters in order to identify inequivalent tori. We can thus identify this moduli space with the complex plane, $\mathfrak{M}(\mathbb{T}^2) \cong \mathbb{C}$. In other words, for two tori to belong to the same equivalence class (with respect to homeomorphisms in this case) we need a total of 2 parameters to coincide.

The particular case of the BZ of U(N) HBT, i.e. the moduli space $\mathfrak{M}(\Sigma_g, U(N))$, is actually an object of remarkable interest in several other areas of mathematics. For example, in complex analysis, the *Narasimhan-Seshadri theorem* states that $\mathfrak{M}(\Sigma_g, U(N))$ is diffeomorphic to the space of stable holomorphic bundles of rank N and first Chern class 0 on Σ_g [573]. Meanwhile, in the context of algebraic geometry, the *Riemann-Hilbert correspondence* says that $\mathfrak{M}(\Sigma_g, U(N))$ isomorphic to space of flat $U(N)$ connections on Σ_g, up to gauge fixing [523, 574] (see [519] for more details). It is known that the dimensionality of the moduli space $\mathfrak{M}(\Sigma_g, U(N))$, which in turn is also the dimensionality of the non-Abelian BZ of HBT, is given by $2N^2(g-1)+2$ [519, 523]. However, a complete and explicit parametrization of this moduli space, necessary to prove the validity of HBT in all its generality and also to better characterize the full spectrum of hyperbolic matter systems, is not currently known.

The lack of such parametrizations for higher-dimensional irreps of Γ is the main obstacle which precludes a direct implementation of this construction for the definition of putative boundary theories in a discrete holography program. A valuable step in this direction has been recently done in [523] where it was shown that the moments of the density of state of hyperbolic tight-binding Hamiltonians can be mapped to expectation values of Wilson loop operators in a quantum gauge theory. This is a consequence of an equivalence between U(N) HBT and two-dimensional quantum U(N) Yang-Mills theory in the large N limit. Nevertheless, for the purposes of explicitly defining boundary fields which covariantly transform under irreps of Γ, this does not necessarily fill in the knowledge gap. However, it may open the door to new connections to string theory which may provide a brand new perspective on how to define discrete versions of holography.

3.2.4. Constructing Hyperbolic Tilings

The properties of hyperbolic $\{p, q\}$ tilings reported in the previous subsections hold when we consider infinite tilings which cover the entirety of hyperbolic space, extending all the way to its circular boundary. However, there are also very rich structures than can be extracted from finite subregions of hyperbolic tilings. More precisely, an equivalent construction to that via reflections is the systematic generation of finite patches of tilings via concentric layers of tiles. The core idea of this construction, which we will denote as *inflation*, is to start with a single p-gonal tile centered at the origin of the Poincaré disk, and subsequently add layers of vertices around it in a systematic manner. By assigning letter labels to these vertices based on a certain notion of connectivity between layers, the inflation procedure generates letter sequences at the boundary of these patches. These are known as *aperiodic sequences* since their

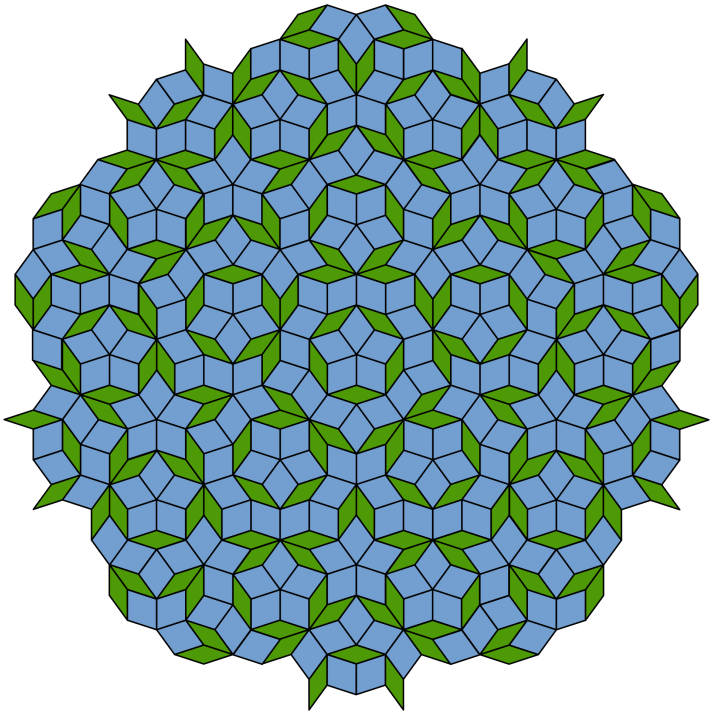


Figure 3.8: Example of a Penrose tiling, an aperiodic tiling of the two-dimensional flat plane, with two types of rhomboidal tiles. Figure courtesy of [575].

subsequences do not follow any repetition patterns. In this subsection, I will explain this inflation method in detail, such as to highlight the interesting features of aperiodic sequences that we can extract from constructing arbitrarily large but finite hyperbolic tilings.

Aperiodic sequences

We begin by introducing some general useful features of binary aperiodic sequences.[8] These are the one-dimensional manifestation of *aperiodic patterns*, structures that arise naturally in the study of so-called *quasi-crystals* [524, 576–578]. The latter describe crystalline-like arrangements of atoms or similar objects in a manner that is ordered but not repetitive, and thus lacks translational invariance. Quasi-crystals were conjectured in the 80's and revolutionized the field of crystallography [579, 580]. There are evidences of their existence in nature [581], and they have also been synthesized artificially, most famously as a result of nuclear bomb testings producing the glass-like material called *Trinitite* [582]. Aperiodic structures can be seen as an interpolation point between fully periodic and fully random distributions. In two dimensions, the

[8] It is possible to consider aperiodic sequences with more than two symbols, as explained in [525], but we will not be needing them in this work.

most celebrated aperiodic pattern is the *Penrose tiling* [512, 583, 584], a tessellation of the flat plane by a pair of irregular tiles in such a way that no arbitrarily large pattern repeats periodically, see Fig. 3.8. Recently, the field of aperiodic tilings has seen a major breakthrough in the discovery of a connected-monotile aperiodic tiling [585, 586], giving a positive answer to the so-called "einstein problem" [587].[9]

For the purposes of this work, we will mainly work with one-dimensional aperiodic sequences, which we denote by $\mathcal{S}$. These are generated by an iterative implementation of a so-called *substitution rule* on an initial collection of letters known as a *seed word* [525]. Our binary sequences will consist of two letters a and b, such that this seed word can be any finite sequence $w_0(a,b) \equiv w_0$ of these letters. The general form of a substitution, or as we will often call it, an *inflation* rule, is given by

$$\sigma : \begin{cases} a \mapsto w_a(a,b)\,, \\ b \mapsto w_b(a,b)\,, \end{cases} \tag{3.44}$$

where $w_a(a,b)$ and $w_b(a,b)$ are the words by which each letter a and b is respectively replaced. One can iteratively apply this rule onto a seed word to generate arbitrarily large letter sequences of the form $\sigma(\cdots\sigma(\sigma(w_0)))$. These sequences, which we will regard as infinitely long, do not have a periodically repeating pattern of any finite length, but they are however *self-similar*. This means that any given subsequence can be found again at any scale. For example, consider the following sequence obtained from applying the substitutions $w_a(a,b) = ab$ and $w_b(a,b) = a$ six times starting from the seed $w_0 = a$,[10]

$$ab\mathbf{ab}\mathbf{a}\mathbf{ab}aababaababaaba\,. \tag{3.45}$$

We see that it contains the subsequence *abaab* (bold), but this same structure can be identified again on the larger scale of the entire sequence, as highlighted by the colored snippets, albeit with newly identified "letters" $\tilde{a} = ababa$ (orange) and $\tilde{b} = aba$ (green). When considering infinite aperiodic sequences, the same sequence can be shown to be generated by different, yet equivalent, inflation rules. Two inflation rules σ and σ' are said to be equivalent, denoted as $\sigma \sim \sigma'$, if they can be mapped to each other via *word conjugation*, i.e. $w_a(a,b) \mapsto w'_a(a,b) = uw_au^{-1}$ and $w_b(a,b) \mapsto w'_b(a,b) = uw_bu^{-1}$ with a finite word $u = u(a,b)$ [525]. Here, the inverse operation effectively amounts to deleting the corresponding word, but practically it is similar to usual matrix multiplication, in the sense that we have $(ab)^{-1} = b^{-1}a^{-1}$ and $a(a^{-1}) = \varnothing$,

[9] Meant as a pun but not named after Albert Einstein, this problem's name is a joint word for the German phrase "ein Stein", meaning "one stone".

[10] To make the example more manifest, we subsequently conjugated the resulting sequence by $u = (aba)^{-1}$ to obtain the order shown in (3.45).

with $\varnothing$ denoting no symbol at all. Moreover, any inflation rule that can be obtained from a shorter rule by applying the latter an integer number of times is also considered to be equivalent. In these cases, e.g. $\sigma'(w_0) \sim \sigma(\sigma(w_0))$. Sometimes, for convenience, we will refer to such rules via powers, for example saying that $\sigma' \sim \sigma^2$.

Although infinite aperiodic sequences generated by iterative application of inflation rules of the form (3.44) do not have any finite periods, their asymptotic structure in the limit of infinitely many iterations can be captured by an object known as the *inflation matrix*

$$M_\sigma = \begin{pmatrix} \#_a(w_a) & \#_a(w_b) \\ \#_b(w_a) & \#_b(w_b) \end{pmatrix}, \tag{3.46}$$

where $\#_i(w_j)$ denotes the number of letters of the i-th type that are present in the word w_j, with $i, j = a, b$ [588–591]. It is instructive to consider an example. Take the following simple substitution rule, which is known as the *Fibonacci rule*

$$\sigma : \begin{cases} a \mapsto ab\,, \\ b \mapsto a\,. \end{cases} \tag{3.47}$$

Its name is due to the fact that the length of the sequence $\mathcal{S}_{\text{Fib}}$ after n iterations is given exactly by the n-th Fibonacci number F_n. Its corresponding inflation matrix is easily identified as being

$$M_{\text{Fib}} = \begin{pmatrix} 1 & 1 \\ 1 & 0 \end{pmatrix}. \tag{3.48}$$

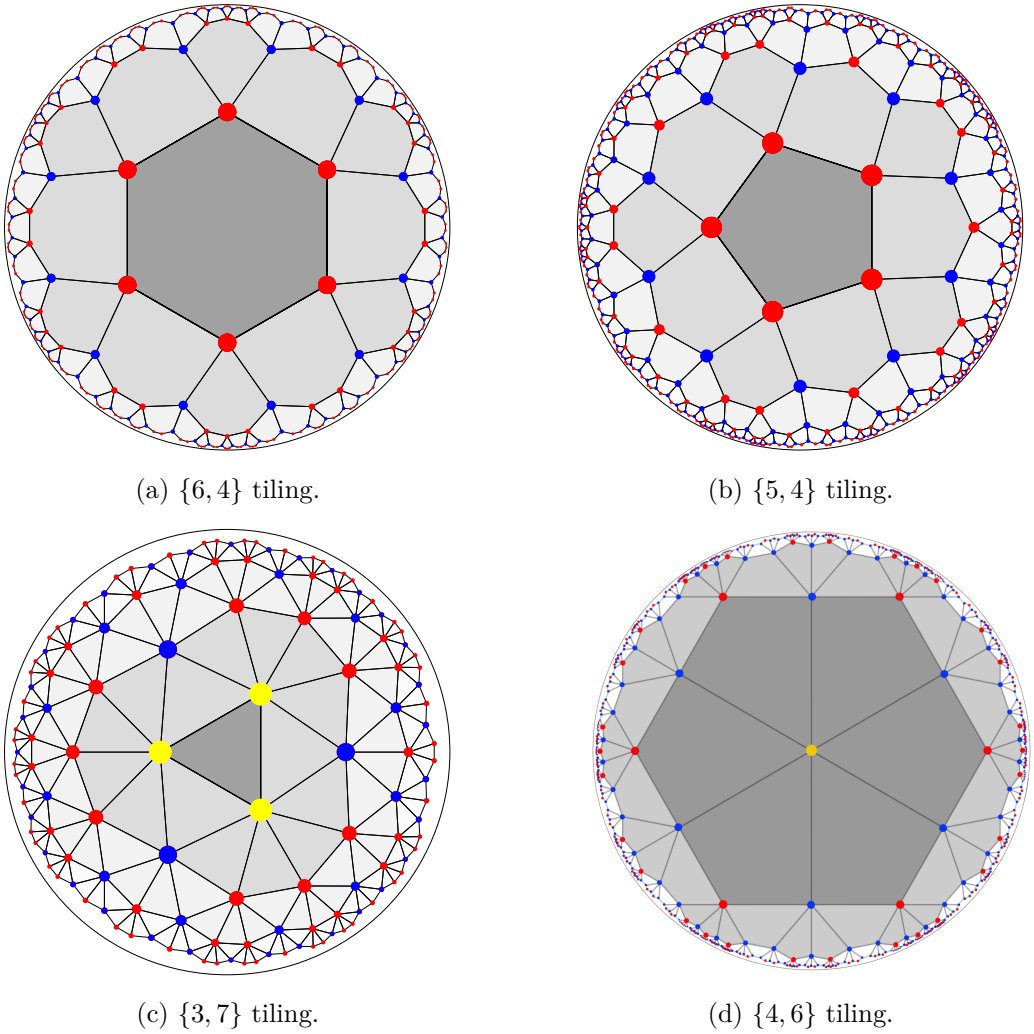
We can readily convince ourselves that inflation matrices as defined in (3.46) are always non-negative and real. As a consequence, the *Perron-Frobenius theorem* [243, 592, 593] guarantees the uniqueness of their largest eigenvalue, λ_+, as well as the positivity of its associated left and right eigenvectors. This eigenvalue describes the asymptotic scaling of the sequence after every iteration step, meaning that the length L_n^σ of the sequence after $n \gg 1$ iterations will be $L_n^\sigma \approx \lambda_+ L_{n-1}^\sigma$. For the Fibonacci sequence, the largest eigenvalue is indeed the golden ratio $\lambda_+ = \frac{1+\sqrt{5}}{2} \equiv \tau$, which is famously the value to which the ratio F_n/F_{n-1} of consecutive Fibonacci numbers converges. The Perron-Frobenius eigenvector corresponding to λ_+ is the statistically normalized right eigenvector of (3.46), denoted as $\mathbf{v}_+ = (p_a, p_b)^{\text{T}}$ with $p_a + p_b = 1$. This vector describes the relative frequencies of the letters a and b in the asymptotic aperiodic sequence. In the case of the Fibonacci sequence, this eigenvector is given by $\mathbf{v}_+ = (\frac{\sqrt{5}-1}{2}, \frac{3-\sqrt{5}}{2})^{\text{T}} \approx (0.618, 0.382)^{\text{T}}$, meaning that the asymptotic sequence obtained from (3.47) will consist of approximately 62% a's and 38% b's. Furthermore, we can also interpret the meaning of the corresponding left eigenvector $\mathbf{u}_+ = (l_a, l_b)$ associated

to λ_+, which is normalized in such a way that $\mathbf{u}_+ \cdot \mathbf{v}_+ = 1$. The entries of this vector describe the characteristic relative length scales associated to each letter in the sequence. Broadly speaking, this is the average relative length of the sequences generated from each of these letters as a fraction of the total length of the sequence, indicating how much of a sequence has been obtained from which letter after an inflation step. Let us stress that the interpretations given above for the eigenvectors and eigenvalues of an inflation matrix are only a good description of the aperiodic sequence in the asymptotic limit of a large number of inflation steps (3.44).

Inflation rules for $\{p, q\}$ tilings

After these general treatment of aperiodic sequences, let us now exploit these inflation rules to construct hyperbolic $\{p, q\}$ tilings discretizing the Poincaré disk $\mathbb{D}^2$, following [158, 159, 437, 439]. This construction starts from a polygon centered at the origin of $\mathbb{D}^2$, and this will denote the zeroth layer of our truncated tiling. By truncated we mean here that the patches constructed via inflation are arbitrarily large but still finite portions of the otherwise infinite $\{p, q\}$ tessellations. The fact that we start with a polygon in the middle is simply a convention and tilings generated in this way are called *polygon-centered tilings* [159]. The benefit of this choice is that it manifestly preserves the symmetry of the central p-gonal tile, which is described by the *dihedral group* D_p [159, 594, 595]. Alternatively, we can also start the construction with a vertex at the origin of $\mathbb{D}^2$, leading to what we will denote as *vertex-centered tilings*. Vertex-centered tilings manifestly preserve the symmetry group of the central vertex, given now by the dihedral group with order q, i.e. D_q. Tilings constructed via these two possible choices are shown in Fig. 3.9, with Fig. 3.9d in particular showing a vertex-centered tiling. As explained in Sec. 3.2.3, the construction of infinite hyperbolic tilings yields a tessellation with the proper triangle group $\Delta^+(p, q, 2)$ as its isometry group. However, for practical computations in AdS/CFT, we typically introduce a UV cutoff to regularize divergent quantities. The analogue of this UV cutoff in the construction of hyperbolic tilings is precisely to consider arbitrarily large but finite truncated tilings, as we construct with the inflation procedure.

The next step of the construction is as follows. We associate the letter a to each vertex of the central p-gon, and define our seed word to be $w_0 = a^p$ (for $p > 3$). Here, we again utilize the shorthand notation of exponents for groups of the same letter, e.g. $a^4 \equiv aaaa$. The construction follows with the subsequent addition of concentric layers of tiles around this central polygon, where the corresponding new vertices are obtained from an inflation rule. These vertex labels follow a binary scheme, and they characterize the vertices at the boundary of each truncated tiling during the inflation



(a) $\{6,4\}$ tiling.

(b) $\{5,4\}$ tiling.

(c) $\{3,7\}$ tiling.

(d) $\{4,6\}$ tiling.

Figure 3.9: Some examples of regular hyperbolic $\{p,q\}$ tilings chosen to showcase the inflation construction. The different types of vertices a and b are shown in red and blue, respectively, while c and d type vertices are both shown in yellow. The labeling of the vertices follows the construction of the tilings according to the inflation rules (3.49) and (3.50). Successive layers obtained during the inflation procedure are shown in different shades of gray, with later layers depicted in lighter tones.

procedure. The inflation rules are based on the following observation: after adding a concentric layer of tiles, some of the vertices at the current boundary of this truncated tiling will have an edge connecting them to the previous layer. Other vertices, however, will only be connected to other boundary vertices on the current layer and will not be connected to the previous layer. These are somewhat equivalent to the vertices of the initial polygon. Therefore, we associate the letter a to vertices which are not connected to the previous layer, and the letter b to those vertices which do have an edge linking them to the previous layer. Note that this is done at each step in the inflation procedure. This construction is valid for any $\{p,q\}$ tilings with $p > 3$. For

the case of $p = 3$, we have to introduce an auxiliary vertex label, denoted by d, which will however only appear in the seed word $w_0 = d^3$ and will vanish after one inflation step. The definition of the a, b vertices above also needs a slight adjustment, since now they will be connected by one and two edges to the previous layer, respectively. Still, taking this special case into account, the inflation construction generates the n-th layer of the tiling by applying a tiling-dependent inflation rule $\sigma_{\{p,q\}}$ to the vertices on the $(n-1)$-th layer. Throughout this procedure, it is implied that each newly generated layer of vertices is "filled" with their corresponding p-gonal tiles, cf. Fig. 3.9. Note that inflation keeps track of the type of vertices, but not necessarily of their position. For the case of $p = 3$ and $q \geq 7$, the inflation rules read

$$\sigma_{\{3,q\}} = \begin{cases} a \mapsto a^{q-5}b\,, \\ b \mapsto a^{q-6}b\,, \\ d \mapsto a^{q-4}b\,, \end{cases} \tag{3.49}$$

where it can be seen that the auxiliary vertex disappears after one inflation step, effectively leading to a binary asymptotic sequence. Meanwhile, for all other hyperbolic $\{p, q\}$ tilings,[11] the inflation rules are given by [158, 159, 437, 439]

$$\sigma_{\{p,q\}} = \begin{cases} a \mapsto a^{p-4}b(a^{p-3}b)^{q-3}\,, \\ b \mapsto a^{p-4}b(a^{p-3}b)^{q-4}\,, \\ c \mapsto (a^{p-3}b)^{q}\,, \end{cases} \tag{3.50}$$

and these determine how each vertex at the boundary of a given layer is to be substituted to generate the next layer of the tiling. Notice that we have incorporated a third vertex type, labeled by c for *center vertex* in (3.50). This label, similarly to the d label in the $p = 3$ case discussed above, is necessary for defining the seed word in the case of vertex-centered tilings, which simply reads $w_0 = c$. However, it also disappears after one inflation step and the inflation rules (3.50) therefore always lead to binary sequences in the asymptotic limit. In particular, in this asymptotic limit and up to a $\mathbb{Z}_n$ $(n = p, q)$ redundancy, the resulting sequence at the boundary of the hyperbolic tilings is well-approximated as being the infinite aperiodic sequence $\mathcal{S}_{\{p,q\}}$. This aperiodic sequence on the boundary encodes information about the way the bulk tiling has been constructed via the parameters p and q. Tilings generated via the inflation rules (3.50) are shown in Fig. 3.9 for the cases of a polygon-centered $\{6, 4\}$,

[11] Actually, the case of $q = 3$ case is somewhat pathological. Its inflation requires three letters, together with a deletion rule that removes a particular letter each step. We will not require it here and therefore we do not go into further details on it. The interested reader can consult [437] for a separate analysis on this case.

$\{5,4\}$, and $\{3,7\}$ tilings, as well as a vertex-centered $\{4,6\}$ tiling. The vertex labels are color-coded by red, blue and yellow dots, representing a-, b- and c,d-type vertices, respectively. Since the latter two types of vertices do not play a significant role in the upcoming analyses, we have taken the liberty of depicting them with the same color. The concentric layers are shaded in different gray tones in Fig. 3.9a-3.9d, and the seed words are a^6, a^5, d^3, and c, respectively. Since there is some ambiguity as to how exactly the vertices should be labeled in the newly generated layer, we adopt the following convention: For the word associated to a given vertex by the inflation rule, we assign the letters to the vertices in a clockwise fashion, starting from the leftmost vertex which is not connected with the previous layer. By construction, this vertex is guaranteed to be of type a. Thus, for the case of the polygon-centered $\{5,4\}$ tiling, the sequence after one inflation step is $abaababaababaababaababaab$, as can be verified by checking the sequence of red and blue dots in the second layer of Fig. 3.9b.
It is again useful to consider some examples of $\{p,q\}$ inflation rules. First, we consider the inflation rule for the $\{3,7\}$ tiling shown in Fig. 3.9c, which according to (3.49) has the inflation rule

$$\sigma_{\{3,7\}} = \begin{cases} a \mapsto aab\,, \\ b \mapsto ab\,, \\ d \mapsto aaab\,, \end{cases} \tag{3.51}$$

where, effectively, we are only interested in the first two lines of the above equation for characterizing the asymptotic sequence $\mathcal{S}_{\{3,7\}}$. The inflation matrix, considering only these two substitutions, reads

$$M_{\{3,7\}} = \begin{pmatrix} 2 & 1 \\ 1 & 1 \end{pmatrix}. \tag{3.52}$$

Interestingly, this inflation rule is equivalent, in the sense explained below (3.50), to the square of the Fibonacci substitution rule, i.e. $\sigma_{\{3,7\}} \sim \sigma^2_{\text{Fib}}$, which can be seen by noticing that $\sigma^2_{\text{Fib}}(a) = aba \sim aab = \sigma_{\{3,7\}}(a)$. Similarly we have $\sigma^2_{\text{Fib}}(b) = ab = \sigma_{\{3,7\}}(b)$. Indeed, the largest eigenvalue of (3.52) is $\lambda_+ = \frac{3+\sqrt{5}}{2} = (1+\tau) = \tau^2$, where $\tau = \frac{1+\sqrt{5}}{2}$ denoted the golden ratio. The square comes from the fact that we have to apply the Fibonacci inflation rule twice in order to realize one substitution step from $\sigma_{\{3,7\}}$. As a second example, let us showcase a further equivalence relation between inflation rules. Namely, take the inflation rule for a $\{5,5\}$ tiling, which according to (3.50) for a polygon-centered tiling reads

$$\sigma_{\{5,5\}} = \begin{cases} a \mapsto abaabaab\,, \\ b \mapsto abaab\,. \end{cases} \tag{3.53}$$

We can show that $\sigma_{\{5,5\}} \sim \sigma^2_{\{3,7\}}$, which in turn makes it also equivalent to the fourth power of the Fibonacci rule, i.e. $\sigma_{\{5,5\}} \sim \sigma^4_{\text{Fib}}$. On the one hand, the Perron-Frobenius eigenvalue of (3.53) is given by $\lambda_+ = \frac{7+\sqrt{5}}{2} = \tau^4$. On the other hand, the inflation matrix corresponding to (3.53) is

$$M_{\{5,5\}} = \begin{pmatrix} 5 & 3 \\ 3 & 2 \end{pmatrix}, \tag{3.54}$$

and, using (3.52) and (3.48), we can find the following relation

$$M_{\{5,5\}} = M^2_{\{3,7\}} = M^4_{\text{Fib}}\,, \tag{3.55}$$

where the powers are taken via standard matrix multiplication. Therefore, the asymptotic sequences generated by these three inflation rules are all asymptotically equivalent $\mathcal{S}_{\{3,7\}} \sim \mathcal{S}_{\{5,5\}} \sim \mathcal{S}_{\text{Fib}}$. Finally, consider the inflation rule generating the vertices of a truncated $\{6,4\}$ tiling.. The seed word is $w_0 = a^6$ and the inflation rule reads

$$\sigma_{\{6,4\}} = \begin{cases} a \mapsto aabaaab\,, \\ b \mapsto aab\,, \end{cases} \tag{3.56}$$

with corresponding inflation matrix

$$M_{\{6,4\}} = \begin{pmatrix} 5 & 2 \\ 2 & 1 \end{pmatrix}. \tag{3.57}$$

This inflation rule can be shown to give rise to a sequence equivalent to that obtained from the so-called *silver mean* sequence [588, 589], which is generated by substitution rule σ_{silver} with $a \mapsto aab$, $b \mapsto a$. This sequence is a close cousin to the Fibonacci sequence, whose ratio of lengths of consecutive layers converges to the so-called silver ratio. The latter belongs to the larger family of *metallic ratios* [596], see Box 3.3 for more details. The Perron-Frobenius largest eigenvalue of (3.57) is indeed the square of the silver ratio $\lambda_+ = 3+2\sqrt{2} = (1+\sqrt{2})^2$. Therefore, we can say that $\sigma_{\{6,4\}} \sim \sigma^2_{\text{silver}}$.

Box 3.3 Metallic Ratios

The Fibonacci sequence is a sequence of natural numbers, where each subsequent number is the sum of the previous two numbers. In other words, the Fibonacci

numbers F_n, with $n \geq 2$, are generated by the following recursion relation

$$F_n = F_{n-1} + F_{n-2}\,, \tag{3.58}$$

with starting conditions $F_0 = 0$ and $F_1 = 1$. The first elements of this sequence read $0, 1, 2, 3, 5, 8, 13, 21, 34, 55, 89, \ldots$. Famously, the ratio of consecutive Fibonacci numbers tends asymptotically to the golden ratio, i.e.

$$\lim_{n\to\infty} \frac{F_n}{F_{n-1}} = \tau = \frac{1+\sqrt{5}}{2}\,. \tag{3.59}$$

The Fibonacci sequence, however, is a special case of a larger class of sequences, known as sequences of metallic means [524, 596]. These sequences are defined by a generalized version of (3.58), namely

$$G_n = kG_{n-1} + m\,G_{n-2}\,, \tag{3.60}$$

with positive integer numbers k, m and with initial conditions $G_0 = 0$ and $G_1 = 1$. One can think of these as weighted versions of the Fibonacci sequence, where the latter is retrieved in the case of $k = m = 1$. It is possible to show that the ratio of subsequent members in these metallic sequences always converges to an irrational number, typically named after a metal, hence their name. More precisely, these ratios are solutions to quadratic equations of the form $x^2 - kx - m = 0$ and read

$$\lim_{n\to\infty} \frac{G_n}{G_{n-1}} = \frac{k+\sqrt{k^2+4m}}{2} \equiv \tau_{k,m}\,. \tag{3.61}$$

Examples of these ratios are the golden ratio $\tau_{1,1} = \frac{1+\sqrt{5}}{2}$, the silver ratio $\tau_{2,1} = 1+\sqrt{2}$, the bronze ratio $\tau_{3,1} = \frac{3+\sqrt{13}}{2}$ and the copper ratio $\tau_{1,2} = 2$. Although in this work we only consider hyperbolic tilings $\{p, q\}$ with $p < \infty$ and $q < \infty$, the cases where one of the Schläfli parameters is infinity can be related to so-called *Farey tessellations*, which have intricate connections to the continued fractions expansions admitted by the metallic ratios. We refer to [596] for a deeper analysis on this.

Having familiarized ourselves with the construction of tilings via inflation rules, and having seen some explicit examples, let us now provide general closed formulas for the most important quantities. The general inflation matrix for a hyperbolic $\{p, q\}$ tiling

constructed via the inflation rules (3.50) is given by

$$M_{\{p,q\}} = \begin{cases} \begin{pmatrix} (p-3)(q-3)+p-4 & (p-3)(q-4)+p-4 \\ q-2 & q-3 \end{pmatrix}, & p>3, \\ \begin{pmatrix} q-5 & q-6 \\ 1 & 1 \end{pmatrix}, & p=3\,, \end{cases} \tag{3.62}$$

and its Perron-Frobenius eigenvalue reads

$$\lambda_+(p,q) = \begin{cases} \frac{1}{2}\left(pq-2p-2q+2+\sqrt{(pq-2p-2q+2)^2-4}\right), & p>3\,, \\ \frac{1}{2}\left(q-4+\sqrt{q^2-8q+12}\right), & p=3\,. \end{cases} \tag{3.63}$$

Notably, we have $\lambda_+(p,q) > 1$ for all p and q, which is to be expected since $\lambda_+ < 1$ would imply that the sequence asymptotically shrinks in size. For the matrices in (3.62), the corresponding properly normalized right and left eigenvectors for $p > 3$ are

$$\mathbf{v}_+ = \begin{pmatrix} \frac{\omega(p,q)}{2(p-2)} - \frac{q}{2} + 2 \\ -\frac{\omega(p,q)}{2(p-2)} + \frac{q}{2} - 1 \end{pmatrix}, \quad \mathbf{u}_+ = \begin{pmatrix} \frac{2}{-p(q-2)+\omega(p,q)+2q} \\ \frac{-p(q-2)+\omega(p,q)+4q-8}{(q-2)(-p(q-2)+\omega(p,q)+2q)} \end{pmatrix}, \tag{3.64}$$

while those for $p = 3$ read

$$\mathbf{v}_+ = \begin{pmatrix} \frac{6+\xi(q)-q}{2} \\ \frac{2}{q+\xi(q)-4} \end{pmatrix}, \quad \mathbf{u}_+ = \begin{pmatrix} \frac{q+\xi(q)-4}{2\xi(q)} \\ \frac{q+\xi(q)-2}{2(q-2)} \end{pmatrix}, \tag{3.65}$$

where we have introduced $\omega(p,q) \equiv \sqrt{(p-2)(q-2)(p(q-2)-2q)}$ as well as $\xi(q) \equiv \sqrt{(q-6)(q-2)}$ for the sake of clarity. The normalization condition $\mathbf{u}_+ \cdot \mathbf{v}_+ = 1$ can be easily verified in both cases.

Let us give a final comment on these aperiodic sequences at the boundary of hyperbolic tilings. Recall the $\mathbb{Z}_n$ redundancy we mentioned below (3.50). This arises from the fact that applying the substitution rules (3.50) on the seed word a large number of times indeed generates a truly aperiodic sequence $\mathcal{S}_{\{p,q\}}$. However, when embedding this sequence on the boundary of a truncated polygon- or vertex-centered hyperbolic tiling, the sequence of letters respectively inherits a $\mathbb{Z}_p$ or $\mathbb{Z}_q$ rotational symmetry. Nevertheless, after an arbitrarily large number $n \to \infty$ of inflation steps, we may restrict ourselves to a p-th or q-th of the tiling's boundary, while still viewing large subsequences of it as good representatives of the aperiodic structure.

Explicit closed formulas on numbers of a and b type vertices

To conclude this subsection, I report the derivation of explicit closed formulas for the exact number of a-type and b-type vertices at any given inflation layer of a general $\{p, q\}$ tiling. To the best of my knowledge, these results have not been published elsewhere in the literature.
Consider the general inflation matrix for $\{p, q\}$ tilings given in (3.62). We can represent the seed word on which such a matrix acts by a two-dimensional vector $v_0 = (p, 0)^T$, whose first and second components count the number of a-type and b-type vertices, respectively. We can then denote a single inflation step as

$$M_{\{p,q\}} v_0 \equiv v_1 = (\mathcal{N}_a(p, q, 1), \mathcal{N}_b(p, q, 1))^T \,. \tag{3.66}$$

The vector v_1 now contains the number of a-type and b-type vertices after one inflation step. The exact number of vertices of both types on the boundary of the n-th layer, denoted by $\mathcal{N}_a(p, q, n)$ and $\mathcal{N}_b(p, q, n)$, can then be obtained by acting on the seed word with the inflation matrix n number of times. Naturally, the total number of vertices on the boundary will be the sum of the vector's components. Therefore, we compute the n-th power of the inflation matrix, which can be worked out in closed form for every p and q. We obtain the following formulas

$$\begin{aligned}
\mathcal{N}_a(p, q, n) &= \frac{p}{2}\left((p-4)(q-2)\frac{\lambda_+^n - \lambda_-^n}{\delta\lambda} + \lambda_+^n + \lambda_-^n\right) , \\
\mathcal{N}_b(p, q, n) &= \frac{p(q-2)}{\delta\lambda}\left(\lambda_+^n - \lambda_-^n\right) , \\
\mathcal{N}(p, q, n) &= \mathcal{N}_a(p, q, n) + \mathcal{N}_b(p, q, n) \\
&= \frac{p}{2(\delta\lambda)}\left(\lambda_+^n\left(\delta\lambda + (p-2)(q-2)\right) + \lambda_-^n\left(\delta\lambda - (p-2)(q-2)\right)\right) ,
\end{aligned} \tag{3.67}$$

with $\delta\lambda \equiv \lambda_+ - \lambda_-$ and where λ_+, λ_- are the largest and smallest eigenvalues of the inflation matrix (3.62) for $p > 3$. The total number of vertices $\mathcal{N}_{\text{tot}}(p, q)$, both boundary and bulk, in a truncated $\{p, q\}$ tiling with M layers is then simply given by

$$\mathcal{N}_{\text{tot}}(p, q) = \sum_{n=0}^{M} \mathcal{N}(p, q, n) \,. \tag{3.68}$$

The analysis is exactly the same for the case $p = 3$ and $q \geq 7$, only this time we use the inflation matrix in the second line of (3.62), together with it's eigenvalues (which we still denote as λ_+ and λ_- in a slight abuse of notation). Moreover, we have to take into account that the original seed word is given by d^3. Applying the inflation rule

(3.49) once, we obtain a new initial vector

$$v_1 = \begin{pmatrix} 3(q-4) \\ 3 \end{pmatrix} , \tag{3.69}$$

which counts our starting number of a- and b-type vertices. From here, we can simply apply the corresponding inflation matrix n times and again obtain closed formulas for the exact number of a-type and b-type vertices after $n+1$ inflation steps in the case of $p = 3$ tilings

$$\begin{aligned} \mathcal{N}'_a(q,n) &= 3\left(\lambda_+^{n+1} + \lambda_-^{n+1}\right) , \\ \mathcal{N}'_b(q,n) &= \frac{3}{\delta\lambda}\left(\lambda_+^{n+1} - \lambda_-^{n+1} + \delta\lambda\right) , \\ \mathcal{N}'(q,n) &= \mathcal{N}'_a(q,n) + \mathcal{N}'_b(q,n) \\ &= 3\left(\lambda_+^{n+1} + \lambda_-^{n+1} + \frac{\lambda_+^{n+1} - \lambda_-^{n+1}}{\delta\lambda} + 1\right) . \end{aligned} \tag{3.70}$$

Note that these are after $n+1$ inflation steps, and not after n, since we had to apply one inflation step to get rid of the d-type vertices. Only after this step we obtain a binary inflation rule. For counting the total number of vertices up to a given inflation layer, we have to sum up the expressions above analogously to (3.68) and then add 3 to take into account the original seed word d^3.

3.3. The Breitenlohner-Freedman Bound on Hyperbolic Tilings

It is apparent that hyperbolic tilings, both in their infinite and truncated manifestations, have a plethora of interesting features and properties. These makes them promising candidates to be the backbone of a discrete holographic duality. Moreover, as we will unveil in the following sections, they open the door to experimental realizations of holography in tabletop experiments. However, before putting our trust into these hyperbolic tessellations, we should benchmark them to see how well they actually approximate the continuum, and if not, how can we characterize the new effects arising from such a discretization. To this end, I will consider a hallmark result of gravity on negatively curved spacetimes, which later experienced a revival for its interpretation within the AdS/CFT correspondence. This is the celebrated *Breitenlohner-Freedman* (BF) [196, 197] bound on the mass of stable scalar field configurations in Anti-de Sitter spacetime. In holography, this bound provides a relation between the mass m

of a scalar field in the bulk and the scaling dimension Δ of its dual operator on the boundary, $\Delta(\Delta - d) = m^2\ell^2$, with ℓ the AdS radius and d the boundary spacetime dimension [86]. The results I report in this section are based on [157] and show how the BF bound can be identified on hyperbolic tilings, and how it is related to its value in the continuum. Moreover, I establish the BF bound on hyperbolic tessellations via an analysis of continuum analytical solutions in the presence of a finite cutoff.

3.3.1. A Scalar Field on AdS

We start our analysis by considering the simple model of a real scalar field Φ defined over a fixed, negatively curved continuous spacetime. In particular, we will consider the Euclidean version of AdS_2, denoted as $EAdS_2$, and recall that $EAdS_2 \cong \mathbb{D}^2$. The metric tensor of this geometry is given by

$$ds^2 = g_{\mu\nu}dx^\mu dx^\nu = \frac{\ell^2}{\cos^2(\theta)}\left(d\theta^2 + \sin^2(\theta)d\phi^2\right) , \tag{3.71}$$

where we have chosen coordinates $\theta \in [0, \frac{\pi}{2})$, $\phi \in [0, 2\pi)$ suitable for our later computations, in which $\theta = \frac{\pi}{2}$ denotes the asymptotic boundary of $EAdS_2$. With this metric, the action functional of a real scalar field on top of this fixed background geometry reads

$$S = \frac{1}{2}\int d^2x\sqrt{g}\left(\partial^\mu\Phi\partial_\mu\Phi + m^2\Phi^2\right) . \tag{3.72}$$

Given any such action, the corresponding equations of motion can be derived via the variation principle. For a scalar field, this equation of motion is given by the *Klein-Gordon* equation, which we take to be defined by the so-called *Laplace-Beltrami operator* $\Box \equiv \frac{1}{\sqrt{g}}\partial_\mu\left(\sqrt{g}g^{\mu\nu}\partial_\nu\Phi\right)$ associated to the given metric. More precisely, we have

$$0 = (\Box - m^2)\Phi = \cos(\theta)^2\partial_\theta^2\Phi(\theta) + \cos(\theta)^2\cot(\theta)\partial_\theta\Phi(\theta) - m^2\ell^2\Phi(\theta) . \tag{3.73}$$

Notice that we have restricted our attention to purely θ-dependent field configurations $\Phi(\theta)$ with no angular dependence for simplicity. This second-order differential equation with variable coefficients admits two linearly independent fundamental solutions in terms of *hypergeometric functions* [597]. Their linear combination yields the general solution to (3.73), which reads

$$\begin{aligned}\Phi(\theta) &= (-1)^{\frac{1}{4}-\frac{1}{4}\sqrt{1+4m^2\ell^2}}\cos(\theta)^{\frac{1}{2}-\frac{1}{2}\sqrt{1+4m^2\ell^2}} \\ &\times\left(\tilde{A}\cdot_2 F_1[a_1, b_1, c_1; \cos(\theta)^2] + \tilde{B}\left(\mathrm{i}\cos(\theta)\right)^{\sqrt{1+4m^2\ell^2}}\cdot_2 F_1[a_2, b_2, c_2; \cos(\theta)^2]\right) ,\end{aligned} \tag{3.74}$$

with coefficients

$$\begin{aligned} a_1 &= \frac{1}{4}\left(1-\sqrt{1+4m^2\ell^2}\right), \quad a_2 = \frac{1}{4}\left(1+\sqrt{1+4m^2\ell^2}\right), \\ b_1 &= \frac{1}{4}\left(3-\sqrt{1+4m^2\ell^2}\right), \quad b_2 = \frac{1}{4}\left(3+\sqrt{1+4m^2\ell^2}\right), \\ c_1 &= \frac{1}{2}\left(2-\sqrt{1+4m^2\ell^2}\right), \quad c_2 = \frac{1}{2}\left(2+\sqrt{1+4m^2\ell^2}\right). \end{aligned} \tag{3.75}$$

The coefficients $\tilde{A}$ and $\tilde{B}$ are integration constants. Ignoring constant prefactors, these solutions have an asymptotic behavior towards the boundary of EAdS_2 as $\cos(\theta)^2 \to 0$ when $\theta \to \frac{\pi}{2}$. This can be seen from the general behavior of hypergeometric functions, which are regular around the origin $z = 0$, with their series expansion given by [597]

$${}_2F_1[a,b,c;z] = 1 + \frac{abz}{c} + \frac{a(a+1)b(b+1)z^2}{2c(c+1)} + \mathscr{O}\left(z^3\right). \tag{3.76}$$

Therefore, the solutions shown in (3.74) have the asymptotic boundary behavior

$$\Phi(\theta) \overset{\theta\to\frac{\pi}{2}}{\approx} A\cos(\theta)^{1-\Delta}\left(1+\mathscr{O}\left(\theta^2\right)\right) + B\cos(\theta)^{\Delta}\left(1+\mathscr{O}\left(\theta^2\right)\right), \tag{3.77}$$

with

$$\Delta = \frac{1}{2} + \frac{1}{2}\sqrt{1+4m^2\ell^2}\,. \tag{3.78}$$

We have also redefined the integration constants to A, B to now include possible constant prefactors. Within AdS/CFT, as reviewed in Sec. 2.2.3, Δ in (3.78) is identified with the scaling dimension of the boundary operator $\mathcal{O}$ which is said to be holographically dual to the bulk field Φ [168]. Moreover, the two terms of the asymptotic expansion (3.77) are usually denoted as *non-normalizable* and *normalizable* modes, respectively. Suitable choices of boundary conditions [598] then allows to identify the coefficient B of the normalizable mode with the vacuum expectation value $\langle\mathcal{O}\rangle$ of the dual operator $\mathcal{O}$, while the coefficient A of the non-normalizable mode is associated to the field J which sources the operator $\mathcal{O}$ in the CFT Lagrangian, cf. Sec. 2.2.3. One would like operators in a CFT to have real valued scaling dimensions, otherwise unitarity can be violated when performing a conformal transformation [599]. We will see the implication of such a statement from the perspective of the bulk gravitational theory in the next section. Inspecting the radicand in (3.78), having a real scaling dimension imposes that the mass of the scalar field must obey

$$m^2\ell^2 \geq -\frac{1}{4}, \tag{3.79}$$

which is exactly the BF bound [196, 197].

From the behavior of hypergeometric functions, we can see that for $\theta \to 0$, the solutions in (3.74) diverge. In fact, each term of the solution exhibits its own logarithmic divergence at this singular point. To ensure the regularity of our solutions in the bulk, meaning $\partial_\theta \Phi(\theta)|_{\theta=0} = 0$, we need to impose a relation between the integration constants $\tilde{A}$ and $\tilde{B}$ such these logarithmic divergences cancel each other, thus guaranteeing that the amplitude of the field at the origin remains finite. Such a condition amounts to imposing Neumann boundary conditions in the bulk when $\theta \to 0$. Doing this, we find

$$\tilde{A} = \frac{(2\mathrm{i})^{\sqrt{1+4m^2\ell^2}} \left(4a_2 - 2m^2\ell^2 c_2\right) \Gamma\left(c_1 + \frac{3}{2}\right) \Gamma\left(c_2 + 1\right)}{\left(-4a_1 + 2c_1 m^2\ell^2\right) \Gamma\left(c_1 + 1\right) \Gamma\left(c_2 + \frac{3}{2}\right)} \tilde{B}\,, \tag{3.80}$$

where $\Gamma(x) = \int_0^\infty dt\, t^{x-1} e^{-t}$ denotes the Euler Gamma function generalizing the notion of the factorial [597]. Finally, any experimental architecture which attempts to probe holographic predictions in a laboratory ought to be of finite extent. When using hyperbolic tilings as a discretization template for EAdS_2, this amounts to considering finite truncated tilings, in the sense explained in Sec. 3.2.4. Since these truncated tilings do not extend all the way to the boundary at $\theta = \frac{\pi}{2}$, this requires the introduction of a UV cutoff $\varepsilon \ll 1$ in the construction, such that the tilings only go up to a radius of $\theta = \theta_c = \frac{\pi}{2} - \varepsilon$. While this cutoff is exact for the continuum EAdS_2 space, the jagged structure of the tiling's boundary at any finite layer necessitates the interpretation of θ_c as an *effective* uniform radial cutoff. The latter detail, however, will only be relevant for later numerical simulations. Thus, coming back to the continuous solutions (3.74), we wish to impose Dirichlet boundary conditions at $\theta = \theta_c$, in such a way that the field value at this point equals unity, i.e. $\Phi(\theta_c) = 1$. In the context of holography, this is equivalent to fixing the boundary source of the operator dual to the bulk field when the cutoff is removed. This boundary condition fixes the remaining integration constant to be

$$\tilde{B} = \frac{(-1)^{-a_1} \cos^{-2a_1}(\theta_c)}{(\mathrm{i}\cos(\theta_c))^{\sqrt{4\ell^2m^2+1}}\, {}_2F_1\left(a_2, b_2; c_2; \cos^2(\theta_c)\right) + \Omega \times {}_2\tilde{F}_1\left(a_1, b_1; c_1; \cos^2(\theta_c)\right)}\,, \tag{3.81}$$

with the regularized hypergeometric function ${}_2\tilde{F}_1[a,b,c;z] = \frac{{}_2F_1[a,b,c;z]}{\Gamma(c)}$ [597] and where we defined the constant coefficient

$$\Omega = \frac{2^{4a_2} e^{\frac{1}{2}\mathrm{i}\pi\sqrt{4\ell^2m^2+1}} \Gamma\left(c_1 + \frac{3}{2}\right) \Gamma\left(c_2 + 1\right) \left(4a_2 - 2c_2\ell^2m^2\right)}{\Gamma\left(c_2 + \frac{3}{2}\right) \left(3 - 4\ell^2m^2\right) \left(-4a_1 - \ell^2m^2\right)}\,, \tag{3.82}$$

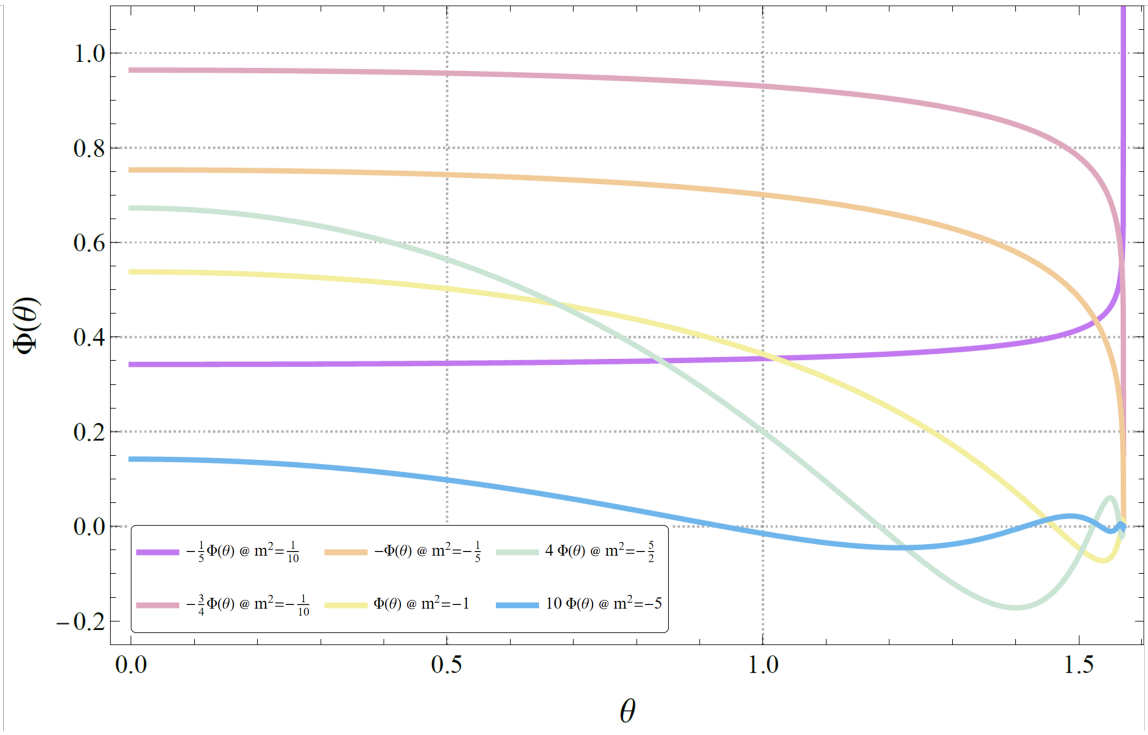


Figure 3.10: Different behavior of the solutions (3.74) to the KG equation for values of the mass-squared above and below the BF bound $m^2\ell^2 = -1/4$. We have rescaled the solutions to aid in the direct visual comparison. Solutions above the BF bound do not exhibit any zeroes, while those below the BF bound do. The curve which diverges towards the boundary $\theta \to \pi/2$ (dark purple) denotes solutions for positive values of the mass-squared, which contain non-normalizable modes as per (3.77).

for display purposes. We thus find that the solutions are fully determined as functions of the mass m^2 and the radial cutoff $\theta_c = \frac{\pi}{2} - \varepsilon$. With these solutions in hand, we can plot their behavior above and below the BF bound. This is shown in Fig. 3.10. Indeed, we observe a notable change in the fundamental behavior of the solutions when the mass-squared goes below the stability threshold, namely they start exhibiting an oscillatory behavior. This is expected, since the exponent governing their behavior towards the boundary is now complex. A more interesting property of the solutions is that they exhibit no zeroes for masses above the BF bound $m^2 \geq m^2_{\text{BF}}$. In contrast, the solutions develop an infinite set of zeroes, which seem to accumulate towards the boundary due to the non-compact nature of EAdS_2 space. A practical and useful way of keeping track of these zeroes for different values of the mass and of the radial cutoff is to observe the value of the field at the origin while varying the aforementioned parameters. The way that we impose Dirichlet boundary conditions at the cutoff $\theta_c = \frac{\pi}{2} - \varepsilon$ amounts to a rescaling of the solutions according to (3.81). However, if the cutoff happens to coincide with one of the zeroes of a solution for masses below the BF

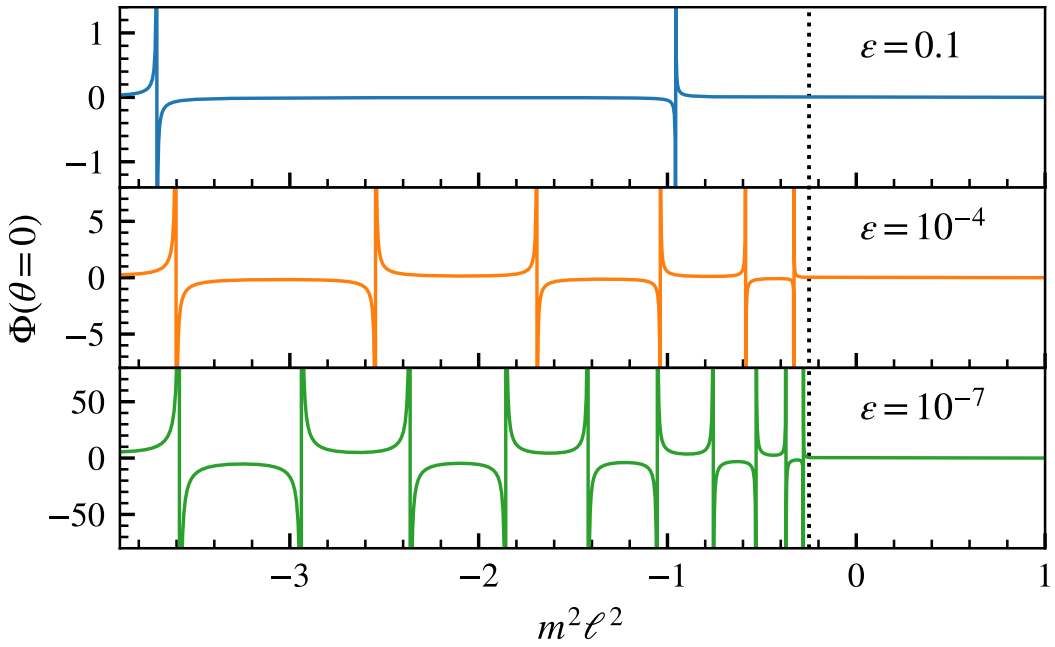


Figure 3.11: Value of the field amplitude at the origin, computed for different values of the cutoff ε. The *Umklapp points* introduced in the text manifest themselves at any finite cutoff as divergences in the field value. The right-most Umklapp point appearing below the dotted line (positioned at the continuum BF bound $m^2\ell^2 = -1/4$) functions as an indicator of the onset of unstable solutions. As the cutoff is removed, we observe an accumulation of the Umklapp points, while the right-most one approaches the continuum BF bound.

bound, this rescaling factor diverges, and so does the value of the field at the origin. We denote the pairs of specific values of the mass-squared and the cutoff (m^2, ε) as *Umklapp points* [157], and we show examples of these in Fig. 3.11. Note that the exact position of the first Umklapp point appearing for masses below $m^2\ell^2 = -\frac{1}{4}$ can be used as an indicator for the onset of the unstable regime, and it corresponds to the zero which is furthest into the bulk, i.e. with the smallest θ coordinate. Given the solutions (3.74) with the coefficients (3.75) and (3.81), we can keep exact analytical tracking of this first (and actually all) Umklapp point. We will later use this as a benchmark reference, shown as a black solid line in Fig. 3.13, for our comparisons with numerical findings on the tilings.

3.3.2. Energy Functional of AdS

Before proceeding to the discretization of the Klein-Gordon equation on hyperbolic tilings, let us briefly review why exactly the BF bound is known as a *stability* bound. The quick & dirty argument states that locally transforming AdS space into flat space induces a shift in the mass-squared of the scalar field of the form $m^2\ell^2 + d^2/4$. This mass term acts as a potential in the Lagrangian, meaning that now there is a stable potential

minimum for the field if $m^2\ell^2 > -d^2/4$. This means that stable field configurations of the bulk scalar field are allowed to have slightly negative mass-squared and still be admissible solutions to the equations of motion. This argument is a nice and short way of describing the origin of the bound, namely the fact that the original space is negatively curved. However, to understand more precisely where a bona fide instability arises, we review parts of the original computation together with an extended analysis done in [600].

From the perspective of the bulk gravitational theory, the BF bound is related to the real-valuedness and positivity of the gravitational energy functional of the scalar field. If the energy is negative or develops a non-vanishing imaginary part, the system is considered to be unstable [196, 197]. Given the action (3.72) with $\mu, \nu = \{\theta, \phi\}$ in the coordinates used in (3.71), we can compute the corresponding stress-energy tensor $T_{\mu\nu}$ through the variation

$$T_{\mu\nu} \equiv \frac{2}{\sqrt{g}} \frac{\delta S}{\delta g^{\mu\nu}} \,. \tag{3.83}$$

Its explicit expression for the scalar field reads

$$T_{\mu\nu} = \partial_\mu \Phi \partial_\nu \Phi + \frac{1}{2} g_{\mu\nu} \left(g^{\rho\sigma} \partial_\rho \Phi \partial_\sigma \Phi + m^2 \Phi^2 \right) \,. \tag{3.84}$$

It turns out that the total energy functional of the full gravitational system plus scalar field decomposes into a contribution from the metric and a contribution from the bulk field. The gravitational contribution was shown to always obey positivity in [601]. As for the contribution from the scalar field, it reads

$$E\left(T_{\mu\nu}\right) = \int_0^{\frac{\pi}{2}} d\theta \, T_{\phi\phi} \,, \tag{3.85}$$

where the integrand denotes the "temporal" component of the stress-energy tensor, which in Euclidean signature is simply given by the angular coordinate ϕ. Plugging (3.84) into (3.85), we find

$$E\left(T_{\mu\nu}\right) = \int_0^{\frac{\pi}{2}} d\theta \left(\frac{3}{2} \left(\partial_\phi \Phi\right)^2 + \frac{1}{2} \left(\partial_\theta \Phi\right)^2 + \frac{1}{2} \frac{m^2 \ell^2}{\cos(\theta)^2} \Phi^2 \right) \,. \tag{3.86}$$

At first glance, it may seem that this expression is manifestly positive and real, but upon closer inspection, we see that the potential term may give negative contributions for negative values of the mass-squared. The first term is however always positive and we may therefore neglect it for our current purposes. We now employ an ansatz for our scalar field of the form $\Phi(\theta) = \cos(\theta)^\Delta \tilde{\Phi}$, with the goal of re-writing the terms

in the functional (3.86) in a properly manifestly positive manner. Notice that, in this ansatz, the exponent Δ is *a priori* not specified, and it's just a parameter of the ansatz. However, we denote it with a suggestive notation in view of the scaling dimension later on. Inserting this ansatz into (3.86), we find the following expression after an integration by parts

$$E\left(T_{\mu\nu}\right)=\int_0^{\frac{\pi}{2}}d\theta\cos(\theta)^{2\Delta}\left(\left(\partial_\theta\tilde{\Phi}\right)^2+\left(\Delta+\frac{\Delta(1-2\Delta)\sin(\theta)^2+\Delta^2+m^2\ell^2}{\cos(\theta)^2}\right)\tilde{\Phi}^2\right)\\ -\left[2\Delta\cos(\theta)^{2\Delta-1}\sin(\theta)\tilde{\Phi}^2\right]_0^{\frac{\pi}{2}}\,. \tag{3.87}$$

For the boundary term, it was proven in [196, 197] that it vanishes for normalizable modes, and later the same was shown in [600] for non-normalizable modes. Therefore, it only remains to guarantee the real-valuedness and positivity of the integrand. By choosing the coefficient in our ansatz to obey $\Delta=\frac{1}{2}+\sqrt{\frac{1}{4}+m^2\ell^2}$, we can write

$$E(T_{\mu\nu})=\int_0^{\frac{\pi}{2}}d\theta\cos(\theta)^{2\Delta}\left((\partial_\theta\tilde{\Phi})^2+\Delta^2\tilde{\Phi}^2\right)\,. \tag{3.88}$$

This last expression is manifestly real and indeed positive as long as Δ is real. This, in turn, requires $m^2\ell^2\geq-\frac{1}{4}$, which is precisely the BF bound (3.79).

3.3.3. The Klein-Gordon Equation on Hyperbolic Tilings

We are now in position to elucidate how the BF bound can be identified on discretizations of EAdS_2 via hyperbolic $\{p,q\}$ tilings. For this, we will work with a discretization of the system where the scalar field is now restricted to take values only on the vertices of the lattice, and we will perform a numerical analysis of a discretized version of the Klein-Gordon equation. More precisely, we will consider a scalar function $\Phi(\theta,\phi)$ which on the tiling takes on a discrete set of values $\Phi_j=\Phi(\theta_j)$, with j simply labeling the vertices of the truncated tiling. Moreover, we denote our discretization of the Laplace-Beltrami operator on hyperbolic $\{p,q\}$ tilings by $\tilde{\Box}$. We define the action of this discrete operator on the scalar field as

$$\left(\tilde{\Box}\,\Phi\right)_j=\sum_{k|j}w_{jk}\ell^{-2}(\Phi_k-\Phi_j), \tag{3.89}$$

where $k|j$ denotes a summation over the q neighboring sites k of site j. This action amounts to a discretization via a weighted finite difference, as is usual in lattice computations, were the weight factors w_{jk} are obtained as follows. First, notice that all

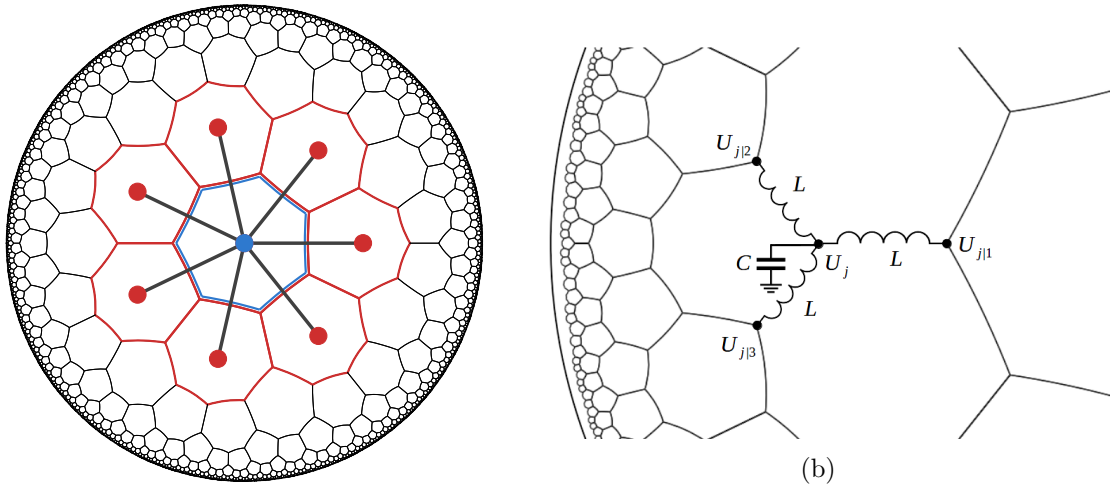


Figure 3.12: Left: Definition of the stencil of weights used for discretizing the Laplace-Beltrami operator in (3.93), shown on the exemplary case of a $\{7,3\}$ hyperbolic tiling [157]. The central node (blue) carries a weight of $-7w^{(7,3)}$, while the neighboring nodes (red) are each associated to constant weights $w^{(7,3)}$. Numerical values for these weights for different choices of Schläfli parameters are given in Tab. 3.1. Right: Schematic illustration of the arrangement of circuit elements according to the geometry of the $\{7,3\}$ tiling, as used in Sec. 3.3.4. U_j denotes the node voltages, while L and C denote inductors and capacitors, respectively.

tiles in a hyperbolic tiling are isometric, in the sense that locally they all look equivalent to one another. Their different aspect ratio in figures is simply an artifact of the embedding of the non-compact $\mathbb{D}^2$ space into a finite disk. Therefore, it is clear that all weights associated to a tile (or, equivalently, a vertex) have to be equal $w_{j,k} \equiv w$, as depicted in the left panel of Fig. 3.12 for the weighing of a $\{7,3\}$ tile. Therefore, we can formally write our lattice operator as a matrix

$$\tilde{\Box} - m^2 \equiv w\ell^{-2}(A - G) + M, \tag{3.90}$$

which acts on a vector of function values $\Phi = (\Phi_0, \Phi_1, \ldots)$. In the equation above, we have $M = \mathrm{diag}(-m^2)$, and the objects A and G denote the so-called *adjacency* and *degree* matrices, respectively. If we take the vertex labels j as naturally defining a set of basis vectors of the form $|0, \ldots, 0, 1, 0, \ldots\rangle$, where the 1 appears at the j-th position, then we can write the adjacency matrix as $A_{ij} = 1$ if there is an edge connecting sites i and j, and 0 otherwise. Similarly, the degree matrix takes into account the connectivity of each vertex, and for hyperbolic $\{p,q\}$ tilings it's simply a multiple of the identity, i.e. $G = q\mathbb{1}$.

Based on this, we compute the weights w by imposing that our discretized Laplace-

Beltrami operator acts on a test function in the same way that a standard second-order differential operator would act in the continuum. For this, recall that for recall approximating a second derivative by finite differences, we write $\tilde{\partial}_x^2\chi(x) = w(\chi(x-h) - 2\chi(x) + \chi(x+h))$. We now look for a test function $\chi(x)$ such that $\partial_x^2\chi(x) = 1$, namely $\chi(x) = \frac{1}{2}x^2$. If we now apply the discretized version of a derivative to this function, we of course find $\tilde{\partial}_x^2\chi(x) = h^2 w$, which therefore fixes $w = h^{-2}$. Thus, we proceed in the same manner for finding the weights appearing in (3.89), albeit here the hyperbolic lattice spacing h is fixed depending on the Schläfli parameters, namely the edge length s_0 computed in (3.22). For the hyperbolic tiling, we have thus to find a radially symmetric test function $\chi(\theta)$ such that

$$\Box\chi(\theta) = \frac{1}{\ell^2}\Big(\cos^2\theta\cot\theta\,\partial_\theta + \cos^2\theta\,\partial_\theta^2\Big)\chi(\theta) \;=\; 1\,. \tag{3.91}$$

One can check that a possible solution is

$$\chi(\theta) = \ell^2\,\log\Big(1 + \frac{1}{\cos\theta}\Big)\,. \tag{3.92}$$

We may now apply our discretized Laplace-Beltrami operator (3.89) to this function to the stencil shown in the left panel of Fig. 3.12, finding

$$\tilde{\Box}\chi(0) = p\,w\Big(\chi(\theta^{(p,q)}) - \chi(0)\Big) = 1. \tag{3.93}$$

Solving for w in the equation above, we can find the corresponding weight factors for every $\{p,q\}$. We list some examples of their exact numerical values in Table 3.1, together with the corresponding values of the lattice constant, denoted by $\theta^{(p,q)}$. Having

$\{p,q\}$	$w^{(p,q)}$	$\theta^{(p,q)}$
$\{3,7\}$	4.213387	0.5382155
$\{4,5\}$	0.928414	0.9045569
$\{4,6\}$	0.616576	1.0471976
$\{5,4\}$	0.541067	1.0147126
$\{6,4\}$	0.240449	1.2309594
$\{7,3\}$	0.503616	0.9224420
$\{8,3\}$	0.233732	1.1437177

Table 3.1: Numerical values for the weights derived from equation (3.93), together with the edge lengths for the tilings used in Fig. 3.13.

found a suitable discretization of the Laplace-Beltrami operator, given by our lattice Laplacian $\tilde{\Box}$ in (3.89) with weights computed as explained above, we are now able to re-express the continuum Klein-Gordon equation on EAdS_2 as an equation on the

finite hyperbolic tiling as

$$\begin{aligned} \tilde{\Box}\,\Phi - m^2\Phi = 0 \quad \text{for} \quad \theta < \theta_c, \\ \Phi(\theta) = \Phi_c \quad \text{for} \quad \theta = \theta_c\,, \end{aligned} \tag{3.94}$$

where the Dirichlet boundary conditions for the field are implemented by assigning constant values to sites of the tiling that lie outside the radial cutoff θ_c. Their role will become clear in the next subsection. The expressions in (3.94) represent a well-defined discrete boundary value problem, which can be tackled with a combination of different numerical methods, the most prevalent one being iterative matrix methods [602, 603]. When applying these methods, their stability needs to be taken into consideration, specially for negative values of m^2, where the lattice operator $\tilde{\Box} - m^2$ becomes indefinite and standard solvers become unstable [604]. This case can be treated with a class of algorithms called Krylow subspace methods [605], of which specifically the GMRES (generalized minimum residual) [606] and BiCGSTAB (biconjugate gradient stabilized) [607] methods were used in our numerical analysis of (3.94). The generation of the tilings and the positions of the coordinates for large system sizes was performed using the *HyperTiling* package [608]. In this way, we are able to numerically find solutions to (3.94) and investigate and extract the positions of the Umklapp points for different choices of hyperbolic $\{p, q\}$ tilings. The combined results from both algorithms mentioned above turn out to be fully compatible with one another, and we present them in Fig. 3.13 for various choices of the Schläfli parameters and values of the cutoff. As a reference, the analytically derived values obtained from the continuum derivation in Sec. 3.3.1 are shown as a black dashed curve. We see that all curves for different values of p and q not only nicely match the continuum prediction, but they also converge towards $m^2\ell^2 = -1/4$ for $\varepsilon \to 0$. This behavior thus confirms that truncated hyperbolic tilings are already a very good approximation of the continuum, and this approximation becomes even better as the lattice size is increased. In fact, we can even give an explanation as to why the results seem to be independent of the choice of Schläfli parameters. This universal behavior is ultimately a consequence of the symmetries of hyperbolic tilings, cf. Sec. 3.2.3. Namely, we have shown that for Fuchsian groups if the first kind, as is the case for the isometry groups of infinite hyperbolic tilings, the limit set at infinity is the entire circle S^1. In turn, this implies conformal invariance of the CFT living on this circle, even though the bulk has been discretized. CFT data like the scaling dimensions of the boundary operators are therefore not affected by the bulk discretization, and thus the threshold at which Δ becomes complex is still given by the continuum BF bound, as per the relation (3.78).

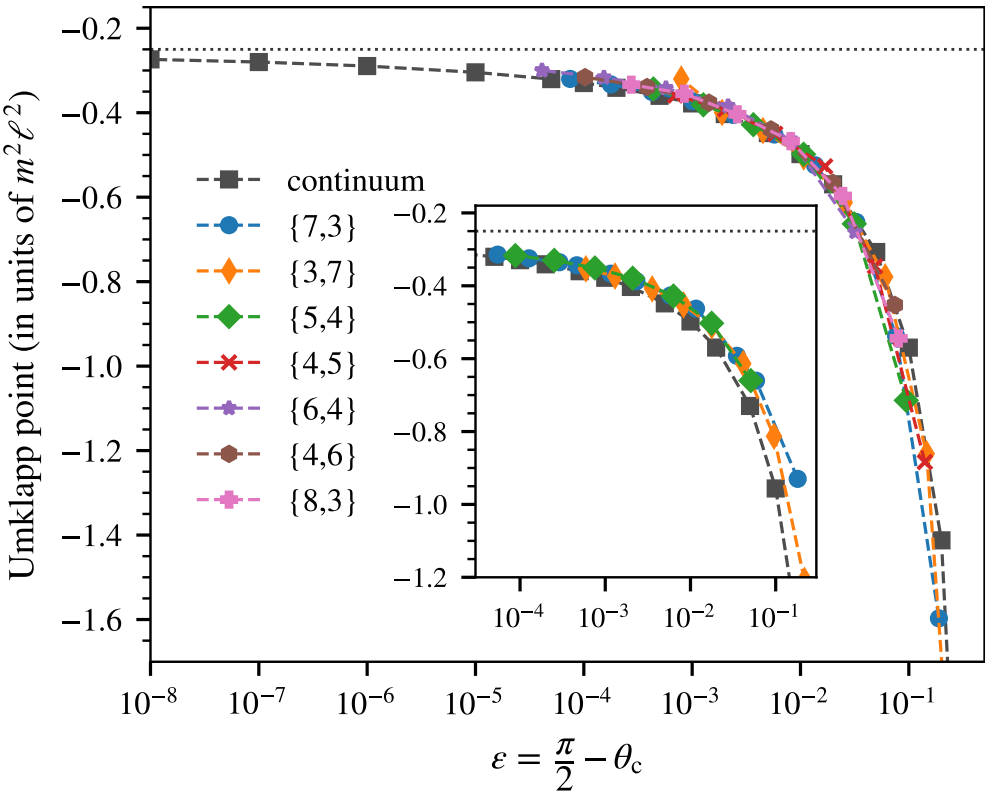


Figure 3.13: Comparison of the results for the dependence of the first Umklapp point on the cutoff, with data obtained from the analytical solutions (3.74) (dashed black line), the numerical simulations based on a discretization of the Laplacian (3.94) (colored markers), and the electric circuit simulations (3.103) (inset) approaches. We observe excellent agreement between all three data sets. Furthermore, we see that all curves tend to the continuum bound $m^2\ell^2 = -1/4$ (dotted horizontal line) as the radial cutoff ε is taken to zero.

This means that the asymptotic value of the first Umklapp point, used here as a signal of the onset of instability, must be the same for any choice of p and q when the cutoff is removed $\varepsilon \to 0$. This approach is universal, and our results shown in Fig. 3.13 indeed indicate that even when a cutoff is present, and the Fuchsian symmetry is broken, the $\varepsilon \to 0$ behavior is preserved for all p and q.

3.3.4. Hyperbolic Electric Circuits

As a final consideration, let us introduce an experimental platform that can be utilized to actually measure the predictions derived above, namely *hyperbolic electric circuits*. These circuits play a key role in several fields of physics, being used as investigation playgrounds for metamaterials, topological properties, lattice symmetries, and of course emulation of negatively curved spaces in view of holography [448, 517–519, 522, 523, 549–560, 563–566, 608–628]. We will encounter them again in the next section, so let us give a brief general introduction into their properties. It is

however worth mentioning that besides the hyperbolic electric circuit implementation shown here, there exist other suggestions for realizing a lattice discretization of hyperbolic space based on differently engineered platforms spanning from circuit quantum electrodynamics and coplanar waveguides [562, 563], to topolectrical circuits [448, 564, 565, 619, 629–633] and topological photonics [561, 634, 635], all the way over to simple mechanical elastic lattices [636].

General Electric Circuits

The idea of hyperbolic electric circuits lies on the integration of classical electrical components, like Ohmic resistors R, capacitors C, inductances L, or even active elements like diodes, on a single motherboard architecture. The layout of these components, in particular their connectivity, follows that of hyperbolic tilings, cf. the right panel of Fig. 3.12. An electric signal, sent through the electrical network and propagating according to the classical Kirchhoff laws, functions as a probe of the underlying curved geometry. Simple voltages and currents passing through the networks nodes mimics the dynamics of a scalar field propagating on a curved space. The simplicity of this platform allows for an ease of manufacture and production, allowing for an unprecedented development and deployment of table-top experiments for the realization of phenomena on negatively curved space.
In the case of a linear RLC electric circuit, the voltages associated the elements mentioned above are known and read

$$U^R = RI\,, \quad U^C = \frac{Q}{C}\,, \quad U^L = -L\dot{I}\,. \tag{3.95}$$

Here, I denotes the current running through the element, which is equal to the time-derivative of the electrical charge Q. The equations describing the flow of current from node i to node j can be derived from Kirchhoff's laws. More precisely, when connecting all three components in parallel, the total current I between two nodes i, j is the sum of the individual currents, while the voltage is equal throughout, i.e. $U^R = U^C = U^L \equiv U$. Therefore, we find

$$C\ddot{U} + \frac{\dot{U}}{R} - \frac{U}{L} = \dot{I}\,, \tag{3.96}$$

where $U \equiv U_i - U_j$ is the voltage difference between the nodes. These equations are readily generalizable to a network of such nodes, i.e. a circuit, where the aforementioned elements can be connected in parallel at each node $i = 1, 2, \ldots$ [565]. The

general Kirchhoff law for the full circuit reads

$$I_i = \sum_j \mu_{ij}(\omega) U_j \,, \tag{3.97}$$

where I_i, U_i are the external input current and the local voltage amplitude at node i, respectively. The matrix $\mu_{ij}(\omega)$ is called the *grounded circuit Laplacian* and is in general dependent on the angular frequency used to drive the system [630]. It is given by

$$\mu_{ij}(\omega) = -\mathrm{i}\omega C_{ij} + \frac{1}{R_{ij}} - \frac{1}{\mathrm{i}\omega L_{ij}} \,, \tag{3.98}$$

where we have used indices in the electrical element symbols to denote that these may in principle vary throughout the network. However, we will only deal with homogeneous networks where $(C, L, R)_{ij} = (C, L, R)$. Given any underlying graph, the equation (3.97) provides the time evolution of currents and voltages throughout the electric circuit.

Hyperbolic Electric Circuits

We now wish to implement the above framework to construct hyperbolic electric circuits. For the purposes of interest in [157], we consider each vertex of a hyperbolic tiling as a node, and we attach grounded capacitors C to each node, while connecting neighboring nodes on the tiling by identical inductances L.[12] One can think of these inductances as running along the edges of the polygons for clarity, but the actual separation of the nodes in the experimental implementation is irrelevant. In such a network, and according to the relations (3.95), the local voltage U_j at site j is related to the capacitor current by

$$I_j = C\dot{U}_j \,, \tag{3.99}$$

and the voltage differences between neighboring sites k of j are given by the induced current

$$(U_k - U_j) = L\dot{I}_{jk} \,. \tag{3.100}$$

Put together, the previous two expressions form a system of $2N$ coupled first-order differential equations, where N is the number of nodes in the truncated tiling. These equations are solved by integrating them using a fourth-order Runge-Kutta method [157, 637, 638]. The Dirichlet boundary conditions of (3.94) are imposed by only iterating the nodes within the cutoff radius $\theta_c < \frac{\pi}{2}$ according to the dynamic rules

[12] This is a matter of convention. Exchanging the role of inductances and capacitors with respect to the ground would only change the dependence of the local impedances $Z_i(\omega) = U_i/I_i$ on the frequency from $\propto \omega^2$ to $\propto 1/\omega^2$ [565].

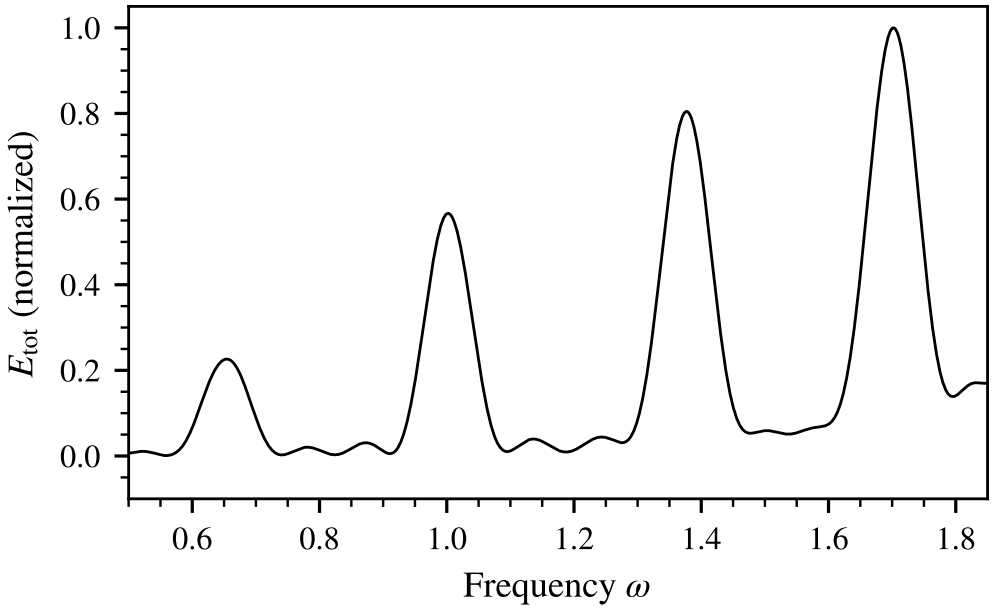


Figure 3.14: Frequency response of the normalized total energy E_{tot} of the circuit as defined in (3.101). The dependence on the driving frequency ω is measured after the external drive has been shut down. Peaks in the plot correspond to resonant frequencies of the system.

(3.99)-(3.100), while nodes outside of this cutoff are grounded without an additional capacitor. They are thus effectively not updated during the simulation. Consequently, their voltages remain constant to a tunable value, i.e. $U_j(t) = \text{const}$ for $\theta(x_j) > \theta_c$, thus imposing the desired boundary conditions. The system is prepared to an initial state with known voltages (usually zero) on all nodes, and then an alternating driving voltage with frequency ω_d is applied to the central site $U(x_0, t) \equiv U_0(t) \propto \sin(\omega_d t)$. This external driving force induces an oscillation of the voltages throughout the network. We want to identify the lowest eigenfrequency of the system, since this will correspond to the first Umklapp point. Thus, we gradually scan the driving frequency ω_d and detect all points $\omega_{c,0} < \omega_{c,1} < \dots$ where the response of the system shows a resonant behavior. A very convenient way of monitoring these resonances is by tracking the total energy, given as

$$E_{\text{tot}} = \frac{1}{2} C \sum_j U_j^2 + \frac{1}{2} L \sum_{k|j} I_{jk}^2. \tag{3.101}$$

This energy is not to be confused with the gravitational energy functional considered in (3.86), since (3.101) is simply the total electric energy in the circuit obtained from Kirchhoff's laws and defined with respect to an auxiliary time parameter. It is a physically independent and different quantity to the gravitational energy of the curved spacetime. The total energy (3.101) is expected to exhibit sharp peaks whenever a

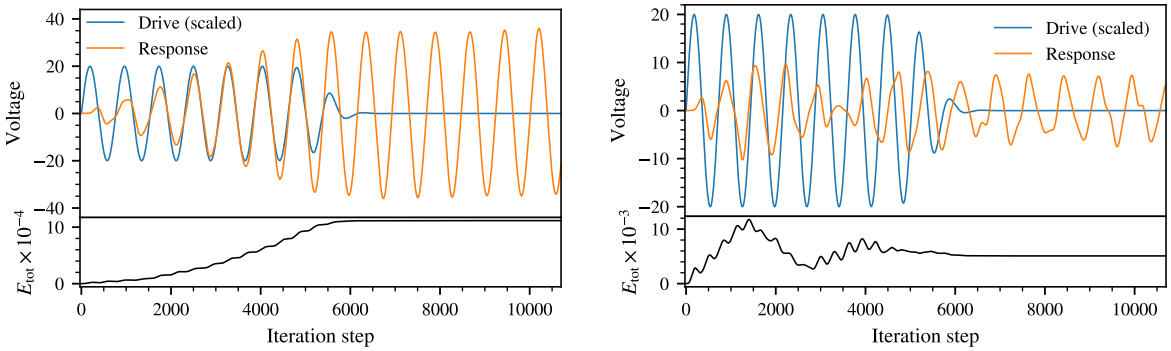


Figure 3.15: Left: Voltage response (orange) of a node in the fourth layer as a response to the driving voltage (blue) over time (measured in iteration steps of the Runge Kutta method). The driving voltage is set to exactly the fundamental resonance frequency of the system, leading to a sustained oscillation even after the driver is shut down. Right: Same quantities but with a driver set away from the resonance frequency, leading to dissipation of the driving and a decay of the total energy of the system, shown below each panel.

resonant frequency is driving the system. The behavior of E_{tot} obtained from our simulations as a function of the driving frequency ω_d is shown in Fig. 3.14 for the exemplary case of a circuit with the connectivity of a $\{7, 3\}$ tiling. We can indeed identify several resonance peaks in the circuit, which we interpret as a physical manifestation of the Umklapp points introduced above. A curious researcher might wonder whether the identified frequencies are real eigenfrequencies of the circuit, or whether they are just artifacts of the driving force. To check this, once the resonant frequency is hit, we shut down the external drive and let the circuit oscillate independently. If the found frequencies are indeed eigenfrequencies of the circuit, then we should expect the steady state to continue oscillating even in absence of a driving force, which is indeed what we observe in Fig. 3.15 by tracking the voltage response of the system. Furthermore, we can perform a second verification by computing the Fourier spectra of the free oscillation of the circuit after shutting down the driving force. The results are shown in Fig. 3.16, and we can see that for the case of the fundamental mode $\omega = \omega_{c,0}$, we indeed find only one sharp peak in an otherwise empty spectrum, indicating that this is an eigenfrequency. Upon identification and verification of this first eigenmode, we compute the corresponding eigenfrequency $\omega_{c,0}$ by fitting a Lorentzian profile to the corresponding peak in Fig. 3.14 and subsequently reading off the maximum value. As we will see below, this frequency can be then related to the corresponding value of the mass-squared of the Klein-Gordon field.

More precisely, we can derive a relation between the eigenfrequencies of the system and the mass-squared parameter in the following way. The equations governing the

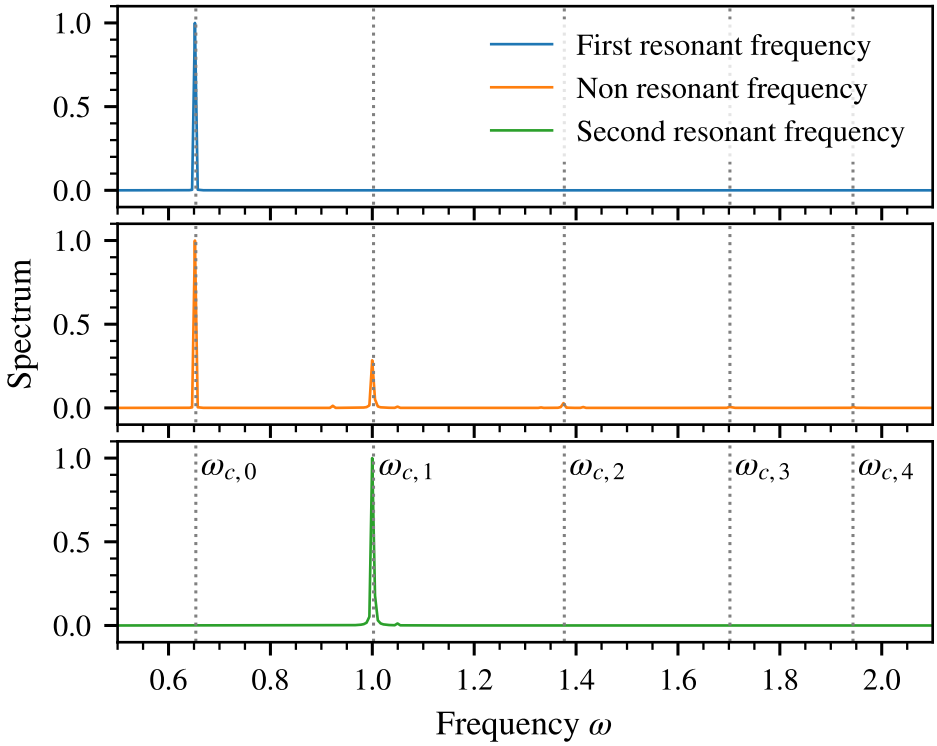


Figure 3.16: Exemplary response spectra when scanning the driving frequency for a circuit with cutoff $\theta_c \approx 1.5644098$. The upper, middle, and lower panels correspond to driving frequencies of $\omega_d = \omega_{c,0}$, $\omega_d = 0.8$, and ≈ 0.653589, respectively. The middle panel shows the response for a non-resonant frequency, yielding multiple response peaks.

time-evolution of circuit voltages derived from (3.97) for this specific circuit read

$$\ddot{U}_j = \frac{1}{LC}\sum_{k|j}(U_k - U_j). \tag{3.102}$$

Note that the time coordinate entering this equation is a simple laboratory time which is used as an auxiliary parameter. We expect solutions to (3.102) to be oscillatory eigenmodes of the $U_j(t) = u_j e^{i\omega t}$, which are obtained from the system of equations

$$-\omega^2 U_j = \frac{1}{LC}\sum_{k|j}(U_k - U_j) = \frac{w^{(p,q)}}{LC}\tilde{\Box}U_j\,, \tag{3.103}$$

where in our case, the weights are constant $w_{jk} = w^{(p,q)}$ and are given in Table 3.1. We can now perform the identification

$$-m^2\ell^2 = \omega^2\frac{LC}{w^{(p,q)}}, \tag{3.104}$$

which allows us to translate the eigenfrequencies of the electric circuit to the values of the mass-squared of the scalar field in the EAdS_2 bulk. We therefore find that our hyperbolic electric circuits as defined in this section provide a realization of the discretized Klein-Gordon equation for $m^2\ell^2 < 0$. We expect that the regime $m^2\ell^2 > 0$ can be attained by introducing active elements into the circuits, or with the use of negative impedance converters to achieve negative values of L or C on the r.h.s. of (3.104). Nevertheless, for the purposes of identifying the BF bound, the regime of (3.104) is sufficient. As can be seen from the identification (3.104), and as alluded to previously in this section, the first Umklapp point corresponds the lowest eigenfrequency of the circuit. We can perform the analysis detailed above for several different hyperbolic $\{p, q\}$ tilings and for different choices of the cutoff radius, and extract the lowest eigenfrequency of the circuit in all these cases. This comprises the final set of data shown in Fig. 3.13, and indeed we observe an excellent agreement with the continuum prediction.

The results reported above show how the celebrated Breitenlohner-Freedman instability bound (3.79) can be realized in lattice discretizations of EAdS_2 via hyperbolic $\{p, q\}$ tilings. Our analysis sheds light on the manifestation of this bound on finite-sized truncated tilings and corresponding passive electric circuits. The presence of a cutoff and a suitable choice of boundary conditions are exploited to keep track of Umklapp points, the first of which signals the onset of unstable solutions below the BF bound. We also clarified the precise nature of this instability, showing that it is related to the threshold where the gravitational energy functional ceases to be real and positive. Both in the presence and upon removal of the finite cutoff, our results show excellent agreement with the continuum, manifesting that hyperbolic tilings are indeed a fine lattice approximation to continuous hyperbolic space.

3.4. Simulating Conformal Field Theories on Hyperbolic Tilings

In the previous section, we saw compelling evidence that hyperbolic tilings are a prominent candidate for discrete realizations of holography. Being able to reproduce a hallmark gravity result such as the BF bound justifies a further investigation into the range of phenomena accessible via hyperbolic tilings. Thus, in this section, which is largely based on the results reported in [160] and follows the presentation therein closely, I showcase the flexibility of hyperbolic tilings by simulating properties of con-

formal field theories. As a by-product of these investigations, we find connections between our lattice realizations of hyperbolic space and some aspects of black holes. Taken as a whole, our findings support the choice of hyperbolic tilings as a cornerstone of the larger discrete holography program pursued in this thesis. Further details to the computations presented here can be found in the Supplemental Material of [160].

3.4.1. Holographic Lattice Model

As a starting point, let us note that Einstein gravity in two-dimensions is a topological theory without propagating degrees of freedom. This is a consequence of the fact that any two metrics g, g' are conformally equivalent, meaning that their respective line-elements can be written as $\mathrm{d}s^2 = e^{\varphi} ds'^2$, where the conformal factor is uniquely defined by a single local field φ. Some properties, like the BF bound, may still be derived, since these rely only on the negative curvature of the space. However, other aspects which are associated to proper fluctuations of the metric tensor g cannot really be investigated. One can, nevertheless, find instances in which even two-dimensional gravity gives rise to interesting physics. One highly celebrated such instance is given by an approach suggested by Polyakov to describe two-dimensional quantum gravity as the geometric world-sheet theory of a critical bosonic string [639]. The details pf this argument are not relevant for our purposes here, but the take-home message is that a good candidate for describing two-dimensional quantum gravity is given by so-called *Liouville gravity* [640, 641]. We review this theory shortly below to show its relation to the theory of Riemann surfaces, and in particular how we can regard EAdS_2 as a solution of this theory.

We follow the presentation of [640] closely. From the point of view of the gravity theory, the idea is to start with an action for a scalar mode describing the fluctuations of the metric, coupled to a fixed but arbitrary curved background. By performing a gauge-fixing, we can first get rid of this arbitrariness, and then solve the resulting equations of motion to find a metric solution, which will turn out to be specifically the metric of EAdS_2. Finally, by considering linearized fluctuations about this EAdS_2 background, we obtain the action of a scalar field living on curved space. More precisely, start by considering a metric g, which we assume to obtain by a conformal rescaling from a chosen reference metric $\hat{g}$ called the *fiducial metric*,

$$g = e^{\varphi} \hat{g}_{(\tau)} \,, \tag{3.105}$$

where the parameter τ is a so-called *modulus*, and it parametrizes all metrics in the moduli space of conformally equivalent metrics. Depending on the community, the

field φ is sometimes called Liouville field or dilaton. The study of Liouville field theory starts from the action

$$S = \int ds^2 \sqrt{\hat{g}} \left(\frac{1}{2} \hat{g}^{ab} \partial_a \varphi \partial_b \varphi + \varphi R(\hat{g}) + \frac{\mu}{2} e^{\varphi} \right) , \tag{3.106}$$

where the parameter μ plays the role of a cosmological constant, and $R(\hat{g})$ denotes the Ricci scalar associated to the fiducial metric. We can now pick a suitable gauge and choose the fiducial metric to be that of Euclidean space, i.e. $\hat{g}_{ab} = \delta_{ab}$. Naturally, this metric is flat, and therefore we have $R(\hat{g}) = 0$. One can then obtain a dynamical variation principle for two-dimensional gravity by minimizing the remaining action

$$S = \int ds^2 \frac{1}{2} \left(\partial_a \varphi \partial_b \varphi + \mu e^{\varphi} \right) . \tag{3.107}$$

It is straightforward to derive the equations of motion for the Liouville field by imposing that the variation of (3.107) vanishes. This yields the so-called *Liouville equation*

$$-e^{-\varphi} \nabla^2 \varphi = -\frac{\mu}{2} . \tag{3.108}$$

Notably, the left-hand side of (3.108) can be identified as the definition of the Gaussian curvature

$$\mathcal{K}[g] = -\frac{1}{2} e^{-\varphi} \nabla^2 \varphi , \tag{3.109}$$

for a metric of the form $ds^2 = e^{\varphi}(dx^2 + dy^2)$. Thus, solutions to the Liouville equation (3.106) are metrics of constant negative curvature. To now make connection with our familiar case of EAdS_2, let us choose complex coordinates for EAdS_2, such that the metric indeed takes on the desired form

$$\mathrm{d}s^2 = (2\ell)^2 \frac{\mathrm{d}z \mathrm{d}\bar{z}}{(1 - |z|^2)^2} , \tag{3.110}$$

from which we can easily identify the form of the Liouville field to be

$$\varphi_\star = \log\left(\frac{(2\ell)^2}{(1 - |z|^2)^2} \right) . \tag{3.111}$$

Plugging (3.111) into (3.108), we can see that EAdS_2 is indeed a solution to the equations of motion, upon identifying the cosmological constant $\mu = -2/\ell^2$.
Thus, by gauge-fixing the original Liouville action (3.106) to a flat fiducial metric, we

obtain EAdS_2 as a solution. We are therefore interested in the resulting action

$$S_{\mathrm{LG}}[\varphi] = \int \mathrm{d}^2 z \, \left[\frac{1}{2}(\nabla\varphi)^2 + \frac{2}{\ell^2}e^{\varphi}\right]. \tag{3.112}$$

Since this action vanishes on-shell, we are particularly curious about fluctuations of it around the EAdS_2 solution given by $\varphi_\star$ in (3.111). More precisely, we consider fluctuations of the form $\varphi = \varphi_\star + \phi$, and we split the action as $S_{\mathrm{LG}}[\varphi] = S_{\mathrm{kin}}[\varphi] + S_{\mathrm{pot}}[\varphi]$ to avoid clutter in the expressions. We will now expand both terms in view of the fluctuation $\varphi = \varphi_\star + \phi$. Expanding upon this fixed solution, the kinetic part of the action S_{kin} reads,

$$S_{\mathrm{kin}}[\varphi_\star + \phi] = \int \mathrm{d}^2 z \left[\frac{1}{2}[\nabla(\varphi_\star + \phi)]^2\right] = \int \mathrm{d}^2 z \; e^{\varphi_\star}\left[-\frac{1}{2}\varphi_\star\frac{2}{\ell^2} - \phi\frac{2}{\ell^2} - \frac{1}{2}\phi(e^{-\varphi_\star}\nabla^2)\phi\right]. \tag{3.113}$$

For the potential part S_{pot} we obtain

$$S_{\mathrm{pot}}[\varphi_\star + \phi] = \int \mathrm{d}^2 z \left[\frac{2}{\ell^2}e^{\varphi_\star}e^{\phi}\right] = \int \mathrm{d}^2 z \; e^{\varphi_\star}\left[\frac{2}{\ell^2}e^{\phi}\right]. \tag{3.114}$$

Notice that terms which are independent of ϕ simply give constant contributions and can therefore be neglected in this linearization. As usual, we are interested only in the dynamics of the fluctuation, which we single out by writing $S_{\mathrm{grav}}[\phi] \equiv \Delta S_{\mathrm{LG}}[\phi] = S_{\mathrm{LG}}[\varphi_\star + \phi] - S_{\mathrm{LG}}[\varphi_\star]$, with

$$S_{\mathrm{grav}}[\phi] = S_{\mathrm{kin}}[\varphi_\star + \phi] + S_{\mathrm{pot}}[\varphi_\star + \phi] - S_{\mathrm{kin}}[\varphi_\star] + S_{\mathrm{pot}}[\varphi_\star]. \tag{3.115}$$

Plugging the results obtained in (3.113) and (3.114) into (3.115), and only keeping terms that have a ϕ-dependence and are not higher-order, we find

$$S_{\mathrm{grav}}[\phi] = \int \mathrm{d}^2 z \; e^{\varphi_\star}\left[-\frac{1}{2}\phi(e^{-\varphi_\star}\nabla^2)\phi + \frac{2}{\ell^2}(e^{\phi} - \phi)\right]. \tag{3.116}$$

Our manipulations have therefore lead us from the Liouville action (3.106) for a scalar field coupled to arbitrary background fiducial metrics to a new action, (3.116) which describes scalar fluctuations around the EAdS_2 solution to the Liouville action, gauge-fixed to flat fiducial metric. Crucially, the resulting action in (3.116) is precisely of the Liouville form once again [641], albeit for a hyperbolic fiducial metric obeying $e^{\varphi_\star} = \frac{(2\ell)^2}{(1-|z|^2)^2}$. Note that the linear term $\frac{2}{\ell^2}\phi$ in the action above comes from the curvature coupling term $\phi R(g)$ of the Liouville action evaluated for the constant curvature EAdS_2 metric. In contrast, our starting action S_{LG} was derived from a flat fiducial metric.

The physical difference in terms of the dynamics of the fields is that the fluctuations can be expected to be small since they arise from a saddle-point approximation, while the same assumption is not true in general for the original field φ. We can therefore expand the exponential potential term in (3.116), such that schematically we have

$$S_{\text{grav}}[\phi] = \int \frac{\mathrm{d}^2 z\ (2\ell)^2}{(1-|z|^2)^2}\left[\frac{1}{2}\phi\left(-\Box + \frac{2}{\ell^2}\right)\phi + \frac{1}{3\ell^2}\phi^3 + \frac{1}{12\ell^2}\phi^4 + \dots\right]. \tag{3.117}$$

In order to obtain the expressions above, we have exploited the Liouville equation (3.108) with the solution (3.111) such as to write $\Box = e^{-\varphi_\star}\nabla^2 = \frac{1}{(2\ell)^2}(1-|z|^2)^2\nabla^2$.

The above considerations are purely from the perspective of a gravity theory in two dimensions. However, the result we obtain in (3.117) appears simple enough to lend itself to direct implementations on discrete hyperbolic lattices, following the dictionary put forward in [611]. The idea here is to realize the gravitational action above by means of a simple model defined on a lattice which discretizes the underlying curved geometry, in this case EAdS_2. In the spirit of this chapter, the canonical choice for such discretizations are regular hyperbolic $\{p,q\}$ tilings. Not only are these graphs great approximations of the continuum underlying geometry, but they also introduce explicit dependences on the Schläfli parameters p and q, which we can tune at will. In particular, upon a suitable choice of constants (m,u,μ), and an according field re-definition, we can bring (3.117) into the form

$$S_{\text{grav}}[\phi] = \int \frac{\mathrm{d}^2 z}{(1-|z|^2)^2}\left[\frac{1}{2}\phi(-\Box + m^2)\phi + \frac{u}{3!}\phi^3 + \frac{\mu}{4!}\phi^4 + \dots\right]. \tag{3.118}$$

The key result of these manipulations is that our dynamical theory of gravity in two dimensions can be re-expressed, at a linearized level, in terms of a real scalar field ϕ defined on top of a fixed hyperbolic background given by $\text{EAdS}_2 \cong \mathbb{D}^2$. This scalar field is massive, with the parameter $\hat{m}^2 = q + qh^2m^2\ell^2$ chosen to be related the physical mass m via a dimensionless lattice constant $h = (1 - \frac{\sin^2(\pi/q)}{\cos^2(\pi/p)})^{1/2}$ which takes into account the effect of the discretization via $\{p,q\}$ hyperbolic tilings [611, 622]. Moreover, the scalar field is interacting given the presence of non-linear terms in the action (3.117). The fact that the action (3.117) describes a simple but interacting scalar field implies that it can be effectively simulated via an elementary model on discrete hyperbolic lattices, exploiting the dictionary introduced in [611]. More precisely, we consider the

lattice model defined by the action

$$S(\{\phi_\mu\}) = -\frac{1}{2}\sum_{\mu,\nu}\phi_\mu A_{\mu\nu}\phi_\nu + \sum_\mu\left(\frac{\hat{m}^2}{2}\phi_\mu^2 + \frac{u}{3!}\phi_\mu^3\right), \tag{3.119}$$

where $A_{\mu\nu}$ denotes the adjacency matrix of the graph or lattice $\mathcal{G}$ on which the model is defined [160]. Moreover, $\phi_\mu = \phi(z_\mu)$ is the scalar field variable which only takes values on the sites $z_\mu \in \mathcal{G}$ of the graph. The virtue of (3.119) as a simple tight-binding Hamiltonian enables its realization in any of the platforms mentioned in the introduction of this section, making it a rich playground for exploring a discrete holographic duality. The parameters $\hat{m}^2$ and u are to be seen as inputs of the theory, and they can be tuned to emulate the effect of the non-linear terms present in (3.117), as well as being adjustable experimentally. For the purposes of our current analysis, it is sufficient to consider cubic interaction terms, and we will thus neglect interaction terms beyond ϕ^3 for simplicity. More explicitly, upon replacing $\sum_\nu A_{\mu\nu}\phi_\nu \to (q + qh^2\ell^2\Box)\phi_\mu$ according to [160, 611] in (3.119), and inserting the aforementioned relation $\hat{m}^2 = q + qh^2m^2\ell^2$, we obtain the expression

$$S(\{\phi_\mu\}) = \sum_\mu\left(qh^2\ell^2\frac{1}{2}\phi_\mu(-\Box + m^2)\phi_\mu + \frac{u}{3!}\phi_\mu^3\right), \tag{3.120}$$

from which a direct mapping between experimental parameters $\hat{m}^2, u$ and those in the gravity action $S_{\text{grav}}[\phi]$ in (3.118) can be obtained. Notice how the resulting model (3.119) deviates from Liouville gravity as a consequence of the omission higher order terms. Instead, it describes the dynamics of a self-interacting scalar field on a negatively curved background, whose equations of motion are however indistinguishable from those of a gravitational mode in two dimensions. Furthermore, notice how the action (3.119) only depends on the choice of graph $\mathcal{G}$. For our purposes, hyperbolic $\{p, q\}$ tilings lend themselves as canonical choices for such graphs, at least for considering discretizations of the Poincaré disk $\mathbb{D}^2$, but we stress that the model is well-defined for any choice of graph $\mathcal{G}$. In fact, we will introduce below a graph related to $\{p, q\}$ tilings which effectively emulates a constant-time slice of a topologically non-trivial spacetime containing a black hole.

3.4.2. Discretizing the BTZ Black Hole

We have stressed the fact that the definition of the lattice model given by (3.119) only requires the input of a graph G and values $\hat{m}^2, u$. This unlocks a plethora of potential implementations of the same model when considered on different choices of graphs, which can lead to drastically different physics. Thus far, we have dealt

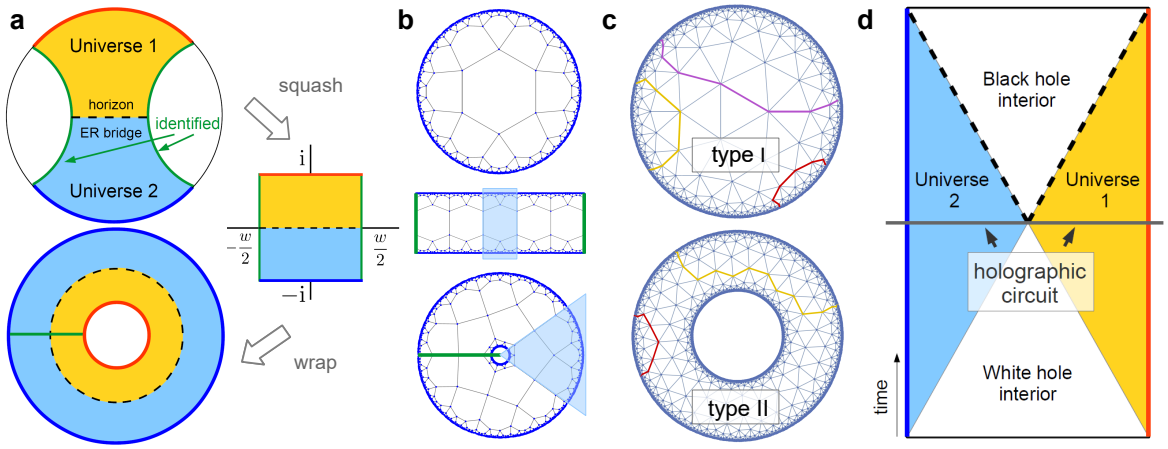


Figure 3.17: (a) Construction from a type-II geometry (coordinates $\hat{z} = \hat{r}e^{i\theta}$) describing a black hole via consecutive squash and wrap transformations on the type-I geometry given by the Poincaré disk (coordinates $z = re^{i\theta}$). The wrap transformation amounts to identifying two geodesics (green) on $\mathbb{D}^2$, which generates two distinct Universes 1 and 2, each with its respective asymptotic boundary, and which are connected by a one-dimensional ER bridge (dashed line) [129, 134]. **(b)** Application of the squash-and-wrap transformation to a type-I hyperbolic flake to generate a type-II flake. This discrete geometry emulates a double-sided BTZ black hole with temperature given by (3.122) with $k = 5$ in this plot. **(c)** Examples of discrete geodesic paths on both type-I and type-II geometries, which are vital for the computation of boundary correlation functions. **(d)** Penrose diagram of a BTZ black hole, with the gray line at $t = 0$ denoting the slice emulated by the type-II hyperbolic lattices. Figure taken from [160].

with hyperbolic $\{p, q\}$ tilings, whose graph tessellates a negatively curved Poincaré disk. We will denote these graphs as *type-I* lattices. A highly intriguing idea, first suggested in [619] and later studied in detail by [160], is that of obtaining a graph which discretizes a time-slice of a black hole. As briefly reviewed in Sec. 2.2.4, black holes are the main ingredient in the holographic dictionary to introduce temperature into holographic dualities, thus lifting their validity from a mere ground-state-to-ground-state identification to a full-fledged correspondence between thermodynamic systems. In lower-dimensions such as AdS_{2+1}, it was shown in 1992 by Bañados, Teitelboim and Zanelli [208, 209] that Einstein's field equations admit a black hole solution, which became to be known as the BTZ black hole. In Sec. 2.2.4, we reviewed in detail how the BTZ black hole can be obtained from the universal cover of AdS spacetime by performing an identification of two geodesics. When working on a constant-time slice, this identification is effected by an element of the hyperbolic translation groups discussed in Sec. 3.2.3 acting on the type-I geometry. The result of this identification is a topologically non-trivial geometry in the form of an annulus, which we obtain by a *squash-and-wrap* procedure as presented in Fig. 3.17. This resulting graph geometry naturally inherits the tiling structure, thus yielding a new graph which tessellates this

annulus. Such a graph was denoted as a *type-II* lattice in [160, 619], and it enjoys two asymptotic boundaries. The squash transformation $z_\mu \mapsto \zeta_\mu = \frac{2}{\pi}\log\left(\frac{1+z_\mu}{1-z_\mu}\right)$,[13] followed by the wrap step $\zeta_\mu \mapsto \hat{z}_\mu = e^{2\pi\mathrm{i}(\zeta_\mu+\mathrm{i})/w}$ maps the Poincaré metric (3.110) to a time-slice of the BTZ black hole [160, 619] given by

$$\mathrm{d}s^2_{\mathrm{II}} = \left(\frac{\ell w}{4}\right)^2 \frac{|\mathrm{d}\hat{z}|^2}{|\hat{z}|^2\cos^2[\frac{\pi}{2}(1-\log|\hat{z}|/\log\hat{r}_{\mathrm{H}})]}\,, \tag{3.121}$$

with $\hat{r}_{\mathrm{H}} = e^{-\frac{2\pi}{w}}$ denoting the position of the black hole horizon. This relation stipulates that, just as we regard type-I lattices as good approximations of the continuum Poincaré disk, we may see type-II lattices as constructed above as discretizations of a constant-time slice of the BTZ black hole. A direct consequence of this finding is the immediate inclusion of black holes into our discrete holographic dictionary, allowing us to bring temperature into discrete realizations of AdS/CFT. In fact, just as in the continuum case, the black hole temperature associated to the type-II geometry can be related to the position of the event horizon and is given by (see Section 3 of the Supplemental Material of [160])

$$T = \frac{w}{8\pi\ell} = -\frac{1}{4\ell\log\hat{r}_{\mathrm{H}}}\,. \tag{3.122}$$

Notice that we have $T \geq 0$ since $\hat{r}_{\mathrm{H}} \leq 1$. In the squash-and-wrap procedure, as well as in numerical simulations to be presented later, we have the relation $w = kP$, where k is a freely chosen integer and $P = P(p,q)$ is a lattice-dependent constant which incorporates the effect of the Schläfli parameters. Upon variation of the parameters (k,p,q), the relation (3.122) grants us access to a large but discrete set of black hole temperatures. An experimental emulation of a black hole is therefore within reach, and we will later provide details on this prospect.

It is now suitable to address a subtle matter regarding the discrete holographic setups based on hyperbolic tilings. All realizations and emulations of negatively curved spaces via discretizations of the Poincaré disk can be seen as instances of what we will denote as *time-slice holography*. The reason is that we typically arrive at the Poincaré disk when viewed as a discretization of a constant-time slice of the larger AdS_{2+1} spacetime. For certain quantities, surprisingly good agreement with theoretical predictions can be found, such as for the Breitenlohner-Freedman bound studied in Sec. 3.3. Nonetheless, it is a greatly valid and non-trivial question to ask which theoretical results exactly should we expect to emulate with lattice models governed

[13] Details can be found in Section 3 of the Supplemental Material of [160].

by adjacency matrices such as that in (3.119). *A priori*, it is not clear whether the result obtained via this approach should reproduce those expected from AdS_3/CFT_2 or rather the more exotic AdS_2/CFT_1. We believe that this is a question of perspective, and it comes down to the precise nature of the physical quantities under consideration. For static quantities which do not directly depend on the behavior of the fundamental degrees of freedom of the theory, as is the case of the BF bound, we have seen that the continuum bound is indeed recovered by the holographic lattice model on the hyperbolic tiling, albeit with a boundary dimension of $d = 1$ instead of the perhaps more naturally expected $d = 2$. In such cases, it is the bulk dimensionality which will determine which theoretical results should be taken as a reference point for comparing with the discrete setup. In contrast, when it comes to dynamical quantities like correlation functions, we have come to the conclusion that the correct way to proceed is to consider derivations and results in AdS_3/CFT_2 and subsequently restrict the solutions to a constant time, usually at $t = 0$. The main reason for this is that correlation functions in holography are computed via smearing kernel functions [642, 643], which take into account contributions from a broad regime in the boundary which extends also in the time direction. In view of comparing the results obtained from the model (3.119) with theoretical predictions, we should consider general results in the complete AdS_{2+1} spacetime and evaluate those at $t = 0$, as sketched in Fig. 3.17d. This is the philosophy we will take in the remaining analysis.

3.4.3. Boundary Correlation Functions

A hallmark result of continuum AdS/CFT is the retrieval of CFT correlation functions from the behavior of bulk fields in the dual gravity theory, as we reviewed in Sec. 2.2.3. To further extend our discrete holographic setup, it is paramount that we investigate how boundary correlation functions can be reproduced by discrete models on hyperbolic lattices such as that given in (3.119). Moreover, the claim that type-II lattices simulate a BTZ black hole can be indeed verified based on the functional form of correlation functions at a finite temperature, as we elucidate below.

Let us begin by splitting the underlying graph on which the model (3.119) is defined into its bulk and boundary components, namely $\mathring{\mathcal{G}}$ and $\partial\mathcal{G}$, such that $\mathcal{G} = \mathring{\mathcal{G}} \cup \partial\mathcal{G}$. In this notation, generic sites of the graph are labeled by the greek indices $\mu, \nu \in \mathcal{G}$, while bulk and boundary sites are labeled by different sets of Roman letters $i, j \in \mathring{\mathcal{G}}$ and $a, b \in \partial\mathcal{G}$, respectively. According to the holographic GKPW dictionary given in (2.23), the AdS/CFT correspondence can be stated as an equivalence between parti-

tion functions of the bulk and boundary theories as

$$Z(\{J_a\}) = \int \Big(\prod_i \mathrm{d}\phi_i\Big) e^{-S(\{\phi_i, \phi_a = J_a\})} \,. \tag{3.123}$$

In other words, the partition function of a holographic CFT is equivalent to a path integral over the configurations of bulk fields in the gravity theory, subject to suitable boundary conditions. For our purposes, these boundary conditions are such that we fix the value of the bulk fields at the boundary sites as $\phi_a = J_a$. Given this constraint, the path integral in (3.123) only runs over bulk field values $i \in \mathring{\mathcal{G}}$. Holography regards $Z(\{J_a\})$ as the generating function for a CFT on the boundary, such that the connected n-point correlation functions of a given CFT operator $\mathcal{O}_a$ can be obtained via standard functional methods

$$\langle \mathcal{O}_{a_1} \dots \mathcal{O}_{a_n} \rangle = \frac{\partial^n \log Z}{\partial J_{a_1} \cdots \partial J_{a_n}}\bigg|_{J=0} \,, \tag{3.124}$$

as we saw in (2.24). Using this prescription, we can study the holographic properties of the lattice model (3.119). For a free model with $u = 0$, we denote the free action by S_0 and write is as

$$S_0(\{\phi_\mu\}) = \frac{1}{2} \sum_{\mu,\nu} M_{\mu\nu} \phi_\mu \phi_\nu \,, \tag{3.125}$$

where $M = -A + \hat{m}^2 \mathbb{1}$ is a real symmetric matrix. In this case, the path integral in (3.119) with $\phi_a = J_a$ on $\partial\mathcal{G}$ can be carried out explicitly due to its Gaussian form as

$$\begin{aligned} Z_0(\{J_a\}) &= \int \Big(\prod_i \mathrm{d}\phi_i\Big) e^{-S_0(\{\phi_i, \phi_a = J_a\})} \\ &= e^{-S_{0,\mathrm{eff}}(\{J_a\})} \,, \end{aligned} \tag{3.126}$$

with the effective generating functional

$$S_{0,\mathrm{eff}} = \frac{1}{2} \sum_{a,b} \Big(M_{ab} - \sum_{i,j} M_{ai} G_{ij} M_{jb} \Big) J_a J_b \,, \tag{3.127}$$

and the bare graph propagator $G_{ij} = (M^{-1})_{ij}$. For the more interesting interacting cases $u \neq 0$, we can study the theory in perturbation theory assuming $u \ll 1$, akin to the semi-classical approximation usually performed in continuous AdS/CFT. This perturbative regime is equivalent to a tree-level truncation of the Feynman diagram expansion for the path integral. This allows us to obtain expressions for the two- and three-point correlation functions of operators on boundary sites given exclusively in

terms of the adjacency matrix governing the model in (3.119). The relevant details to these computations can be found in Section 4 of the Supplemental Material of [160]. The main results are a formula for the two-point function, given by

$$\langle \mathcal{O}_a \mathcal{O}_b \rangle = -M_{ab} + \sum_{i,j} M_{ai} G_{ij} M_{jb} \,, \tag{3.128}$$

where we recall that $M_{\mu\nu} = (G^{-1})_{\mu\nu} = -A_{\mu\nu} + \hat{m}^2 \delta_{\mu\nu}$. An approximate expression reading $\langle \mathcal{O}_a \mathcal{O}_b \rangle \approx G_{ab}$ yields the bulk propagator extrapolated to the boundary sites a, b. As for the three-point function in the presence of interaction $u \neq 0$, we obtain

$$\langle \mathcal{O}_a \mathcal{O}_b \mathcal{O}_c \rangle = u \sum_i B_{ai} B_{bi} B_{ci} \,, \tag{3.129}$$

where $B_{ai} = \sum_j M_{aj} G_{ji}$ denotes the boundary-to-bulk propagator, i.e. the bulk propagator with one of its insertion points extrapolated to the boundary. The expression in (3.129) is a discrete version of a Witten diagram [168] where the bulk site i is summed over, thus incorporating the contributions of bulk-to-boundary propagators to all three boundary sites a, b, c. In the perturbative regime that we are working with, the largest contribution to these diagrams comes from graph-geodesic paths, as shown in Fig. 3.19a. The formula (3.129) lays out a way to compute boundary three-point functions directly from the lattice model (3.119). Since there are no higher-order interaction terms in the action (3.119), all connected n-point functions with $n \geq 4$ vanish identically in our case, while the three point function in (3.129) also vanishes if $u = 0$, as expected from a free theory.

The above derivations give a clear way of computing the boundary correlation functions of the holographic lattice model (3.119), exploiting the fact that the partition function entering the GKPW relation in (3.123) is discrete and finite, and can thus be accessed explicitly. In parallel, however, it is known that conformal invariance in two dimensions starkly constrains the form of two- and three-point correlation functions, as reviewed in Sec. 2.2.2. Their specific forms partly contain parameters of the theory which enable a distinction between different conformal field theories in two dimensions, the so-called *CFT data*. This set of parameters contains objects like the central charge, the spectrum of primary operators and their scaling dimensions, and the leading coefficients of three-point functions, also known as the structure constants [172]. The precise nature of the central charge in the context of discrete holography still remains an intriguing open question, and we will consider it in more detail in later sections, as well as in the outlook of the thesis. On the contrary, access to scaling dimensions and three-point coefficients can be gained taking the expected behavior of

continuous correlation functions and suitably comparing it to the results obtained from the holographic lattice model (3.119). More precisely, two- and three-point correlation functions of a two-dimensional CFT are given by

$$\langle \mathcal{O}_a \mathcal{O}_b \rangle \simeq \frac{1}{(d_{ab})^{2\Delta}}, \quad \langle \mathcal{O}_a \mathcal{O}_b \mathcal{O}_c \rangle \simeq \frac{C_3}{(d_{ab} d_{ac} d_{bc})^{\Delta}}, \tag{3.130}$$

where Δ denotes the scaling dimension of the operator $\mathcal{O}$ (cf. Sec. 2.2.2 and C_3 is the structure constant coefficient. We have taken the liberty of normalizing the boundary fields $\mathcal{O}_a$ such that the numerator of the two-point function is equal to unity. In continuous CFTs, as we saw in Sec. 2.2.2, the functions d_{ab} characterize the distance between the boundary sites a, b, and their exact expression is known, e.g. $d_{ab} = |a - b|$ as measured on the CFT spacetime. Our strategy for the current analysis is to leave these functions undetermined at first, and obtain their expressions based on the data delivered by the holographic model. This test will quantify how well our model can actually reproduce CFT correlation functions. Furthermore, it is a celebrated result of the AdS/CFT correspondence that the scaling dimension of the operator $\mathcal{O}$ and the mass of its holographically dual bulk scalar field are related by (2.27). Moreover, the three-point coefficient C_3 should also be sensitive to the bulk interactions. We will therefore assess the validity of these relations on the discrete setting by varying the bulk parameters $m^2\ell^2$ and u.

To this goal, we compute the two- and three point correlation functions from the holographic model using (3.128) and (3.129), respectively, on both type-I and type-II lattices. The obtained behavior is shown in Figs. 3.18 and 3.19. Remarkably, they show an excellent agreement with the expected behavior in (3.130) upon performing the identifications

$$d_{ab} = \begin{cases} |e^{\mathrm{i}\theta_a} - e^{\mathrm{i}\theta_b}| & \text{type-I} \\ \dfrac{\sinh(\pi T \ell |\theta_a - \theta_b|)}{\pi T \ell} & \text{type-II} \end{cases}, \tag{3.131}$$

where $\theta_{a,b}$ are the angle coordinates of the boundary sites, and the parameter T is precisely the temperature derived in (3.122). A detailed derivation of these two formulas is contained in Section 4 of the Supplemental Material in [160].

The results shown in Figs. 3.18 and 3.19 lead to several key insights which lay the foundations of our model, and it is worth it to go through them individually.
First, the main statement of our results can be highlighted in the following way: Starting from the holographic lattice model (3.119), one can compute two- and three-

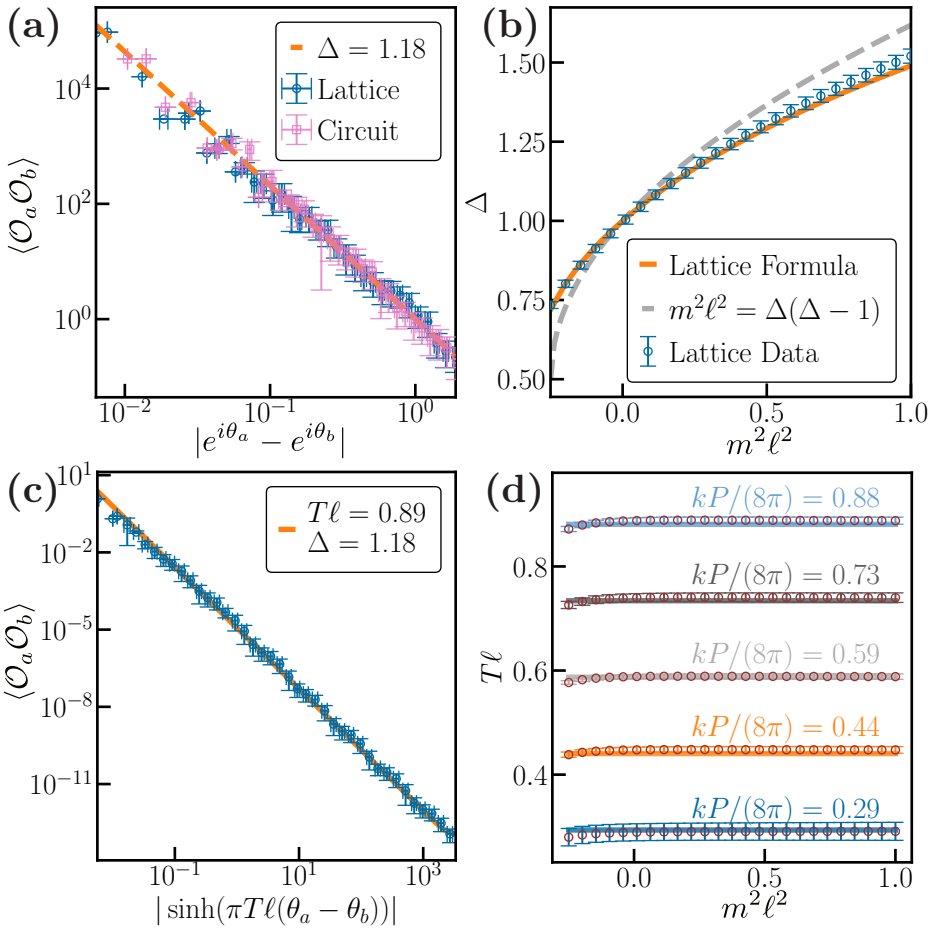


Figure 3.18: (a) Results for the boundary two-point function as a function of the boundary distance for $m^2\ell^2 = 0.271$, as obtained from (3.128) (blue) and from numerical simulations of the electric circuit (3.133)-(3.141) (pink). Binning of lattice coordinates θ_a is the source of the scattering of the results. A fitted power-law behavior (orange), expected from (3.130), allows us to extract the scaling dimension $\Delta = 1.18$ for this example. **(b)** Fitted dependence of the conformal dimension Δ on the mass $m^2\ell^2 > -1/4$ (blue). The lattice corrections (3.132) (orange) lead to a better description of the data by taking into account lattice effects, which lead to a deviation from the continuum relation $m^2\ell^2 = \Delta(\Delta - 1)$ (gray dashed). **(c)** Boundary two-point function for the same mass as in **a** but on the type-II flake. The behavior exhibited coincides with that of a thermal CFT, in agreement with (3.130). **(d)** Black hole temperature (3.122) for several values of k, showing that the latter parameter controls the value of T while it being approximately insensitive to the value of m (and thus Δ). Here, $P \approx 1.845$ for $\{3, 7\}$ and $k = 4, 6, 8, 10, 12$. All results are shown for the exemplary case of a $\{3, 7\}$ hyperbolic flake. Figure taken from [160]

point correlation functions when $u = 0$. Fitting the numerical results to the ansatz given in (3.130), we find that the distance functions d_{ab} governing the decay of these correlations functions have precisely the form (3.131), which presents a discrete version of the standard behavior of correlation functions in two-dimensional CFT. Therefore, we find that the lattice model (3.119) emulates the correlation functions of CFTs

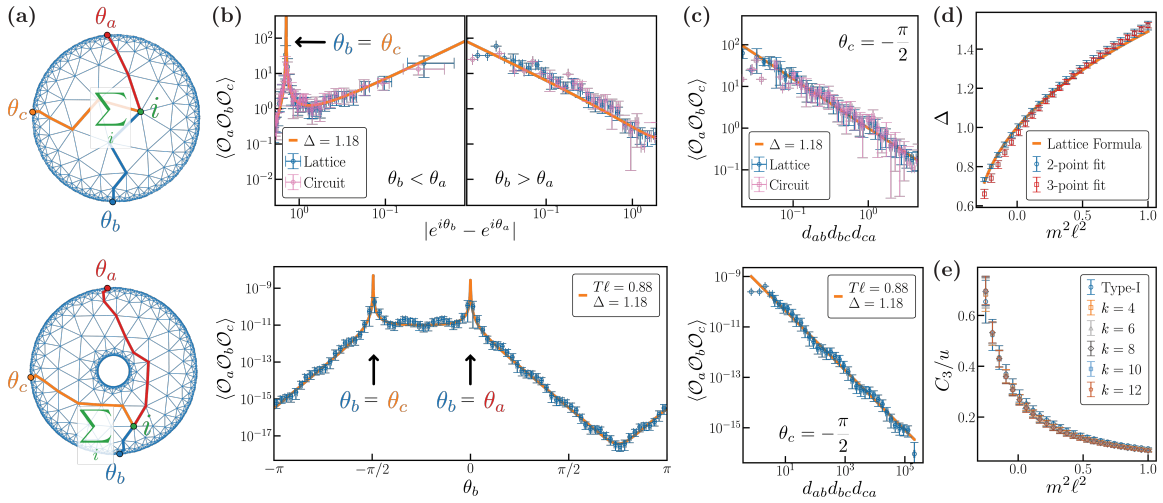


Figure 3.19: Results for the three-point correlation function for type-I (top row) and type-II (bottom row) geometries. In all simulations, the angles θ_a, θ_c of $\mathcal{O}_a, \mathcal{O}_c$ are fixed, while the position of $\mathcal{O}_b$ at angle θ_b is varied. **(a)** Largest contributions to the Witten diagram in (3.129) come from discrete graph-geodesic paths between boundary insertion sites and an arbitrary bulk site i. **(b)** Boundary three-point functions for type-I and type-II flakes, with parameters as in Fig. 3.18, obtained from (3.129) (blue) and electric circuit simulations (3.133)-(3.141) with a realistic diode (pink). The theory prediction is shown in orange, with Δ and T obtained from the two-point function, such that C_3 is the only fitted parameter. Divergences occur when two insertion angles coincide (arrows). **(c)** Fitted characteristic power-law decay $\langle \mathcal{O}_a \mathcal{O}_b \mathcal{O}_c \rangle \propto (d_{ab} d_{ac} d_{bc})^{-\Delta}$ (orange), where $d_{ab} = |e^{i\theta_a} - e^{i\theta_b}|$ for type-I and $d_{ab}(T) = \sinh(\pi T\ell|\theta_a - \theta_b|)/\pi T\ell$ for type-II geometries, respectively, with both lattice and circuit data. **(d)** Compatible dependence of the scaling dimension $\Delta(m^2\ell^2)$ as extracted from both two- and three-point functions on type-I flakes, showing consistency of our approach. **(e)** Extracted dependence of the normalized three-point structure constant C_3/u on the mass from both type-I and type-II lattices. The agreement of the data indicates that the CFTs emulated by both graphs are indeed equal. Figure taken from [160].

on a circle at zero and at finite temperature (3.122). Let us comment that (3.130) with (3.131) are a very good approximation even in type-II lattices, in particular for the two-point functions, although the correct formula for continuous CFTs at finite temperature requires a replacement $\theta_a - \theta_b \to \theta_a - \theta_b + 2\pi n$ in d_{ab} and a subsequent sum over $n \in \mathbb{Z}$ such as to ensure the periodicity of the functions [229]. This sum arises from the method of images required to properly derive correlation functions on the boundary of a double-sided BTZ black hole. Nonetheless, the convergence of the sum over $n \in \mathbb{Z}$ is extremely rapid, meaning that we can focus on the leading terms in (3.130) (a detailed discussion is provided in [160]).

Second, continuing our analysis of the correlation functions shown in Fig. 3.18 and 3.19, we can extract the relation between the bulk mass and the scaling dimension of the boundary operators by varying the parameter m^2 and retrieving the associated Δ

from the numerical simulations. The resulting relation $\Delta(m^2\ell^2)$, extracted from both two- and three-point functions independently for type-I and type-II lattices, is shown in Fig. 3.18b and Fig. 3.19d, where we can see a good agreement between lattice data and the continuous relation (2.27). The fact that we retrieve the same CFT data separately from two- and three-point functions demonstrates the consistency of the emulated CFT, and, vitally, it shows that both type-I and type-II lattices simulate *the same* CFT. The agreement of $\Delta(m^2\ell^2)$ can even be improved by taking into account lattice corrections to this formula. Namely, the continuous relation between Δ and $m^2\ell^2$ is of the form $m^2\ell^2 = f(\Delta(\Delta-1))$ with $f_{\text{cont}}(X) = X$ in the continuum. However, in [611], a gradient expansion for functions on hyperbolic $\{p, q\}$ lattices was derived, which related them to action of the continuous Laplace operator. Taking this gradient expansion into account in the case of the $\{3, 7\}$ tiling yields

$$f(X) \simeq X + \frac{h^2}{4}(X^2 + 2X) + \frac{h^4}{36}(X^3 + 10X^2 + 12X) \tag{3.132}$$

with $h = 0.497$ [157, 160, 551, 615].[14] This relation is shown as a solid orange line in Fig. 3.18b, and an enhanced agreement with the lattice data is then made manifest. Notice that the precise value of h, as well as the form of the function $f(X)$, depend on the specific $\{p, q\}$ lattice, yet a universal continuum limit can be formally recovered for $h \to 0$. Notice that a similar agreement between data for type-I and type-II lattices is observed for the coefficient C_3/u of the three-point function, shown in Fig. 3.19e. In order to retrieve C_3 in a way that reduces scattering of the data as a consequence of the lattice discretization, we construct the function $F_{abc} = \langle \mathcal{O}_a \mathcal{O}_b \mathcal{O}_c \rangle / [\langle \mathcal{O}_a \mathcal{O}_b \rangle \langle \mathcal{O}_a \mathcal{O}_c \rangle \langle \mathcal{O}_b \mathcal{O}_c \rangle]^{1/2}$, which we average over a, b, c to obtain $\langle F_{abc} \rangle \simeq C_3$, cf. the discussion in Section 7 of the Supplemental Material of [160].

Finally, we have stressed that the parameter T appearing in (3.131) is exactly the temperature derived in (3.122). In particular, the parameter k introduced in the transformation from type-I to type-II lattices, governs the resulting temperature at which the emulated CFT is defined via the formula $T\ell = kP/8\pi$, as we show in Fig. 3.18d. Crucially, changing the temperature does not affect the CFT data obtained from the lattice simulations, a behavior that is congruent with that of continuous CFTs. These findings indicate that, just as type-I tilings of the Poincaré disk successfully emulate the physics of a constant-time slice of AdS_{2+1}, type-II lattices are an incredibly good platform for simulating a constant-time slice of a double-sided BTZ black hole, as visualized in the Penrose diagram in Fig. 3.17d. The fact that the squash-and-wrap procedure yields a discretization of a double-sided BTZ black hole, which has an in-

[14] Details can be found in Section 5 of the Supplemental Material of [160].

terior region connecting both Universes, is highly non-trivial, and indeed a separate check for this claim is required. Fortunately, the expected correlations across the horizon for simultaneous operator insertions on opposite boundaries were also computed in [229], and, surprisingly, they are non-vanishing. In the original setting of the AdS/CFT correspondence considered in [229], these non-zero correlations between the two boundaries are a consequence of the entanglement between them, realized geometrically by the ER bridge connecting both exterior regions in the Penrose diagram of Fig. 3.17d. For our lattice model, which can only access the $t = 0$ slice of the Penrose diagram, the ER bridge consists of a single point and has no volume, as portrayed by the horizon line on the annulus shown in Fig. 3.17a. Crucially, our results for the correlation functions (3.130) with (3.131) on type-II lattices yield non-vanishing correlations even if the sites a, b are on different boundaries. This validates our claim that type-II lattices indeed emulate the double-sided geometry instead of two disconnected one-sided black holes.

3.4.4. Measurement Protocol on Electric Circuits

In a similar fashion to Sec. 3.3, we envision an experimental implementation of the conceptual model (3.119) by means of electric circuits. The logic to obtain this such a realization is to derive a map from the equation of motion of the scalar field ϕ_μ, obtained by varying the action (3.119), and an equation of motion for the voltages U_μ. In the following, we present the derivation of these two expressions separately, before imposing their equivalence in order to acquire an explicit mapping.
On the one hand, from the point of view of the lattice model, the equation of interest is

$$-\sum_\nu A_{\mu\nu}\phi_\nu + \hat{m}^2\phi_\mu + \frac{u}{2}\phi_\mu^2 = 0\,, \tag{3.133}$$

where ϕ_μ is the scalar field defined at node z_μ. For a circuit realization, we think of this scalar field as being implemented by a normalized voltage at every node, such that we identify $\phi_\mu \sim \bar{U}_\mu$. The required boundary conditions $\bar{U}_a = J_a$ for the bulk field can be imposed by applying voltage sources on the boundary sites. The equation (3.133) can be realized in an electrical circuit consisting of resistors and diodes. This is different than the RLC circuit we used in Sec. 3.3.4, the reason being that the diodes allow us to introduce non-linearities into the system, which was not possible using only inductors and capacitors. More precisely, the circuits consists of resistors R_0 connecting adjacent nodes of the graph realized by the chosen adjacency matrix, resistors R_g grounding each node, and an additional diode between each node of the graph and ground. The

role of these circuit elements is to realize specific parts of the equation of motion, with resistors yielding the linear couplings $\sum_\nu(-A_{\mu\nu}+\hat{m}^2\delta_{\mu\nu})U_\nu$, while the diodes generate the non-linear potential uU_μ^2. More precisely, the current-voltage relation of a diode is well-approximated by the Schokley equation $I(U)=I_\mathrm{S}(\mathrm{e}^{\frac{U}{U_\mathrm{S}}}-1)$, which reproduces the quadratic interaction terms in the equation of motion when expanded to second order. In this case, we have $I(U)=c_1U+c_2U^2+\mathscr{O}(U^3)$, where c_1,c_2 are diode-dependent constants. Given the boundary conditions, the equation of motion (3.133) only needs to be implemented for bulk nodes $\bar{U}_i$, and we can re-write it as

$$\sum_\nu M_{\mu\nu}\bar{U}_\nu+\frac{u}{2}\bar{U}_\mu^2=0\,, \tag{3.134}$$

with $M_{\mu\nu}=-A_{\mu\nu}+\hat{m}^2\delta_{\mu\nu}$, such that we can obtain

$$\sum_j M_{ij}\bar{U}_j+\frac{u}{2}\bar{U}_i^2=I_i^\mathrm{eff}\,, \tag{3.135}$$

for the bulk sites. The effective bulk source term above reads

$$I_i^\mathrm{eff}\equiv I_i^\mathrm{eff}(\{J_a\})=-\sum_a M_{ia}J_a\,. \tag{3.136}$$

On the other hand, from the point of view of the circuit, we can separately derive the equation of motion for the voltages by adding up all currents flowing out from a given node. Similarly as in Sec. 3.3.4, their behavior is governed by Kirchhoff's current law, which, to second order in the voltages U_i, imposes

$$I_i=\frac{1}{R_0}\sum_j(q\,\delta_{ij}-A_{ij})\,U_j+\frac{1}{R_\mathrm{g}}U_i+c_1U_i+c_2U_i^2\,. \tag{3.137}$$

In this expression, I_i denotes some external current fed into the circuit nodes via a connected fix-voltage source. For no external sources, we have $I_i=0$, while a fixed voltage J_a gives the corresponding current $I_i=I_i^\mathrm{eff}(\{J_a\})$. Note that in any practical or numerical simulations, small parasitic capacitances will arise at each node, which would technically contribute a term of the form $C_i\dot{U}_i(t)$ to (3.137). We will assume these to be sufficiently small such that the circuit reaches its equilibrium state with $\dot{U}_i=0$ instantaneously [160]. Based on these considerations, we can complete the mapping between (3.133) and (3.137) by matching

$$\sum_j(-A_{ij}+\hat{m}^2\delta_{ij})\bar{\phi}_j+\frac{u}{2}\bar{\phi}_i^2\overset{!}{=}c\left[\frac{1}{R_0}\sum_j(q\,\delta_{ij}-A_{ij})\,U_j+\frac{1}{R_\mathrm{g}}U_i+c_1U_i+c_2U_i^2\right]. \tag{3.138}$$

Here, $c = R_0/U_0$ is an arbitrary proportionality constant, while U_0 is a voltage scale that can be set to $U_0 = 1$ without the loss of generality. The matching of coefficients in (3.138) yields the following relations

$$\bar{\phi}_\mu \mapsto U_\mu/U_0\,, \quad \hat{m}^2 \mapsto q + R_0(R_{\mathrm{g}}^{-1} + c_1)\,, \quad u/2 \mapsto U_0 R_0 c_2\,. \tag{3.139}$$

More details on the specific choice and calibration of diodes required to reproduce the values of the mass used in Figs. 3.18 and Fig. 3.19 can be found in the Supplemental Material of [160], but these are not imperative for our current analysis.

The above analysis shows how the equation of motion (3.133) for the bulk scalar field of the holographic lattice model (3.119) can be realized experimentally via an appropriate electric circuit with parameters given in (3.139). It is apparent that the solution $\bar{U}_\mu$ of (3.133) will parametrically depend on the boundary sources J_a, as expected from continuum AdS/CFT. By introducing an auxiliary implementation of time-dependent boundary conditions, i.e. $J_a(t)$, it is possible to conveniently map derivatives in the ancillary parameter t to functional derivatives with respect to J_a, as required by the relation (3.124). More precisely, we can compute the circuit generating functional from the voltage signal $\bar{U}_\mu$ as

$$W_{\mathrm{circ}}(t) = -S(\{\bar{U}_\mu(t)\}), \tag{3.140}$$

where $S(\{\phi_\mu\})$ is the action of our lattice model (3.119). Consequently, in the saddle-point approximation considered here, we have $W_{\mathrm{circ}} \simeq \log Z$. Using (3.140), we propose the following protocol for computing two-point correlation functions from $W_{\mathrm{circ}}(t)$: Apply a linear-ramp drive to the voltages as $(J_a(t), J_b(t)) = (K_a, K_b)(t - t_0)$, crossing zero at $t = t_0$, while the remaining sources are set to $J_\mu(t) \equiv 0$ for $\mu \neq a, b$. This allows us to effectively compute functional derivatives, exploiting the fact that all second-order t-derivatives vanish. In this manner, we obtain

$$\begin{aligned} \frac{\mathrm{d}^2 W_{\mathrm{circ}}}{\mathrm{d}t^2}\bigg|_{t=t_0} &= \sum_{\mu,\nu} \dot{J}_\mu \dot{J}_\nu \frac{\partial^2 W_{\mathrm{circ}}}{\partial J_\mu \partial J_\nu}\bigg|_{J=0} \\ &= K_a^2 \langle \mathcal{O}_a^2 \rangle + 2K_a K_b \langle \mathcal{O}_a \mathcal{O}_b \rangle + K_b^2 \langle \mathcal{O}_b^2 \rangle\,. \end{aligned} \tag{3.141}$$

A system of three linear equations can be obtained by running the above protocol in a series of subsequent measurements for three linearly independent ramps, e.g. $(K_a, K_b) = (1, 0), (0, 1), (1, 1)$. The solution to this system of equations finally yields the two-point function $\langle \mathcal{O}_a \mathcal{O}_b \rangle$ exclusively from voltages on the circuit. We would like to mention that the generic case of n-point functions can be straightforwardly

obtained via the same protocol by linearly ramping the voltages of n boundary sites $J_{a_1}(t), \ldots, J_{a_n}(t)$ in specific independent combinations. For example, the three-point function $\langle \mathcal{O}_a \mathcal{O}_b \mathcal{O}_c \rangle$ is obtained from $\mathrm{d}^3 W_{\mathrm{circ}}/\mathrm{d}t^3|_{t=t_0}$ by using ten linearly independent ramps. The results obtained using this protocol, numerically implemented in the software LTspice, are shown in Fig. 3.18 and 3.19. The excellent agreement with numerical simulations and the analytic predictions provides a clear proof of principle that our holographic lattice model is experimentally realizable.

Our results show that a genuine table-top realization of certain aspects of the AdS/CFT correspondence is realistically attainable via a combination of a holographic model on hyperbolic lattices and non-linear electric circuits. Our widely applicable framework emulates many properties of holographic CFTs with unprecedented accuracy, such as correlation functions, scaling dimensions, and structure constants. Moreover, our technique allows for the realization of thermal CFT behavior emergent from the presence of a double-sided black hole. Together with our proposed measurement protocol, investigations into holographic CFTs using simple electric circuits are within the realm of present-day experimental capabilities.

3.5. Aperiodic Quantum Spin Chains

The previous two sections have showcased the incredible flexibility of hyperbolic tilings when it comes to reproducing holographic features. These results where mostly focused on phenomena which are attainable via bulk computations, such as the gravitational energy and the BF bound in Sec. 3.3, as well as the holographic models based on the adjacency matrix considered in Sec. 3.4. In this final section, we will shift our focus from the bulk to the boundary of hyperbolic tilings. In particular, given that the effectiveness of hyperbolic tilings as discretization schemes has been thoroughly verified in the previous sections, we will know consider the more ambitious goal of developing concrete instances of a discrete holographic duality by constructing explicit boundary theories. More precisely, based on the results reported in [158, 159], I will explain how to construct aperiodic spin chain models at the boundary of truncated hyperbolic tilings in a way that encodes information about the tiling's construction via the inflation rules introduced in Sec. 3.2.4. This encoding of information in the boundary theory is largely motivated by the holographic nature of the AdS/CFT correspondence, and should thus play a pivotal role in any discrete version of the duality. I will first provide a general construction of these spin models, together with general strong-disorder renormalization group (SDRG) techniques to access their ground state

properties. Then, I will show how the ground state entanglement entropy and the mutual information can be computed for a large class of aperiodic spin models obeying certain criteria. I will continue by displaying the applicability of these methods in three explicit models. Finally, a tensor network construction associated to the ground state of these models will be introduced, motivated by the goal of reconstructing a bulk dual for these ground states.

3.5.1. The Jeweler's Dream: Constructing Aperiodic Chains

Our old friend the tiler turns out to have a very close companion of hers who is a jeweler. This is a person who manufactures jewelry like necklaces, rings, and in particular, chains. Similarly to the tiler, they are also bored of the usual diamond and gold chains they typically sell to their customers day in and day out. One night, they also had a dream about a more exciting type of chain, one that has no repeating patterns. They were ecstatic at this idea of being able to simply slightly move their chain around their neck and seeing a pattern of jewels that is not the same as before. Yet, having completely new designs every time seemed too much of a gamble, so they imagined that these hypothetical chains would show some of the same patterns after a while. To make it exciting however, one would never know when a pattern would arise again. In other words, there would not be any fixed periods in these chains, they would be *aperiodic*. Engulfed by the beautiful idea of an aperiodic necklace, they too started to buy the required pieces, until the morning alarm went off. Back in the real world, our jeweler grasped that in order to actually realize their dream, such a necklace would necessarily have to be infinite. Otherwise, the whole chain would start repeating after a predictable amount of time. After telling the tiler about their dream, she introduced the jeweler to the concept of aperiodic sequences at the boundary of hyperbolic tilings, which we have already encountered in Sec. 3.2.4. These are exactly what the jeweler was dreaming of! To cheer up the jeweler, with whom we now share a passion for aperiodic sequences and hyperbolic tilings, we will now construct chains based on these aperiodic sequences. These will however not consist of diamonds, but rather of spin degrees of freedom. Nevertheless, the jeweler will be happy to see that such object can indeed be constructed, and moreover they will be fascinated by the interesting physical phenomena that arise in such systems.

We begin with the construction of aperiodic spin chains based on the inflation procedure for generating hyperbolic tilings. As explained in Sec. 3.2.4, the vertex-inflation of both polygon-centered and vertex-centered $\{p, q\}$ tilings via the general inflation matrix (3.62) generates an aperiodic sequence $\mathcal{S}_{\{p,q\}}$ on the asymptotic boundary layer.

This boundary will consist of a set of edges $\{e_i\}_{i=1}^N$ and a set of vertices $\{v_i\}_{i=1}^N$. The inflation procedure is such that every vertex v_i is labeled by a letter $x_i \in \{a, b\}$ in such a way that the sequence $\{x_i\}_{i=1}^N$ is precisely the aperiodic sequence $\mathcal{S}_{\{p,q\}}$ associated to the inflation rule (3.50). This is depicted in the top part of Fig. 3.20. As mentioned in Sec. 3.2.4, truncated tilings obtained from inflation rules enjoy $\mathbb{Z}_n$ rotational symmetry, with $n = p, q$. However, we may restrict to one n-th of the boundary in any case, where the asymptotic sequence is a proper aperiodic sequence with no finite-sized periods. Under the assumption of infinitely many inflation steps, we may regard the boundary chain as being infinite and the approximation of the entire boundary as carrying the aperiodic sequence $\mathcal{S}_{\{p,q\}}$ is well-founded. More precisely, we may consider infinite sets of edges and vertices, $\{e_i\}_{i\in\mathbb{Z}}$ and vertices $\{v_i\}_{i\in\mathbb{Z}}$, wherein the vertices follow the infinite aperiodic sequence $\{x_i\}_{i\in\mathbb{Z}} \cong \mathcal{S}_{\{p,q\}}$. This allows us to fully exploit the properties of these aperiodic sequences reviewed in Sec. 3.2.4, encapsulated in the inflation matrix (3.62) and its statistics given by the left and right eigenvectors (3.64). It is this structure which we now employ to define spin chain models. Namely, we utilize the aperiodic distribution of letters at the asymptotic boundary of hyperbolic tilings to define the set of couplings in a quantum chain, an assignment which we depict in Fig. 3.20. To be precise, we assign spin degrees of freedom, encapsulated in a vector $\vec{\sigma}_i$, to each edge e_i of the tiling's boundary. This vector will contain the degrees of freedom localized at site i of the chain. At the same time, we associate a chain bond to every vertex v_i of the boundary, where the bond coupling μ is given by the label of the associated vertex. In other words, we have μ_a if $x_i = a$ and μ_b if $x_i = b$, where the precise nature of these couplings will vary depending on the microscopic details of the model. We consider them as being generic coupling parameters of the theory, whose role is to encode the information about the bulk's tiling. The outlined construction defines so-called *aperiodic quantum chains*, which are a class of models previously investigated in the context of condensed matter physics [576, 644–648]. For the purposes of this work, we will focus solely on the cases where the aforementioned couplings describe nearest-neighbor hopping parameters, such that the aperiodic modulation represents an instance of *spatial disorder* or *inhomogeneity* [649–651]. In particular, if $\mu_a = \mu_b$, we recover the case of a homogeneous spin chain. We will consider these homogeneous chains as being in a regime of their parameters such that the system find itself in a gapless phase. This will typically be the case when the system is close to a critical point, where universal effective descriptions in the continuum limit via CFTs with central charge c are admissible [172, 652]. Throughout the subsequent analysis, an underlying question will be whether the introduction of aperiodicity into an otherwise homogeneous model affects the critical properties of the system. This behavior can

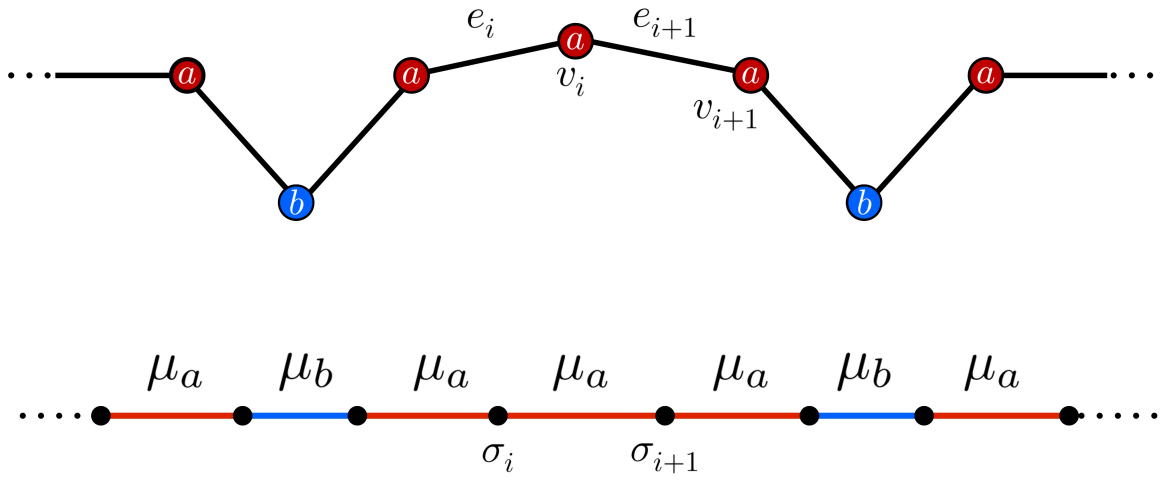


Figure 3.20: Sketch for the construction of aperiodic spin chains (bottom) from a given letter sequence produced by inflation rules (3.50) on the boundary of $\{p, q\}$ hyperbolic tilings (top). According to the letter sequence, we associate a corresponding hopping parameter μ_k with $k = a, b$ (red and blue) connecting two sites of the spin chain. In this way, the hopping parameters of the spin chain are aperiodically modulated.

generally be classified based on the relevance of the modulation in the following way: an aperiodic modulation is denoted as *relevant* if it changes the critical behavior of the underlying homogeneous system, such that the physics of the new disordered model are governed by a new disorder-induced fixed point. If this is not the case, and the properties of the system are left unchanged by the introduction of aperiodicity, we call the modulation *irrelevant*. Lastly, it might be the case that the critical behavior of the system, described by its set of critical exponents, develops a dependence on the original values of the hopping parameters μ_a, μ_b. In this case, we say that the aperiodicity is a *marginal* modulation.

General Aperiodic Hamiltonians

Let us now define the class of boundary models we will be dealing with in the following. In general, the precise nature of the spin degrees of freedom defined on each site is not fixed *a priori*, and this is indeed one of the aspects that we will exploit when considering explicit examples later on. Moreover, the actual form of the Hamiltonian governing the aperiodic chain is also not fixed, and so this is a further characteristic which we can tune in order to define explicit boundary theories. The only feature which is universal to all models considered in this section is the aperiodic modulation of the nearest-neighbor hoppings, which will always be determined by the choice of $\{p, q\}$ tessellation in the bulk. Based on these considerations, we define our general class of

aperiodic spin chains at the boundary of hyperbolic $\{p, q\}$ tilings as spin Hamiltonians with nearest-neighbor interactions of the form

$$H_{\{p,q\}} = \sum_{i\in\mathbb{Z}} \mu_i \, h(\vec{\sigma}_i, \vec{\sigma}_{i+1}; \theta_i) \, . \tag{3.142}$$

Here, $\vec{\sigma}_i$ is the vector of spin variables located at site i, whose exact nature we will discuss below. The fact that the interactions are nearest neighbor is encoded in the second argument of the function h, which denotes the set of degrees of freedom at the neighboring site $i + 1$. As mentioned before, the hopping parameters $\mu_i \in \{\mu_a, \mu_b\}$ and $\theta_i \in \{\theta_a, \theta_b\}$ are spatially distributed following the aperiodic sequence $\mathcal{S}_{\{p,q\}}$. In particular, we include the latter set of parameters θ_i to cover instances of anisotropies in the chain. For the moment, we also leave the exact form of the function h unspecified, the only restriction on the model is that this function takes two spin vectors as an argument.

The precise nature of the local spin degrees of freedom can be determined from several perspectives, depending on the features we would like our spin chain to have. For example, as alluded to previously, we may require the spin chain to have a gapless regime for some choice of the system parameters. This would consequently impose constraints on the form of the local spin degrees of freedom, as well as on the allowed form of the Hamiltonian. A very common choice is to consider SU(2) spins, i.e. where the local degrees of freedom are matrix operators which obey the $\mathfrak{su}(2)$ Lie algebra. These are the familiar spins in terms of local Pauli matrices at each lattice site. Among the possible multiplets which furnish irreducible representations of this algebra, we are free to choose specific ones according to their associated conserved quantum number. In the case of SU(2), this is the spin quantum numbers, which can be either an integer or a half integer. It is known, even in the absence of aperiodic modulation, that different choices of representation can drastically affect the physical properties of the system [653–655]. Another possibility is to allow the spins to take on more internal values, something that can be achieved by representing local degrees of freedom using generators of SU(N) [656–672] or SO(N) groups [673–680]. In these cases, there are again different physical consequences to choosing local degrees of freedom as transforming under the adjoint or the fundamental representation of the underlying Lie algebra, leading to non-trivial phenomena like dimerization and symmetry-protected topological phases. Finally, one can also think of defining the local spin degrees of freedom based on spatial symmetries of the system. This is rather unorthodox for quantum spin chains, but the idea is motivated by relativistic field theories, whose fields furnish irreducible representations of the Poincaré or conformal groups.

It is apparent that the nature of the local spin degrees of freedom of our chain is non-unique. For the purposes of the current analysis, we will constrain this daunting ambiguity by imposing certain general constraints on models of the form (3.142), which will guarantee that we can analyze them with the SDRG methods explained below. These general aperiodic spin chains, which encode information about the bulk's discretization in their aperiodic modulation, will be the main subject of investigation of the following sections. In the end, we will give three explicit examples of aperiodic spin chains, with explicit choices of local spin degrees of freedom, which fall under the large umbrella of our framework.

Finally, let us return to the assumption that the aperiodic model (3.142) is in a gapless regime. Although it is not *a priori* clear whether aperiodic modulations will keep the system within its critical window, it was argued in [681, 682] (for the spin-1/2 representation of the XXZ model) that the system will continue to be critical under binary aperiodic modulations if the sequence has equal fractions of letters a or b at even and odd sites. In other words, criticality is maintained if, for example, the a (or b) letters in the sequence are uniformly distributed between even and odd numbered sites of the full chain. Although this might seem as an extremely niche property to ask for, there exists a criterion to check whether a given aperiodic sequence fulfills this property or not, which was derived in [648] based on previous work [576, 683]. Thus, it was shown in [158] that for all the aperiodic modulations given by the sequences $\mathcal{S}_{\{p,q\}}$ obtained from hyperbolic tilings, this criterion is fulfilled. Therefore, assuming that the aperiodic model (3.142) is critical amounts to assuming that the underlying homogeneous chain was critical as well [158, 591, 648].

3.5.2. The Strong-Disorder Renormalization Group and Aperiodic Singlet Phases

With the general structure of aperiodic spin chains given by the Hamiltonian (3.142), we now explain how to access the low-energy properties of such chains. In particular, we will employ a tool called *strong-disorder renormalization group* (SDRG), first developed in [681, 682] in the context of randomly disordered spin chains (see [651] for a review). This real-space renormalization approach is one of the most powerful techniques to analytically tackle inhomogeneous quantum spin chains, and its overall philosophy is as follows. For binary aperiodic sequences, the core of this perturbative approach is the identification of chain sites which are coupled by a hopping parameter which is assumed to be much larger than the other one, hence the strong disorder. Under this strong-disorder assumption, one can see the blocks of strongly coupled spins as being only weakly connected to their surrounding neighbors, and thus, to the

rest of the chain. Accordingly, we may describe this situation within perturbation theory in the weak hopping parameter. The low-energy properties of the chain can then be accessed by considering that the spins connected by strong hoppings will couple into their local ground state, and they can thus be decimated from the system. More precisely, consider a block of n-spins which are connected by strong hoppings among themselves and are connected to their nearest neighbors to the left and the right by weak bonds. This block will be described by a local Hamiltonian H_n, which is simply obtained from the restriction of the general Hamiltonian to the given sites. We can treat the neighboring sites to this block as a perturbation $\delta H_{\mathrm{l,l}}$, where l and r stand for the left and right nearest neighbors to the strongly coupled block. The decimation of this strongly coupled block induces a new renormalized hopping (and possibly renormalized anisotropies) between the left and right neighbors. A schematic representation of such a decimation steps is shown in Fig. 3.21, whose notation is introduced below. This renormalized hopping is obtained from second-order perturbation theory with the weak hopping as the perturbative parameter, in which the total Hamiltonian of $n+2$ sites is projected onto the ground state of the local Hamiltonian H_n. It is worth noting that such a decimation is indeed removing degrees of freedom from the system, since it is an RG step after all. More precisely, given the local Hilbert space dimension d, the original Hamiltonian of the block under consideration is a $d^{n+2} \times d^{n+2}$ matrix, while the Hamiltonian after the projection due to decimation is only a $d^2 \times d^2$ or $d^3 \times d^3$ matrix, depending on the parity of n. Thus, in principle, the chain will have less degrees of freedom after a decimation step. However, if we consider our chains to be infinite, the resulting chain after the RG step will once again be infinite. The consequences of the decimation are therefore fully encapsulated in the renormalization of the parameters. It is worth mentioning that the decimation may generate new terms in the Hamiltonian which where not present in the original form. However, as we will show in detail below, all models considered here are such that the decimation steps lead to a Hamiltonian with precisely the same form as before the decimation, up to the renormalized hoppings and anisotropies. Finally, the perturbative assumption needs to be verified *a posteriori* by checking that the renormalized parameters obey the original claim of being strongly disordered. If this is the case, and we can still identify one renormalized hopping being much larger than the other one, we can iterate the decimation procedure and gain access into the low-energy properties of the system. Specifically, the flow of the system's parameters induced by the SDRG will drive the chain into a so-called *disorder-induced fixed point*, where the critical properties of the model can be analyzed.

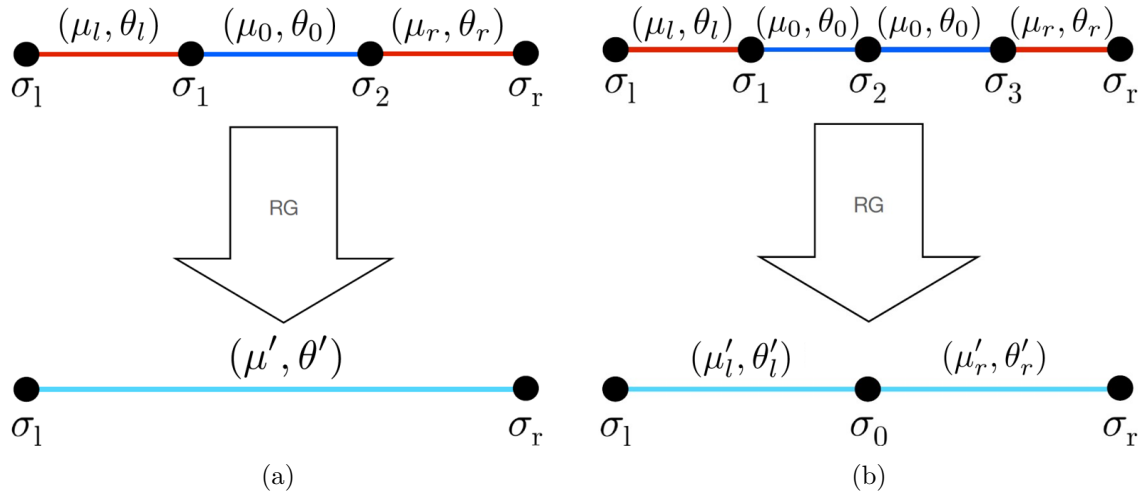


Figure 3.21: Depiction of the fundamental decimation steps involved in the SDRG in the exemplary cases of two (a) and three (b) strongly coupled spins. Weak and strong hoppings are depicted in red and blue, respectively. The cyan bonds can only be determined to be weak or strong *a posteriori*, once the renormalized couplings have been computed via (3.146).

SDRG Decimation Steps

Let us give a more quantitative exposition of the SDRG procedure, particularly focusing on its application to aperiodic spin chain, following [158, 159, 590, 591]. The aperiodic Hamiltonian of interest is given by (3.142). We assume that the parameters of the model are such that the system is in a gapless regime in the absence of aperiodicity, a requirement we explained in detail above. To keep our discussion as general as possible, we will introduce a slight change of notation, and denote the strong hopping parameter by μ_0. The strong-disorder assumption is that μ_0 is much larger than any other hopping parameter present in the theory. Consider now a generic block consisting of $n+2$ consecutive sites in our spin chain, where the central n sites are connected by strong hoppings μ_0. The left- and rightmost sites of the block, which we denote by σ_l and σ_r, respectively, are connected to this central piece via weak hoppings $\mu_{\mathrm{l,r}} \ll \mu_0$. Notice that, in general, these need not be equal, although we will later mostly deal with the case where $\mu_\mathrm{l} = \mu_\mathrm{r}$. Moreover, according to (3.142), the spin chain may also have anisotropy parameters, which we accordingly label as $\theta_0, \theta_\mathrm{l}, \theta_\mathrm{r}$. However, their hierarchy among themselves does not enter the perturbative assumptions. The aforementioned local Hamiltonian for the strongly coupled sites reads

$$H_n = \mu_0 \sum_{i=1}^{n-1} h(\vec{\sigma}_i, \vec{\sigma}_{i+1}; \theta_0)\,, \tag{3.143}$$

while the coupling of this central block to the external neighbors $\vec{\sigma}_{\mathrm{l,r}}$ is given by

$$\delta H \equiv \delta H_{\mathrm{l}} + \delta H_{\mathrm{r}} = \mu_{\mathrm{l}} h(\vec{\sigma}_{\mathrm{l}}, \vec{\sigma}_1; \theta_{\mathrm{l}}) + \mu_{\mathrm{r}} h(\vec{\sigma}_n, \vec{\sigma}_{\mathrm{r}}; \theta_{\mathrm{r}}) \,. \tag{3.144}$$

The essence of the SDRG is to view (3.144) as a perturbation to the local Hamiltonian (3.143), since $\mu_0 \gg \mu_{\mathrm{l,r}}$. Within this approximation, the central n spins will not be affected by the left- and rightmost spins, and they will rather couple among themselves to their local ground state. This means that central block will thus give a fixed contribution to the thermodynamic properties of the system and can be therefore decimated out after taking this into account. In other words, the decimation projects the strongly-coupled block onto the ground state of the corresponding local Hamiltonian (3.143). In general, H_n is a $d^n \times d^n$ matrix whose set of eigenstates we can schematically denote as $\{|g\rangle, |e_i\rangle\}$, containing the local n-site ground state $|g\rangle$ (which we assume to be non-degenerate) and local excited states $|e_i\rangle$, with $i = 0, \ldots, d^n - 2$. The exact form of this step and of the aforementioned states depends on whether n is even or odd, as we explain below. In any case, this elimination of the central degrees of freedom induces a set of renormalized hopping and anisotropy parameters, which we denote by (μ', θ'), between the external sites $\vec{\sigma}_{\mathrm{l}}$ and $\vec{\sigma}_{\mathrm{r}}$. The magnitudes of these new parameters can be estimated through second-order perturbation theory [590, 591].

Let us first consider the case where n is even. The ground state $|g\rangle_{\mathrm{even}}$ of the local Hamiltonian for an even number of spins, if it is non-degenerate, is going to be the generalization of the singlet state familiar from spin-1/2 SU(2) spins. We can schematically write this state as

$$|g\rangle_{\mathrm{even}} \equiv |T\rangle = \sum_{m_1=1}^{d} \cdots \sum_{m_n=1}^{d} T_{m_1 \ldots m_n} |m_1\rangle \ldots |m_n\rangle \,, \tag{3.145}$$

where we have introduced the notation $|T\rangle$ for later convenience, and where $|m_i\rangle$ denotes a generic choice of basis for the local Hilbert space of dimension d. This can be made more explicit once a representation for the spins is chosen, and we will later return to it in our exemplary models. The real-space decimation step from the SDRG procedure is performed on the Hamiltonian operator of the $(n+2)$-site block by projecting it onto the local ground state (3.145). Specifically, at second order in perturbation theory, we have

$$H'_{\mathrm{even}} = \sum_{i=0}^{d^n-2} \frac{\langle T| \, H_{\mathrm{l}} + H_{\mathrm{r}} \, |e_i\rangle \, \langle e_i| \, H_{\mathrm{l}} + H_{\mathrm{r}} \, |T\rangle}{E_g - E_{e_i}} \equiv \mu' h(\vec{\sigma}_{\mathrm{l}}, \vec{\sigma}_{\mathrm{r}}; \theta') \,, \tag{3.146}$$

where we recall that $|e_i\rangle$ are the excited states of the local Hamiltonian H_n. Notice how the decimation step induces an effective hopping between the external sites, such that they such that they can be described via the Hamiltonian H'_{even}, which is itself a $d^2 \times d^2$ operator of the exact same form as the original one (3.143), albeit now with renormalized parameters (μ', θ'). This decimation is shown in Fig. 3.21a for the case of a block of $n = 2$ spins. It is quite reasonable that H'_{even} is now $(d^2 \times d^2)$ since it acts on the two remaining sites of the original $(n + 2)$-site block which have survived the decimation. Once again, the explicit form of the renormalized couplings and their dependence on the original couplings $\mu_0, \mu_{\text{l,r}}$ is going to be particular to the specific model of choice, and we will report them in our examples section. The key point is that we obtain functionally the same Hamiltonian as before.

Let us now turn to the case of odd values of n. Here, the typical ground state of the central n sites will be a generalized version of a doublet state, i.e. a linear superposition of two states with the schematic form

$$|T^{m_0}\rangle = \sum_{m_1=1}^{d} \cdots \sum_{m_n=1}^{d} T^{m_0}_{m_1 \ldots m_n} |m_1\rangle \ldots |m_n\rangle \ , \tag{3.147}$$

where the sum does not run over $m_0 = \{1, \ldots, d\}$, regarded here as a free index labeling each of the two ground states. Notice that the coefficients $T^{m_0}_{m_1 \ldots m_n}$ are not specified yet, since they depend on the specific form of the Hamiltonian. The way to fix them within the SDRG procedure [590, 591] is by imposing that the block of an odd number of spins has a total spin operator (or a corresponding Casimir operator for more general spin degrees of freedom) which is equal to an single effective spin degree of freedom, denoted by $\vec{\sigma}_0$. The schematic form of this condition, in the notation of (3.147), reads

$$\left\langle T^{m_0} \left| \mathcal{C}^{(\alpha)}_n \right| T^{m'_0} \right\rangle \propto \eta^{(\alpha)}_n(\theta_0) \, \langle m_0 | \, \sigma^{(\alpha)}_0 \, | m'_0 \rangle \ , \tag{3.148}$$

where $\mathcal{C}^{(\alpha)}_n$ is a Casimir operator generalizing the notion of the total spin operator, and α is an index running through all the species of local spin degrees of freedom, i.e. the number of components of the $\vec{\sigma}$ vector for the given representation. For example, $\alpha = x, y, z$ in the case of spin-1/2 SU(2) spins. The function $\eta^{(\alpha)}_n(\theta_0)$ is a proportionality factor which will typically depend on the anisotropy parameter and the number of spins in the block. By imposing (3.148), the SDRG implies that we can decimate the block of n strongly coupled spins in its ground state by the effective spin degree of

freedom $\vec{\sigma}_0$, such that it is coupled to the neighboring sites via

$$H'_{\text{odd}} = \mu'_{\text{l}} h(\vec{\sigma}_{\text{l}}, \vec{\sigma}_0; \theta_{\text{l}}) + \mu'_{\text{r}} h(\vec{\sigma}_0, \vec{\sigma}_{\text{r}}; \theta'_{\text{r}}) \,. \tag{3.149}$$

In this expression, which is obtained analogously to (3.146), $\mu'_{\text{l,r}}$ and $\theta'_{\text{l}}, \theta'_{\text{r}}$ are the renormalized hoppings and anisotropies describing the coupling of the new effective degree of freedom to its nearest neighbors after the decimation step. Interestingly, even in cases where the original chain did not have aperiodically modulated anisotropies, the decimation induces an effective modulation on θ_i, which gets renormalized into two distinct anisotropies $\theta'_{\text{l}}, \theta'_{\text{r}}$. Importantly, (3.149) has once again the same functional form as the original Hamiltonian (3.142), which allows us to repeat the decimation steps detailed above. The decimation of a block of $n = 3$ spins is shown schematically in Fig. 3.21b. However, in this work, we will mostly restrict our attention to those aperiodic modulations for which only singlet states are produced during the SDRG procedure, as we discuss below. Cases where doublet states are generated will only be considered when we introduce a tensor network approach to aperiodic spin chains.

Singlet-producing self-similar sequences

From the analysis given above, we can summarize the application of the SDRG to Hamiltonians of the form (3.142) as follows. Once an aperiodic modulation for the hopping parameters (and anisotropies) is specified, the decimation procedure is carried out simultaneously as explained above on all blocks of consecutive strongly coupled spins. This leads to the renormalization of the hoppings throughout the chain, and we denote a single decimation as an *RG step*. From the renormalized parameters after the RG step, assuming that the strong-disorder assumption holds true, we are able to identify again strong and weak hoppings. Their spatial distribution after a single RG step, however, need not immediately correspond to the original aperiodic sequence. In other words, not all aperiodic sequences will be left invariant by decimation steps of the type described above. The class of aperiodic sequences which are indeed invariant under such RG steps are called *self-similar*, and these have been studied previously in [588–591, 684, 685]. In particular, since we mentioned above that we will focus on aperiodic sequences where only singlets are generated in the SDRG procedure, we denote these as *singlet-producing self-similar sequences* [589]. However, it was pointed in [158, 590, 591] that there exists examples where self-similarity is attained after a finite number $k > 1$ of consecutive RG steps. In other words, the distribution of bonds on the chain returns to being described by the original aperiodic sequence after we have performed a number k of decimation steps. Indeed, this distribution is then

reached every k steps, thus repeating periodically throughout the SDRG trajectory. We denote such aperiodic sequences as *attractors*, and more specifically we will call them *k-cycle bond distribution attractors* [158]. Regarding a single RG step as its own transformation, it is apparent that the combined operation consisting of k such RG steps is the transformation which will leave the spatial distribution of hoppings of the original chain invariant. We denote these as *sequence-preserving SDRG transformations*, and they will be denoted by Ξ. In other words, when an aperiodic sequence is a k-cycle attractor, Ξ is obtained as the composition of k individual RG steps, i.e. $\Xi = \mathrm{RG}_k \circ \mathrm{RG}_{k-1} \circ \cdots \circ \mathrm{RG}_1$. We will see that infinitely many families of k-cyclic aperiodic sequences can be found within the large family of $\{p, q\}$ aperiodic sequences. For the most part of the remaining analysis in this chapter, we will focus on aperiodic modulations which act as k-cycle bond distribution attractors with either $k = 1$ or $k = 2$, since they allow for the explicit computation of the entanglement entropy. For higher k, the computations we will introduce in Sec. 3.5.4 cannot be straightforwardly generalized. These cases, however, can be treated within the tensor network approach introduced later in Sec. 3.5.7.

Let us now return to the iterative application of decimation steps within the SDRG procedure. Focusing on the hopping ratio $r = \mu_a/\mu_b$ and the set of anisotropies θ_i, the consecutive application of the decimation steps detailed above will induce a flow of these parameters which looks like $r \to r' \to r'' \to \cdots \to r^*$ and $\theta_i \to \theta_i' \to \theta_i'' \to \cdots \to \theta_i^*$, with $i \in \{a, b\}$. Here, the star denotes the values of these parameters at the SDRG fixed point. More precisely, after applying a sequence-preserving SDRG transformation M times, the renormalized parameters will be formally given by

$$r^{(M)} = F_M(r, \{\theta_j\}), \qquad \theta_a^{(M)} = G_M^{(a)}(r, \{\theta_j\}), \qquad \theta_b^{(M)} = G_M^{(b)}(r, \{\theta_j\}), \tag{3.150}$$

where $\{\theta_j\}$ denotes here the complete set of possibly distinct anisotropy parameters of the original chain. The explicit forms of the functions F_M, $G_M^{(a)}$ and $G_M^{(b)}$ depend both on the specific aperiodic modulation and the local spin degrees of freedom chosen. In any case, the strong-disorder induced fixed point, which perturbatively describes the critical properties of the system at low energies, is obtained by taking the limit $M \to \infty$, i.e. as the limiting points of the flow equations

$$r^* = \lim_{M\to\infty} F_M(r, \{\theta_j\}), \qquad \theta_a^* = \lim_{M\to\infty} G_M^{(a)}(r, \{\theta_j\}), \qquad \theta_b^* = \lim_{M\to\infty} G_M^{(b)}(r, \{\theta_j\}). \tag{3.151}$$

The nature of these fixed point values allows us to further clarify the aforementioned classification of aperiodic modulations based on their relevance. In particular, if r^*

and $\theta^*_{a,b}$ still exhibit an explicit dependence on the original values of r and $\{\theta_j\}$, the aperiodic modulation is said to be marginal. If however, the SDRG flows (3.150) lead to a certain value of $\theta^*_{a,b}$ and $r^* \to 0$ independently of the initial parameters, the modulation is relevant. Naturally, if the decimations do not induce a renormalization of the couplings, the modulation is irrelevant. Let us stress that the whole discussion given here is valid within the perturbative of the SDRG. However, in the case of relevant modulations, the strong-disorder assumption gets enhanced with every decimation step, meaning that the SDRG becomes asymptotically exact as $M \to \infty$.

The Ground State

We are now in position to introduce one of the main concepts in this section. Given the definition of the parameters at the strong-disorder induced fixed point, and considering aperiodic sequences in which only singlets arise throughout the SDRG trajectory, the ground state of aperiodic spin chains with Hamiltonian (3.142) will have a factorized form. More precisely, at the SDRG fixed point, the ground state will be given by the product of all singlet states $|T_s\rangle$ generated throughout the SDRG procedure. Formally, this ground state has the form

$$|\psi\rangle = \bigotimes_{i=1}^{\infty} \bigotimes_{s_i \in G_i} |T_{s_i}\rangle \ , \tag{3.152}$$

where the index s_i runs over the set G_i of all the pairs of sites which are coupled into a singlet during the ith generation of the SDRG. In particular, these singlets will connect spins at arbitrarily large distances. We denote this by saying that the system is in an *aperiodic singlet phase* (ASP) [588, 589]. A schematic depiction of a generic ASP ground state in shown in Fig. 3.22. The ultimate goal of the following sections will be to exploit the properties of this ASP, together with the analytical tractability offered by the SDRG, to characterize several physical quantities such as correlation functions, entanglement entropy and mutual information in aperiodic spin chains.

Having introduced all the general features of the aperiodic spin chains needed for this section, let us summarize the main four criteria that aperiodic chains with Hamiltonians of the form (3.142) must obey for the results in the following subsections to be valid:

I *Criticality:* The model must be critical, which for the aperiodic modulations following sequences $\mathcal{S}_{\{p,q\}}$ requires the homogeneous model underlying (3.142) to be gapless as well.

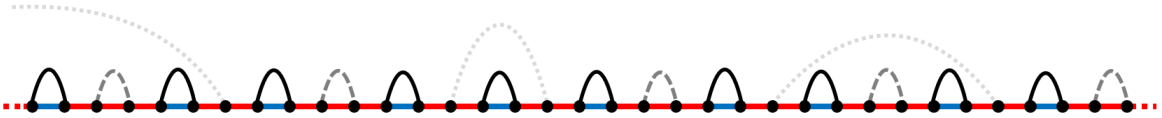


Figure 3.22: Sketch of the factorized structure of a ground state in an aperiodic singlet phase, as defined by (3.152). All singlets generated during the SDRG are shown on top of the original aperiodic chain for reference, with weak and strong bonds denoted in red and blue, respectively. Singlets which are generated during the first, second and n-th SDRG steps ($n \geq 3$) are depicted by black solid lines, dark gray dashed lines, and light gray dotted lines, respectively. On an infinite chain, the SDRG can be iterated indefinitely as the system flows towards the strong-disorder fixed point, generating singlets which couple spins at arbitrarily large distances along the way. Shorter singlets appear early in the SDRG, while longer singlets are generated in later generations.

II *Relevance:* The modulation induced by $\mathcal{S}_{\{p,q\}}$ must be relevant.

III *Cyclicity:* The SDRG flow must follow either a one-cycle or a two-cycle bond-distribution attractor.

IV *ASP:* The ground state of (3.142) must be in an aperiodic singlet phase (ASP).

These criteria are an amalgamation of conditions both on the specific dynamics of the function h in (3.142), as well as on the aperiodic sequences $\mathcal{S}_{\{p,q\}}$ used in their modulation. Even though criteria **I**-**IV** may seem unexpectedly restrictive, it was shown in [158] that there are infinitely many $\{p, q\}$ tilings whose inflation rules obey all four criteria. Moreover, there exists also a different infinite class of substitution rules, considered in [589], which by construction are self-similar and obey the criteria above. However, only a few of them can are equivalent to inflation rules for $\{p, q\}$ tilings. Since we are interested in keeping the connection to these discretizations of hyperbolic space, we will not consider this additional class of substitution rules. For hyperbolic $\{p, q\}$ tilings, the complete list of inflation rules obeying our criteria encompasses the aperiodic sequences associated to the

$$\{5, 4\},\ \{5, 5\},\ \{3, 7\},\ \{3, 8\},\ \text{and}\ \{6, q\} \tag{3.153}$$

hyperbolic tilings. In the remainder of this work, we will often refer to these as the *admissible* modulations, for which the criteria **I**-**IV** are obeyed. In particular, note how $\{6, q\}$, with $q \geq 4$, is an infinite family of tilings. Thus, in addition to a vast flexibility in the specific choice of Hamiltonian function h and of spin degrees of freedom $\vec{\sigma}$, we have an infinite class of aperiodic modulations for which we can analytically access the ground state of aperiodic spin chains using SDRG techniques.

3.5.3. Correlation Functions in Aperiodic Singlet Phases

As a first quantity of interest, we compute the correlation functions of two spin degrees of freedom in ASPs of general aperiodic Hamiltonians (3.142). More precisely, we consider the two-point function of spins which are coupled into a singlet at some stage throughout the SDRG procedure. As we will see later, other two-point functions between spins not in a singlet are subleading. Higher-point correlation functions are of course also of interest, but these cannot be easily accessed via SDRG methods, and so we restrict ourselves to two-point correlation functions. For this, I first review the results presented in [591] for the case of one-cycle aperiodic modulations under SDRG. Then, I report on the extension of these computations to the case of aperiodic modulations which are two-cycle attractors under the SDRG. This scenario introduces different correlation functions for singlets generated in consecutive steps of the SDRG, as we elucidate below. Finally, a qualitative relation between the two-point function and the discrete geodesic distance of boundary points on hyperbolic tilings is presented. Motivated by a similar relation within AdS/CFT [686], I argue that an effective scaling dimension of boundary operators will increase as a consequence of the discretization.

Correlation functions in one-cycle SDRG for ASP

The original analysis of two-point correlation functions in ASPs was first done in [591]. Although this work considered specifically a spin-1/2 XXX spin chain, the general argument can indeed be extended to all aperiodically modulated Hamiltonians of the form (3.142), under the assumption that the criteria **I**-**IV** are satisfied. Given the factorized structure of ASPs, in which spins are coupled into singlets at arbitrarily large distances, the dominant contribution to the two-point functions will come precisely from spins connected by said singlets. All other correlations between spin degrees of freedom which are not connected by a singlet throughout the SDRG will be exponentially suppressed in comparison and can therefore be neglected. For general Hamiltonians (3.142), we can write a generic form of the two-point function of interest without specifying the nature of the spin degrees of freedom. This is given by

$$C^{\alpha\beta}(\Lambda) \equiv \overline{\langle \sigma_i^\alpha \sigma_{i+\Lambda}^\beta \rangle} = \delta_{\alpha\beta} C(\Lambda)\,, \tag{3.154}$$

with Λ a parameter describing the typical length of a singlet in an aperiodic sequence, and α, β two indices which label the components of the spin vector $\vec{\sigma}$. The last equality in (3.154) assumes that only spins belonging to the same components in the spin vector can have non-vanishing correlations. While this may not be true in general, all models considered in this work exhibit this feature as a consequence of symmetries present

in their Hamiltonians, and we will therefore assume it from the beginning. This can be easily pictured in the case of spin-1/2 Hamiltonians, where correlations like $\langle \sigma_i^x \sigma_j^z \rangle$ vanish. Notice that, due to the aperiodic nature of our systems, an average over the whole chain needs to be computed for the correlation functions to capture generic features of the ASP. This is what the bar denotes in (3.154). This averaged value of the correlation function is captured by the function $C(\Lambda)$, which sensibly only depends on the distance between the spins, determined by the singlet length Λ. As explained in [591], $C(\Lambda)$ can be obtained from the correlation c_0 between two spins in a singlet, which is a fixed number, and the relative density of singlets generated at any given step in the SDRG. More precisely, the singlet correlation value c_0 can be directly computed from the local Hamiltonian h in (3.142), although its precise numerical value depends on the specific representation of the spin degrees of freedom. As for $C(\Lambda)$, we first need to recall that the typical length of the singlets generated during the SDRG will depend on their *generation*, i.e. after how many RG steps they arise. Thus, let Λ_j denote the typical length of singlets created in the j-th generation. We can readily convince ourselves that this length will be inversely proportional to the number ρ_j of spins that belong to singlets in that same generation, meaning that $\rho_j \sim 1/\Lambda_j$ [591]. This is because the more spins are already part of a singlet, given the structure of aperiodic sequences, the spins which are not yet coupled into singlets will generally be further apart. An important point to highlight here is that the singlets are always generated *after* a decimation step, such that their typical length will correspond to the typical length of strong bonds in the previous generation. Under this approximation, the correlation function of two spins in a singlet can be written as

$$C(\Lambda_j) \approx c_0(\rho_j - \rho_{j+1}) = \frac{c_0}{\Lambda_j}\left(1 - \frac{\Lambda_j}{\Lambda_{j+1}}\right). \tag{3.155}$$

In the case of one-cycle SDRG modulations, we can derive that the quotient of typical lengths Λ_j/Λ_{j+1} of consecutive generations tends to a constant as $j \to \infty$. Therefore, the whole bracket in (3.155) tends to a constant value $\Upsilon(p,q)$, which depends on the Schläfli parameters, and is given by [591]

$$C(\Lambda_j) = \frac{c_0 \Upsilon(p,q)}{\Lambda_j}. \tag{3.156}$$

Remarkably, the full dependence on the Schläfli parameters, and thus on the aperiodic modulation, is mostly encapsulated in a numerical prefactor if we regard the singlet length Λ_j as simply a reference scale. We will use this interpretation in forthcoming discussions. This is because the dependence of the correlation function on the singlet

length, i.e. the distance between spins the spins, turns out to be the same as that known from continuum systems, with a scaling exponent equal to one.

Correlation functions in two-cycle SDRG for ASP

We will now generalize the computation above to the cases of aperiodic modulations which are two-cycle bond attractors under the SDRG. For this, let us first generally characterize two-cycle modulations in more detail by considering their associated sequence-preserving transformation Ξ. More precisely, two-cycle modulations have a sequence-preserving transformation which is the composition of two individual RG steps, i.e. $\Xi = \mathrm{RG}_2 \circ \mathrm{RG}_1$. This means that the original sequence is renormalized into itself only after the application of these two decimations. We can interpret each of these RG steps as inverse inflation steps, although they do not need to be exactly equivalent as matrices. In other words, a generic decimation will take the form $w_1(a,b) \mapsto a'$, $w_2(a,b) \mapsto b'$, where some pair of given words describe the decimated blocks and these are replaced by renormalized couplings a', b'. We will often use the short-hand notation $a \equiv \mu_a$ and $b \equiv \mu_b$ by which the letters and their associated hoppings are addressed interchangeably. For the current analysis, we are only interested in the fact that we recover a binary sequence, so we will momentarily drop the primes. This observation implies that we can associate to each RG step the inverse of an inflation matrix M which implements the corresponding inflation rule. More precisely, we can schematically write

$$\mathrm{RG} = \begin{cases} w_1(a,b) \mapsto a \\ w_2(a,b) \mapsto b \end{cases} \quad \Longleftrightarrow \quad M = \begin{pmatrix} \#_a(w_1) & \#_a(w_2) \\ \#_b(w_1) & \#_b(w_2) \end{pmatrix} . \tag{3.157}$$

In this sense, and returning to the two-cycle modulations, let M_1 and M_2 be the inflation matrices implementing the inverse of the two RG steps RG_1 and RG_2 which constitute the sequence-preserving transformation Ξ. Accordingly, we have that $\Xi = M_2^{-1} M_1^{-1} = (M_1 M_2)^{-1}$. Notice that when $M_1 = M_2$, this effectively returns to the one-cycle case and thus the results of [588, 589] summarized above would hold. As inflation matrices on their own right, we can assume that M_1 and M_2 are both symmetric, and indeed this is the case for all examples we consider. Based on this assumption, the matrices $M_2 M_1$ and $M_1 M_2$ will share the same eigenvalues, the largest of which we will denote by $\lambda_+^{(12)}$. Importantly, this will generally not be the product of the largest eigenvalues of M_1 and M_2, because the matrices do not necessarily commute.

During an SDRG procedure on a two-cycle attractor modulation, the distribution of the hoppings throughout the chain will alternate between two versions which we associate to the even and odd generations. By the latter we mean the sequences obtained

after an even or an odd numbers of applied RG steps, respectively. As a consequence, the k-th even generation, corresponding to the $2k$-th overall generation with $k \in \mathbb{N}$, is obtained by applying the matrix $(M_1 M_2)^{-1}$ on the $(k-1)$-th even generation. As discussed in Sec. 3.2.4, this implies that the system undergoes a rescaling of $\left(\lambda_+^{(12)}\right)^{-1}$. In a similar fashion, the k-th odd generation, corresponding to the $(2k-1)$-th overall generation, is obtained from the application of the matrix $(M_2 M_1)^{-1}$ to the $(k-1)$-th odd generation. Again, the system gets rescaled by a factor of $\left(\lambda_+^{(12)}\right)^{-1}$. However, an initial condition on the relative scaling between the first even and odd generations is necessary. This again has to do with the fact that the singlets of the first generation are determined by the distribution of strong hoppings in the original chain, and this very first step requires a single application of M_1. However, we cannot immediately extract the corresponding scaling associated to this step from the eigenvalues of M_1, because the latter does not asymptotically generate the even generations. This is once more due to the fact that $[M_1, M_2] \neq 0$. For now, we will denote this unspecified scaling factor by $\tilde{\lambda}$. We will show later how we can determine its exact value.

Let us now individually investigate the behavior of the even and odd generations. As mentioned before, the singlets in the k-th generation are associated with the strong bonds in the $(k-1)$-th generation. As a sort of initial condition, we will denote as the 0-th generation the distribution of strong bonds on the original chain. The characteristic length Λ_k of singlets in the k-th generation is then given by

$$\Lambda_{2k-1} = l_b^{(e)} \left(\lambda_+^{(12)}\right)^{k-1}, \tag{3.158}$$

$$\Lambda_{2k} = l_b^{(o)} \left(\lambda_+^{(12)}\right)^{k-1} \tilde{\lambda}, \tag{3.159}$$

with $l_b^{(o)}$ and $l_b^{(e)}$ the b-th components of the left eigenvectors associated to $\lambda_+^{(12)}$ of $M_2 M_1$ and $M_1 M_2$, respectively. Notice that this automatically takes care of our initial condition, which implies $\Lambda_1 = l_b^{(e)}$. We have chosen the superscripts in (3.158) and (3.159) accordingly, again keeping in mind that the characteristic length of the odd generations will be determined by the distribution of strong hoppings of the previous generation, i.e. the even generation with $l_b^{(e)}$. The lengths of the even generations are obtained analogously. From similar arguments, we have that the singlet concentration in the k-th generation is given by

$$\rho_{2k-1} = p_b^{(e)} \left(\lambda_+^{(12)}\right)^{-k+1}, \tag{3.160}$$

$$\rho_{2k} = p_b^{(o)} \left(\lambda_+^{(12)}\right)^{-k+1} \tilde{\lambda}^{-1}, \tag{3.161}$$

where $p_b^{(o)}$ and $p_b^{(e)}$ represent now the b-th component of the right eigenvectors asso-

ciated to $\lambda_+^{(12)}$ of M_2M_1 and M_1M_2, respectively. We are now in position to derive the value of the undetermined scaling parameter $\tilde{\lambda}$, and we do this based on the expected properties that an ASP ought to have. Namely, since the ASP ground state will factorize into singlet contributions, the sum of the singlet concentrations of all the generations throughout the SDRG must yield $\frac{1}{2}$. More precisely,[15] this normalization condition imposes

$$\sum_{k=1}^{\infty} \left(p_b^{(o)}\tilde{\lambda}^{-1} + p_b^{(e)}\right) \left(\lambda_+^{(12)}\right)^{-k+1} = \left(p_b^{(o)}\tilde{\lambda}^{-1} + p_b^{(e)}\right) \frac{\lambda_+^{(12)}}{\lambda_+^{(12)} - 1} = \frac{1}{2}\,. \tag{3.162}$$

We can invert this relation to find

$$\tilde{\lambda} = \frac{2p_b^{(o)}\lambda_+^{(12)}}{\lambda_+^{(12)}\left(1 - 2p_b^{(e)}\right) - 1}\,. \tag{3.163}$$

Given that M_1 and M_2 are assumed to be symmetric, we can furthermore check that the following relation holds

$$p_b^{(o)} l_b^{(o)} = p_b^{(e)} l_b^{(e)}\,. \tag{3.164}$$

Based on these parameters, we can obtain the relative fraction of the chain which is covered by singlets of the k-th generation, which is given by $W_k = \rho_k \Lambda_k$. Thus, exploiting (3.158)-(3.161), we have

$$W_{2k-1} = p_b^{(e)} l_b^{(e)}\,, \qquad W_{2k} = p_b^{(o)} l_b^{(o)}\,, \tag{3.165}$$

for all $k \in \mathbb{N}$. In particular, note how W_k does not depend on k. This concludes our characterization of two-cycle aperiodic modulations under the SDRG.

With the characteristic parameters of two-cycle modulations derived above, we may now return to our extension of the analysis of [591] to the two-cycle case. First of all, let us recall the fact that a two-point function will only be non-vanishing for spin degrees of freedom belonging to the same generation, i.e. there are no correlations across different RG steps. As a consequence, in the treatment of two-cycle modulations under SDRG, we may fully characterize the correlation functions by consider two separate families, one for the even and one for the odd generations. It will be sometimes useful and more concise to encapsulate this dependence into the overall generation index $j \in \mathbb{N}$

[15] Notice that this normalization condition is enough to find the scaling coefficient $\tilde{\lambda}$ only for the case of $k = 2$ cycles, while the same condition would not be sufficient once we consider modulations with higher cyclicities $k \geq 3$. This technical obstacle can be overcome by the tensor network construction introduced in Sec. 3.5.7.

which takes on the value $j = 2k$ for the even generations and $j = 2k - 1$ for the odd ones. In a similar fashion as for the one-cycle case, the correlation function can be well-approximated by multiplying the constant correlation of an individual singlet, c_0, by the density of singlets in the given generation. Importantly, this is not a cumulative counting, and only the singlets of the current generation need to be taken into account, while previously generated singlets are independent. Similarly to (3.156), we can thus approximate this density of singlets in the j-th generation as the difference between the numbers of spins which belong to a singlet in the current generation and the number of spins that will become part of a singlet in the next generation, i.e.

$$C(\Lambda_j) \approx c_0 \left(\rho_j - \rho_{j+1}\right) . \tag{3.166}$$

This is because the next generation will have in some sense "less" degrees of freedom due to the decimation, implying precisely that a certain number if these spins coupled into singlets and where removed from the system. The crucial difference to the one-cycle case is that this difference is always taken with respect to the immediate next generation, which is now different depending on whether j is even or odd. Luckily, we have characterized each of these generations individually above. Thus, exploiting the results in (3.158)-(3.161), we can provide expressions for these concentrations of singlets as functions of the typical singlet length associated to each type of generation. Doing this, we obtain

$$\rho_{2k} = \frac{p_b^{(o)} l_b^{(o)}}{\Lambda_{2k}} , \qquad \rho_{2k-1} = \frac{p_b^{(e)} l_b^{(e)}}{\Lambda_{2k-1}} . \tag{3.167}$$

We can now use the previously found relation in (3.164) by writing $p_b^{(e)} l_b^{(e)} = p_b^{(o)} l_b^{(o)} \equiv p_b \, l_b$. Plugging this, together with (3.167) into (3.166), we obtain an expression for the two-point function that reads

$$C(\Lambda_j) = \frac{c_0 \, l_b \, p_b}{\Lambda_j} \left(1 - \frac{\Lambda_j}{\Lambda_{j+1}}\right) . \tag{3.168}$$

Note that although this is similar to (3.156), the quotient of typical singlet lengths tends to a constant when $j \to \infty$, but this constant is now dependent on the parity of the generation index j. More precisely, we have

$$\frac{\Lambda_{2k}}{\Lambda_{2k+1}} = \frac{l_b^{(o)} \tilde{\lambda}}{l_b^{(e)} \lambda_+^{(12)}} \equiv \alpha^{(e)} , \qquad \frac{\Lambda_{2k-1}}{\Lambda_{2k}} = \frac{l_b^{(e)}}{l_b^{(o)} \tilde{\lambda}} \equiv \alpha^{(o)} , \tag{3.169}$$

for $j = 2k$ and $j = 2k - 1$, respectively, and with the parameter $\tilde{\lambda}$ given in (3.163). The expressions above show the explicit dependence of our correlation functions on

the Schläfli parameters p and q, such that we effectively have $\alpha^{(e)} = \alpha^{(e)}_{(p,q)}$ and $\alpha^{(o)} = \alpha^{(o)}_{(p,q)}$. In turn, our final expression for the two-point functions in ASPs for aperiodic modulations which are two-cycle attractors also depends on the Schläfli parameters, and reads

$$C(\Lambda_j) = \begin{cases} \dfrac{c_0\, l_b\, p_b\, \left(1 - \alpha^{(e)}_{(p,q)}\right)}{\Lambda_{2k}}\,, & j = 2k\,, \\ \dfrac{c_0\, l_b\, p_b\, \left(1 - \alpha^{(o)}_{(p,q)}\right)}{\Lambda_{2k-1}}\,, & j = 2k-1\,. \end{cases} \tag{3.170}$$

It is instructive to check that the formulas in (3.170) are indeed compatible with the one-cycle cases. In particular, whenever the aperiodic modulation is a one-cycle attractor, we have that $\tilde{\lambda}^2 = \lambda_+^{(12)}$, $l_b^{(o)} = l_b^{(e)}$ and therefore $\alpha^{(o)} = \alpha^{(e)}$, and thus (3.170) indeed reduces to (3.156). Moreover, the functional dependence of we find in (3.170) on the distance between spins is in agreement with that found in [590] for one-cycle modulations. All in all, the effect of the aperiodic modulations on the correlation functions in the two-cycle case is also entirely encapsulated in constant prefactors which explicitly depend on the Schläfli parameters.

We should also emphasize the fact that the ASP describes a factorized ground state for the aperiodic spin chains under consideration. More precisely, the density matrix of the ASP ground state is given by the tensor product of individual singlet density matrices entangling two spins. As a consequence of this structure, all the $2n+1$-point correlation functions of the model vanish. Meanwhile, $2n$-point correlation functions are non-zero only if all the spins in the correlators are pairwise coupled in the ground state density matrix. It is in this latter case where the results given in (3.170) can be applied to compute the $2n$-point correlation functions. Remarkably, this factorization is a universal feature of the ASP and it will arise even for interacting Hamiltonians, as long as criteria **I-IV** are satisfied.

Let us now give some explicit examples of two-cycle aperiodic modulations and their corresponding expressions for the two-point functions as per (3.170). We start with the two specific instances of modulations corresponding to the hyperbolic tilings $\{5,4\}$ and $\{3,8\}$. These are both two-cycle attractors under the SDRG (in the sense discussed above (3.150)), but they share an even more interesting connection. Namely, it turns out that their decimation matrices M_1 and M_2, associated with the respective decimation steps of odd and even generations, are the same up to re-ordering. More precisely, we have that $M_1^{\{3,8\}} = M_2^{\{5,4\}}$ and $M_2^{\{3,8\}} = M_1^{\{5,4\}}$. Notice that this is true even though $\sigma_{\{5,4\}} \nsim \sigma_{\{3,8\}}$ as inflation rules. What this behavior implies is that the distribution of bonds in even generations of the $\{3,8\}$ chain is equal to the distribution of odd bonds for the $\{5,4\}$ chain and vice-versa. Therefore, this means that we can

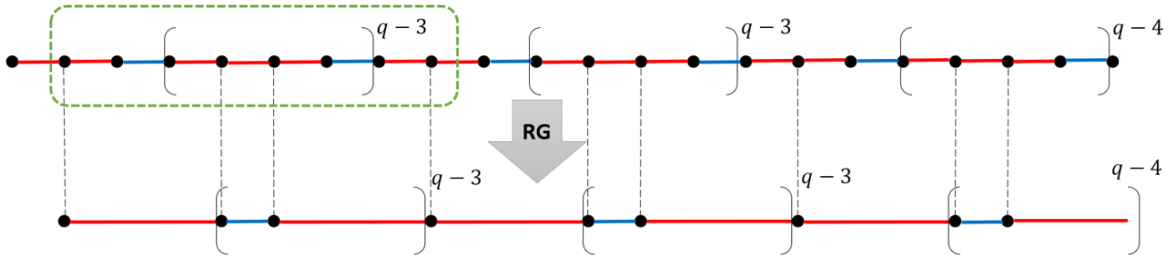


Figure 3.23: Top line: Snippet of the aperiodic sequence generated by the $\{6, q\}$ inflation rule (3.173). Weak and strong bonds are shown in red and blue, respectively. Subsequences enclosed in brackets with an exponent imply that these are to be repeated, e.g. $(abb)^2 \equiv abbabb$. We perform a decimation step as defined by (3.174), whereby particular subsequences like the one enclosed in the green box can be seen to be renormalized into a specific new subsequence. Bottom line: Sequence obtained after one decimation step, which is manifestly different from the original sequence. For instance, the sequence after the decimation step does no have any consecutive a letters.

compute their correlation functions by the methods explained above, but the results will slightly differ, given that, e.g. $p_b^{(0)}$ and $p_b^{(e)}$ will appear interchanged. Thus, plugging the corresponding typical singlet lengths and concentrations given above for these two modulations into (3.170), we obtain the following the two-point functions

$$C_{\{5,4\}}(\Lambda_j) = \begin{cases} \frac{c_0}{6}\left(5 - \frac{7}{\sqrt{3}}\right)\dfrac{1}{\Lambda_{2k}}\,, & j = 2k\,, \\ c_0\left(\frac{13}{2} - \frac{11}{\sqrt{3}}\right)\dfrac{1}{\Lambda_{2k-1}}\,, & j = 2k-1\,, \end{cases} \tag{3.171}$$

and

$$C_{\{3,8\}}(\Lambda_j) = \begin{cases} c_0\left(\frac{5}{2} - \frac{4}{\sqrt{3}}\right)\dfrac{1}{\Lambda_{2k}}\,, & j = 2k\,, \\ \frac{c_0}{6}\left(9 - 5\sqrt{3}\right)\dfrac{1}{\Lambda_{2k-1}}\,, & j = 2k-1\,. \end{cases} \tag{3.172}$$

Let us now turn to the case of the infinite class of admissible modulations in (3.153) given by $\{6, q\}$ tilings. The particularly attractive feature of this family is that it allows us to retrieve formulas with an explicit q dependence and study their behavior with q viewed as a discrete variable. In fact, this will be a prime example to which we will come back several times throughout the upcoming sections, so it is both instructive and pedagogical to describe the decimation steps of this case in detail, such as to shed light into the nuances of the RG procedure in the case of two-cycle bond attractors. From (3.50), the inflation rules for $\{6, q\}$ tilings are given by

$$\sigma_{\{6,q\}} = \begin{cases} a \mapsto aab(aaab)^{q-3}\,, \\ b \mapsto aab(aaab)^{q-4}\,. \end{cases} \tag{3.173}$$

By simply applying this substitution rule 4 or 5 times, we can already get a glimpse of the overall structures that will play a role in the decimation procedure. We show an exemplary snippet of the asymptotic sequence $\mathcal{S}_{\{p,q\}}$ in the top line of Fig. 3.23. One can verify by mere inspection the following features of $\mathcal{S}_{\{6,q\}}$:

- $\mathcal{S}_{\{6,q\}}$ will not have any isolated a letters.
- $\mathcal{S}_{\{6,q\}}$ will never have consecutive strong bonds, i.e. no subsequences of the form b^n with $n \geq 2$.
- The $aab(aaab)^{q-4}$ subsequence never appears consecutively, or in other words, $aab(aaab)^{q-4}aab(aaab)^{q-4}aab$ is not present in the asymptotic sequence.
- Powers of the $(aaab)$ blocks are always either $(q-3)$ or $(q-4)$, separated by aa strings. In particular, concatenations to a $(2q-7)$ block do not appear.

Based on these observations, and following the general decimation rules detailed in the beginning of this section, we can identify the decimation block for general in the general $\mathcal{S}_{\{p,q\}}$ sequences. First of all, notice that the effective spins of the renormalized chain will be defined on the two spins of the middle weak bond of all aaa subsequences, as well as the middle spin of all the aa subsequences. By identifying that the subsequences $(aaab)^{q-3}$ and $(aaab)^{q-4}$ are mere repetitions of these original spin-block structures, we can readily see that their decimation can be performed independently of each other. Each of the aforementioned subsequences will then yield new subsequence blocks of the form $(ba)^{q-3}$ and $(ba)^{q-4}$, respectively (cf. the green dashed box in Fig. 3.23). We can thus write down the first RG transformation corresponding to this decimation step,[16] which turns out to be independent of q, as

$$\mathrm{RG}_1^{\{6,q\}} = \begin{cases} aba \mapsto a \\ a \mapsto b \end{cases} \quad \Longleftrightarrow \quad M_1^{\{6,q\}} = \begin{pmatrix} 2 & 1 \\ 1 & 0 \end{pmatrix}, \tag{3.174}$$

where, as explained in (3.157), $M_1^{\{6,q\}}$ is the substitution matrix associated to the inflation rule which implements the inverse of $\mathrm{RG}_1^{\{6,q\}}$. The sequence we obtain after this first decimation step, a snippet of which is shown in the bottom line of Fig. 3.23, is again a binary sequence, and no new types of bonds arise. However, by comparing the top and bottom lines of Fig. 3.23, one can easily see that these sequences are

[16] Technically, at this point we would need to pick a specific Hamiltonian and carry out the perturbation theory to identify the new strong and weak hoppings in this renormalized chain. We will do this later in the examples section, and we will verify that the decimation given in (3.174) is correct. We can do this because in this simple decimation block, one can make an educated guess for the renormalized hoppings which can be then explicitly checked *a posteriori*.

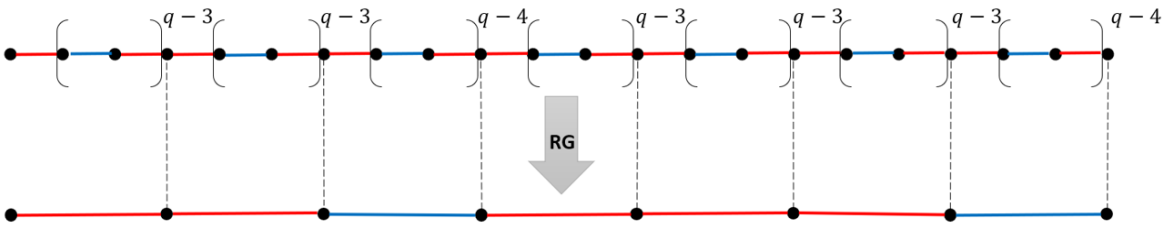


Figure 3.24: Top line: Snippet of the sequence after one decimations step, obtained by rescaling the sequence at the bottom line of Fig. 3.23. We show the application of the second RG step given in (3.175), where $(q-3)$ blocks and their preceding bonds get renormalized to a weak coupling μ_a'', while the $(q-4)$ blocks are renormalized to a strong coupling μ_b''. This identification of weak and strong bonds required the specification of the model, but we show here the behavior encountered in all explicit models we consider for clarity. Bottom line: Resulting sequence after two RG steps, which can be seen to be identical to the original sequence, thus showing that the bond distribution attractor for the for $\{6, q\}$ modulations is a two-cycle.

manifestly different, hence indicating that the single decimation step (3.174) is not a sequence-preserving transformation. This implies that we are dealing with at least a two-cycle bond distribution attractor. To verify the order of the cyclicity, we perform a decimation step again on the sequence obtained after the first RG step. We show this in Fig. 3.24, where the top line represents an extended version of the bottom line of Fig. 3.23. The second decimation step has the form

$$\mathrm{RG}_2^{\{6,q\}} = \begin{cases} a(ba)^{q-3} \mapsto a \\ a(ba)^{q-4} \mapsto b \end{cases} \quad \Longleftrightarrow \quad M_2^{\{6,q\}} = \begin{pmatrix} q-2 & q-3 \\ q-3 & q-4 \end{pmatrix} . \tag{3.175}$$

Upon inspection, we can now verify that the resulting sequence after applying $\mathrm{RG}_2^{\{6,q\}}$ is indeed the original $\mathcal{S}_{\{6,q\}}$ aperiodic sequence. We conclude that the combined action of both decimation steps is now a proper sequence-preserving transformation, i.e. $\Xi^{\{6,q\}} = \mathrm{RG}_2^{\{6,q\}} \circ \mathrm{RG}_1^{\{6,q\}}$. In particular, notice that $M_2^{\{6,4\}} = M_1^{\{6,4\}}$ when $q = 4$, indicating that this case reduces to a one-cycle attractor under the SDRG.

Having demonstrated the RG steps of a two-cycle bond attractor in detail, let us return to the evaluation of the correlation functions in the ASP of $\{6, q\}$ aperiodic spin chains. The parameters $p_b^{(o)}, p_b^{(e)}, l_b^{(o)}, l_b^{(e)}, \tilde{\lambda}$ and $\lambda_+^{(12)}$ can be straightforwardly derived in this case for all $q \geq 4$ using the formulas (3.163), (3.174), and (3.175). Based on these, we can compute the prefactors in (3.170) as a function of q, which read

$$l_b p_b (1 - \alpha_{(6,q)}^{(e)}) = \frac{q^2 - \left(\sqrt{(q-3)(q-2)} + 4\right) q + 2\sqrt{(q-3)(q-2)} + 3}{2(q-3)} , \tag{3.176}$$

$$l_b p_b (1 - \alpha^{(o)}_{(6,q)}) = \frac{-3q + 3\sqrt{(q-3)(q-2)} + 8}{2\sqrt{(q-3)(q-2)}} \,. \tag{3.177}$$

These fully determine the correlation functions via (3.170). Interestingly, note that the limit of these expressions when $q \to \infty$ is 1/4 for (3.176) and 0 for (3.177), suggesting that for large q only singlets in even generations have non-vanishing correlations. At the moment, we do not have a clear understanding of the physical mechanism behind this behavior. However, the $q \to \infty$ limit of $\{p, q\}$ tilings has been related to interesting mathematical structures known as Thompson and Ptolemy groups [433]. It would therefore be highly interesting to study this relation in more detail and see if the properties of these groups can give an intuitive explanation for the behavior of the correlations in (3.176) and (3.177) for large q.

Boundary correlation functions in holography

As advertised in the beginning of this section, we would like to make a comparison between our results for the correlation functions in ASPs and the behavior expected from holography. The following is such a qualitative comparison, which incorporates our previously derived results in Sec. 3.2.2 on the length of discrete geodesics on hyperbolic $\{p, q\}$ tilings.

First, recall that within the AdS/CFT correspondence, the two-point correlation function of an operator O_Δ in the boundary CFT with scaling dimension Δ admits a simplified form in the regime $\Delta \gg 1$ [686, 687]. In particular, it can be written as a function of the continuous bulk geodesic distance $\gamma(x, y)$ between the two boundary points x and y as

$$\langle O_\Delta(x) O_\Delta(y) \rangle \propto e^{-\Delta \frac{\gamma(x,y)}{L_{\text{AdS}}}} \,. \tag{3.178}$$

We omit the introduction of cut-offs for the proper evaluation of the geodesic distance since they will not affect our heuristic argument. If we assume the validity of the formula (3.178) even after the discretization of the spacetime, we can exploit our result (3.28) for the length γ of a discrete geodesic Γ on a generic $\{p, q\}$ tiling. Recall that this explicitly depends on the Schläfli parameters since it is a function of the edge length $s(p, q)$, the asymptotic scaling factor $\lambda_+(p, q)$, and a parity function $\nu(p, q)$, cf. Sec. 3.2.2. Replacing the continuous geodesic length $\gamma(x, y)$ by its discrete counterpart (3.28), we can identify an *effective* scaling dimension which depends on the Schläfli parameters p and q, as

$$\langle O(x) O(y) \rangle_{\text{discr}} \propto \frac{1}{|x-y|^{2\Delta_{\text{eff}}(p,q)}} \,, \qquad \Delta_{\text{eff}}(p, q) = \frac{s(p, q)\nu(p, q)}{\ell \log \lambda_+(p, q)} \Delta \,, \tag{3.179}$$

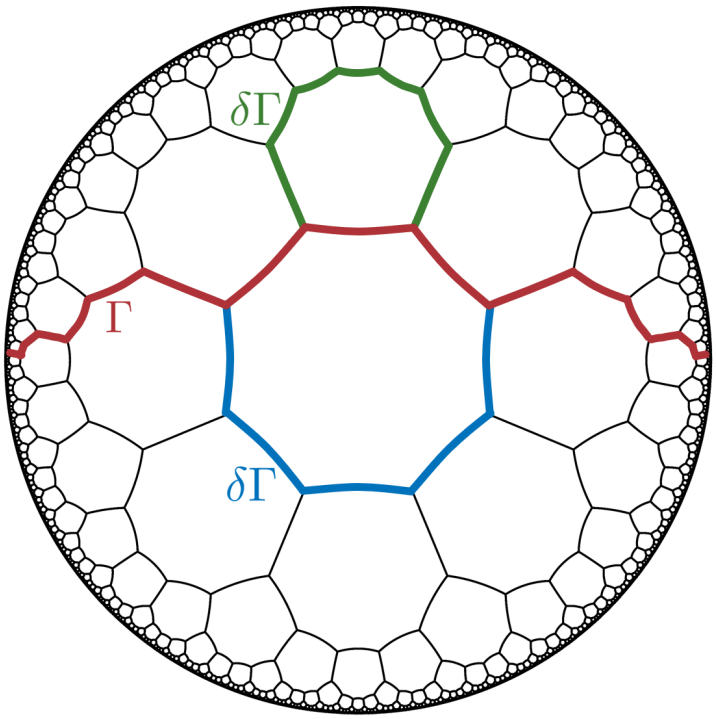


Figure 3.25: Example of a discrete geodesic Γ (red) on an $\{8,3\}$ tiling, together with two cases of small admissible fluctuations $\delta\Gamma$ compatible with the tiling structure. The green fluctuation is 6 edges longer than Γ, while the blue one is 2 edges longer. Since each edge has a geodesic length of the order of the AdS radius, any fluctuation in the geodesic path drastically alters the admissible fluctuations for a scalar field localized on Γ. In particular, there are no infinitesimally small fluctuations.

where ℓ denotes the AdS radius. Here, the norm-distance $|x-y|$ simply counts the number of vertices or sites between x and y on the discrete boundary of the hyperbolic tiling. Evaluating the ratio $\Delta_{\text{eff}}/\Delta$ through explicit insertion of the functions s, ν and λ derived in Sec. 3.2.2, we find that the effective scaling dimension is always larger than the original one. In other words, the discretization via hyperbolic tilings induces an increase of the scaling dimension of operators. We remain agnostic to the precise nature of the operators O in this discussion, since our arguments should hold in general. A possible interpretation for this behavior is as follows: In continuum holography, the large scaling dimension limit $\Delta \gg 1$ implies that the bulk field which is holographically dual to O is extremely localized around the continuum geodesic. This is the reason why the two-point function is dominated by the contribution weighted by the geodesic length. However, in the continuum case, infinitesimal fluctuations away of this geodesic only induce perturbatively small corrections to the two-point function (3.178). We find a starkly contrasting behavior in the discrete setup. Here, any fluctuation of the discrete geodesic Γ has to necessarily run along the $p-1$ or $p-2$ edges of a neighboring

tile, given that the tiles themselves are not part of our discrete space. An exemplary discrete geodesic Γ and two possible fluctuations $\delta\Gamma$ thereof are shown in Fig. 3.25. Such deviations $\delta\Gamma$ change the length of the geodesic by an amount of order $\mathscr{O}(\ell)$, given that each edge length is of order of the AdS radius. This drastically restricts the allowed fluctuations of a scalar field defined on the tilings vertices. In particular, admissible fluctuations in the discrete case cannot be infinitesimal, and indeed need to be rather large to affect the discrete geodesic. This effectively implies a higher degree of localization of the scalar field on the discrete geodesic Γ with respect to the continuum case. In turn, this localization can be associated to an effectively larger mass of the scalar field, in the sense that the inertia of a field excitation towards being moved away from the discrete geodesic is increased. By the mass-dimension relation (2.27), a larger mass corresponds to a larger scaling dimension, which is precisely what our result (3.179) indicates.

3.5.4. Entanglement Entropy in Aperiodic Singlet Phases

We turn to the investigation of entanglement entropy in aperiodic singlet phases, which represent the ground states of our general aperiodic spin chains (3.142). In particular, we elucidate how the entanglement properties of such ground states depend on the Schläfli parameters dictating the modulation of the couplings. At the strong-disorder induced fixed points, governed by ASPs, we expect that the entanglement entropy only depends on p and q due to the previously shown relevance of modulations based on aperiodic sequences $\mathcal{S}_{\{p,q\}}$. We consider Hamiltonians of the form (3.142) and assume that the criteria **I**-**IV** are fulfilled. Consequently, the ground state of the model is described by an ASP. Given a subregion A consisting of L consecutive sites, its entanglement entropy with respect to its complement B can be simply obtained by counting the number of singlets that are shared between A and B. By this we mean that one of the sites in a singlet is located in A while the other is in B, and vice-versa. This way of computing the entanglement entropy was originally implemented for randomly disordered chains [688], where the corresponding ground states obtained through SDRG are known as *random singlet phases* [651, 689–692]. The validity of this methodology is intuitively clear: the correlations in an ASP are dominated by the singlet contributions, but a singlet which is entirely contained in a given subregion cannot contribute to the correlations across a bipartition. If all singlets in the ground state are equivalent, as is the case in the ASP, then the entanglement entropy between A and B can only originate from shared singlets which are cut by the entangling points, cf. Fig. 3.26. We denote this number of shared singlets between both subsystems by $n_{A:B}$. We further denote the entanglement entropy of an individual singlet by s_0 and

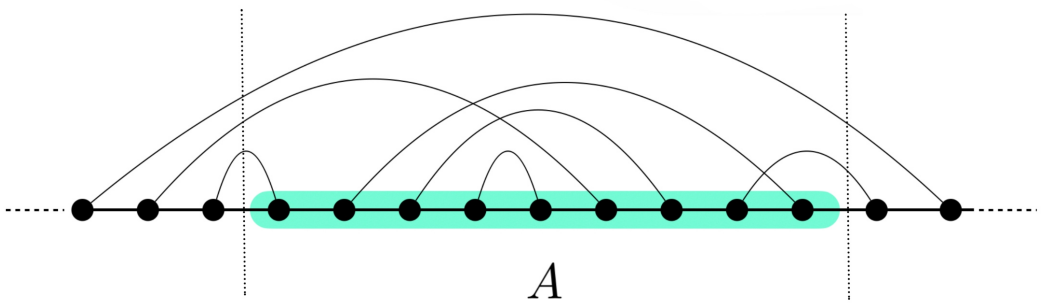


Figure 3.26: Schematic depiction of the typical setup for computing entanglement entropy in aperiodic singlet phases. We consider a subregion A consisting of L sites ($L = 9$ here), with the entangling points coinciding with two bonds on the chain. The factorized structure of a ground state in an ASP, as per (3.152), is superimposed on the chain. The entanglement entropy of the degrees of freedom within A with respect to those outside of A will be given by the number of singlets cut by the entangling points (dotted lines), whereas every singlet gives a contribution of s_0 to the entanglement entropy. Singlets connecting sites which are both within or both outside A do not contribute to S_A. In this example, the entanglement entropy is $S_A = 3s_0$.

its value depends on the explicit form of the singlet state (3.145). For reference, for a chain of spin-1/2 SU(2) spins, the singlet state is a Bell pair and therefore we have $s_0 = \log 2$. Given that the spin chain is not homogeneous, even after fixing the subsystem size L, the exact value of $n_{A:B}$ can vary throughout the chain. It is therefore more proper to work with the number of shared singlets averaged over all possible positions of the subregion A along the chain, a quantity that we denote by $\bar{n}_{A:B}$. This averaging procedure is precisely the point where the statistics associated to the aperiodic sequence enter and bestow a $\{p, q\}$-dependence upon the number of singlets. Accordingly, the entanglement entropy computed from this quantity is also an average entropy, but we will simply refer to it as the entanglement entropy of the system. By the philosophy explained above, this entanglement entropy for a subregion A of size L in an ASP is given by

$$S_A(L) = s_0\, \bar{n}_{A:B}(L)\,. \tag{3.180}$$

Remarkably, notice that this quantity does not depend on the explicit form of the function h in the Hamiltonian (3.142). Rather, it only depends on the properties of the aperiodic modulation based on the aperiodic sequence $\mathcal{S}_{\{p,q\}}$. In the following, we show how $\bar{n}_{A:B}$, and thus $S_A(L)$, are computed explicitly in ASPs.

It is worth to briefly comment on the entire entanglement spectrum of ground states described by ASPs, based on the general result (3.180). This spectrum consists of not

only the entanglement entropy, but all Rényi entropies (2.57) with $\alpha > 1$. Given the factorized structure of the ground state in ASPs (3.152), the reduced density matrix ρ_A of subregion A will also factorize. More precisely, ρ_A will have a tensor product structure containing singlet (pure state) density matrices $\rho_i^{(2s)}$ and reduced density matrices $\rho_j^{(1s)}$ of individual spins belonging to singlets cut by the entangling points, cf. the ASP structure shown in Fig. 3.26,

$$\rho_A = \left(\bigotimes_{i \in \text{singlets}} \rho_i^{(2s)} \right) \otimes \left(\bigotimes_{j \in \text{cut singlets}} \rho_j^{(1s)} \right) . \tag{3.181}$$

This factorized structure implies that all higher Rényi entropies with $\alpha > 1$ will can be broken down into the Rényi entropies of individual singlets. However, the entanglement entropy of an individual singlet is s_0, which is also the value of all its higher Rényi entropies. In other words, we say that the entanglement spectrum is *flat*. This means that a generalization of our results to include the Rényi entropies is trivial as long as we stay within the perturbative assumptions. This is indeed quite different from the behavior of the Rényi entropies for homogeneous critical systems where they exhibit an explicit dependence on the Rényi index [117]. This is a consequence of the factorized structure of the ASP.

The entanglement entropy in ASPs for one-cycle SDRG modulations has been previously studied for specific models, such as the aperiodic XXZ chains [588, 589]. In particular, these works considered the singlet-producing self-similar sequences mentioned in Sec. 3.5.2. Here, we report the results of [158, 159], where the computation of entanglement entropy in ASPs was generalized to two-cycle SDRG modulations and generic aperiodic Hamiltonians of the form (3.142) obeying the criteria **I**-**IV**.

Our goal is to explicitly evaluate the expression (3.180), which requires the knowledge about the precise counting of singlets which are produced during the SDRG procedure and are shared between A and B, thus contributing to the entanglement entropy. To do this, we exploit the previously derived quantities (3.158)-(3.165) which capture the letter statistics of the aperiodic sequence $\mathcal{S}_{\{p,q\}}$ obtained after an asymptotically large number of inflation steps. In particular, these quantities are valid for two-cycle aperiodic modulations under SDRG. To evaluate (3.180), we follow [589] and recall that the fraction W_k of the chain which is covered by singlets of the k-th SDRG generation is given by the values (3.165), which in particular indicated that it is not dependent on the generation index k. Given a subregion A consisting of L sites, we can split the number of singlets contributing to the entanglement entropy into those whose length is smaller $\Lambda_k < L$ and larger $\Lambda_k > L$ than the subregion size. Moreover, recall that

each singlet gives a constant contribution s_0 to the entanglement entropy, whose value depends on the specific model and choice of degrees of freedom. The contributions of the generations containing singlets smaller than L is then given by

$$S_{A,<} = 2s_0\, p_b^{(e)} l_b^{(e)} \left(n^{(e)}(L) + n^{(o)}(L) \right) \equiv 2s_0\, p_b^{(e)} l_b^{(e)} n(L)\,, \tag{3.182}$$

where $n^{(e)}(L)$ and $n^{(o)}(L)$ respectively denote the number of even and odd generations of singlets with $\Lambda_k < L$. Their expressions can be derived from the statistics of the aperiodic sequence and read

$$n^{(e)}(L) = \left\lfloor \frac{\log\left(L/l_b^{(o)}\right) - \log\tilde{\lambda}}{\log \lambda_+^{(12)}} \right\rfloor\,, \qquad n^{(o)}(L) = \left\lfloor \frac{\log\left(L/l_b^{(e)}\right)}{\log \lambda_+^{(12)}} \right\rfloor + 1\,, \tag{3.183}$$

with $\lfloor\cdot\rfloor$ the floor function. Similarly, we can obtain the contributions of generations of singlets with $\Lambda_k > L$ from the expression

$$S_{A,>} = 2Ls_0 \sum_{k=n(L)+1}^{\infty} \rho_k = 2Ls_0 \left(\frac{1}{2} - \sum_{k=1}^{n(L)} \rho_k \right)\,. \tag{3.184}$$

To further manipulate this expression, we need to differentiate between even and odd values of $n(L)$. For odd $n(L)$, we have

$$\begin{aligned} S_{A,>} &= 2Ls_0 \left[\frac{1}{2} - \sum_{k=1}^{[n(L)+1]/2} p_b^{(e)} \left(\lambda_+^{(12)}\right)^{-k+1} - \sum_{k=1}^{[n(L)-1]/2} p_b^{(o)} \tilde{\lambda}^{-1} \left(\lambda_+^{(12)}\right)^{-k+1} \right] \\ &= 2Ls_0 \frac{p_b^{(e)} + p_b^{(o)} \tilde{\lambda}^{-1} \lambda_+^{(12)}}{\lambda_+^{(12)} - 1} \left[\lambda_+^{(12)}\right]^{-(n(L)-1)/2} \equiv S_{A,>}^{(o)}\,, \end{aligned} \tag{3.185}$$

whereas for even values of $n(L)$ even we have

$$\begin{aligned} S_{A,>} &= 2Ls_0 \left[\frac{1}{2} - \sum_{k=1}^{n(L)/2} p_b^{(e)} \left(\lambda_+^{(12)}\right)^{-k+1} - \sum_{k=1}^{n(L)/2} p_b^{(o)} \tilde{\lambda}^{-1} \left(\lambda_+^{(12)}\right)^{-k+1} \right]\,, \\ &= 2Ls_0 \frac{p_b^{(e)} + p_b^{(o)} \tilde{\lambda}^{-1}}{\lambda_+^{(12)} - 1} \left[\lambda_+^{(12)}\right]^{-n(L)/2+1} \equiv S_{A,>}^{(e)}\,. \end{aligned} \tag{3.186}$$

The last equality in (3.162) was used in obtaining both expressions. The total contribution to the entanglement entropy is of course the sum of the singlets with larger and shorter lengths than the subsystem size, i.e. $S_A = S_{A,<} + S_{A,>}$, and we therefore

find

$$S_A = 2s_0\, p_b^{(e)} l_b^{(e)} n(L) + \begin{cases} S_{A,>}^{(e)} & \text{when } n(L) \text{ is even}\,, \\ S_{A,>}^{(o)} & \text{when } n(L) \text{ is odd}\,, \end{cases} \tag{3.187}$$

with the individual terms $S_{A,>}^{(o)}$ and $S_{A,>}^{(e)}$ defined in (3.185) and (3.186), respectively. Equation (3.187) represents the entanglement entropy of a subregion of size L in aperiodic singlet phases associated to two-cycle modulations under the SDRG, generalizing [589]. It is a straightforward check that our results indeed reduce to those of [589] in the case of a one-cycle modulation, since all properties derived above depend on the eigenvalues and eigenvectors of the matrices M_1 and M_2 associated with the decimation steps, which for one-cycle modulations obey $M_1 = M_2$.

We can in fact perform a further analysis of the result (3.187) which yields not only a simpler form, but one that is familiar form continuum results on entanglement entropy in CFTs. For this, notice that the entanglement entropy given in (3.187) has a dependence on the subsystem size which enters via a floor function in $n(L)$. This implies that we can expect the entanglement entropy to exhibit a piece-wise behavior as a function of L, a feature that is known to arise in aperiodically disordered systems [588, 589]. Such a piece-wise linear behavior is drastically different from the homogeneous counterparts of such one-dimensional systems, where entanglement entropy typically exhibits a logarithmic growth with the subsystem size [116, 263], which can be seen as a consequence of the continuum description of such critical systems in terms of CFTs [116–118]. Moreover, this logarithmic dependence has also been found to hold in random singlet phases using SDRG [688], a result that shows perfect agreement with numerical simulations in the case of the XX chain [693]. Given our description of aperiodic disorder as a qualitative interpolation between homogeneous and fully random disorder, one may find the absence of a logarithmic growth in the entanglement entropy (3.187) puzzling.

It turns out, however, that we can indeed make contact with this expected behavior via the following observations. The function (3.187), being piece-wise linear, has breaking points where the slope changes in a non-analytic way. Since the piece-wise function counts the number of singlets of a given length, these breaking points correspond to $L = \Lambda_k$, where Λ_k is defined in (3.158)-(3.159). Upon specifying a set of points $\{\Lambda_{2k-1}\}$ and $\{\Lambda_{2k}\}$ for the even (e) and odd (o) generation singlets, respectively, we can uniquely identify two logarithmic enveloping functions of (3.187). Each of these envelopes will smoothly connect the corresponding set of breaking points. These two functions will share the same coefficient for the logarithmic term, but differ by an additive constant κ_i. More precisely, the entanglement entropy in ASPs obtained through

two-cycle SDRG reads

$$S^{(i)}_{\text{env}}(L) = \frac{c_{\text{eff}}}{3}\log L + \kappa_i, \quad i = e, o\,, \qquad c_{\text{eff}} = \frac{12 p_b^{(e)} l_b^{(e)} s_0}{\log \lambda_+^{(12)}}\,. \tag{3.188}$$

Several comments are in order. First, the coefficient c_{eff} in front of the logarithm is *not* the central charge of a CFT. However, inspired by the aforementioned connections to results in homogeneous critical systems [116–118], we denote it as *effective central charge*. This terminology originated from studies of the entanglement entropy in critical quantum chains with defects, where the prefactor of the logarithmic dependence depends on the defect strength defect strength [694–697]. It was then also adopted in the literature on aperiodic spin chains [437, 588, 589].

We see that although aperiodic spin chains do not enjoy a clear continuum description, their entanglement entropy still captures the functional dependence on the subsystem size known from homogeneous systems at criticality. Remarkably, the effective central charge c_{eff} we obtain is explicitly dependent on the Schläfli parameters via the quantities $p_b^{(e)}, l_b^{(e)}$ and $\lambda_+^{(12)}$. This means that the entanglement entropy of the aperiodic spin chain indeed carries an imprint of the discretization used in the bulk, and different $\{p, q\}$ tilings will lead to different values of the central charge. We will indeed study this quantity in more detail in the following subsection. Second, the non-universal additive constants are also dependent on the specific choice of aperiodic sequences, and we can indeed derive their analytic expression based on the letter statistics of the sequence. The interested reader can find the details of this derivation in Appendix C of [159]. Third, the sets of breaking points converge to a unique set of points when $M_1 = M_2$, meaning that the corresponding envelopes (3.188) coalesce into a single logarithmic envelope, reproducing the results of [589] for the one-cycle SDRG case.

The effective central charge c_{eff}

Let us provide a more detailed study of the effective central charge c_{eff} governing the logarithmic behavior of the entanglement entropy in ASPs. In particular, we are interested in the dependence of this quantity on the Schläfli parameters associated with the hyperbolic $\{p, q\}$ tilings in the bulk. Recall that these parameters determine the inflation rule $\sigma_{\{p,q\}}$ which in turn fixes the aperiodic sequence $\mathcal{S}_{\{p,q\}}$. A particularly instructive starting point is the inflation rule $\sigma_{\{6,q\}}$ with $q \geq 4$, which is the infinite family contained in our admissible modulations (3.153). Recall that if $q = 4$, this sequence describes a one-cycle bond distribution attractor, while for $q > 4$ it is a two-cycle. In this latter case, the matrices M_1 and M_2 describing the sequence-preserving

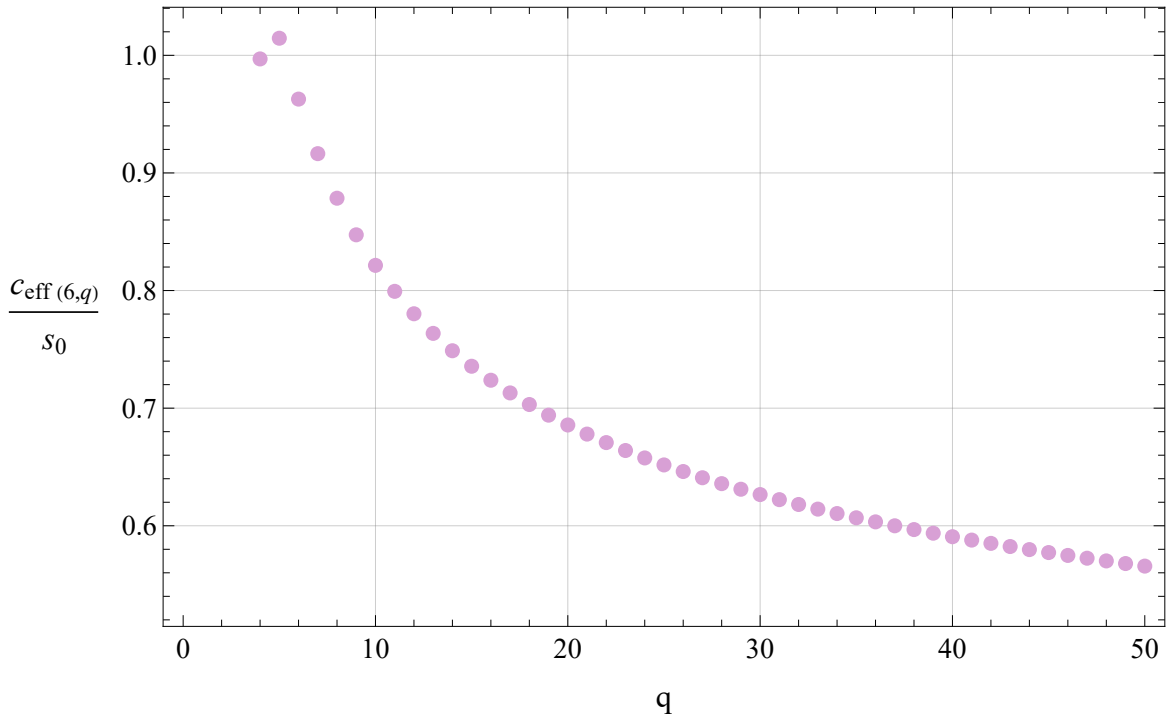


Figure 3.27: Normalized effective central charge $c_{\text{eff}}(6,q)/s_0$ for $\{6,q\}$ aperiodic spin chains for values of $q \in [4,50]$. A maximum is reached early for $q = 5$ with $c_{\text{eff}}(6,q)/s_0 \approx 1.0145$, followed by the onset of a logarithmic decay, as can be expected from (3.189).

transformation are given by (3.174) and (3.175), respectively. Their corresponding characterizing quantities $p_b^{(e)}$, $l_b^{(e)}$, $p_b^{(o)}$, $l_b^{(o)}$, $\tilde{\lambda}$, and $\lambda_+^{(12)}$ can be easily computed using (3.63), (3.64), and (3.163) on these matrices, wherein a q-dependence will be present. Thus, plugging in the resulting expression into (3.187), we find an explicit form of the effective central charge

$$c_{\text{eff}}(6,q) = \frac{6-2q+\sqrt{q^2-5q+6}}{\log\left(2q-5+2\sqrt{q^2-5q+6}\right)}\frac{6s_0}{6-2q}\,, \tag{3.189}$$

which, again, has a non-trivial dependence on the Schläfli parameter q. The unknown value of s_0 in the above expression precludes a full-fledged characterization of the effective central charge for arbitrary values. However, since s_0 only appears as a prefactor in (3.189), it will merely re-scale the overall form of the remaining function. We may therefore plot the q-dependent part of the effective central charge (3.189), i.e. $c_{\text{eff}}(6,q)/s_0$, which is shown in Fig. 3.27. From this figure we see that the function reaches its maximum value of $c_{\text{eff}}(6,q)/s_0 \approx 1.0145$ for $q = 5$, before entering a logarithmic decay for larger q. This behavior has also been observed in [437]. The case of $q = 4$ is that of a one-cycle sequence, namely the silver mean sequence, in which $M_1^{\{6,4\}} = M_2^{\{6,4\}}$. The value of the q-dependent part of the effective central charge in

this case is given by $c_{\text{eff}}(6,q)/s_0 \approx 0.9969$. Being lower than that for $q = 5$, but still larger than for any other $q \geq 6$, it alludes to a special behavior of the one-cycle modulation as compared with the two-cycle one, although the origin of this is not physically clear. Nevertheless, in the case of $s = 1/2$ SU(2) spin singlets, for which $s_0 = \log 2$, we obtain an effective central charge of $c_{\text{eff}}(6,4) \approx 0.6910$, which consistently reproduces the results obtained in [589].

For the sake of completeness, we provide the effective central charges of the other admissible modulations in (3.153). First, we consider the modulation associated to $\{3,8\}$ and $\{5,4\}$ tilings. Though not asymptotically equivalent as inflation rules, both these modulations were two-cycle bond distribution attractors under the SDRG, and their decimation matrices were related via $M_1^{\{3,8\}} = M_2^{\{5,4\}}$ and $M_2^{\{3,8\}} = M_1^{\{5,4\}}$. Mathematically, this means that the quantities $\tilde{\lambda}$ and $\lambda_+^{(12)}$ are the same for both modulations, while the corresponding $p_b^{(e)}$, $l_b^{(e)}$ and $p_b^{(o)}$, $l_b^{(o)}$ vectors alternate in their appearance, as we mentioned previously in our discussion of the correlation functions. Physically, this implies that the distribution of singlets for both aperiodic chains throughout the SDRG is the same upon exchanging even and odd generations. Therefore, the resulting entanglement entropies (3.187) for both modulations enjoy the same effective central charge

$$c_{\text{eff}}(3,8) = c_{\text{eff}}(5,4) = \frac{2(3-\sqrt{3})}{\operatorname{arcosh} 7} s_0 \,, \tag{3.190}$$

but their envelopes differ by the additive constants contained in Appendix C of [159]. Again focusing only on the (p,q)-dependent part, it has a value of $c_{\text{eff}}(3,8)/s_0 = c_{\text{eff}}(5,4)/s_0 \approx 0.6674$. Finally, we have the pair of aperiodic sequences associated to the tilings $\{3,7\}$ and $\{5,5\}$. Recall that their inflation rules were equivalent $\sigma_{\{3,7\}} \sim \sigma_{\{5,5\}}$ in the sense explained in (3.55), an in particular they are both equivalent to the Fibonacci inflation rule as well. The Fibonacci sequence is a one-cycle modulation under the SDRG, since its decimation matrix is sequence-preserving. Indeed, for the Fibonacci XXX chain, the entanglement entropy of a block of L consecutive spin was computed in the ASP ground state in [588, 589], where they find an expression which is entirely consistent with our result in (3.187) applied to the Fibonacci inflation rule. There is a unique envelope for the piece-wise linear entanglement entropy in that case, and the effective central charge, now for arbitrary singlet contributions s_0 generalizing [588, 589], is given by

$$c_{\text{eff}}(3,7) = c_{\text{eff}}(5,5) = \frac{5-\sqrt{5}}{5} \frac{3}{\operatorname{arcsinh} 2} s_0 \,. \tag{3.191}$$

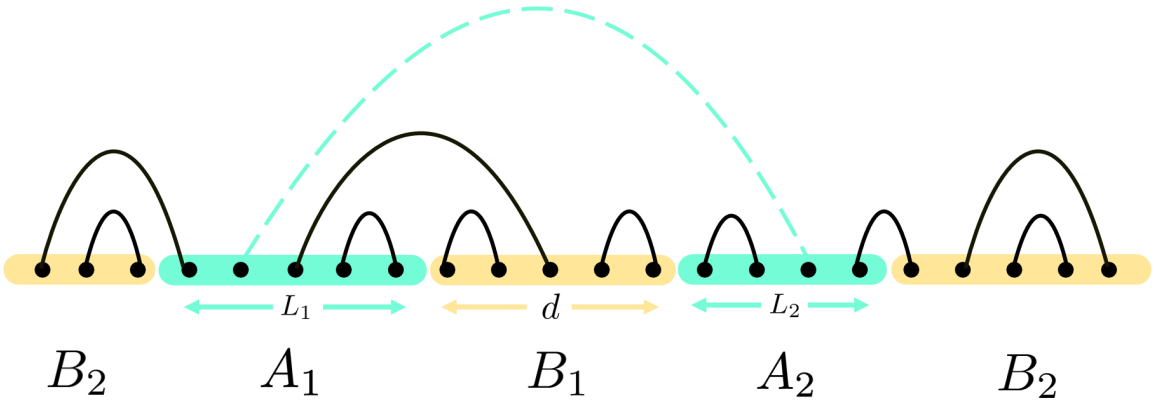


Figure 3.28: Setup for computing the mutual information between two subregions A_1 and A_2 consisting of L_1 and L_2 consecutive sites, respectively, and separated by a region B_1 consisting of d sites. Two adjacent intervals correspond to the case $d = 0$. The complement of the union $A_1 \bigcup A_2$ is the region $B_1 \bigcup B_2$. We have superimposed the factorized structure of the ASP (3.152) onto the chain, with solid arcs denoting spins that are coupled into singlets during the SDRG. In the ASP, the mutual information is proportional to the number of shared singlets between A_1 and A_2, which in this case is equal to one (dashed arc).

For the XXX chain, we have $s_0 = \log 2$ and we retrieve the result $c_{\text{eff}}(3, 7) = c_{\text{eff}}(5, 5) \approx 0.7962$ as in [588, 589].

3.5.5. Mutual Information in Aperiodic Singlet Phases

As we reviewed in Sec. 2.3.1, entanglement entropy ceases to be a good measure of correlations when considering more than one subsystem within a larger system. In these cases, the quantity known as mutual information, introduced and discussed in Sec. 2.3.3, is defined in terms of individual entanglement entropies and provides a better quantitative measure of correlations. Given the results for the entanglement entropy in ASPs obtained in the previous section, it seems natural to explore the mutual information in these states as well. This quantity has been previously studied for random singlet phases [698], and it will prove instructive to first briefly review their construction before we apply it to the aperiodic case. The novel results for aperiodic spin chains with one- and two-cycle modulations were first derived in [159]. At the end, we will compare our results for the mutual information of disjoint intervals separated by d sites to holographic predictions from continuum AdS/CFT [270].

Mutual Information in Random Spin Chains

We review the approach for computing mutual information in random spin-1/2 XXX chains put forward in [698], since the philosophy will be quite similar for the aperiodic case, and we can furthermore generalize it to all models of the type (3.142). We

consider two disjoint subregions A_1 and A_2 containing L_1 and L_2 consecutive sites, respectively, in an infinite aperiodic chain. They are separated by a region B_1 consisting of d sites, while the remaining complement is denoted by B_2. This setup is shown in Fig. 3.28, where we have taken the liberty to already show the structure of aperiodic singlet phases for later reference. Random disorder means that the couplings μ_i in the Hamiltonian are randomly drawn from a fixed distribution instead of being determined by the aperiodic sequence. It is known that this type of disorder can drive lattice systems into an infinite-randomness fixed point, which is described by the aforementioned random singlet phase [688]. The only difference between random singlet phases and ASPs is that the final distribution of singlets is random in the former, while it follows the structure of the aperiodic sequence in the latter. Modulo this distinction, the entanglement structure is the same in both cases [589, 688], such that the very same formulas may be applied. We recall the definition of the mutual information between A_1 and A_2 given in Sec. 2.3.3, which reads

$$I(A_1 : A_2) = S_{A_1}(L_1) + S_{A_2}(L_2) - S_{A_1 \cup A_2}(L_1, L_2, d)\,. \tag{3.192}$$

It is shown in [698] that in the singlet phase, the mutual information $I(A_1 : A_2)$ is proportional to the average number $\bar{n}_{A_1:A_2}$ of singlets shared between the subregions. This proportionality constant is derived to be twice the entanglement entropy s_0 of an individual singlet, which can in fact be left generic as we have done throughout our computations. The mutual information is then given by [698]

$$I(A_1 : A_2) = 2\, s_0\, \bar{n}_{A_1:A_2}\,. \tag{3.193}$$

As in (3.180), $\bar{n}_{A_1:A_2}$ is the average number of singlets shared between the two subsystems. The physical interpretation of this counting can also be borrowed from the entanglement entropy computations. In particular, we can intuitively understand that all correlations between the two subregions can only arise from those singlets which are shared among them. The computational difficulty for the mutual information arises from the precise computation of this average number of singlets $\bar{n}_{A_1:A_2}$. While this number is relatively simple to access for counting singlets between a given region and its complement, it is not *a priori* clear how to obtain it for two generic subregions. To circumvent this difficulty, the authors in [698] suggested a way of re-writing this number into a specific combination of single-region number of shared singlets, which themselves can be expressed in terms of single contiguous-region entanglement entropies. However, these single-regions do not necessarily coincide with the subregions

A_1, A_2, B_1, B_2 shown in Fig. 3.28, but rather they are rather a combination thereof. More precisely, we can re-write $\bar{n}_{A_1:A_2}$ in terms of a sum of numbers of shared singlets $\bar{n}_{\Omega:\Omega^c}$ of contiguous regions $\Omega = \{A_1 \cup B_1, B_1 \cup A_2, B_1, B_1 \cup A_1 \cup A_2\}$ with lengths $L_\Omega = \{L_1 + d, d + L_2, d, d + L_1 + L_2\}$ and their respective complements. The benefit of this is that now the only objects entering the computation are the numbers of singlets between a single interval and its complement. Up to the proportionality constant s_0, these are precisely the entanglement entropies $S_\Omega(L_\Omega)$ of these regions, which we have obtained in Sec. 3.5.4 and is given by (3.180) in general. The final result for the mutual information in given by [698]

$$I(A_1 : A_2) = S_{B_1 \cup A_1}(d+L_1) + S_{B_1 \cup A_2}(d+L_2) - S_{B_1}(d) - S_{B_1 \cup A_1 \cup A_2}(d+L_1+L_2)\,. \quad (3.194)$$

We can therefore immediately implement our results for the single-interval entanglement entropy in ASPs obtained in Sec. 3.5.4 to this formula to compute the mutual information in aperiodic singlet phases, as we do in the following.

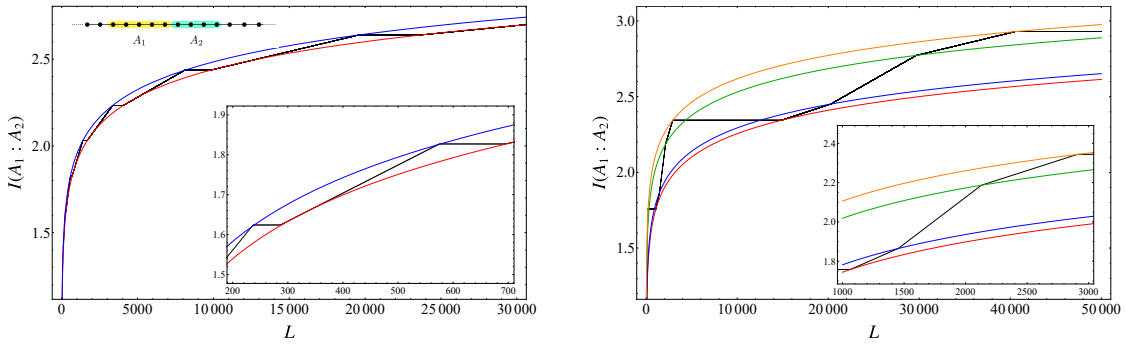
Mutual Information in ASP

We are in position to compute the mutual information in ASPs which appear as strong-disorder fixed points of one- and two-cycle SDRG flows. It is convenient to study the cases of adjacent ($d = 0$) and disjoint ($d > 0$) intervals separately.

Adjacent intervals: For adjacent subregions, we can write the length of one subregion as a multiple of the other without the loss of generality, e.g. $L_1 \equiv L$, $L_2 \equiv aL$, with $a > 0$. This simplifies the formula (3.194) to

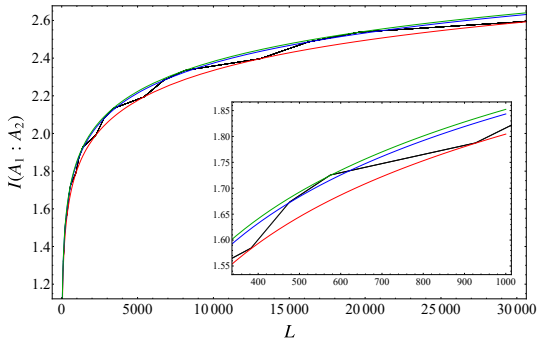
$$I(A_1 : A_2) = S_{A_1}(L) + S_{A_2}(aL) - S_{A_1 \cup A_2}((1+a)L)\,. \quad (3.195)$$

Each of the terms in this expression can be explicitly evaluated using our results (3.188) and (3.187) for the single-interval entanglement entropy in ASPs. Up to the choice of s_0, we can thus derive the general value of the mutual information, which we show in the panels of Fig. 3.29 for the exemplary cases of $\{6, 4\}$ and $\{6, 6\}$ modulations. The distinction between the panels of the same modulation is due to the precise value of the proportionality factor a, and we will explain it in detail below. Generally, we observe in Fig. 3.29 that the mutual information retains the piece-wise linear behavior of the entanglement entropy with associated enveloping functions. Moreover, we can analytically track the positions of all breaking points by the behavior of the floor functions entering (3.183), as explained in Appendix C of [159]. Given the structure of the mutual information (3.194), we may expect that the enveloping functions of $I(A_1 : A_2)$

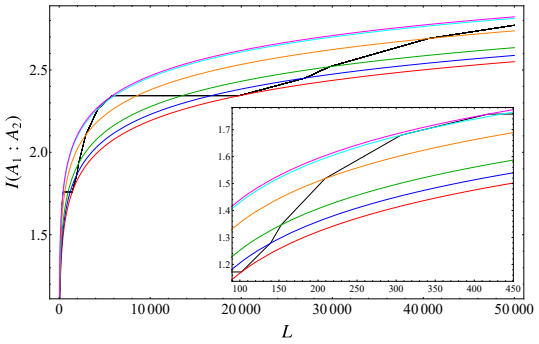


(a) $\{6, 4\}$, $a = 1$.

(b) $\{6, 6\}$, $a = 1$.



(c) $\{6, 4\}$, $a = \frac{1}{2}$.



(d) $\{6, 6\}$, $a = \frac{1}{2}$.

Figure 3.29: Mutual information $I(A_1 : A_2)$ in an ASP for the case of two adjacent intervals with $L_1 \equiv L$ and $L_2 \equiv aL$, obtained for two different aperiodic modulations via (3.193) with $s_0 = \log 2$. We have chosen a one-cycle ($\{6, 4\}$) and a two-cycle ($\{6, 6\}$) modulation as examples such as to cover the four cases of interest given in Table 3.2 for equal and unequal subsystem sizes.

are simply the sum of the individual envelopes of the entanglement entropies. This, however, turns out not to be the case, and their treatment is much more subtle. This is because the expression (3.195) has in general three length scales, namely L, $a\,L$ and $(1 + a)L$. Each of these length scales has an associated set of breaking points $\{x_k\}$, which are the points at which the logarithmic envelope (3.188) and the corresponding entropy $S_\alpha(x_k)$, with $\alpha = \{A_1, A_2, A_1 \cup A_2\}$ *exactly* match. In the case of adjacent intervals, the lack of an extra reference length scale due to $d = 0$ allows us to exploit the properties of the logarithm function. More precisely, we can manipulate the expressions for $\log aL$ and $\log(1 + a)L$ and extract an overall $\log L$ factor, while simultaneously keeping careful track of the non-universal constants κ of the envelopes corresponding to all three length scales. In this way, we are able to find the set of envelopes corresponding to the entire mutual information, implying that we can derive

	one-cycle	two-cycle
$a = 1$	2	4
$a \neq 1$	3	6

Table 3.2: Total number of enveloping functions for the mutual information of two adjacent intervals in an ASP, for both the cases of equal and unequal interval lengths, and one- and two-cycle modulations. We choose $L_1 \equiv L$ and $L_2 \equiv aL$, such that $a = 1$ and $a \neq 1$ denote the equal and unequal length cases, respectively. The number of envelopes also indicates the number of different additive constants $\beta^{(i)}$ in (3.196).

a result similar to (3.188) for $I(A_1 : A_2)$ which reads

$$I^{(i)}_{\text{env}}(A_1 : A_2) = \frac{c_{\text{eff}}}{3} \log L + \beta^{(i)} , \quad i = 1, \ldots, k ; \qquad k \in \{2, 3, 4, 6\} . \tag{3.196}$$

Here, a new set of non-universal additive constants $\beta^{(i)}$ has been defined (also contained in Appendix C of [159]), whose number of elements denotes the total number of enveloping functions. As alluded to previously, this number is related to the proportionality factor a and we summarize this relation in Table 3.2. The coefficient c_{eff} of the logarithmic term is precisely the effective central charge previously obtained in (3.187). As we did for the entanglement entropy, it is interesting to compare our result (3.196) to that obtained from continuous CFT computations [290, 292, 699, 700]. In particular, we find that the mutual information $I(A_1 : A_2)$ exhibits the same functional dependence on the subsystem size as the continuum result, albeit with a different multiplicative prefactor. The latter, together with the non-universal additive constants, carries the dependence of the mutual information on the Schläfli parameters of the bulk discretization. Surprisingly, we find a direct relation between the number of total envelopes for the mutual information, the number of length scales in the setup, and the cyclicity of the corresponding modulation under SDRG. We summarize this relation in Table 3.2, as well as in Fig. 3.29, where each panel showcases one of the entries of this table. In particular, for unequal subsystem sizes $a \neq 1$ and one-cycle modulations like $\{6, 4\}$, there exist three length scales in the system and the mutual information has three enveloping functions, cf. Fig. 3.29c. These envelopes coalesce into only two when the intervals become equal in length, i.e. $a = 1$, as seen in Fig. 3.29a. For two-cycle modulations such as $\{6, 6\}$, we observe a doubling effect with respect to the one-cycle case, due to the fact that even and odd generations each have a corresponding set of envelopes. Thus, we expect to see four envelopes when $a = 1$ and six envelopes when $a \neq 1$, which is precisely the behavior seen in Fig. 3.29b and Fig. 3.29d, respectively.

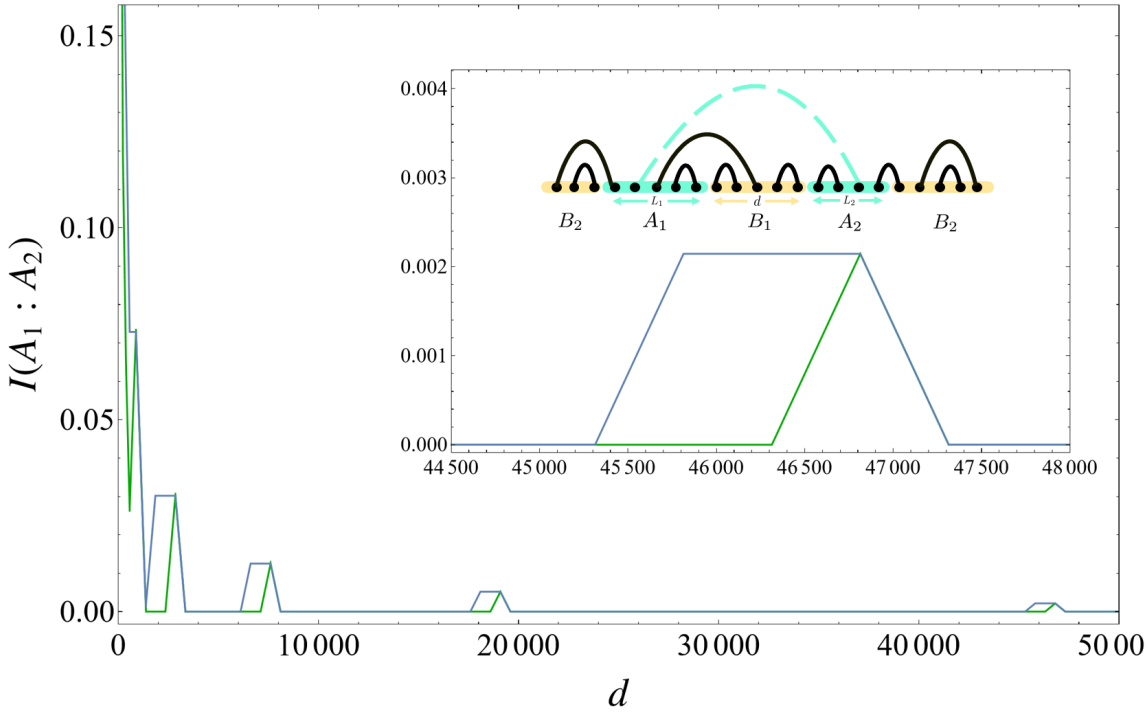


Figure 3.30: Mutual information $I(A_1 : A_2)$ as a function of d in an ASP for two disjoint intervals with equal (green line, $L_1 = L_2 = 500$) and unequal (blue line, $L_1 = 500$, $L_2 = 1500$, $a = 3$) length for the case of the one-cycle $\{6, 4\}$ modulation, as computed from (3.194). Inset: Example of peak (hill) of non-vanishing mutual information at around $d \approx 47000$ after a large regime of vanishing $I(A_1 : A_2)$, showcasing the properties of the ASP. The schematic structure of the latter is recalled along with the setup as in Fig. 3.28. We have once again chosen $s_0 = \log 2$ for concreteness.

Disjoint intervals: We turn our attention to the case of two disjoint intervals, i.e. $d \neq 0$, as per the original setup of Fig. 3.28. As previously appraised, the presence of an additional length scale $d \neq 0$ complicates the evaluation of terms like $S(aL + d)$ appearing in (3.194). Technical details on this complication are given in Appendix C of [159], where it is explained how d enters additively in the floor functions in (3.183) and does no longer allow for the identification of enveloping functions. Nevertheless, we still have analytical access to the expressions of each of the terms appearing in (3.194), meaning that we may directly evaluate the mutual information. Since we are interested in the dependence of the mutual information on the distance d, we may fix the ratio of the subsystem sizes without the loss of generality. The resulting behavior is shown in Fig. 3.30 for the exemplary case of a $\{6, 4\}$ modulation. We include two curves for the cases of equal (green line) and unequal (blue line) subsystem sizes. Fig. 3.30 displays a remarkably interesting behavior for the mutual information $I(A_1 : A_2)$, namely a piece-wise linear decay but without enveloping functions and

with regions of vanishing mutual information. The absence of enveloping functions obstructs a direct quantitative comparison with continuum results from CFT [247, 290, 292, 699, 700], where it is expected that mutual information decays algebraically with the distance. Furthermore, the vanishing mutual information for certain ranges of d is intriguing and seems to mirror a feature unique to aperiodically disordered systems. In particular, notice that these regions where $I(A_1 : A_2) = 0$ are separated by either "peaks", in the case of equal-sized subsystems, or "hills", for instances of unequal interval lengths. The visualization in Fig. 3.30 shows that the appearance of these two isolated behaviors becomes sparse as $d \to \infty$, and their corresponding amplitudes decrease as well with increasing distance. This is a unique feature of the ASP and is a consequence of the existence of singlets at arbitrary scales [159]. Namely, as we move the subregions further apart, we can expect to find a singlet which is shared between them at arbitrarily large distances, but their contribution to the mutual information will be minor as d increases. This prevents $I(A_1 : A_2)$ from remaining zero after any finite critical distance d_c and explains the surfacing of peaks and hills after arbitrarily large distances. The behavior we find for the mutual information is starkly distinct from that expected from holographic theories. More precisely, it is a consequence of the RT formula [114, 115] for holographic entanglement entropy that holographic mutual information between two intervals in a CFT should experience a sharp transition after a finite critical distance d_c [270]. In particular, holographic mutual information is expected to vanish identically for $d > d_c$. The reason for this is that the corresponding RT surface in the bulk undergoes a first-order phase transition from a single connected to two disconnected geodesics [270]. It is nevertheless intriguing to see that the aperiodic spin chains proposed in [158, 159] as possible boundary theories in a discrete holographic duality exhibit a behavior which in some sense interpolates between that of holographic [270] and non-holographic theories [247, 290, 292, 699, 700].

3.5.6. Explicit Models

The previous sections have provided a broad overview of the general results that can be obtained for several quantities in ground states of aperiodic Hamiltonians of the form (3.142) which obey the criteria **I-IV**. Such an overarching platform opens the door for studying several specific models. In the following, I show three explicit examples of such models and report on their ground state properties by directly applying the results derived above. All three of these models can be thought as starting points for discrete holographic dualities, and we elucidate more on their respective potential below.

Aperiodic XXZ Spin Chains

We begin with aperiodic XXZ chains, which correspond to the choices $\theta_x = \Delta_0$ and $h(\vec{\sigma}_i, \vec{\sigma}_{i+1}; \Delta_0) = X_i X_{i+1} + Y_i Y_{i+1} + \Delta_0 Z_i Z_{i+1}$ in the general aperiodic Hamiltonian (3.142). Here, X_i, Y_i, Z_i denote the Pauli matrices in the local Hilbert space at site $i \in \mathbb{Z}$ and describe spin degrees of freedom furnishing a spin-1/2 irreducible representation of the SU(2) group. Concretely, the aperiodic XXZ Hamiltonian reads

$$H = \sum_{i \in \mathbb{Z}} \mu_i \left[X_i X_{i+1} + Y_i Y_{i+1} + \Delta Z_i Z_{i+1} \right] , \tag{3.197}$$

where the hopping parameters μ_i are modulated according to an aperiodic sequence $\mathcal{S}_{\{p,q\}}$. The initial anisotropy parameter is homogeneous throughout the chain and we take it to lie in the window $0 \leq \Delta_0 \leq 1$. This guarantees that the underlying homogeneous XXZ chain is in its gapless regime, where it enjoys a continuum description in terms of a compactified free boson CFT with $c = 1$ and a the compactification radius determined by Δ_0 [652]. The XXZ model (both in its homogeneous and disordered versions) is an interacting model, as can be seen by applying a Jordan-Wigner (JW) transformation to spinless fermions. When $\Delta_0 = 0$, the model (3.197) reduces to the Hamiltonian of the aperiodic XX model, which is a free model after mapping it via the JW to a chain of free fermions. Instead, when $\Delta_0 = 1$, the model (3.197) describes the so-called aperiodic XXX spin chain.

The XXZ model remains critical upon introducing aperiodic disorder for all $\{p, q\}$ modulations [158, 590, 591, 684], as we discussed below (3.142). Rather interestingly, however, this is not guaranteed if we consider other types of spin degrees of freedom, like integer-spin irreps of SU(2). In fact, aperiodic spin-1 XXX chains were found to have a finite gap in their spectrum in the thermodynamic limit, in contrast to their spin-1/2 counterparts [655]. We are therefore motivated to consider spin-1/2 XXZ chains where the criticality condition is well understood [590, 648, 684], but we will later see that other choices of local degrees of freedom are possible for other models.

We can readily apply the formulas derived in Sec. 3.5.2 to the aperiodic XXZ chain modulated by any of the admissible sequences (3.153). The latter restriction implies that only singlets arise throughout the SDRG procedure, corresponding to decimation blocks of the form in Fig. 3.21a. This analysis was done in [590, 591] for one-cycle modulations and was extended to two-cycle modulations in [158]. A feature of the SDRG on aperiodic XXZ chains is that the anisotropy parameter, which was originally homogeneous, inherits an aperiodic disorder upon decimation and gets renormalized into to two different anisotropies Δ_{l}, Δ_{r}. Using (3.146), the renormalized parameters μ' and

Δ' of the system after a single decimation of a block of n strongly-coupled spins read

$$\mu' = \gamma_n(\Delta_0)\frac{\mu_\mathrm{l}\mu_\mathrm{r}}{\mu_0}\,, \qquad \Delta' = \delta_n(\Delta_0)\Delta_\mathrm{l}\Delta_\mathrm{r}\,, \tag{3.198}$$

where γ_n and δ_n are functions of the anisotropy Δ_0 and the number n of strongly-coupled spins. In general, they should obey $|\delta_n(\Delta_0)| < 1$ when $0 \leq \Delta_0 < 1$ and $\delta_n(1) = 1$. However, since these functions are obtained from perturbation theory, we do not have access to their analytical expression for arbitrary values of n to check the aforementioned constraints. For small values of n like $n = 2$, their expressions are indeed known [590, 591, 681, 682] and read

$$\gamma_2(\Delta_0) = \frac{1}{1+\Delta_0}\,, \qquad \delta_2(\Delta_0) = \frac{1+\Delta_0}{2}\,. \tag{3.199}$$

For larger values of n, we are forced to evaluate the constraints $\delta_n \leq 1$ when $0 \leq \Delta_0 \leq 1$ and $\gamma_n(1) < 1$ numerically. This is done in Appendix B of [158], to which we refer the reader for technical details. For the admissible aperiodic modulations given in (3.153), however, the only decimation blocks that are needed are those with $n = 2$ or blocks of type $a(ba)^k$ with $k \geq 1$, whose expression for the renormalized coupling is similar to that in (3.198) and can also be found through perturbation theory.

Based on the above equations, we can already describe the main properties of aperiodic XXZ spin chains at criticality, which can be visualized in the parameter space (r, Δ_a, Δ_b) shown in Fig. 3.31. These qualitative properties are valid regardless of the specific form of the aperiodic modulation, but we should keep in mind that different Schläfli symbols will give rise to distinct phase diagrams with the same general features. First, the top face of the phase diagram corresponds to a hopping ratio $r \equiv \mu_a/\mu_b = 1$, which further implies that the models along the diagonal $\Delta_a = \Delta_b = \Delta_0$ are homogeneous. Each value of the anisotropy Δ_0 gives rise to a different fixed point (yellow dots in Fig. 3.31), described by a free compactified boson CFT with a different compactification radius. Second, note that the constraint $\delta_n(\Delta_0) < 1$ when $0 \leq \Delta_0 < 1$ implies that the anisotropy parameter flows to a fixed point characterized by $\Delta_a^* = \Delta_b^* = 0$ according to (3.198). Therefore, in the presence of aperiodicity $r < 1$, the aperiodic XXZ model with $0 \leq \Delta_0 < 1$ enjoys the same critical behavior as the aperiodic XX model. We visualize this behavior for an exemplary point in the phase diagram by the light blue arrow in the bottom part of Fig. 3.31. Since the SDRG is a perturbative approach, this picture is technically only reliable in the bottom part of the phase diagram where $r \ll 1$. If we directly start with an aperiodic XX chain, meaning $\Delta_0 = 0$, the critical behavior under aperiodic modulations can be determined exactly

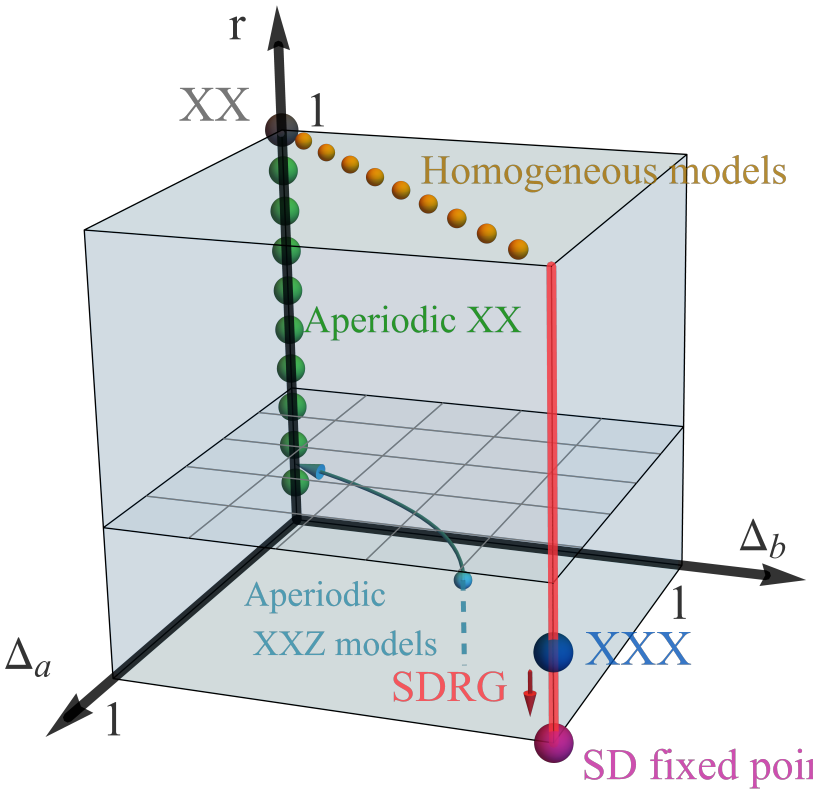


Figure 3.31: Portion of the phase diagram of the aperiodic XXZ chain (3.197) in its critical window. The horizontal grid plane broadly indicates the regime where the perturbative assumption of the SDRG is valid and the results are reliable. The marginality of aperiodic disorder for XX chains with $0 \leq r < 1$ leads to a line of r-dependent fixed points (green) and can be derived using the exact methods of [648]. The distinct axes for the anisotropies Δ_a and Δ_b are required due to the effective aperiodicity induced on the original homogeneous anisotropy Δ_0 by the SDRG procedure. The top face of the diagram describes models with $r = 1$. Along the diagonal with $\Delta_a = \Delta_b \equiv \Delta_0$, the homogeneous XXZ chain is known to have a continuum description at its fixed points (yellow) in terms of a compact boson with a Δ_0-dependent compactification radius [652]. For disorder values $r \ll 1$ below the grid plane, the aperiodic XXZ model with any initial anisotropy $\Delta_0 < 1$ will flow towards an XX fixed point (light blue arrow) as a consequence of the marginality of the modulation. In contrast, when $\Delta_0 = 1$, the aperiodic XXX chain is driven by the SDRG towards a new, strong-disorder fixed point with $r^* = 0$ (dark blue dot, red arrow, and purple dot).

via the methods of [648], and one can show that the aperiodic modulations associated to $\sigma_{\{p,q\}}$ inflation rules are marginal for any pair $\{p, q\}$. This means that the fixed point r^* reached by the hopping ratio under the SDRG is a finite constant value which depends on the initial value of r. The marginality of the aperiodic modulations on the XX chain are depicted in Fig. 3.31 by the line of fixed points denoted by green dots

along the vertical line $\Delta_a = \Delta_b = 0$. Finally, when we have $\Delta_0 = 1$, corresponding to an aperiodic XXX chain, we have $\delta(1) = 1$ and the anisotropy parameter does not get renormalized at all and therefore does not flow under SDRG. Instead, it stays at its fixed original value of unity and remains homogeneous throughout the chain. As for the coupling ratio $r \equiv \mu_a/\mu_b$, a proof that all the aperiodicities generated by $\{p, q\}$ inflation rules lead the system to a fixed point different from the homogeneous one, meaning that all these modulations are relevant, can be found in Appendix B of [158]. In particular, we will show below for the exemplary case of the $\{6, q\}$ modulation that the new strong-disorder fixed point is characterized by $r^* = 0$ as defined in (3.151). This is represented in the phase diagram in Fig. 3.31 by the dark blue dot flowing towards the strong-disorder fixed point (purple dot) along the red vertical edge at $\Delta_a = \Delta_b = 1$. In the case of such relevant modulations, the perturbative assumption is reinforced after every decimation step, meaning that the SDRG method presented here becomes asymptotically exact. The generalization to any pair $\{p, q\}$ is quite challenging using the standard methods presented here. In Sec. 3.5.7 we will introduce an equivalent graphical approach using the language of tensor networks, which allows to prove the relevance of all $\{p, q\}$ modulations in aperiodic XXX spin chains.

Let us now explicitly apply the formulas of Sec. 3.5.2 to the aperiodic XXZ chain, in the specific case of the infinite family of admissible modulations $\{6, q\}$ with $q > 4$. Our goal is to explicitly show how the couplings are renormalized and thus verify the qualitative considerations performed above. For this, we will make use of the properties of this aperiodic sequence, which we have previously discussed in Sec. 3.5.3, specifically in the expressions (3.173)-(3.175). Recall that a sequence-preserving transformation is obtained after two RG steps, since the modulation is a two-cycle attractor. After the first decimation step, described by (3.174) and shown in Fig. 3.23, the renormalized parameters read

$$\begin{aligned} \mu_a' &= \gamma_2(\Delta_0)\frac{\mu_a^2}{\mu_b}\,, \quad \mu_b' = \mu_a\,, \\ \Delta_a' &= \delta_2(\Delta_0)\Delta_0^2\,, \quad \Delta_b' = \Delta_0\,, \end{aligned} \tag{3.200}$$

with the functions $\gamma_2(\Delta_0)$ and $\delta_2(\Delta_0)$ reported in (3.199). Already we can see that in the case of the XXX chain, i.e. $\Delta_0 = 1$, the anisotropies do not get renormalized, as foreshadowed above. We however continue the treatment with arbitrary values of Δ_0. After the second RG step, described by the q-dependent decimation matrix in (3.175)

and depicted in Fig. 3.24, the renormalized couplings are given as follows

$$\begin{aligned} \mu_a'' &= \Big(\gamma_2(\Delta_b')\Big)^{q-3} \frac{\mu_a'^{q-2}}{\mu_b'^{q-3}}\,, \quad \mu_b'' = \Big(\gamma_2(\Delta_b')\Big)^{q-4} \frac{\mu_a'^{q-3}}{\mu_b'^{q-4}}\,, \\ \Delta_a'' &= \Big(\delta_2(\Delta_b')\Big)^{q-3} \Delta_a'^{q-2}\,, \quad \Delta_b'' = \Big(\delta_2(\Delta_b')\Big)^{q-4} \Delta_a'^{q-3}\,. \end{aligned} \tag{3.201}$$

Since we now recover the original sequence, we can directly relate the parameters in (3.201) to the original ones (μ_a, μ_b, Δ_0), finding

$$\begin{aligned} \mu_a'' &= \Big(\gamma_2(\Delta_0)\Big)^{2q-5} \frac{\mu_a^{q-1}}{\mu_b^{q-2}}\,, \quad \mu_b'' = \Big(\gamma_2(\Delta_0)\Big)^{2q-7} \frac{\mu_a^{q-2}}{\mu_b^{q-3}}\,, \\ \Delta_a'' &= \Big(\delta_2(\Delta_0)\Big)^{2q-5} \Delta_0^{2q-4}\,, \quad \Delta_b'' = \Big(\delta_2(\Delta_0)\Big)^{2q-7} \Delta_0^{2q-6}\,. \end{aligned} \tag{3.202}$$

In particular, the RG flow of the hopping ratio after a single sequence-preserving transformation $\Xi^{\{6,q\}} = \mathrm{RG}_2^{\{6,q\}} \circ \mathrm{RG}_1^{\{6,q\}}$ reads

$$r'' = \Big(\gamma_2(\Delta_0)\Big)^2 r\,. \tag{3.203}$$

Iterating this procedure, we can obtain the fixed points in analogy with (3.151) to which the system flows under SDRG, which we see are entirely determined by the functions γ and δ. In a similar fashion as described above while discussing the phase diagram, we see that for an initial anisotropy $0 \leq \Delta_0 < 1$, we have $\delta_2(\Delta_0) < 1$ as per (3.199), meaning that the anisotropies flow towards a XX chain fixed point with $\Delta_a^* = \Delta_b^* = 0$. In this case, the hopping ratio flows to a non-vanishing r^*, which depends on the initial value of r, in agreement with the marginality of the $\{6, q\}$ modulation for XX chains. The more interesting case is when $\Delta_0 = 1$, i.e. the XXX chain, where we have $\gamma_2(\Delta_0 = 1) = \frac{1}{2}$ and $\delta_2(\Delta_0 = 1) = 1$. Here, the anisotropy remains equal to unity throughout the SDRG procedure, while the bare hopping ratio is driven to the strong-disorder fixed point $r \to r^* = 0$, consistent with the relevance of the $\{6, q\}$ modulation for XXX chains. Let us recall that in the case of $q = 4$, the $\{6, 4\}$ modulation is a one-cycle under the SDRG, and the decimation (3.174) is sequence-preserving by itself. This means that the entire RG flow can be obtained from the renormalized couplings in (3.200) alone, but the entire discussion given above is still valid. The behavior found here and summarized in the phase diagram in Fig. 3.31 motivates us to focus on the study of the aperiodic XXX chain, since this model has a ground state described by an aperiodic singlet phase.

We continue our investigation of the aperiodic XXX chain with the computation of

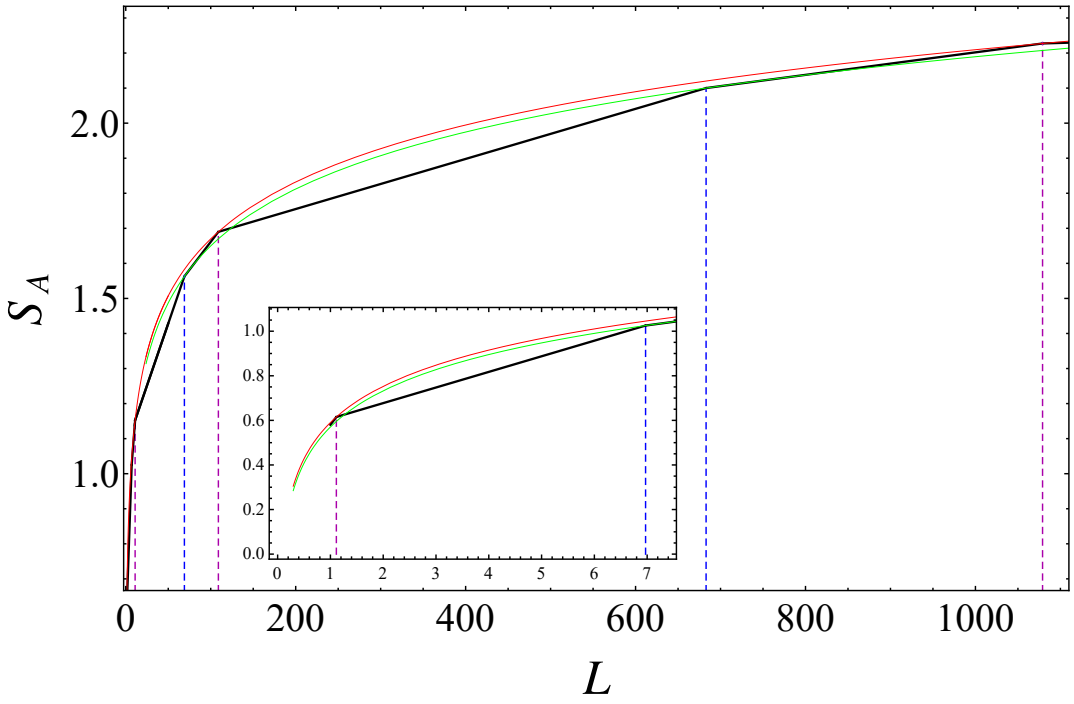


Figure 3.32: Behavior of the entanglement entropy of a block of L consecutive sites on an aperiodic XXX chain in an ASP, shown here for the case of the two-cycle $\{6, 5\}$ modulation. The solid black line shows the piece-wise linear behavior obtained from (3.187), while the colored curves depict the logarithmic envelopes of (3.188) with additive constants $\kappa_1 \simeq 0.576$ (green) and $\kappa_2 \simeq 0.591$ (red). The effective central charge of both curves is given by (3.189) with $q = 5$. The breaking points of the black curve occurring at $L = \Lambda_{2k-1}$ (3.158) and $L = \Lambda_{2k}$ (3.159) are indicated by the dashed blue and purple lines, respectively.

the correlation functions in the ASP ground state. For one-cycle modulations, these were first computed in [590, 591]. The generalized results for two-cycle bond attractors under SDRG are those derived in (3.170), where the singlet correlation takes on the value $c_0 = -1$.[17] For the specific case of the $\{6, q\}$ modulations, the correlation functions are those in (3.170) with the specific coefficients derived in (3.176)-(3.177).

Let us now shift our focus to the study of entanglement entropy in the ASP ground state of aperiodic XXX chains. Since the criteria **I**-**IV** are fulfilled, the entanglement entropy of a block of L consecutive spins is given by the results derived in [589] for one-cycle modulations, and their generalization given in (3.187) for the two-cycle case. The quantity s_0 is now given by $s_0 = \log 2$, since this is the entanglement entropy of an SU(2) singlet, i.e. the Bell state $|\psi\rangle = \frac{1}{\sqrt{2}}(|01\rangle - |10\rangle)$. For our favorite example of two-cycle modulations, namely the $\{6, q\}$, we plot the entanglement entropy (3.187) with

[17] Note the difference with respect to [590, 591] where the correlation of two spins in a singlet was $c_0 = -1/4$. This apparent discrepancy lies simply in the normalization of the spin operators appearing in the Hamiltonian, which the author of [590, 591] takes to be $\vec{S} = \frac{1}{2}\vec{\sigma}$.

the envelopes (3.188) for $q = 5$ in Fig. 3.32. The black line showcases the predicted piece-wise linear behavior, with breaking points occurring at the positions $L = \Lambda_{2k-1}$ (blue vertical dashed lines) and $L = \Lambda_{2k}$ (purple vertical dashed lines) given in (3.158) and (3.159), respectively. The two-cycle nature of the $\{6, 5\}$ modulation is made manifest by the presence of the two enveloping functions (3.188) in Fig. 3.32, which we depict as colored curves. More precisely, the green envelope is the function touching the piece-wise linear entanglement entropy at the breaking points $L = \Lambda_{2k-1}$, while the red one touches the black curve at the breaking points at $L = \Lambda_{2k}$. The coefficient of the logarithm is the effective central charge c_{eff} given in (3.189) evaluated for $q = 5$ and $s_0 = \log 2$. The additive constants were obtained analytically in Appendix B of [159].

As for the mutual information in the ASP ground state of aperiodic XXX chains, the results are those reported in Sec. 3.5.5 upon imposing $s_0 = \log 2$ in all instances where the effective central charge appears. Indeed, all figures in that subsection where computed for this choice of s_0, and we will therefore not discuss them further here. This concludes our discussion of the ground state properties of aperiodic XXZ chains for modulations which are both one- and two-cycle bond distribution attractors under the SDRG.

Aperiodic Spin Chains with Dihedral Symmetry

Next, we will consider a model which is inspired by the original matching of symmetries that makes the AdS/CFT correspondence so robust, as explained in Sec. 2.2. The results presented here were originally published in [159]. Following the paradigm of AdS/CFT, we would like to define boundary degrees of freedom in such a way that they transform under irreducible representations of the isometry group of the bulk. As we have mentioned already in Sec. 3.2.4, whenever we deal with truncated hyperbolic $\{p, q\}$ tilings, the Fuchsian isometry group is broken down to a cyclic group $\mathbb{Z}_n$, with $n = p$ or $n = q$ depending on whether we consider polygon-centered or vertex-centered tilings, respectively. Cyclic groups are, however, Abelian, meaning that they only admit one-dimensional irreducible representations. To make our putative model have a slightly richer structure, we will allow also for orientation-reversing transformations. This enhances the symmetry group to the dihedral group D_n, which is defined by the presentation

$$D_n = \langle r, s | r^n = s^2 = e,\, rs = sr^{-1} \rangle \,, \tag{3.204}$$

with e denoting the identity element of the group. The presentation (3.204) makes manifest that the generators r, s act by implementing a rotation by an angle $\frac{2\pi}{n}$ and a reflection with respect to a fixed axis, respectively. Fortunately, the representation

theory of dihedral groups is known explicitly, as we review in the following. We will later exploit this to construct a boundary Hamiltonian whose local degrees of freedom arrange into multiplets of D_n irreps.

Let us review the representation theory of D_n. It is known that, depending on the parity of the order n of the group, there is a different, yet finite number of unitary irreps. Namely, for even n there exist $\lceil n/2 \rceil + 3$ irreps, while for odd n there are $\lceil n/2 \rceil + 1$, where $\lceil \cdot \rceil$ denotes the ceiling function. A large number $\lceil n/2 \rceil - 1$ of the irreps are two-dimensional, and there are only 4 one-dimensional irreps when n is even and 2 one-dimensional irreps when n is odd [701, 702]. The way to uniquely identify a representation, up to basis changes, is by their action on the generators r, s of the group. In particular, for even n, we denote the 4 one-dimensional irreps by Φ_l, $l = 1, 2, 3, 4$ and their action on the generators is given by

$$\Phi_1(r) = 1\,, \qquad \Phi_1(s) = 1\,, \tag{3.205}$$

$$\Phi_2(r) = -1\,, \qquad \Phi_2(s) = 1\,, \tag{3.206}$$

$$\Phi_3(r) = 1\,, \qquad \Phi_3(s) = -1\,, \tag{3.207}$$

$$\Phi_4(r) = -1\,, \qquad \Phi_4(s) = -1\,. \tag{3.208}$$

As for the case of odd n, only two of the irreps in (3.205)-(3.208) are to be considered, namely Φ_1 and Φ_3. Going over to the two-dimensional unitary irreps, we will label these by $m = 1, \ldots, \lceil n/2 \rceil - 1$, and there is no distinction between odd or even n. Their action on the generators reads

$$\rho_m(r) = \begin{pmatrix} e^{2\pi \mathrm{i} m/n} & 0 \\ 0 & e^{-2\pi \mathrm{i} m/n} \end{pmatrix}\,, \tag{3.209}$$

$$\rho_m(s) = \begin{pmatrix} 0 & 1 \\ 1 & 0 \end{pmatrix}\,, \tag{3.210}$$

where we have chosen a suitable basis where $\rho_m(r)$ is diagonal.

Having characterized all unitary irreps of the dihedral isometry group $D_{n=p,q}$ of both polygon- and vertex-centered truncated tiling, let us proceed with the construction of an associated boundary aperiodic spin chain. Let us stress that the dihedral symmetry is an isometry in the bulk, while for the boundary chain it is a spatial symmetry acting on the coordinates of the local degrees of freedom. It is the latter which we construct as multiplets of the irreps given in (3.205)-(3.210), in a way which generalizes the spin-1/2 XXX chain considered in previous sections. The benefit of having an explicit parametrization of these irreps for every value of n is that we can access the limit

$n \to \infty$. Mathematically, this number increases the number of irreps, while physically it means that we enter a regime where the number of local degrees of freedom of the theory is large. This can qualitatively be thought as an analogy with the large N typically encountered in holographic boundary theories. To start our construction, consider the spin-1/2 XXX Hamiltonian

$$H^{\text{XXX}}_{\{p,q\}} = \sum_{i\in\mathbb{Z}} \mu_i \, \vec{\sigma}_i \cdot \vec{\sigma}_{i+1} \,, \tag{3.211}$$

which is a special instance of the general Hamiltonian given in (3.142) with the choice $h(\vec{\sigma}_i, \vec{\sigma}_{i+1}; \theta_i) = \vec{\sigma}_i \cdot \vec{\sigma}_{i+1}$. In particular, it is the Hamiltonian given in (3.197) with $\Delta_0 = 1$, such that the entries of the vector $\vec{\sigma}_i$ are the three standard Pauli matrices (X, Y, Z), but for the purposes of the current analysis it is more convenient to leave the notation generic. The idea of the construction is to first study the way the multiplets of irreps transform under the action of D_n, and then define D_n-invariant terms from combinations of these multiplets. These will be the terms entering our Hamiltonian. We begin with the one-dimensional irreps, and we denote one-dimensional multiplets transforming under these irreps as $\vec{\sigma}_l$, with $l = 1, \ldots, 4$ or $l = 1, 2$ depending on whether n is even or odd, respectively. Note that each of these multiplets contains a single vector of Pauli matrices, hence the one-dimensional label. Let us now act on such a multiplet with a unitary representation $U(\lambda)$ of a generator $\lambda = r, s$ of the dihedral group. The transformation law reads

$$U_l(\lambda)\vec{\sigma}_{i,l}U_l(\lambda^{-1}) = \Phi_l(\lambda)\vec{\sigma}_{\lambda(i),l} \,, \tag{3.212}$$

where the U_l matrices act on the local Hilbert space at site i of the chain, and $\lambda(i)$ is the site resulting from the application of the generators on the i-th site. Recall the explicit form of the one-dimensional irreps $\Phi_l(\lambda)$ given in (3.205)-(3.208). Even though we have 4 one-dimensional irreps for even n, notice that only two of them, Φ_1 (3.205) and Φ_3 (3.207), transform trivially under the action of the generator r. We will thus only consider these in our construction, since we expect on physical grounds that a rotation of the bulk should not induce a phase on the scalar boundary degrees of freedom. Fittingly, these are also the only irreps present in the case of odd n, which can be seen as a further justification of our constraint. Since we now have no reason to distinguish between even and odd values of n, let us relabel the one-dimensional irreps by their eigenvalue under the action of s, namely $\Phi_1 \equiv \Phi_+$ and $\Phi_3 \equiv \Phi_-$, together with their spin multiplets $\vec{\sigma}_\pm$. Then, using the transformation law (3.212), we can

write the action of D_n generators on our one-dimensional multiplets as

$$U_\pm(r)\vec{\sigma}_{i,\pm}U_\pm(r^{-1}) = \vec{\sigma}_{r(i),\pm}\,, \qquad U_\pm(s)\vec{\sigma}_{i,\pm}U_\pm(s^{-1}) = \pm\vec{\sigma}_{s(i),\pm}\,. \tag{3.213}$$

We can give a physical meaning to these multiplets based on their transformation behavior under reflections or parity transformations. In fact, using (3.205) and (3.207), we can see $\vec{\sigma}_{i,+}$ as a scalar while $\vec{\sigma}_{i,-}$ is a pseudo-scalar. Both $\vec{\sigma}_{i,+}$ and $\vec{\sigma}_{i,-}$ act non-trivially on two different Hilbert spaces, and we may therefore regard them as independent degrees of freedom. We can now construct D_n-invariant combinations of these one-dimensional multiplets, which in general read

$$(\vec{\sigma}_{i,l}\cdot\vec{\sigma}_{i+1,l})^{P_1}\,,\ (\vec{\sigma}_{i,l_1}\cdot\vec{\sigma}_{i+1,l_2})^{2P_2}\,, \qquad P_1, P_2 \in \mathbb{N}_0 \ \text{ and } l_1 \neq l_2\,. \tag{3.214}$$

We will mostly only consider terms with $P_1 = 1$ and $P_2 = 0$, since these represent a straightforward generalization of the XXX spin chain with Hamiltonian (3.211).
Let us now proceed with a quite analogous construction for the two-dimensional irreps of D_n. These will be labeled by $m = 1, \ldots, \lceil \frac{n}{2} \rceil - 1$, and the corresponding multiplets at each site of the chain read

$$\vec{T}_{i,m} \equiv \begin{pmatrix} \vec{\tau}_{i,m} \\ \vec{\tilde{\tau}}_{i,m} \end{pmatrix}\,, \qquad \vec{T}^\dagger_{i,m} = \begin{pmatrix} \vec{\tau}^\dagger_{i,m} & \vec{\tilde{\tau}}^\dagger_{i,m} \end{pmatrix} = \begin{pmatrix} \vec{\tau}_{i,m} & \vec{\tilde{\tau}}_{i,m} \end{pmatrix}\,. \tag{3.215}$$

These are two-dimensional vectors where each entry is a vector of Pauli matrices. As such, we may define an inner product between multiplets as

$$\vec{T}^\dagger_{i,m}\cdot\vec{T}_{i+1,m} = \vec{\tau}_{i,m}\cdot\vec{\tau}_{i+1,m} + \vec{\tilde{\tau}}_{i,m}\cdot\vec{\tilde{\tau}}_{i+1,m}\,. \tag{3.216}$$

As before, we may impose a transformation law for these two-dimensional multiplets (3.215) under the action of the generators r, s of the dihedral group,

$$U_m(r)\vec{T}_{i,m}U_m(r^{-1}) = \rho_m(r)\begin{pmatrix} \vec{\tau}_{r(i),m} \\ \vec{\tilde{\tau}}_{r^{-1}(i),m} \end{pmatrix} = \begin{pmatrix} e^{\frac{2\pi i m}{n}}\vec{\tau}_{r(i),m} \\ e^{\frac{-2\pi i m}{n}}\vec{\tilde{\tau}}_{r^{-1}(i),m} \end{pmatrix}\,, \tag{3.217}$$

$$U_m(s)\vec{T}_{i,m}U_m(s^{-1}) = \rho_m(s)\begin{pmatrix} \vec{\tau}_{s(i),m} \\ \vec{\tilde{\tau}}_{s(i),m} \end{pmatrix} = \begin{pmatrix} \vec{\tilde{\tau}}_{s(i),m} \\ \vec{\tau}_{s(i),m} \end{pmatrix}\,, \tag{3.218}$$

with $\rho_m(r)$ and $\rho_m(s)$ given in (3.209) and (3.210). Note that once again we may interpret the components of these multiplets in physical terms. For example, the component $\vec{\tilde{\tau}}_{i,m}$ in (3.217) is evaluated at $r^{-1}(i)$ after the action of the generator, while $\vec{\tau}_{i,m}$ is evaluated in $r(i)$. Moreover, the phase factors picked up by each component

are equal but inverse to each other as well. This behavior allows us to regard the two components of the multiplet as right and left mover degrees of freedom with respect to the rotations by $2\pi/n$ contained in D_n. As was the case for the one-dimensional irreps, the two matrices $\vec{\tau}_{i,m}$ and $\vec{\tilde{\tau}}_{i,m}$ act on different local Hilbert spaces, and we therefore regard them as different degrees of freedom. In total, this means that we have $2(\lceil n/2 \rceil - 1)$ distinct two-dimensional Hilbert spaces at each site of the chain, spanned by the two-dimensional multiplets. The construction of D_n-invariant terms from two-dimensional multiplets is slightly more convoluted. We must consider general combinations of the form $\vec{T}^{\dagger}_{i,m}\, g^{(m)}\, \vec{T}_{i+1,m}$, where $g^{(m)}$ is a coupling matrix. This matrix is necessary since *a priori* we have no reason to prohibit terms with mixed representations. Once again acting with a unitary transformation matrix $U_m(\lambda)$ on this combination, we obtain

$$\vec{T}^{\dagger}_{i,m}\, g^{(m)}\, \vec{T}_{i+1,m} \to \vec{T}^{\dagger}_{i,m}\, \rho_m^{-1}(\lambda) g^{(m)} \rho_m(\lambda)\, \vec{T}_{i+1,m}. \tag{3.219}$$

We can now impose restrictions on the coupling matrix such that the multiplet actually remains invariant under the transformation law. More precisely, if

$$\rho_m^{-1}(\lambda) g^{(m)} \rho_m(\lambda) = g^{(m)} \qquad \Longrightarrow \qquad g^{(m)} \rho_m(\lambda) = \rho_m(\lambda) g^{(m)}\,, \tag{3.220}$$

then the transformation law (3.219) leaves the multiplet invariant. In (3.220), we have exploited the fact that $\rho_m(\lambda)$ is a unitary representation. Upon closer inspection, we see that the condition (3.220) imposes that $g^{(m)}$ needs to commute with the generators of the group in their two-dimensional irrep for it to define properly invariant terms of the form $\vec{T}^{\dagger}_{i,m}\, g^{(m)}\, \vec{T}_{i+1,m}$. Although this might seem like an unlikely condition, Schur's lemma [703] guarantees that any element which commutes with all the generators has to be proportional to the identity operator. Thus, we can set $g^{(m)} = \mathbb{1}_m$ and our invariant term is simply given by $\vec{T}^{\dagger}_{i,m}\, \vec{T}_{i+1,m}$. By the same chain of logical arguments, one can show that terms of the type $\vec{T}^{\dagger}_{i,m_1}\, \vec{T}_{i+1,m_2}$, with $m_1 \neq m_2$ are not invariant.
Now that we have constructed a set of local degrees of freedom as multiplets transforming under irreps of the dihedral group, we can define the Hamiltonian governing our boundary theory. It acts on a Hilbert space with the following structure

$$\mathcal{H}_n = \bigotimes_{i\in\mathbb{Z}} \left[\mathcal{H}_{i,+} \otimes \mathcal{H}_{i,-} \bigotimes_{m=1}^{\lceil n/2 \rceil - 1} \left(\mathcal{G}_{i,m} \otimes \tilde{\mathcal{G}}_{i,m} \right) \right], \tag{3.221}$$

where our local degrees of freedom $\vec{\sigma}_{i,\pm}$, $\vec{\tau}_{i,m}$ and $\vec{\tilde{\tau}}_{i,m}$ act non-trivially only on $\mathcal{H}_{i,\pm}$, $\mathcal{G}_{i,m}$ and $\tilde{\mathcal{G}}_{i,m}$, respectively. Naturally, each of these Hilbert spaces is two-dimensional, and

therefore the dimension of the local Hilbert space at each site of the chain is $2^{2\lceil \frac{n}{2} \rceil}$. As mentioned above, we only want to consider terms in (3.214) with $P_1 = 1$ and $P_2 = 0$ for the one-dimensional multiplets. For the two-dimensional multiplets, we have terms of the form (3.219) with $g^{(m)} = \mathbb{1}_m$. Using these building blocks, we construct the following D_n-invariant aperiodic Hamiltonian

$$H^{\text{dih}}_{\{p,q\}} = \sum_i \left[\mu_i^{(+)} \vec{\sigma}_{i,+} \cdot \vec{\sigma}_{i+1,+} + \mu_i^{(-)} \vec{\sigma}_{i,-} \cdot \vec{\sigma}_{i+1,-} + \sum_{m=1}^{\lceil \frac{n}{2} \rceil - 1} \mu_i^{(m)} \vec{T}^{\dagger}_{i,m} \cdot \vec{T}_{i+1,m} \right] , \quad (3.222)$$

where we take all couplings $\mu_i^{(+)}$, $\mu_i^{(-)}$ and $\mu_i^{(m)}$ to be modulated according to a given aperiodic sequence $\mathcal{S}_{\{p,q\}}$ at the boundary of a hyperbolic tiling. Besides being by construction invariant under the action of the dihedral group, the Hamiltonian (3.222) can be seen as a sum of $2\lceil \frac{n}{2} \rceil$ independent XXX Hamiltonians of the form (3.211). Each of the copies of this XXX chain acts non-trivially on one of the local Hilbert spaces entering the decomposition (3.221). This is however a consequence of our restriction to only consider terms in (3.214) with $P_1 = 1$ and $P_2 = 0$. Relaxing this constraint, we can build even more general D_n-invariant Hamiltonians. Some examples of possible terms that can be added to our Hamiltonian consist of simple powers of the terms appearing in (3.222).

Given that the Hamiltonian (3.222) can be written as the sum of independent aperiodic XXX Hamiltonians, all subject to the same aperiodic modulation $\mathcal{S}_{\{p,q\}}$ we can readily report the results for the correlation functions and the entanglement entropy of the dihedral-invariant model. Beginning with the correlation functions, we exploit the results obtained in Sec. 3.5.3 to compute the spin-spin two-point correlation functions in the Hamiltonian (3.222). As one would expect, thanks to the aforementioned splitting of the Hamiltonian into copies of XXX chains, the behavior of the correlation functions remains unchanged. The only aspect that is different is that now we have $(\lceil \frac{n}{2} \rceil + 1)$ distinct species of degrees of freedom, and one may expect new correlations between different species to contribute to the overall correlation structure of the ground state. However, this is not the case, and only degrees of freedom which belong to the same multiplet can exhibit non-vanishing correlations. Even more restrictive, within the same multiplet component, the correlation functions are non-vanishing only between degrees of freedom of the same entry. In the notation of (3.154), this imposes $\alpha = \beta$. Some of these non-vanishing two-point functions are $\langle \sigma_{i,+} \sigma_{i+r,+} \rangle$ and $\langle \tilde{\tau}_{i,m} \tilde{\tau}_{i+r,m} \rangle$. The computation of the disorder averaged two-point function can therefore be carried out exactly as explained in Sec. 3.5.3, using (3.156) for one-cycle modulations, and (3.170) for two-cycle ones. In particular, since the non-vanishing correlators are still those

between two Pauli matrices, both in the one- and the two-dimensional multiplets, the coefficient $c_0 = -1$ remains unchanged.

Let us now investigate the entanglement entropy in the ground state of the D_n-invariant Hamiltonian (3.222), implementing the general results reported in Sec. 3.5.4. As we saw for the correlation functions, the computation is straightforward due to the factorized structure of the Hamiltonian (3.222). In particular, for those aperiodic modulations that are relevant and drive the ground state of each of the individual XXX spin chains into an ASP, the entanglement entropy is given by the formulas provided in Sec. 3.5.4. Therefore, the total entanglement entropy of a block of consecutive spins in the ground state of the D_n-invariant Hamiltonian is $s_0 = \log 2$ times $2\lceil \frac{n}{2} \rceil$, which is the number of copies of XXX chains. This extensive behavior carries through to the effective central charge of the model (3.222), such that we obtain $2\lceil \frac{n}{2} \rceil c_{\text{eff}}$, with c_{eff} given in (3.188). Finally, as mentioned in the beginning of this section, the explicit parametrization of irreps of D_n for every value of n enables an investigation of the $n \to \infty$ regime. Although this was originally motivated by the desire to mimic, at least as an analogy, the large N limit of holographic theories, we find that the $n \to \infty$ limit has an interpretation with no actual counterpart in continuous AdS/CFT. More precisely, since n can be either one of the Schläfli parameters, varying n amount to simultaneously change the aperiodic modulation of the couplings appearing in the Hamiltonian (3.222). Moreover, this also amounts to a change in the underlying bulk geometry, since a different hyperbolic tiling is being used as a discretization. While from the boundary point of view $n \to \infty$ indeed describes a limit of a large number of local degrees of freedom, for the bulk this indicates discretizations of $\mathbb{D}^2$ via $\{\infty, q\}$ or $\{p, \infty\}$ tilings. In continuous AdS/CFT, such a change is not possible, since the isometry group of the spacetime does not posses such a tunable parameter, nor does the conformal group on the boundary. Thus, this seems to be a novel property arising solely in the discrete setting. We can even analyze this behavior in more detail by exploiting our analytic access to an infinite family of aperiodic modulations which are compatible with ASP ground states, namely the class of tilings $\{6, q\}$ with $q \geq 4$. By taking $n = q$, the effective central charge for these aperiodic modulations and for spin-1/2 XXX chains was given in (3.189), and we repeat it here for convenience,

$$c_{\text{eff}}(6, q) = \frac{6 - 2q + \sqrt{q^2 - 5q + 6}}{\log\left(2q - 5 + 2\sqrt{q^2 - 5q + 6}\right)} \frac{6 \log 2}{6 - 2q} \,. \tag{3.223}$$

This is the result for a single XXX chain, and we see that $c_{\text{eff}}(6, q)$ goes to zero as $1/\log q$ when $q \to \infty$, cf. Fig. 3.27. However, in the case of the ground state of the

D_n-invariant Hamiltonian, where there is a rescaling of the effective central charge by the number of irreps in the multiplet, we find that now $c_{\text{eff}}(6,q)$ actually diverges with q for $q \to \infty$. Thus, the enhancement of the symmetries has a drastic consequence on the scaling of the local degrees of freedom of the boundary theory.

SO(N) Aperiodic Spin Chains

As a final example to showcase the framework developed in Sec. 3.5.2 through Sec. 3.5.5, we consider aperiodic spin chains with a global SO(N) symmetry, as presented in [159]. The motivation for choosing this model is once again rooted in continuum AdS/CFT, where the notion of the large N limit is of utmost importance. Typical boundary theories in holographic dualities are gauge theories with SU(N) as their gauge group, where the fields are part of the adjoint representation of SU(N). In the large N limit, the $1/N$ double-line diagrammatic expansion of such theories can be mapped to the genus expansion in string theory [168, 184]. This is a crucial ingredient in the original formulations of AdS/CFT. We would therefore like to introduce a similar feature in our putative boundary models for discrete holography. Therefore, we study aperiodic spin chains whose local degrees of freedom are generators of a global SO(N) symmetry, given in their fundamental representation. As we will clarify in detail later, this specific choice of symmetry group and representation is inexpendable if we want to have a critical lattice model as per criterion **I**, thus ensuring that the low-energy properties of the model are described by an ASP at the SDRG fixed point. Keeping the rank N of the group generic throughout our calculations allows us to attain the $N \to \infty$ limit. It is however important to mention that, although inspired by continuous AdS/CFT, the large N limit of our approach is slightly different, since it pertains the rank of a global symmetry group rather than a local gauge symmetry.
Our model of interest was previously introduced in [676, 679] and is given by a specific instance of (3.142) with h chosen as

$$h\left(\vec{\sigma}_i, \vec{\sigma}_{i+1}; \theta\right) = \cos\theta\, \vec{\sigma}_i \cdot \vec{\sigma}_{i+1} + \sin\theta \left(\vec{\sigma}_i \cdot \vec{\sigma}_{i+1} + \frac{2\left(\vec{\sigma}_i \cdot \vec{\sigma}_{i+1}\right)^2}{N-2} \right), \quad N > 2\,. \tag{3.224}$$

While the XXZ chain had spin degrees of freedom belonging to the spin-1/2 fundamental representation of SU(2), the local degrees of freedom of the model (3.224) are the $N(N-1)/2$ generators of the group SO(N), which we group into the vector

$$\vec{\sigma}_i = \left(\sigma_i^{(1)}, \sigma_i^{(2)}, \ldots, \sigma_i^{\left(\frac{N(N-1)}{2}\right)} \right)^{\mathrm{T}}. \tag{3.225}$$

In particular, we choose these degrees of freedom to be in the fundamental representation of SO(N) [704], meaning that each generator in (3.225) is given by an $N \times N$ matrix. The Hamiltonian (3.224) enjoys a global SO(N) symmetry which is made manifest by acting on $\vec{\sigma}_i$ with a unitary representation of an element of SO(N). More precisely, the global invariance of the Hamiltonian is realized via

$$\vec{\sigma}_i \to U_{\vec{k}}^\dagger \vec{\sigma}_i U_{\vec{k}} \,, \qquad U_{\vec{k}} \equiv e^{\mathrm{i} \sum_{j\in\mathbb{Z}} \vec{k}\cdot\vec{\sigma}_j} \,, \tag{3.226}$$

with the vector $\vec{k}$ which is comprised of $N(N-1)/2$ real entries. It is a straightforward computation to check that the Hamiltonian (3.224) commutes with all the components of $\sum_{j\in\mathbb{Z}} \vec{\sigma}_j$, thus implying its invariance under (3.226). Remarkably, we can show that (3.224) is the most general SO(N)-invariant Hamiltonian with nearest-neighbor interactions [676, 679]. To see this, notice that terms of the form $(\vec{\sigma}_i \cdot \vec{\sigma}_{i+1})^n$ with $n > 2$ can be expressed in terms of $\vec{\sigma}_i \cdot \vec{\sigma}_{i+1}$ and $(\vec{\sigma}_i \cdot \vec{\sigma}_{i+1})^2$ for any pair of spins, cf. [676, 679]. Besides the aperiodically modulated hopping parameters μ_i in (3.142), the Hamiltonian (3.224) further contains a coupling parameter $\theta \in [0, 2\pi)$, which we assume to be homogeneous throughout the chain. The phase diagram of homogeneous SO(N) chains, i.e. with $\mu_i = \mu$ on all sites, has been previously investigated in [676]. The model exhibits several phases governed by the value of θ, the most relevant ones for our purposes being $\pi/4 \leq \theta \leq \pi/2$ and $-\pi/2 \leq \theta \leq -\pi/4$ where the homogeneous model is gapless. For our analysis, we assume θ in (3.224) to lie in this range such that the chain remains critical upon introducing aperiodic disorder, as per criterion **I**. Let us mention that SO(N) spin chains with random disorder have been previously considered in [679], where the SDRG procedure was adapted to the presence of SO(N) degrees of freedom. The results presented here, which are contained in [159], generalize these to the case of aperiodic modulations. As in the previous sections, we will focus on the admissible modulations (3.153) only, such as to guarantee that only one- or two-cycle SDRG flows with exclusively two-spin decimation blocks arise. As discussed around (3.152), the ASP requires that the local ground state of h in (3.224) on such a two-spin system be a singlet. While the identification of this singlet was straightforward for the SU(2) spins of the XXZ chain, we need to specify its form more precisely in the case of SO(N). In particular, due to the invariance of h under SO(N) transformations (3.226), the eigenstates of the Hamiltonian will be arranged into degenerate multiplets of SO(N) irreps. In particular, these irreps are those appearing in the tensor product decomposition for two spins in the fundamental representation [704]. From group-theoretic arguments involving Young-Tableaux, it is known that this tensor product decomposition for SO(N) gives rise to an $(N+2)(N-1)/2$-dimensional,

an $N(N-1)/2$-dimensional, and a one-dimensional irrep. This latter one-dimensional representation is precisely the one containing the state we denote as *singlet*. The fact that this singlet is always present in the tensor product decomposition for any value of N is a consequence of the fundamental representation of SO(N) being *self-conjugate* [704]. Notice that this is also the case for SU(2), giving a mathematical justification for the existence of the singlet state in XXZ chains. However, the fundamental representation of SU(N) with $N > 2$ is not self-conjugate, and its tensor product decomposition does not contain singlets. This is the reason why Hamiltonians of the form (3.142) with $\vec{\sigma}_i$ containing SU(N) generators in their fundamental representation do not lead to ASPs and are therefore not considered in this work. Although the aforementioned argument for the existence of the singlet in SO(N) has technical caveats for the specific cases of $N = 4$ and $N = 8$ [704], the existence of a singlet state is still guaranteed and we thus include these cases in our analysis. However, the fact that this singlet is present in the tensor product decomposition does not immediately imply that it is the actual ground state of the two-spin system. The eigenenergies of h for this two-spin case depend on θ, and it was shown in [679] that for $-3\pi/4 < \theta < \arctan\left(\frac{N-2}{N+2}\right)$, the singlet state is indeed the local ground state of the system. This means that SO(N)-invariant aperiodic spin chains obey the criteria **III** (SDRG cyclicity) and **IV** (ASP ground state) in the range $-\pi/2 \leq \theta \leq -\pi/4$, where the model is also critical.

To be able to full apply the notions discussed in Sec. 3.5.2 to the aperiodic SO(N), we need to verify that the modulations described by aperiodic sequences $\mathcal{S}_{\{p,q\}}$ with admissible $\{p, q\}$ pairs are relevant. To show this, we explicitly compute the RG flow of the models parameters under SDRG. By explicitly evaluating the expression (3.146), the renormalized couplings were found in [679] to be

$$\mu' \cos\theta' = f_1(N) \frac{\mu^2 (\cos\theta)^2}{\mu_0 (g(N) - \tan\theta_0)}, \qquad \mu' \sin\theta' = f_2(N) \frac{\mu^2 (\sin\theta)^2}{\mu_0 (1 - \tan\theta_0)}, \tag{3.227}$$

with the functions

$$f_1(N) \equiv \frac{4}{N(N+2)}, \qquad f_2(N) \equiv -\frac{4}{N^2}, \qquad g(N) \equiv \frac{N-2}{N+2}. \tag{3.228}$$

In these expressions, we use θ_0 and μ_0 to denote the couplings in the two-spins block before the decimation, while θ and μ are the couplings connecting the block to the rest of the chain. The symbols θ' and μ' are the renormalized couplings after the decimation step. Notice that the presence of two terms in the Hamiltonian (3.224) induces an separate renormalization of μ and θ. The flow of these parameters under iteration of these decimation steps throughout the SDRG for both one- and two-cycle modulations

was given in [159], generalizing the results of [159, 676, 679]. It is pedagogical to choose a specific modulation for the following computations, which we take to be our prime example of $\mathcal{S}_{\{6,q\}}$, with $q \geq 4$. Remember that this class contains both one-cycle ($q = 4$) and two-cycle ($q > 4$) instances. A careful evaluation of (3.146) yields the renormalization of the coupling parameters after a sequence-preserving transformation Ξ, which read

$$\mu'_a \cos\theta'_a = \frac{\mu_a^{q-1}}{\mu_b^{q-2}} \frac{f_1(N)^{2q-5}(\cos\theta_a)^{q-1}}{(\cos\theta_b\,(g(N)-\tan\theta_b))^{q-2}\,(g(N)+B(N,\theta_a,\theta_b))^{q-3}}\,, \tag{3.229}$$

$$\mu'_a \sin\theta'_a = \frac{\mu_a^{q-1}}{\mu_b^{q-2}} \frac{(\tan\theta_a)^{q-3}\,f_2(N)^{2q-5}(\sin\theta_a)^{q-1}}{(\cos\theta_b\,(1-\tan\theta_b))^{q-2}\,(1+B(N,\theta_a,\theta_b))^{q-3}}\,, \tag{3.230}$$

and

$$\mu'_b \cos\theta'_b = \frac{\mu_a^{q-2}}{\mu_b^{q-3}} \frac{f_1(N)^{2q-7}(\cos\theta_a)^{q-2}}{(\cos\theta_b\,(g(N)-\tan\theta_b))^{q-3}\,(g(N)+B(N,\theta_a,\theta_b))^{q-4}}\,, \tag{3.231}$$

$$\mu'_b \sin\theta'_b = \frac{\mu_a^{q-2}}{\mu_b^{q-3}} \frac{(\tan\theta_a)^{q-4}\,f_2(N)^{2q-7}(\sin\theta_a)^{q-2}}{(\cos\theta_b\,(1-\tan\theta_b))^{q-3}\,(1+B(N,\theta_a,\theta_b))^{q-4}}\,, \tag{3.232}$$

where

$$B(N,\theta_a,\theta_b) \equiv (\tan\theta_a)^2 \left(\frac{N+2}{N}\right) \frac{(g(N)-\tan\theta_b)}{(1-\tan\theta_b)}\,, \tag{3.233}$$

and f_1, f_2 and g are defined in (3.228). Since the sequence-preserving transformation may contain the decimation of several strongly-coupled blocks at the same time, the relations (3.227) need to be appropriately combined in order to obtain (3.229)-(3.232). This is to be done in a similar way as we obtained (3.201). Similarly to the case of the XXZ chain, also here we see that the decimation induces an effective aperiodicity on the parameter θ, even though it was originally homogeneous throughout the chain. Upon iterated application of the sequence-preserving transformations to the entire chain, we can exploit the formulas (3.229)-(3.232) to obtain the RG flow of the hopping ratio $r = \mu_a/\mu_b$ and the coupling parameter θ. In particular, one finds that the angle θ has two SDRG fixed points, which can be unveiled by inspecting the following equation

$$\tan\theta'_i = \left(\frac{f_2(N)}{f_1(N)}\right)^{2(q-k_i)+1} \left[\frac{(\tan\theta_a)^2(g(N)-\tan\theta_b)}{1-\tan\theta_b}\right]^{q-k_i+1} \left[\frac{g(N)+B(N,\theta_a,\theta_b)}{1+B(N,\theta_a,\theta_b)}\right]^{q-k_i}. \tag{3.234}$$

with $i = a, b$ and $k_a = 3$ and $k_b = 4$. This expression was studied for random disorder in [679] and later applied to the two-cycle aperiodic case in [159]. The fixed points of the equation (3.234) simultaneously represent the SDRG fixed points for the coupling θ. In particular, restricting to the window of interest for our model given

by $-\pi/2 \leq \theta \leq -\pi/4$, we find an unstable fixed point $\theta_a = \theta_b = -\pi/4$ and a stable fixed point at $\theta_a = \theta_b = -\pi/2$. This stability can be thought of in a similar way as for the anisotropy Δ_0 in the XXZ chain, where the value $\Delta_0 = 1$ was an unstable, or *repulsive* fixed point of the SDRG meaning that any slight deviation $\Delta_0 = 1 - \epsilon$ with $\epsilon \ll 1$ drives the anisotropy to a new fixed point $\Delta^* = 0$. For the aperiodic SO(N) spin chains (3.224), any deviation from $\theta_a = \theta_b = -\pi/4$ drives the coupling to the stable, or *attractive* fixed point $\theta_a = \theta_b = -\pi/2$ under SDRG. We can also study the renormalization flow for the hopping ratio, which after a single RG step $r \to r'$ reads

$$r' = r\, C(q, N, \theta_a, \theta_b)\,, \tag{3.235}$$

where the explicit form of the function $C(q, N, \theta_a, \theta_b)$ can be derived from (3.229)-(3.232), although it is not particularly illuminating. For our purposes, we are only interested in the important feature that $C(q, N, \theta_a, \theta_b) < 1$ for any values $-\pi/2 \leq \theta_a, \theta_b \leq -\pi/4$, $q \geq 4$ and $N > 2$. Therefore, the renormalized hopping ratio is smaller than the original one, meaning that the strong-disorder fixed point as per (3.151) is given by $r^* = 0$. This fixed point is attractive with respect to r, and any slight deviation from homogeneity $r \neq 1$ will drive the system into this new fixed point. In analogy with our analysis of the XXZ chain, we can conclude that the aperiodic $\{6, q\}$ modulations are relevant when acting on the Hamiltonian given by (3.142) with (3.224) and they ultimately drive the system to an aperiodicity-induced fixed point under SDRG. This shows that criterion **II** (relevance) is also fulfilled. Let us stress that analogous results can be obtained for the other examples of admissible modulations (3.153) as well, namely those associated with $\{5, 4\}, \{5, 5\}, \{3, 7\}$, and $\{3, 8\}$ tilings.

The considerations above show that the SO(N)-invariant spin chain with Hamiltonian (3.142) and (3.224) satisfies all criteria **I**-**IV** when subject to the admissible aperiodic modulations (3.153). Therefore, our results for the correlation functions, entanglement entropy, and mutual information obtained in sections 3.5.3-3.5.5 can be readily applied. First, for the two-point correlation functions of spins belonging to the same singlet, these are given by (3.170) upon inserting the correlation of two SO(N) spins in a singlet, which is given by $c_0 = -2/N$ [159]. All remaining coefficients are left untouched, in particular the dependence on the Schläfli parameters. Second, the entanglement entropy of a block of L consecutive spins in this SO(N)-invariant spin chain is given by (3.180), where a straightforward computation yields the entanglement entropy of an individual SO(N) singlet to be $s_0 = \log N$ [688]. Again, the expression of the entanglement entropy as a function of p and q is unchanged by the specification of the model. It does, however, introduce a dependence of the effective

central charge c_{eff} appearing in (3.180) on the additional parameter N. An interesting consequence of this is that the effective central charge now diverges logarithmically in the $N \to \infty$ limit. This behavior is significantly different from the power-law dependence of the central charge on N predicted by the Brown-Henneaux formula in continuum $\text{AdS}_3/\text{CFT}_2$ [86, 168, 705]. However, this can hardly be seen as a surprise after recalling the different interpretation of the parameter N in the spin chain and in continuous AdS/CFT explained in the introductory paragraph to this section. Finally, the mutual information in the ground state of aperiodic SO(N) spin chains is given by (3.193), again upon replacing $s_0 = \log N$. This concludes our treatment of aperiodic spin chains with a global SO(N) symmetry.

3.5.7. Tensor Networks for Aperiodic Spin Chains

We conclude this section on aperiodic spin chains by introducing a powerful equivalent description of ASPs using the language of tensor networks (TNs). We have reviewed the fundamentals of TNs in Sec. 2.3.4. They provide an effective way of representing the ground states of the aperiodic spin chains considered above. A particularly insightful benefit of TNs is that they efficiently encode both the symmetries and entanglement structures of the quantum states they simulate. One of the main results of [158, 159], which we report in this section, was the construction of TNs which exactly reproduce the ground states of aperiodic spin chains. A consequence of this analysis is a graphical representation of the tensor network, the *TN graph*, which we interpret as a discrete hyperbolic geometry encapsulating the properties of the boundary state.

As for several quantities encountered in the previous sections, the properties of the TNs describing ASP ground states do not vary drastically when considering different models, as long as they are of the form (3.142) and obey criteria **I**-**IV**. In principle, the effects of the Schläfli parameters associated to the discretization of the bulk are the same for every model, while the only parameter that has to be computed anew, besides of course the actual decimation steps involved in the SDRG, is s_0. While the latter can be associated with the bond dimension of the TN, the overall network structure is entirely determined by the aperiodic sequence $\mathcal{S}_{\{p,q\}}$ and through the decimation steps of the SDRG procedure. It was therefore pointed out in [159] that the TN describing generic ground states of aperiodic chains possesses certain universal features shared among different models of the form (3.142). Thus, for concreteness, we will report the results of [158] using the specific example of the aperiodic XXX chain given by (3.197) with $\Delta_0 = 1$, but keep in mind that the entire discussion is readily adjusted to cover also other examples of aperiodic spin chains.

SDRG as a Tensor Network

We begin with the construction of the tensor networks to recover the exact ground states of aperiodic spin chains obtained from SDRG. As commented in Sec. 2.3.4, TNs inherently encode ideas of real space RG in their goal of approximating ground states of quantum systems by a construction extending one dimension higher [152, 417, 420, 430, 438–440, 706–712]. Therefore, it is natural to wonder whether the RG steps involved in the SDRG procedure, as detailed in Sec. 3.2.4, admit such a description in terms of tensors. To tackle this, the authors of [158] built upon the ideas previously developed in [430], as we report in the following. Recall how, within the SDRG perturbative assumption, the decimation of a spin of n strongly coupled spins amounts to project the local Hamiltonian (3.143) onto either the singlet ground state (3.145) (if n is even) or a superposition of doublet states (3.147) (if n is odd). These states can indeed be interpreted as tensors, which explains the suggestive notation $|T\rangle$ used in (3.145) and (3.147). For the concrete case of the aperiodic XXX chain with spin-1/2 SU(2) spins, we introduce a collective notation for these tensors, based on the value of n,

$$|T_n\rangle = \begin{cases} \dfrac{1}{\sqrt{2}} \displaystyle\sum_{\{m_i=\pm\}} \delta^{m_0}_{m_1} |m_0\rangle\, |m_1\rangle \ , & n = 1\,, \\ \displaystyle\sum_{\{m_i=\pm\}} T_{m_1\dots m_n} |m_1\rangle \dots |m_n\rangle \ , & n \text{ even}\,, \\ \dfrac{1}{\sqrt{2}} \displaystyle\sum_{\{m_i=\pm\}} T^{m_0}_{m_1\dots m_n} |m_0\rangle\, |m_1\rangle \cdots |m_n\rangle \ , & n \text{ odd } \neq 1\,. \end{cases} \tag{3.236}$$

Naturally, these expressions can also be given in the more general notation used in (3.145), but we restrict to the XXX case for clarity. Note that we have introduced an additional state in the first line of (3.236) which describes the action of the TN on spins that are not renormalized in a given RG step. The state $|T_n\rangle$ for n even is precisely (3.145), while a summation over the free index m_0 is implied for the n odd state, thus defining a superposition of the degenerate doublet states $|T^{m_0}\rangle$ given in (3.147). The benefit of this notation is that it allows us to identify the coefficients $\delta^{m_0}_{m_1}$, $T_{m_1\dots m_n}$, $T^{m_0}_{m_1\dots m_n}$ of the states in (3.236) as tensors of rank 2, n and $n+1$, respectively, similarly to the MPS states (2.86) reviewed in Sec. 2.3.4. Depending on the computation at hand, we may consider these tensors, or their corresponding states, which of course are in a one-to-one equivalence. We will therefore use both terminologies interchangeably. Recall that each index m_i corresponds to a local Hilbert space $\mathcal{H}$ of dimension two, and at the same time we use it to label the complete basis of states $\{|m_i = \pm\rangle\}$ in $\mathcal{H}$. Therefore, the tensor state $|T_n\rangle$ lives in a local product Hilbert

space spanned by all its tensor legs, i.e. $|T_n\rangle \in \mathcal{H}^{\otimes 2\lfloor (n+1)/2 \rfloor}$. The key point for our purposes is that the tensors defined in (3.236) are linear maps that implement the fundamental operations involved in an SDRG. These decimations were previously shown in Fig. 3.21, and we visualize them again in Fig. 3.33, where the tensors $\delta^{m_0}_{m_1}$, $T_{m_1 m_2 \ldots m_n}$ and $T^{m_0}_{m_1 m_2 \ldots m_n}$ are depicted by the symbols $\bigcirc, \triangle, \square$, respectively. Within the philosophy of the SDRG inducing an RG flow, we will denote the chain before the application of an SDRG step as the *UV chain*, while the resulting sequence of spins after the decimation will be denoted as the *IR chain*. Accordingly, in the visualization shown in Fig. 3.33, the lower indices of the tensors correspond to tensor legs connected to spins on the UV chain, while upper indices correspond to tensor legs connected to spins on the IR chain. If we now assign the tensors (3.236) throughout the full chain according to the way we would typically implement decimation steps, we can indeed realize a full RG step. Repeating this procedure iteratively, the full SDRG flow can be generated. In this way, we obtain a collection of tensors, each of which represents a local state at some point during the SDRG as per (3.236). We label the location of a tensor in this generated graph by the index b. Then, the entire state corresponding to the collection of tensors in the graph is given by their tensor product

$$\bigotimes_b |T_n\rangle_b \ . \tag{3.237}$$

Gathering the position indices of all tensors in this collection gives rise to a disconnected graph, where each node of the graph corresponds to a tensor. This situation is visualized in Fig. 3.33, which already hints at the network structure that can arise from this construction. The next step to attain the full TN graph pertains the connection of tensors via internal lines. These lines represent the instances in the network where two neighboring tensors share a common leg as dictated by the geometry of the TN graph. At the same time, these lines denote precisely the positions of the spin degrees of freedom throughout the RG flow. This can be made more precise by labeling the tensor leg Hilbert spaces according to the vertices of the graph which they connect. For instance, for two tensors at positions b and b' on the graph, we label the Hilbert spaces of their shared legs as $\mathcal{H}_{bb'}$ and $\mathcal{H}_{b'b}$, respectively. Though most of the legs in the graph are internal, we also have some legs which only connected to a single tensor. We denote these as *open* or *dangling* legs, and they represent precisely the starting point of the SDRG, i.e. they describe the initial degrees of freedom on what we will denote as the *original UV chain*. The simultaneous application of decimation steps contained in the SDRG is described in the language of tensors by computing the outer product of the tensors decimating individual spin-blocks. This is precisely the

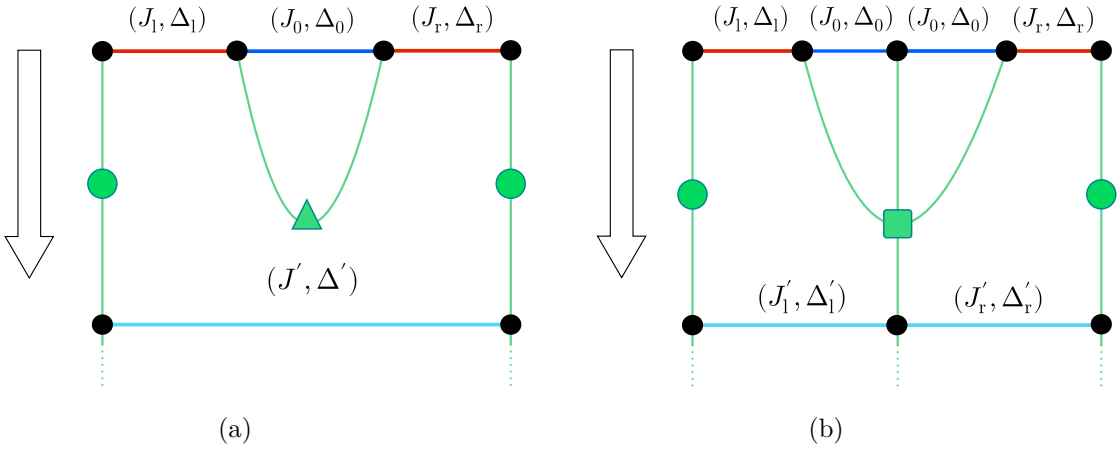


Figure 3.33: The same fundamental SDRG transformations as shown in Fig. 3.21, but now depicting the tensor representation of these steps. The tensor states $|T_n\rangle$ defined in (3.236) are depicted as green circles ($n = 1$), triangles (n even) and squares ($n \neq 1$ odd), with the green legs representing their indices. The outermost spins $\sigma_{\mathrm{l,r}}$ remain unchanged by the decimation, and are therefore contracted with the identity tensor $|T_1\rangle$. (a) Decimation step for a two-spin singlet via contraction of the two central spins with the rank-2 tensor given by $|T_2\rangle$. (b) Decimation step for a three-spin doublet via contraction of the three central spins with the rank-4 tensor given by $|T_3\rangle$. We will drop the green squares, circles, and triangles from later figures in view of avoiding clutter.

operation that leads to the product state (3.237). The final network is obtained upon contracting all upper and lower indices of tensors which share a leg in the TN graph. This contraction operation is effectively carried out by projecting the local product Hilbert space, say, $\mathcal{H}_{bb'} \otimes \mathcal{H}_{b'b}$, onto a maximally entangled state denoted by $|bb'\rangle$ [158, 430]. Since all local Hilbert spaces in our network are identical and of dimension two, this maximally entangled state is indeed an EPR pair in the local basis

$$|bb'\rangle = \frac{1}{\sqrt{2}} \left(|+\rangle\,|+\rangle + |-\rangle\,|-\rangle \right) . \tag{3.238}$$

Of course, for more general spin chains, like the SO(N)-invariant spin chain considered in Sec. 3.5.6, we would need to accordingly take the maximally entangled state of the higher-dimensional local Hilbert space. Performing such contractions on all tensors sharing internal legs, we obtain the full *tensor network state* $|\Psi\rangle$ of the network

$$|\Psi\rangle = \left(\bigotimes_{\langle bb' \rangle} \langle bb'| \right) \left(\bigotimes_{b} |T_n\rangle_b \right) , \tag{3.239}$$

where $\langle bb' \rangle$ denotes a shared leg, and the labels b, b' run over all the tensor positions in the TN graph. The TN state $|\Psi\rangle$ given in (3.239) is an element of the product Hilbert space of all dangling legs of the original UV chain, i.e. the Hilbert space of

the aperiodic XXX chain. Given that the TN graph exactly implements the SDRG procedure by construction, we conclude the $|\Psi\rangle$ reproduces precisely the ground state of the aperiodic XXX chain.

While the above conclusions concern the UV end of our TN, it remains to be clarified how exactly the uncontracted indices on the last IR chain are affected. At this stage, it is necessary to distinguish between two cases, namely the XXX chain defined on the circle, or it being an infinite line. In the latter case, the IR chain after indefinitely iterating the SDRG procedure will still be an infinite chain. The remaining uncontracted legs in this case will have no bearing on any local measurement at any finite scale on the UV chain. These uncontracted legs are therefore not relevant for us. However, in the case of an XXX chain defined on a circle, the SDRG procedure ought to finalize in a finite amount of steps due to the finite nature of the circle. The remaining upper indices of the final IR chain in this situation need to be contracted in order to finalize the construction of the TN state. Recalling the construction of hyperbolic tilings via inflation rules detailed in Sec. 3.2.2, the associated dangling legs of the IR chain are governed by an IR XXX Hamiltonian, whose couplings are modulated according to the seed sequence of the inflation rule. As we saw in Sec. 3.2.2, this seed sequence for $\{p, q\}$ tilings is a^p for $p > 3$ and d^3 for $p = 3$, cf. the discussion above (3.49). The corresponding IR Hamiltonian is therefore a homogeneous XXX chain with p sites, with a ground state given by either the singlet state (3.145) for even $p = n$ or one of the doublet states in (3.147) for odd $p = n$. As a consequence, we can contract the dangling tensor legs of this final IR chain with the corresponding rank-p tensor describing the ground state of the IR Hamiltonian. This final tensor, which is similar to the "top-level tensor" introduced in [423] for the MERA tensor network on a circle, caps off our TN state.

SDRG Cyclicity and TN Classes

The TN constructed above provides a graphical implementation of the SDRG, and thus we ought to provide an interpretation for the notions of cyclicity explained in Sec. 3.5.2. In particular, we know that the decimation steps shown in Fig. 3.21 and Fig. 3.33 do not necessarily effect a sequence-preserving transformation on the chain. This lead us to define a cyclicity notion which relates inflation steps to decimation steps, which specifically introduced the cycle number k to count how many RG steps are required to recover the original sequence. Such a sequence-preserving transformation Ξ then corresponds to the concatenation of k individual RG transformations, which we denoted by their associated decimation matrices M. We can, however, find an equivalent relation between sequence-preserving transformations and proper

inverse inflation, i.e. *deflation* steps. Crucially, the latter are different than the RG steps related to decimations, and they are literally described by the inverse of the inflation matrix (3.62) associated to a given $\{p, q\}$ inflation rule. We can thus define the integer m as the number of deflation steps required to implement a sequence-preserving transformation. More specifically, we say that the Ξ transformation for a given $\{p, q\}$-modulated chain is always equivalent to m deflation steps as

$$\Xi^{\{p,q\}} \sim \sigma_{\{p,q\}}^{-m} . \tag{3.240}$$

Surprisingly, we find that m only takes on the values $m = 1, 2, 3$ for any possible $\{p, q\}$ symbol, and we can thus categorize sequence-preserving SDRG transformations, and their corresponding TN implementations, into three classes denoted by I, II and III, respectively. In particular, we can directly express this classification in terms of the Schläfli parameters as

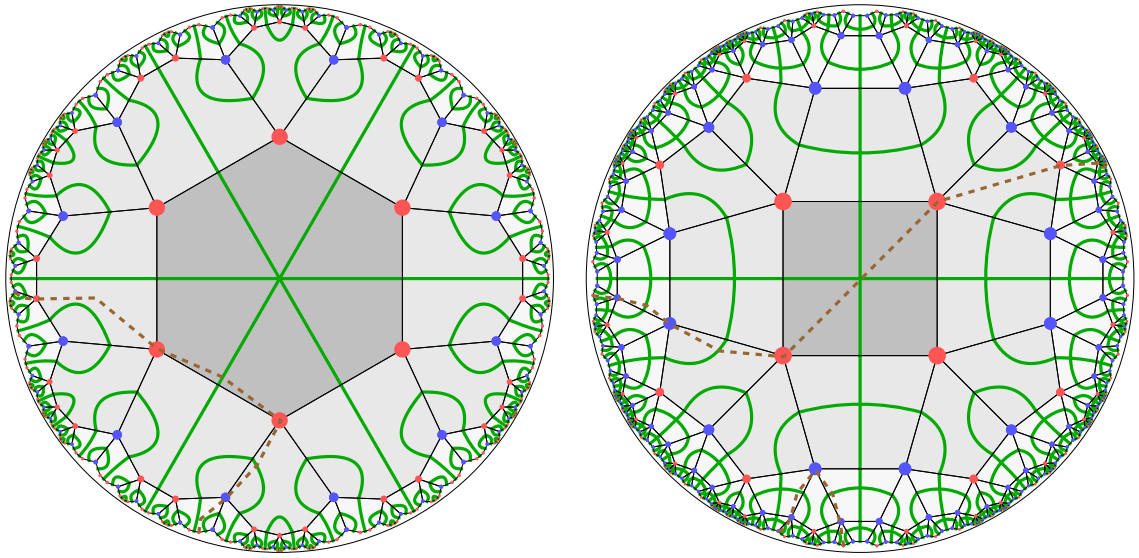
- $\{p, q\}$ with p even $\rightarrow$ Class I, i.e. $m = 1$ in (3.240).
- $\{p, q\}$ with p odd and q even $\rightarrow$ Class II, i.e. $m = 2$ in (3.240).
- $\{p, q\}$ with p odd and q odd $\rightarrow$ Class III, i.e. $m = 3$ in (3.240).

For the admissible modulations given in (3.153), we can see that the infinite family $\{6, q\}$ belongs to class I, the pair $\{3, 8\}$ and $\{4, 5\}$ are class II, and the pair $\{3, 7\}$ and $\{5, 5\}$ are in class III. Nonetheless, the great benefit of (3.240) is that it holds for all $\{p, q\}$ tilings, a fact that is highly non-trivial due to some rather technical issues, as discussed in Appendix B of [158].

A particularly useful consequence of the classification given by (3.240) is that we may place the TN on top of the $\{p, q\}$ tilings graph in a commensurable way due to the finite integer nature of m. The equivalence (3.240) then implies that a layer of tensors implementing the sequence-preserving transformation Ξ coincides with m layers of polygons on the tiling. This graphical embedding of the TNs reproducing the ground states of the $\{6, 4\}$ and $\{4, 5\}$ XXX chains is shown in Fig. 3.34. Note that both these TNs are class I since their sequence-preserving transformations are given by $\Xi^{\{6,4\}} = \sigma_{\{6,4\}}^{-1} = \{abaaaba \mapsto a,\ aba \mapsto b\}$ and $\Xi^{\{4,5\}} = \sigma_{\{4,5\}}^{-1} = \{babab \mapsto a,\ bab \mapsto a\}$.

Symmetries of TN states

It is evident from Fig. 3.34 that the graph structure from the TN does not coincide with the graph of the hyperbolic tiling. It is worth providing a more detailed dive into this discrepancy by investigating our tensor network construction in view of two types of



(a) $\{6,4\}$ XXX chain (b) $\{4,5\}$ XXX chain

Figure 3.34: Graphical representation of the tensor networks reproducing the ground state of aperiodic $\{p,q\}$ chains, embedded onto the Poincaré disk. These TNs are represented y the green lines, and the TN graph fits the underlying tiling commensurately. Red and blue vertices, according to the inflation procedure, respectively denote weak and strong bonds along the SDRG. TNs for all aperiodic chains have the same structure, with the specific details of the models like XXX of SO(N) chains only affecting the inner structure of the tensors via a different bond dimension. (a) TN of the aperiodic $\{6,4\}$ XXX chain, whose constituents are identical rank-2 tensors, without including the central top-level tensor. (b) TN of the aperiodic $\{4,5\}$ XXX chain, made up of identical rank-4 tensors together with rank-2 tensors. We show some examples of minimal cuts through the TN with brown dashed polylines. These are all homologous to a corresponding boundary subregion.

symmetries: internal and spatial. By internal symmetries we denote those which act on the local Hilbert spaces of the boundary theory, irrespective of the spatial coordinates on the chain. We have already encountered many examples of such internal symmetries in Sec. 3.5.6, such as global SU(2), U(1) and SO(N) symmetries of XXX, XXZ and SO(N) aperiodic spin chains, respectively. Meanwhile, the spatial symmetries, as the name suggests, are those associated to transformations which involve the spatial coordinates both on the chain and within the TN graph. These can be interpreted as discrete counterparts to the bulk isometries.

Let us begin by considering internal symmetries. For this, consider the fundamental tensor states in (3.236) together with the EPR state in (3.238). The singlet ground states $|T_n\rangle$ for even n will enjoy the same symmetry as the local Hamiltonian H_n of the block of spins on which the tensor is acting, which is either a global SU(2) symmetry for $\Delta_0 = 1$ or a global $\mathrm{U}(1)_z$ symmetry for $\Delta_0 \neq 1$. The z subscript in the latter denotes that the U(1) rotation is performed around the z-direction of the

spin variables. On the other hand, the individual doublet ground states $|T^{m_0}\rangle$ (3.147) for odd n only possess the $\mathrm{U}(1)_z$ symmetry. However, the enlargement of the Hilbert space given by the superposition in (3.236) restores the SU(2) symmetry such that $|T_n\rangle$ enjoys the same symmetries as H_n. We may therefore provide a collective account of the symmetries of all the tensor states in (3.236) as

$$|T_n\rangle = \mathcal{G}^{(n)}\,|T_n\rangle\,, \quad \mathcal{G}^{(n)} \equiv \begin{cases} G^{\otimes n}, & \text{even } n \\ G^* \otimes G^{\otimes n}, & \text{odd } n \end{cases}, \quad G \in \begin{cases} \mathrm{SU}(2), & \Delta_0 = 1 \\ U(1)_z, & \Delta_0 \neq 1 \end{cases}, \tag{3.241}$$

where G^* denotes the conjugation of G in the local $|\pm\rangle$ basis. The symmetries summarized in (3.241) can be thought of as *local* symmetries in the bulk TN graph since the tensor states $|T_n\rangle$ are located at different points throughout the network. Simultaneously, the same symmetries (3.241) realize precisely the *global* symmetries of the aperiodic Hamiltonian on the boundary. This situation is quite reminiscent of that in continuous AdS/CFT, where the global symmetries of the boundary theory elegantly match with local symmetries in the bulk [168]. We can check that the EPR states (3.238) used throughout the TN to contract tensors also enjoy the symmetry

$$G^* \otimes G\,|bb'\rangle = |bb'\rangle\,, \quad G \in SU(2)\,. \tag{3.242}$$

It remains to address the symmetries associated with the somewhat distinguished top-level tensor at the center of the tiling. In resemblance of the notation used above, we denote this tensor by $|T_p^{\mathrm{top}}\rangle$ and it represents the ground state of the IR Hamiltonian H_p with periodic boundary conditions. Similarly to the definition of the states in (3.236), $|T_p^{\mathrm{top}}\rangle$ is a singlet sharing the same symmetries as H_p when p is even, while it is a general linear combination of doublet states when p is odd. In the latter case, however, it is now imperative to specify the precise linear combination of doublet states, since this will dictate the symmetries of the state. This elevates the importance of $|T_p^{\mathrm{top}}\rangle$ in the analysis of the global symmetries of the TN state $|\Psi\rangle$ given in (3.239). It is therefore pertinent to explicitly highlight this dependence notationally by writing $\left|\Psi\left(|T_p^{\mathrm{top}}\rangle\right)\right\rangle$. Making use of (3.241), we can provide a relation for the action of the symmetry group of the boundary Hamiltonian on the TN state,

$$G^{\otimes L}\left|\Psi\left(|T_p^{\mathrm{top}}\rangle\right)\right\rangle = \left(\bigotimes_{\langle bb'\rangle} \langle bb'|\,G_b^T \otimes G_{b'}^\dagger\right)\left(\bigotimes_b \mathcal{G}_b^{(n)}\,|T_n\rangle_b\right) = \left|\Psi\left(G^{\otimes p}\,|T_p^{\mathrm{top}}\rangle\right)\right\rangle\,. \tag{3.243}$$

In this expression, L denotes the total number of sites on the boundary chain, while the labels b in $\mathcal{G}_b^{(n)}$ and G_b make clear that these symmetry operators are acting on

the legs of a tensor state located at position b in the TN graph. Quite remarkably, the expression (3.243) describes an instance of operator propagation by means of which a transformation $G^{\otimes L}$, originally acting on the boundary Hilbert space, can be propagated into the bulk of the TN until it hits the top-level tensor $|T_p^{\text{top}}\rangle$. This operator propagation thus manifestly shows that the symmetry of $|\Psi\rangle$ depends solely on $|T_p^{\text{top}}\rangle$. As a consequence, notice how our TN state $|\Psi\rangle$ enjoys the same symmetries as the aperiodic boundary Hamiltonian when p is even. A similar statement for p odd is subtle, since it depends on the details of the superposition defining $|T_p^{\text{top}}\rangle$ and whether it shares the same symmetries as G.

To round off our discussion on the internal symmetries of our TN states, we comment on their relevance in view of extending a possible discrete holographic dictionary. An aspect that immediately lends itself to scrutiny is an analogous expression for the GKPW relation given in (2.23), which can be implemented in the TN language via inner products of states on both sides of the correspondence. For instance, an SU(2)-valued bulk field ϕ can be defined as a linear map from the set of tensor legs $\{bb'\}$ to the symmetry group SU(2) as

$$bb' \mapsto \phi(bb') \in SU(2)\,. \tag{3.244}$$

The insertion of such a field at any point in the TN graph can be viewed as a bulk excitation in the standard holographic language. From the perspective of the tensor network, this insertion amounts to a deformation of the TN state (3.239) of the form

$$|\Psi,\phi\rangle \equiv \left(\bigotimes_{\langle bb'\rangle} \langle bb'|\, 1\otimes\phi(bb')\right)\left(\bigotimes_{b}|T_n\rangle_b\right) = \Phi_\partial[\phi]\,|\Psi\rangle\ . \tag{3.245}$$

In order to obtain the final equality, we have propagated $\phi(bb')$ from the bulk to the boundary by exploiting the symmetries (3.241) and (3.242). This manipulation allows us to obtain a boundary operator Φ_∂ which now acts on the undeformed TN state $|\Psi\rangle$. For the reader with a more quantum-information theoretic background, this operation can be regarded as *quantum error-correction* (QEC) in the philosophy of [152, 428]. Typically, such boundary operators constructed from QEC are highly complicated objects. However, we are aided by the tree-like structure of the TN which implements the SDRG, cf. Fig. 3.34, such that the boundary operator Φ_∂ can be given the relatively simple form of

$$\Phi_\partial[\phi] = \bigotimes_{b\in\partial}\left[\phi(bb^{(1)})\phi(b^{(1)}b^{(2)})\phi(b^{(2)}b^{(3)})\cdots\right]^{\otimes n}\ , \tag{3.246}$$

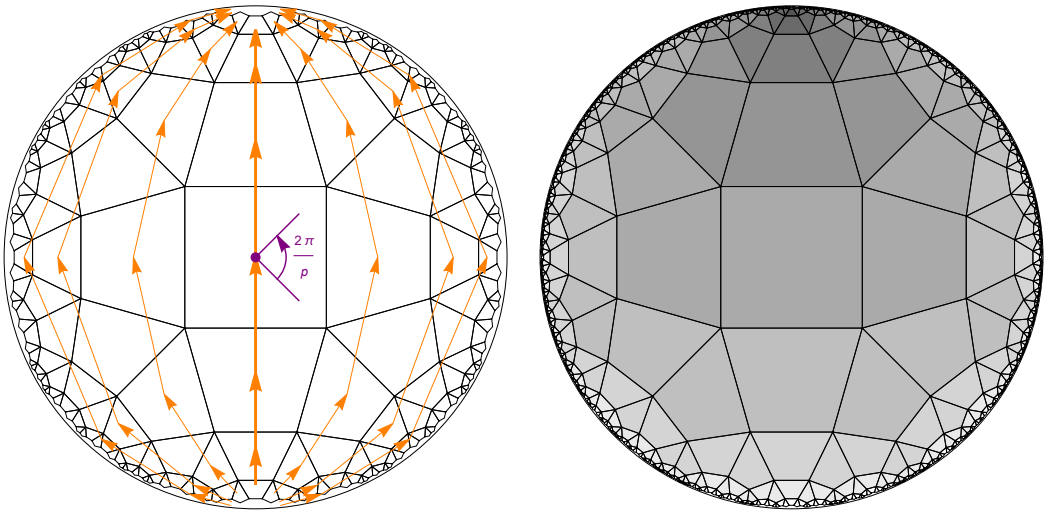


Figure 3.35: Left: Graphical representation of two elements of the Fuchsian group of isometries of a $\{p, q\}$ tiling. A rotation around the origin of $\mathbb{D}^2$ by an angle $2\pi/p$ (cf. Fig. 3.6) is shown in purple, while the orange arrows showcase the effect of a hyperbolic translation or boost $\gamma \in \Gamma$ (cf. Fig. 3.7). Right: Depiction of the Poincaré foliation, where different leafs are shown in different shades of gray, going from darker to lighter tones. This specifies a preferred inflation direction different from the radial foliation shown in Fig. 3.9.

with a tensor product exhausting all nodes along the TN boundary ∂. In (3.246), $b^{(m)}$ denotes the node of the TN graph which is attained by implementing m sequence-preserving SDRG transformations on $b \equiv b^{(0)}$. Instances may arise where factors in the tensor product (3.246) result in 2×2 identity matrices. The presence of such trivial factors is explicitly dependent on the choice of the SU(2)-valued function (3.244) and thus cannot be determined *a priori* on general grounds. As a final consideration, we write down an expression for the inner product of two such SU(2) fields, reading

$$\langle \Psi, \phi | \Psi, \phi' \rangle = \langle \Psi | \, \Phi_\partial[\phi]^\dagger \Phi_\partial[\phi'] \, | \Psi \rangle \ . \tag{3.247}$$

In this way, we can provide an explicit relation between correlation functions both in the bulk and on the boundary. For the future, we envision a systematic step-by-step construction of a discrete holographic GKPW dictionary by using formulas akin to (3.247) for other types of fields and operators.

We continue our symmetry analysis by considering the spatial symmetries of the TN graph, in particular in view of elucidating the discrepancy between the TN structure and the bulk hyperbolic tiling. Recalling our discussion in Sec. 3.2.2, the original isometry group of the full AdS_{2+1} spacetime has been broken down by the discretization to the class of Fuchsian groups reviewed in Sec. 3.2.3 describing the remnant

symmetries on the constant-time slice. Despite these groups begin infinite, we will focus on two specific elements of it for the current discussion, whose respective actions on the tiling consist of rotations around the origin by $\frac{2\pi}{p}$, and a boost of the central tile to the center of any other tile.[18] These actions are depicted in Fig. 3.35 by purple and orange arrows, respectively. Additionally, the construction of hyperbolic tilings via inflation rules explained in Sec. 3.2.4 inherently introduces a *discrete foliation* of the hyperbolic space, where each inflation layer defines a *leaf* of the foliation. Given the radial construction of tilings by the systematic addition of layers beginning from the center, it is evident that the inflation procedure naturally singles out a particular direction for this foliation. Be that as it may, there is no fundamental obstruction to the definition of alternative foliations of the Poincaré disk starting from points other than the origin. For instance, we may act on the entire tiling with an element of the hyperbolic translation groups reviewed in Sec. 3.2.3, thus boosting the central polygon to a new position close to the boundary. The inflation procedure initiated from this new point would give rise to a different foliation of the Poincaré disk. We show an example of this in the right panel of Fig. 3.35, where subsequent inflation layers are depicted in increasingly light shades of gray, similarly to our visualizations in Fig. 3.9. By analogy with the system of coordinates denoted as the Poincaré patch (2.13), obtained from the global coordinates (2.8) by a boost towards the boundary, we denote the resulting foliation starting from this boundary point as "Poincaré foliation". The Poincaré foliation also appoints a preferred inflation direction, albeit a different one to that of the radial foliation. Though both foliations indubitably give rise to the same hyperbolic tiling asymptotically, it is evident from our discussion in Sec. 3.5.7 that the SDRG flow is indeed dependent on the specific foliation we choose due to its direct relation to the inflation rules. Thus, given that the TN is a graphic embodiment of the inflation procedure, we may expect that it too is sensitive to the choice of foliation.

It is worth commenting that TNs which exactly coincide with the underlying hyperbolic tilings have indeed been constructed in previous literature [430, 435, 437–439, 709, 711–713]. Though such TNs automatically share the same spatial symmetries as the tilings, they typically only realize quantum states with unknown parent Hamiltonians. In our construction, we present an explicit Hamiltonian that governs the boundary theory, and our TN is such that it exactly reproduces its ground state. As a result, the TN graph does not coincide with the tiling. It is thus worth discussing this dependence of our TNs symmetries on the choice of foliation in more detail.

To this end, we will further differentiate between *global* and *local* spatial symmetries of

[18] We use rotations by $\frac{2\pi}{p}$ here as a concrete example, but of course all arguments in this discussion can be applied to vertex-centered tilings with corresponding rotations by $\frac{2\pi}{q}$.

the TN. More precisely, we denote as global symmetries those transformations which preserve the entirety of the TN graph, while transformations that only map subregions of the TN to each other, preserving the tensor structure, are considered as local symmetries. It is clear that the latter do not depend on the chosen foliation, since they only act locally. Based on these definitions, the symmetries of the TN representing the ground state of an aperiodic XXX chain are as follows:

Global symmetries in radial foliation: rotational $\mathbb{Z}_p$ symmetry Recalling our discussion of the dihedral symmetries of truncated tilings in Sec. 3.5.6, we can easily see that in the radial foliation the central p-gon carries the seed word a^p (or d^3 for $p = 3$). The corresponding TN thus has a central top-level tensor of rank p. It is thus manifest that the TN only inherits the global $\mathbb{Z}_p$ rotational symmetry around the central rank-p tensor, as can be seen in Fig. 3.34.

Global symmetries in Poincaré foliation: $\mathbb{Z}$ scaling symmetry This situation is slightly different for the Poincaré foliation. Here, even though the boost transformation of the central tile to the boundary leaves the tiling itself invariant, the central rank-p tensor is shifted. As a consequence, a new preferred direction for the inflation and the SDRG arises in the TN, cf. the left panel of Fig. 3.35. The hyperbolic boost maps all but one leg of the rank-p tensor to the infinite boundary, meaning that it no longer enjoys the $\mathbb{Z}_p$ symmetry present in the radial foliation. Nonetheless, there is a remnant symmetry along the one surviving tensor leg, which itself runs diametrically through the Poincaré disk. Along this leg, the entire TN enjoys a global $\mathbb{Z}$ scaling symmetry.

Local symmetries Finally, the TN naturally inherits the self-similar structure enjoyed by the aperiodic sequences defining the modulation of the boundary chain. The repercussions of this are that any arbitrarily large substructure of the TN can always be found at infinitely many other locations throughout the TN graph. We can in fact identify two types of such local symmetries: if a given substructure can be found within the same leaf of the foliation, we may regard the associated transformation as an instance of a local translational symmetry. Transformation of this kind have been previously denoted as "approximate" or "quasi" translational symmetries [439, 525]. In contrast, if the given substructure con only be found in a different leaf of the foliation, we consider this transformation as being a local scaling symmetry. In Fig. 3.36, we visualize both these types of local symmetries arising from the self-similar properties of aperiodic sequences.

This concludes our discussion on the symmetries of TN states reproducing the

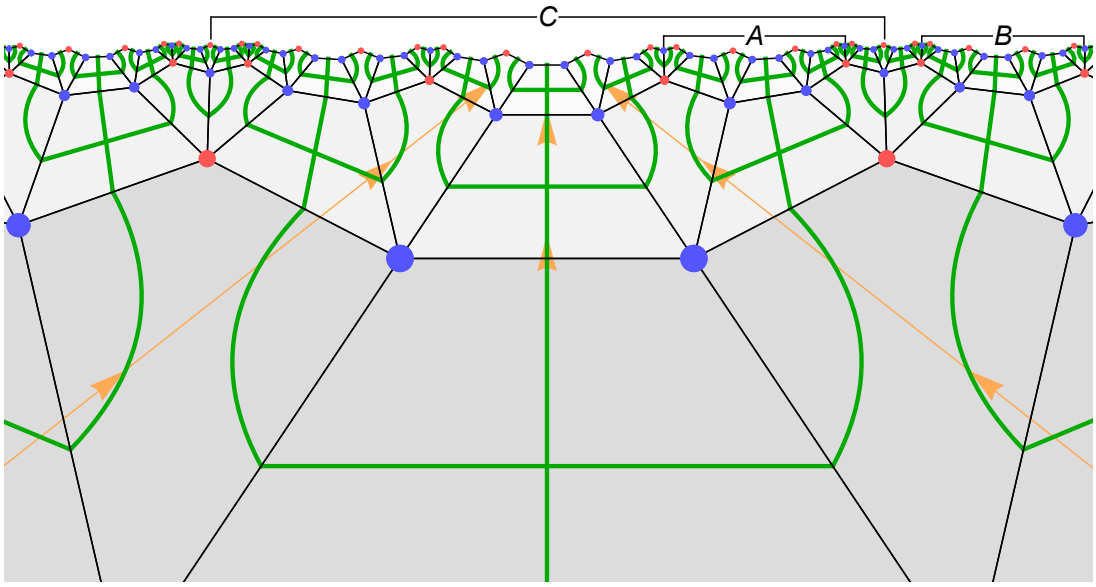


Figure 3.36: Portion of the TN reproducing the ground state of the $\{4,5\}$ aperiodic XXX chain, together with its underlying hyperbolic tiling. The snippet is obtained by zooming in on a region of the TN close to the boundary, such that the local structure is agnostic to the chosen foliation. The orange arrows are those of Fig. 3.35. TN substructures ending on the boundary subregions A and B are related by local translational symmetry on the TN graph, and they are both related to the substructure ending on boundary subregion C by a local scaling transformation.

ground states of aperiodic spin chains. In the following, we quantitatively support our claims that the TN implements the SDRG by providing an algorithm to systematically and explicitly generate the SDRG flows of the couplings.

Algorithm of RG flow from tensor networks

To showcase the computational power of our TN construction, we will now provide a graphical algorithm to explicitly determine the coupling flows along the SDRG for $\{p,q\}$-disordered XXX chains. Begin by considering a portion of a layer of tiles on the Poincaré disk which connects a UV chain to an IR chain, together with its corresponding set of tensors, thus consolidating a graphical depiction of an RG decimation step. This setup is shown in Fig. 3.37 for the exemplary case of the $\{8,4\}$ tiling, with black lines denoting (deformed) polygon edges, and green lines depicting the tensors as defined previously in Fig. 3.33. The upper line, representing the UV chain, carries on each edge a pair of couplings (μ_i, Δ_i), with $i \in \{a,b\}$, according to the usual color coding of these letters. The function of the algorithm is to translate the graphical distribution of the tensors into an explicit renormalization of the couplings along the UV chain into the ones in the IR chain, which we will denote by (μ', Δ'). By construction, the exact positions of the renormalized degrees of freedom in the IR chain

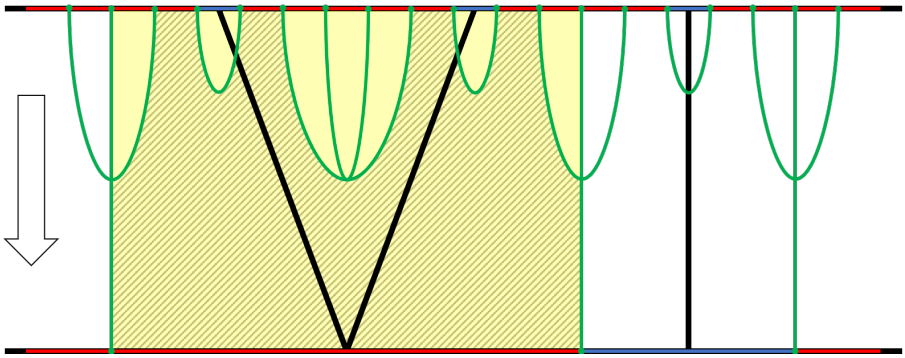


Figure 3.37: Sketch of a generic layer of tiles (delimited by black lines) of an $\{8,4\}$ tiling, together with the corresponding tensors (green lines). The figure is stretched to aid visualization of a decimation step as done in Figs. 3.21 and 3.33. Upper and lower horizontal lines therefore depict the UV and IR chains, respectively. Red and blue horizontal lines respectively represent weak and strong hopping parameters, associated to a- and b-type vertices on the tiling as per Fig. 3.20. The RG direction is downwards (arrow). The yellow shaded region encompasses the letter sequence and spins that are renormalized, while the gray striped region highlights those couplings which effectively enter the RG flow algorithm given in (3.248)-(3.251).

coincide with the positions at which the legs of the tensors intersect said chain, as can be seen from the bottom line of Fig. 3.37. This construction distinguishes a specific region of the tilings, represented by the yellow domain in Fig. 3.37, which we define to be bounded by the following elements: the IR edge with couplings (μ', Δ') (bottom), the TN legs carrying the renormalized spins (left and right) and the sequence of edges in the UV chain encompassed by these legs (top). Notice how the sequence of couplings of the UV chain delimited by this region are precisely the word that will be renormalized to the new pair of couplings (μ', Δ') upon implementing a deflation step. Exploiting the RG rules (3.198), we are able to formulate an algorithm to compute the explicit values of (μ', Δ'), which reads [158]:

- a singlet of n spins connected by couplings (μ_i, Δ_i) contributes to μ' with a factor $\gamma_n(\Delta_i)/\mu_i$ and to Δ' with $\delta_n(\Delta_i)$.
- a doublet of n spins connected by couplings (μ_i, Δ_i) contributes to μ' with a factor $\gamma_n(\Delta_i)$ and to Δ' with $\delta_n(\Delta_i)$.
- An isolated bond with couplings (μ_i, Δ_i) contributes to μ' with a factor μ_i and to Δ' with a factor Δ_i.

This elegantly simple algorithm is to be performed under the additional restriction that only the internal couplings in the gray striped region in Fig. 3.37 should be taken into account. It turns out that this distinction is inessential for class I TNs, but it

becomes relevant for studying the RG flow of the couplings in class II and III tensor networks, cf. (3.240), where the definition of the gray striped region is non-trivial. We exemplify the implementation of our algorithm by applying it to the $\{8,4\}$ tiling and its corresponding class I TN, as shown in Fig. 3.37. We will write the results of applying the algorithm to this case in a somewhat pedantic manner in order to facilitate the identification of the origin of every term according to their appearance in the rules of the algorithm. After a single decimation step, which for class I TNs equals a sequence-preserving transformation, we find that the renormalized couplings in the IR chain are given by

$$\mu_a' = \Big(\gamma_3(\Delta_a)\Big)\mu_a\left(\frac{\gamma_2(\Delta_b)}{\mu_b}\right)\mu_a\left(\frac{\gamma_4(\Delta_a)}{\mu_a}\right)\mu_a\left(\frac{\gamma_2(\Delta_b)}{\mu_b}\right)\mu_a\Big(\gamma_3(\Delta_a)\Big), \tag{3.248}$$

$$\Delta_a' = \Big(\delta_3(\Delta_a)\Big)\Delta_a\Big(\delta_2(\Delta_b)\Big)\Delta_a\Big(\delta_4(\Delta_a)\Big)\Delta_a\Big(\delta_2(\Delta_b)\Big)\Delta_a\Big(\delta_3(\Delta_b)\Big), \tag{3.249}$$

$$\mu_b' = \Big(\gamma_3(\Delta_a)\Big)\mu_a\left(\frac{\gamma_2(\Delta_b)}{\mu_b}\right)\mu_a\Big(\gamma_3(\Delta_a)\Big), \tag{3.250}$$

$$\Delta_b' = \Big(\delta_3(\Delta_a)\Big)\Delta_a\Big(\delta_2(\Delta_b)\Big)\Delta_a\Big(\delta_3(\Delta_b)\Big)\,. \tag{3.251}$$

We explained in Sec. 3.5.6 that the entire RG flow of the couplings can be obtained by iteratively applying the algorithm an asymptotically large number of times. In fact, we showed that the relevance of a modulation can already be extracted from the behavior of the couplings after a single sequence-preserving decimation, given the properties of the coefficients γ_n and δ_n. Thus, it is possible to analyze the relevance of all $\{p,q\}$ modulations on aperiodic chains via our graphical TN algorithm, a computation that is technically involved and is explained in Appendix B of [158]. Nonetheless, the results of that Appendix based on the TN algorithm are fully compatible with those obtained following the more standard approach given in Sec. 3.5.2, and in fact we can show that all the modulations induced by $\sigma_{\{p,q\}}$ on XXX chain are relevant, while on the XX chain they are marginal. Though effectively equivalent, the TN algorithm provides a much more accessible and intuitive proof for generic values of p and q.

Effective central charge from tensor networks

Much in the original spirit of tensor networks, we now exploit the TN constructed above to study the entanglement entropy of the ground state of aperiodic XXX chains. As reviewed in Sec. 2.3.4, the entanglement entropy of a boundary subregion A of general TNs with uniform bond dimension χ is bounded from above in a way reminiscent

of the RT formula for holographic entanglement entropy. From (2.88), we have

$$S_A \leqslant |\gamma_A| \log \chi \,, \tag{3.252}$$

where $|\gamma_A|$ denotes the minimal number of tensor legs cut by a curve in the bulk which is anchored at the entangling points of region A. If such a curve is furthermore homologous to A, we call it the *minimal cut* and denote it by γ_A. The exact type of tensors of which the network is built will determine the level of saturation of the inequality (3.252), with so-called *perfect tensors* fully saturating the bound [430]. In the TNs we are considering, the bond dimension is fixed and constant throughout the entire TN, since it represents the dimensionality of the local Hilbert space at each site of the chain. We have previously denoted this dimensionality in the general case by d, while in the specific example of the XXX chain we have $\chi = d = 2$, and for the SO(N)-invariant spin chains considered in Sec. 3.5.6 we would have $\chi = d = N$. Given the simple interpretation of this parameter, however, it is pertinent to continue our discussion for arbitrary values of the bond dimension χ.

As done throughout the previous sections, we consider a subregion A of the original UV chain consisting of L consecutive sites. The entangling points denoting the boundary ∂A of the subregion are the two outermost vertices of the block. Any candidate for γ_A should be anchored at these points. To now construct the minimal cut through the TN, starting from either vertex in ∂A, we connect it to its corresponding image in the TN graph according to the SDRG transformation. In particular, we choose this segment of γ_A such that it performs this connection while cutting the minimal number of tensor legs. After arriving at this next site of the chain after a sequence-preserving transformation, we can repeat the process and iteratively construct two RG trajectories, one for each vertex in ∂A, that run deeper into the bulk. There are two ways that this process can end: either the two trajectories meet at a given intermediate layer in the bulk, or they both reach up to the central tile. Any which way, both scenarios yield a complete minimal cut γ_A which is anchored at ∂A and which runs through the TN graph. We show some examples of minimal cuts created in this way in Fig. 3.34, where we have depicted them by brown dashed lines. We should stress that RG trajectories which start from different sites in the original chain are completely independent from each other, and may in principle lead to drastically different minimal cuts. Since our goal is to obtain an upper bound for the entanglement entropy in the spirit of (3.252), we should estimate the *average* number $\tilde{n}$ of legs cut by an individual step in the aforementioned construction of these RG trajectories. For the models considered here, such an estimation of $\tilde{n}$ was reported in [158] following previous constructions

put forward in [437], and we now proceed to explain this.

To provide an estimate of $\tilde{n}$, it is pertinent to introduce a more refined labeling of the vertices in a $\{p,q\}$ tiling, and we will use the letters $\{a_i\}_{i\in\mathbb{N}_0}$, $\{b_i\}_{i\in\mathbb{N}_0}$ for this purpose. While the a- and b-type vertices retain their original properties explained in Sec. 3.2.4, the subscript i denotes the number of tensor legs cut by one step along the RG trajectory when starting from the corresponding vertex. For instance, the portion of the minimal cut constructed as detailed above, when starting from a vertex labeled by a_2, will cut two tensor legs before reaching the corresponding IR chain. Of course, these subscripts are only allowed to be non-negative integers, and we denote their respective sets of possible values by K_a and K_b, respectively. This finer resolution of the vertices is naturally accompanied by a generalization of the inflation rules (3.49) and (3.50), which we will denote by $\tilde{\sigma}_{\{p,q\}}$. These are obtained from the original substitution words $w_a(a,b)$, $w_b(a,b)$ upon replacement of each a and b with a_i and b_i, respectively, according to the criteria explained above. An explicit form of the new rules $\tilde{\sigma}_{\{p,q\}}$ is not particularly enlightening, specially for class II and III TNs, and we will therefore not report them here, although we will give one explicit example later. Regardless, we stress that these can be obtained for every p and q, and in particular we may construct their associated substitution matrix $\widetilde{M}$ in exactly the same way as in Sec. 3.2.4. The difference is that now $\widetilde{M}$ is $(K_a+K_b)\times(K_a+K_b)$ matrix, while the original inflation matrix M was only 2×2. It turns out that M and $\widetilde{M}$ can be related since both admit a decomposition as $\widetilde{M}=\tilde{A}\tilde{B}$ and $M=\tilde{B}\tilde{A}$, where $\tilde{A}$ and $\tilde{B}$ are $(K_a+K_b)\times 2$ and $2\times(K_a+K_b)$ matrices, respectively. The nice consequence of this is that $\widetilde{M}$ and M share the same largest eigenvalue λ_+ given in (3.63). Consequently, we have that the left and right eigenvectors $\tilde{\mathbf{u}}_+$ and $\tilde{\mathbf{v}}_+$ of $\widetilde{M}$ corresponding to λ_+ are constructed as $\tilde{\mathbf{u}}_+=\mathbf{u}_+\tilde{B}$ and $\tilde{\mathbf{v}}_+=\tilde{A}\mathbf{v}_+$ respectively, with $\mathbf{u}_+$ and $\mathbf{v}_+$ the left and right eigenvectors of M corresponding to λ_+, given in (3.64). These quantities can be exploited to define a corresponding deflation matrix $\widetilde{D}$, which will allow us to study the RG trajectories, given by

$$\widetilde{D}_{ij}=\frac{\widetilde{M}_{ij}\tilde{v}_j}{\lambda_+\tilde{v}_i}\,. \tag{3.253}$$

We can interpret each entry $\widetilde{D}_{ij}$ of this deflation matrix as the probability of reaching a j-labeled vertex from a i-type vertex within one deflation step. The overall probability of reaching an i-type vertex at all from deflating any starting point is encoded in the components $p_i=\tilde{u}_i\tilde{v}_i$ of the left eigenvector $\mathbf{p}$ of the deflation matrix $\widetilde{D}$ with eigenvalue 1. Finally, a full characterization of the network structure requires the definition of a

$(K_a + K_b) \times (K_a + K_b)$ entanglement matrix $\widetilde{E}$. Its components $\widetilde{E}_{ij}$ are equal to the minimal number of legs cut by any curves connecting the vertex i in the UV chain and the vertex j in the IR chain.

The remaining part of our analysis will benefit from a distinction between the different classes of SDRG flows defined in (3.240). Starting with inflation rules $\tilde{\sigma}_{\{p,q\}}$ whose SDRG flows belong to class I, the deflation matrix $\widetilde{D}$ actually provides a direct upper bound for the entanglement entropy. The average number of cut legs $\tilde{n}$ in this case is simply given by

$$\tilde{n} = \frac{\sum_{ij} \widetilde{D}_{ij} \widetilde{E}_{ij} p_i}{\sum_{ij} \widetilde{D}_{ij} p_i} = \frac{\sum_{ij} \widetilde{E}_{ij} \widetilde{M}_{ij} \tilde{u}_i \tilde{v}_j}{\lambda_+ \sum_i \tilde{u}_i \tilde{v}_i} \,, \tag{3.254}$$

a result which is entirely determined by the network structure. Therefore, recalling the expression in (3.252), a single sequence-preserving transformation carries an associated decrease of the entanglement entropy which is bounded by

$$\Delta S_A \leqslant 2\tilde{n} \log \chi \,. \tag{3.255}$$

Based on this expression, we can obtain a bound for the effective central charges considered in Sec. 3.5.4, which we recall were defined as the coefficient in front of the logarithmic dependence of the entanglement entropy on the subsystem size, i.e. $S_A \simeq \frac{c_{\text{eff}}}{3} \log L$. Given that under a sequence-preserving transformation the subsystem size L is re-scaled to L/λ_+, we find the following bound for the effective central charge

$$c_{\text{eff}} = \frac{3\Delta S_A}{\log \lambda_+} \leqslant \frac{6\tilde{n}}{\log \lambda_+} \log \chi = \frac{6 \sum_{ij} \widetilde{E}_{ij} \widetilde{M}_{ij} \tilde{u}_i \tilde{v}_j}{\lambda_+ \log \lambda_+ \sum_i \tilde{u}_i \tilde{v}_i} \log \chi \,, \tag{3.256}$$

where the case of the XXX chain is obtained by setting $\chi = 2$. Notice that the inequality in (3.256) is a consequence of (3.252), and it is therefore only saturated in the case of perfect tensors [152]. The bound (3.256) is generalized to class II and III SDRG flows upon replacing $\left(\widetilde{M}, \lambda_+\right)$ with $\left(\widetilde{M}^2, \lambda_+^2\right)$ and $\left(\widetilde{M}^3, \lambda_+^3\right)$, respectively.

As forecasted above, we showcase this construction in an explicit example belonging to class I, namely that of TN states implementing the SDRG procedure of $\{p = 2k, q \geq 4\}$-aperiodic XXX chains. The fine-grained inflation rule in this case reads

$$\tilde{\sigma}^{\text{I}}_{\{2k,q\}} = \begin{cases} \{a_0 \mapsto (b_1 a_0)^{q-3} b_1, \;\; b_1 \mapsto (b_1 a_0)^{q-4} b_1\} \,, & k = 2 \\ \{a_i \mapsto a_{k-3} \cdots a_1 a_0 b_1 (a_0 a_1 \cdots a_{k-2} \cdots a_1 a_0 b_1)^{q-3} a_0 a_1 \cdots a_{k-3}, \\ \;\; b_1 \mapsto a_{k-3} \cdots a_1 a_0 b_1 (a_0 a_1 \cdots a_{k-2} \cdots a_1 a_0 b_1)^{q-4} a_0 a_1 \cdots a_{k-3}\}, & k \geqslant 3 \end{cases} \tag{3.257}$$

with $i = 0, 1, ..., k-2$, and we have $\Xi = \tilde{\sigma}^{-1}_{\{2k,q\}}$ since the modulation is class I. The physical action of the SDRG associated to the sequence generated by (3.257) is to map the spins in the word $a_0 b_1 a_0$ to a 2-spin singlet, the spins in the word $a_0 a_1 \cdots a_{k-2} \cdots a_1 a_0$ to a $(2k-4)$-spin singlet and the spins in the word $a_0 a_1 \cdots a_{k-3} a_{k-3} \cdots a_1 a_0$ to a $(2k-5)$-spin doublet. The case of $k = 3$, i.e. $\{6, q\}$, is a special one where the SDRG only generates 2-spin singlets, meaning that the associated 2-rank tensors are perfect and therefore the inequalities in (3.252) and (3.256) are saturated. The fact that the tensors (3.236) appearing in all our TNs are perfect only when $n = 2$ is shown in detail in Appendix C of [158] based on a numerical analysis, together with an overall discussion on the entanglement structure of TN states. From (3.257) we readily obtain the $k \times k$ inflation matrix

$$\widetilde{M} = \begin{pmatrix} 2q-4 & \cdots & 2q-4 & 2q-6 \\ \vdots & \ddots & \vdots & \vdots \\ 2q-4 & \cdots & 2q-4 & 2q-6 \\ q-3 & \cdots & q-3 & q-4 \\ q-2 & \cdots & q-2 & q-3 \end{pmatrix} , \tag{3.258}$$

where we have arranged the rows and columns such that they follow a lexicographic order in the fine-grained letters $a_0, a_1, a_2, ..., a_{k-2}, b_1$. Using (3.63), the largest eigenvalue of (3.258) immediately follows, together with its corresponding left and right eigenvectors

$$\tilde{\mathbf{u}} = \big(1, \cdots 1, 1, x\big) , \quad \tilde{\mathbf{v}} = \big(2, \cdots 2, x, 1\big)^{\mathrm{t}} , \tag{3.259}$$

$$\text{with} \quad x = 2 - k + \sqrt{(k-1)\left(k - \frac{q}{q-2}\right)} . \tag{3.260}$$

The $x \times k$ entanglement matrix is thus derived to be

$$\widetilde{E} = \begin{pmatrix} 0 & \cdots & 0 \\ 1 & \cdots & 1 \\ \vdots & \ddots & \vdots \\ k-2 & \cdots & k-2 \\ 1 & \cdots & 1 \end{pmatrix} . \tag{3.261}$$

Finally, exploiting (3.256) with $\chi = 2$, we attain an inequality for effective central

charge, which reads

$$c_{\text{eff}}^{\text{I}} \leqslant \frac{3\log 2}{\log \lambda_+} \frac{(k-1)x + (k-3)(k-2)}{(k-2)+x} \,. \tag{3.262}$$

We will provide a detailed discussion of this result in the following paragraph. Here, let us simply highlight that when $k = 3$, corresponding to $p = 6$, the effective central charge (3.262) is saturated, thus reproducing the result obtained in (3.189) of Sec. 3.5.4 for $\{6, q\}$ modulations. This represents a highly non-trivial consistency check between the two methods we have described in this section.

Comparison of different effective central charges

To conclude this section on TN states and aperiodic spin chains, we provide an encompassing comparison between effective central charges obtained via three distinct approaches. More precisely, we will contrast the dependence on the Schläfli parameters for the coefficients c_{eff} obtained in Sec. 3.5.4 through the analytic SDRG, that obtained above in (3.262) from the TN, and one that we will now derive via a geometric argument, using results from Sec. 3.2.2. In addition, we will juxtapose our findings with those of [437] and highlight the main aspects that differentiate our results.

Let us commence by providing a geometric derivation of entanglement entropy on hyperbolic tilings by means of a discrete analogue of the RT formula (2.63). For this, we will exploit the results of Sec. 3.2.2 on the length of a discrete geodesic path on arbitrary hyperbolic $\{p, q\}$ tilings. Our assumption is that the holographic RT formula for the entanglement entropy of a subregion A of the boundary CFT still holds after the discretization. This means that the key quantity entering the RT formula should now be length of the discrete geodesic Γ_A anchored at the entangling points of A, whose expression we derived in (3.31) in Sec. 3.2.2. Inserting this into the RT formula (2.63), we obtain its discrete analogue as

$$S_A = \frac{|\Gamma_A|}{4G_N} = \frac{2\ell\, s(p,q)\, \nu(p,q)}{4G_N\, t(p,q)} \log\left(\frac{l}{\epsilon}\right) \,. \tag{3.263}$$

As a first remark, note that the discrete geodesic Γ_A shares the same anchoring points as its continuous counterpart γ_A. By construction, a discrete path will end at a vertex of the hyperbolic tiling, thus making the definition of a subregion on the quantum chain well-defined. Furthermore, to properly complete our analysis, we ought to relate the lengths notions in the bulk and on the boundary systems. From the inflation procedure by which we construct the tiling, we know that lengths towards the asymp-

totic boundary are to be rescaled by a factor of λ_+, which is the largest eigenvalue of the corresponding inflation matrix and is given in (3.63). Any measurement of distances on the boundary performed using the bulk metric needs to take this rescaling into account. This technicality is discussed in detail in Appendix A of [158], where the relation $\log(L) = \mathfrak{d}\log(l/\epsilon)$ between the number of sites L in subregion A and its length l is derived, with $\mathfrak{d} = \log(\lambda_+)/t$ a type of fractal dimension associated to the self-similar structure of the boundary. If we include this scaling behavior into our expression for the entropy, we finally obtain a tiling-dependent expression for the entanglement entropy which reads

$$S_A = \frac{2\ell}{4G_N}\frac{s(p,q)\,\nu(p,q)}{t(p,q)}\frac{t(p,q)}{\log\lambda_+(p,q)}\log(L) \equiv \frac{c_{\text{eff,bulk}}(p,q)}{3}\log(L)\,, \tag{3.264}$$

from which we can read off the effective central charge

$$c_{\text{eff,bulk}}(p,q) = \frac{c\,s(p,q)\,\nu(p,q)}{\log\lambda_+(p,q)}\,. \tag{3.265}$$

In the last step, we have made use of the continuum Brown-Henneaux formula $c = \frac{3\ell}{2G_N}$ relating the proper central charge of the CFT to the AdS radius, although the precise value of c is left undetermined.

We may now compare all the results we obtained for the effective central charge. First of all, we can contemplate the effective central charge $c_{\text{eff,bulk}}$ obtained in (3.265) in the context of a similar quantity derived from TNs in [437]. Recall that our $c_{\text{eff,bulk}}$ quantifies, in a $\{p,q\}$-dependent way, the length of a discrete path on the hyperbolic tilings which is taken as the closest approximation to the continuum geodesic γ_A. This quantification occurs specifically in units of the polygon edge lengths $s(p,q)$ given (3.22). This is amply different from the quantification of lengths used in [437], where the logarithm of the bond dimension $\log\chi$ acted as a "length unit". As canonical as such a choice may seem from the perspective of the tensor network used in [437], the bond dimension is not a naturally arising quantity in any hyperbolic $\{p,q\}$ tiling. Nonetheless, we may bridge this gap in interpretation by invoking the Brown-Henneaux formula, which we assumed to remain true and unchanged by the discretization when deriving (3.265). Our results actually support this conjecture, since we see that the effect of the discretization always manifests itself via tiling-dependent multiplicative factors, e.g. $c_{\text{eff,bulk}} = c \cdot f(p,q)$, while the proper central charge of the CFT is left unaltered. In contrast, the TN constructed in [435] explicitly assumes a fixed bond dimension χ for any choice of Schläfli parameters. In order for this to be the case, an

implicit dependence of Newton's constant on the tilings parameters $G_N \equiv G_N(p,q)$ needs to be assumed, such that $\log \chi = \frac{s(p,q)}{4G_N(p,q)}$ is constant. Assuming this relation, we can indeed make contact between our expression for $c_{\text{eff,bulk}}$ with that of [437], and both approaches can be shown to be equivalent up to a constant numerical prefactor. Second, we would like to bring attention to the fact that the tensors of class I TNs have generally a lower rank than those considered in [152, 437]. As a consequence, the entries of the entanglement matrix (3.261) are smaller in value as compared with the entanglement matrix of TNs associated to HaPPY codes [152] or Majorana dimers [437]. We can therefore generally conclude that the resulting maximal value for the effective central charge in (3.262), at least for the class I SDRG flows, will also be smaller than for the other mentioned TN constructions. However, it is relevant to mention that even though we mostly focused on the XXX chain for clarity, it is straightforward to extend our TN construction to other aperiodic Hamiltonians of the form (3.142). For instance, we have shown in Sec. 3.5.6 that the admissible modulations (3.153) are all relevant when acting on SO(N)-invariant Hamiltonians, such that criteria **I-IV** are fulfilled and the general results from the SDRG in Sec. 3.5.2 are valid. The TN which exactly reproduces the ground state of the Hamiltonian (3.224) is therefore exactly the one constructed in this section, upon setting the bond dimension to $\chi = N$. The maximal entanglement contribution of a cut tensor leg will therefore be $\log N$, but besides this modification, all other considerations and properties of the TNs introduced above retain their validity. As a consequence, we may view our TN construction as an exact geometric description of the correlation and entanglement structure of general ground states of aperiodic spin chains. This role as geometric embodiment naturally carries over to the mutual information, such that we may relate the appearance of peaks in Fig. 3.30 with the presence of TN legs connecting spins at arbitrarily large distances through the bulk.

Third, we mentioned above that (3.262) reproduces the effective central charge (3.189) obtained in Sec. 3.5.4. In fact, the TN construction is even more powerful and allows to obtain upper bounds for the effective central charge for SDRG flows belonging to the classes II and III. A detailed analysis in contained in Appendix B of [158]. Further consistency checks obtained in this way in fact recover the effective central charges for the admissible modulations $\{p,q\} = \{3,7\},\{5,5\},\{3,8\},\{5,4\}$ obtained in Sec. 3.5.4 via the traditional SDRG approach.

Finally, we may extend our comparison of the results obtained in this section and those resulting from the traditional SDRG approach presented in Sec. 3.5.4 for ground states of aperiodic spin chains. The TN construction presented in this section lead us to the upper bound (3.262) for the effective central charge $c_{\text{eff}}^{\text{I}}$ of class I TNs. Our

upper bound (3.262) depends on p and q, as expected, and indeed is saturated in the case of $\{6, q\}$ modulations, where the result (3.189) of Sec. 3.5.4 is recovered. We note that our result (3.262) was obtained exploiting the expression (3.256) on our particular TN. However, the formula (3.256) was first derived in [437] and applied to a drastically different type of TNs where each polygon of the $\{p, q\}$ tiling is identified with a tensor. It is therefore not difficult to imagine that (3.256) provides different results when applied to differently constructed TNs, since it is an expression which depends on the internal structure of both the tensors and the graph associated to a TN. This explains the discrepancies between the maximal effective central charges obtained from (3.262) and those reported in [437]. On a more general level, the fact that our TN is different from that in [437] is also a reflection of the fact that they are reproducing different ground states on their boundary, and we should thus not expect the entanglement structure of different states to be equal.

We have thus provided an explicit construction of a TN which implements the SDRG procedure and thus exactly reproduces the ground state of $\{p, q\}$ aperiodic spin chains. We achieved this by associating tensor states (3.236) to the fundamental decimation steps involved in the SDRG (cf. Fig. 3.33), and building a TN graph by contracting these tensor states according to the RG flow. Although the resulting TN graph can be obtained independently from the discrete geometry utilized to tessellate the Poincaré disk, we showed that it can nonetheless be embedded onto the corresponding $\{p, q\}$ tiling of $\mathbb{D}^2$ whose inflation rule gives rise to the associated modulation of the spin chain. Whilst it is manifest that the TN graph and the tiling do not coincide (cf. Fig. 3.34), the discrete bulk structure provided by the TN still enjoys some of the spatial symmetries of the tiling. Moreover, the relations (3.241) and (3.242) show that the global symmetries of the boundary theory are in fact encapsulated in the TN states (3.236) localized in the bulk. Overall, our TN captures the RG flow of the couplings on the original chain via a graphical representation which extends into the bulk, much in the spirit of holographic RG flows known from AdS/CFT [168, 714, 715]. Our construction further allowed us to derive an upper bound for the effective central charges of aperiodic spin chains, thus taking us one step closer to a complete characterization of putative boundary theories for the discrete holography program.

3.6. Discussion

We close this chapter by providing an overview of the results obtained, with en emphasis on their overall relevance and pertinence within the broader landscape of discrete holography, cf. Sec. 3.1.

A discrete holographic duality necessitates first and foremost a description of *how* the underlying continuum variables will be discretized. In the approach to discrete holography presented in this chapter, we have chosen regular hyperbolic tilings, characterized by their Schläfli symbol $\{p, q\}$ with $(p-2)(q-2) > 4$, as our discretization scheme. As discussed in Sec. 3.2, these tessellations provide a canonical way of breaking down the continuous Poincaré disk $\mathbb{D}^2$, arising as a constant-time slice of the larger AdS_{2+1} spacetime, into a discrete but infinite set of points. Infinitely many choices of such $\{p, q\}$ tilings are possible, each of them crucially retaining a large amount of the isometries of the original continuous space, encapsulated in so-called Fuchsian groups. The desire to consider discretizations with large amounts of symmetry fits well within the original versions of AdS/CFT, and it seems to be a beloved characteristic shared by many approaches to discrete holography, such as modular discretization, hyperbolic buildings, and p-adic AdS/CFT. Our review in Sec. 3.2.3 revealed the vast and intricate mathematical structures associated with Fuchsian groups, something that can hopefully be exploited in greater detail in future investigations. We will address this point again in Chapter 5. Furthermore, hyperbolic tilings can be systematically constructed from substitution rules in a procedure called *inflation*, which we have thoroughly detailed in Sec. 3.2.4. This procedure induces captivating mathematical structures known as aperiodic sequences on the boundary of truncated but arbitrarily large hyperbolic tilings. The absence of translation invariance, together with a notion of self-similarity at all scales, make these sequences highly intriguing. In a hypothetical scale measuring the amount of disorder that can be associated with a binary sequence of variables, going from perfectly homogeneous to completely random, aperiodic sequences provide an exciting middle-ground due to their non-homogeneous yet deterministic nature. Self-similar structures such as fractals play a role in other approaches to discrete holography such as that of hyperbolic buildings.

Notwithstanding, a discretization alone does not yet define a discrete holographic duality. For this, concrete models with specific degrees of freedom need to be considered. Moreover, the overall capability of such discretizations to even capture well-established phenomena from their continuous counterparts needs to be verified. To this end, in Sections 3.3 and 3.4, we have presented simple yet powerful proofs of principle that straightforward lattice models of a scalar field defined on such hyperbolic tilings indeed are capable of reproduce many hallmarks behaviors of the continuous AdS/CFT correspondence. In particular, we considered the Breitenlohner-Freedman stability bound, the mass-to-scaling-dimension formula, and boundary correlation functions. All of these not only reproduce the continuum results to a high degree of accuracy, but the precise effect of the discretization, if present, can also be precisely quantified. The cul-

mination of these investigations lies in a concrete proposal for table-top realizations in terms of electric circuits, via which these previously experimentally inaccessible predictions from AdS/CFT can be drawn within the reach of current technologies in the laboratory. This feature poses a major advancement in the overall program of discrete holography, since none of the approaches mentioned in Sec. 3.1 has been able to showcase such an immediate connection to feasible experiments.

While these foundational lattice models have far-reaching consequences for future experimental investigations of discrete holography, they do not directly address the nature of potential boundary theories. In the spirit of seeing holographic dualities as a kind of quantum error-correcting code which redundantly encodes information of the boundary within the bulk spacetime, we may expect that discrete boundary theories should also carry knowledge about their dual geometry. In fact, as we explained above, the main benefit of aperiodic sequences is their rich structure which can be accessed from a very simple construction. Guided by this dogma, in Sec. 3.5 we have introduced and explored a general class of disordered quantum spin chains with nearest-neighbor hopping where the hopping parameters are disordered following an aperiodic letter sequence. The useful properties of aperiodic sequences allow for analytical tractability and explicit computations in these systems. At low energies, the physics of these models can be accessed via the powerful tool of the strong-disorder renormalization group (SDRG), which consists of a systematic decimation of degrees of freedom associated to high energies, as we elucidated in Sec. 3.5.2. Under certain criteria, the ground states of this vast class of aperiodic spin chains will take on a factorized form (3.152) corresponding to what is known as an aperiodic singlet phase (ASP). Generalizing previous known results, we have used the SDRG to compute several quantities in such ASPs for an infinite class of admissible modulations associated with hyperbolic $\{p, q\}$ tilings, such as correlation functions in Sec. 3.5.3, entanglement entropy in Sec. 3.5.4, and mutual information in Sec. 3.5.5. We have moreover applied our results to three explicit examples of aperiodic spin chains with vastly different characteristics and local degrees of freedom. To complete our investigations of aperiodic spin chains at the boundary of hyperbolic tilings, in Sec. 3.5.7 we have constructed tensor networks (TNs) which implement the SDRG procedure and thus exactly reproduce the ground states of these boundary theories, even when these are not given explicitly. Our results enhance those of previous works with TNs in that we know exactly the form of the parent Hamiltonian, while other approaches merely reproduce a ground state whose physical origin is unknown. Moreover, we have discussed the interpretation of our TNs as providing a discrete geometric dual to ground states of aperiodic spin chains, both from the perspective of symmetries and the formulation of a discrete analogue

of the GKPW dictionary. Our overarching combined framework of hyperbolic tilings, aperiodic spin chains, and tensor networks provides an unprecedented and pioneering exploration of an explicit discrete holographic duality, which at the same time paves the way for deeper studies in the future.

Quantum Information and Holography

4

"Young man, in mathematics, you don't understand things. You just get used to them."

John von Neumann

The AdS/CFT correspondence was born as a duality between two theories which, though quite different at first glance, turn out to be fundamentally related on several levels. Moreover, it quickly became apparent that the overall validity of the holographic principle is indeed extremely broad. The results of Chapter 3, exhibiting this validity of the holographic principle beyond continuum formulations, are an explicit testament to this seemingly universal principle. About a decade after its inception, the foundations of a new pillar to the holographic paradigm started to be laid. Initiated by the seminal work of Ryu and Takayanagi (RT) [114, 115] on holographic entanglement entropy, this pillar consists of incorporating aspects and ideas of quantum information theory and quantum computing [165–167, 260] into the AdS/CFT correspondence. Beyond entanglement entropy [114, 115, 169, 228, 319, 331, 335–337], other quantities such as mutual information [270, 307, 716–720], entropy inequalities [333, 721–727], relative entropy and Rényi entropies [271, 272, 338, 339, 728, 729], circuit complexity [138–141, 161, 357–371, 373–393, 730–743], entanglement negativity [744–748], as well as quantum error-correction and tensor networks [133, 152, 153, 287, 420–424, 428–431, 436–442, 709, 710, 749–752] have found their way into new entries of the holographic dictionary. More recently, the quest for understanding general properties of entanglement in quantum gravity has experienced a revival via a new take on an old paradigm, namely the theory of local operator algebras [142–145, 265, 753, 754].
The driving question for these investigations into the role of quantum information quantities in holography can be summarized as follows

What can quantum information teach us about black holes?

As the quantum information entries into the holographic dictionary started to be filled, it became clear that the question could be divided to ask for specific aspects of black holes in quantum gravity. Each of these aspects will turn out to be related to a specific quantum information quantity, as we describe as follows. The present Chapter is de-

voted to presenting my contribution to the investigation of these quantum information quantities and their role within the AdS/CFT correspondence.

The first insight was that of holographic entanglement entropy and it's role into the description of how *space* emerges in the bulk. The description of entanglement provided by the RT formula and its generalizations hints at how the geodesics and other geometric surfaces can be thought of as emergent quantities sourced from quantum correlations in boundary subregions. A celebrated example of this is the duality between an eternal traversable wormhole and two copies of a holographic CFT in a specific, maximally entangled state called the *thermofield double (TFD) state* [129, 130]. The culmination of this dogma was summarized in the conjecture that Einstein–Rosen bridges in the bulk are equivalent to Einstein–Podolski–Rosen entangled states in the boundary. This came to be known as the ER=EPR conjecture [132, 134, 755].

Though convincing, ER=EPR quickly raised further questions into the properties of wormholes and their role in holographic dualities. Namely, since the two copies of a CFT which go into the definition of the TFD state are not explicitly interacting, the boundary Hilbert space is assumed to factorize, i.e. $\mathcal{H}_{\text{bdry}} = \mathcal{H}_L \otimes \mathcal{H}_R$, where $\mathcal{H}_{L,R}$ denote the individual Hilbert spaces of the left and right CFTs. However, the dual bulk Hilbert space does not admit such a factorized structure $\mathcal{H}_{\text{bdry}} \neq \mathcal{H}_L \otimes \mathcal{H}_R$, the reason being that the wormhole, in particular including its interior, is a smooth continuous geometry. This apparent contradiction is known as the *factorization puzzle* [135]. It is apparent that there are pieces of information missing, and we are lead to ask what quantities can be used to either diagnose or explain non-factorization. As we will see in Sec. 4.2, the quantum information quantity of quantum discord, and a derivative of it known as *geometric quantum discord*, can be utilized for precisely this purpose. To show this, I report the results of [162] on geometric quantum discord and its connection to factorization properties of the partition function.

On a parallel vein, after it was understood that entanglement entropy can be used to describe the emergence of space outside of the horizon, it was argued that this description falls short when it comes to the region behind the horizon. In particular, it has been argued that the time evolution of boundary entanglement entropy in the TFD state reaches a constant value, i.e. thermalizes, at relatively short time scales. Here, this is meant to be relative to the time scales in which the interior of the black hole, or alternatively the length of the ER bridge, increases in size. Put succinctly, "entanglement is not enough" [138] to fully capture the emergence of space behind black hole horizons. To remedy this situation, a concept of quantum computation science known as *circuit complexity* was borrowed. Given a quantum operation, this quantity measures how difficult it is to implement based on certain criteria. Quantum

circuit complexity is an inherently ambiguous quantity, which makes its proper definition difficult and non-unique. Some desired properties for a holographic measure of complexity have been proposed, based on the properties of the black hole interior that it ought to describe. In this respect, in Sec. 4.1, I present the results of [161] where a notion of complexity for infinite-dimensional Hilbert spaces, exhibiting these desired features, was introduced. Remarkably, this introduces interesting connections to the theory of classical hydrodynamics and also sub-Riemannian geometry.
Finally, it remains to be addressed how the notion of *time* itself emerges in the bulk, and more specifically, in the interior of a black hole. It has been recently proposed [146, 148, 756, 757] that a proper understanding of the algebras of local operators on both sides of the duality will play a paramount role in tackling this question. In particular, it seems that *transitions* between different types of operator algebras carry information about the emergence of time within the black hole interior, as well as the emergence of the singularity. Studies on such transitions have been mostly performed in the context of quantum gravity [146, 148, 756–762], but having a simpler system on which to investigate this phenomenon is highly valuable. Therefore, in Sec. 4.3, I report the results derived in [163] on an exactly solvable, interacting quantum many-body system whose phase diagram allows for the identification of several transitions of operator algebras.

4.1. Quantum Complexity: When Entanglement is not Enough

Our first stop along the quantum information path to holography is quantum complexity. We have reviewed this quantity in detail in Sec. 2.3.2, together with its role in the present state of holography, which arose from the desire to probe black hole interiors at times much larger than the thermalization times of the boundary theory. A main obstacle to the explicit evaluation of complexity is its ambiguous nature, which hinders a consistent definition for arbitrary systems. While for finite-dimensional systems one may rely on physical justifications to narrow down admissible definitions of complexity, such constructions are entirely not clear when dealing with infinite-dimensional Hilbert spaces. A specific instance of this is when dealing with QFTs, where complexity can only be evaluated in particularly simple situations such as free theories.
It is therefore natural to ask whether a sensible definition of complexity for infinite-dimensional Hilbert spaces may be obtained as a limit of the more well-established finite-dimensional scenarios. However, this turns out to be extremely subtle, and

often such a limit is not well-defined. More precisely, the notion of k-locality is a basic feature of circuit complexity for finite systems of qubits, following the idea that if an operation acts on more than k qubits simultaneously, it should be considered hard [359, 361–363, 763]. The problem is that the cost functions associated with this penalization scheme diverge and become discontinuous in the thermodynamic limit, resulting in singular geometries on the manifold of unitaries and obstructing the definition of Nielsen complexity as geodesic length. Moreover, even if a complexity measure could hypothetically be defined in this case, it is not guaranteed that it would exhibit the features desired for it to be a *holographic* complexity measure. These key features, discussed in Sec. 2.3.2, were ergodicity and the existence of conjugate points.

To address this issue, in this section I report the results contained in [161], where a generalization of Nielsen complexity for unitaries $U \in \mathrm{SU}(N)$ acting on N-level quantum systems was proposed. The proposed cost function on $\mathrm{SU}(N)$, which assigns polynomial penalty factors to unitaries departing from the identity operator e,[1] exhibits both ergodicity and conjugate points in the limit $N \to \infty$. Moreover, this limit gives rise to an emergent interpretation of complexity in terms of classical hydrodynamics of an ideal, i.e. inviscid and incompressible, fluid flowing on a torus. Our construction involves a description of geodesic motion on curved manifolds known as the *Euler-Arnold* (EA) approach [764, 765], which allows for the analysis of geodesics entirely within the Lie algebra $\mathfrak{su}(N)$. The EA approach has been previously implemented in studies of complexity for CFTs [369–371, 735]. We show how the complexity geometry arising in the large N limit is well-defined and non-singular, thus preserving a sensible notion of complexity as geodesic length. In particular, we show how the low-energy sector of $\mathrm{SU}(N \to \infty)$ is isomorphic to the manifold $\mathrm{SDiff}(\mathbb{T}^2)$ of volume-preserving diffeomorphisms on the torus, on which the EA equation reduces to the well-known Euler equation of the ideal fluid. This emergent hydrodynamic theory is classically chaotic as a consequence of the hyperbolic nature of its phase space, which we probe by a numerical curvature analysis on the $\mathrm{SU}(N)$ manifold for large N.

4.1.1. The Euler-Arnold Approach to Nielsen Complexity

We review the Euler-Arnold (EA) approach for describing the geodesic trajectories of the $\mathrm{SU}(N)$ group manifold purely in terms of dynamics of elements of the Lie algebra $\mathfrak{su}(N)$. This framework was originally developed by Arnold in 1966 [764] to study geodesic flows on Lie group manifolds and their close relation to the Eulerian motion of a rigid body. This analysis culminates in the EA equation, which is the main object

[1] For this section, we denote the identity operator by e instead of $\mathbb{1}$ to notationally distance ourselves from matrix representations in view of the large N limit.

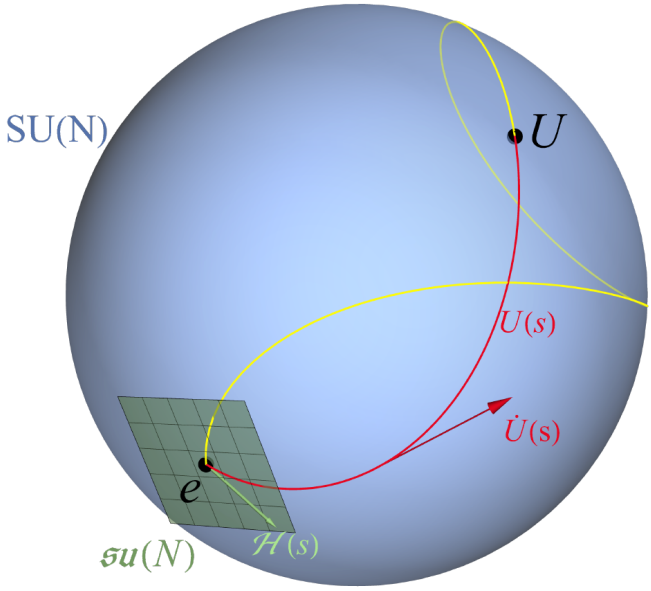


Figure 4.1: Illustration of the SU(N) Lie group manifold, highlighting its compact nature by plotting it as a sphere, familiar from the SU(2) $\cong$ SO(3) case. The tangent vector space at the identity e is isomorphic to the $\mathfrak{su}(N)$ algebra (dark green). Every point on the sphere represents a unitary gate acting on an N-level qudit, and we exemplify this by the target unitary U (black dot). Nielsen's geometric notion of complexity considers geodesics on SU(N), of which we have shown two examples, representing a minimal (red) and a non-minimal (yellow) trajectory connecting the identity with the target unitary. The EA approach exploits the group structure and translates the generation of a geodesic curve $U(s)$ onto the evolution of the control Hamiltonian $\mathcal{H}(s)$ (light green) with respect to the circuit time s. The latter is obtained as the pull-back of the tangent vector $\dot{U}(s)$ onto $\mathfrak{su}(N)$ as $\mathcal{H}(s) = \dot{U}(s)U^{-1}(s)$. The dynamics of $\mathcal{H}(s)$ are then governed by the EA equation (4.3).

of study in the subsequent sections.

We consider a quantum system with N levels, which generalizes the notion of the typical two-level system described by qubits. Borrowing the usual notation from quantum information theory, we denote our system as a *qudit*, with dimension $d = N$. Quantum gates acting on the qudit are unitary operators belonging to the SU(N) group. As a Lie group, SU(N) admits a description in terms of a smooth differentiable manifold, where each point corresponds to a specific unitary. A point of particular interest on this manifold is the identity operator e, whose tangent vector space is isomorphic to the Lie algebra $\mathfrak{su}(N)$. We can reach any target unitary operation $U \in \mathrm{SU}(N)$ of our interest by following a geodesic trajectory $U(s) \in \mathrm{SU}(N)$ parametrized by a value $s \in [s_i, s_f]$, see Fig. 4.1. Typically, in the context of the AdS/CFT correspondence, we are particularly interested in a specific unitary, namely the time-evolution operator $U = e^{Ht}$, with H the *physical* Hamiltonian of the system.[2] Nonetheless, all the fol-

[2]For this section only, due to the direct implementation of many results in the mathematical literature, we consider the algebra $\mathfrak{su}(N)$ to contain anti-Hermitian generators rather than the more

lowing arguments are valid for any unitary gate. The parameter s is sometimes called "circuit time", but let us stress that it does not necessarily coincide with the physical time t of the time evolution. We will however often simply refer to s as time when the context is clear. Without the loss of generality, we may take $s_i = 0$ and $s_f = 1$, such that the trajectory obeys the boundary conditions $U(0) = e$ and $U(1) = U$. This geodesic trajectory can be thought of as being infinitesimally generated by an (anti-Hermitian) *control* Hamiltonian denoted by $\mathcal{H}(s)$ via the Schrödinger equation $\frac{dU}{ds} = \mathcal{H}(s)U(s)$, as we reviewed in Box 2.2. The Euler-Arnold formalism [764, 765] capitalizes on the group structure of the manifold of unitaries and identifies the control Hamiltonian with the pull-back of the tangent vector $\dot{U}(s)$ of the geodesic trajectory $U(s)$ onto the tangent space at the identity via

$$\mathcal{H}(s) = \dot{U}(s)U^{-1}(s)\,. \tag{4.1}$$

In this way, it becomes clear that the control Hamiltonian is an element of the Lie algebra $\mathcal{H} \in \mathfrak{su}(N)$, which itself depends on the circuit time s, and whose image under the exponential map generates the trajectory $U(s)$. Note that the pull-back (4.1) is defined by right-multiplication. This is related to the fact that we choose to work with a right-invariant metric on the manifold of unitaries.[3] More precisely, we consider the inner product $\langle\cdot,\cdot\rangle_\gamma$ of two vectors ζ, η at some point $\gamma \in \mathrm{SU}(N)$. Right-invariance implies that we only need to define this inner product on a specific tangent space, namely the one at the identity $\gamma = e$, and then we can utilize the push-forward operation to define it on the entire $\mathrm{SU}(N)$ manifold. In other words, we have

$$\langle\zeta,\eta\rangle_\gamma = \left\langle \zeta\gamma^{-1}, \eta\gamma^{-1}\right\rangle_e\,. \tag{4.2}$$

We will drop the subscripts of the inner product in the following and always refer to the one defined on $\mathfrak{su}(N)$. The entire evolution of $\mathcal{H}$ as a function of the circuit time s within this approach is governed by the *Euler-Arnold* (EA) equation

$$\dot{\mathcal{H}} = -\kappa(\mathcal{H},\mathcal{H})\,, \tag{4.3}$$

with $\kappa : \mathfrak{su}(N)\times\mathfrak{su}(N) \longrightarrow \mathfrak{su}(N)$ a quadratic bilinear two-form defined on the $\mathfrak{su}(N)$ algebra [764]. It is implicitly defined in terms of both the Lie bracket $[\cdot,\cdot]$ and the

usual choice of Hermitian ones used in standard physics literature.

[3] This is mostly convention. Analogous constructions are possible by choosing a left-invariant metric. The case of bi-invariant metrics on $\mathrm{SU}(N)$, induced by the Killing form on $\mathfrak{su}(N)$, are not interesting from the point of view of complexity, since they do not apply any penalty factors and lead to a trivial EA equation [766].

chosen inner product $\langle \cdot, \cdot \rangle$ on $\mathfrak{su}(N)$ as

$$\langle [X, Y], Z \rangle = \langle \kappa(Z, X), Y \rangle \ , \tag{4.4}$$

with $X, Y, Z \in \mathfrak{su}(N)$. Note that while the Lie bracket is fixed by the algebra structure, we are free to choose any inner product we desire. Since any choice of inner product on $\mathfrak{su}(N)$ induces a corresponding Riemannian metric on $\mathrm{SU}(N)$, selecting a given product implies choosing a specific set of penalty factors. Different choices of $\langle \cdot, \cdot \rangle$ will provide distinct κ forms and thus lead to different cost functions in Nielsen's setup. On the one hand, at the level of the $\mathrm{SU}(N)$ Lie group, the inner product determines the cost associated to an infinitesimal transformation generated by the control Hamiltonian $\mathcal{H}$. On the other hand, from the perspective of the $\mathfrak{su}(N)$ algebra, the inner product controls the time evolution of $\mathcal{H}$. We therefore see that the task of finding geodesics on $\mathrm{SU}(N)$ boils down to computing those Lie algebra elements which solve the EA equation. In this sense, note that the EA equation (4.3) presents an advantageous way of finding geodesics on $\mathrm{SU}(N)$ as compared to solving the nested commutators appearing in a generic solution of the Schrödinger equation given above [365]. We will come to our specific choice of inner product on the $\mathfrak{su}(N)$ algebra in a later section.

4.1.2. An Algebra of N-level Qudits

Having stressed the relevance of the choice of inner product for the computation of complexity in the EA approach, we now turn our attention to the set of gates that we wish to allow in our quantum circuits. Since the control Hamiltonian is an element of the $\mathfrak{su}(N)$ algebra, we may always expand it as a linear combination of a set of generators for this algebra, which act as a basis for the corresponding $(N^2 - 1)$-dimensional vector space. These are our fundamental quantum gates from which the target unitary U will be synthesized. In this section, we present the construction of a particular set of anti-Hermitian generators of $\mathfrak{su}(N)$ [161], expanding on previous work [767–770], which has a well-defined large N limit.

We begin by introducing the so-called "shift" and "clock" matrices h and g. These are $N \times N$ matrices of the form

$$h = \begin{pmatrix} 0 & 1 & 0 & \dots & 0 \\ 0 & 0 & 1 & \dots & 0 \\ \vdots & \vdots & \vdots & \ddots & \vdots \\ 0 & 0 & 0 & \dots & 1 \\ 1 & 0 & 0 & \dots & 0 \end{pmatrix}, \qquad g = \begin{pmatrix} 1 & 0 & 0 & \dots & 0 \\ 0 & \xi & 0 & \dots & 0 \\ 0 & 0 & \xi^2 & \dots & 0 \\ \vdots & \vdots & \vdots & \ddots & \vdots \\ 0 & 0 & 0 & \dots & \xi^{N-1} \end{pmatrix}, \tag{4.5}$$

with $\xi = \exp\frac{2\pi \mathrm{i}}{N}$ a primitive N-th root of unity. A short-hand notation for these matrices reads $h_{ij} = \delta_{i+1,j}$ and $g_{ij} = \xi^j \delta_{i,j}$, with $i, j = 0, \ldots, N-1 \bmod N$. The modularity of the indices is related to the fact that these matrices obey $g^N = h^N = \mathbb{1}$. The naming convention of these matrices is due to their action on momentum and position eigenstates in a finite-dimensional Hilbert space. More precisely, the shift matrix h shifts from one momentum eigenvector to the next one, while the clock matrix g has the effect of multiplying position eigenstates by a phase, the set of which looks like a clock when shown on the complex unit disk. In fact, in the large N limit, these matrices transition to exactly the position and momentum modes of a plane wave, as we will see later in more detail. Crucially, the shift and clock matrices do not commute but rather obey a deformed commutation relation $hg = \xi\, gh$. As pointed out in [767–770], the matrices (4.5) can be used to define a set of unitary but not necessarily anti-Hermitian matrices as

$$J_{\vec{m}} = \xi^{\frac{m_1 m_2}{2}} g^{m_1} h^{m_2} \,. \tag{4.6}$$

These matrices are labeled by a two-vector $\vec{m} = (m_1, m_2)$ on the integer lattice $\mathbb{Z}^2$. Given the interpretation above in terms of momentum and position operators, and due to the fact that they do not commute, the matrices $J_{\vec{m}}$ can be seen as non-commutative plane waves with wave vector $\vec{m}$. The matrices in (4.6) are traceless and obey the relation $J_{\vec{m}}^\dagger = J_{-\vec{m}}$. Moreover, they inherit the N-modularity from the shift and clock matrices, which induces the following transformation law

$$J_{\vec{m}+\vec{t}N} = (-1)^{(Nt_1t_2+m_1t_2+m_2t_1)}\, J_{\vec{m}} \,, \tag{4.7}$$

under suitable N-translations characterized by an arbitrary vector $\vec{t} = (t_1, t_2) \in \mathbb{Z}^2$. This is a key relation which will ensure the closure of the $\mathfrak{su}(N)$ algebra. More precisely, the law (4.7) effectively divides the $\mathbb{Z}^2$-lattice into $N \times N$ cells. We may therefore focus our attention to the central one, defined by $m_1, m_2 = -\frac{N}{2}, \cdots, \frac{N}{2} + 1$ for even N and $m_1, m_2 = -\frac{N-1}{2}, \cdots, \frac{N-1}{2}$ for N odd, which we will denote as the *fundamental cell*. We note that the generators $J_{(0 \bmod N, 0 \bmod N)}$ are proportional to the $N \times N$ identity matrix. Therefore, they decouple from the algebra, reducing the total number of generators to $N^2 - 1$, as expected for the $\mathfrak{su}(N)$ algebra. Putting all these relations together, the set of matrices (4.6) closes under matrix multiplication and realizes the algebra

$$[J_{\vec{m}}, J_{\vec{n}}] = -2\mathrm{i} \sin\left(\frac{\pi}{N}(\vec{m} \times \vec{n})\right) J_{\vec{m}+\vec{n}} \,, \tag{4.8}$$

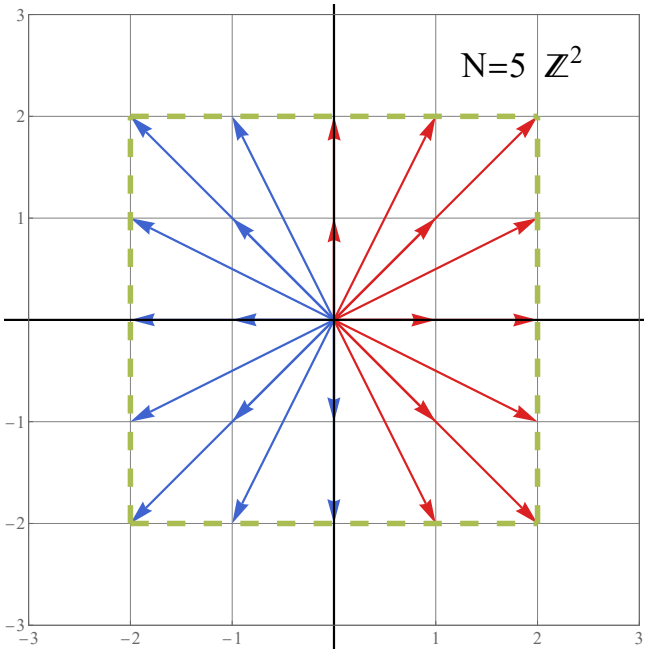


Figure 4.2: Fundamental cell (green dashed) in the $\mathbb{Z}^2$ lattice containing the final distribution of generators for the $\mathfrak{su}(N=5)$ algebra. Red arrows denote vectors $\vec{m}$ associated with $C_{\vec{m}}$ generators, while blue arrows are those points where $S_{\vec{m}}$ generators are allocated.

where $\vec{m}\times\vec{n}\equiv m_1n_2-m_2n_1$. Note the interesting trigonometric form of the structure constants in the algebra (4.8), which will play a major role in our later arguments. As noted in [767–770], this is indeed a realization of the $\mathfrak{su}(N)$ algebra, albeit one based on unitary generators. This is sufficient for the description of $\mathfrak{su}(N)$ as a vector space, but it falls short when trying to specify the usual relation between algebra generators and group elements via the exponential map. Of course, for a basis of $\mathfrak{su}(N)$ to act as proper generators of SU(N) elements, it needs to consist of N^2-1 traceless *anti-Hermitian* generators. In view of this, we construct new generators from two possible anti-Hermitian linear combinations of J's, namely one for each vector-index $\vec{m}$,

$$C_{\vec{m}}\equiv \mathrm{i}(J_{\vec{m}}+J_{\vec{m}}^\dagger)\,,\quad S_{\vec{m}}\equiv (J_{\vec{m}}-J_{\vec{m}}^\dagger)\,. \tag{4.9}$$

The chosen notation alludes to the usual Euler decomposition of exponentials into cosine and sine functions. It is evident that by doing this, we have doubled the number of elements in our basis, thus making it over-complete. This is because every point $\vec{m}$ on the fundamental cell is now associated once to a C generator and once to an S generator. Even worse, some of the C's and S's are linearly dependent. Though it might seem that we have only complicated the situation, we will now show that these issues can be overcome to obtain a final set of N^2-1 generators for the $\mathfrak{su}(N)$ algebra.

Let us now find this definitive set of generators, which we will denote as the *final*

distribution. This final distribution amounts to having a unique anti-Hermitian generator associated to each of the N^2-1 points contained in the fundamental cell on the $\mathbb{Z}^2$-lattice. Although in (4.9) we have given two possible generators $C_{\vec{m}}$ and $S_{\vec{m}}$ for each index vector, we can provide a systematic way of finding the final distribution by starting from the case of $N=2$ and subsequently extending the cell with linearly independent generators for higher values of N. More precisely, since $S_{\vec{m}}$ for $\vec{m} \in \left\{\left(-\frac{N}{2},-\frac{N}{2}\right),\left(-\frac{N}{2},0\right),\left(0,-\frac{N}{2}\right),\left(-\frac{N}{2},\frac{N}{2}\right),\left(\frac{N}{2},\frac{N}{2}\right),\left(\frac{N}{2},0\right),\left(0,\frac{N}{2}\right),\left(\frac{N}{2},-\frac{N}{2}\right)\right\}$ vanish identically for all even N, we only have C's generators at our disposal for $N=2$. The distribution is therefore unambiguous in this case. Going over to $N=3$, the corresponding fundamental cell now extends from -1 to 1 in both directions, and non-vanishing S are now present. We could try to derive a completely new distribution of generators for this case, but it would be more systematical if the structure of the final distribution for larger values of N preserves that derived for lower values, while only taking care of the newly added points to the unit cell. We denote this feature as the "compatibility" of a distribution. To ensure such compatibility of the $N=3$, we appoint a C generator to the vectors $(0,1),(1,0)$ and $(1,1)$ of the final distribution, since these were there already in the distribution for $N=2$. The remaining points of the new unit cell are to then be carefully filled with S generators. We say carefully because not all these newly added points host an $S_{\vec{m}}$ generator which is linearly independent from all others. This follows from the symmetry conditions

$$C_{-\vec{m}} = C_{\vec{m}}\,, \quad S_{-\vec{m}} = -S_{\vec{m}}\,. \tag{4.10}$$

which are a consequence of (4.7) and (4.9), and which we denote as the *linear dependence condition* (LDC). From the LDC (4.10), we can readily see that $S_{(1,-1)} \propto S_{(-1,1)}$, and therefore the point $(1,-1)$ in the $N=3$ fundamental cell must be associated with a C generator, which is by construction linearly independent from the S generator. In this way, we may fill out all points of the $N=3$ fundamental cell to obtain the final distribution of generators. Once these distributions have been set for the cases $N=2$ and $N=3$, the above construction may be iterated to systematically find the final distribution for $N \geq 4$. In the general case of odd values of N, where the fundamental cell is particularly symmetric around the origin, our construction based on compatibility and imposition of the LDC (4.10) effectively assigns C generators to all points on the right half-plane together with the positive m_2-axis, while allocating S generators to all points on the left half-plane and the negative m_2-axis. An illustrative example of this for the final distribution in the case of $N=5$ is shown in Fig. 4.2. Crucially, the generators C and S constructed in (4.9) obey similar commutation re-

lations inherited from (4.8), albeit in a slightly more intricate way. The corresponding structure constants are more involved than those in (4.8), which is a consequence of the over-completeness of the C, S basis at first glance. Nevertheless, a systematic approach can be written down via an algorithm which computes the structure constants for the C, S version of the $\mathfrak{su}(N)$ algebra, cf. the Supplemental Material of [161].

It was shown in [769] that in the large N limit, the algebra we obtained in (4.8) for the unitary matrices J defined in (4.6) becomes isomorphic to the algebra $\mathrm{SVect}(\mathbb{T}^2)$ of divergence-free vector fields X_f on the torus defined as

$$\mathrm{SVect}(\mathbb{T}^2) := \left\{ X_f \in T_{\mathbf{id}} \,\mathrm{SDiff}(\mathbb{T}^2) \,|\, \nabla \cdot X_f = 0 \right\} , \tag{4.11}$$

where $\mathrm{SDiff}(\mathbb{T}^2)$ is the corresponding Lie group of volume-preserving diffeomorphisms on $\mathbb{T}^2$, and $T_{\mathbf{id}}$ denotes the tangent vector space at the identity map $f = \mathbf{id}$. If we imagine such vector fields as describing the motion of a fluid on the surface of the torus, the condition of vanishing divergence can be physically interpreted as imposing that the fluid with velocity field X_f is incompressible. It is therefore also known as the incompressibility condition [765]. Note that, in two dimensions, all divergence-free vector fields are automatically Hamiltonian vector fields in the classical sense, i.e. they obey Hamilton's equations [771]. This explains the subscript f of the vector fields X, implying that any Hamiltonian vector field X_f is uniquely determined by its associated *stream function* $f \in \mathscr{C}^\infty(\mathbb{T}^2)$. More precisely, they are defined as

$$\iota_{X_f}\omega = -\mathbf{d}f \,, \tag{4.12}$$

where ω denotes the symplectic two-form on the torus, $\mathbf{d}$ is the exterior derivative, and ι represents the interior product. Note that the symplectic form ω is used to define the Poisson bracket of Hamiltonian stream functions as $\{f, g\} = \omega(X_f, X_g)$, implying that the commutator of Hamiltonian vector fields is itself again a Hamiltonian vector field. In particular, the latter vector field has a stream function given by the Poisson bracket of the Hamiltonian functions f and g,

$$\begin{aligned} \iota_{[X_f,X_g]}\omega &= \mathscr{L}_{X_f}\iota_{X_g}\omega - \iota_{X_g}\mathscr{L}_{X_f}\omega \\ &= \mathbf{d}\iota_{X_f}\iota_{X_g}\omega + \iota_{X_f}\underbrace{\mathbf{d}\iota_{X_g}\omega}_{=0} - \iota_{X_g}\underbrace{\mathbf{d}\iota_{X_f}\omega}_{=0} - \iota_{X_g}\iota_{X_f}\underbrace{\mathbf{d}\omega}_{=0} \\ &= -\mathbf{d}\omega(X_f, X_g) = -\mathbf{d}(\{f, g\}) = \iota_{X_{\{f,g\}}}\omega \,. \end{aligned} \tag{4.13}$$

In the expression above, $\mathscr{L}_Y h = Y(h)$ is Lie derivative of a smooth function h in

the direction of the vector field Y. Moreover, we have used Cartan's magic formula $\mathscr{L}_X = \mathbf{d}\,\iota_X + \iota_X \mathbf{d}$ to relate the Lie derivative to a linear combination of interior products and exterior derivatives [771].

On the torus $\mathbb{T}^2$, there is a canonical basis in which we may expand any such smooth function, namely plane waves. In particular, these automatically take care of the periodicity of the coordinates. Coincidentally, any such plane wave can also be indexed by a two-vector, whose components are integers due to the modularity. This is very similar to the discrete wave vector we have introduced for our generators of the $\mathfrak{su}(N)$ algebra, i.e. $\vec{k} \sim \vec{m}$, making our previous analogy between generators and noncommutative plane waves more clear. Any stream function can therefore be generically expanded in this basis of plane waves on $\mathbb{T}^2$ as [765]

$$f \equiv f_{\vec{m}} = -\exp(\mathrm{i}\,\vec{m}\cdot\vec{x}) = -\exp(\mathrm{i}(m_1 x + m_2\, p))\,. \tag{4.14}$$

This allows us to use f and $\vec{m}$ interchangeably, meaning that Hamiltonian functions (stream functions) and their wave vectors are equivalent. The algebra $\mathrm{SVect}(\mathbb{T}^2)$ is itself a Lie algebra, spanned by Hamiltonian vector fields. It can be shown [161, 765] that the commutation relations for the $\mathrm{SVect}(\mathbb{T}^2)$ algebra are given by

$$[X_{\vec{m}}, X_{\vec{n}}] = (\vec{m}\times\vec{n})X_{\vec{m}+\vec{n}}\,, \tag{4.15}$$

where the Lie bracket in this case is not given by a matrix commutator, but rather by the Poisson bracket. The aforementioned isomorphism between the $\mathfrak{su}(N)$ algebra and $\mathrm{SVect}(\mathbb{T}^2)$ in the large N limit is a consequence of Taylor expanding the sine function in (4.8) to first order in $1/N$. This yields the identification

$$J_{\vec{m}} \overset{N\to\infty}{\longrightarrow} \frac{2\pi}{\mathrm{i}N} X_{\vec{m}}\,. \tag{4.16}$$

This isomorphism manifestly relates Hamiltonian vector fields, spanning the algebra $\mathrm{SVect}(\mathbb{T}^2)$, with generators of the $\mathfrak{su}(N)$ algebra in the large N limit. There is, however, a slight subtlety to the identification (4.16), which was not originally addressed in [767–770], but it was indeed pointed out in [772]. Namely, the Taylor expansion of the trigonometric structure constants in (4.8) is not valid for certain classes of vector pairs $\vec{m}, \vec{n}$. More precisely, we can consider parametric types of vectors which are defined for every value of N, such as $\vec{m} = (\frac{N-1}{2}, 0)$ and $\vec{n} = (0, \frac{N-1}{2})$, whose cross product is of order $\mathscr{O}(N^2)$ or $\mathscr{O}(N)$. The structure constants for these instances cannot reliably be expanded in a series when $N \to \infty$. We are therefore obliged to restrict the isomorphism (4.16) to only those pairs of vectors which are of $\mathscr{O}(1)$. As N is taken to infinity,

a hierarchy will emerge between the region of the fundamental cell containing $\mathscr{O}(1)$ and $\mathscr{O}(N)$ or $\mathscr{O}(N^2)$ vectors. We will come back to this technical aspect later, and we will see that the vectors for which the isomorphism (4.16) can be reliably applied are indeed the low-momentum modes typically relevant for hydrodynamics.
Importantly, the new generators C and S are a linear combination of J's in (4.9). Therefore, the isomorphism (4.16) can be equivalently applied to the set of C and S generators, thus bestowing a well-defined structure upon them in the large N limit. Vitally, the relation to Hamiltonian vector fields, and therefore the theory of hydrodynamics of an incompressible two-dimensional fluid on a torus, remains unchanged.

4.1.3. A Cost Function from Hydrodynamics

The EA Equation for the SVect($\mathbb{T}^2$) Algebra

The relation between the $\mathfrak{su}(N)$ algebra and the algebra of volume-preserving diffeomorphisms on a torus presents an intriguing situation in view of complexity and the EA equation. More precisely, while canonical inner products on $\mathfrak{su}(N)$ give rise to bi-invariant Riemannian metrics on the manifold of unitaries, which yield trivial complexity, this is not the case for the algebra of Hamiltonian vector fields. This suggests a particular penalization scheme in the language of Nielsen complexity, together with a natural extension of it for finite values of N. Thus, in this section, we show how the natural inner product on the algebra SVect($\mathbb{T}^2$) gives rise to a simple Euler-Arnold equation. Moreover, it also provides a natural extrapolation of this hydrodynamic cost function to a choice of penalty factors for the $\mathfrak{su}(N)$ algebra at finite N, in a way that these have a well-defined large N limit.
The SVect($\mathbb{T}^2$) algebra of Hamiltonian vector fields is naturally equipped with an L^2 inner product, which can be written in terms of the Laplacian operator acting on the stream functions as

$$\langle X_f, X_g\rangle = \int_\omega X_f \cdot X_g = -\int_\omega f\Delta g\,, \tag{4.17}$$

with $\omega = dx \wedge dp$. Notice how for $f = g$, the expression (4.17) yields twice the kinetic energy of the fluid. As an inner product, (4.17) induces a right-invariant Riemannian metric on the manifold SDiff($\mathbb{T}^2$) of volume-preserving diffeomorphisms [764, 765], therefore assigning a length and a cost to geodesics. From the point of view of the EA approach, however, the inner product specifies a κ form. This can be seen by exploiting the relation (4.13) and using it together with (4.17) to obtain

$$\langle [X_f, X_g], X_f\rangle = \left\langle X_{\{f,g\}}, X_f\right\rangle = -\int_\omega \{f,g\}\Delta f = \int_\omega g\Delta\Delta^{-1}\{f,\Delta f\} \overset{!}{=} \langle X_g, \kappa(f,f)\rangle\,. \tag{4.18}$$

To obtain the expression above, we have used the Leibniz rule for the Poisson bracket, as well as the property that $\{f, g\}\omega$ can be expressed as the exterior derivative of a 1-form $\mathbf{d}(g\,\iota_{X_f}\omega)$ for any Hamiltonian functions f and g via Cartan's formula. Subsequently, we can employ the generalized Stokes' theorem stating that $\int_{\mathcal{M}} \mathbf{d}\alpha = \int_{\partial\mathcal{M}} \alpha$ for any 1-form α, where the boundary integral over α actually vanishes on the torus since $\partial\mathcal{M} = 0$. Finally, we have also inserted an identity operator via $\Delta\Delta^{-1}$ to recover the original form of the inner product given in (4.17). The expressions in (4.18) makes manifest that the κ form induced by the inner product (4.17) reads

$$\kappa(f, f) = -\Delta^{-1}\{f, \Delta f\}\,. \tag{4.19}$$

Since the control Hamiltonian $\mathcal{H}$ is an element of the $\mathfrak{su}(N)$ algebra, it will be identified with a Hamiltonian vector field $X_{\mathcal{H}}$ in $\mathrm{SVect}(\mathbb{T}^2)$ after the large N limit is taken. Correspondingly, it will have an associated stream function, denoted by $\mathfrak{h}$, defined via the symplectic form as $\iota_{X_{\mathcal{H}}}\omega = -d\mathfrak{h}$, cf (4.12). Making use of (4.19) and (4.3), we can thus obtain the associated EA equation for $\mathfrak{h}$, which reads

$$\Delta\dot{\mathfrak{h}} = -\{\mathfrak{h}, \Delta\mathfrak{h}\}\,. \tag{4.20}$$

Remarkably, the expression (4.20) is precisely the stream function form of the incompressible Euler equation in $(2+1)$ dimensions [765, 773]. Moreover, since there are not other terms present in (4.20), such as pressure or viscosity terms, we conclude that (4.20) describes the hydrodynamics of an incompressible and inviscid fluid, which is also known as an *ideal* fluid, flowing on $\mathbb{T}^2$.

By virtue of the isomorphism (4.16), we have argued that the $N \to \infty$ limit of the $\mathfrak{su}(N)$ algebra yields a simplification of the EA equation to the Euler equation for an ideal fluid on a torus. In terms of complexity, this means that the Nielsen complexity of very large qudit-unitaries can be equivalently evaluated in an effective hydrodynamic theory for which the control Hamiltonian is straightforwardly accessible via (4.20). In fact, we can make this mapping to the hydrodynamic setup even more precise via the following considerations: If we recall the Schrödinger equation associated with the target unitary U, it provided a direct relation to its control Hamiltonian. In hydrodynamics, this relation is precisely the mapping between the Eulerian and the Lagrangian frames of reference of the fluid $\frac{df}{ds} = \mathcal{H}(s, f(s))$ [774]. Here, $\mathcal{H}$ denotes the control Hamiltonian obtained from the solution $\mathfrak{h}$ to the Euler equation (4.20), while f is the target diffeomorphism on $\mathrm{SDiff}(\mathbb{T}^2)$ that we are aiming to synthesize. By subjecting the EA equation to the boundary conditions $f(0) = \mathbf{id}$, and $f(1) = f_{\text{target}}$ (the target

diffeomorphism), we obtain initial velocities $v^{\vec{m}} \equiv v^{\vec{m}}(s, f_{\text{target}})$ for geodesics as functions of f_{target}. Armed with these initial velocities, we may plug them into the length functional induced by our choice of cost function (inner product) $\ell = \int_0^1 ds\sqrt{G_{\vec{m}\vec{n}}v^{\vec{m}}v^{\vec{n}}}$ to compute their geodesic length. In the latter expression, we use $G_{\vec{m}\vec{n}}$ to denote the Riemannian metric induced on $\text{SDiff}(\mathbb{T}^2)$ by the inner product (4.17). A minimization procedure of this functional over all solutions of the EA equation (4.20) finally yields the complexity $\mathcal{C}(f_{\text{target}})$ of f_{target}.

In other words, the Nielsen complexity of very large qudit unitaries with $N \to \infty$ is given by the length of the minimal geodesic connecting the Lie algebra $\text{SVect}(\mathbb{T}^2)$ with our desired target diffeomorphism $f \in \text{SDiff}(\mathbb{T}^2)$. This geodesic is generated by control Hamiltonian which solves the hydrodynamic EA equation, i.e., the Euler equation (4.20). The target diffeomorphism f is associated to the large N limit of the unitary U that we wish to synthesize. In particular, our construction provides a smooth complexity geometry in the limit $N \to \infty$, in contrast to previous approaches for which the cost functions in this limit develop singularities.

Polynomial Penalty Factors for $\mathfrak{su}(N)$

Our successful description of complexity of $\text{SU}(N)$ unitaries in the strict large N limit readily suggests a natural extrapolation to finite N. In particular, it encourages the choice of a particular inner product on the $\mathfrak{su}(N)$ algebra at finite N which implements *polynomial* penalty factors in any direction of the tangent space. This is in stark contrast to previous approaches based on notions of k-locality, where hard directions are typically penalized exponentially in k. The strength of our approach lies in the well-defined behavior of complexity in the large N limit, ensuring a smooth transition from the finite- to the infinite-dimensional case, and leading to the hydrodynamic theory discussed above. Furthermore, we show how both our cost functions at finite and infinite N exhibit desired properties for holographic complexity measures, namely ergodic geodesic flows and conjugate points.

Inspecting the hydrodynamic inner product (4.17), we see that it is governed by two ingredients: the stream functions f, g, and the Laplacian operator Δ. The adaptation of these elements to finite N can be done by exploiting the interpretation of the set of matrices $J_{\vec{m}}$ as non-commutative plane waves. This is readily applied to the stream functions, given their natural expansion in commutative plane waves as in (4.14). At finite N, we can immediately replace the position and momentum modes of the plane waves by their non-commutative counterparts contained in the J matrices. As for the choice of inner product on the $\mathfrak{su}(N)$ algebra, we take inspiration in the way that the

standard Laplacian acts on commutative plane waves $f_{\vec{k}}$, namely as

$$\Delta f_{\vec{k}} = (\partial_x^2 + \partial_p^2) f_{\vec{k}} = -k^2 f_{\vec{k}} \,. \tag{4.21}$$

It is therefore natural to now define the action of a discrete Laplacian $\tilde{\Delta}$ at finite N on the basis of non-commutative plane waves as

$$\tilde{\Delta} J_{\vec{m}} = -m^2 J_{\vec{m}} \,. \tag{4.22}$$

Although the definition of a finite-dimensional Laplacian is not unique (see [772] for a different one), our choice (4.22) is a canonical one for plane waves on the torus. Based on the action of the discrete Laplacian (4.22) and the form of the hydrodynamic inner product (4.17), we define an inner product on the $\mathfrak{su}(N)$ algebra at finite N as

$$\langle \mathcal{T}_{\vec{m}}, \mathcal{T}_{\vec{n}} \rangle := -\frac{1}{2N} \operatorname{Tr}\left(\mathcal{T}_{\vec{m}} \Delta \mathcal{T}_{\vec{n}}^{\dagger} \right) . \tag{4.23}$$

Since the Lie algebra is a vector space, it is sufficient to define the action of the inner product on the generators $\mathcal{T} \in \{C, S\}$ of the algebra. Exploiting the Lie group structure, the inner product (4.23) induces a right-invariant metric $\tilde{G}_{\vec{m}\vec{n}}$ on the $\mathrm{SU}(N)$ manifold, where the tilde simply emphasizes that it is associated to the discrete Laplacian $\tilde{\Delta}$. This metric acts as a cost function, with its individual components denoting the penalty factors assigned to each of the N^2-1 linearly independent directions $\vec{m}$ on the tangent space to $\mathrm{SU}(N)$. In particular, these penalties are given by the eigenvalues of the discrete Laplacian acting on the generators, i.e.

$$\tilde{G}_{\vec{m}\vec{n}} = m^2 \delta_{\vec{m}\vec{n}} \,, \tag{4.24}$$

where we have defined $m = |\vec{m}|$. Crucially, these penalty factors are polynomial weights for every direction $\vec{m}$, the latter denoting the fundamental gates admitted by our construction. The penalty scheme applied by our cost function (4.24) causes the metric to be homogeneous, i.e. equal at every point on the manifold, but *not* isotropic, because different directions get penalized differently. More precisely, the only directions on the tangent space which get assigned equal penalty factors are those vectors which are related by parity or conjugation transformations, e.g. $\vec{m} = (1, 2)$, $\vec{n} = (2, 1)$ and $\vec{l} = (-2, -1)$. This is not a coincidence and it mirrors the classical Hamiltonian structure of our metric in the sense that the Laplacian is invariant under symplectic transformations. As a consequence of this symmetry, every single direction $\vec{m}$ on the Lie algebra, or any tangent space on $\mathrm{SU}(N)$ for that matter, is weighted by a

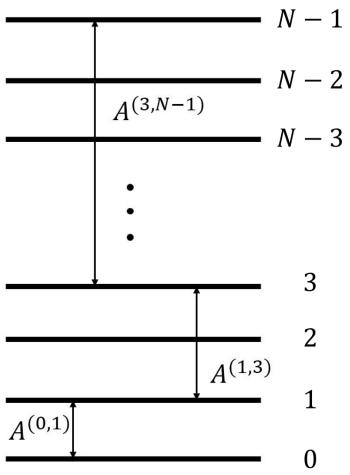


Figure 4.3: Sketch of an N level qudit decorated with exemplary transitions between different levels, labeled by the vector $\vec{m} = (m_1, m_2)$, with m_1, m_2 denoting the initial and final levels ofthe transition, respectively. These represent fundamental gates that may be realized in experiment when using such a qudit for the implementation of quantum algorithms. We assume that all-to-all interactions are possible, such that each of the $N^2 - 1$ transitions may arise. Our cost function (4.23) assigns, up to eight-fold degeneracy, a polynomial penalty of m^2 to each one of these transitions, such that higher-energy excitations are less preferred.

distinct penalty factor with at most an eight-fold degeneracy. This indicates that our choice of cost function corresponds to a maximally anisotropic metric on the unitary manifold. This is a highly desired characteristic as anisotropy is known to lead to negative curvature, which in turn is a robust indicator of ergodic geodesic flow [360].

Furthermore, the assignment of penalties by our cost function (4.24) can also be given a physical interpretation in view of experimental qudit realizations with a large number N of levels [775–781], as depicted in Fig. 4.3. Each of the directions $\vec{m}$ on the Lie algebra can be associated with a transition between two levels in the qudit, for example $\vec{m} = (0, 1)$ describing an excitation from the ground state to the first excited state of the system. The energy associated to such a transition can be naturally interpreted with a cost of implementing it, in particular of we think of them as gates which are realized via, e.g. radio-frequency pulses. Coincidentally, this energy difference between the levels is given precisely by m^2 for a given transition, in accordance with the penalty factors imposed by our cost function (4.24). This scheme naturally punishes the implementation of gates which are associated with high-energy excitations within the N-level qudit. This may be seen as a notion of smeared locality, indicating that fundamental gates implementing $\mathcal{O}(1)$ transitions are preferable in terms of cost as compared to gates effecting $\mathcal{O}(N)$ transitions, which are highly penalized. Naturally, the exact restriction as to which directions are $\mathcal{O}(1)$ and which are $\mathcal{O}(N)$ is relative and it varies for every finite value of N. While some vectors are $\mathcal{O}(N)$ for a given

value of N, they may wander into the $\mathscr{O}(1)$ sector as N grows large. We will return to this matter when discussing the curvatures associated with our cost function.

Let us stress the fundamental differences between our penalty scheme and previous ones found in the literature on the subject of Nielsen complexity in finite-dimensional systems [351, 359–362]. These works based their cost functions on the notion of k-locality, which is also rooted in experimental realizations of quantum computer using qubit registries. In this case, an operation which acts on k or more qubits simultaneously is considered hard, and these are correspondingly penalized *exponentially* with penalty factors $p \sim \alpha^k \sim e^{k \log \alpha}$. The Pauli weight of a many-qubit gate is defined via its decomposition into tensor products of standard Pauli matrices, together with the two-dimensional identity matrix. A k-local gate thus contains up to k Pauli matrices, with all other qubits being acted on by the identity. It is worth mentioning that the idea that polynomial penalty schemes might be better suited in certain circumstances was first pointed out in [365], since the typical exponential penalty factors diverge in an uncontrollable manner when the system size grown large. In turn, this leads to singular geometries in the $N = 2^n \to \infty$ limit [361–363], as we have mentioned before. In this respect, our construction comes to shine since our penalty factors remain finite in the $N \to \infty$ limit, where they acquire an interpretation in terms of wave vectors for the momentum and position modes of Hamiltonian vector fields on the torus. A crucial step in this identification is that the isomorphism (4.16) is naturally restricted to the set of vectors in the algebra which are of $\mathscr{O}(1)$. This is because certain families of vectors in $\mathfrak{su}(N)$ give rise to cross products of order $\mathscr{O}(N)$ or $\mathscr{O}(N^2)$, which scale in a way that impedes the truncation of the series expansion of the structure constants. In these instances, an identification with Hamiltonian vector fields is not proper. From the point of view of the hydrodynamic theory, this implies that the hydrodynamical phase space only contains low-momentum modes, which we will denote as the *admissible* directions on the $\mathrm{SVect}(\mathbb{T}^2)$ algebra. As a consequence, there are no infinitely-penalized directions on any tangent space of the manifold of diffeomorphisms $\mathrm{SDiff}(\mathbb{T}^2)$, thus ensuing a regular geometry.

The Strict Large N Limit and Sub-Riemannian Geometry

One may wonder what happens with the vectors of $\mathscr{O}(N)$ or $\mathscr{O}(N^2)$, which are definitely part of the $\mathfrak{su}(N)$ algebra at finite N but seem to get lost in the $N \to \infty$ limit and are not present in the $\mathrm{SVect}(\mathbb{T}^2)$. This is a very subtle matter which has to do with the delicate nature of the strict large N limit, as it often occurs when considering transitions between very large, but finite, and actually infinite quantities. The key point is that the $\mathrm{SU}(N \to \infty)$ manifold may cease to be compact when N is strictly

infinite. In this sense, even though the algebras $\mathfrak{su}(N \to \infty)$ and $\mathrm{SVect}(\mathbb{T}^2)$ are indeed isomorphic, the manifolds $\mathrm{SU}(N \to \infty)$ and $\mathrm{SDiff}(\mathbb{T}^2)$ are not. Rather, in the strict large N limit, $\mathrm{Diff}(\mathbb{T}^2)$ emerges as a so-called *sub-Riemannian* manifold of the larger and possibly non-compact $\mathrm{SU}(\infty)$ manifold [782, 783]. On the tangent bundle of the latter, there are admissible directions, i.e. the ones associated with the hydrodynamical phase space of $\mathrm{SVect}(\mathbb{T}^2)$, but there are also *inadmissible* directions arising from the high-energy sectors of the $\mathfrak{su}(N)$ algebra containing $\mathscr{O}(N)$ and $\mathscr{O}(N^2)$ modes. Since all natural numbers have been exhausted for the penalties m^2 along the admissible directions, these inadmissible directions are associated with penalty factors which are *at least* infinite. Note that the potential role of sub-Riemannian geometry within the study of complexity measures has been indeed highlighted in [743], although it was also originally mentioned in [349] as well. Within this framework, we can think of our cost function (4.24) as defining a family of metrics $\{\tilde{G}^{(N)}_{\mu\nu}\}$ for every finite value of N. The above-mentioned notion of smeared locality, as opposed to the sharp k-locality, will be imposed by each of these metrics by imposing large penalties to the $\mathscr{O}(N), \mathscr{O}(N^2)$ directions. In the transition from finite- to infinite-dimensional setups effected by the strict large N limit, our family of approximately sub-Riemannian metrics converges to a genuine sub-Riemannian metric on the $SU(\infty)$ manifold, namely

$$\lim_{N\to\infty} \{\tilde{G}^{(N)}_{\mu\nu}\} = \mathfrak{G}_{\mu\nu}\,. \tag{4.25}$$

The metric $\mathfrak{G}_{\mu\nu}$ is defined on the large $\mathrm{SU}(\infty)$ manifold, and it has two constituents. The first one is the $G_{\vec{m}\vec{n}}$ hydrodynamics metric with the standard Laplacian operator, imposing m^2 penalties to all directions $\vec{m}$ in the hydrodynamical phase space encompassing the entire $\mathbb{Z}^2$ lattice. These are the admissible directions for $\mathfrak{G}_{\mu\nu}$. The second constituent is a so-called *hard-wall* metric which assigns (at least) infinite penalties to all remaining directions which are associated to the strict large N limit of the $\mathscr{O}(N)$ and $\mathscr{O}(N^2)$ sectors. These are precisely the inadmissible directions mentioned above. In this sense, the hydrodynamics theory contained in the $\mathrm{SDiff}(\mathbb{T}^2)$ manifold emerges as the low-energy $\mathscr{O}(1)$ sub-Riemannian manifold of the larger $SU(N \to \infty)$.

Given the above considerations, it is a valid concern whether some of the large N unitaries, which may be of interest at finite N, could become entirely inaccessible in the strict large N limit. This would be quite undesirable, since it would drastically constrain the applicability of our approach. This notion within Nielsen's approach that any target transformation may be reached by geodesics starting from the identity is known as *controllability*. A fundamental result regarding controllability on finite-dimensional manifolds is the *Chow-Rashevskii theorem* [784, 785], which ensures con-

trollability under the requirement that the basis for the tangent bundle is a so-called *bracket-generating distribution*. Without entering into technicalities, let us state that this is always fulfilled in the absence of inadmissible directions on the tangent space. If there exist inadmissible directions, then the bracket-generating condition means that every direction on the tangent space may be equivalently obtained from a finite chain of commutators of generators in admissible directions. In our case of interest, one can check that our basis (4.9) is indeed a bracket-generating distribution for any finite N, as a consequence of $\mathfrak{su}(N)$ being a simple Lie algebra. Even so, the genuine sub-Riemannian metric $\mathfrak{G}_{\mu\nu}$ arises in our setup only in the strict large N limit. Luckily, a version of the Chow-Rashevskii theorem also exists for infinite-dimensional manifolds [786], guaranteeing that controllability properties present for finite N also survive the transition to infinite N. This ensures that we can still reach any point of the large SU(∞) manifold by means of geodesics which only run along admissible directions, namely those spanned by the hydrodynamic phase space.

4.1.4. Complexity Geometry at Large N

We conclude our analysis of the cost function (4.24) with a detailed study of its curvature properties and a characterization of the associated complexity geometry at large N. Such curvature analyses have become increasingly important in the general study of complexity [359–363, 743, 763, 787]. In this manner, we show how our cost function exhibits ergodic geodesic flows, as well as conjugate points, both sought-after characteristics of any potential holographic complexity measure.

The local curvature properties of a manifold are a key factor governing the flow of geodesic trajectories, and they can be used to distinguish between geometries where two nearby geodesics will typically flow away from each other and those where they may perhaps cross after a finite time. The main object of study in recent explorations of curvature in complexity geometries [359–363, 743, 763, 787] are the *sectional curvatures* $K(\vec{m},\vec{n})$ of the manifold of unitaries with respect to the chosen cost function. This object takes as arguments two tangent vectors and outputs the scalar curvature of the manifold in the direction of the two-plane spanned by them. In our case, for finite N, each tangent space is isomorphic to the $\mathfrak{su}(N)$ algebra and thus has N^2-1 independent directions, as determined by the index-vectors $\vec{m}$ in the fundamental cell. Having chosen two such directions, their sectional curvature is defined as [765]

$$K_{\vec{m}\vec{n}} = \frac{\langle R(\vec{m},\vec{n})\vec{m},\vec{n}\rangle}{\langle\vec{m},\vec{m}\rangle\langle\vec{n},\vec{n}\rangle} = \frac{1}{m^2n^2}\left(-\langle\nabla_{[\vec{m},\vec{n}]}\vec{m},\vec{n}\rangle - \langle\nabla_{\vec{m}}\nabla_{\vec{n}}\vec{m},\vec{n}\rangle + \langle\nabla_{\vec{n}}\nabla_{\vec{m}}\vec{m},\vec{n}\rangle\right), \tag{4.26}$$

where $\nabla_{\vec{m}}$ denotes the covariant derivative associated to the chosen metric on the SU(N) manifold, and the normalization is due to the fact that our set of generators provides an orthogonal, but not necessarily orthonormal basis for $\mathfrak{su}(N)$. The inner product $\langle \cdot \cdot \rangle$ is the one we defined in (4.23) for the $\mathfrak{su}(N)$ algebra. For any value of N, the algebra contains $N^2 - 1$ independent directions, but the sectional curvatures are symmetric under the exchange of their arguments, since the orientation of the two-plane spanned by the argument vectors does not change the underlying curvature. Due to this symmetry, and taking into account that $K(w, w) = 0$ for any vector w in the tangent plane, the total number of possible non-trivial sectional curvatures is given by $\frac{(N^2-2)(N^2-1)}{2}$. Provided with our choice of generators $C_{\vec{m}}, S_{\vec{m}}$ for the $\mathfrak{su}(N)$ algebra and our chosen inner product (4.23), an explicit expression for the sectional curvatures (4.26) can be obtained as

$$K_{\vec{m}\vec{n}} = \frac{1}{m^2 n^2}\left(\sum_{\vec{k}} \frac{1}{2}\alpha_{\vec{m}\vec{n}\vec{l}}\left(-\alpha_{\vec{m}\vec{n}\vec{l}}l^2 + \alpha_{\vec{n}\vec{l}\vec{m}}m^2 + \alpha_{\vec{l}\vec{m}\vec{n}}n^2\right) - \frac{1}{k^2}\alpha_{\vec{k}\vec{m}\vec{m}}\alpha_{\vec{k}\vec{n}\vec{n}}m^2 n^2 \right.$$
$$\left. - \frac{1}{4k^2}\left(\alpha_{\vec{m}\vec{n}\vec{k}}k^2 - \alpha_{\vec{n}\vec{k}\vec{m}}m^2 + \alpha_{\vec{k}\vec{m}\vec{n}}n^2\right)\left(\alpha_{\vec{m}\vec{n}\vec{k}}k^2 + \alpha_{\vec{n}\vec{k}\vec{m}}m^2 - \alpha_{\vec{k}\vec{m}\vec{n}}n^2\right)\right). \tag{4.27}$$

Here, the coefficients $\alpha_{\vec{m}\vec{n}\vec{l}}$ are the structure constants of the $\mathfrak{su}(N)$ algebra with respect to our set of generators, i.e. they are obtained from the commutation relations $[\mathcal{T}_m, \mathcal{T}_{\vec{n}}] = \alpha_{\vec{m}\vec{n}\vec{l}}\mathcal{T}_{\vec{l}}$, with $\mathcal{T} \in \{C, S\}$, cf. the Supplemental Material of [161]. The formula (4.27) enables an explicit evaluation of all the sectional curvatures induced by our choice of cost function with polynomial penalty factors. The sign of these sectional curvatures can be used as an indicator for the divergence (negative sign) or convergence (positive sign) of nearby geodesics along that particular direction in the tangent space [788]. This, in turn, gives a diagnostic for the "chaoticness" of the motion of a geodesic, given that a trajectory moving along a direction with negative sectional curvature will be very sensitive to the initial conditions on its velocity v, and will thus be classically chaotic. However, we should stress that this stability cannot be fully assessed by only considering the sign of the sectional curvature in the direction parallel to the tangent velocity vector. Rather, any emergent chaotic behavior will be sensitive to the sign of the sectional curvatures along *all* two-planes which contain this velocity vector v [765]. We should therefore take all these contributions into account when analyzing the stability of geodesics, which strongly suggests the use of the quantity

known as the *normalized Ricci curvature* $\mathrm{Ric}(v)$ [789]. It is defined as

$$\mathrm{Ric}(v) = \lim_{N\to\infty} \frac{1}{N^2-2} \sum_{\vec{m}} K(v, \mathcal{T}_{\vec{m}}) \,, \tag{4.28}$$

and it represents an average of all sectional curvatures K with a fixed first argument with respect to all possible orthogonal directions $\mathcal{T}_{\vec{m}}$ on the tangent space. The normalization takes into account the dimension of this tangent space, as well as the fact that $K(w,w) = 0$ for any vector w. Moreover, it ensures that the normalized Ricci curvature remains a well-defined even in the large N limit.

The mathematical literature on differential geometry contains the highly pertinent result that $\mathrm{Ric}(v) \leq 0$ for $\mathrm{SDiff}(\mathbb{T}^2)$ [789]. The well-known statement that two-dimensional hydrodynamics is a classically chaotic theory is quantified precisely by this result, which states that the average curvature experienced by any geodesic on $\mathrm{SDiff}(\mathbb{T}^2)$ is negative. In other words, the phase space of a fluid is hyperbolic, leading to generically unstable trajectories. In our setup, given that we have full control over the sectional curvatures at finite N by means of (4.27), we can also access and compute the normalized Ricci curvatures of our complexity geometry. Moreover, the isomorphism (4.16) to the algebra $\mathrm{SVect}(\mathbb{T}^2)$ suggests that we can extrapolate our results for very large N and compare with the one known from hydrodynamics. For this, we numerically evaluate the normalized Ricci curvatures using (4.28) and (4.27) for odd values $N \in [3, 39]$.[4] For simplicity, we take the vector v to be each of the orthogonal directions $\vec{m}$. Naturally, since the dimensionality of the tangent space grows with N, some vectors will only arise as directions in the final distribution after a certain value $N = N_0(\vec{m})$, and this values depends on the specific vector in the $\mathbb{Z}^2$ lattice. Their Ricci curvature can correspondingly only be defined for values $N \geq N_0(\vec{m})$, after which it will continue to vary as more and more directions contribute to the average given in (4.28). From our numerical data, we observe that the Ricci curvature of all newly added directions to the $\mathfrak{su}(N)$ algebra at any given $N = N_0$ are always positive. However, they all eventually turn negative at some higher *critical value* $N = N_c(\vec{m})$, as more directions contribute to the average. To the extent of our numerical analysis, we have plotted this value of N_c for every direction $\vec{m} \in \mathfrak{su}(N)$ in Fig. 4.4. Even though $N = 39$ is respectably large, notice that the identification of the critical value $N_c(\vec{m})$ not only requires that the corresponding direction be within one of the reached fundamental cells (i.e. $N_0 \leq 39$), but it further necessitates data on that particular

[4] The odd N case is simply technically easier to implement, as a consequence of the symmetry of the fundamental cell. We perform all computations for odd N, but of course the setup equally valid for even values of N.

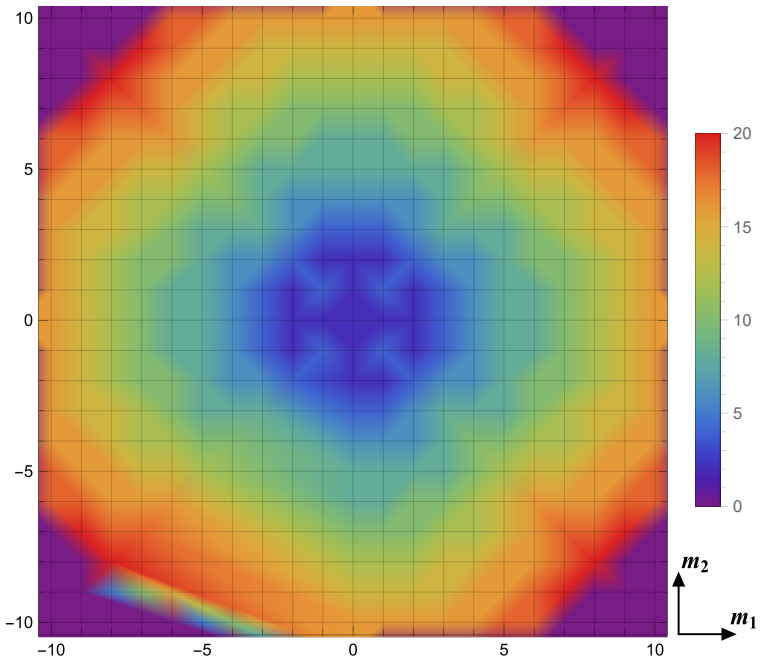


Figure 4.4: Density plot for the computed critical values $N_c(\vec{m})$ at which the normalized Ricci curvature (4.28) for a given direction $\vec{m}$ within the $\mathfrak{su}(N)$ algebra becomes negative. The plot shows values for a region around the origin of the $\mathbb{Z}^2$ lattice, spanned by the vector components m_1, m_2. Numerical evaluation of the sectional curvatures (4.27) up to $N = 39$ allow for the identification of N_c for vectors obeying $|\vec{m}| \lesssim 10$. We interpolate the data defined on the integer lattice points with a color density to guide the eye. Notice that the color flare at the bottom-left corner is only an artifact of this interpolation. The eight-fold symmetry of the penalty factors imposed by our cost function is manifest.

vector for several larger values of N such as to identify when $\mathrm{Ric}(\vec{m})$ turns negative. Due to this restriction, the characterization of the critical values N can only be done for vectors within the fundamental cell of $N \approx 10$. Still, even within this restricted set of data, we can identify a trend that every single vector $\vec{m} \in \mathbb{Z}^2$ has indeed a finite critical value N_c after which its corresponding normalized Ricci curvature turns negative. This is represented by the color scale in Fig. 4.4, which can indeed be used to give a visual and qualitative definition for the $\mathscr{O}(1)$ and $\mathscr{O}(N)$ subsectors. More precisely, notice from Fig. 4.4 that the critical value N_c for vectors appears to grow only slowly for vectors that denote points further away from the origin. In spite of this, all critical values N_c remain finite. The blue region of Fig. 4.4, together with its extrapolation for large N, can be then interpreted as the definition of the $\mathscr{O}(1)$ subsector from which the hydrodynamic theory emerges when $N \to \infty$. In other words, every direction within the $\mathfrak{su}(N)$ algebra will start by having a positive normalized Ricci curvature as soon as it appears for a given N_0, but it will turn negative at a higher, finite value N_c. As we increase N, new directions will enter the fundamental

cell as the dimension of the tangent space increases, and these will have positive Ricci curvature, as mentioned above. These are precisely the families of vectors which make up what we denoted previously as the $\mathscr{O}(N)$ subsector. However, as we increase N, directions $\vec{m}$ which previously had $\mathrm{Ric}(\vec{m}) > 0$ will now turn to negative curvature, thus transitioning to the $\mathscr{O}(1)$ sector. In the subtle transition from finite but large to infinite N, the resulting $SU(\infty)$ will contain those directions associated to the $\mathscr{O}(1)$ subsector, which are those that can be isomorphically identified with Hamiltonian vector fields as per (4.16). These are the directions giving rise to the phase space of the hydrodynamic theory, which is spanned by all vectors in $\mathbb{Z}^2$. The limit of the directions in the $\mathscr{O}(N)$ subsector are then associated with the inadmissible directions on the larger SU(N) manifold, in the sense of sub-Riemannian geometry explained above.

These results lead to several interesting properties of the complexity geometry associated with our specific choice of cost function. First, we can conclude that the geometry associated to the low-energy sector of $\mathscr{O}(1)$ indeed exhibits negative Ricci curvatures in the large N limit, thus providing a numerical confirmation of the mathematical results for the hydrodynamics theory [789]. Moreover, this indicates the emergence of chaotic behavior of trajectories on the manifold of unitaries, which in the strict large N limit results in the known chaotic behavior of the hydrodynamical phase space. This behavior indicates that a given geodesic, if given enough finite time, will explore the entirety of the manifold, indicating the ergodicity of the geodesic flow. This key property is thus inherited by our cost function, induced by the inner product (4.23) imposing polynomial penalty factors, strongly suggesting its potential as a holographic complexity measure [358, 359]. Second, we highlight that although all the average Ricci curvatures of the low-energy sector turn negative at some finite value of N, directions with positive sectional curvature are guaranteed to appear at any value of N. Rather than a bug, this is a feature of our cost function in view of being a candidate for a holographic complexity measure for two reasons: On the one hand, while it is true that a geometry with strictly negative curvature will be ergodic [362, 790], any Riemannian metric on a Lie group without any positive sectional curvature has been proven to necessarily be flat [363, 791]. From the perspective of Nielsen complexity, a flat metric is not of interest. Therefore, it is a highly beneficial trait of our cost function that it combines the negative average Ricci curvature required for ergodicity with the existence of positive sectional curvatures to avoid triviality. On the other hand, purely negative geometries lack a key property expected for any geometric complexity measure, namely *conjugate points*. These are the points on a manifold where the a given geodesic ceases to be globally minimal, i.e. there exists an alternative geodesic

which reaches the target point with a smaller geodesic length [782]. A clear example of conjugate points are any antipodal points on a sphere, e.g. the North and South pole. Starting from the South pole and going West, the typical arc segment geodesic ceases to be the minimal trajectory exactly when we go pass the North pole. At this point, the arc segment geodesic starting from the South pole and going East is the globally minimal path. The existence of such conjugate points are considered to be a necessary feature of any holographic complexity measure, since they effectively stop the complexity from displaying an unbounded growth with time [351, 361–363, 743], making it reach a plateau instead. For our emergent hydrodynamic theory in the strict large N limit, it is known in the mathematical literature that the manifold $\mathrm{SDiff}(\mathbb{T}^2)$ indeed exhibits conjugate points [765, 792]. As for finite N, we can expect these to exist given the presence of positive sectional curvatures, but their exact position on the manifold of unitaries is unclear.

Let us conclude our analysis by discussing our results in view of the universality classes for complexity measures introduced in [743]. The authors of that work conjecture the existence of certain families of complexity metrics of the same dimension $\{(g_{\mu\nu})_{\mathcal{I}}\}$, which are labeled by the penalty factor $\mathcal{I}$ assigned by the cost function to the hard directions. The general case where $\mathcal{I}$ turns into a multi-index is treated in [743], but for the purposes of the present discussion we may take all hard directions to be degenerate with the same penalty $\mathcal{I}$ for simplicity. The main claim of [743] is that for large values of the hard penalties $\mathcal{I}$ and long geodesic distances on the manifold of gates, the complexity measures should exhibit a universal hierarchy of the form

$$\mathcal{C}_{\mathcal{I}=\infty} = \mathcal{C}_{\mathcal{I}} + \mathscr{O}\left(\left(\frac{1}{\sqrt{\mathcal{I}}}\right)\right) . \tag{4.29}$$

In other words, one can approximate a hard-wall metric with infinite penalty $\mathcal{I}$ by $\mathscr{O}\left(1/\sqrt{\mathcal{I}}\right)$ corrections to the complexity computed with finite but large penalty $\mathcal{I}$. Notice that the label $\mathcal{I}$ can also be related to the leading order behavior of the sectional curvatures for large penalty $\mathcal{I}$, yielding the schematic relation $K \sim \mathcal{I}$ [743]. From the perspective of our construction, we see that our cost function (4.24) imposes penalties which grow with N, in particular making $\mathscr{O}(N)$ directions on the tangent space increasingly more expensive in terms of geodesic length on the $\mathrm{SU}(N)$ manifold. Put differently, we naturally expect that unitaries at large geodesic distance from the identity will necessarily involve the implementation of increasingly complex fundamental gates, namely those which are strongly penalized with factors which grow with N. In particular, any given geodesic will prefer to develop indirectly in an $\mathscr{O}(N)$ direction

by alternatively moving along cheaper $\mathscr{O}(1)$ directions. As we mentioned before, the Chow-Rashevskii theorem guarantees that any point on the manifold can be reached in this manner. The conjecture (4.29) makes this heuristic understanding more clear in the following way. Namely, we can confirm both analytically and through our numerical computations that we have $\mathcal{I} \sim N^2$ as a label for our class of cost functions $\{\tilde{G}^{(N)}_{\mu\nu}\}$. We can then exploit this, together with (4.29), to devise a relation between complexity on the SU(N) manifold at large N and large geodesic distances and the complexity on the manifold of diffeomorphisms, as

$$\mathcal{C}(\mathrm{SU}(N)) \simeq \mathcal{C}(\mathrm{SDiff}(\mathbb{T}^2)) + \mathscr{O}(1/N) \ . \tag{4.30}$$

A consequence of this relation is that we can expect a specific finite value of $N \equiv N^*$ to exist, such that the complexity $\mathcal{C}(\mathrm{SU}(N^*))$ at short distances is equivalent to $\mathcal{C}(\mathrm{SDiff}(\mathbb{T}^2))$ at long distances, in spite of the fact that both manifolds are not isomorphic. Let us also stress that even though the original conjecture of [743] was made for families of metric of the same dimensions, we use it in (4.30) for a class of metrics whose dimension varies with N. This is, however, not a contradiction, but rather a corroboration of the expectations of the authors as they elucidate in the discussion of the relation (4.29) in [743].

Driven by the quest of understanding possible definitions of quantum complexity for infinite-dimensional systems such as QFTs, in this section we have presented a cost function for SU(N) unitary gates acting on an N-level qudit and showed that its Nielsen complexity remains well-defined even in the large N limit. Introducing a suitable basis (4.9) for the $\mathfrak{su}(N)$ algebra in terms of non-commutative plane waves labeled by $\vec{m} \in \mathbb{Z}^2_{\mathrm{mod}\,N}$, we exploit the isomorphism (4.16) to relate it in the large N limit to the algebra SVect($\mathbb{T}^2$) of Hamiltonian vector fields on the torus. The latter algebra describes the hydrodynamic phase space of an ideal fluid flowing on $\mathbb{T}^2$, and it is the tangent space of the manifold SDiff($\mathbb{T}^2$) [765]. This emergent description in the large N limit suggests a natural cost function (4.17) in terms of the kinetic energy of the fluid, which we utilize within the Euler-Arnold approach to show that the EA equation of this theory is precisely the Euler equation of (2+1)-dimensional hydrodynamics of an ideal fluid (4.3). Motivated by this well-behaved construction at infinite N, we define a cost function (4.23) for the $\mathfrak{su}(N)$ algebra at finite N, which imposes polynomial penalty factors m^2 for the infinitesimal gates belonging to the $\mathfrak{su}(N)$ algebra. We characterize the complexity geometry induced by this choice of cost function by a curvature analysis, in particular by computing its sectional (4.27) and normalized Ricci curvatures (4.28). Our numerical results show that our cost function always exhibits

positive sectional curvatures, ensuring the existence of conjugate points, but overall it has an negative average curvature for large N, thus guaranteeing the ergodicity of the geodesic motion. We find that these two features of our complexity geometry of large qudit unitaries, which are highly desired (if not necessary) for any putative holographic complexity measure, are naturally inherited from the hyperbolic nature of the phase space of ideal hydrodynamics.

We have thus constructed a setup for Nielsen operator complexity which behaves well when transitioning from finite to infinite N. The complexity of large qudit unitaries can be equivalently computed by solving for the corresponding control Hamiltonian stream function in (4.3), an aspect that greatly simplifies the usual computation of complexity on the SU(N) manifold. Crucially, our framework ensures that even in the large N limit, every unitary on the SU(∞) manifold can be reached in a cost-effective way by following admissible directions within the SDiff($\mathbb{T}^2$), which emerges as a sub-Riemannian manifold of SU(N) containing the low-momentum modes $\mathscr{O}(1)$ which are preferred by our cost function. All in all, our work shows that a definition of complexity for QFTs can greatly benefit from cost functions defined in terms of the Laplacian acting on infinitesimal gates, in particular in view of eventually developing consistent complexity measures for holographic CFTs to probe interior black hole geometries at late times. Let us finally point out that the behavior of holographic systems at doubly-exponential times is poorly understood, and the precise meaning of a Poincaré recurrence for the bulk is not at all clear. Given that there exist some results in the mathematical literature [793, 794] regarding the late-time behavior of certain solutions to the Euler equation (4.20), it is highly intriguing if these can be used to elucidate the details of Poincaré recurrences via our Nielsen complexity measure.[5]

4.2. Geometric Quantum Discord: When Entanglement Connects Universes

Within the ER = EPR paradigm [132, 134, 755], the emergence of spacetime is seen as a consequence of the quantum correlations between systems. Usually, this is associated to entanglement being shared between degrees of freedom defined on different subregions of a larger system. As discussed in Chapter 2, the prototypical realization of the ER = EPR conjecture is the duality between two entangled CFTs in their TFD state and an eternal two-sided black hole in AdS [129]. In this case, the quantum correlations between the two boundaries support the emergent smooth and continuous

[5] I am very thankful to Arnab Kundu for bringing this to my attention.

geometry which is the wormhole in the bulk. This is, however, the root of the factorization puzzle: the boundary Hilbert space is expected to factorize as $\mathcal{H}_{\text{TFD}} = \mathcal{H}_L \otimes \mathcal{H}_R$, since the two CFTs do not explicitly interact. However, the dual wormhole geometry defines a Hilbert space which does not admit such a factorization.[6] It became apparent that a resolution of this contradiction relies on a detailed understanding of the nature of the correlations supporting the presence of the wormhole.

We are in particular interested in quantifying how much of the correlations embodied by the wormhole are of pure quantum mechanical origin, and which could effectively be described by classical correlations. While it is true that the two copies of the CFT in the TFD state are entangled, this state is by itself a very fine-tuned pure state with a vanishing total entanglement entropy. More realistic black holes are quite unlikely to end up in such a refined configuration. It is more natural to expect that a black hole, as the macroscopic object with tremendous amount of entropy it is, will be better represented by a mixed state. Moreover, it should be a type of mixed state that is decohered in such a way that any asymptotic observer which has access to correlations only one side of the black hole cannot possibly tell the difference between this state and the TFD state. These considerations lead to the proposal of the so-called *thermomixed double* (TMD) state in [164]. For a low-energy one-sided observer, this state is indistinguishable from the TFD state while only containing purely classical correlations. More precisely, the TMD state does not support any kind of quantum correlations and only classical Shannon mutual information is shared between the two sides. Yet, the TMD state maintains a gravity interpretation as a smooth geometry connecting both boundaries. Because of this, the bulk Hilbert space will still not factorize, but it would however not obey the EPR side due to the absence of entanglement. This indicates that quantum correlations not encompassed by entanglement entropy are pivotal for a deeper understanding of the factorization puzzle.

Several measures for correlations beyond quantum entanglement have been suggested in the literature, in particular in view of quantifying these correlations in mixed states. Some of these are the entanglement of formation [250, 251] and the entanglement negativity [795], but these generalizations are typically tailored to address only a certain class of all possible quantum correlations [258]. With the goal of having a single measure that is sensitive to *any* type of correlation that is purely of quantum mechanical origin, the notion of quantum discord was introduced in [256–258], as we reviewed in Sec. 2.3.3. For example, it was shown that quantum discord in non-vanishing in isotropic states, which are a one-parameter class of states interpolating between

[6] However, see [137] for a recent discussion on how factorization of the bulk trace can be explained through non-perturbative wormhole contributions to the gravitational path integral.

pure and mixed states, while other measures such as entanglement of formation and entanglement negativity are zero [257, 795, 796]. However, while insightful, the computation of quantum discord for general quantum states is highly involved and can only be accessed analytically in a handful of simple cases. This is due to the minimization procedure involved in its definition (2.78), and it has actually been proven that the computation of quantum discord for generic states is an NP complete problem [797]. To circumvent this issue, [798, 799] introduced an alternative quantity known as *geometric quantum discord* (GQD), which can be shown to provide a necessary and sufficient condition for non-vanishing quantum discord. Moreover, GQD acts as an upper bound on the entanglement negativity [255]. The key computational advantage of GQD is the replacement of a complicated minimization over measurements by a much simpler minimization over states in terms of the Hilbert-Schmidt norm [800].
Inspired by this state of affairs in both quantum information and high-energy physics communities, in this section we report the results obtained in [760], where GQD was proposed as an easily computable indicator of non-factorization in the boundary.[7] More precisely, we begin by computing GQD for arbitrary pure states in Sec. 4.2.1, and subsequently apply our results to the prime example of the TFD state in Sec. 4.2.2. We derive the way in which a non-vanishing GQD implies the non-factorization of the modular or thermal partition function by relating it to the second Rényi entropy of a specific classical state, which can be interpreted as the closest classical approximation to the TFD state. In particular, our results show that this is precisely the TMD state of [164]. In parallel, we demonstrate that GQD for pure states is equivalent to the "geometric measure of quantum correlation" first introduced in [801]. Finally, we relate the computation of GQD to certain microstates of realistic black holes created by gravitational collapse, and also comment on potential bulk duals of GQD.

4.2.1. Geometric Quantum Discord for Pure States

We begin by computing GQD for arbitrary pure quantum states. Recall that quantum discord, by construction, only captures purely quantum correlations, since it is literally defined as the difference between the total and the purely classical correlations between two subsystems, cf. (2.78). Woefully, the complicated minimization over measurements involved in the quantum conditional entropy (2.74) hinders the general analytical treatment of quantum discord. In contrast, the quantity of GQD, introduced in [798]

[7] Many insights regarding this analysis were patiently explained to me by Moritz Dorband, for which I am extremely grateful. A discussion of the results in this section in the broader context of geometric phases is contained in his PhD thesis [394].

and denoted by $Q^{(2)}$, requires a much more feasible minimization over states, namely

$$Q^{(2)}(A:B) = \min_{\chi \in \Omega^{(\text{q-c})}} ||\rho_{AB} - \chi||^2 \,. \tag{4.31}$$

Here, ρ_{AB} is the density matrix of the full quantum system, which we assume to be bipartite, i.e. $\mathcal{H} = \mathcal{H}_A \otimes \mathcal{H}_B$. Moreover, we use the Hilbert-Schmidt norm for an arbitrary operator X, defined as

$$\|X\| = \sqrt{\text{Tr}\,(X^\dagger X)}\,. \tag{4.32}$$

The set $\Omega^{(\text{q-c})}$ is that containing all quantum states with vanishing discord, which we have argued in Sec. 2.3.3 is equivalent to the set of all the (q-c) states. These zero-discord (q-c) states are of the form.

$$\chi \equiv \chi^{\text{q-c}} = \sum_k q_k \rho_k^A \otimes |\phi_k^B\rangle\langle\phi_k^B|\,, \tag{4.33}$$

where $q_k \geq 0$, $\sum_k q_k = 1$ and $\langle\phi_k^B|\phi_l^B\rangle = \delta_{kl}$. In this expression, the density operator $\chi^{\text{q-c}}$ is bipartite and consists of a linear combination between reduced density matrices ρ_k^A of subsystem A and pure states $\left\langle \phi_k^B \middle| \phi_k^B \right\rangle$ in subsystem B. Note that, if we were to compute GQD with respect to subsystem A instead of B, this definition of zero-discord states can be changed accordingly by exchanging $\rho_k \leftrightarrow |\phi_k\rangle\langle\phi_k|$, leading to so-called (c-q) states. In this language, it becomes apparent that the essence of the GQD (4.31) is to minimize over the set of coefficients $\{q_k\}$ of χ such as to find the zero-discord state which is closest to ρ_{AB} in the sense of distance as measured by the Hilbert-Schmidt norm. This then suggests the interpretation of χ as the (q-c) state that best approximates the generic state ρ_{AB}. Recalling the definition of the Hilbert-Schmidt norm in (4.32), we have

$$\|\rho_{AB} - \chi^{\text{q-c}}\|^2 = \text{Tr}\Big(\rho_{AB}^2\Big) - 2\,\text{Tr}(\rho_{AB}\chi^{\text{q-c}}) + \text{Tr}\Big((\chi^{\text{q-c}})^2\Big)\,, \tag{4.34}$$

since both ρ_{AB} and $\chi^{\text{q-c}}$ are Hermitian. Since we are assuming that ρ_{AB} is a pure state, the first term is given by $\text{Tr}(\rho_{AB}^2) = 1$. More precisely, as we saw in Sec. 2.3.1, any pure state $|\psi\rangle$ in a bipartite $\mathcal{H} = \mathcal{H}_A \otimes \mathcal{H}_B$ can be written in Schmidt decomposition

$$|\psi\rangle = \sum_k \lambda_k |\phi_k^A\rangle|\phi_k^B\rangle\,, \tag{4.35}$$

where $\left|\phi^A\right\rangle$ and $\left|\phi^B\right\rangle$ are two orthonormal bases for the respective subsystems, as they appeared also in (4.33). Its corresponding density matrix is then given by

$$\rho_{AB} = \sum_{k,l} \lambda_k \lambda_l |\phi_k^A\rangle|\phi_k^B\rangle\langle\phi_l^A|\langle\phi_l^B| \,. \tag{4.36}$$

Here, the set of coefficients λ_k are the Schmidt coefficients characterizing the entanglement properties of $|\psi\rangle$. They obey $\sum_k \lambda_k^2 = 1$ which amounts to the normalization of the density matrix $\mathrm{Tr}\left(\rho^{AB}\right) = 1$. Plugging (4.36) and (4.33) into (4.34), we obtain

$$\|\rho_{AB} - \chi^{\text{q-c}}\|^2 = 1 - 2\sum_k \lambda_k^2 q_k \,\mathrm{Tr}_A(\rho_k^A) + \sum_k q_k^2 \,\mathrm{Tr}_A(\rho_k^A \rho_k^A) \,. \tag{4.37}$$

Since all reduced density matrices obey $\mathrm{Tr}\left(\rho_k^A\right) = 1$, the second term is readily evaluated. In contrast, the third terms requires a more careful analysis. We identify the third term as being precisely the definition of the *purity* of the state $\chi^{\text{q-c}}$. This quantity describes, in some sense, how close a given state ρ is to being pure, with $\mathrm{Tr}(\rho^2) = 1$ holding if and only if ρ is pure, and $0 < \mathrm{Tr}(\rho^2) < 1$ if it is mixed. In general, we do not know the purity of $\chi^{\text{q-c}}$. In order to then find the minimum of (4.37), we ought to compute its derivatives with respect not only to the coefficients q_k of $\chi^{\text{q-c}}$, but also all possible entries of the matrices ρ_k^A. The system of equations to solve is thus given by

$$\frac{\partial}{\partial q_m}\|\rho_{AB} - \chi^{\text{q-c}}\|^2 \stackrel{!}{=} 1 \,, \quad \frac{\partial}{\partial (\rho_m^A)_{ij}}\|\rho_{AB} - \chi^{\text{q-c}}\|^2 \stackrel{!}{=} 1 \,. \tag{4.38}$$

Fortunately, this system is determined and has a unique solution, which is given by

$$q_k = \lambda_k^2 \,, \quad \left\langle \phi_k^A \right| \rho_k^A \left| \phi_k^A \right\rangle = \delta_{kl} \,, \quad \mathrm{Tr}\left((\rho_k^A)^2\right) = 1 \,. \tag{4.39}$$

This is quite an interesting result, where the third relation in (4.39) tells us that all ρ_k^A are actually pure, and the second relation further imposes the form

$$\rho_k^A = \left|\phi_k^A\right\rangle \left\langle \phi_k^B \right| \,. \tag{4.40}$$

These results are not merely coincidental. Indeed, for pure states we know that any non-vanishing quantum discord is precisely the entanglement entropy, i.e. $Q(A:B) = S(\rho^A)$. From the definition of $Q(A:B)$ given in (2.78), this is a consequence of the conditional entropy being $S(A|B) = 0$, which precisely vanishes only when each ρ_k^A is pure. This shows the consistency of our results (4.39) obtained through minimization. We may now plug the coefficients (4.39) into (4.37) and subsequently into the GQD

given in (4.31). We find that the GQD of an arbitrary pure state (4.35) reads

$$Q^{(2)}(A:B) = 1 - \sum_k \lambda_k^4 \,. \tag{4.41}$$

We may perform a further consistency check on this last result, observing that $Q^{(2)}(A:B)$ given in (4.41) vanishes if and only if a single Schmidt coefficient is non-zero $\lambda_{k^*} = 1$ with all other $\lambda_{k\neq k^*}$ vanishing. This is a consequence of the normalization condition $\sum_k \lambda_k^2 = 1$ obeyed by the Schmidt coefficients. According to (4.35), this is precisely the case where $|\psi\rangle$ is a product state and therefore $Q(A:B) = S(\rho_A) = 0$.
A further consequence of our result (4.39) is that the minimization procedure imposes that the (q-c) state which is closest in Hilbert-Schmidt distance to ρ_{AB} is given by

$$\chi_0^{\text{q-c}} = \sum_k \lambda_k^2 |\phi_k^A\rangle\langle\phi_k^A| \otimes |\phi_k^B\rangle\langle\phi_k^B| \;\widehat{=}\; \chi_0^{\text{c-c}} \,, \tag{4.42}$$

which is actually a classical-classical (c-c) state! Stated another way, we see that the original minimization, which was over the set $\Omega^{(\text{q-c})}$ of all zero-discord states, in fact constrains $\chi^{\text{q-c}}$ to be a (c-c) state in the subset $\Omega^{(\text{c-c})} \subset \Omega^{(\text{q-c})}$, as we depicted in Fig. 2.6. This is somewhat counter-intuitive, since it states that if we add some "quantumness" to our (c-c) state by turning into a (q-c) state, this will not provide us with a better approximation to the generally (q-q) state ρ_{AB}. A by-product of this finding is an interesting connection to another measure of correlations introduced in [801] denoted as "geometric measure of quantum correlations" and defined as

$$\bar{Q}^{(2)}(A:B) = \min_{\chi\in\Omega^{(\text{c-c})}} \frac{\|\rho_{AB} - \chi\|^2}{\|\rho_{AB}\|^2} \,. \tag{4.43}$$

Of course, a quick comparison reveals that this quantity is equivalent to the GQD in (4.31) with the only difference being that the minimization is done over the set $\Omega^{\text{c-c}}$, whose elements are of the general form

$$\chi^{\text{c-c}} = \sum_{k,l} q_{kl} |\phi_k^A\rangle\langle\phi_k^A| \otimes |\phi_l^B\rangle\langle\phi_l^B| \,. \tag{4.44}$$

Therefore, we find that for an arbitrary pure state ρ_{AB}, the expressions for $Q^{(2)}(A:B)$ and $\bar{Q}^{(2)}(A:B)$ are equivalent in spite of the set hierarchy $\Omega^{(\text{c-c})} \subset \Omega^{(\text{q-c})}$. Thus, the state minimizing $Q^{(2)}(A:B)$ is the same state minimizing $\bar{Q}^{(2)}(A:B)$.
Notice that the above is only valid for pure states, and for mixed states $Q^{(2)}(A:B)$ and $\bar{Q}^{(2)}(A:B)$ will be different in general. For example, consider the one-parameter

family of isotropic states for a two-spin system [802], given by

$$\rho_{\text{iso}} = \frac{1-a}{4}\mathbb{1}_4 + \frac{a}{2}\Big(|00\rangle + |11\rangle\Big)\Big(\langle 00| + \langle 11|\Big)\,, \tag{4.45}$$

written in the product basis $|00\rangle \equiv |0\rangle_A \otimes |0\rangle_B$ of the two spins. These states are pure when $a = 1$ and mixed for $0 < a < 1$, since it describes a parametrized linear combination of the maximally mixed state $\mathbb{1}$ and the pure state $|\psi\rangle = 1/\sqrt{2}(|00\rangle+|11\rangle)$, which is additionally also maximally entangled. It can be shown that this state is separable for $a \leq \frac{1}{3}$ by computing its entanglement of formation [802]. However, the quantum discord of the isotropic state (4.45) is non-zero unless $a = 0$ [257], showing that the system contains quantum correlations not captured by entanglement entropy. To compute the GQD of isotropic states, we use the ansatz

$$\chi = q\,\rho_0^A \otimes |0\rangle\langle 0| + (1-q)\rho_1^A \otimes |1\rangle\langle 1|\ , \tag{4.46}$$

with a further parametrization of the 2×2 reduced density matrices $\rho_{0,1}^A$ in terms of three real parameters a_i, b_i, c_i, with $i = 0, 1$, as

$$\rho_i^A = \begin{pmatrix} a_i & b_i + \mathrm{i}c_i \\ b_i - \mathrm{i}c_i & 1 - a_i \end{pmatrix}\ , \tag{4.47}$$

where we have already imposed the normalization condition. Based on these two ansätze, we can explicitly compute the Hilbert-Schmidt norm $\|\rho_{\text{iso}} - \chi\|^2$ and subsequently perform a minimization over the coefficients q, a_i, b_i, c_i in a similar fashion as we did in (4.38). In this way, we find

$$q = \frac{1}{2}\,, \quad a_0 = \frac{1+a}{2}\,, \quad a_1 = \frac{1-a}{2}\,, \quad b_0 = b_1 = c_0 = c_1 = 0\,. \tag{4.48}$$

Notice that ρ_i^A are not pure states for general values of a, and therefore the state $\chi \equiv \chi^{(\text{q-c})}$ does not reduce to a (c-c) state, implying that it cannot arise as a solutions to the geometric measure of quantum correlations $\bar{Q}^{(2)}(A:B)$ given in (4.43). In fact, the ρ_i^A are only pure if $a = 1$, which is precisely the case where the isotropic state (4.45) itself becomes pure, and we again retrieve the equivalence to GQD. The GQD of the isotropic state obtained from the above coefficients (4.48) reads $Q_{\text{iso}}^{(2)}(A:B) = \frac{a^2}{2}$, from which it is manifest that it only vanishes for $a = 0$.

We wrap up our analysis on GQD for pure states by highlighting a relation of our

result (4.41) with Rényi entropies (2.57), in particular the second Rényi entropy

$$S^{(2)}(\rho) = -\log \mathrm{Tr}\left(\rho^2\right). \tag{4.49}$$

Inspecting our result (4.41), we can see that, in terms of the minimizing state (4.42), it can be equivalently written as $Q^{(2)}(A:B) = 1 - \mathrm{Tr}\left(\left(\chi_0^{(\text{c-c})}\right)^2\right)$. Then, it is straightforward to see that we can express the GQD found in (4.41) as

$$Q^{(2)}(A:B) = 1 - e^{-S^{(2)}\left(\chi_0^{(\text{q-c})}\right)} = 1 - e^{-S^{(2)}(\rho_{AB})}, \tag{4.50}$$

where the last equality is true because of the simple structure of (c-c) states (4.44), which leads to $\mathrm{Tr}\left(\left(\chi_0^{(\text{c-c})}\right)^2\right) = \mathrm{Tr}\left((\rho_{AB})^2\right)$. This intriguing expression lends itself to consider the computation of GQD in the context of QFTs, where the Rényi entropies are known to be accessible via the replica trick [116, 117]. This is certainly a promising task for future explorations. The connection between GQD and the second Rényi entropy can be used as a starting point to a further generalization as follows. Let us introduce the so-called *modular Hamiltonian* associated to the minimizing state as $H_{\text{mod}} \equiv -\log \chi_0^{\text{q-c}}$, with the help of which we can further define the *modular partition function* $Z_{\text{mod}}(H_{\text{mod}}) = \sum_k e^{-h_k}$. Here, h_k are the eigenvalues of the modular Hamiltonian. The modular partition function can also be interpreted as the physical partition function in the sense of statistical mechanics of a system at temperature $T = 1$. Given these objects, and after some simple manipulations, we can again re-write the GQD as

$$Q^{(2)}(A:B) = 1 - \frac{Z_{\text{mod}}(2H_{\text{mod}})}{Z^2_{\text{mod}}(H_{\text{mod}})}. \tag{4.51}$$

Note that this expression vanishes if and only if the modular partition function factorizes, i.e. $Z_{\text{mod}}(2H_{\text{mod}}) = Z^2_{\text{mod}}(H_{\text{mod}})$. Therefore, our results state that any non-vanishing amount of GQD, which in turn implies a non-vanishing quantum discord, amounts to a non-factorization of the modular partition function of the system. Conversely, if the modular partition function does not factorize, then there exist purely quantum correlations between the subsystems A and B.

4.2.2. Geometric Quantum Discord for the Thermofield Double State

Our derivations above hold for any arbitrary pure states. Within the AdS/CFT correspondence, few pure states play a more ubiquitous role than the TFD state. Indeed, this is precisely the setup which gives rise to the factorization puzzle after all. It is

therefore enticing to apply our results and study the GQD associated to the TFD state, such as to potentially elucidate key aspects about the factorization properties of the system. This analysis will also establish an interesting connection to the ideas about Euclidean wormholes put forward in [164], in particular in view of the TMD state introduced therein.

Considering two copies of a CFT, the TFD state is defined as

$$|\text{TFD}\rangle = \frac{1}{\sqrt{Z(\beta)}} \sum_n e^{-\beta \frac{E_n}{2}} |n_L\rangle |n_R\rangle^* , \tag{4.52}$$

where the normalization factor is the thermal partition function $Z(\beta) = \sum_n e^{-\beta E_n}$ at inverse temperature β. The TFD state can be seen as a purification since tracing out any one of the two CFTs results in a thermal reduced density matrix at inverse temperature β. The basis chosen in (4.52) is that of the energy eigenstates $|n_i\rangle$ of each CFT, with corresponding eigenvalues $E_{n,i}$, where $E_{n,L} = E_{n,R}$ and we denote $E_n = \frac{1}{2}(E_{n,L} + E_{n,R})$. The conjugation in $|n_R\rangle^*$ is to be taken with respect to an anti-unitary operation $|n_R\rangle^* = \Theta|n_R\rangle$, typically taken to be $\Theta = \mathcal{CPT}$. The weighted superposition of energy eigenstates in the TFD state resembles that of statistical mechanics, therefore suggesting the identification of $p_n = \frac{1}{\sqrt{Z(\beta)}} e^{-\beta \frac{E_n}{2}}$ as Boltzmann weights. By construction, these p_n are precisely the Schmidt coefficients of the TFD. It is accepted that the TFD state provides a possible pure state description, from the boundary perspective, of the two-sided eternal black hole [129]. However, as briefly touched upon in the introduction to this section and as argued in [164], it can be argued that as soon as a black hole comes in contact with its environment, interactions should lead to a decoherence of this originally pure state. This decoherence amount to the state becoming mixed, and is a process that turns quantum correlations into classical ones. Nonetheless, from the perspective of either one of the CFTs, such a decoherence should not be detectable. In fact, both before and after the decoherence, the black hole simply looks thermal to any one-sided low-energy observer. It turns out that a simple way of encoding purely quantum information into the TFD state is by adding phases α_n to the superposition as

$$|\text{TFD}\rangle_\alpha = \sum_n p_n e^{\mathrm{i}\alpha_n} |n_L\rangle |n_R\rangle^* . \tag{4.53}$$

These phases can help us understand how the decoherence affects the quantum information stored in the state. They can be thought of as arising from a time evolution of the TFD state under the action of the global operator $H_L + H_R$, with $H_{L,R}$ being the boundary Hamiltonians on each CFT. It is here where the highly chaotic nature

of the spectrum of CFTs comes into play, allowing us to assume that for any value of time t, there is a phase factor $e^{i\alpha_n}$ for the corresponding energy level E_n. Though the time coordinate t is not defined globally due to the absence of a global time-like Killing vector in the bulk, any local observer is agnostic to this fact [803]. This is why the phases α_n can be thought of as storing quantum information [164]. A consequence of this is that any low-energy one-sided observer will not be able to tell the difference between the classical geometries associated to the TFD and TFD_α states, for any set of phases $\{\alpha\}$. This ignorance means that it is reasonable to consider an incoherent sum over all such TFD_α states rather than a specific instance of it. This consideration lead the author of [164] to define the *thermomixed double* (TMD) state as

$$\rho_{\text{TMD}} = \frac{1}{N}\sum_{\{\alpha\}} |\text{TFD}\rangle_{\alpha\,\alpha}\langle\text{TFD}|\,, \tag{4.54}$$

where the sum is to be read as a sum over N different complete sets $\{\alpha\}$ of phases, each of them having their internal counting index n. Plugging (4.53) into (4.54), and exploiting the chaotic nature of the CFT spectra, we can write $\frac{1}{N}\sum_{\{\alpha\}} e^{i(\alpha_n-\alpha_m)} = \delta_{nm}$, and thus find

$$\rho_{\text{TMD}} = \sum_n p_n^2 |n_L\rangle\langle n_L| \otimes |n_R\rangle\langle n_R|\,. \tag{4.55}$$

This is the proper state describing the black hole after it has fully decohered due to interactions with its environment. The TMD state thus contains exclusively classical correlations, and indeed we can see from the form of (4.55) that $\rho_{\text{TMD}} \in \Omega^{(\text{c-c})}$. A useful way to characterize the correlations contained in ρ_{TMD} is via mutual information, in particular when comparing it to the standard TFD state and the completely factorized state $\rho = \rho_L \otimes \rho_R$. More precisely, the mutual information between the two CFTs in the TFD state (4.52) or its time-shifted version (4.53) is equal to twice the entanglement entropy $S(\rho_{L/R})$. This is also twice the Bekenstein-Hawking entropy S_{BH} of an AdS black hole, consistent with the fact that the TFD state is holographically dual to the double-sided geometry. On the other hand, the completely factorized state unsurprisingly has vanishing mutual information, manifesting that the two subsystems are not correlated at all. Meanwhile, the mutual information in the TMD state is given by $S(\rho_{L/R})$, and can thus justify the role of the TMD state as a sort of middle ground between the product state and the entangled TFD state.

Given this setup, we are ready to compute the GQD for the TFD state. Plugging the

Schmidt coefficients p_n of the TFD state into our result (4.41), we obtain

$$Q^{(2)}(L:R) = 1 - \sum_n p_n^4 \,. \tag{4.56}$$

Although we have derived (4.56) using the un-shifted TFD state (4.52), the exact same result can be obtained for its time-shifted version (4.53), since the additional phases drop out in the definition of the Hilbert-Schmidt norm. The result (4.56) is what we should have expected, and it tells us that a non-vanishing GQD signals the presence of quantum correlations in any instance of the TFD. Of course, these are precisely the known quantum correlations between the left and right CFTs. What is perhaps not as expected is the precise state singled out by the minimization procedure, which we know from our analysis in Sec. 4.2.1 that should be a (c-c) state. In particular, using (4.42), we find that the (c-c) state minimizing the GQD, and therefore providing the best classical approximation to the TFD state, is *precisely* the TMD state,

$$\chi_0^{\text{c-c}} = \sum_n p_n^2 |n_L\rangle\langle n_L| \otimes |n_R\rangle\langle n_R| = \rho_{\text{TMD}} \,. \tag{4.57}$$

It is worth stressing that we have obtained the TMD via a purely quantum information-theoretic calculation, which is completely agnostic to any holographically dual interpretations. In other words, it was not necessary to invoke the notion of a decohered black hole, as done in [164], to find the TMD state. Of course, we reviewed it for pedagogical purposes, but our results provide the novel interpretation of the TMD state as the state which best approximates the TFD state without including any quantum correlations. Furthermore, exploiting our result (4.41) with the explicit Schmidt coefficients p_n of the TFD state, we find

$$Q^{(2)}(L:R) = 1 - \frac{\sum_n e^{-2\beta E_n}}{Z^2(\beta)} = 1 - \frac{Z(2\beta)}{Z^2(\beta)} \,, \tag{4.58}$$

which precisely realizes (4.51) for the case where the modular Hamiltonian is given by the thermal one, i.e. $H_{\text{mod}} = \beta H_{L/R}$. This is because the entanglement spectrum of the TFD state is thermal, while that of an arbitrary pure state will have a more general form. Therefore, the typical modular partition function entering (4.51) is only given exactly by the thermal one in the case of the TFD state. We note that the expression we obtain in (4.58) resembles that obtained from Euclidean path integral considerations in [164, 804, 805]. In fact, this is not merely coincidental, since it was shown in [164, 804] that powers of the TMD state can be utilized in such a context to define the gravitational partition function of wormhole geometries with k throats.

More precisely, we have that

$$\mathrm{Tr}\left(\rho_{\mathrm{TMD}}^{k}\right)=\frac{Z(k\beta)}{Z^{k}(\beta)}\,, \tag{4.59}$$

which for $k=2$ can be combined with our relation between GQD and Rényi entropies obtained in (4.50) in order to retrieve (4.58).

Several comments are in order regarding our result (4.58). First, it is evident that (4.58) is non-vanishing in general, and therefore also the quantum discord will be generically non-zero. This is a natural consequence given that the TFD state is pure and therefore we have $Q(L:R)=S(\rho_L)$, which is non-zero since the reduced density matrix of the TFD state is thermal and thus $S(\rho_L)\neq 0$. Second, notice how, similarly to (4.51), $Q^{(2)}(L:R)$ in (4.58) is an indicator of non-factorization given that it vanishes if and only if $Z(2\beta)=Z^2(\beta)$, which is exactly the case where there are no correlations at all between the subsystems. To check the consistency of this claim, note that in the zero-temperature limit, the TFD state reduces to a product state, i.e. $\lim_{\beta\to\infty}|\mathrm{TFD}\rangle=|0_L\rangle|0_R\rangle$, where no EPR pairs are shared between the two boundaries. This is because the lowest energy E_0 approaches 1 in this limit, while all higher Schmidt coefficients vanish. Holographically, the $\beta\to\infty$ limit removes the wormhole, since there are no longer any quantum correlations to support it, resulting in factorization in the bulk as well. As a consequence of these observations, we can conclude that GQD is a useful quantity in the diagnostic of non-factorization for generic pure states, and in particular for the holographically relevant case of the TFD state. The connection of our results with those in [164, 804, 805] also allows an interpretation of GQD in terms of wormholes. Our results in (4.51) and (4.58) explicitly show how a non-vanishing quantum discord, signaled by non-zero GQD, can be achieved if and only if the modular or thermal partition function does not factorize. Based on our results, we can make the general claim that *non-zero quantum discord implies non-factorization due to the presence of quantum correlations* [162]. In other words, whenever a system exhibits quantum correlations manifesting themselves in the non-factorization of the partition function, the GQD, and thus the quantum discord of that state, will be non-zero. Given the relative ease with which we can compute GQD, our results provide a useful tool to diagnose non-factorization for generic pure states. It is however worth noticing that non-factorization may arise as a consequence of classical correlations, although in that case, the off-diagonal components of $\rho_{\mathrm{TFD}_\alpha}$ go to zero, implying that $\rho_{\mathrm{TFD}_\alpha}\to\rho_{\mathrm{TMD}}$ as a state.

The practical relevance of the results of this section can be accentuated as follows. Suppose you are given a pure quantum state ρ_{AB} describing the entirety of a bipar-

tite system. Does its corresponding modular partition factorize? While this question may be addressed explicitly in low-dimensional systems, obtaining an answer in general holographic settings is quite non-trivial. The reason is that we do not usually have concrete arguments as to whether or not the partition function should factorize. Fortunately, our results provide an accessible alternative way of answering this question by computing the GQD of the state. In particular, after obtaining the closest classical approximation ρ_{AB}^{c-c} to the original quantum state ρ_{AB}, we can readily insert it into (4.50) to verify the factorization of the partition function. This verification works because if the partition function of ρ_{AB}^{c-c} does not factorize, then that of ρ_{AB} is guaranteed to not factorize either, given that both states share the same Schmidt coefficients. We have therefore boiled down the diagnostic of non-factorization for arbitrary pure states to the computation of the second Rényi entropies of their closest classical approximations.

Finally, let us comment on the connection (4.50) between GQD and the second Rényi entropy in view of a potential holographic dual. It has been shown that the bulk duals of Rényi entropies $S^{(n)}$ can be given by the areas of cosmic branes of tension $T_n = \frac{n-1}{4nG_N}$ which back-react on the bulk geometry, generating in this way conical defects $\Delta\phi = 2\pi\frac{n-1}{n}$ [729]. If we consider the limit of vanishing defect, the associated cosmic brane becomes tension-less and reduces to the standard RT minimal surface [729]. It is therefore not far-fetched to think of a bulk dual for GQD which is in some way related to such a cosmic brane with a tension $T_2 = \frac{1}{8G_N}$ and creating a conical defect of $\Delta\phi = \pi$ in the bulk. A more detailed appraisal of this conjecture in a specific holographic system would be extremely alluring.

4.2.3. Black Hole Microstates from Geometric Quantum Discord

The results presented above gain a new glance when interpreted deeper in a holographic context. From this point of view, recall that both the TFD state (4.52), its time-shifted version (4.53), and the TMD state (4.54) are all indistinguishable for a one-sided low-energy observer [803]. An immediate consequence of this is that observables such as a two-point functions will yield the same results when evaluated on any of these states. This situation changes if we consider a high-energy observer, modeled perhaps as a so-called *heavy* operator which scales at least with N. She would indeed be able to tell these states apart, implying that the quantum correlations stored in the phases of the TFD_α state can be interpreted as $1/N$ corrections. In the following, we study these corrections in more detail, relating them and an extension of the GQD to certain black hole microstates mentioned in [803]. Our results will ultimately reveal an intriguing

connection to factorization diagnosis in terms of the gravitational path integral.

Overlaps of Black Holes Microstates and GQD

Recall that any particular set of phases $\{\alpha\}$ in a TFD_α state contains the information about how both boundaries share correlations, and it specifies the way that they are connected to the bulk geometry. This is a consequence of the phases being an explicit parametrization of the time-slice t, thus specifying the microstate of the TFD state under consideration. Correspondingly, we may interpret the TMD state (4.54) as an ensemble average over many instances of these microstates TFD_α. The precise overlap between the averaged TMD state and any specific microstate TFD_α turns out to play a crucial role in the computation of the GQD of these time-shifted states. To see this, let us revisit the results (4.41) and (4.58), which implied the relation $Q^{(2)}(L:R) = 1 - \text{Tr}(\rho_{\text{TMD}}^2)$ for the GQD of the TFD state. Inspecting this result carefully, the relative sign can be seen to arise from an overlap term $\text{Tr}(\rho_{\text{TFD}_\alpha}\rho_{\text{TMD}})$ in the Hilbert-Schmidt norm, namely

$$||\rho_{\text{TFD}_\alpha} - \rho_{\text{TMD}}||^2 = 1 - 2\,\text{Tr}(\rho_{\text{TFD}_\alpha}\rho_{\text{TMD}}) + \text{Tr}\Big(\rho_{\text{TMD}}^2\Big)\,, \tag{4.60}$$

with $\rho_{\text{TFD}_\alpha} = |\text{TFD}\rangle_\alpha\,{}_\alpha\langle\text{TFD}|$. As mentioned before, the inclusion of the phases does not affect the result for the GQD. This can be interpreted in the present context as an implicit self-averaging carried out by the trace in the definition of the GQD. This averaging, and the role played by the $1/N$ corrections, can be brought to light by inspecting the overlaps terms more carefully and writing the TMD state as a linear combination of general microstates $|\text{TFD}\rangle_\gamma$ as in (4.54).[8] More precisely, we have

$$\text{Tr}\Big(\rho_{\text{TFD}_\gamma}\rho_{\text{TMD}}\Big) = \frac{1}{N}\sum_{\{\alpha\}} {}_\gamma\langle\text{TFD}|\text{TFD}\rangle_\alpha\,{}_\alpha\langle\text{TFD}|\text{TFD}\rangle_\gamma\,, \tag{4.61}$$

where we can now make use of the fact that, up to $1/N$ corrections, any two microstates are orthogonal, i.e. we have ${}_\alpha\langle\text{TFD}|\text{TFD}\rangle_\gamma \simeq \delta_{\alpha\gamma} + \mathscr{O}\,(1/N)$. However, it is precisely these subleading corrections which imply that the naive application of this relation does not lead to the above mentioned result for the GQD. In particular, if we were to directly apply the orthogonality condition to leading order in (4.61), we would find

$$\text{Tr}\Big(\rho_{\text{TFD}_\gamma}\rho_{\text{TMD}}\Big) = \frac{1}{N}\sum_{\{\gamma\}} \delta_{\alpha\gamma}\delta_{\gamma\alpha} = 1\,, \tag{4.62}$$

[8] We use the label γ here to avoid confusion with the temperature β.

which leads to a manifestly incorrect GQD of $Q^{(2)}(L:R) = 2 + \mathrm{Tr}(\rho^2_{\mathrm{TMD}})$. In other words, performing the average of the square of such an overlap does not equate to the product of Kronecker deltas, since the sums over the phases do not commute with the leading order approximation of the orthogonality condition. This is exactly the non-factorizing property of the state in disguise. We should thus include the $1/N$ corrections by computing the overlap before implementing the orthogonality condition,

$$ {}_\gamma\langle \mathrm{TFD}|\mathrm{TFD}\rangle_\alpha = \sum_n p_n^2 e^{\mathrm{i}(\alpha_n - \gamma_n)} \,. \tag{4.63} $$

Exploiting this result, together with $\frac{1}{N}\sum_{\{\alpha\}} e^{\mathrm{i}(\alpha_n - \alpha_m)} = \delta_{nm}$, we have

$$ \begin{aligned} \mathrm{Tr}\Big(\rho_{\mathrm{TFD}_\gamma}\rho_{\mathrm{TMD}}\Big) &= \frac{1}{N}\sum_{\{\alpha\}}\sum_{n,m} p_n^2 e^{\mathrm{i}(\alpha_n-\beta_m)} p_m^2 e^{\mathrm{i}(\alpha_m-\beta_n)} \\ &= \sum_{n,m} p_n^2 p_m^2 e^{\mathrm{i}(\alpha_n-\alpha_m)}\delta_{mn} = \sum_n p_m^4 = \frac{Z(2\beta)}{Z^2(\beta)} \,. \end{aligned} \tag{4.64} $$

This result shows how the phases indeed cancel in (4.61), leaving only the $\sum_n p_n^4$. The sign in front of the overlap term in (4.60) then leads to the correct expression for the GQD given in (4.58).

Similar considerations to the above hold for the more general case of the overlap between a given microstate and any power of the TMD state,

$$ \begin{aligned} \mathrm{Tr}\Big(\rho_{\mathrm{TFD}_\gamma}\rho^{n-1}_{\mathrm{TMD}}\Big) &= \frac{1}{N^{n-1}} \sum_{\{\alpha\}_1,\ldots,\{\alpha\}_{n-1}} {}_\gamma\langle \mathrm{TFD}|\mathrm{TFD}\rangle_{\alpha_1\ldots\,\alpha_{n-1}}\langle \mathrm{TFD}|\mathrm{TFD}\rangle_\gamma \\ &= \sum_m p_m^{2n} = \frac{Z\big(n\beta\big)}{Z^n(\beta)} \,, \end{aligned} \tag{4.65} $$

with $n \in \mathbb{N}$. In connection with the relation (4.59), which had an interpretation as the partition function of a k-fold wormhole geometry, we can see the result (4.65) as including these types of wormhole contributions. However, in our setup, these arise from a state-averaging procedure in (4.63), in contrast to typical constructions which implement an ensemble average [806–808]. Moreover, the structure we find in (4.65) of a ratio of partition functions given by the overlap of TMD states bears a striking resemblance to that of the microstates of astrophysical black holes considered in [809, 810]. There, the authors present a microstate counting to estimate the entropy of such realistic black holes created from gravitational collapse. More precisely, the collapse of shells of dust $|\psi_{m_k}\rangle$ of mass m_k into a black hole is a unitary process, enabling the description of such black holes as pure states, just before decoherence sets

in. We may therefore relate our results to those of [809, 810] in the limit $m_n \gg M$, where M is the total mass of the black hole. In this limit, the overlaps $\langle\psi_{m_k}|\psi_{m_l}\rangle$ take on the same form as those in (4.65). We may therefore apply our arguments for the GQD to this case as well, with a corresponding (c-c) state akin to the TMD state playing the role of the closest classical approximation to the dual state to astrophysical black holes. Even though our analysis was done for an eternal black hole, we still believe that the logic of [809, 810] can be mirrored in our scenario. In particular, we need to perform an identification of the set of phases $\{\alpha\}_n$ as a collapsing shell of mass m_n. Moreover, we note that the normalization $1/N$ of (4.54), associated to the corrections containing the purely quantum correlations in the TMD state, is a vital ingredient imposing that there are N different sets of phases which can be interpreted as N different microstates [164]. Ultimately, this gives the correct microstate counting leading to a thermodynamic black hole entropy of $S = S_{\rm BH} = \log N$.

The inclusion of $1/N$ corrections and their associated microstate contributions is paramount for obtaining the correct expression for GQD, even though they do not appear explicitly in the final result. In fact, the higher overlaps (4.65) can be generalized by considering the natural extension of the Hilbert-Schmidt norm to its own higher powers. More precisely, the Hilbert-Schmidt norm used in the definition of the GQD is a special case of the so-called *Schatten norm*, defined for a given matrix X as

$$||X||_{(n)} = \left[\mathrm{Tr}\left(\sqrt{X^\dagger X}^{\,n}\right)\right]^{\frac{1}{n}} . \tag{4.66}$$

For Hermitian operators where $X = X^\dagger$ we have the simplification $\sqrt{X^\dagger X} = X$. The Hilbert-Schmidt norm (4.32) corresponds to the case $n = 2$. In view of this, it is natural to consider a new notion of distance between the two states $\rho_{\mathrm{TFD}_\alpha}$ and $\rho_{\rm TMD}$ given by higher powers of such Schatten norms, namely

$$Q^{(n)}(L:R) = \|\rho_{\mathrm{TFD}_\alpha} - \rho_{\rm TMD}\|^n_{(n)} . \tag{4.67}$$

Explicitly evaluating this quantity, we find the schematic expression

$$Q^{(n)}(L:R) = 1 + \#_1 \frac{Z(2\beta)}{Z^2(\beta)} + \ldots + \#_n \frac{Z(n\beta)}{Z^n(\beta)} . \tag{4.68}$$

Here, we have used the symbols $\#_k$ to denote numerical factors appearing in each term, which are such that the $Q^{(n)}(L:R)$ vanishes if and only if all the individual partition functions (modular or thermal) factorize, i.e. when $Z(k\beta) = Z^k(\beta)$ for $1 \leq k \leq n$. Importantly, note how all such intermediate contributions need to be taken into

account, since every single one of them contributes to the total quantum correlations between the subsystems. Furthermore, similarly to the situation in (4.50), each one of the ratios of partition functions appearing in (4.68) can be equivalently expressed in terms of Rényi entropies $S^{(n)}$ of the same index. This again suggests an immediate bulk interpretation in terms of cosmic branes [729], as mentioned previously.

Microstate Wormholes in the Path Integral

We conclude this section by providing a complementary take on the connection between GQD and wormhole physics unveiled above, in particular from the perspective of the path integral. Based on the studies in [804], and as alluded to previously when discussing (4.59), the appearance of wormholes in the path integral of any quantum system can be related to a non-exact of symplectic form. For the specific case of the TFD state, this non-exactness argument was further investigated in [811, 812]. We will now discuss this for the case of the black hole microstates TFD_α. For this, we will review the construction of Hamiltonians whose ground states are the TFD state given in [813], and combine this with the arguments of [804] about non-exact symplectic forms in order to shed light on the non-factorization properties of the partition function. This will nicely wrap up our discussion on the correspondence between the non-vanishing of GQD, the consequent non-factorization of the partition function $Z(2\beta) \neq Z^2(\beta)$, and the existence of wormhole microstates. For these considerations, it is enough to study the standard TFD state rather than its time-shifted version, since we have seen above that the GQD is the same for both.

We begin by showing that the Hamiltonian considered in [813], whose ground state is the TFD state, indeed possesses an associated non-exact symplectic form. The construction in [813] considers operators d_k of the form

$$d_k = e^{-\frac{\beta}{4}(H_L^0+H_R^0)}\left(\mathcal{O}_{L,k} - \Theta\mathcal{O}_{R,l}^\dagger\Theta^{-1}\right)e^{\frac{\beta}{4}(H_L^0+H_R^0)}\,, \tag{4.69}$$

where $H_{L/R}^0$ and $\mathcal{O}_{L/R,k}$ are the Hamiltonians and exemplary operators of the left and right theories, respectively. The Θ is that appearing in the definition (4.52). The key observation of [813] is that such operators obey $d_k|\text{TFD}\rangle = 0$ by construction. This immediately allows for the definition of a Hamiltonian as

$$H = c_k d_k^\dagger d_k\,, \tag{4.70}$$

with c_k being positive constants, which has precisely the TFD state as its ground state. This rather straightforward construction is guaranteed to work in principle, but in practice it is quite challenging to access the exponential of an operator as appearing

in (4.69). A simpler ansatz for the same construction considers the operators

$$d_k = \mathcal{O}_{L,k} - \Theta \mathcal{O}_{R,k}^\dagger \Theta^{-1} \,, \tag{4.71}$$

with which a different Hamiltonian can be defined as

$$H = H_L^0 + H_R^0 + c_k' d_k^\dagger d_k \,, \tag{4.72}$$

with c_k' again being positive constants, which are now to be chosen appropriately such as to ensure that the ground state of (4.72) is indeed the TFD state. It was shown in [813] that this constraint on the coefficients amounts to assuming that the eigenstate thermalization hypothesis [814–817] holds for the system under consideration. Note that this is a sufficient condition, but it is not necessary, as we can explicitly show by considering the case of two coupled harmonic oscillators. For this, consider the Hamiltonian given by [813]

$$H = \frac{1+c}{2}\left(p_L^2 + p_R^2\right) + \frac{(1+c)\omega^2}{2}\left(q_L^2 + q_R^2\right) + c p_L p_R - c\omega^2 q_L q_R \,, \tag{4.73}$$

with $c = \frac{1}{2}\operatorname{csch}^2 \frac{\beta\omega}{4}$. Upon diagonalizing this Hamiltonian in terms of the canonical position and momentum variables $p_\pm, q_\pm$, we may write it in the form

$$H = \epsilon_+ a_+^\dagger a_+ + \epsilon_- a_-^\dagger a_- \,, \tag{4.74}$$

where $\epsilon_+ = \frac{1}{\omega}\coth\frac{\beta\omega}{4}$ and $\epsilon_- = \frac{1}{\omega}\tanh\frac{\beta\omega}{4}$. In order to finally bring this expression into the form considered in [804], we define the operators $J = a_k^\dagger a_k$ and $X_I = \frac{1}{2} a_k^\dagger \sigma_I^{kl} a_l$ such that $J^2 = \sum_{I=1}^3 X_I^2$. In terms of these operators, the Hamiltonian (4.74) reads

$$H = \gamma J + \epsilon X_3 \,, \tag{4.75}$$

where $\gamma = \frac{1}{\omega}\coth\frac{\beta\omega}{2}$ and $\epsilon = \frac{1}{\omega}\operatorname{csch}\frac{\beta\omega}{2}$. These rather cumbersome manipulations show that our Hamiltonian, which has the TFD state as its ground state, is precisely of the form considered in [804]. It was shown in that work that the corresponding symplectic form to (4.75) is in fact non-exact when the system is restricted to a quantizable orbit with $J = j$ with $2j \in \mathbb{N}$, in the context of geometric quantization [818–820]. In fact, in this case the symplectic form can be seen as the volume form on the two-sphere, which is non-exact. The upshot of this is that the non-exactness of the symplectic form implies the non-factorization of the partition function due to the presence of replica wormholes (4.59) in the path integral [804]. Note that this independent argument is

fully in agreement with our expectations from computing the GQD for the TFD state, which also showed that the partition function does not factorize.
Given that our method of diagnosing non-factorization yields the same results as that put forward in [804], one may ask why one should be preferred over the other. The answer boils down to ease of implementation in practical computations. For the method of [804], we need to show that a given form ω is exact (or not), which amounts to finding a suitable surface S such that the integral $\int_S \omega$ vanishes. For general systems, this task is quite challenging, in particular because it needs to be shown to hold for any choice of S, such that an exemplary proof for specific surfaces S is not enough. In these instances, the diagnosis of non-factorization using GQD offers a more accessible alternative, specially when considering arbitrary pure states as per Sec. 4.2.1.

Let us sum up the results of this section. We have proposed the quantity of geometric quantum discord (4.31) as an accessible way to diagnose the factorization properties of the partition function of a quantum system. We provided an explicit formula for the GQD of arbitrary pure states (4.41), which manifestly implies that the existence of purely quantum correlations between subsystems leads to a non-factorizing modular or thermal partition function. As a by-product of our analysis, we have given a novel, purely quantum information-theoretic interpretation of the TMD state introduced in [164] as the classical state that best approximates the TFD state. Non-vanishing GQD can further be related to the appearance of state-averaged replica wormholes in the path integral, a perspective that may potentially lead to a deeper understanding of the factorization puzzle from the role of quantum correlations within the TFD state. We believe that future investigations of the latter would benefit from the study of holographic duals to the Schatten norms describing higher overlaps given in (4.68).

4.3. Local Operator Algebras: When Entanglement is Infinite

Entanglement entropy is a ubiquitous phenomenon in quantum systems, and it is clear that this quantity has permeated a big part of the current thesis. Within the AdS/CFT correspondence, we have established the relevance of entanglement as the quantity describing the emergence of both space and time in the bulk. However, outside the realm of holography, entanglement entropy also enjoys a highly regarded status, in particular in the context of condensed matter and many-body physics. Specifically, entanglement can be used to detect phase transitions in quantum systems [155, 156, 821–824]. An

example of this are the ground states of local gapped many-body Hamiltonians, in which entanglement entropy is expected to obey an area law [156]. However, when these systems approach a critical point, the long-ranged correlations may lead to violations of this area law [116, 263], which can be used as heralds for the onset of critical phenomena and phase transitions. Moreover, entanglement can also be exploited to characterize systems with disorder [825, 826] (as we have also seen in Sec. 3.5.4) or even characterizing topological order [264, 827].
In parallel, many problems in many-body physics which are intractable via exact diagonalization methods can acquire simpler, effective descriptions in the thermodynamic limit. Such a limit can be associated with the limit of an infinitely extended system, or also with a divergence in the number of degrees of freedom in the theory. In any case, this leads to the problem of generic states having an *infinite* amount of entanglement due to the infinite-dimensional nature of the underlying Hilbert space. A further problematic aspect, which becomes even more evident in the context of QFTs, is the issue of how to perform a bipartition of a continuous spacetime, and whether or not this corresponds to a bipartition of the Hilbert space. The reduced density matrix ρ_A associated to a subsystem is the key ingredient for entanglement entropy, yet its definition in a specific subregion of a spacetime is precisely the source of the universal divergence of entanglement in QFT [261, 278, 757]. The question arises as to how we can properly define a notion of entanglement in the thermodynamic limit of quantum many-body systems, an issue concretely addressed for the first time in [828]. It turns out that the correct language to describe this is that of *local operator algebras* [265, 754, 754, 829], and, more precisely, so-called *von Neumann algebras* [142–145] (see [757, 830, 831] for a modern review). Thus, though long-standing, the study of algebraic properties emerging in quantum systems in the limit of infinitely many degrees of freedom, which enables phenomena such phase transitions, has now received novel interest. Therefore, in the following sections, we investigate these von Neumann algebras and study a quantum many-body system which admits analytical tractability into not only their existence, but also into different transitions between them.

4.3.1. Local Operator Algebras and Holography

The purpose of this section is twofold. First, I give a crash course into the main definitions involved in the theory of von Neumann algebras, mainly focusing on the statements and constructions which we will exploit in the following subsections. This is by no means an exhaustive nor a mathematically rigorous review, and we refer the interested reader to [754, 830–834] for a more thorough introduction to the topic. Second, I briefly touch upon the recent investigations which have sparked the interest

into these mathematical aspects of operator algebras. In particular, I discuss the main results of [146, 148, 756] and their significance in the context of holography, laying the motivational foundations for our studies in the coming sections.

Brief History of Operator Algebras

Let us historically contextualize the study of local operator algebras before we present some of their more technical aspects. In the late 1920's, John von Neumann was interested in providing a mathematically sound description of physical systems of infinite nature. Nowadays we may think of quantum field theories as a prototypical example for such systems, yet the considerations of von Neumann vastly predate the first commonly accepted formulations of quantum field theory. In parallel, the theory of quantum mechanics was contemporary to von Neumann, and a proper mathematical understanding of infinite quantum mechanical systems underlied his work. The language developed by von Neumann to rigorously treat these systems is that of *operator rings* [835]. In the later period of the 1930's and early 1940's, von Neumann entered a vivid collaboration with Francis Murray, together with whom he developed the foundations of the theory of operator algebras [142–145, 753]. They quickly realized that these formal mathematical analyses are closely related to very physically relevant problems, such as the deceivingly simple task of dividing a quantum mechanical system into two subsystems, i.e. a *bipartition*. While it seemed straightforward to deal with bipartitions for quantum states belonging to finite-dimensional Hilbert spaces, many subtleties arise when considering thermodynamic limits of such systems. In fact, such considerations are absolutely necessary for providing a quantum mechanical description of typical systems in nature which are at a finite temperature. The consistency of this interplay between statistical mechanics and formal aspects of quantum mechanics in terms of operator algebras was first explored in [836, 837] for a free Bose gas, and later generalized in [828] for generic quantum systems in thermal equilibrium.

Almost in parallel, during the 1960's, a great deal of attention was given to the axiomatic formulation of the recently developed theory of quantum fields. In particular, the community of axiomatic QFT (AQFT) addressed the question of how to mathematically define QFTs in such a way that the mere notion of a subregion of spacetime is consistent, see e.g. [265, 829, 838–840]. Without introducing a UV cutoff, the inherent fluctuations of continuum quantum fields throughout spacetime make such a construction highly non-trivial. Indeed, an immediate consequence of the Reeh-Schlieder theorem [841] is that the entanglement between quantum fields on adjacent spacetime regions is so intense that the entanglement entropy in generic quantum field theories is a UV divergent quantity, as pointed out in many instances

[116, 261, 277, 278, 310, 311, 842, 843]. Several sets of axioms were developed for this purpose, such as the Gårding-Wightman axioms [844], the Osterwalder-Schrader axioms [845], and the Haag-Kastler axioms [846]. While the first two sets take an approach based on the systematic construction of a Hilbert space based on correlation functions for Lorentzian and Euclidean QFTs, it is the latter Haag-Kastler axioms which propose a definition of QFTs based on their algebra of observables. The idea is to rigorously define a QFT by associating a von Neumann algebra of local operators to every subregion of the spacetime. Physically, this amounts to regarding bounded observables as the fundamental objects of any theory, and constructing the physical Hilbert space as that generated by the action of these operators on certain states.
It is clear that the history of local operator algebras is very rich, and these objects have been the subject of research, with varying levels of activity, for the last 80 years. Recently, they have seen an unexpected revival driven by new perspectives on condensed-matter and high-energy physics as seen through the lens of operator algebras. From the point of view of the former, studies on symmetry protected topological phases of quantum matter [847] have been tackled using operator algebra techniques [848, 849]. As for high-energy physics, recent studies of the von Neumann operator algebras in holographic contexts have yielded promising insights into the emergence of time behind the black hole horizons [146, 147, 756, 830, 850–852], as well as the properties that entanglement ought to have in quantum gravity [758–760, 853–858]. A prime playground for these arguments was the detection of changes of von Neumann algebras across phase transitions within holography, in particular the Hawking-Page phase transition reviewed in Box 2.1. In this case, it was found [146, 147, 756] that the von Neumann algebra of single-trace operators at $N = \infty$ for the TFD state (cf. (2.39)) of two copies of $\mathcal{N} = 4$ Super-Yang-Mills theory changes drastically across the Hawking-Page temperature. This was then interpreted as the emergence of a new arrow of time behind the black hole horizon for temperatures above the Hawking-Page temperature. These results motivate us to investigate similar occurrences of changes in von Neumann algebras in simpler setups without invoking quantum gravity considerations, such as quantum many-body systems. Before that, it is necessary to review some basic definitions regarding operator algebras, and we do this in the following.

Fundamentals on Operator Algebras

Having provided plenty of historical evidence to motivate the study of von Neumann algebras, we now turn our attention to their mathematical aspects. We restrict our review to those ingredients that will be of importance for later analysis in this section, and the reader is directed to [757, 831, 858] for a more complete exposition. In par-

ticular, we partially follow the presentations in [757, 830, 858].
Operator algebras are concerned with the abstract description of quantum systems based on their fundamental local observables. These observables are described by a set $\mathcal{B}(\mathcal{H})$ of bounded linear operators acting on a given Hilbert space $\mathcal{H}$. We will be specially interested in *von Neumann* algebras, denoted by $\mathcal{A}$ which are defined in Definition 7 [142–145, 835, 859].

Definition 7 (von Neumann Operator Algebra)**:** *Let $\mathcal{A}$ be a set of bounded operators, equipped with an involutive operation $\maltese : \mathcal{A} \to \mathcal{A}$ which maps $a \mapsto a^*$ and a commutation operation such that*

$$\mathcal{A}' = \{\mathfrak{a}' \,|\, [\mathfrak{a}, \mathfrak{a}'] = 0 \ \forall \mathfrak{a} \in \mathcal{A}\}\,, \tag{4.76}$$

denotes the commutant of $\mathcal{A}$, i.e. the set of all bounded operators that commute with every element of $\mathcal{A}$. Let $\mathbb{1}$ denote the identity operation which acts as $\mathbb{1}\mathfrak{a} = \mathfrak{a}$ for any element $\mathfrak{a} \in \mathcal{A}$. Further, let $\|\cdot\|$ denote a norm for algebra elements which obeys

$$\|\mathfrak{a}^*\mathfrak{a}\| = \|\mathfrak{a}^*\| \cdot \|\mathfrak{a}\| = \left\|\mathfrak{a}^2\right\| \quad \textit{for all} \ \ \mathfrak{a} \in \mathcal{A}\,. \tag{4.77}$$

Then, $\mathcal{A}$ is a von Neumann algebra if for all $\mathfrak{a}, \mathfrak{b} \in \mathcal{A}$ and $\lambda \in \mathbb{C}$ it obeys:

i) $(\mathfrak{a} + \mathfrak{b})^* = \mathfrak{a}^* + \mathfrak{b}^* \in \mathcal{A}$ *and* $(\mathfrak{a}\mathfrak{b})^* = \mathfrak{b}^*\mathfrak{a}^* \in \mathcal{A}$

ii) $(\mathfrak{a}^*)^* = \mathfrak{a}$ *and* $(\lambda\mathfrak{a})^* = \lambda^*\mathfrak{a}^* \in \mathcal{A}$

iii) $\mathbb{1} \in \mathcal{A}$

iv) $\mathcal{A} = (\mathcal{A}')'$

An alternative but completely equivalent definition of a von Neumann algebra is a unital C^*-algebra which is closed under the weak operator topology, but our Definition 7 is better suited for our current purposes. For the discussions in this thesis, we can take the operation $\maltese$ to denote Hermitian conjugation $\maltese = \dagger$, although this need not be the case in general [831]. Note that the $*$ symbol in criterion *ii)* indeed denotes complex conjugation for λ. Although the requirements in Definition 7 might seem rather abstract, von Neumann algebras are not entirely exotic. In fact, if we consider a typical quantum many-body system with complex two-dimensional Hilbert spaces spanned by the Pauli matrices, one can readily verify that the set of all bounded operators constructed from these matrices indeed forms a von Neumann algebra.
Definition 7 clarifies the properties of the algebra of observables of a quantum system, but it does not address what the Hilbert space of the theory is. Within the theory

of operator algebras, the philosophy for this is that a Hilbert space $\mathcal{H}$ of *uncountably* infinite dimension (which arises naturally in QFTs) can nevertheless be tamed by constructing a "smaller" Hilbert space $\mathcal{H}_0$ of *countably* infinite dimension, based on the action of our algebra of local observables. The Hilbert space $\mathcal{H}_0$ of the theory is such that it contains any physically relevant vector which can be reached by acting with the algebra of observables on a particular state vector $|\psi\rangle$. The general notion of a state in the language of algebras is given by any positive and normalized linear functional $\omega : \mathcal{A} \to \mathbb{C}$ from the algebra to the complex numbers, such that it obeys [830, 831]

$$\omega(\mathfrak{a}^\dagger \mathfrak{a}) \geq 0\,, \quad \omega(\mathbb{1}) = 1\,, \quad \omega(\mathfrak{a} + \mathfrak{b}) = \omega(\mathfrak{a}) + \omega(\mathfrak{b})\,. \tag{4.78}$$

The construction of the Hilbert space $\mathcal{H}_0$ generated by a von Neumann algebra $\mathcal{A}$ is known as the Gelfand-Naimark-Segal (GNS) construction [860, 861], and it is based on a specific class of states called *cyclic and separating vectors*. A detailed review of the GNS construction is outside of the scope of this thesis. For our current purposes, it suffices to know that a state $|\psi\rangle$ in the algebra $\mathcal{A}$ is *separating* if the relation $\mathfrak{a}\,|\psi\rangle = 0$ uniquely implies that $\mathfrak{a} = 0$, and it is *cyclic* if the linear space spanned by $\{\mathfrak{a}\,|\psi\rangle \mid \mathfrak{a} \in \mathcal{A}\}$ is dense in $\mathcal{H}$. The latter condition generalizes the notion of basis vectors to the case of infinite-dimensional spaces. The cyclicity property is key, since it implies that while we might not have access to arbitrary states in the uncountably infinite Hilbert space $\mathcal{H}$, we may just as well define a physical Hilbert space $\mathcal{H}_0$ by restricting to a countably-infinite and dense subspace of it. By construction, this subspace will contain all physically relevant states that we may be interested in and which are obtained by acting with our entire algebra of observables $\mathcal{A}$ on the cyclic and separating vector $|\psi\rangle$. For generic QFTs in Minkowski spacetime, the Reeh-Schlieder theorem [841] states that the vacuum state is guaranteed to be cyclic and separating state vector for the operator algebras of any subregion U a spatial Cauchy slice [757]. This statement has been shown to hold also in curved spacetimes under suitable circumstances [862–865]. We will later encounter some other examples of such cyclic and separating states in our investigations on quantum many-body systems.

While the first three requirements in Definition 7 are shared by any unital C^*-algebra [860, 861], it is the final requirement which characterizes von Neumann algebras. Note that the commutant of a von Neumann algebra is itself a von Neumann algebra. Requirement *iv)* does not rule out the case that both $\mathcal{A}$ and its commutant share elements. This intersection $\mathcal{A} \cap \mathcal{A}'$ is known as the *center* $\mathcal{Z}(\mathcal{A})$ of $\mathcal{A}$. Special instances of von Neumann algebras are those where the center only contains complex scalars. Such von Neumann algebras are known as *factors*, and they can be thought

of as foundational objects in the theory of local operator algebras, whose study is key to the understanding of properties of general von Neumann algebras. In fact, von Neumann algebras that are not factors can be constructed from factors [757]. We will therefore focus on von Neumann algebras which are factors for the remainder of this chapter, without explicitly naming them as such. In [142], it was shown that von Neumann algebras can be classified into three distinct types, denoted as type I, II and III, and this characterization was further investigated and refined in several instances [831, 832, 866–870]. Though there exist many equivalent forms of this classification in the literature, we choose the version which will better suit our analysis of quantum many-body systems, as formulated in [757, 832, 833]. There, the classification of von Neumann operator algebras associated to a subregion A is based on two ingredients: the entanglement entropy of the degrees of freedom in A with the rest of the system, and the ability to define a normalized trace functional on the algebra. The latter is a positive-definite, linear, and cyclic functional on the algebra. Broadly speaking, type I von Neumann algebras encapsulate a finite amount of entanglement entropy and are typically associated to finite-dimensional quantum systems.[9] For type II and type III algebras, the entanglement entropy is infinite when computed with respect to the typical trace functional "Tr" of quantum mechanics. In this case, the existence of a normalized trace functional, denoted by a lower case "tr", is the key aspect distinguishing between type II (tr exists) and type III (tr does not exist) algebras.
Let us provide more details on this classification, following [757]. Consider a subregion A of a quantum system consisting of a number n of qubits and associate to it a von Neumann algebra of local operators $\mathcal{A}$. Its commutant $\mathcal{A}'$ is also a von Neumann algebra for some other subregion B of the system, which may or may not be the complement of A. The dimension of the Hilbert space of this model is given by $d = 2^n$. This system will be our playground to exemplify the appearance of different types of algebras.[10] The properties of the Hilbert space containing the ground state of our theory depend on the type of von Neumann algebra describing local observables restricted to subregion A, whose classification can be summarized as follows:

Type I: If the Hilbert space is finite-dimensional, i.e. $d < \infty$, then all operators acting on it will necessarily be bounded. As a consequence, also the entanglement entropy of any subregion will be finite. Moreover, we are guaranteed to find a trace

[9] More precisely, type I algebras may also describe systems where *some* state have infinite entanglement, but the key point is that there exist states with finite entanglement. In contrast, type II and III algebras only describe states with infinite entanglement.
[10] This type of operator algebras that can be constructed as limits of matrix algebras are known as *hyperfinite factors* [832, 833, 859], but we will not require this terminology here.

functional tr on the algebra $\mathcal{A}$, which we can take to be the standard trace Tr from quantum mechanics. The von Neumann algebra of any subregion, i.e. a subset of the spins, is in this case of type I, and more specifically it is denoted as type I_d to emphasize the dimensionality. In the limit of infinitely many qubits $n \to \infty$, the dimension of the Hilbert space $d = 2^n$ becomes uncountably infinite, but we can still find states within it which have finite entanglement entropy (any generic eigenstate of the Hamiltonian will have this property). The algebras underlying this scenario are still type I, in particular they are type I_∞. In this case, a trace functional can still be defined for some elements in a given subalgebra (so-called *trace-class* operators), while there may be other elements, like the identity operator, which have infinite trace.

Type II: The next non-trivial type of von Neumann algebras are type II algebras, which can only arise in infinite-dimensional systems. In fact, we will now construct an instance of this type of algebra by taking the limit $n \to \infty$ of our qubit system in a specific manner. In infinite-dimensional spaces, the trace Tr we typically use when dealing with matrix algebras is no longer useful, since it can only take the values 0 or ∞. It is here that the notion of a normalized trace functional tr, as mentioned above, comes into play. Before describing this trace, let us define the types of operators that belong to our algebra. Every local Hilbert space of two entangled qubits is a 2×2 dimensional complex space V on which the algebra of 2×2 complex matrices acts. For concreteness, we can think of this algebra as being generated by the Pauli matrices and any linear combination of them together with the 2×2 identity operator $\mathbb{1}_2$. Within this local space, we have one vector (corresponding to one operator) which can be associated to the normalized maximally entangled state namely $J_2 \equiv \mathbb{1}_2/\sqrt{2}$. This interpretation comes from the fact that the identity matrix can be seen as the reduced density matrix for a single qubit in the maximally entangled two-qubit Bell state. The naive Hilbert space of the entire model, constructed as the tensor product $V^{(1)} \otimes V^{(2)} \otimes \cdots \otimes V^{(n)}$ in the limit $n \to \infty$ has uncountable infinite dimension. Following the general considerations above, we construct a Hilbert space of countably infinite dimension, within which all our observables of physical interest will be contained. More precisely, consider a subspace which is spanned by vectors of the form

$$\lim_{n\to\infty} v_1 \otimes v_2 \otimes \cdots \otimes v_{k-1} \otimes v_k \otimes J_2 \otimes \cdots \otimes J_2 \in V^{(1)} \otimes V^{(2)} \otimes \cdots \otimes V^{(n)}\,, \qquad (4.79)$$

where the vector spaces of the first $k < n$ qubits are generic, while all the remaining ones $j > k$ are fixed to be in the maximally entangled state J_2. In particular, notice that only finitely many qubits are left unfixed. Note that the indices used here do

not necessarily correspond to a spatial arrangement of the qubits, they are merely a counting label for them. The space spanned by vectors of the form (4.79), which is technically a pre-Hilbert space, can be completed to a Hilbert space [757]. The operators that enter our algebra are defined in a similar manner, highlighting that the observables of interest to us are only those acting on a finite number of qubits at the same time. To be precise, the operators contained in our algebra $\mathcal{A}$ are of the form

$$\lim_{n\to\infty} O_1 \otimes O_2 \otimes \cdots \otimes O_{k-1} \otimes O_k \otimes \mathbb{1}_2 \otimes \cdots \otimes \mathbb{1}_2 \in \mathcal{A}\,. \tag{4.80}$$

Also here, notice how all but finitely many of the elements in the tensor product are fixed to act through the identity $\mathbb{1}$, while the remaining k qubits may be acted upon by any local operator built from Pauli matrices and the identity. It can be shown that the algebra (4.80) can be closed upon inclusion of weak or strong limits [757]. This is a consequence of the bicommutant theorem [835].

We can now return to the notion of a trace in the algebra. This trace is associated with the existence of a particular state, called the *tracial state* ω_{tr}, in the algebra $\mathcal{A}$. This is a particular state with the usual properties outlined above in (4.78) (positivity, linearity, normalization), with the added condition that it needs to be cyclic, i.e.

$$\omega_{\mathrm{tr}}(\mathfrak{a}\mathfrak{b}) = \omega_{\mathrm{tr}}(\mathfrak{b}\mathfrak{a})\,, \quad \forall\, \mathfrak{a}, \mathfrak{b} \in \mathcal{A}\,. \tag{4.81}$$

If the Hilbert space constructed from the action of $\mathcal{A}$ on a cyclic and separating vector $|\psi\rangle$ contains such a tracial state, then the algebra is said to be type II. In our specific example of the qubit system, an explicit example of such a tracial state was given in [757]. This state is given by

$$|\Psi\rangle = J_2 \otimes J_2 \otimes \cdots \otimes J_2 \otimes \cdots\,, \tag{4.82}$$

and we will denote it as the *maximally entangled state*, since it consists of an infinite collection of qubits entangled into Bell pairs. It was shown in [757] that the state $|\Psi\rangle$ in (4.82) is cyclic and separating for both $\mathcal{A}$ and $\mathcal{A}'$. Moreover, it was also shown that the natural definition of a trace functional as an expectation value in this state, i.e.

$$\mathrm{tr}(\mathfrak{a}) = \langle\Psi|\,\mathfrak{a}\,|\Psi\rangle\,, \tag{4.83}$$

is cyclic, thus providing a normalized trace functional on the algebra. Notice that the entanglement entropy in the state $|\Psi\rangle$ of (4.82) is infinite, yet we are still able to define a trace functional (4.83) on the algebra. This will be our working definition of type II

von Neumann algebra. Crucially, any other vector within the restricted Hilbert space constructed from our algebra $\mathcal{A}$ will also have infinite entanglement entropy [757]. Finally, let us note that the trace functional given in (4.83) is defined for every operator in the algebra $\mathcal{A}$, and it is normalized such that $\mathrm{tr}(\mathbb{1}) = 1$. This property is notationally highlighted by denoting $\mathcal{A}$ as a type II_1 von Neumann algebra. If a trace functional defined via a different tracial state is only defined for a certain subset of the operators in the algebra, while being infinite for operators that are not trace-class, we denote the associated von Neumann algebra as type II_∞.

Type III: The final type of algebras is type III, and these turn out to be the types of algebras which appear generically as algebras of observables in QFTs [265, 757, 871–873]. Their construction follows very similar steps as those outlined above, with the difference that now we reduce the amount of entanglement between the qubits. More precisely, the fixed elements in the tensor products of the form (4.79) will now be given by the matrix

$$K_{2,\lambda} = \frac{1}{\sqrt{1+\lambda}} \begin{pmatrix} 1 & 0 \\ 0 & \sqrt{\lambda} \end{pmatrix} , \tag{4.84}$$

with $0 < \lambda \leq 1$, describing a pair of qubits with a finite, but not maximal, amount of entanglement [757]. Notice how we recover the maximally entangled case of J_2 when $\lambda = 1$. The constructions above for the type II algebras can be repeated upon replacing $J_2 \to K_{2,\lambda}$. They will, however, lead to a different Hilbert space $\mathcal{H}_\lambda$, and consequently to a different algebra, since the closure of operators of the form (4.80) will be taken with respect to a different Hilbert space. The crucial consequence of this is that this new Hilbert space $\mathcal{H}_\lambda$ will *not* contain the maximally entangled state $|\Psi\rangle$ (4.82). Physically, this implies that the maximally entangled state $|\Psi\rangle$ cannot be reached from the analogous cyclic and separating vector

$$|\Psi\rangle_\lambda = K_{2,\lambda} \otimes K_{2,\lambda} \otimes \cdots \otimes K_{2,\lambda} \otimes \cdots , \tag{4.85}$$

by applying an element of the algebra, since these are by definition bounded operators in subregion A. This means that they cannot generate the infinite amount of entanglement required for transforming all $K_{2,\lambda}$ elements into J_2. Crucially, the state (4.85) induces a functional on the algebra which is linear and positive, but not cyclic. In these circumstances, the definition of the trace functional as (4.83) is not possible.[11] This, in turn, implies that the definition of density operators is not viable. Such von Neumann algebras which encapsulate an infinite amount of entanglement but do not

[11] According to [830], it can be shown that indeed no other choice of trace functional can be defined in this case, and not only the trace functional (4.83). This is based on previous studies in [867].

	Entropy	Maximally Entangled State	Trace functional
Type I	$S(\rho_A) < \infty$	$\|\Psi\rangle \in \mathcal{H}$	✅ $\mathrm{tr}(\mathfrak{a}) = \langle\Psi\|\,\mathfrak{a}\,|\Psi\rangle$
Type II	$S(\rho_A) = \infty$	$\|\Psi\rangle \in \mathcal{H}$	✅ $\mathrm{tr}(\mathfrak{a}) = \langle\Psi\|\,\mathfrak{a}\,|\Psi\rangle$
Type III	$S(\rho_A) = \infty$	$\|\Psi\rangle \notin \mathcal{H}$	❌

Figure 4.5: Practical summary of the classification of the type of a von Neumann algebra $\mathcal{A}$ associated to a subregion A of a quantum system. ρ_A denotes the reduced density matrix of the system, and the maximally entangled vector $|\Psi\rangle$ is defined in (4.82). The Hilbert space $\mathcal{H}$ is that obtained from the action of the algebra $\mathcal{A}$ on a cyclic and separating vector. The existence of states with finite entanglement entropy $S(\rho_A)$, together with the existence (or non-existence) of a normalized trace functional as in (4.83) are the key ingredients we will use to identify the type of von Neumann algebras.

allow for the definition of a normalized trace functional tr are called type III. There exists a more refined classification of type III algebras due to Powers [833], and Araki and Woods [832], which we will review at a later stage in this section. For later reference, we have schematically summarized the main ingredients of this version of the type classification of von Neumann algebras in Fig. 4.5. In the later sections, we will often refer to this figure when identifying the von Neumann algebras underlying a certain class of interacting quantum many-body models.

von Neumann Algebras and Holography

Lastly, we briefly review the recent interest in von Neumann operator algebras within the AdS/CFT correspondence. In [146, 756], the Hawking-Page phase transition in AdS, together with its holographically dual deconfinement transition, were studied under the lens of operator algebras. It was found that this phase transition is accompanied by a transition from type I_∞ to type III_1 of the von Neumann operator algebra of single-trace operators in the dual $\mathcal{N} = 4$ super-Yang-Mills theory. This algebra can equivalently be seen to describe the algebra of quantum fields in the bulk gravity theory, restricted to the region outside of the black hole horizon. In particular, the results of [146, 756] hold in the strict large N limit, where this algebra is type I_∞ below the Hawking-Page temperature, but becomes type III_1 in the black hole phase. The emergence of a new time behind the horizon is based on the existence of the extension of a *half-sided modular inclusion* along the black hole horizon [146, 756], which is an algebraic structure capturing the creation of an event horizon in the bulk

and only exists for algebras of type III_1. It was suggested in [858, 874, 875] that a similar analysis, based on the Källén-Lehman spectral density, could be carried out for finite 't Hooft coupling on the boundary as well, providing insights into the features of stringy black hole horizons. These studies lead to the general expectation that such algebra transitions hint at the appearance of black hole horizons in the bulk, although it is unclear whether the appearance of algebras specifically of type III_1 is a sufficient condition for this [858].

Later, the analysis of [146, 756] was extended to include $1/N$ corrections in [148], where it was found that these corrections cause the type III_1 algebra to deform into a type II_∞ factor. This type II_∞ algebra has the structure of a crossed product between the type III_1 algebra at strict large N and its modular automorphism group [866, 867]. This structure indicates that the entanglement entropy of the black hole can be well-defined independently of the choice of cyclic and separating vector, thus providing an algebraic definition for this quantity which was not accessible in the type III_1 description. This comes closer to a full-fledged understanding of the origin of black hole entropy, although only to the point where it is akin to a thermodynamic entropy, without providing explicit knowledge about the microstates. It is conjectured that such an microscopic description of the black hole states will yield a type I von Neumann algebra, which in turn is the algebra type expected for quantum gravity.

These paradigm shifting developments were quickly followed by investigations on the role of operator algebras in models of quantum gravity [137, 758, 762, 854, 855, 857, 876], de Sitter space [759, 761, 856, 877], SYK models [878, 879], and other quantum systems [852, 853, 858, 880]. Motivated by this state of the art, I report the results of [163] on von Neumann algebras in interacting models of Majorana fermions.

4.3.2. Large-N Interacting Majorana Models

The recent studies into von Neumann algebras in the context of holography showcase the importance of operator algebras for the description of entanglement in infinite-dimensional Hilbert spaces. In particular, Sec. 4.3.1 made clear that transitions between different types of von Neumann algebras can provide us with new insights into the entanglement properties of a system. These recent developments, together with a general interest in entanglement as a diagnosing tool for phase transitions, motivates us to study transitions of operator algebras in interacting many-body quantum systems. In particular, we are interested in quantum systems whose Hilbert space structure allows for a controlled analysis of entanglement as the dimensionality of said Hilbert space becomes infinite. For this, we consider a lattice model with L sites with N Majorana fermions ψ_x^j on each site. These obey the anti-commutation relations

$\left\{\psi_x^j, \psi_y^k\right\} = \delta^{jk}\delta_{xy}$. The microscopic Hamiltonian of the theory allows the Majoranas to interact via a general potential involving multi-body hoppings, which reads

$$H = \frac{N}{2}\sum_{x,y=1}^{L} h_{xy}\left(\frac{2}{\mathrm{i}N}\sum_{j=1}^{N}\psi_x^j\psi_y^j\right) . \tag{4.86}$$

Here, h_{xy} is a general interaction potential, which we may take to obey $h_{xy}(\xi) = h_{yx}(-\xi)$ and $h_{xx}(\xi) = 0$ without the loss of generality. Besides this constraint, this function can be quite general, and indeed we only need it to be an analytic function for it to define an instance of our model.

The Hamiltonian (4.86) can be related to many other models. For any choice of h_{xy} other than $h_{xy}(\xi) = \xi$, the model (4.86) represents an interacting system and is invariant under a global $O(N)$ rotation $\psi_x^j \to \sum_k O^{jk}\psi_x^k$, where O is an orthogonal matrix, due to the argument of the interaction potential being a fermion bilinear. Our model can thus be regarded as a lattice counterpart of the Gross–Neveu model [881], albeit with a general interaction potential. We will see later that this analogy can be made precise in terms of how the Feynman diagram expansion looks like. Also, choosing $h_{xy}(\xi) \propto \xi^q$, the model (4.86) is equivalent to a replicated Brownian Sachdev-Ye-Kitaev (SYK$_q$) model, when considered in disorder averaging [882]. However, in our case, $h_{xy}(\xi)$ always includes a linear term in ξ.

For generic values of N, the model (4.86) is quite hard to solve. However, in the large N limit, its partition function $Z = \int D\psi e^{-S}$ in Euclidean time τ admits an effective description in terms of two auxiliary bilocal fields (also known as *master fields*), namely the Green's function $G_{xy}(\tau_1, \tau_2) = 1/N\sum_j \psi_x^j(\tau_1)\psi_y^j(\tau_2)$ and the self-energy $\Sigma_{xy}(\tau_1, \tau_2)$. The latter introduced as a Lagrange multiplier, such that the original action $S = \int d\tau L = \int d\tau \left(\sum_{xj} \frac{1}{2}\psi_x^j\partial_\tau\psi_x^j + H\right)$ can be re-written into an effective action which is manifestly of $\mathscr{O}(N)$. More precisely, considering the model in the canonical ensemble at a finite temperature $1/\beta$, we have the thermal partition function

$$Z = \int \mathcal{D}\tilde{G}\mathcal{D}\tilde{\Sigma}e^{-S_E[\tilde{G},\tilde{\Sigma}]} , \tag{4.87}$$

where the tildes denote integration variables, and with the effective action

$$\begin{aligned} -\frac{S_E}{N} &= \log \mathrm{Pf}(\partial_\tau\delta_{xy} - \Sigma_{xy}) - \frac{1}{2}\sum_{x,y}\int_0^\beta d\tau_1 d\tau_2 G_{xy}(\tau_1-\tau_2)\Sigma_{xy}(\tau_1-\tau_2) \\ &\quad - \frac{1}{2}\sum_{x,y}\int_0^\beta d\tau h_{xy}(-2\mathrm{i}G_{xy}(0)) , \end{aligned} \tag{4.88}$$

where $G_{xy}(\tau) = -G_{yx}(-\tau)$ and Pf denotes the Pfaffian determinant defined as the square root of the usual determinant, i.e. $\mathrm{Pf}(A) \equiv \sqrt{\det(A)}$. Note that we have assumed time-translation invariance. The partition function (4.87), together with the effective action (4.88), allow us to either access the ground state when $\beta \to \infty$, or the thermodynamic properties of the system at finite temperature. Taking the large N limit allows us to do a saddle-point approximation on the partition function and derive the equations of motion by imposing that the variations $\frac{\partial S_E}{\partial G}$, $\frac{\partial S_E}{\partial \Sigma}$ vanish. The resulting equations of motion for the master fields are known as the *Schwinger-Dyson* (SD) equations, and read

$$G'_{xy}(\tau_{12}) - \sum_z \int d\tau_3 \Sigma_{xz}(\tau_{13}) G_{zy}(\tau_{32}) = \delta_{xy}\delta(\tau_{12}), \tag{4.89}$$

$$\Sigma_{xy}(\tau_{12}) = 2\mathrm{i}\, h'_{xy}(-2\mathrm{i}G_{xy}(0))\delta(\tau_{12})\,, \tag{4.90}$$

where the assumed time-translational invariance allows us to write $\tau_{ij} \equiv \tau_i - \tau_j$, and $\Sigma_{xy} = -\Sigma_{yx}$ due to the conditions on h_{xy} mentioned above. Crucially, this model exhibits large-N factorization and is thus exactly solvable when $N \to \infty$. By this we mean that all n-point functions with $n \geq 3$ factorize into products of two-point functions. From the Lagrangian of the model, given by

$$L = \sum_x \sum_j \frac{1}{2} \psi^j_x \partial_\tau \psi^j_x + H\,, \tag{4.91}$$

we can derive the Feynman diagrams describing the interaction terms of the model in the perturbative expansion in $1/N$. More precisely, these Feynman diagrams are made out of the bare propagator $G_0(\tau_1, \tau_2) = \frac{1}{2}\mathrm{sgn}(\tau_1 - \tau_2)$, together with the simultaneous but non-local interactions given by the series expansion of the potential

$$\frac{N}{2} \sum_{xy} h_{xy} \left(\frac{2}{iN} \sum_j \psi^j_x \psi^j_y \right) = \frac{N}{2} \sum_{p=0} \sum_{xy} h^{(p)}_{xy} \left(\frac{2}{iN} \sum_j \psi^j_x \psi^j_y \right)^p , \tag{4.92}$$

where $h^{(p)}_{xy}$ are expansion coefficients. We visualize the $p = 1, 2, 3$ order terms via the interaction vertices shown in Fig. 4.6. In the presence of interactions, the bare propagator gets dressed to the Green's function $G_{xy}(\tau_1, \tau_2) = \left\langle \frac{1}{N} \sum_j \psi^j_x \psi^j_y \right\rangle$, whose expression we can obtain from the sequence of iterated Feynman diagrams shown in Fig. 4.7. In this diagrammatic expression, the dashed lines indicate the bare propagators G_0, while the blob indicates the one-particle irreducible (1PI) diagram. Meanwhile, the self-energy $\Sigma(\tau_1, \tau_2)$ is obtained from the 1PI diagram shown in Fig. 4.8. The order of each of the diagrams in the $1/N$ expansion can be obtained by simply counting the

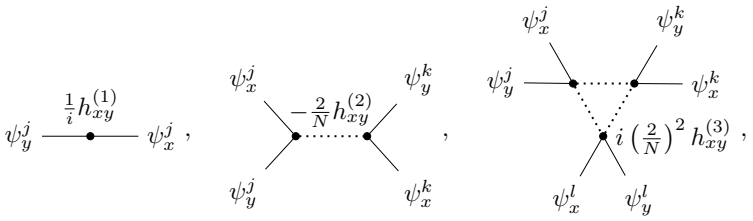


Figure 4.6: Diagrams for the interaction vertices appearing in (4.92) for $p = 1, 2, 3$. Each individual dot denotes the non-local bilinear operator $\psi^j_x \psi^j_y$, while the dotted lines indicate that the interactions between operators occur synchronously, i.e. at the same time.

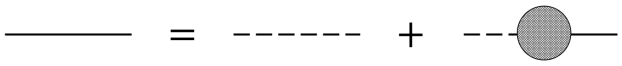


Figure 4.7: Dressing of the bare propagator (dashed line) G_0 by the iterated 1PI diagrams (blob), to obtain the Green's function $G_{xy}(\tau_1, \tau_2) = \left\langle \frac{1}{N} \sum_j \psi^j_x \psi^j_y \right\rangle$ in presence of interactions.

summation over the color indices $j, k, l, \ldots$. Doing this, we find the bubble diagrams depicted in the first line of Fig. 4.8 to be of $\mathcal{O}(N^0)$. It is precisely these diagrams which give rise to the SD equations (4.89)-(4.90). All Green's functions considered here will receive contributions from these bubble diagrams. By the same counting, we can see that the diagrams in the second line of Fig. 4.8 are $\mathcal{O}(N^{-1})$ and are therefore suppressed in the large N limit. The fact that only the bubble diagrams contribute to two-point functions at leading order in $1/N$ is the feature alluded to before in the comparison to the Gross-Neveu model.

We now proceed to solve the SD equations (4.89)-(4.90). In Fourier space, we have

$$G_{xy}(\omega_n) = \left[\frac{1}{-\mathrm{i}\,\omega_n - \Sigma(\omega_n)} \right]_{xy} , \tag{4.93}$$

where the Fourier transforms of $G(\tau_1, \tau_2)$ and $\Sigma(\tau_1, \tau_2)$ are given by

$$\begin{aligned} G(\tau_1, \tau_2) &= \sum_{n \in \mathbb{Z}} e^{-\mathrm{i}\omega_n(\tau_1 - \tau_2)} G(\omega_n) \equiv G(\tau_{12}) , \\ \Sigma(\tau_1, \tau_2) &= \sum_{n \in \mathbb{Z}} e^{-\mathrm{i}\omega_n(\tau_1 - \tau_2)} \Sigma(\omega_n) \equiv \Sigma(\tau_{12}) . \end{aligned} \tag{4.94}$$

Here, $\omega_n = 2\pi(n + 1/2)/\beta$ are the fermionic Matsubara frequencies to take into account the fermionic anti-commutation relations of our variables [883]. In the zero-temperature limit $\beta \to \infty$, these frequencies ω_n become continuous and we may do the replacement $\sum_{n \in \mathbb{Z}} \to \int_0^\beta d\omega$ in (4.94). Naturally, the Green's function in the Euclidean time domain $G(\tau_{12})$ is retrieved by taking the inverse Fourier transform of

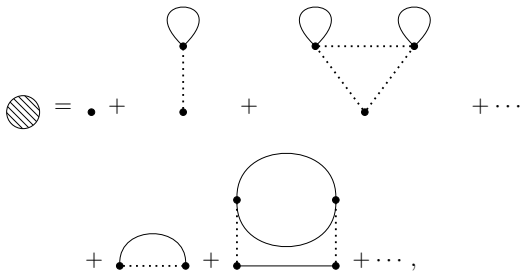


Figure 4.8: Construction of the 1PI diagram from a combination of the diagrams in Fig. 4.6 and a subsequent amputation of external legs.

(4.93). A crucial feature of our model is that the self-energy in (4.90) has a simple time-dependence given by a δ-function. As a consequence, $\Sigma(\omega)$ in (4.94) is independent of the frequency. Moreover, its time-domain counterpart does not depend on the entire Green's function, but rather it is solely determined by $-2\mathrm{i}G_{xy}(0)$. We can leverage this fact to solve for $G(0)$ by imposing *self-consistency* (SC) conditions. In particular, from (4.93) we have

$$G_{xy}(0) = \frac{1}{\beta}\sum_n \left[\frac{1}{(-\mathrm{i}\omega_n - \Sigma(\omega_n))^{-1}}\right]_{xy} . \tag{4.95}$$

Since Σ only depends on $G(0)$ as per (4.90), the equation above imposes a self-consistency condition for the matrix $G(0)$ which allows to find its value. The Green's function $G(\tau)$ is subsequently obtained by inserting $G(0)$ back into (4.90) and (4.89). We do this for two explicit systems below.

4.3.3. Thermodynamics and Phase Diagram

The techniques detailed above enjoy a vast regime of applicability, both from the perspective of working for generic choices of interaction potential h, as well as from the access to, in principle, generic lattice choices. In practice, however, it may be that solving the self-consistency equations (4.95) poses a challenging task all by itself. Still, computationally, the corresponding system of equations will be easier to solve numerically than an exact diagonalization of the Hamiltonian, providing in this way many advantages. Nonetheless, we will show below that extremely rich physics can be extracted from the model (4.86), even for small lattices. In doing this, we will access the thermodynamics of the system, unveiling the existence of a phase transition.

Two-site Chain: Green's Function

We first focus on an instance of our model governed by the general Hamiltonian H (4.86) defined on a 1D chain consisting of $L = 2$ sites and at a finite temperature $1/\beta$.

Without loss of generality, β can be absorbed into the general form of the Hamiltonian (4.86), such that we effectively set $\beta = 1$. The density matrix of the system reads

$$\rho = \frac{e^{-H}}{Z}, \qquad H = Nh\left(\frac{2}{\mathrm{i}N}\sum_j \psi_1^j \psi_2^j\right), \tag{4.96}$$

where $Z = \mathrm{Tr}\left(e^{-H}\right)$ is the partition function and we have used the symmetry $h(\xi) \equiv h_{12}(\xi) = h_{21}(-\xi)$. Utilizing the general methods detailed above, we can exactly solve the model and obtain the Green's function. More precisely, for the two-site system, the self-energy is given by

$$\Sigma_{xy}(\tau) = 2\mathrm{i}\delta(\tau)\begin{pmatrix} 0 & -h'(X) \\ h'(X) & 0 \end{pmatrix}, \tag{4.97}$$

where we have defined the quantity $X \equiv -2\mathrm{i}G_{12}(0)$ representing a slight redefinition of the 1-2 component of the Green's function. Plugging the Fourier transform of (4.97) into the expression (4.93), we find

$$G_{xy}(\omega_n) = \frac{\mathrm{i}}{\omega_n^2 + 4[h'(X)]^2}\begin{pmatrix} \omega_n & 2h'(X) \\ -2h'(X) & \omega_n \end{pmatrix}. \tag{4.98}$$

We now make use of (4.94) to obtain the Green's function at finite temperature $\beta^{-1} = 1$ for any value of $\tau \geq 0$, which reads

$$G_{xy}(\tau) = \frac{1}{2}\begin{pmatrix} \frac{e^{2h'(X)\tau}+e^{-2h'(X)(\tau-1)}}{1+e^{2h'(X)}} & \mathrm{i}\frac{\sinh\left[h'(X)(1-2\tau)\right]}{\cosh\left(h'(X)\right)} \\ -\mathrm{i}\frac{\sinh\left[h'(X)(1-2\tau)\right]}{\cosh\left(h'(X)\right)} & \frac{e^{2h'(X)\tau}+e^{-2h'(X)(\tau-1)}}{1+e^{2h'(X)}} \end{pmatrix}. \tag{4.99}$$

To get to this expression, recall that the sums over n in (4.94) can be evaluated by rewriting them as a contour integral of a function with simple poles along the imaginary axis. Notice how (4.99) is still a function of the interaction potential h, and derivatives thereof h', which themselves are functions of G. In other words, G is given as a function of itself, in particular of the entry $G_{12}(0)$. Therefore, we can impose the self-consistency of this solution as explained in (4.95) by evaluating (4.99) at $\tau = 0$. This yields,

$$G_{xy}(0) = \frac{1}{2}\begin{pmatrix} 1 & -\mathrm{i}\tanh\left(h'(X)\right) \\ \mathrm{i}\tanh\left(h'(X)\right) & 1 \end{pmatrix}, \tag{4.100}$$

from which we can immediately extract the self-consistency condition for X, given by

$$X = -\tanh\left(h'(X)\right). \tag{4.101}$$

Note that, due to the symmetries of G and the choice of $L = 2$, this condition suffices to determine G in its entirety. Once solutions of (4.101) are found, these can be inserted back into (4.99) to retrieve the full Green's function for any time $\tau > 0$. Analyzing (4.101) more closely, we see that $-1 < X < 1$ independently of the explicit form of the interaction potential h. This symmetric domain hints at the fact that two relevant regimes to consider for (4.101) are when $|X| \to 0$ and $|X| \to 1$. These correspond to the regimes where the correlations $G_{12}(0)$ between the two sites of this system are weak and strong, respectively.

Two-site Chain: Thermodynamics

Based on these self-consistency conditions, we can investigate the thermodynamic properties of the system at finite temperature by exploiting its path integral description in the large N limit. Namely, we derive the free energy of this two-site system for generic interaction potentials, for which it will be instructive to reinstate the physical temperature parameter $1/\beta$. Furthermore, it will prove convenient to introduce a function describing the derivative of the interaction potential as $h'(\xi) \equiv \mu\, m(\xi)$, where $m(\xi)$ is a dimensionless function encapsulating the dependence on the fermion bilinear. This definition allows us to extract the explicit dependence on the energy scale μ, which denotes the hopping parameter between sites 1 and 2, and it will be sometimes useful to use the dimensionless quantity $\hat{\mu} \equiv \mu\beta$. Of course, the original interaction potential can be recovered from this notation by integration $h(\xi) = \mu \int d\xi' m(\xi')$.
In the saddle-point approximation to the path integral enabled by the large N limit,

$$Z = e^{-\beta F} = \int \mathcal{D}\tilde{G}\mathcal{D}\tilde{\Sigma}\, e^{-S_E[\tilde{G},\tilde{\Sigma},\hat{\mu}]}\,, \tag{4.102}$$

and the free energy can thus be obtained via the on-shell effective action given in (4.88). By on-shell we mean here all possible solutions to the SC equation (4.101). Using $X = -2\mathrm{i}G_{12}(0)$, we can re-write the last term in the effective action (4.88) as

$$\begin{aligned} -\frac{1}{2}\sum_{x,y}\int_0^\beta d\tau h_{xy}(-2\mathrm{i}G_{xy}(0)) &= -\frac{\beta}{2}\left(h_{12}(X) + h_{21}(-X)\right) \\ &= -\beta h(X) = -\hat{\mu}\int^X d\tilde{X} m(\tilde{X}) \equiv S_m[G](\hat{\mu})\,. \end{aligned} \tag{4.103}$$

The reason for doing this is that we can now split the effective action (4.88) into three terms which can then be analyzed separately, namely

$$-S_E \equiv S_{\mathrm{Pf}}[\Sigma] + S_G[G,\Sigma] + S_m[G](\hat{\mu})\,. \tag{4.104}$$

where $S_{\rm Pf}$ and S_G are identified with the first two terms of (4.88). In the large N limit, the saddle-point of the path integral (4.102) yields

$$\log Z = -\beta F \approx -S_E[G, \Sigma, \hat{\mu}]\,, \tag{4.105}$$

where $S_E[G, \Sigma, \hat{\mu}]$ is the effective action evaluated on solutions to the SC equation, which can be written explicitly as

$$\hat{\mu} = -\frac{\tanh^{-1}(X)}{m(X)}\,. \tag{4.106}$$

However, a direct evaluation of the effective action is hindered by the presence of the Pfaffian term, as pointed out in [884]. Still, we can find a way around this, which broadly speaking involves a differentiation and subsequent integration of the effective action with respect to a parameter not present in the Pfaffian, such as to functionally get rid of it. More precisely, we consider the derivative with respect to $\hat{\mu}$,

$$\hat{\mu}\frac{\partial}{\partial\hat{\mu}}\left(-S_E\right) = \hat{\mu}\frac{\partial\Sigma}{\partial\hat{\mu}}\left(\frac{\delta S_{\rm Pf}}{\delta\Sigma} + \frac{\delta S_G}{\delta\Sigma}\right) + \hat{\mu}\frac{\partial G}{\partial\hat{\mu}}\left(\frac{\delta S_G}{\delta G} + \frac{\delta S_m}{\delta G}\right) + \hat{\mu}\left(\frac{\partial S_m}{\partial\hat{\mu}}\right)\,. \tag{4.107}$$

When we now evaluate this expression on-shell, we see that the first two terms vanish due to the SD equations, and they would only contribute a constant which is independent of X and $\hat{\mu}$. The only remaining contribution is therefore

$$\frac{\partial}{\partial\hat{\mu}}\left(-\frac{S_E}{N}\right)\Big|_{\text{on-shell}} = \frac{\partial}{\partial\hat{\mu}}\left(\frac{S_m[G](\hat{\mu})}{N}\right)\Big|_{\text{on-shell}} = -\int^X d\tilde{X} m(\tilde{X}) = -\frac{h(X)}{\mu}\,. \tag{4.108}$$

We can recover the free energy by integrating (4.108) with respect to $\hat{\mu}$. This needs to be done carefully since, on-shell, X itself is a function of $\hat{\mu}$ as per (4.106), and so we have $h(X) \equiv h(X(\hat{\mu}))$. We deal with this by a change of integration variable using $\frac{d\hat{\mu}}{\mu} = d\beta = \frac{\partial\beta(X)}{\partial X}dX$. Using the SC equation (4.106), and recalling that $h'(X) = \mu\, m(X)$, we see that $\frac{\partial\beta(X)}{\partial X} = \frac{\partial}{\partial X}\left(-\frac{\tanh^{-1}(X)}{h'(X)}\right)$. Thus, the free energy reads

$$\frac{\beta F}{N} = \int_{X_0}^{X} d\tilde{X}\left(\frac{\partial\beta}{\partial X}\right)_{|X=\tilde{X}} h(\tilde{X}) = -\frac{h(X)\tanh^{-1}(X)}{h'(X)} + \frac{1}{2}\log\left(1-X^2\right) + X\tanh^{-1}(X)\,, \tag{4.109}$$

where we again remind ourselves that this expression is to be evaluated on those values of X which solve the SC equation (4.106). From the free energy (4.109), we can further

derive the internal energy E of the two-site system, which is given by

$$E = -\partial_\beta \log Z = \mu \partial_{\hat{\mu}} S_E \implies \frac{\beta E}{N} = \frac{\beta h(X)}{N} . \tag{4.110}$$

Finally, we can obtain the entropy S at leading order in $1/N$, which we express as an entropy density $s = S/N$ and reads

$$\frac{S}{N} = \frac{\beta E}{N} - \frac{\beta F}{N} = -X \tanh^{-1} X - \frac{1}{2} \log\left(1 - X^2\right) + \log 2 + h(X) \left(\frac{\tanh^{-1}(X)}{h'(X)} + \beta \right) . \tag{4.111}$$

Notice the factor of $\log 2$, which is added based on physical considerations on the maximal and minimal values that a thermodynamic entropy ought to have. This factor fixes the additive constant of the free energy mentioned above. A quite remarkable feature of (4.109) is that the expression in brackets in the last term vanishes identically due to the SC condition (4.106). We thus obtain our final result for the entropy of the two-site system for generic interaction potentials at a finite temperature, given by

$$s(X) = -\frac{1+X}{2} \log \frac{1+X}{2} - \frac{1-X}{2} \log \frac{1-X}{2} . \tag{4.112}$$

A highly remarkable feature of the entropy (4.112) is that it does not depend explicitly on the interaction potential. It takes the same functional form regardless of the choice of h. However, this independence is only a feature of the entropy, since other quantities like the free energy (4.109), and of course the internal energy (4.110), do indeed exhibit an explicit dependence on h. Moreover, we will see below that this independence of the entropy is spoiled by $1/N$ corrections.

Two-site Chain: Subleading Corrections

In order to properly assess the behavior of the entropy (4.112) in the regimes of interest $|X| \to 0$ and $|X| \to 1$, we compute the subleading corrections in the $1/N$ expansion. For this, recall that the density matrix of the system is given by (4.96). In this expression, the bilinear operator $\chi = \frac{2}{\mathrm{i}N} \sum_{j=1}^{N} \psi_1^j \psi_2^j$ can be expressed as the fermionic occupation number n via $\chi = 2n/N - 1$. When expressed in terms of the occupation basis $\{|n_1, n_2, \cdots, n_N\rangle \,|\, n_j \in \{0,1\}, \forall j\}$, the Hamiltonian is diagonal with eigenvalue $Nh(2n/N-1)$, where $n = \sum_j n_j$. The partition function of the system then reads

$$Z = \sum_{n=0}^{N} \binom{N}{n} e^{-Nh(2n/N-1)} \to \int_{-1}^{1} d\chi \sqrt{\frac{N}{2\pi(1-\chi^2)}}\, e^{-Nf(\chi)} , \tag{4.113}$$

where we have fixed $0 < n/N = (\chi+1)/2 < 1$ and the arrow represents the limit $N \to \infty$. Moreover, we have introduced the function

$$f(\chi) = h(\chi) - s(\chi)\,, \quad s(\chi) = -\frac{1+\chi}{2}\log\frac{1+\chi}{2} - \frac{1-\chi}{2}\log\frac{1-\chi}{2}\,, \tag{4.114}$$

which can be thought of as a free energy density. The similarity of s with (4.112) will become apparent shortly. The integral obtained in (4.113) can be well approximated in the large N limit by its saddle-point value, which is precisely the condition imposing $\chi = X$, as we know from the SC condition (4.101).
In order to analyze this saddle-point approximation, and subleading terms thereof, it is convenient to first introduce a generic functional $Y(\chi)$ in the following way

$$\langle Y(\chi)\rangle = \frac{1}{Z_0}\sqrt{\frac{N}{2\pi}}\int_{-\infty}^{\infty} d\chi\, Y(\chi)\, e^{-Nf(X)-\frac{N}{2}f''(x)(\chi-X)^2}\,, \tag{4.115}$$

$$Z_0 = \sqrt{\frac{N}{2\pi}}\int_{-\infty}^{\infty} d\chi\, e^{-Nf(X)-\frac{N}{2}f''(x)(\chi-X)^2} = \frac{e^{-Nf(X)}}{\sqrt{f''(X)}}\,. \tag{4.116}$$

The Gaussian form of the integral allows us to establish

$$\langle 1\rangle = 1, \quad \langle \chi - X\rangle = 0, \quad \left\langle (\chi-X)^2\right\rangle = \frac{1}{Nf''(X)}\,. \tag{4.117}$$

This implies that the generic functional can be expanded in a series as

$$\langle Y(\chi)\rangle = \sum_n \frac{1}{n!} Y^{(n)}(X)\,\langle(\chi-X)^n\rangle\,, \tag{4.118}$$

which in turn gives us access to the thermodynamic properties of the system order by order. More precisely, the saddle-point contributions to the partition function Z, the energy E, and the entropy S are given by

$$Z = Z_0\left\langle\frac{1}{\sqrt{1-\chi^2}}\right\rangle, \quad E = \frac{\left\langle h(\chi)/\sqrt{1-\chi^2}\right\rangle}{\left\langle 1/\sqrt{1-\chi^2}\right\rangle}, \quad S = E + \log Z\,. \tag{4.119}$$

To obtain the subleading corrections to this contribution, we consider the $(\chi-X)^2$ order of the series expansions of the averaged quantities in (4.119). In particular, we are interested in the corrections to the entropy, which read

$$S = Ns(X) + \frac{1}{2}\left(1 + \log\frac{f''(X)}{1-X^2} + \frac{2Xh'(X)-1}{f''(X)(1-X^2)}\right)\,. \tag{4.120}$$

Notably, we find that these subleading corrections to the entropy density are of $\mathcal{O}\left((1/N)^0\right)$ for $|X| < 1$. In particular, this means that $S \to N \log 2 + \mathcal{O}(1)$ when $|X| \to 0$. However, the situation when $|X| \to 1$ is a bit more subtle. In this limit, the subleading corrections given in (4.120) diverge, implying that the computation is not valid anymore. Specifically, this behavior signals the breakdown of our ansatz (4.96) for the density matrix. This general form of the density matrix is admissible when the system is in a mixed state, but ceases to be valid when the state becomes pure. The divergent behavior of the subleading corrections (4.120) when $X \to 1$ indicates that the system asymptotes to a pure state. This can be further justified by the behavior of the SC solutions to (4.101) from which, when reinstating the temperature β, one can see that $X \to 1$ forces $\beta \to \infty$. This means that the system reaches its ground state, which is of course a pure state. The crucial consequence of this is that for a pure state, $S = 0$ to all orders in the $1/N$ expansion. This is furthermore consistent with the fact that $\lim_{X\to 1} s(X) = 0$. Below, we will encounter further evidence as to why this pure state limit is well-justified. Our results for the entropy of the two-site chain for generic interaction potentials can be thus summarized by (4.112), together with the limiting behaviors $S \to N \log 2 + \mathcal{O}(1)$ when $|X| \to 0$, and $S \to 0$ when $|X| \to 1$.

Four-site chain: Green's Function

Although the two-site system might seem rather simple by itself, it develops a new level of relevance when considering this two-site chain as a subsystem of larger chains. In particular, the results we obtained for the entropy of the two-site chain will prove extremely useful to study the entanglement structure of these larger systems. As an explicit example, we will now consider an open chain with $L = 4$ sites at zero temperature, again described by a Hamiltonian of the form (4.86) with a nearest-neighbor interaction potential obeying $h_{x,x+1}(\xi) = h_{x+1,x}(-\xi)$, with all the other components of $h_{xy}(\xi)$ equal to zero. As a slight simplification, we choose the hopping parameters of the four-site chain obey a reflection symmetry $\mu_1 = \mu_3 \equiv \mu_a$, $\mu_2 \equiv \mu_b$, which implies $h_{12}(\xi) = h_{34}(\xi)$. It will prove convenient to again define a dimensionless parameter, which for the four-site chain we take to be the hopping ratio $r \equiv \mu_a/\mu_b$. From (4.90), we can readily find the expression of the self-energy to be

$$\Sigma_{xy}(\tau) = 2\mathrm{i}\delta(\tau) \begin{pmatrix} 0 & -h'_{12}(-2\mathrm{i}G_{12}(0)) & 0 & 0 \\ h'_{12}(-2\mathrm{i}G_{12}(0)) & 0 & -h'_{23}(-2\mathrm{i}G_{23}(0)) & 0 \\ 0 & h'_{23}(-2\mathrm{i}G_{23}(0)) & 0 & -h'_{12}(-2\mathrm{i}G_{12}(0)) \\ 0 & 0 & h'_{12}(-2\mathrm{i}G_{12}(0)) & 0 \end{pmatrix}. \tag{4.121}$$

Inserting its Fourier transform in (4.93), we obtain

$$G_{xy}(\omega_n) = \alpha \begin{pmatrix} w_n\left(r^2+w_n^2+1\right) & r\left(r^2+w_n^2\right) & rw_n & r^2 \\ -r\left(r^2+w_n^2\right) & w_n\left(r^2+w_n^2\right) & w_n^2 & rw_n \\ rw_n & -w_n^2 & w_n\left(r^2+w_n^2\right) & r\left(r^2+w_n^2\right) \\ -r^2 & rw_n & -r\left(r^2+w_n^2\right) & w_n\left(r^2+w_n^2+1\right) \end{pmatrix}, \tag{4.122}$$

where we have defined the prefactor

$$\alpha = \frac{\mathrm{i}}{b[(r^2+w_n^2)^2+w_n^2]}, \tag{4.123}$$

to avoid clutter. We have defined the short-hand notation $b \equiv 2h'_{23}(-2\mathrm{i}G_{23}(0)))$. Note that the frequencies ω_n have also been re-scaled as $w_n \equiv \omega_n/b$, and we are using the parametrization $r = \frac{h'_{12}(-2\mathrm{i}G_{12}(0))}{h'_{23}(-2\mathrm{i}G_{23}(0)))} = \frac{1}{2}\tan\theta$, which will prove useful later. We have written the above expression for a finite temperature β, but we are interested in the ground state of the system, and so we take the limit $\beta \to \infty$. Similarly to the case of the two-site chain, the sums over the frequencies in (4.94) can be replaced by continuous integrals over $w \in [-\infty, \infty]$. This time, evaluating these integrals on the complex plane requires the identification of poles of the Green's function (4.94), of which there are exactly four for each entry, as can be seen from the prefactor α in (4.123). These poles are given by

$$w_{\pm\pm} = \pm\frac{\mathrm{i}}{2}(\sec\theta \pm 1)\,. \tag{4.124}$$

For $\tau > 0$, we may close the integration contour on the lower-half plane and pick up the residues of the two poles with negative imaginary part. The two-point functions are then given by

$$G_{xy}(\tau) = \tilde{\alpha} \begin{pmatrix} (s+1)e^{b\tau}+s-1 & \mathrm{i}\sqrt{s^2-1}\left(e^{b\tau}+1\right) & \sqrt{s^2-1}\left(e^{b\tau}-1\right) & \mathrm{i}\left((s+1)e^{b\tau}-s+1\right) \\ \mathrm{i}\sqrt{s^2-1}\left(e^{b\tau}+1\right) & (s-1)e^{b\tau}+s+1 & -\mathrm{i}\left((s-1)e^{b\tau}-s-1\right) & \sqrt{s^2-1}\left(e^{b\tau}-1\right) \\ \sqrt{s^2-1}\left(e^{b\tau}-1\right) & \mathrm{i}\left((s-1)e^{b\tau}-s-1\right) & (s-1)e^{b\tau}+s+1 & \mathrm{i}\sqrt{s^2-1}\left(e^{b\tau}+1\right) \\ -\mathrm{i}\left((s+1)e^{b\tau}-s+1\right) & \sqrt{s^2-1}\left(e^{b\tau}-1\right) & -\mathrm{i}\sqrt{s^2-1}\left(e^{b\tau}+1\right) & (s+1)e^{b\tau}+s-1 \end{pmatrix}, \tag{4.125}$$

with a new prefactor $\tilde{\alpha} = \frac{e^{-\frac{1}{2}(s+1)b\tau}}{4s}$ and where we have introduced s such that $\frac{1}{2}\tan\theta = \frac{1}{2}\sqrt{s^2-1}$, which is merely a more convenient parametrization for this result. Similarly to the two-site chain, we see that also the Green's function of the four-site chain depends on itself, namely on its values at $\tau = 0$. This dependence is encoded in the parameters s, b and, in turn, θ, which itself parametrizes a quotient of the interaction potential with arguments $-2\mathrm{i}G_{12}(0)$ and $-2\mathrm{i}G_{23}(0)$. More specifically, evaluating

(4.125) at $\tau = 0$ and exploiting the relation between s and θ, we find

$$G_{xy}(0) = \frac{1}{2}\begin{pmatrix} 1 & \mathrm{i}\sin\theta & 0 & \mathrm{i}\cos\theta \\ -\mathrm{i}\sin\theta & 1 & \mathrm{i}\cos\theta & 0 \\ 0 & -\mathrm{i}\cos\theta & 1 & \mathrm{i}\sin\theta \\ -\mathrm{i}\cos\theta & 0 & -\mathrm{i}\sin\theta & 1 \end{pmatrix} . \tag{4.126}$$

Once more, we can impose that both sides of this equation are equivalent, which leads to a self-consistency condition. Thanks to a our convenient choice of parametrization, and due to the reflection symmetry of the chain, we obtain a single SC equation even for the $L = 4$ case, which reads

$$\frac{\tan\theta}{2} = \frac{G_{12}(0)}{2G_{23}(0)} = \frac{h'_{12}(-2\mathrm{i}G_{12}(0))}{h'_{23}(-2\mathrm{i}G_{23}(0)))} . \tag{4.127}$$

As for the two-site chain, once solutions to the SC equation (4.127) are found, these yield the full Green's function for $\tau > 0$ via (4.125).

Four-site Chain: Self-consistent Solutions

It is pertinent to investigate the SC condition (4.127) in more detail. Although our methods are valid for generic choices of the interaction potential, and we will indeed keep most of the derivations general, it is pedagogical to also consider a specific example of a potential. In particular, we will consider the choice of an exponential interaction potential as our prime example for many explicit computations in this section. This potential reads

$$h_{x,x+1}(\xi) = \mu_x \left(1 - e^{J\xi}\right)/(2J) = h_{x+1,x}(-\xi) , \tag{4.128}$$

where $J > 0$ plays the role of an interaction strength. As for the two-site chain, it will prove helpful to extract the hopping parameters from the potential and define $h'_{x,x+1}(\xi) = \mu_x m(\xi)$, where the function $m(\xi)$ is given by $m(\xi) = -e^{J\xi}/2$ in the case of the exponential potential. The SC condition (4.127) now reads

$$r\, e^{J(\sin\theta - \cos\theta)} = \frac{1}{2}\tan\theta . \tag{4.129}$$

This is a transcendental equation for the parameter θ which has no solutions in closed form. Nonetheless, it can be solved numerically. We do this and plot the resulting solutions for different values of the interaction strength in Fig. 4.9. From this, we see that all curves pass through the point $(r = 1/2, \tan\theta = 1)$, because this is a fixed

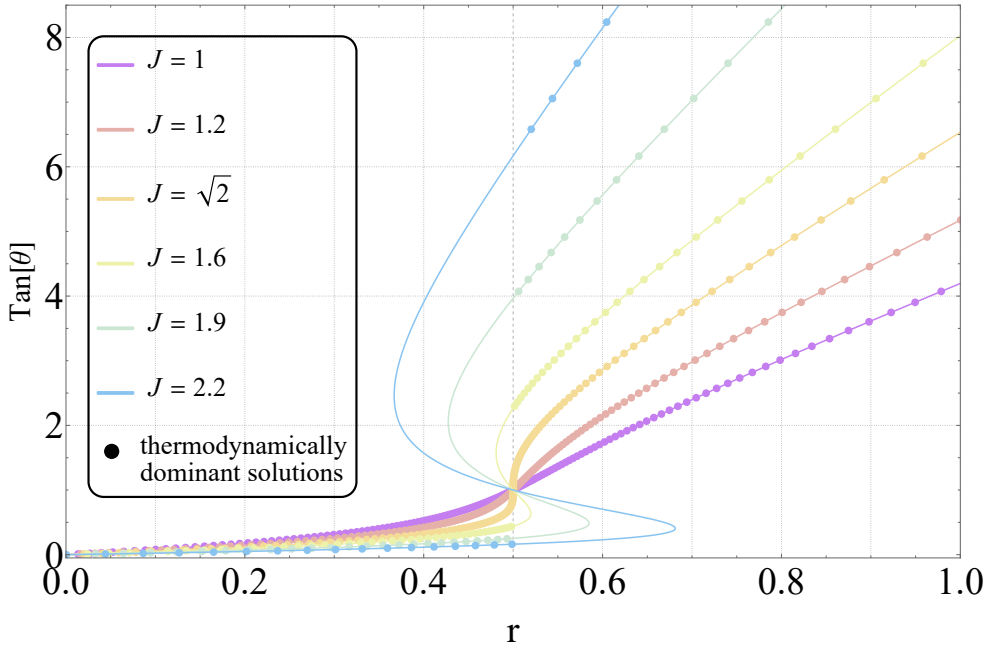


Figure 4.9: Exemplary set of solutions to the self-consistency equation (4.129) for an exponential potential with different interaction strengths, plotted as a function of the hopping ratio $r \equiv \mu_a/\mu_b$. We see that above a certain characteristic value $J = J_c = \sqrt{2}$, the SC equation admits three possible solutions, which are denoted by the solid lines. The solutions which minimize the free energy (4.139), which we derive in the next section, are represented by dots on these lines. We observe that these thermodynamically dominant solutions to the SC equation exhibit a discontinuous jump at $r = 1/2$ for $J > J_c$, foreshadowing that the systems undergoes a phase transition.

point of the SC equation due to $\sin(\pi/4) = \cos(\pi/4)$, which means that the equation is obeyed for any value of J. Furthermore, we observe that the set of solutions becomes multi-valued for large interaction strengths. This multi-valuedness is an explicit signal of a discontinuous behavior that the system exhibits as a function of r, which we may now see as a control parameter. More precisely, we can identify a critical value $J \equiv J_c = \sqrt{2}$ above which the SC equation has three possible solutions, while it only has a single solution for $J < J_c$.

In fact, we can exploit the fixed point of the SC equation to derive this critical interaction strength J_c for general forms of the interaction potential. Consider the generic potential $h'_x(\xi)$ with $x = a, b$ and ξ either $\sin\theta$ or $\cos\theta$. The SC equation (4.129) fixes the dependence of the hopping ratio r as a function of θ as

$$r(\theta) = \frac{1}{2}\tan\theta\frac{m(\cos\theta)}{m(\sin\theta)}\,, \tag{4.130}$$

where, importantly, only the function m appears, since we have explicitly extracted the hopping ratio. The critical point of the solutions can be attained by studying

the inflection points of the function $r(\theta)$ in (4.130). To do this, we impose that the first and second derivatives of the general function m vanish. In principle, this yields only two equations with three unknowns, namely $m(\xi(\theta^*))$, $m'(\xi(\theta^*))$ and $m''(\xi(\theta^*))$. Here, θ^* is a solution of (4.130), and ξ can be either $\sin(\cdot)$ or $\cos(\cdot)$. It is here that we can exploit the fixed point of the SC equation. Namely, given that all curves pass through the fixed point $(r, \theta) = (1/2, \pi/4)$, we may study the behavior of the system of equations derived above at exactly this point of $\theta^* = \pi/4$. This works because J_c is precisely an inflection point of $r(\theta)$, meaning that both its first and second derivatives should vanish. For the first derivative, we have

$$r'(\theta)|_{\theta=\frac{\pi}{4}} = 1 - \frac{m'\left(\frac{1}{\sqrt{2}}\right)}{\sqrt{2}m\left(\frac{1}{\sqrt{2}}\right)} \stackrel{!}{=} 0\,. \tag{4.131}$$

Note that in this expression, the arguments of $1/\sqrt{2}$ arise from evaluating $\sin(\pi/4) = \cos(\pi/4) = 1/\sqrt{2}$. Crucially, these last two functions yield the same value at $\theta^* = \pi/4$. For practical evaluations of explicit potentials, one should always first compute the derivative of the function $m(\xi)$ and only subsequently evaluate it at $1/\sqrt{2}$. This order is relevant because only after the insertion of an explicit potential do we introduce the interaction strength J into the equation. Based on this, (4.131) singles out the value J_c for that specific potential. The reason why this is now computable is because the constraint (4.131) is an ordinary algebraic equation, and no longer a differential equation. The general solution to this algebraic equation is given by $m'(1/\sqrt{2}) = \sqrt{2}\,m(1/\sqrt{2})$. Using this, we can evaluate the second derivative of $r(\theta)$ as

$$r(\theta)''|_{\theta=\pi/4} = \frac{m'\left(\frac{1}{\sqrt{2}}\right)^2}{m\left(\frac{1}{\sqrt{2}}\right)^2} - \frac{2\sqrt{2}m'\left(\frac{1}{\sqrt{2}}\right)}{m\left(\frac{1}{\sqrt{2}}\right)} + 2 \stackrel{!}{=} 0\,. \tag{4.132}$$

We can readily see that the equation (4.132) is immediately solved by the same solution as (4.131), namely a generic potential $m(\xi)$ evaluated at $r = 1/2$ and $\theta = \pi/4$. As a consequence, whenever the potential $m(\xi)$ obeys the condition $m'(1/\sqrt{2}) = \sqrt{2}\,m(1/\sqrt{2})$, as imposed by (4.131), then it is this condition which determines the value J_c for which the function $r(\theta)$ has an inflection point at $\theta = \pi/4$.

We can now exploit this general analysis and compute the critical interaction strengths for several different potentials. In our prime example of the exponential potential, we have $m(\xi) = -e^{J\xi}/2$, and one can straightforwardly solve (4.131) to obtain $J_c = \sqrt{2}$, as predicted above. We can also consider a more general class of potentials defined by truncations of the series expansion of the exponential function. Members of this class

of exponentials are labeled by their maximal order n and read

$$m(\xi) = -\frac{1}{2}\sum_{k=0}^{n}\frac{1}{k!}(J\xi)^k\,. \tag{4.133}$$

Physically, these truncations represent the cases where we have a finite number of interaction terms in the Hamiltonian (4.86). Plugging (4.133) into the condition (4.131), we obtain an equation determining J_c which reads

$$\sum_{k=0}^{n}\frac{k-1}{k!}\frac{1}{(\sqrt{2})^{k-1}}J^k = 0\,. \tag{4.134}$$

Therefore, the value of J_c for a generic member of the class of truncated polynomial potentials (4.133) is obtained by finding the roots of an exponential of order n with constant coefficients. Notably, this can be done analytically.

Four-site Chain: Free Energy and Phase Transition

Recall that the critical values of the interaction strength denote the point where the SC condition (4.127) starts to exhibit three possible solutions, signaling the onset of a new physical behavior in the system. To better characterize these solutions, and in particular to identify the self-consistent solution physically realized by the system, we to compute the free energy of the four-site chain for general interaction potentials. The upshot of this analysis is the identification of a phase transition of the system.
For this derivation, we follow the same steps as for the two-site chain in spirit, with the key difference being the effective action and the physical parameters entering the calculation. Namely, the last term of the effective action for the four-site chain reads

$$\begin{aligned}-\frac{1}{2}\sum_{x,y}\int d\tau h_{xy}(-2\mathrm{i}G_{xy}(0)) &= -\mathrm{Vol}(\tau)\Big(2h_a(-2\mathrm{i}G_{12}(0)) + h_b(-2\mathrm{i}G_{23}(0))\Big)\\ &= -\mathrm{Vol}(\tau)\mu_b\Big(2r\int^{X_{12}} d\xi m(\xi) + \int^{X_{23}} d\xi m(\xi)\Big) \equiv S_h[G](r)\,.\end{aligned} \tag{4.135}$$

To obtain this result, we have exploited the symmetries of G, those of the potential $h_{x,x+1}(\xi) = h_{x+1,x}(-\xi)$, and the reflection symmetry $G_{12}(0) = G_{34}(0)$. We are also using a similar form of writing the potential as in the two-site chain case, namely $h_{a,b}(\xi) = \mu_{a,b}\int^{\xi} d\xi' m(\xi')$. Here, we slightly abuse our notation in that the integrals are to be evaluated over the same function m, but they should be evaluated at different values $\xi = X_{12} \equiv -2\mathrm{i}G_{12}(0)$ and $\xi = X_{23} \equiv -2\mathrm{i}G_{23}(0)$. Since we are interested in the ground state of the four-site chain, the integrals over Euclidean time appearing in

(4.88) are to be seen as a formality. These are trivial to evaluate due to the δ-function dependence of the self-energy (4.121) on τ, and they yield a divergent yet constant contribution, which we denote as $\int d\tau \equiv \mathrm{Vol}(\tau)$. Finally, a factor of μ_b has been extracted from the expression in (4.135) in order to identify the hopping ratio r in the first term of the second line. The action can now be again split into three terms $-S_E/N \equiv S_{\mathrm{Pf}}[\Sigma] + S_G[G,\Sigma] + S_h[G](r)$, just as for the two-site chain case. In fact, we again avoid the evaluation of the Pfaffian determinant by performing a derivative with respect to the dimensionless hopping ratio r, which yields

$$r\frac{\partial}{\partial r}\left(-\frac{S_E}{N}\right) = r\frac{\partial\Sigma}{\partial r}\left(\frac{\delta S_{\mathrm{Pf}}}{\delta\Sigma} + \frac{\delta S_G}{\delta\Sigma}\right) + r\frac{\partial G}{\partial r}\left(\frac{\delta S_G}{\delta G} + \frac{\delta S_h}{\delta G}\right) + r\left(\frac{\partial S_h}{\partial r}\right). \tag{4.136}$$

Also in this case, the first two terms vanish when evaluated on-shell due to the fields G, Σ obeying the SD equations. The non-vanishing contribution to this derivative thus comes from the third term in its explicit dependence on the hopping ratio

$$\frac{\partial}{\partial r}\left(-\frac{S_E}{N}\right)_{|\text{on-shell}} = \frac{\partial}{\partial r}\left(S_h[G](r)\right)_{|\text{on-shell}} = -2\mathrm{Vol}(\tau)\mu_b\int^{X_{12}} d\xi m(\xi)\,. \tag{4.137}$$

As in the case of the two-site chain, evaluating this expression on-shell imposes $X_{12} = -2\mathrm{i}G_{12}(0)$, with the difference that now this entry is that of the four-site Green's function at $\tau = 0$, i.e. it is the $G_{12}(0)$ entry of (4.126).

The free energy of the system is now obtained by integrating back over r, for which we introduce a suitable parametrization in terms of θ. More precisely, we use $-2\mathrm{i}G_{12}(0) = \sin\theta$ and the fact that θ itself depends on r and the interaction potential via the relation (4.130). We can thus perform a change of variables which allows us to find the general form of the free energy for the four-site chain

$$\begin{aligned}\frac{\mathrm{Vol}(\tau)F}{N} &= 2\mathrm{Vol}(\tau)\mu_b\int_{r_0}^{r} dr'\left[\int^{X_{12}} d\xi\, m(\xi)\right]_{X_{12}=\sin\theta} \\ &= 2\mathrm{Vol}(\tau)\mu_b\int_{\theta_0}^{\theta} d\theta'\left[\frac{\partial r(\theta'')}{\partial\theta''}\right]_{\theta''=\theta'}\left[\int^{X_{12}} d\xi\, m(\xi)\right]_{X_{12}=\sin\theta}.\end{aligned} \tag{4.138}$$

We encountered a similar expression to (4.138) for the two-site system, although in that case, the integral was simple enough to be evaluated without an explicit choice of the functions h or m. The four-site case is slightly less straightforward in this sense, and an explicit evaluation of (4.138) requires the choice of a specific interaction potential. Nonetheless, the expression is general and works for any such choice.

We are now in position to evaluate the free energy (4.138) for different interaction potentials and study the behavior of the system while tuning the interaction strength

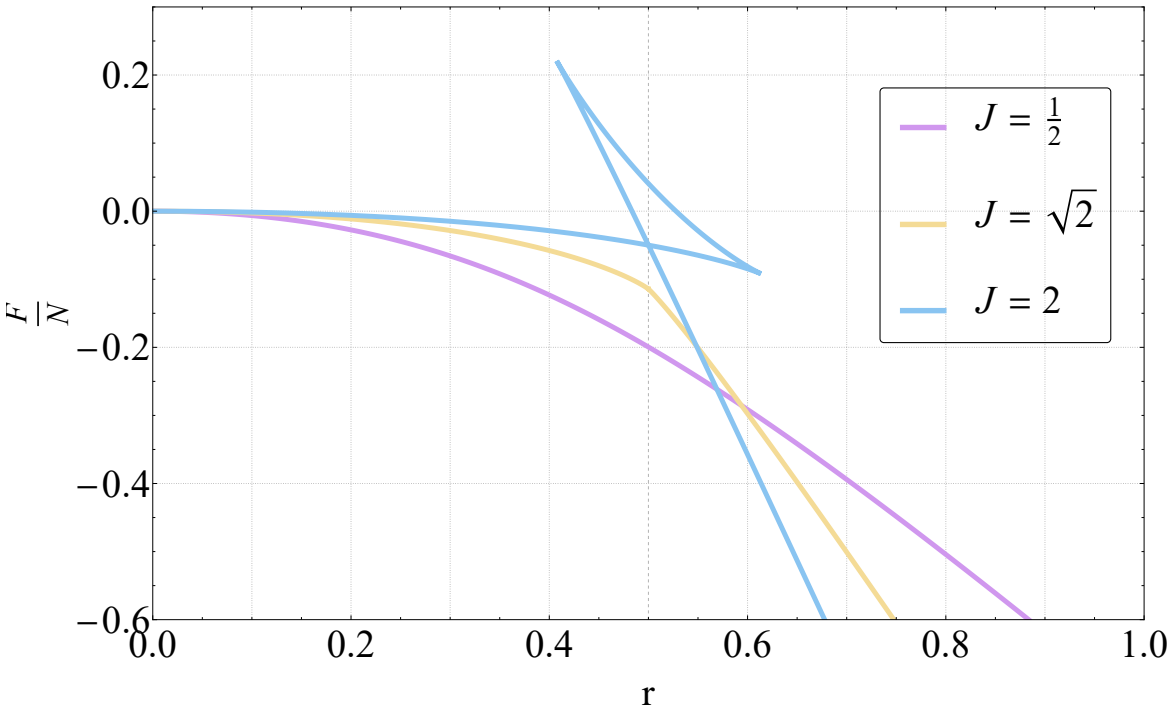


Figure 4.10: Free energy (4.139) of the four-site chain with exponential potential $h_{x,x+1}(\xi) = \mu_x \left(1 - e^{J\xi}\right)/(2J)$ for different interaction strengths $J = \{\frac{1}{2}, \sqrt{2}, 2\}$ as a function of the hopping ratio r. The free energy functional exhibits non-analytic behavior at $r \equiv \mu_a/\mu_b = 1/2$ for J above the critical value $J_c = \sqrt{2}$, indicating that the system undergoes a first order phase transition. At the critical point $J = \sqrt{2}$, the transition is second order.

across its critical value derived from (4.131). Recall that for $J > J_c$, the self-consistent solution which minimizes the free energy functional is the thermodynamically dominant configuration actually realized by the system. We begin with our familiar example of the exponential interaction potential, for which we have $m(\xi) = -e^{J\xi}/2$, with integral form given by $h_x(\xi) = \mu_x \int d\xi' m(\xi') = \frac{\mu_x}{2J}(1 - e^{J\xi})$, as in (4.128). Evaluating (4.138) with these expressions, we obtain the free energy

$$\frac{F}{N} = \frac{\mu_b}{2J}\left[\tan(\theta)e^{J(\cos(\theta)-\sin(\theta))} - (\tan(\theta)+1)e^{J\cos(\theta)} + e^{J}\right], \tag{4.139}$$

where the last term e^J is a consequence of evaluating the integration constant at $\theta = 0$,

$$\left[\tan(\theta_0)e^{J(\cos(\theta_0)-\sin(\theta_0))} - (1+\tan(\theta_0)e^{J\cos(\theta_0)})\right]\Big|_{\theta_0=0} = -e^{J}. \tag{4.140}$$

We plot the free energy (4.139) for $\mu_b = 1$ in Fig. 4.10 for different values of the interaction strength J above, at, and below the critical value J_c. Indeed, we find confirmation that the system undergoes a quantum phase transition [885] at $r = 1/2$ for

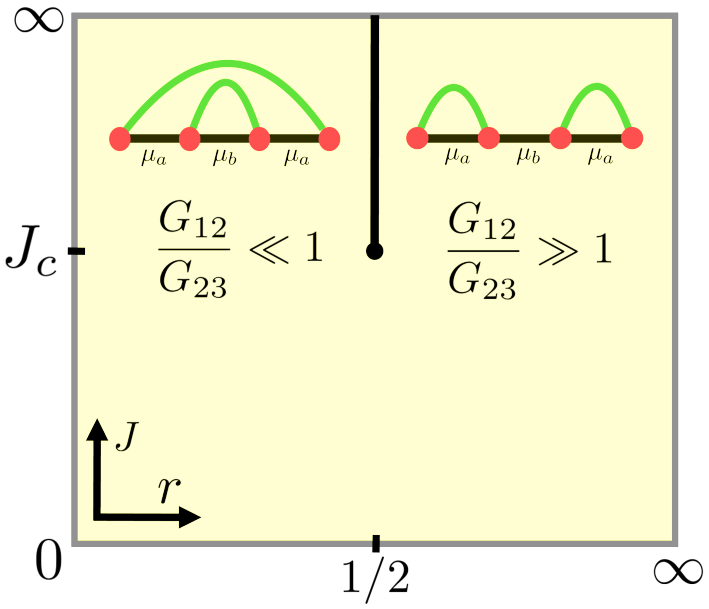


Figure 4.11: Phase diagram for the four-site chain spanned by the hopping ratio r and the interaction strength J. At $r = 1/2$ and at the critical interaction strength $J = J_c$, a black dot denotes a second order phase transition, while the solid black line for $J > J_c$ represents the continuous line of first order phase transitions. We expect similar phase diagrams for any choice of interaction potentials, upon substitution of the corresponding value of J_c (if it is not infinite).

$J \geq J_c$, which manifests itself in a non-analyticity of the on-shell free energy. This is a consequence of the multi-valuedness of the solutions to the SC equation (4.127). The thermodynamically dominant SC solutions are those which minimize the free energy, and we have preemptively depicted these as dots in Fig. 4.9. This then manifestly shows a discontinuity in the physically realized solutions to the SC condition, which is a further manifestation of the phase transition undergone by the system. More precisely, from the form of the free energy in Fig. 4.10, we can see that at the critical point $J = J_c$, the quantum phase transition is of second order, while it is first order for $J > J_c$. The system is then characterized by two phases, namely for $r < 1/2$ and $r > 1/2$, where the distinguishing features of the system in each phase can be retrieved from the function $(\tan(\theta))(r)$. In particular, in the $r < 1/2$ phase, $\tan\theta$, and therefore also θ, is small. As a consequence, the correlations dominating the system according to (4.126) are G_{23} and G_{14}. In contrast, in the phase with $r > 1/2$, the parameter $\tan\theta$ is large, implying that θ is close to $\pi/2$. Comparing once again with the Green's function of the four-site system given in (4.126), this implies that the correlations $G_{12} = G_{34}$ are the dominant ones in this phase. This correlation structure arising in the limiting regimes of $r \to 0$ and $r \to \infty$, which characterizes the two phases of the system, is embedded within the phase diagram of the model shown in Fig. 4.11.

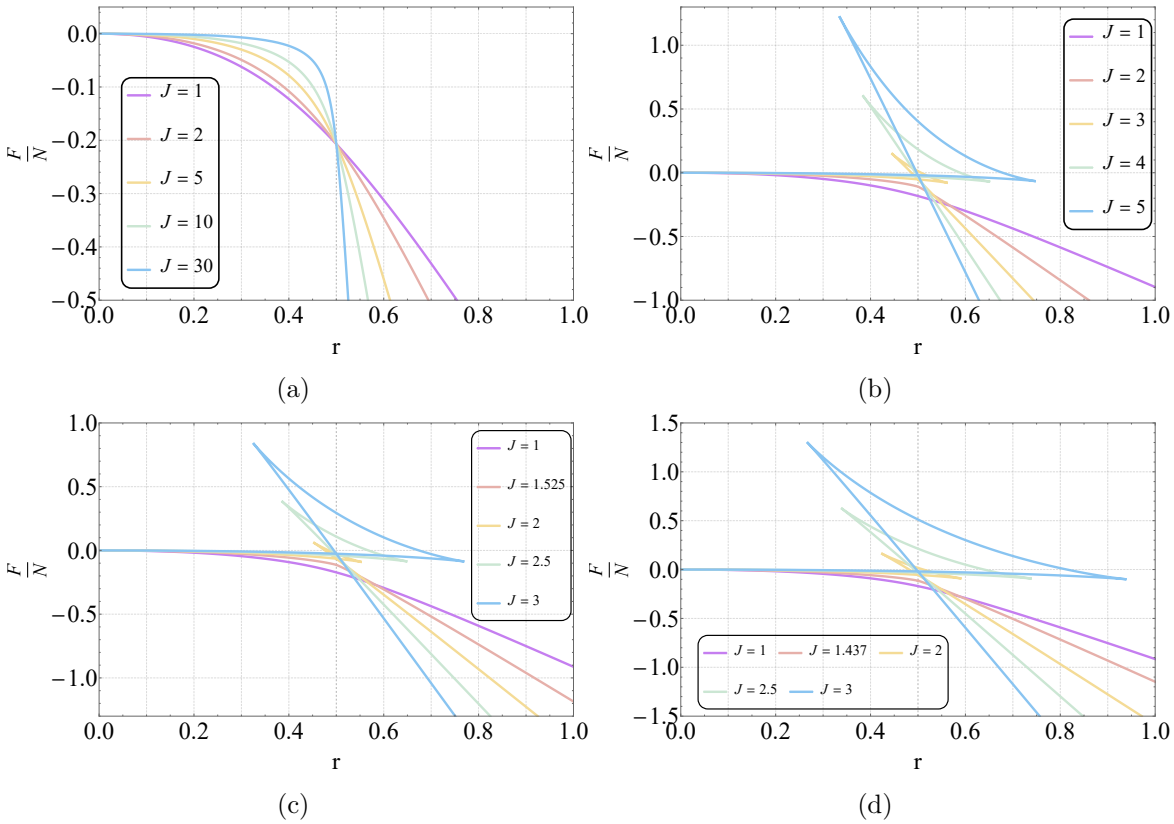


Figure 4.12: Free energies computed from (4.138) for linear (4.12a), quadratic (4.12b), cubic (4.12c), and quartic (4.12d) interaction potentials, as specified by the function m in the form (4.133). The critical interaction strengths vary for each truncation, with $J_c = \infty$ for the linear, $J_c = 2$ for the quadratic, $J_c \sim 1.525$ for the cubic, and $J_c \sim 1.437$ for the quartic potential. For higher-order potentials, these values tend to $J_c = \sqrt{2}$ which is the critical interaction for the exponential potential.

Finally, let us highlight that this phase transition is indeed a generic feature of our model, and we can find it also for other examples of interaction potentials. To exemplify this, we will exploit our derivation of the critical interaction strength for truncated potentials m of the form (4.133) given in (4.131), to evaluate the general free energy (4.138) for this class of potentials. In particular, we consider the specific examples where m is a linear, quadratic, cubic and quartic potential, corresponding to the choices $n = 1, 2, 3, 4$ in (4.133), respectively. We restrict ourselves to a graphical analysis for these cases, since the analytical expression of the free energy functional is not very enlightening. The free energy obtained from (4.138) for these four potentials is shown in Fig. 4.12. The critical interaction strengths J_c were obtained from (4.134), and each plot shows the free energy below, at, and above this value to manifestly illustrate the onset of the phase transition. Notice that the case of a linear interaction potential is the only one which does not exhibit such a phase transition, since its corresponding interaction strength is $J_c = \infty$. The linear potential m with $n = 1$ in

(4.133) still describes an interacting Hamiltonian, since h is obtained by integrating m, which effectively yields a four-fermion interaction in (4.86). Still, this interaction seems to not be drastic enough to induce a phase transition at any finite value of the interaction strength. As one may have expected from their functional form, the critical values for the truncated potentials approach that of the exponential potential as their order is increased. This is of course a consequence of the fact that the series (4.133) approaches the series expansion of the exponential function when $n \to \infty$. For the other three choices of interaction potential shown in Fig. 4.12, we in fact observe a phase transition at $r = 1/2$ for $J \geq J_c$. Also in these cases the object characterizing the respective phases is the dominant correlation structure shown in Fig. 4.11, as we have explained above for the case of the exponential potential.

Four-site Chain: Entanglement Entropy

Following the motivation put forward in the beginning of this section, we turn our attention to the study of the entanglement entropy in the ground state of the four-site chain, in the hope that it can function as a detector of the phase transition found above. We consider a connected subregion A consisting of two sites, which we take to be $x = 1, 2$. When seen as a subsystem of a larger chain, we expect to reduced density matrix ρ_A associated to subregion A to take the form of a thermal density matrix of the form given in (4.96). However, now we can give a new interpretation to the function H, namely it plays the role of the so-called *one-sided modular Hamiltonian*, also known as the *entanglement Hamiltonian*, cf. (2.55) in Sec. 2.3.1. We will use these terms interchangeably in the following, and also refer to the one-sided modular Hamiltonian simply as the modular Hamiltonian. It is a celebrated result from Peschel [886] that this entanglement Hamiltonian is entirely determined by the Green's function restricted to subregion A in the case where H describes a free model, i.e. a free fermionic system with $J = 1$. In fact, it is instructive to consider this free case in more detail, as many conclusions may be drawn from it which we can later use for our analysis of the general interacting case.

In the free case, the ground state of the model (4.86) factorizes into the individual contributions from each of the Majorana fermion colors $j = 1, \ldots, N$, implying that the model can be solved exactly for any value of N. The function $h(\xi)$ is simply a linear function, and the Hamiltonian is quadratic in the fermions. This quadratic structure of the model allows us to write an ansatz for the reduced density matrix of

the two-site subsystem A of the form

$$\rho_A = \frac{e^{-\sum_{x,y=1}^{2} K_{xy} \sum_{j=1}^{N} \psi_x^j \psi_y^j}}{Z}\,, \tag{4.141}$$

where the 2×2 matrix K_{xy} is the only unknown object governing this ansatz for ρ_A. In (4.141), the sites in the subsystem are sites 1 and 2, and Z ensures the normalization $\mathrm{Tr}\rho_A = 1$. In the sum over the colors, we can exploit the fact that $(\psi_x^j)^2 = 1/2$ due to the anti-commutation relations, and the constant resulting from these terms can be reabsorbed in the normalization. This simplifies the expression for ρ_A to

$$\rho_A = \frac{e^{-(K_{21}-K_{12})\sum_{j=1}^{N} \psi_2^j \psi_1^j}}{Z} = \frac{e^{-2\mathrm{i}\kappa \sum_{j=1}^{N} \psi_2^j \psi_1^j}}{Z}\,, \tag{4.142}$$

where we defined $K_{12} = -K_{21} \equiv -\mathrm{i}\kappa$. We can now see explicitly that ρ_A factorizes into N identical terms because $[\psi_2^j\psi_1^j, \psi_2^i\psi_1^i] = 0$. Correspondingly, the partition function of the system factorizes as well into equal contributions from each color, leading to

$$Z = (2\cosh\kappa)^N\,. \tag{4.143}$$

In the absence of interactions, it is an acclaimed result that the matrix K, which is the entanglement Hamiltonian of our system, is entirely determined by the two-point functions of degrees of freedom within the subsystem A [886], effectively as a consequence of Wick's theorem [44, 887]. More precisely, for fermionic Gaussian states, we have the relation

$$K^{\mathrm{T}} = \frac{1}{2}\log\left([G_A(0)]^{-1} - \mathbb{1}\right)\,, \tag{4.144}$$

where $G_A(0)$ is the matrix of two-point functions with indices restricted to the subsystem A and $\mathbb{1}$ is the identity matrix of the same size as $G_A(0)$. This relation also fixes the parameter κ. We can relate κ to the Green's function within subsystem A by using (4.142), finding

$$G_{21}(0) \equiv \frac{1}{N}\sum_{j=1}^{N}\langle\psi_2^j\psi_1^j\rangle = \frac{\mathrm{i}}{2}\tanh\kappa\,. \tag{4.145}$$

For the free case, the above equation is fulfilled by the mere construction of (4.141) [886]. However, as we will see later, in the interacting case it can be interpreted as a constraint on our original ansatz, imposing that the reduced density matrix reproduces the two-point functions we obtain from the SD equations. Knowing $G_{21}(0)$ from

(4.126), we can determine the parameter κ in terms of the parameters of the model as

$$\kappa = \frac{1}{4}\log\left(\frac{\cos(2\theta)+4\sin(\theta)-3}{\cos(2\theta)-4\sin(\theta)-3}\right), \tag{4.146}$$

where we recall that θ is related to the hopping ratio via $\frac{\mu_a}{\mu_b} = \frac{1}{2}\tan\theta$ in the free case. Having determined the parameter κ, we can proceed to compute the entanglement entropy by simply inserting κ back into our ansatz (4.141), diagonalizing the associated entanglement Hamiltonian K, and plugging the results into the definition of the entanglement entropy (2.53) [230]. Doing this, we obtain the following expression for the entanglement entropy between subsystem A and its complement

$$S_A = N\left[\log\left(1+e^{2\kappa}\right) - \kappa\left(1+\tanh\kappa\right)\right]. \tag{4.147}$$

A few comments on this result are in order. First, since the only non-vanishing two-point functions are those between Majoranas of the same color index $j = 1,\ldots,N$, their contributions are equal for any j and factorize, meaning that $G_{xy}(0) = \langle\psi_x^j\psi_y^j\rangle$ for any $j = 1,\ldots,N$. This justifies our use of the result (4.144), which lead us to (4.147). Second, in the interacting case, our ansatz for the reduced density matrix (4.141) is no longer valid. This is because, in the presence of interactions, the correlations between subsystem A and its complement can be created by any function of operators of degrees of freedom within A, and not only the fermion bilinear. In fact, for a general interacting system, as is the case for our model (4.86) when h is generic, the explicit form of the entanglement Hamiltonian K is not known. We may only assume that K will be a function of all the possible observables we can construct from Majoranas living in subregion A, since these are the ones that can potentially contribute to the entanglement entropy. This is precisely what the general ansatz (4.96) takes into account. Note that although we introduced (4.96) for the isolated two-site chain, it can be more generally interpreted as an ansatz for the reduced density matrix of any two-site subregion embedded in a larger chain. The constraint (4.145) can now be generalized to impose that the ansatz reproduce the correlations given by the Green's function (4.126) restricted to the subregion A, which we know from their independent computation via the SD equations. The general constraint is

$$G_{xy}(0) = \frac{1}{N}\sum_j \mathrm{Tr}\left(\rho_A\psi_x^j\psi_y^j\right), \qquad x,y\in A, \tag{4.148}$$

with ρ_A given in (4.96). Remarkably, this constraint imposes that κ is related to θ in exactly the same way as in (4.146), with the only difference being that the parameter

θ should now be a solution to the general self-consistency equations in the interacting case (4.127). As a consequence, the expression (4.147) for the entanglement entropy holds also in the interacting case, and in fact it has the given form for any choice of the interaction potential. In accordance with our expectation that the reduced density matrix of a subregion should generally look thermal, we can indeed verify that the entanglement entropy (4.147) for subregion A in the four-site chain at zero temperature is precisely the entropy (4.112) of an isolated two-site chain at finite temperature upon identifying $\kappa = \operatorname{arctanh}(X)$, with $X = -2\mathrm{i}G_{12}(0)$ a solution of (4.127). However, although (4.147) is valid for any value of N in the free case, it is only true at leading order in N in presence of interactions. This is simply a consequence of the fact that the SD equations, which give rise to our self-consistency conditions, are valid only at large N. Nevertheless, the result (4.147) is highly remarkable in that even without knowing the explicit form of ρ_A (remember, we did not specify K, but only constrained it via (4.148)) we are able to compute the entanglement entropy of a two-site subregion for arbitrary choices of interaction potentials in (4.86).

Having derived the entanglement entropy of subregion A, it is instructive to plot it as a function of the hopping ratio r, similarly to how we have done it for the free energy. If our expectations are correct, the entanglement entropy should be able to detect that the system is undergoing a phase transition. In Fig. 4.13, we plot the entanglement entropy as per (4.147) (or, respectively (4.112)) as a function of r for different values of the interaction strength J. Note that we have chosen the exponential potential for the explicit evaluation of S_A shown in Fig. 4.13. Although the functional dependence of S_A on κ, and subsequently on θ, is the same for every interaction parameter, the fact that θ is a solution to the SC equations (4.127) implicitly introduces a dependence on the particular critical value for each given potential. In other words, even though $\theta \in [0, \pi/2)$ always, the precise value at which we start having multiples self-consistent solutions, i.e. J_c, depends on the specific choice of the potential, and this dependence gets reflected in the behavior of the entropy. From the behavior in Fig. 4.13, we see that the entanglement entropy indeed detects the phase transition of the system, a fact manifested by the discontinuous jump of S_A at $r = 1/2$ for $J > J_c = \sqrt{2}$.

Let us conclude this discussion on the entanglement entropy by considering some limiting behaviors of this quantity, which can, in part, be already deduced from the plots in Fig. 4.13. First, let us consider the case $r \to 0$. From the relations (4.130) and (4.146), we see that $r \to 0$ also implies $\theta \to 0$ and $\kappa \to 0$. As a consequence, we also have $X \to 0$ due to (4.145). In this case, and at leading order in N, the entanglement entropy approaches its maximal value of $\log 2$, as can be seen from (4.147). More precisely, we have $S \to N \log 2 + \mathscr{O}(1)$ when $|X| \to 0$, where the

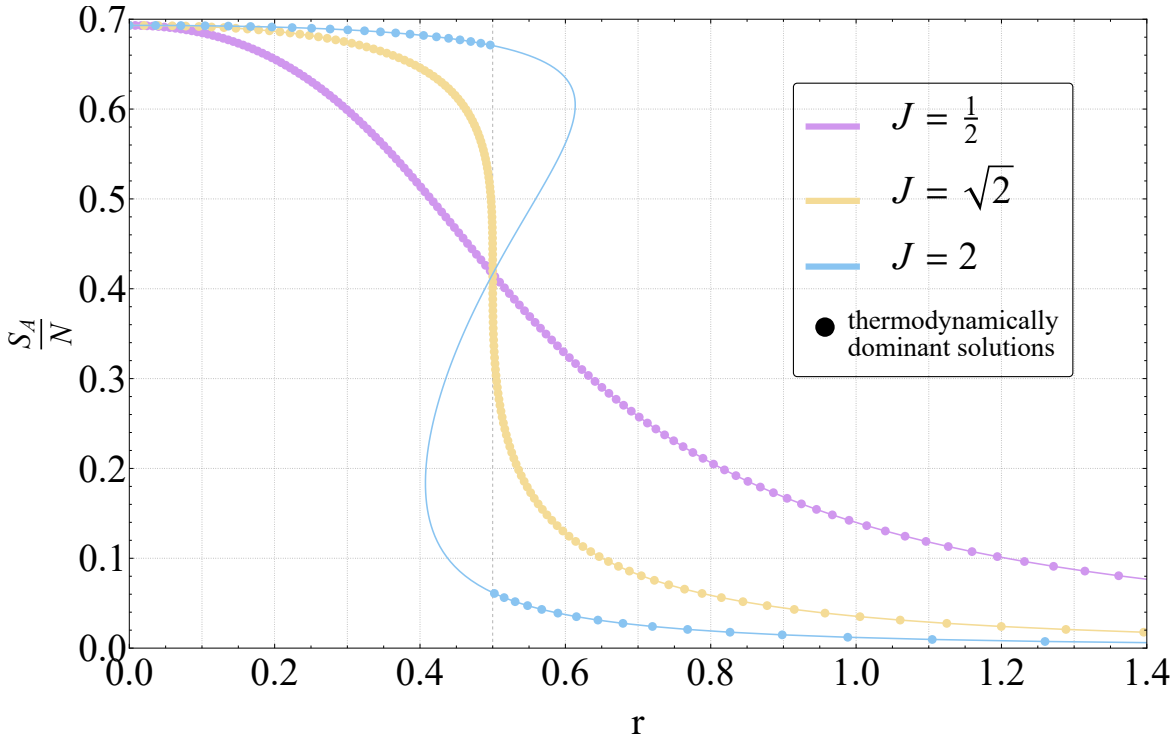


Figure 4.13: Entanglement entropy of subregion A of the four-site chain computed from (4.147) evaluated on self-consistent solutions $\kappa(\theta)$ to (4.127), plotted as a function of the hopping parameter $r \equiv \mu_a/\mu_b$ for different values of the interaction strength $J = \{\frac{1}{2}, \sqrt{2}, 2\}$. These values are exemplary for the exponential potential, but the results hold for any interaction potential. We use solid lines to denote the entanglement entropy evaluated on all SC solutions, while a sample of physical solutions minimizing F in Fig. 4.10 is denoted by dots. The discontinuous jump of the latter at $r = 1/2$ for $J > J_c$ manifestly shows how the entanglement entropy indeed detects the phase transition undergone by the system.

subleading corrections are given by (4.120). For the opposite case of $r \to \infty$, we have the following implied behaviors according to (4.130), (4.145) and (4.146): $\theta \to \pi/2$, $\kappa \to -\infty$ and consequently $X \to 1$. In this case, the entanglement entropy (4.147) goes to zero, which can also be at least qualitatively expected from Fig. 4.13. We can in fact be more precise about this limiting behavior. Namely, $r \to \infty$ corresponds to $\mu_b \to 0$ in terms of the hopping parameters of the chain. Setting $\mu_b = 0$ in the Hamiltonian (4.86), and only subsequently taking the large N limit, it turns out that we again retrieve the same SD equations (4.89)-(4.90). This means that the limit $\mu_a/\mu_b \to \infty$ and $N \to \infty$ commute. However, if $\mu_b = 0$ in the Hamiltonian (4.86), this means that we have two completely decoupled blocks consisting of sites 1 and 2 on the one side and sites 3 and 4 on the other, each coupled by a hopping parameter μ_a. This system is manifestly factorized with an evidently separable ground state, and therefore $S_A = 0$. Since the limits commute, we expect this result to remain present

even if we first take $N \to \infty$ and then $\mu_a/\mu_b \to \infty$, i.e. $X \to 1$. In parallel, the diagrammatics of the self-energy shown in Fig. 4.8 imply that the self-energy Σ_{xy} with $x = 1, 2$ and $y = 3, 4$, including the $1/N$ series expansion, vanishes when $\mu_b \to 0$. As a consequence, the correlations G_{xy} with $x = 1, 2$ and $y = 3, 4$, including their $1/N$ corrections, also vanish in the limit $\mu_b \to 0$. Thus, we can claim that $S_A \to 0$ exactly when $X \to 1$ at all orders in $1/N$.

4.3.4. Transitions of von Neumann Algebras

The analysis of Sec. 4.3.3 reveals that rich physical phenomena arise in our model even for the case of small system sizes like $L = 2$ and $L = 4$. The limit of large N takes on the role of a thermodynamic limit and, in combination with the presence of interactions, it allows us to find a quantum phase transition between two starkly different correlations structures. Moreover, we have shown that the entanglement entropy S_A, which we compute for an arbitrary choice of interaction potentials, can detect this phase transition by becoming a discontinuous function of the hopping ratio r above a critical interaction strength J_c. However, since the large N limit is to be taken first for all our calculations, the entanglement entropy diverges. This is a known feature appearing both in quantum field theory [757, 830], and in quantum systems in the thermodynamic limit [828]. As foreshadowed in Sec. 4.3.1, the language of local operator algebras plays an important role in these instances, allowing to still retrieve meaningful information about the entanglement properties of a system, even when the dimensionality of the Hilbert space is infinite. We are therefore motivated to apply the content of Sec. 4.3.1 to our interacting Majorana models and investigate the different types of local operator algebras that underlie it.

Modular Operator for Free Case

We begin by briefly defining the operators that will play a role in the following construction. Our construction here parallels that of [830], which we have reviewed in Sec. 4.3.1. Similarly to our exposition above for the entanglement Hamiltonian, it is instructive to perform our analysis first on the free case, where the arguments of [754, 832, 833, 859] can be reproduced exactly in our context. In particular, we can study the modular operator Δ, together with its spectrum, to deduce the types of von Neumann algebras underlying our model.

We consider the four-site chain, and are interested in the two-site subregion A consisting of sites $x = 1, 2$. We associate to this subregion an algebra of bounded local operators, denoted by $\mathcal{A}_A$. The operators contained in $\mathcal{A}_A$ are all products of finitely many Majorana fermions located in subregion A. Examples of these operators are a

single Majorana fermion of color j on the first site, ψ_1^j, or the product the fermion bilinear in A for five different Majorana colors, i.e. $\prod_{j=1}^5 \psi_1^j \psi_2^j$. Following [830], we think of these operators as acting non-trivially only on a finite number of indices j of color space (or limits of such operators). In turn, they will act trivially, e.g. via the identity operator, on a countably infinite number of indices j. At finite N, this algebra fulfills the requirements of being a von Neumann algebra, and in particular it is a von Neumann algebra of type I_d, where $d = 2^{2N}$ is the dimension of the Hilbert space of the four-site chain. We are interested in identifying the von Neumann type of the algebra $\mathcal{A}_A$ when taking the strict large N limit, and in particular whether this type changes for different points throughout the phase diagram.
For this, we study the object known as the modular operator Δ, defined as

$$\Delta = \lim_{N\to\infty} \rho_A \otimes \rho_B^{-1} \,, \tag{4.149}$$

where ρ_A, ρ_B are the reduced density matrices of subregion A and its complement B, respectively, and ρ_A is given by (4.142) in the absence of interactions. In our four-site chain, the matrix ρ_B is of the same form as ρ_A. When the system is free, i.e. $J = 0$, the ground state of the four-site chain factorizes into infinitely many individual contributions from each color, where each contribution is however associated to a vector in a finite-dimensional Hilbert space. This is precisely the structure that allows us to exploit the arguments put forward in [832, 833, 859] to identify the von Neumann algebra type of $\mathcal{A}_A$ based on the spectrum of the modular operator (4.149). Using (4.142) and inserting it into (4.149), we find

$$\Delta = \lim_{N\to\infty} \bigotimes_{j=1}^{N} \begin{pmatrix} 1 & 0 & 0 & 0 \\ 0 & e^{-2\kappa} & 0 & 0 \\ 0 & 0 & e^{2\kappa} & 0 \\ 0 & 0 & 0 & 1 \end{pmatrix} . \tag{4.150}$$

The spectrum of this operator is given by

$$\mathrm{Spec}(\Delta) = \lim_{N\to\infty} \{\lambda^n\}_{n=-N}^{N} \,, \tag{4.151}$$

where we defined $\lambda = e^{2\kappa}$, and degeneracies of eigenvalues are not taken into account. We see that the eigenvalues λ^n explicitly depend on the parameter κ which determines our ansatz for the reduced density matrix via (4.142). Moreover, recall that this parameter is uniquely tied to the entanglement entropy as computed in (4.147), emphasizing once more the connection between entanglement and von Neumann algebras. Exploit-

ing the relation between κ and the two-point function within the subregion A, given by $X = -2\mathrm{i}G_{12}(0)$, we find a direct relation between the eigenvalues of the modular operator and the correlation functions, which reads

$$\lambda = \frac{1-X}{1+X}\,. \tag{4.152}$$

It is pertinent to discuss the behavior of the spectrum for some of the special values of κ, or equivalently X, for which we have also studied the value of the entanglement entropy. In particular, based on the results of [832, 833, 859], the values of the spectrum of Δ can be used to immediately classify the type of von Neumann algebra for $\mathcal{A}_A$. When $\kappa = 0$, we also have $X = 0$ and thus all eigenvalues (4.152) of the modular operator Δ are equal to one. This means that the underlying operator algebra $\mathcal{A}_A$ is of type II_1. For the intermediate regime where $-\infty < \kappa < 0$, we correspondingly have $0 < X < 1$ (we drop the absolute value for clarity). The spectrum (4.152) in this case is of the form λ^n with $n \in \mathbb{Z}$, where $0 < \lambda \equiv e^{2\kappa} < 1$. This exact form of the spectrum of the modular operator corresponds to von Neumann algebras of type III_λ. Finally, in the limit of $\kappa \to -\infty$, we have $X = 1$, which is the case where our reduced density matrix (4.142) turns into a product of projectors, yielding a vanishing entanglement entropy as a consequence. Since the entanglement entropy vanishes, it is in particular finite while the Hilbert space is still infinite-dimensional, thus indicating that the operator algebra $\mathcal{A}_A$ is of type I_∞.

These quantitative results show that the phase diagram Fig. 4.11 supports several types of von Neumann algebras, at least at the very bottom where $J = 0$, i.e. the free case. The argument given above is completely equivalent to that put forward in [830] in terms of the trace functional on the algebra, which we have also reviewed in Sec. 4.3.1. In fact, we will use the latter to extend our analysis also to the interacting case and find the type of von Neumann algebra associated to $\mathcal{A}_A$ throughout the entire phase diagram. This is because, in the interacting case, the modular operator is not known, since we do not have access to the explicit form of the reduced density matrix for general interacting models. Nevertheless, in the next section, we provide heuristic arguments based on our results for the entanglement entropy that allow us to also deduce the von Neumann type of $\mathcal{A}_A$ in the presence of interactions.

Algebra Typification Throughout the Phase Diagram

We proceed with the algebra typification of $\mathcal{A}_A$ for generic interaction potentials. Our classification is founded on the quantitative results found above for the free case, but it is more amenable to express it in the terms used in [830]. More precisely, as ex-

plained in Sec. 4.3.1, the three types of von Neumann algebras can be identified by their amount of entanglement entropy and the existence or non-existence of a trace functional on the algebra. For this, we will exploit our results (4.147) on the entanglement entropy of the ground state of the four-site chain to argue for the properties of the Hilbert space $\mathcal{H}$ constructed from acting with the algebra $\mathcal{A}_A$ on this ground state. In this way, we identify the type of von Neumann operator algebra associated to subregion A for different values of the correlation function $X = -2iG_{12}(0)$ throughout the phase diagram of the model. The resulting classification is shown in Fig. 4.14.

Let us begin by stressing that the operators in the algebra are fixed throughout this entire construction. Different types of von Neumann algebra are not a consequence of the algebra $\mathcal{A}_A$ containing new operators. Rather, it is a consequence of how the fixed set of operators of the algebra acts on the ground state of the theory, such that different ground states will give rise to Hilbert spaces with distinct structure, even though they were constructed from the action of the very same operators. By changing the value of r, we simultaneously vary the quantity X describing the two-point function within subregion A. This itself changes the precise ground state on which the algebra $\mathcal{A}_A$ acts, and can therefore lead to $\mathcal{A}_A$ being a different type of von Neumann algebra depending on the value of X. Having emphasized this formal aspect, we proceed with the classification of von Neumann algebras throughout the phase diagram of our model. Consider the limit $X \to 1$. As we showed in Sec. 4.3.3 and can also be seen from (4.147), the entanglement entropy vanishes $S_A \to 0$ identically to all orders. We have also argued above that this is quite reasonable since $X \to 1$ implies $r \to \infty$ by (4.129)), meaning that $\mu_b \to 0$, and we therefore expect the two subsystems A and B to completely factorize. Due to the large N limit, which is to be taken first throughout these computations, the Hilbert space of the model is infinite-dimensional. Nevertheless, the vanishing entropy is in particular finite, and we therefore conclude that $\mathcal{A}_A$ is a type I_∞ algebra when $X \to 1$. Let us now turn to the other end of the phase diagram and examine the limit $X \to 0$, which also implies $r \to 0$. As a first observation, we notice that the ground state is no longer factorized as soon as $X < 1$. Moreover, the entropy (4.147) is infinite due to the large N limit, which immediately rules out $\mathcal{A}_A$ being of type I for any value $X < 1$. Following the arguments of [830], we may specify the type of von Neumann algebra by the possibility of constructing a proper trace functional tr on $\mathcal{A}_A$. In particular, whenever the maximally entangled state $|\Psi\rangle$, defined in (4.82), is contained in the Hilbert space generated by the algebra $\mathcal{A}_A$ acting on the ground state of our model, we can use it to define such a trace functional via $\mathrm{tr}(\mathfrak{a}) \equiv \langle\Psi|\mathfrak{a}|\Psi\rangle$, with $\mathfrak{a} \in \mathcal{A}_A$, as done in (4.83) [830]. Note that when $X = 0$, although we do not know the explicit expression of our ground state, we know

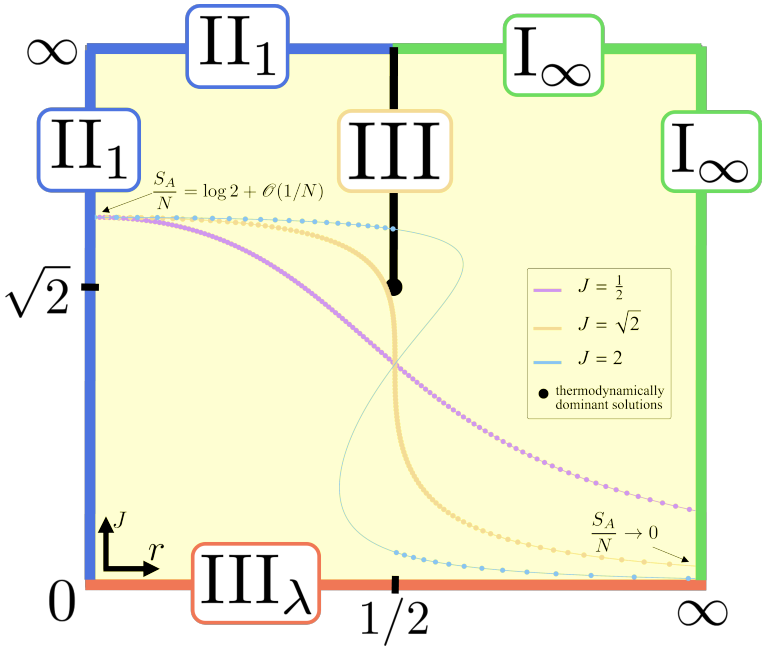


Figure 4.14: Phase diagram of the four-site chain decorated with the type of the von Neumann algebra $\mathcal{A}_A$ associated with subregion A, in the exemplary case of an exponential potential. Several transitions between different types of algebras are observed. The results for the free $J = 0$ case based on the spectrum (4.151) of the modular operator yield the type III_λ region at the bottom of the diagram (red). Given the key role of the entanglement entropy density S_A/N in this classification, we overlay the main curves of Fig. 4.13 onto the diagram. This overlay shares the $r = 0$ and $r = 1/2$ points with the axis of the phase diagram, while the $r > 1/2$ region of the curves is meant as a mere hint at the overall behavior of the curves when $r \to \infty$. At $r = 0$, we have $S_A/N = \log 2 + \mathscr{O}(1/N)$ for any value of J as per (4.147) and (4.120), and the underlying algebra is a von Neumann algebra of type II_1 (blue). In contrast, when $r \to \infty$, we have a vanishing entanglement entropy at all orders and for all J, implying a von Neumann algebra of type I_∞ (green). For finite interaction strengths $J < \infty$, the intermediate region $0 < r < \infty$ exhibits infinite but not maximal entanglement entropy. Its underlying algebra is therefore of type III (entire yellow region). Finally, in the strong coupling limit $J \to \infty$ (top of diagram), where the entropy becomes a step function $S_A/N = \log 2\,\Theta(1/2 - r)$, we unveil a direct transition of algebras $\mathrm{II}_1 \leftrightarrow \mathrm{I}_\infty$ at $r = 1/2$, which precisely coincides with the phase transition of the system.

that the entanglement entropy in this state is infinite *and maximal* up to subleading corrections in $1/N$, as shown in (4.120). Therefore, we can argue that our ground state can be mapped to the maximally entangled state $|\Psi\rangle$ by applying a finite number of Majorana operators located in subregion A, i.e. elements of the algebra $\mathcal{A}_A$. This is possible because such operators cannot change the amount of entanglement, something that would require operators acting on both A and B simultaneously. Since $|\Psi\rangle$ can be attained from our ground state by acting solely with algebra operators $a \in \mathcal{A}_A$, it is part of the corresponding Hilbert space. Therefore, the functional tr can be defined as above and we may conclude that $\mathcal{A}_A$ is of type II_1 at the point $X = 0$. Finally,

we turn to the intermediate regime of $0 < X < 1$, which corresponds the hopping ratios $0 < r < \infty$ by virtue of (4.129). From (4.147), with $\kappa = -\text{arctanh}X$, we see that the entanglement entropy is infinite, but it is not maximal at leading order when $N \to \infty$. This can also be qualitatively extracted from the plot of Fig. 4.13. Running the same argument used above for the $X = 0$ case, we can now see that the maximally entangled state $|\Psi\rangle$ is not contained within the Hilbert space generated by $\mathcal{A}_A$ acting on the ground state for $0 < X < 1$. Following [830] and Fig. 4.5, the algebra $\mathcal{A}_A$ does not admit the definition of a trace and is thus of type III.

This classification is summarized in the phase diagram shown in Fig. 4.14, where we have embedded the entanglement entropy shown in Fig. 4.13 as a visual guide. Remarkably, our model (4.86) exhibits all three types of von Neumann algebras throughout its phase diagram. In particular, we observe transitions between different types of algebras in the form of $\text{II}_1 \leftrightarrow \text{III} \leftrightarrow \text{I}_\infty$. Interestingly, the entire regime $0 < X < 1$ has an underlying type III algebra for any value of the interaction strength. Even when the system transitions across the critical point at $r = 1/2$ for $J > J_c$, the type of algebra does not change. This is in stark contrast with the observations of [146, 756] on the change of algebra type at the Hawking-Page phase transition. It turns out that this behavior can be different for a specific choice of the interaction potential, as we investigate in the following paragraph. It is worth reiterating that we do not know the precise form of the modular Hamiltonian in the interacting case. Therefore, a quantitative analysis of the spectrum of the modular operator as done in (4.152) for the free case, and a subsequent classification of the von Neumann types following [832, 833, 859], is out of reach in the presence of interactions. Nevertheless, we have provided solid heuristic arguments akin to those of [830] to still perform a classification of the von Neumann algebras in the presence of interactions. The fact that our results on the entanglement entropy (4.147) is valid for any choice of interaction potentials presents further evidence supporting our analysis in the interacting case.

Strong Coupling Limit

We conclude this subsection with a detailed analysis of the strong coupling limit $J \to \infty$. Our motivation is to better understand the point $(r, J) = (1/2, \infty)$ in the phase diagram in Fig. 4.14 from the point of view of algebra transitions. For finite values of J, we expect to see similar phase diagrams for any choice of interaction potentials, not only the exponential one (4.128) used as an example in our figures. This is because the behavior of the entanglement entropy for $r \to 0$ and $r \to \infty$ is exactly the same for other types of potentials. However, the solutions to the SC equation (4.129) shown in Fig. 4.9 as J is increased hints at an interesting behavior of

the system in the limit $J \to \infty$. Moreover, the entanglement entropy shown in Fig. 4.13 seems to approach a step-function behavior as J grows large, which would have drastic implications on the types of underlying operator algebras. We can therefore exploit the analytical tractability of our framework to study this regime in detail.

Recall the SC equation for the exponential interaction potential, which is given by (4.129) but we recall here for convenience

$$re^{J(\sin\theta-\cos\theta)} = \frac{1}{2}\tan\theta\,. \tag{4.153}$$

When $J \to \infty$, we in particular have $J > J_c$, such that (4.153) has three possible solutions. Moreover, we know that (4.153) has a fixed point which is independent of J, namely $\theta^* = \pi/4$ at $r = 1/2$. We perform a perturbative analysis of slight deviations from this fixed point of the form $\theta_\pm = \theta^* \pm \epsilon$, with $\epsilon \ll 1$. Naturally, each of these deviations imposes a restriction of our analysis to values of r slightly above or below $1/2$, respectively. For the case of θ_+, we see that the exponent on the left-hand side of (4.153) is positive, i.e. $(\sin\theta - \cos\theta) > 0$, implying $e^{J(\sin\theta-\cos\theta)} \to \infty$ as $J \to \infty$. The right-hand side of the SC equation (4.153) must therefore also diverge in order to guarantee self-consistency, despite the fact that it has no explicit J-dependence. Therefore, we can see that the self-consistent solution must tend to $\theta \to \pi/2$ such that $\tan\theta \to \infty$. We may now plug this value into the relation (4.146), leading to $\kappa \to -\infty$, which implies $X \to 1$. We find that the entanglement entropy vanishes for the deviation θ_+. A similar argument can be performed for θ_-, where we encounter the opposite behavior of $e^{J(\sin\theta-\cos\theta)} \to 0$ as $J \to \infty$, implying that the self-consistent solution tends to $\theta \to 0$. By the same relation as above, we have $\kappa \to 0$ ($X \to 0$) and therefore entanglement $S_A/N \to \log 2$ in the case of θ_-. We have thus shown that, for the exponential interaction potential in the strong coupling limit $J \to \infty$, the entanglement entropy is maximal (at leading order when $N \to \infty$) in the whole regime $0 \leq r < 1/2$, while it is vanishing for $r > 1/2$. This behavior can be summarized in the Heaviside step function dependence $S_A/N = \log 2\,\Theta(1/2 - r)$.

We can be even more precise about this behavior of the entropy when $J \to \infty$ in the case of the exponential potential. In fact, we can derive it explicitly at the level of the formula for the entanglement entropy. For this, we consider the deviation θ_+ once again. Our analysis above indicates that the self-consistent solution ought to be $\theta = \pi/2$ for $r > 1/2$. We thus perform an expansion of the SC condition around this

value by a different infinitesimal value $\varepsilon \ll 1$. To leading order, we have

$$r = e^{-J}\left(-\frac{1}{2\left(\theta-\frac{\pi}{2}\right)}+\frac{J}{2}\right)\,, \tag{4.154}$$

which is explicitly solvable for θ as a function of r and the interaction strength J. Specifically, we find

$$\theta\left(r,J\right)=\frac{-2\pi e^{J}r+\pi J+2}{2\left(J-2e^{J}r\right)}\,. \tag{4.155}$$

Subsequently, and upon application of the formulas (4.146) and (4.145), we can obtain explicit expressions for both $\kappa(\theta)$ and $X(\kappa(\theta))$. We may insert these relations into (4.112), or equivalently, (4.147), to unveil an explicit formula for the entanglement entropy at large J and for $r > 1/2$. It reads

$$\frac{S_A}{N}=-2\log\left(\cos\left(\frac{\zeta}{2}\right)\right)+\left(1-\cos\left(\zeta\right)\right)\tanh^{-1}\left(\cos\left(\zeta\right)\right)\,, \tag{4.156}$$

where, for clarity, we have defined the parameter

$$\zeta\equiv\frac{1}{2e^{J}r-J}\,. \tag{4.157}$$

It is worth stressing that this expression was obtained from two distinct expansions, and is therefore not an exact solution to the SC equation. Nevertheless, the accuracy of this approximation is very high for values of r away from $1/2$. Around $r = 1/2$, the approximation becomes increasingly accurate as J gets larger. Given the analytical expression of (4.157), we may be tempted to set $r = 1/2$ and evaluate the limit $J \to \infty$. It is however more proper to leave the value of the hopping ratio unfixed, and study the behavior of the entanglement entropy (4.156) when $J \to \infty$. This can be straightforwardly evaluated by noticing that

$$\lim_{J\to\infty}\zeta=0\,,\quad\forall\, r\,, \tag{4.158}$$

such that the first term in (4.156) vanishes for $J \to \infty$. Evaluating the limit of the second term is slightly more subtle, since it leads to an indeterminate expression of the type $0\cdot\infty$. We write $f(\zeta)/(1/g(\zeta))$, with $f(\zeta) = \tanh^{-1}(\cos(\zeta))$ and $g(\zeta) = (1-\cos(\zeta))$ such as to obtain an indeterminate expression of type $\frac{\infty}{\infty}$, which allows us to apply L'Hôpital's rule, obtaining

$$\lim_{J\to\infty}f(\zeta)g(\zeta)=\lim_{J\to\infty}\frac{f(\zeta)}{1/g(\zeta)}=\lim_{J\to\infty}\frac{\partial_J f(\zeta)}{\partial_J(1/g(\zeta))}=\lim_{J\to\infty}\tan^2(\zeta)=0\,. \tag{4.159}$$

This result shows that the entanglement entropy for values of the hopping ratio r infinitesimally larger than $1/2$ tends to zero when $J \to \infty$. By the nature of the approximations done above, we can conclude that the entire branch of the entanglement entropy for values $r > 1/2$ tends to zero in the strong coupling limit.

Not surprisingly, we can perform an analogous evaluation for the other branch of the entanglement entropy. More precisely, we consider the other relevant solution to the SC equation, $\theta = 0$, which is the value towards which θ_- is pushed when we slightly deviate the hopping ratio from $r = 1/2$ by $-\epsilon$. Upon expanding the SC equation around this point, we can once more obtain an explicit relations $\theta(r, J)$ and $X(\kappa(\theta))$ and insert them into the entanglement entropy. This yields

$$\frac{S_A}{N} = \log\left(\frac{2}{\sin\left(\tilde{\zeta}\right)+1}\right) + \left(1-\sin\left(\tilde{\zeta}\right)\right)\tanh^{-1}\left(\sin\left(\tilde{\zeta}\right)\right), \tag{4.160}$$

where we have now defined the parameter

$$\tilde{\zeta} = 2\,r\,e^{-J}. \tag{4.161}$$

It is straightforward to evaluate the $J \to \infty$ limit of (4.160) since no indefinite expressions arise. We have,

$$\lim_{J\to\infty}\frac{S_A}{N} = \log 2, \tag{4.162}$$

which indeed confirms that the value of the entanglement entropy for $r = 1/2 - \epsilon$ tends to $\log 2$ for $J \to \infty$. Thus, we conclude that the entanglement entropy tends to this value for the entire branch $r < 1/2$ in the strongly coupled limit.

We have thus proved that the entanglement entropy for the exponential potential tends to a step function $S_A/N = \log 2\,\Theta(1/2 - r)$ in the limit $J \to \infty$. This has interesting consequences for the von Neumann algebra typification in the phase diagram of our model. Indeed, in the limit $J \to \infty$, corresponding to the top line of the phase diagram, the local operator algebra $\mathcal{A}_A$ is of type II_1 for $r < 1/2$ and of type I_∞ for $r > 1/2$, as indicated in Fig. 4.14 by a change in color at $r = 1/2$ along the top line. Thus, we observe a direct transition of the type of von Neumann algebra which coincides with the phase transition undergone by the system at $r = 1/2$. The intermediate regime where the underlying algebra is of type III ceases to be present. The resulting behavior is qualitatively similar, but not equivalent, to that observed for the Hawking-Page phase transition. The difference is that when $J \to \infty$, we observe a transition of the form $\mathrm{II}_1 \leftrightarrow \mathrm{I}_\infty$ while the Hawking-Page system exhibits a transition $\mathrm{III}_1 \leftrightarrow \mathrm{I}_\infty$.

It is quite remarkable that the above phenomenon is a unique feature of the class of

exponential interaction potentials (4.128). The mathematical origin of this different behavior lies in the SC equation for truncated potentials given by finite-order series expansions as in (4.133). More precisely, for these potentials, the $J \to \infty$ behavior of the SC equation (4.127) does not impose any constraints on the dependence $\theta(r, J)$. While for the exponential potentials we had the expression $e^{J(\sin\theta - \cos\theta)}$, which enjoys a clear limiting behavior when $J \to \infty$ depending on the value of θ, this is no longer the case for truncated potentials. Specifically, when $J \to \infty$, the leading behavior of (4.130) will be simply dominated by the highest-power term, i.e.

$$\frac{m(\sin\theta)}{m(\cos\theta)} = \frac{\sum_{k=0}^{n} \frac{J^k}{k!}(\sin\theta)^k}{\sum_{k=0}^{n} \frac{J^k}{k!}(\cos\theta)^k} \overset{J\to\infty}{\sim} (\tan\theta)^n > 1\,, \quad \forall\ \theta \in [0, \frac{\pi}{2})\,. \tag{4.163}$$

In this limit, the SC equation takes on the form

$$r(\tan\theta)^n = \frac{1}{2}\tan\theta\,, \tag{4.164}$$

which has a unique solution given by the smooth function $\theta = \tanh^{-1}((2r)^{\frac{1}{1-n}})$. In particular, this solution is valid for any value of θ, and we do not encounter a sudden transition in the SC solutions which may eventually lead to a discontinuous behavior of the entanglement entropy. Therefore, even in the large J limit, the regime $0 < r < \infty$ in the phase diagram for truncated potentials is still governed by a type III von Neumann algebra, and no change of the algebra occurs across the phase transition. Qualitatively speaking, we can expect that the exponential potential in the large J limit describes a situation which is physically much more drastic, in such a manner that it alters the way the operator algebra acts on the ground state for the two different phases of the system. In contrast, any truncated potential will not describe interactions that can change this behavior, even when taking $J \to \infty$.

4.3.5. Closed Periodic Chains

We devote the final part of this section to show how our techniques can be applied to extended systems beyond $L = 2$ and $L = 4$ sites. In particular, the generality of our methods allows us to consider closed chains, which in the thermodynamic limit can be equivalently taken to describe infinitely extended one-dimensional systems.
We consider a closed periodic chain consisting of L sites and governed by a general Hamiltonian of the form (4.86) and with staggered hopping parameters given by

$$\begin{aligned} h_{xy}(\xi) &= \delta_{x+1,y}(h_b(\xi)\delta_{\mathrm{mod}_2 x,0} + h_a(\xi)\delta_{\mathrm{mod}_2 x,1}) \\ &+ \delta_{x-1,y}(h_a(-\xi)\delta_{\mathrm{mod}_2 x,0} + h_b(-\xi)\delta_{\mathrm{mod}_2 x,1})\,. \end{aligned} \tag{4.165}$$

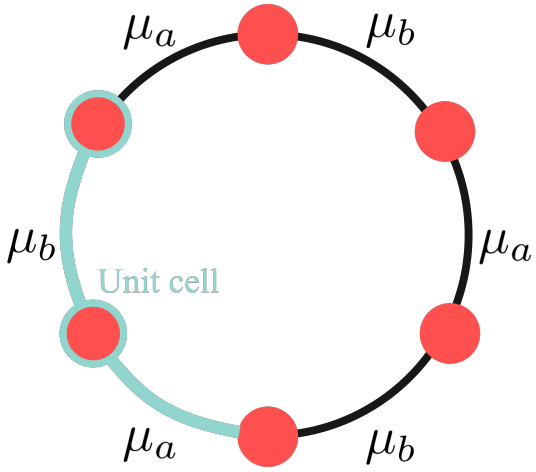


Figure 4.15: Closed periodic chain with $L = 6$ with staggered interactions as given in (4.165). The system exhibits translation invariance with respect to a unit cell (green) consisting of two sites connected by a strong hopping μ_b, together with the subsequent weak hopping μ_a.

Here, $x = 0, \ldots, L-1$ labels the site of the chain, h_a and h_b are generic functions, and the periodicity of the chain is encapsulated in the identification $L+x \sim x$. This system is schematically represented in Fig. 4.15. The periodic nature of the hoppings inherent to the staggering indicates that we can define *unit cells* consisting of those pairs of adjacent sites which interact via h_b. With respect to these cells, the entire chain enjoys translation invariance, thus allowing for a solution of the model in momentum space. More precisely, we introduce new coordinates r, s which take into account the unit cell along the chain, and the site within a respective unit cell, respectively. These read $r = 0, \ldots, \frac{L}{2} - 1$, such that $x = 2r + s$, with $s \in \{0, 1\}$. Translation invariance is then manifest with respect to r. Writing $x = 2r_1 + s_1$ and $y = 2r_2 + s_2$, $h_{xy} \equiv h^{s_1 s_2}_{r_1 r_2}$ we can express the derivative of (4.165) with respect to ξ as

$$h'^{s_1 s_2}_{r_1 r_2} = M_b \delta_{r_1 r_2} \epsilon^{s_1 s_2} + M_a \left(\delta_{r_1 - r_2, -1} \delta_{1,s_1} \delta_{0,s_2} - \delta_{r_1 - r_2, 1} \delta_{0,s_1} \delta_{1,s_2} \right) , \tag{4.166}$$

with $\epsilon^{s_1 s_2}$ the totally anti-symmetric symbol such that $\epsilon^{01} = 1$. Moreover, we define

$$M_a \equiv h'_a \left(-2\mathrm{i} G^{1,0}_{r,r+1}(0) \right) , \qquad M_b \equiv h'_b \left(-2\mathrm{i} G^{0,1}_{r,r}(0) \right) , \tag{4.167}$$

by making use of the aforementioned translational invariance, by which the components of $h'^{s_1 s_2}_{r_1 r_2}$ depend on the indices r_1 and r_2 only through their differences $r_1 - r_2 \equiv \delta r$. We also express the spatial dependence of G_{xy} in terms of r_1, r_2, s_1 and s_2 for convenience. It is particularly convenient to express the entries of $h'^{s_1 s_2}_{r_1 r_2}$ uniquely as functions of δr, which allows us to collect them into 2×2 matrices in the basis of the

intra-cell indices s_1 and s_2. These read

$$h'^{s_1 s_2}_{r_1 r_2} = \begin{pmatrix} 0 & M_b\delta_{\delta r,0} - M_a\delta_{\delta r,1} \\ -M_b\delta_{\delta r,0} + M_a\delta_{\delta r,-1} & 0 \end{pmatrix} \equiv (h'_{\delta r})_{s_1 s_2}\,. \tag{4.168}$$

Due to the translational invariance enjoyed by the system in both the spatial and Euclidean time coordinates, we can define two distinct types of Fourier transform for the Green's function, given by

$$G^{s_1 s_2}_{r+\delta r,r}(\tau) = \frac{2}{L}\sum_{k=-L/4}^{L/4-1} G^{s_1 s_2}_k(\tau)\, e^{-2\pi \mathrm{i}\frac{k\delta r}{L/2}}\,, \qquad G^{s_1 s_2}_k(\tau) = \frac{1}{2\pi}\int_{-\infty}^{\infty} G_k(\omega) e^{-\mathrm{i}\omega\tau} d\omega\,, \tag{4.169}$$

where the transform with respect to Euclidean time is continuous, whereas that in the spatial coordinates is discrete. Analogous definitions hold for the self-energy $\Sigma_{xy}(\tau) = 2\mathrm{i}h'_{xy}(G_{xy}(0))\delta(\tau)$, where we can further employ (4.168) to write

$$\Sigma^{s_1 s_2}_k(\omega) = 2\mathrm{i}\begin{pmatrix} 0 & M_b - M_a e^{\mathrm{i}4\pi k/L} \\ -M_b + M_a e^{\mathrm{i}4\pi k/L} & 0 \end{pmatrix} = \mathrm{i}\begin{pmatrix} 0 & \varepsilon_k e^{\mathrm{i}\varphi_k} \\ -\varepsilon_k e^{-\mathrm{i}\varphi_k} & 0 \end{pmatrix}\,, \tag{4.170}$$

with the convenient parametrization

$$\varepsilon_k \equiv \sqrt{M_b^2 + M_a^2 - 2M_a M_b \cos(4\pi k/L)}\,, \qquad e^{\mathrm{i}\varphi_k} \equiv \frac{M_b - M_a e^{\mathrm{i}4\pi k/L}}{M_b - M_a e^{-\mathrm{i}4\pi k/L}}\,. \tag{4.171}$$

Correspondingly, we can write the SD equations in Fourier space as

$$G_k(\omega) = \frac{\mathrm{i}}{\omega + 2h'_{\delta r}} = \mathrm{i}\frac{\omega + 2h'_{\delta r}}{\omega^2 + \varepsilon_k^2}\,, \tag{4.172}$$

where ω is implicitly multiplied by the 4×4 identity matrix, and the last step was obtained exploiting (4.168) and (4.170). The equation at $\tau = 0$ is a boundary condition, while for $\tau > 0$ we can insert (4.172) into the second equation of (4.169), yielding

$$G^{s_1 s_2}_k(\tau) = \frac{e^{-\tau\varepsilon_k}}{2}\begin{pmatrix} 1 & \mathrm{i}e^{\mathrm{i}\varphi_k} \\ -\mathrm{i}e^{-\mathrm{i}\varphi_k} & 1 \end{pmatrix}\,. \tag{4.173}$$

The Green's function of the ground state of the system can now be found from the first equation of (4.169), obtaining

$$\begin{aligned} G^{s_1 s_2}_{r+\delta r,r}(\tau) =& \frac{1}{L}\sum_{k=-L/4}^{L/4-1} e^{-\tau\varepsilon_k - 4\pi \mathrm{i}\frac{k\delta r}{L}} \begin{pmatrix} 1 & \mathrm{i}e^{\mathrm{i}\varphi_k} \\ -\mathrm{i}e^{-\mathrm{i}\varphi_k} & 1 \end{pmatrix} \\ &\longrightarrow \int_{-\frac{1}{2}}^{\frac{1}{2}} dp \frac{e^{-\tau\varepsilon(p) - 2\pi \mathrm{i} p\delta r}}{2} \begin{pmatrix} 1 & \mathrm{i}e^{\mathrm{i}\varphi(p)} \\ -\mathrm{i}e^{-\mathrm{i}\varphi(p)} & 1 \end{pmatrix}, \end{aligned} \tag{4.174}$$

where we have taken the thermodynamic limit $L \to \infty$ in the last step, which allows us to integrate over the momentum variable $p = 2k/L$. We have also introduced $\varepsilon(p) \equiv \lim_{L\to\infty} \varepsilon_{k=pL/2}$ and $\varphi(p) \equiv \lim_{L\to\infty} \varphi_{k=pL/2}$. The above construction enables the identification of a self-consistent system of equations, much in the spirit of our analysis for the smaller chains. More specifically, notice that the functions $\varepsilon(p)$ and $\varphi(p)$ in (4.174) are not yet determined, but they depend themselves on entries of the Green's function evaluated at $\tau = 0$ via M_a and M_b. A more explicit SC condition can be found by noticing that, from (4.167), M_a and M_b each only depend on a single but distinct entry of the Green's function at $\tau = 0$. In particular, G is given by an implicit function of only the correlations within a given cell $G_{2x,2x+1}(0)$, and those connecting adjacent cells $G_{2x-1,2x}(0)$. Their form can be obtained from (4.174) and reads

$$G^{0,1}_{r,r}(0) = \frac{\mathrm{i}}{2}\int_{-\frac{1}{2}}^{\frac{1}{2}} dp e^{\mathrm{i}\varphi(p)} = G_{2x,2x+1}(0)\,, \quad G^{1,0}_{r,r+1}(0) = -\frac{\mathrm{i}}{2}\int_{-\frac{1}{2}}^{\frac{1}{2}} dp e^{2\pi \mathrm{i} p - \mathrm{i}\varphi(p)} = G_{2x-1,2x}(0)\,, \tag{4.175}$$

where we have restored the spatial dependence on the spatial coordinates x in the last step. Upon shifting the integration variable $p \to p + 1/2$ and employing the parametrization (4.171), we find

$$\begin{aligned} -2\mathrm{i}G_{2x,2x+1}(0) &= \int_0^1 dp \frac{1 - R\cos(2\pi p)}{\sqrt{R^2 - 2R\cos(2\pi p) + 1}}\,, \\ -2\mathrm{i}G_{2x-1,2x}(0) &= \int_0^1 dp \frac{R - \cos(2\pi p)}{\sqrt{R^2 - 2R\cos(2\pi p) + 1}}\,, \end{aligned} \tag{4.176}$$

with the parameter R given by

$$R \equiv \frac{M_a}{M_b} = \frac{h_a'\left(-2\mathrm{i}G_{2x-1,2x}(0)\right)}{h_b'\left(-2\mathrm{i}G_{2x,2x+1}(0)\right)}\,. \tag{4.177}$$

The above equation is precisely the SC condition for the closed periodic chain. We can introduce a further parametrization via the value v such that $R = \frac{1-v}{1+v}$ with $v \in [-1, 1]$,

which allows us to re-write (4.176) in the form

$$G_{2x-1,2x}(0) = \frac{\mathrm{i}}{2} g\left(-v\right) , \quad G_{2x,2x+1}(0) = \frac{\mathrm{i}}{2} g(v) , \tag{4.178}$$

$$g(v) = \frac{2\,\mathrm{sgn}(v)}{\pi} \left[\frac{E(1-1/v^2)}{1+1/v} + \frac{K(1-1/v^2)}{1+v} \right] , \tag{4.179}$$

where $K(\xi)$, $E(\xi)$ are the complete elliptic integrals of the first and second kind, respectively [597]. Notice how $v \to -v$ merely exchanges $G_{2x-1,2x}(0)$ and $G_{2x,2x+1}(0)$ by virtue of (4.178), and therefore it simply amounts to exchanging h_a and h_b. Given that $g(1) = 1$, the limit $v \to 1$ and $v \to -1$ correspond to a maximal value of the correlations between nearest neighbor sites within and across unit cells, respectively.

With the above equations, the model is exactly solved upon finding the expression of the two-point functions, and so it is necessary to find expressions of $\varepsilon(p)$ and $\varphi(p)$ in terms of the parameters of the microscopic Hamiltonian. For this, the solution for v is required, and the model is completely solved once v has been found. To do this, we insert (4.178) into the SC equation (4.177), yielding an explicit equation for v. Solving this equation, we fully determine $G_{2x,2x+1}(0)$ and $G_{2x-1,2x}(0)$, which, in turn, are required to obtain the functions $\varepsilon(p)$ and $\varphi(p)$. Finally, inserting $\varepsilon(p)$ and $\varphi(p)$ into (4.174) allows us to compute all two-point functions of the system, which in the large N limit suffices to solve the model in its entirety.

We find it worth mentioning that, although we have generalized the computation of the Green's function to this larger system given by a closed chain of L sites, the analysis of the entanglement entropies for longer chains is a formidable challenge. While we can indeed parallel our discussions in Sec. 4.3.4 on the entanglement entropy and algebra typification for periodic chains with $L = 4$ sites, the case of $L > 4$ remains inaccessible with current methods. The main obstacle is the computation of the entanglement entropy for subregions consisting of more than 2 sites. In the $L = 4$ case, such a bipartition is the only non-trivial one, but for $L > 4$, subregions with 3 or more sites are possible. Their entanglement entropy requires the knowledge of the entanglement Hamiltonian, for which we cannot use the ansatz (4.96) anymore. This is because, in principle, the entanglement Hamiltonian should be a function of all possible local operators located in the subregion, which for more than 2 sites are not entirely captured by our fermion bilinear ansatz. For example, the operator $\psi_1^j \psi_2^j \psi_3^j$ cannot be obtained from a function whose argument is the fermion bilinear, but it most certainly can contribute to the entanglement entropy of a three-site subregion. Thus, a more general ansatz for the entanglement Hamiltonian for generic interacting systems is required, a problem that is to this day an active field of research.

In this section, we have introduced and investigated a vast class of models of interacting Majorana fermions, whose intricate phase diagram has allowed us to realize transitions between different types of local operator algebras. More specifically, the large N description of our model (4.86) in terms of the SD equations (4.89)-(4.90), together with the self-consistency conditions (4.95), allowed us to solve the model exactly for any choice of interaction potentials. We unveiled a phase transition by computing the free energy of the model in a four-site chain, a system which we further investigated in view of its ground state entanglement entropy. The latter turned out to exhibit a highly non-trivial structure, which manifested itself in the different types of underlying operator algebras, summarized in Fig. 4.14. Our results showcase the high versatility of our model and our techniques, enabling the study of von Neumann algebras, and transitions thereof, in a well-controlled quantum many-body setup.

4.4. Discussion

To end this chapter, we provide an overarching discussion of the presented results. In particular, we return to the question asked at the beginning of the chapter and embed our findings within the larger paradigm of quantum information within holography.
We began with the motivation of understanding the emergence of spatial dimensions behind the event horizons of black holes. A double-sided black hole geometry, dual to the TFD state of a holographic CFT, was the original setup where the growth of the wormhole for late times was identified. In particular, this inner geometry of an ER bridge continues to grow even for times much larger than the thermalization time of the boundary CFT. This pointed to a shortcoming of observables like the entanglement entropy, indicating that they cannot capture the entirety of the geometry behind the horizon. It was suggested that a suitable notion of quantum circuit complexity of the time-evolution operator may be able to probe this late time growth of the ER bridge. However, the exact implementation of this proposal is not immediately clear, given the rather arbitrary nature of complexity, as well as the specific properties that a *holographic* complexity measure ought to have. Moreover, the mere definition of complexity for infinite-dimensional Hilbert spaces such as those appearing in QFTs is not clear a priori. To advance this program, in Sec. 4.1 we provided a novel setup for Nielsen complexity of $\mathrm{SU}(N)$ qudit unitaries which enjoys a well-defined large N limit. To this goal, as explained in Sec. 4.1.1, we worked within the Euler-Arnold approach to geodesic motion on Lie group manifolds, where the definition of Nielsen operator complexity boils down to the choice of a set of generators in the $\mathfrak{su}(N)$ algebra (fun-

damental gates) and an inner product (cost function). In Sec. 4.1.2, we constructed a basis for the $\mathfrak{su}(N)$ algebra which, in the large N limit, admits an isomorphism to the algebra of Hamiltonian vector fields on a torus. The latter characterizes the hydrodynamical phase space of a classical ideal fluid flowing on $\mathbb{T}^2$. As explained in Sec. 4.1.3, this emergent hydrodynamic theory is equipped with a natural cost function given by the kinetic energy of the fluid, governed by the Laplacian. Motivated by this, we defined an inner product on the $\mathfrak{su}(N)$ algebra at finite N as a discrete analog to it, and which implemented polynomial penalty factors to fundamental gates. Our construction thus provided a well-defined notion of complexity which not only survives the transition from finite- to infinite-dimensional Hilbert spaces, but gives rise to a well-known theory in the $N \to \infty$ limit. Finally, via a refined curvature analysis given in Sec. 4.1.4, we showed that this cost function exhibits two key features of holographic complexity measures, namely ergodicity and conjugate points. While the search for *the* holographic complexity measure remains open, our results give compelling evidence that choices of cost functions motivated by hydrodynamics are promising candidates to capture operator complexity in holographic CFTs, potentially shedding light on the intricacies of spatial geometries behind black hole horizons.

In parallel, another intriguing dilemma appears in the context of the eternal black hole in AdS. Known as the factorization puzzle, this issue addresses the fact that the bulk Hilbert space describing a smooth wormhole geometry does not factorize, while the boundary Hilbert space sees no obstruction to factorization given that the two copies of the CFT do not interact. To make progress in this direction, in Sec. 4.2 we proposed a simple diagnostic of the factorization of modular partition functions of arbitrary pure states. More precisely, in Sec. 4.2.1, we showed how these objects factorize if and only if the geometric quantum discord (GQD) of the corresponding arbitrary (q-q) pure state vanishes. Physically, this implies that the mere presence of purely quantum correlations between subsystems leads to a non-factorization of the modular partition function. In Sec. 4.2.2, we applied our results to the holographically relevant case of the TFD state. Via the minimization involved in the computation of the GQD, we found a novel interpretation of the TMD state as the closest classical approximation to the TFD state. Moreover, in this case the modular partition function can be identified with the thermal partition function of the TFD state. Additionally, exploiting a relation between the higher Rényi entropies of the TMD state and the partition functions of multi-throat wormhole geometries, we were able to find a bridge between yet another quantum information quantity and gravitational physics. This was further supported by our findings in Sec. 4.2.3, where we provided clear connections between GQD (and generalizations thereof) and the higher overlaps

of microstates of astrophysical black holes. All in all, our investigations extend the ER=EPR dogma showing that *any* quantum correlations, and not only entanglement, are deeply related to the non-factorization properties of states, as signaled by their modular partition functions. The possibility of finding geometric bulk duals for the GQD based on conical defects created by cosmic branes further supports the relevance of our results. Extended considerations of GQD within holography certainly provide a promising avenue to unveil a full understanding of the factorization puzzle.

At last, in Sec. 4.3, we concerned ourselves with the question regarding emergence of time behind black hole horizons, a topic which has recently gained plenty of attention. A predominant mathematical tool in the analysis of this complicated issue is the theory of operator algebras, which we reviewed from both a historical and technical point of view in Sec. 4.3.1. The main objects of study from this perspective were von Neumann algebras, which provide a mathematically rigorous description of physically relevant observables. It became clear that von Neumann algebras are deeply related to the entanglement properties of quantum states. Studies on the types of von Neumann algebras appearing in certain holographic settings indicate that situations where there are changes in the type of an operator algebra can be directly associated with interesting physical phenomena. The prime example of this was the emergent type III_1 algebra for the quantum fields in the outside region of the AdS black hole above the Hawking-Page phase transition, which provided an explanation of how the notion of time arises behind the horizon. Based on these explorations, it became clear that such transitions of von Neumann algebras are highly interesting, in particular when they coincide with physical phase transitions. A simple model to study these objects without the intricacies of quantum gravity would therefore be tremendously desirable. This is precisely what we provided in Sec. 4.3.2 by introducing a model of interacting Majorana fermions which becomes exactly solvable in a certain thermodynamic limit. More precisely, the model consists of N Majoranas living on each lattice site and interacting via an arbitrary interaction potential. In the large N limit, the dynamics of the theory is governed by the Schwinger-Dyson equations, and large-N factorization ensures exact solvability after computing the matrix of two-point correlation functions, i.e. the Green's function. We investigated the thermodynamics of this theory for the case of a four-site chain in Sec. 4.3.3, unveiling the presence of a quantum phase transition driven by the interaction strength. The two phases of the system are respectively characterized by their factorized and non-factorized correlation structures. Moreover, we analytically computed the entanglement entropy of the left half of the chain with respect to the right half in the ground state, obtaining a closed expression for this quantity which is manifestly independent on the form of the interaction

potential. The resulting entanglement entropy not only detects the phase transition undergone by the system, but it hinted at non-trivial entanglement properties of the ground state throughout the phase diagram of the model. In Sec. 4.3.4, we quantitatively characterized this observed behavior by identifying the types of von Neumann algebras underlying our model throughout the entire phase diagram. In particular, we find instances of type I, II, and III von Neumann algebras, together with transitions and crossovers between them for varying values of the hopping ratio. Specifically, we quantify an entire range of type III_λ algebras in the absence of interactions, and we unveil type II_1 and type I_∞ algebras in the case of vanishing and infinitely large hopping ratios, respectively. For finite interaction strength and finite hopping ratio, the algebra of observables of a subregion of the model is generically of type III, even across the quantum phase transition. Nonetheless, for the case of an exponential interaction potential, we were able to show that a direct algebra transition of type $\mathrm{II}_1 \leftrightarrow \mathrm{I}_\infty$ exactly coincides with the phase transition of the system, in resemblance to the situation for the Hawking-Page setup. However, notice that the latter involved a transition to a type III_1 algebra, which is not present in our approach. We concluded in Sec. 4.3.5 by showcasing the wide range of applicability of our setup, at least to the extent of exactly computing the correlation functions, by solving the model on a closed periodic chain with staggered interactions. Our investigations provide a significant step towards the algebraic analysis of black holes by supplying an exactly solvable and controllable quantum many-body model where the intricate relations between entanglement and von Neumann algebras can be studied. It is an intriguing question for the future to explore the potential significance of algebra transitions involving types other than III_1 and their role in the broader scrutiny of black holes using quantum information tools.

Conclusions and Outlook 5

"Failure of existing rules is the prelude to a search for new ones."

Thomas Kuhn

In our everlasting quest to understand Nature, we have come to accept the scientific method as a fundamental logical tool to decipher the inner workings of the world around us. Both precise and attentive observations, together with logical reasoning and diligent skepticism, underlie the very essence of this empiric approach to reality. It is precisely this last aspect which indicates that we may learn more from what a theory *does not* explain than what it *does* explain. In particular, understanding the limits and ranges of validity of our models is a key ingredient in the further development of scientific cognizance. Therefore, let us summarize the main results obtained in this work in view of identifying the open questions that remain. The overarching questions addressed in this thesis were concerned with the extension of the AdS/CFT correspondence and the holographic principle to discrete settings in Chapter 3, and contributions to the ever-increasing role of quantum information quantities in understanding properties of black holes via holographic dualities in Chapter 4.

In Chapter 3, I have presented an encompassing description of the discrete holography program, together with a collection of novel results in the field. I introduced regular hyperbolic tilings as a main platform for discretizing negatively curved hyperbolic space, arising in constant-time slices of AdS_{2+1}. My investigations show that these tilings are not only excellent approximations to the continuum geometry, reproducing pivotal predictions of AdS/CFT such as the Breitenlohner-Freedman bound and CFT-like correlation functions, but they also allow for a natural imprinting of bulk information onto their boundary, in a vivid resemblance of the error-correction properties of holography. This is achieved via the construction of hyperbolic tilings based on inflation rules, which bestows an aperiodic structure upon the boundary sites. Exploiting this, I have presented a large class of explicit boundary Hamiltonians for this discrete holographic setting in terms of aperiodically disordered quantum spin chains. I thoroughly characterized the ground states of these boundary theories in terms of their correlation functions, ground state factorization structure, entanglement entropy, and mutual information. Together with a tensor network realization

of these ground states, which provide a geometric description of the boundary state extending into the bulk, our models reproduce holographic behaviors for the entanglement entropy in a discrete setting. At the same time, I studied holographic lattice models defined on regular hyperbolic tilings, as well as their counterpart for a hyperbolic annulus geometry discretizing a constant-time slice of an eternal black hole in AdS. I showed how both discretizations reproduce the correlation functions expected for operators in a CFT at zero and finite temperature, respectively. Moreover, this holographic lattice model admits efficient, controllable, and readily implementable experimental realizations via electric circuits, paving the way for measurable verifications of holographic predictions.

These results provide concrete instances of discrete holographic setups, both from the bulk and the boundary point of view. The outcomes of my studies offer many interesting paths to further develop the discrete holography program, which I list in what follows. The discrete and explicit nature of holographic lattice models on hyperbolic tilings can be exploited to further characterize the class of CFTs that can be simulated with this approach, for example by deriving an explicit form of the boundary Hamiltonian from the discrete path integral. Another idea is to identify an explicit CFT by introducing more bulk fields, thus allowing for the insertion of multiple CFT operators and the better characterization of CFT data. As for the aperiodic spin chains, while we have showed how to include a large number of degrees of freedom via a large N limit, it is key to study extensions of these models that allow to also access some notion of strong coupling. This would come closer to the standard regime of validity of continuous AdS/CFT, as reviewed in Sec. 2.2. Finally, it is a highly interesting question whether the explicit Hamiltonians I propose as boundary theories can be exploited to establish the dynamics of discrete holographic dualities. This notion of dynamics is one of the biggest open questions when it comes to discrete approaches to AdS/CFT. I believe that the large amount of controllability present for aperiodic quantum chain Hamiltonians should allow for a canonical time-evolution on the boundary. The less straightforward task is to obtain a dual notion of time evolution either for the hyperbolic tiling or, more promisingly, the dual tensor network. Recent proposals to include dynamics into holographic tensor networks can be found in [433, 436, 888, 889].

In Chapter 4, I reported the results on three distinct quantum information measures, namely quantum complexity, geometric quantum discord, and von Neumann algebras, and discussed their role within holography as potential probes of black hole properties. I explained how these quantities shed light on the factorization puzzle, as well as the emergence of space and time behind black hole horizons. I introduced an explicit construction for Nielsen complexity which is well-defined both for finite- and infinite-

dimensional Hilbert spaces, thus presenting a promising reference for definitions of complexity for QFTs. Moreover, the suggested cost function induces a complexity geometry that exhibits desired properties of holographic complexity measures, such as ergodic geodesic flows, conjugate points, and even a possible concrete realization of the Poincaré recurrence. Then, I showed how the quantity of geometric quantum discord (GQD) can be used as an easily implementable diagnose for the factorization properties of modular partition functions. After deriving a general expression for GQD, I applied these results to the holographically relevant case of the TFD state, where I found a novel interpretation of the TMD state as the closest classical state approximating the TFD state. This connection allows to relate GQD to wormhole physics arising in the gravitational path integral, thus bringing us closer to understanding the structures responsible for the factorization puzzle. Finally, I discussed an exactly solvable model of interacting Majorana fermions whose non-trivial phase diagram exhibits a quantum phase transition, as well as several different types of von Neumann operator algebras. In particular, in the strongly coupled regime, we find a direct transition between two types of von Neumann algebra which coincides with the phase transition undergone by the system, a behavior resembling that found for the Hawking-Page phase transition in AdS, although our case occurs at zero temperature. This model provides a rich playground to investigate operator algebras, which have seen much interest in view of describing the emergence of time behind the horizon.
Once more, the results I presented in this thesis allow for some prompt extensions in view of deepening our understanding of black holes and quantum gravity via quantum information quantities. First, it would be interesting to find explicit chaotic Hamiltonians for the dynamics of a large qudit, in order to compute its complexity via the EA approach we introduce. Moreover, a generalization of our framework to a collection of qudits seems promising to find a quantum field theory analogue of our cost function. On a more abstract level, it is intriguing to study the long-time behavior for generic solutions of the Euler equation in order to understand better the recurrence of complexity expected at doubly-exponential times. While some results exist in the mathematical literature [793, 794], it remains to be investigated which specific property of the dual wormhole geometry captures this recurrence. For the GQD, an explicit gravity construction in terms of bulk branes would prove extremely useful to complete the entry of GQD in the holographic dictionary. Moreover, the relation between higher Schatten norms providing straightforward extensions of GQD needs to be explored further in order to clarify the physical meaning of these quantities, as well as their potential gravitational duals. Finally, our interacting Majorana model could be potentially generalized to higher dimensions or larger chains. This is technically

challenging since the entanglement Hamiltonian would not have a simple structure, making the analysis of entanglement entropies, and thus of the von Neumann algebras, very complicated. Still, such generalizations may allow to find similar non-trivial phase diagrams exhibiting behaviors closer to those observed in holography, see [858] for recent works in this direction.

Outlook

Beyond the above-mentioned immediate extensions to the results presented in this thesis, we find it instructive to point out some more general ideas within the discrete holography program that are worth to explore in the future.

Fractional Calculus and Discrete Holography Although not discussed in this thesis, the results of [890] regarding fractional Klein-Gordon equations in AdS_{d+1} could potentially be exploited for discrete holography. Fractional calculus [891, 892] generalizes standard calculus to allow for non-integer derivatives by smearing out the weighing domain of differential operators, and it can be used to describe non-local long-range interactions with power law decays in physical systems. For instance, the action of a fractional derivative on plane waves is given by $\Delta^\alpha e^{\mathrm{i}\vec{k}\vec{x}} = -(k^2)^\alpha e^{\mathrm{i}\vec{k}\vec{x}}$, where Δ^α is the fractional Laplacian and $\alpha > 0$ is the control exponent describing the order of the derivative ($\alpha = 1$ is the standard calculus case). Given that the boundary of hyperbolic tilings can be associated with a fractal dimension $\mathfrak{d}$, future investigations into notions of discrete boundary field theories may profit from dynamics described via fractional calculus, with a suitable choice of $\alpha(\mathfrak{d})$. Connections between fractional calculus and fractal structures have been studied before [893, 894] and may thus prove useful for this vein of the discrete holography program.

Time, Optical Realizations and Entanglement In this thesis, we have realized negatively curved spaces implementing electric circuits. However, these offered discretizations for constant-time slices of AdS spacetime only, and accessing phenomena which extend in the time direction is unclear with this approach. There exist other experimental platforms which are particularly well-suited to study discrete realizations of AdS spacetime, including the time direction, something that is beyond the current power of hyperbolic tilings. One of these is provided by optical lattices of coupled femtosecond-laser-written photonic waveguides [895]. Based on a paraxial approximation of the Helmholtz equation, the equations of motion describing the *spatial* propagation of light through such coupled waveguide arrays can be shown to

be functionally equivalent to a discretized version of the Dirac equation of a fermion propagating in a curved spacetime. This is achieved by suitably modulating the refractive index n of the waveguides, which in turn also tunes the evanescent overlaps between the electric field amplitude of neighboring waveguides. While this has been studied for waveguide arrays emulating fermion propagation in some (1+1) and (2+1)-dimensional curved spacetimes [896, 897], the specific case of AdS spacetime has not been considered yet. Already a two-dimensional $N \times M$ waveguide array, with coupling constants κ_{nm}, $n = 1, \dots N$, $m = 1, \dots M$ chosen appropriately, would be enough to mimic the confining-box gravitational potential of AdS and experimentally emulate the propagation of fermions through AdS_{2+1}. Key ingredients for such a realization are the precise relation between theory parameters such as the fermion mass m and the AdS radius ℓ and experimental parameters such as the wavelength λ of the light, the refractive index n, and the coupling constants κ_{nm}. This platform has the promising potential of eventually working with entangled photons propagating in such waveguides, which could lead to new insights about bulk entanglement in holography.

Hyperbolic Buildings, Edge Length Dynamics, and SDRG The hyperbolic buildings considered in [482], which we briefly reviewed in Sec. 3.1 as a part of the current discrete holography landscape, are intriguing mathematical objects generalizing the concept of hyperbolic tilings. Their boundary has a very explicit fractal structure being homeomorphic to the so-called Menger sponge. It was shown in [482] that a generalization of the HaPPY code [152] to hyperbolic buildings gives rise to an RT-like behavior of the entanglement entropy which interestingly can detect the fractal dimension of the boundary. This fractal dimension depends on the way in which the hyperbolic building is constructed, with the method used in [482] being via reflections according to the generators of the Coxeter group of isometries of specific hyperbolic buildings known as Bourdon's buildings [487, 488]. It strikes us as intriguing to obtain similar fractal dimensions by generalizing the inflation rules of $\{p, q\}$ in such a way that they incorporate the local branching of hyperbolic buildings. The growth rate of such generalized inflation rules would be analogous to the largest eigenvalue λ_+ of the inflation matrix, and it would induce a specific fractal dimension on the boundary. Subsequently, it is highly compelling to adapt the SDRG to this setting in such a way that we can define models analogous to aperiodic spin chains on the boundary of these hyperbolic buildings and study their ground state properties via this approach. This is very technically challenging since the decimation steps of such models would not preserve the connectivity of the spin degrees of freedom. Nonetheless, such an explicit construction would allow to detect novel fractal dimensions via the entanglement en-

tropy, perhaps even extending the range of validity of the area-law to fractal systems. In parallel, the notion of edge length dynamics introduced in [478] in the context of p-adic AdS/CFT is a promising avenue to include metric fluctuations into our hyperbolic tilings. A full-fledged holographic duality naturally necessitates a bulk theory, and including metric fluctuations governed by a discrete Einstein-Hilbert action on hyperbolic tilings is a great candidate for this goal. While the setup of [478] covers the case of tree graphs, the generalization to graphs with closed loops has not been explored yet. The key technical aspect here is the evaluation of the expression

$$W(\psi_{v_1}, \psi_{v_2}) \equiv \sup_{f \in \mathcal{L}^1} \sum_{v \in \mathcal{G}} f(v) \left(\psi_{v_1} - \psi_{v_2}\right) , \tag{5.1}$$

where $W(\psi_{v_1}, \psi_{v_2})$ denotes the Wasserstein distance between two probability distributions ψ_{v_1}, ψ_{v_2} on two different vertices v_1, v_2 of the graph $\mathcal{G}$ associated to hyperbolic tilings, and the supremum is to be taken over the set $\mathcal{L}^1$ of all 1-Lipschitz functions [478]. The Wasserstein distance defines a discrete notion of Ricci curvature on graphs, but the supremum in (5.1) is highly non-trivial to carry out when the graph $\mathcal{G}$ has closed loops [478]. Still, up to this technical mathematical detail, an extension of the results of [478] to hyperbolic tilings does not seem forbiddingly difficult and it would prove immensely useful to advance the bulk side of discrete holographic dualities.

Continuum Limits of Aperiodic Sequences The aperiodic sequences exploited in this thesis are manifestly not translation-invariant, which hinders the analysis of aperiodic chains via standard methods in reciprocal space. In particular, a continuum limit of such chains is non-trivial, since functions describing binary aperiodic modulations in the limit of vanishing lattice spacing would necessarily be highly non-continuous and nowhere differentiable, obscuring any further manipulations. Nonetheless, some methods to construct aperiodic sequences through projections from higher-dimensional embedding spaces at irrational angles might provide access to Fourier techniques in these ambient spaces. These are related to the study of Fourier spectra of quasi-crystalline structures,[1] see for instance [577, 898, 899]. A continuum limit of aperiodic chains could then be achieved by first reversing this projection, applying Fourier techniques, and subsequently projecting the result once again. Obtaining access to continuum limits of aperiodic systems in this way would be extremely useful to study whether these models also admit a continuum CFT description at criticality, and if so, to better understand how the CFT structure is affected by the introduction of aperiodicity with respect to the homogeneous case. Understanding whether these

[1] I am very thankful to Lizzy Rieth for pointing these out to me.

"aperiodic CFTs" belong to known universality classes would greatly refine our understanding of discrete holographic boundary theories.

Higher-Dimensional Representations of Fuchsian Groups As we saw in Sec. 3.2.3, the Fuchsian groups capturing the isometries of regular hyperbolic tilings are highly complex mathematical structures. Little is known about explicit parametrizations of higher-dimensional irreducible representations of them, which would be necessary to construct covariantly transforming degrees of freedom for putative boundary theories in the original spirit of the AdS/CFT correspondence. Recently, a map between the moduli space of $U(N)$ irreducible representations and topological two-dimensional Yang-Mills theory with $U(N)$ gauge group was derived in [523]. The former is the higher-dimensional analogue of the Brillouin zone and plays a role in the hyperbolic version of Bloch's theorem, while the latter is an exactly solvable quantum theory defined on a Riemann surface of genus $g \geq 2$. It was shown that the moments of the density of states of arbitrary tight-binding Hamiltonians on regular hyperbolic lattices can be equivalently computed via expectation values of Wilson loops in the Yang-Mills theory [523]. In particular, computations requiring the integration over the moduli space can be circumvented in this way and replaced by actually computable partition functions of the topological theory. It seems very promising to study this novel alternative description of hyperbolic band theory in future definitions of theories at the boundary of hyperbolic tilings, perhaps exploiting new techniques to define degrees of freedom which furnish multiplets of irreducible representations of Fuchsian isometry groups. On an orthogonal vein, it is an interesting question whether gauge symmetries can be incorporated into the discrete holography program. One promising idea would be the definition of a discrete Chern-Simons theory on hyperbolic tilings, where the gauge degrees of freedom are defined on the edges of the tiles, now seen as plaquettes. Though technically challenging, this idea might equally benefit from some of the techniques used in [523]. A particularly intriguing one is the so-called Migdal's lattice gauge theory [900, 901], a toy model for gauge theories in two dimensions which enjoys the remarkable property known as *subdivision invariance*, meaning that its partition function is independent of the discretization chosen. An adaptation of these techniques to gauge theories on hyperbolic tilings is a highly relevant goal that would substantially enlarge the discrete holographic dictionary.

Wormhole Networks There exists a celebrated example of a simple quantum mechanical model which admits a holographic dual in a certain low-energy regime. The Sachdev-Ye-Kitaev (SYK) model [902, 903] is a $(0+1)$-dimensional model of N

randomly interacting Majorana fermions ψ, whose large N and low-energy sector can be shown to be described by the same effective action governing the IR sector of so-called Jackiw-Teitelboim (JT) [904, 905] dilaton gravity in nearly AdS_2 spacetime [884]. Remarkably, it was also shown that two coupled SYK dots have a holographic dual description in terms of a traversable wormhole connecting two nearly AdS_2 geometries [906], providing a realization of the ER=EPR conjecture. Motivated by the previous independent results on aperiodic spin chains [158, 159] and interacting Majorana [163] models, it seems highly promising to study spatial generalizations of the SYK model to aperiodic SYK chains with Hamiltonian

$$H = \sum_{x=1}^{L} \left(\mathrm{i}^{q/2} \sum_{1\leq j_1<j_2<\cdots<j_q\leq N} s_x J_{j_1 j_2 \cdots j_q, x} \psi_x^{j_1} \psi_x^{j_2} \cdots \psi_x^{j_q} + \mathrm{i} \sum_{1\leq j\leq N} \mu_x \psi_x^j \psi_{x+1}^j \right). \tag{5.2}$$

In this expression, $s_x = (-1)^{(x-1)q/2}$ and q (assumed even) describes the q-body SYK interaction, which is governed by the coupling parameter $J_{j_1 j_2 \cdots j_q, x}$. The latter is randomly drawn from a Gaussian distribution with zero mean value and correlation

$$\left\langle J_{j_1 j_2 \cdots j_q, x} J_{j_1 j_2 \cdots j_q, y} \right\rangle = \frac{(q-1)!}{N^{q-1}} J^2 e^{-\frac{|x-y|^2}{\zeta^2}} = \frac{(q-1)! 2^{q-1}}{q N^{q-1}} \mathcal{J}^2 e^{-\frac{|x-y|^2}{\zeta^2}}, \tag{5.3}$$

where ζ is a finite correlation length between Gaussian distributions of spatially separated on-site interactions. The $\{\mu_x\}$ are spatially inhomogeneous hopping parameters, which can be taken to be aperiodically modulated. This model is being currently studied in [907] and the results will soon be published, although I have not discussed them in this thesis. Preliminary results which merge the SDRG with the effective description of the model (5.2) at large N in terms of Schwinger-Dyson equations show that the ground state of the SYK chain (5.2) admits a partially geometric interpretation consisting of an aperiodic wormhole network, largely extending the results of [906]. This work, and extensions thereof, are promising avenues to find discrete holographic bulk duals to aperiodic spin chains.

Future Horizons for Discrete Holography

The list of outlooks given above solidifies not only the established nature of discrete holography as a field of research, but it further manifests its untapped potential. It is imperative to continue with our investigations into discrete holography, both for exploring the true limits of the holographic principle, as well as devising ever-more faithful and detailed experimental platforms to test the AdS/CFT correspondence. It is also not unthinkable that advancements towards explicit discrete holographic dual-

ities could shed light into certain aspects of quantum gravity, such as the microscopic emergence of spacetime from discrete degrees of freedom. The aid of quantum information theory in the pursuit of this goal cannot be overstated. Questions regarding the true factorization and entanglement properties of quantum gravity can only be answered in this language, as has become clear by the solidified role of quantum information within holography. It is thus our strong belief that through this quantum information looking-glass, the future of discrete holography is perhaps bright enough to illuminate the many obscure mysteries of black holes in quantum gravity.

Publications

A

This thesis is based on the following original works published in scientific journals:

- [161]: P. Basteiro, J. Erdmenger, P. Fries, F. Goth, I. Matthaiakakis and R. Meyer. *Quantum Complexity as Hydrodynamics*, Phys. Rev. D **106** (2022) 065016, [2109.01152].
- [157]: P. Basteiro, F. Dusel, J. Erdmenger, D. Herdt, H. Hinrichsen, R. Meyer and M. Schraut. *Breitenlohner-Freedman Bound on Hyperbolic Tilings*, Phys. Rev. Lett. **130** (2023) 091604, [2205.05081].
- [158]: P. Basteiro, G. Di Giulio, J. Erdmenger, J. Karl, R. Meyer and Z-Y. Xian. *Towards Explicit Discrete Holography: Aperiodic Spin Chains from Hyperbolic Tilings*, SciPost Phys. **13** (2022) 103, [2205.05693].
- [159]: P. Basteiro, R. N. Das, G. Di Giulio and J. Erdmenger. *Aperiodic Spin Chains at the Boundary of Hyperbolic Tilings*, SciPost Phys. **15** (2023) 218, [2212.11292].
- [162]: S. Banerjee, P. Basteiro, R. N. Das and M. Dorband. *Geometric Quantum Discord Signals Non-Factorization*, *JHEP* **08** (2023) 104, [2305.04952].
- [163]: P. Basteiro, G. Di Giulio, J. Erdmenger and Z-Y. Xian. *Entanglement in Interacting Majorana Chains and Transitions of von Neumann Algebras*, Phys. Rev. Lett. **132** (2024) 161604, [2401.04764].

I have also contributed to the following pre-print published on arXiv, which is currently under peer-review and whose contents are also included in this thesis:

- [160]: S. Dey, A. Chen, P. Basteiro, A. Fritzsche, M. Greiter, M. Kaminski, P. M. Lenggenhager, R. Meyer, R. Sorbello, A. Stegmeier, R. Thomale, J. Erdmenger and I. Boettcher. *Simulating Holographic Conformal Field Theories on Hyperbolic Lattices,* [2404.03062].

Finally, I have also contributed to the following publication, whose contents are only briefly alluded to in this thesis:

- [890]: P. Basteiro, J. Elfert, J. Erdmenger and H. Hinrichsen. *Fractional Klein-Gordon Equation on AdS_{2+1}*, J. Phys. A **55** (2022) 364002, [2201.10870].

Bibliography

[1] R. P. Feynman, *The pleasure of finding things out*, Perseus Books, Boulder, CO, Oct., 1999. (Cited on p. 1).

[2] A. Einstein, *Zur Allgemeinen Relativitätstheorie*, *Sitzungsber. Preuss. Akad. Wiss. Berlin (Math. Phys.)* **1915** (1915) 778–786. (Cited on pp. 1 and 2).

[3] A. Einstein, *The Field Equations of Gravitation*, *Sitzungsber. Preuss. Akad. Wiss. Berlin (Math. Phys.)* **1915** (1915) 844–847. (Cited on pp. 1 and 2).

[4] A. Einstein, *The foundation of the general theory of relativity.*, *Ann. Phys.* **49** (1916) 769–822. (Cited on pp. 1 and 2).

[5] M. Planck, *On the Law of Distribution of Energy in the Normal Spectrum*, *Ann. Phys.* **4** (1901) 553. (Cited on pp. 1 and 4).

[6] N. Bohr, *On the Constitution of Atoms and Molecules*, *Phil. Mag. Ser. 6* **26** (1913) 1–24. (Cited on pp. 1 and 4).

[7] W. Heisenberg, *Über den anschaulichen Inhalt der quantentheoretischen Kinematik und Mechanik*, *Z. Phys.* **43** (1927) 172–198. (Cited on pp. 1 and 4).

[8] E. Schrödinger, *Quantisierung als Eigenwertproblem*, *Ann. Phys.* **384** (1926) 361–376. (Cited on pp. 1 and 4).

[9] P. A. M. Dirac and N. H. D. Bohr, *The quantum theory of the emission and absorption of radiation*, *Proc. Roy. Soc. London Series A, Containing Papers of a Mathematical and Physical Character* **114** (1927) 243–265. (Cited on pp. 1, 4, 5, and 6).

[10] P. A. M. Dirac and R. H. Fowler, *The quantum theory of the electron*, *Proc. Roy. Soc. London Series A, Containing Papers of a Mathematical and Physical Character* **117** (1928) 610–624. (Cited on pp. 1 and 4).

[11] D. Harlow et al., *TF1 Snowmass Report: Quantum gravity, string theory, and black holes*, 2210.01737. (Cited on p. 2).

[12] I. Newton, *Philosophiæ Naturalis Principia Mathematica*, Jussu Societatis Regiæ ac Typis Josephi Streater, 1687. (Cited on p. 2).

[13] A. Einstein, *Explanation of the Perihelion Motion of Mercury from the General Theory of Relativity*, *Sitzungsber. Preuss. Akad. Wiss. Berlin (Math. Phys.)* **1915** (1915) 831–839. (Cited on p. 2).

[14] A. Einstein, *On The influence of gravitation on the propagation of light*, *Annalen Phys.* **35** (1911) 898–908. (Cited on p. 2).

[15] A. Einstein, *Über Gravitationswellen*, *Sitzungsber. Preuss. Akad. Wiss. Berlin (Math. Phys.)* **1918** (1918) 154–167. (Cited on p. 2).

[16] A. Einstein, *Approximative Integration of the Field Equations of Gravitation*, *Sitzungsber. Preuss. Akad. Wiss. Berlin (Math. Phys.)* **1916** (1916) 688–696. (Cited on p. 2).

[17] F. W. Dyson, A. S. Eddington and C. Davidson, *A Determination of the Deflection of Light by the Sun's Gravitational Field, from Observations Made at the Total Eclipse of May 29, 1919*, *Phil. Trans. Roy. Soc. Lond. A* **220** (1920) 291–333. (Cited on p. 2).

[18] R. D. Reasenberg, I. I. Shapiro, P. E. MacNeil, R. B. Goldstein, J. C. Breidenthal, J. P. Brenkle et al., *Viking relativity experiment: Verification of signal retardation by solar gravity*, *Astrophys. J. Lett.* **234** (1979) L219–L221. (Cited on p. 2).

[19] D. E. Lebach, B. E. Corey, I. I. Shapiro, M. I. Ratner, J. C. Webber, A. E. E. Rogers et al., *Measurement of the Solar Gravitational Deflection of Radio Waves Using Very-Long-Baseline Interferometry*, *Phys. Rev. Lett.* **75** (1995) 1439–1442. (Cited on p. 2).

[20] B. Bertotti, L. Iess and P. Tortora, *A test of general relativity using radio links with the Cassini spacecraft*, *Nature* **425** (2003) 374–376. (Cited on p. 2).

[21] J. B. Holberg, *Sirius B and the Measurement of the Gravitational Redshift*, *Journal for the History of Astronomy* **41** (2010) 41–64, [https://doi.org/10.1177/002182861004100102]. (Cited on p. 2).

[22] S. G. Turyshev, *Experimental Tests of General Relativity*, *Ann. Rev. Nucl. Part. Sci.* **58** (2008) 207–248, [0806.1731]. (Cited on p. 2).

[23] J. Antoniadis et al., *A Massive Pulsar in a Compact Relativistic Binary*, *Science* **340** (2013) 6131, [1304.6875]. (Cited on p. 2).

[24] LIGO Scientific, Virgo collaboration, B. P. Abbott et al., *Observation of Gravitational Waves from a Binary Black Hole Merger*, *Phys. Rev. Lett.* **116** (2016) 061102, [1602.03837]. (Cited on p. 2).

[25] Event Horizon Telescope collaboration, K. Akiyama et al., *First M87 Event Horizon Telescope Results. I. The Shadow of the Supermassive Black Hole*, *Astrophys. J. Lett.* **875** (2019) L1, [1906.11238]. (Cited on p. 2).

[26] Event Horizon Telescope collaboration, K. Akiyama et al., *First Sagittarius A* Event Horizon Telescope Results. I. The Shadow of the Supermassive Black Hole in the Center of the Milky Way*, *Astrophys. J. Lett.* **930** (2022) L12. (Cited on p. 2).

[27] K. Schwarzschild, *On the gravitational field of a sphere of incompressible fluid according to Einstein's theory*, *Sitzungsber. Preuss. Akad. Wiss. Berlin (Math. Phys.)* **1916** (1916) 424–434, [physics/9912033]. (Cited on p. 3).

[28] K. Schwarzschild, *On the gravitational field of a mass point according to Einstein's theory*, *Sitzungsber. Preuss. Akad. Wiss. Berlin (Math. Phys.)* **1916** (1916) 189–196, [physics/9905030]. (Cited on p. 3).

[29] R. Penrose, *Gravitational Collapse and Space-Time Singularities*, *Phys. Rev. Lett.* **14** (Jan, 1965) 57–59. (Cited on p. 3).

[30] S. W. Hawking and R. Penrose, *The Singularities of gravitational collapse and cosmology*, *Proc. Roy. Soc. Lond. A* **314** (1970) 529–548. (Cited on p. 3).

[31] S. W. Hawking and G. F. R. Ellis, *The Large Scale Structure of Space-Time*, Cambridge Monographs on Mathematical Physics, Cambridge University Press, 2, 2023, 10.1017/9781009253161. (Cited on pp. 3 and 39).

[32] J. J. Thomson, *Cathode Rays*, *Philosophical Magazine and Journal of Science* **44** (1897) 293–306. (Cited on p. 3).

[33] E. Rutherford, *The scattering of alpha and beta particles by matter and the structure of the atom*, *Phil. Mag. Ser. 6* **21** (1911) 669–688. (Cited on p. 3).

[34] A. Einstein and M. Born, *Born–Einstein Letters, 1916–1955*, Macmillan Science, Palgrave Macmillan New York, 1 ed., 2005. (Cited on p. 4).

[35] A. Einstein, *On the electrodynamics of moving bodies*, *Ann. Phys.* **17** (1905) 891–921. (Cited on p. 5).

[36] A. Einstein, *Ist die Trägheit eines Körpers von seinem Energieinhalt abhängig?*, *Ann. Phys.* **323** (1905) 639–641. (Cited on p. 5).

[37] J. S. Bell, *On the Einstein Podolsky Rosen paradox*, *Physics Physique Fizika* **1** (Nov, 1964) 195–200. (Cited on p. 5).

[38] A. Einstein, B. Podolsky and N. Rosen, *Can quantum mechanical description of physical reality be considered complete?*, *Phys. Rev.* **47** (1935) 777–780. (Cited on p. 5).

[39] B. Hensen et al., *Loophole-free Bell inequality violation using electron spins separated by 1.3 kilometres*, *Nature* **526** (2015) 682–686, [1508.05949]. (Cited on p. 5).

[40] M. Giustina et al., *Significant-Loophole-Free Test of Bell's Theorem with Entangled Photons*, *Phys. Rev. Lett.* **115** (2015) 250401, [1511.03190]. (Cited on p. 5).

[41] L. K. Shalm, E. Meyer-Scott, B. G. Christensen, P. Bierhorst, M. A. Wayne, M. J. Stevens et al., *Strong Loophole-Free Test of Local Realism*, *Phys. Rev. Lett.* **115** (Dec, 2015) 250402. (Cited on p. 5).

[42] W. Heisenberg and W. Pauli, *Zur Quantendynamik der Wellenfelder*, *Zeitschrift für Physik* **56** (Jan., 1929) 1–61. (Cited on p. 5).

[43] R. P. Feynman, *Space-time approach to nonrelativistic quantum mechanics*, *Rev. Mod. Phys.* **20** (1948) 367–387. (Cited on pp. 5 and 6).

[44] M. E. Peskin and D. V. Schroeder, *An Introduction to quantum field theory*, Addison-Wesley, Reading, USA, 1995. (Cited on pp. 5, 35, and 319).

[45] R. P. Feynman, *Mathematical Formulation of the Quantum Theory of Electromagnetic Interaction*, *Phys. Rev.* **80** (Nov, 1950) 440–457. (Cited on p. 6).

[46] R. P. Feynman and M. Gell-Mann, *Theory of the Fermi Interaction*, *Phys. Rev.* **109** (Jan, 1958) 193–198. (Cited on p. 6).

[47] S. L. Glashow, *The renormalizability of vector meson interactions*, *Nucl. Phys.* **10** (1959) 107–117. (Cited on p. 6).

[48] A. Salam and J. C. Ward, *Weak and electromagnetic interactions*, *Nuovo Cim.* **11** (1959) 568–577. (Cited on p. 6).

[49] S. L. Glashow, *Partial Symmetries of Weak Interactions*, *Nucl. Phys.* **22** (1961) 579–588. (Cited on p. 6).

[50] S. Weinberg, *A Model of Leptons*, *Phys. Rev. Lett.* **19** (1967) 1264–1266. (Cited on p. 6).

[51] A. Salam, *Weak and Electromagnetic Interactions*, *Conf. Proc. C* **680519** (1968) 367–377. (Cited on p. 6).

[52] M. Gell-Mann, *A Schematic Model of Baryons and Mesons*, *Phys. Lett.* **8** (1964) 214–215. (Cited on p. 6).

[53] H. Fritzsch, M. Gell-Mann and H. Leutwyler, *Advantages of the Color Octet Gluon Picture*, *Phys. Lett. B* **47** (1973) 365–368. (Cited on p. 6).

[54] D. J. Gross and F. Wilczek, *Ultraviolet Behavior of Nonabelian Gauge Theories*, *Phys. Rev. Lett.* **30** (1973) 1343–1346. (Cited on p. 6).

[55] H. D. Politzer, *Asymptotic Freedom: An Approach to Strong Interactions*, *Phys. Rept.* **14** (1974) 129–180. (Cited on p. 6).

[56] K. G. Wilson, *Confinement of Quarks*, *Phys. Rev. D* **10** (1974) 2445–2459. (Cited on p. 6).

[57] Particle Data Group collaboration, K. A. Olive et al., *Review of Particle Physics*, *Chin. Phys. C* **38** (2014) 090001. (Cited on p. 6).

[58] ATLAS collaboration, G. Aad et al., *Observation of a new particle in the search for the Standard Model Higgs boson with the ATLAS detector at the LHC*, *Phys. Lett. B* **716** (2012) 1–29, [1207.7214]. (Cited on p. 6).

[59] CMS collaboration, S. Chatrchyan et al., *Observation of a New Boson at a Mass of 125 GeV with the CMS Experiment at the LHC*, *Phys. Lett. B* **716** (2012) 30–61, [1207.7235]. (Cited on p. 6).

[60] J. W. Rohlf, *Modern physics from alpha to Z0*, John Wiley & Sons, Nashville, TN, Mar., 1994. (Cited on p. 6).

[61] A. Zee, *Quantum field theory in a nutshell*, In a Nutshell, Princeton University Press, Princeton, NJ, 2 ed., Feb., 2010. (Cited on pp. 6, 7, and 35).

[62] A. H. Guth, *The Inflationary Universe: A Possible Solution to the Horizon and Flatness Problems*, *Phys. Rev. D* **23** (1981) 347–356. (Cited on p. 7).

[63] M. H. Goroff and A. Sagnotti, *The Ultraviolet Behavior of Einstein Gravity*, *Nucl. Phys. B* **266** (1986) 709–736. (Cited on p. 7).

[64] A. E. M. van de Ven, *Two loop quantum gravity*, *Nucl. Phys. B* **378** (1992) 309–366. (Cited on p. 7).

[65] J. F. Donoghue, *Leading quantum correction to the Newtonian potential*, *Phys. Rev. Lett.* **72** (1994) 2996–2999, [gr-qc/9310024]. (Cited on p. 7).

[66] J. F. Donoghue, *General relativity as an effective field theory: The leading quantum corrections*, *Phys. Rev. D* **50** (1994) 3874–3888, [gr-qc/9405057]. (Cited on p. 7).

[67] J. F. Donoghue, *Introduction to the effective field theory description of gravity*, in *Advanced School on Effective Theories*, 6, 1995, [gr-qc/9512024]. (Cited on p. 7).

[68] I. B. Khriplovich and G. G. Kirilin, *Quantum power correction to the Newton law*, *J. Exp. Theor. Phys.* **95** (2002) 981–986, [gr-qc/0207118]. (Cited on p. 7).

[69] N. E. J. Bjerrum-Bohr, J. F. Donoghue and B. R. Holstein, *Quantum gravitational corrections to the nonrelativistic scattering potential of two masses*, *Phys. Rev. D* **67** (2003) 084033, [hep-th/0211072]. (Cited on p. 7).

[70] C. P. Burgess, *Quantum Gravity in Everyday Life: General Relativity as an Effective Field Theory*, *Living Reviews in Relativity* **7** (Apr., 2004) . (Cited on p. 7).

[71] J. Polchinski, *String theory. Vol. 1: An introduction to the bosonic string*, Cambridge Monographs on Mathematical Physics, Cambridge University Press, 12, 2007, 10.1017/CBO9780511816079. (Cited on pp. 7 and 30).

[72] J. Polchinski, *String theory. Vol. 2: Superstring theory and beyond*, Cambridge Monographs on Mathematical Physics, Cambridge University Press, 12, 2007, 10.1017/CBO9780511618123. (Cited on p. 7).

[73] B. Zwiebach, *A first course in string theory*, Cambridge University Press, 7, 2006, 10.1017/CBO9780511841682. (Cited on p. 7).

[74] G. Veneziano, *Construction of a crossing - symmetric, Regge behaved amplitude for linearly rising trajectories*, *Nuovo Cim. A* **57** (1968) 190–197. (Cited on p. 7).

[75] Z. Koba and H. B. Nielsen, *Reaction amplitude for n mesons: A Generalization of the Veneziano-Bardakci-Ruegg-Virasora model*, *Nucl. Phys. B* **10** (1969) 633–655. (Cited on p. 7).

[76] M. A. Virasoro, *Alternative constructions of crossing-symmetric amplitudes with regge behavior*, *Phys. Rev.* **177** (1969) 2309–2311. (Cited on p. 7).

[77] J. A. Shapiro, *Electrostatic analog for the virasoro model*, *Phys. Lett. B* **33** (1970) 361–362. (Cited on p. 7).

[78] J. Scherk and J. H. Schwarz, *Dual Models for Nonhadrons*, *Nucl. Phys. B* **81** (1974) 118–144. (Cited on p. 7).

[79] T. Yoneya, *Connection of Dual Models to Electrodynamics and Gravidynamics*, *Prog. Theor. Phys.* **51** (1974) 1907–1920. (Cited on p. 7).

[80] M. B. Green and J. H. Schwarz, *Anomaly Cancellation in Supersymmetric D=10 Gauge Theory and Superstring Theory*, *Phys. Lett. B* **149** (1984) 117–122. (Cited on p. 7).

[81] D. J. Gross, J. A. Harvey, E. J. Martinec and R. Rohm, *The Heterotic String*, *Phys. Rev. Lett.* **54** (1985) 502–505. (Cited on p. 7).

[82] P. Candelas, G. T. Horowitz, A. Strominger and E. Witten, *Vacuum configurations for superstrings*, *Nucl. Phys. B* **258** (1985) 46–74. (Cited on pp. 7 and 8).

[83] P. Horava and E. Witten, *Heterotic and type I string dynamics from eleven-dimensions*, *Nucl. Phys. B* **460** (1996) 506–524, [hep-th/9510209]. (Cited on p. 8).

[84] E. Witten, *String theory dynamics in various dimensions*, *Nucl. Phys. B* **443** (1995) 85–126, [hep-th/9503124]. (Cited on p. 8).

[85] J. M. Maldacena, *The Large N limit of superconformal field theories and supergravity*, *Adv. Theor. Math. Phys.* **2** (1998) 231–252, [hep-th/9711200]. (Cited on pp. 8, 21, 25, 32, and 33).

[86] S. S. Gubser, I. R. Klebanov and A. M. Polyakov, *Gauge theory correlators from noncritical string theory*, *Phys. Lett. B* **428** (1998) 105–114, [hep-th/9802109]. (Cited on pp. 8, 21, 25, 33, 35, 124, and 217).

[87] E. Witten, *Anti-de Sitter space and holography*, *Adv. Theor. Math. Phys.* **2** (1998) 253–291, [hep-th/9802150]. (Cited on pp. 8, 21, 25, 33, 35, and 36).

[88] S. A. Hartnoll, C. P. Herzog and G. T. Horowitz, *Building a Holographic Superconductor*, *Phys. Rev. Lett.* **101** (2008) 031601, [0803.3295]. (Cited on pp. 8 and 34).

[89] S. A. Hartnoll, C. P. Herzog and G. T. Horowitz, *Holographic Superconductors*, *JHEP* **12** (2008) 015, [0810.1563]. (Cited on pp. 8 and 34).

[90] S. A. Hartnoll, *Lectures on holographic methods for condensed matter physics*, *Class. Quant. Grav.* **26** (2009) 224002, [0903.3246]. (Cited on pp. 8 and 34).

[91] J. McGreevy, *Holographic duality with a view toward many-body physics*, *Adv. High Energy Phys.* **2010** (2010) 723105, [0909.0518]. (Cited on pp. 8, 22, and 34).

[92] S. Sachdev, *Condensed Matter and AdS/CFT*, *Lect. Notes Phys.* **828** (2011) 273–311, [1002.2947]. (Cited on pp. 8 and 34).

[93] J. Erdmenger, C. Hoyos, A. O'Bannon and J. Wu, *A Holographic Model of the Kondo Effect*, *JHEP* **12** (2013) 086, [1310.3271]. (Cited on pp. 8 and 34).

[94] J. Zaanen, Y.-W. Sun, Y. Liu and K. Schalm, *Holographic Duality in Condensed Matter Physics*, Cambridge Univ. Press, 2015, 10.1017/CBO9781139942492. (Cited on p. 8).

[95] S. A. Hartnoll, A. Lucas and S. Sachdev, *Holographic quantum matter*, 1612.07324. (Cited on pp. 8 and 34).

[96] O. Aharony, *The NonAdS / nonCFT correspondence, or three different paths to QCD*, in *NATO Advanced Study Institute and EC Summer School on Progress in String, Field and Particle Theory*, pp. 3–24, 12, 2002, [hep-th/0212193]. (Cited on p. 8).

[97] J. Erlich, E. Katz, D. T. Son and M. A. Stephanov, *QCD and a holographic model of hadrons*, *Phys. Rev. Lett.* **95** (2005) 261602, [hep-ph/0501128]. (Cited on pp. 8 and 34).

[98] L. Da Rold and A. Pomarol, *Chiral symmetry breaking from five dimensional spaces*, *Nucl. Phys. B* **721** (2005) 79–97, [hep-ph/0501218]. (Cited on pp. 8 and 34).

[99] A. Karch, E. Katz, D. T. Son and M. A. Stephanov, *Linear confinement and AdS/QCD*, *Phys. Rev. D* **74** (2006) 015005, [hep-ph/0602229]. (Cited on pp. 8 and 34).

[100] J. Erdmenger, N. Evans, I. Kirsch and E. Threlfall, *Mesons in Gauge/Gravity Duals - A Review*, *Eur. Phys. J. A* **35** (2008) 81–133, [0711.4467]. (Cited on pp. 8 and 34).

[101] J. Casalderrey-Solana, H. Liu, D. Mateos, K. Rajagopal and U. A. Wiedemann, *Gauge/String Duality, Hot QCD and Heavy Ion Collisions*, Cambridge University Press, 2014, 10.1017/CBO9781139136747, [1101.0618]. (Cited on p. 8).

[102] G. 't Hooft, *Dimensional reduction in quantum gravity*, *Conf. Proc. C* **930308** (1993) 284–296, [gr-qc/9310026]. (Cited on pp. 8 and 22).

[103] L. Susskind, *The World as a hologram*, *J. Math. Phys.* **36** (1995) 6377–6396, [hep-th/9409089]. (Cited on pp. 8 and 22).

[104] R. Bousso, *The holographic principle*, *Rev. Mod. Phys.* **74** (2002) 825–874, [hep-th/0203101]. (Cited on pp. 8, 23, and 24).

[105] J. D. Bekenstein, *Black Holes and the Second Law*, *Lett. Nuovo Cim.* **4** (1972) 737–740. (Cited on pp. 8 and 23).

[106] J. D. Bekenstein, *Black Holes and Entropy*, *Phys. Rev. D* **7** (1973) 2333–2346. (Cited on pp. 8, 23, 24, and 43).

[107] J. D. Bekenstein, *Universal upper bound on the entropy-to-energy ratio for bounded systems*, *Phys. Rev. D* **23** (1981) 287–298. (Cited on pp. 8, 23, 24, and 25).

[108] S. W. Hawking, *Black holes in general relativity*, *Communications in Mathematical Physics* **25** (June, 1972) 152–166. (Cited on pp. 8 and 23).

[109] S. W. Hawking, *Gravitational radiation from colliding black holes*, *Phys. Rev. Lett.* **26** (1971) 1344–1346. (Cited on pp. 8, 23, and 39).

[110] S. W. Hawking, *Black hole explosions*, *Nature* **248** (1974) 30–31. (Cited on pp. 8, 9, and 23).

[111] S. W. Hawking, *Particle Creation by Black Holes*, *Commun. Math. Phys.* **43** (1975) 199–220. (Cited on pp. 8, 9, and 23).

[112] A. Strominger and C. Vafa, *Microscopic origin of the Bekenstein-Hawking entropy*, *Phys. Lett. B* **379** (1996) 99–104, [hep-th/9601029]. (Cited on pp. 9 and 24).

[113] A. Strominger, *Black hole entropy from near horizon microstates*, *JHEP* **02** (1998) 009, [hep-th/9712251]. (Cited on p. 9).

[114] S. Ryu and T. Takayanagi, *Holographic derivation of entanglement entropy from AdS/CFT*, *Phys. Rev. Lett.* **96** (2006) 181602, [hep-th/0603001]. (Cited on pp. 9, 47, 58, 60, 198, and 243).

[115] S. Ryu and T. Takayanagi, *Aspects of Holographic Entanglement Entropy*, *JHEP* **08** (2006) 045, [hep-th/0605073]. (Cited on pp. 9, 47, 58, 59, 60, 198, and 243).

[116] C. Holzhey, F. Larsen and F. Wilczek, *Geometric and renormalized entropy in conformal field theory*, *Nucl. Phys. B* **424** (1994) 443–467, [hep-th/9403108]. (Cited on pp. 9, 14, 53, 55, 56, 188, 189, 276, 288, and 290).

[117] P. Calabrese and J. L. Cardy, *Entanglement entropy and quantum field theory*, *J. Stat. Mech.* **0406** (2004) P06002, [hep-th/0405152]. (Cited on pp. 9, 14, 47, 56, 186, 188, 189, and 276).

[118] P. Calabrese and J. Cardy, *Entanglement entropy and conformal field theory*, *J. Phys. A* **42** (2009) 504005, [0905.4013]. (Cited on pp. 9, 14, 47, 56, 188, and 189).

[119] S. W. Hawking, *Breakdown of predictability in gravitational collapse*, *Phys. Rev. D* **14** (Nov, 1976) 2460–2473. (Cited on pp. 10 and 23).

[120] G. Penington, *Entanglement Wedge Reconstruction and the Information Paradox*, *JHEP* **09** (2020) 002, [1905.08255]. (Cited on p. 10).

[121] A. Almheiri, N. Engelhardt, D. Marolf and H. Maxfield, *The entropy of bulk quantum fields and the entanglement wedge of an evaporating black hole*, *JHEP* **12** (2019) 063, [1905.08762]. (Cited on p. 10).

[122] A. Almheiri, R. Mahajan, J. Maldacena and Y. Zhao, *The Page curve of Hawking radiation from semiclassical geometry*, *JHEP* **03** (2020) 149, [1908.10996]. (Cited on p. 10).

[123] G. Penington, S. H. Shenker, D. Stanford and Z. Yang, *Replica wormholes and the black hole interior*, *JHEP* **03** (2022) 205, [1911.11977]. (Cited on p. 10).

[124] A. Almheiri, T. Hartman, J. Maldacena, E. Shaghoulian and A. Tajdini, *The entropy of Hawking radiation*, *Rev. Mod. Phys.* **93** (2021) 035002, [2006.06872]. (Cited on p. 10).

[125] N. Engelhardt and A. C. Wall, *Quantum Extremal Surfaces: Holographic Entanglement Entropy beyond the Classical Regime*, *JHEP* **01** (2015) 073, [1408.3203]. (Cited on p. 10).

[126] D. N. Page, *Information in black hole radiation*, *Phys. Rev. Lett.* **71** (1993) 3743–3746, [hep-th/9306083]. (Cited on p. 10).

[127] H. Geng and A. Karch, *Massive islands*, *JHEP* **09** (2020) 121, [2006.02438]. (Cited on p. 10).

[128] J. Martín García, *Quantum Complexity and Holography*. PhD thesis, U. Autonoma, Madrid (main), 2020. 2209.04632. (Cited on p. 11).

[129] J. M. Maldacena, *Eternal black holes in anti-de Sitter*, *JHEP* **04** (2003) 021, [hep-th/0106112]. (Cited on pp. 10, 11, 38, 43, 44, 45, 46, 146, 244, 269, and 277).

[130] W. Israel, *Thermo field dynamics of black holes*, *Phys. Lett. A* **57** (1976) 107–110. (Cited on pp. 11, 38, 44, and 244).

[131] M. Van Raamsdonk, *Comments on quantum gravity and entanglement*, 0907.2939. (Cited on p. 11).

[132] M. Van Raamsdonk, *Building up spacetime with quantum entanglement*, *Gen. Rel. Grav.* **42** (2010) 2323–2329, [1005.3035]. (Cited on pp. 11, 21, 244, and 269).

[133] B. Swingle, *Constructing holographic spacetimes using entanglement renormalization*, 1209.3304. (Cited on pp. 11, 75, and 243).

[134] J. Maldacena and L. Susskind, *Cool horizons for entangled black holes*, *Fortsch. Phys.* **61** (2013) 781–811, [1306.0533]. (Cited on pp. 11, 46, 146, 244, and 269).

[135] J. M. Maldacena and L. Maoz, *Wormholes in AdS*, *JHEP* **02** (2004) 053, [hep-th/0401024]. (Cited on pp. 11 and 244).

[136] D. Harlow, *Wormholes, Emergent Gauge Fields, and the Weak Gravity Conjecture*, *JHEP* **01** (2016) 122, [1510.07911]. (Cited on p. 11).

[137] J. Boruch, L. V. Iliesiu, G. Lin and C. Yan, *How the Hilbert space of two-sided black holes factorises*, 2406.04396. (Cited on pp. 11, 270, and 298).

[138] L. Susskind, *Entanglement is not enough*, *Fortsch. Phys.* **64** (2016) 49–71, [1411.0690]. (Cited on pp. 12, 60, 61, 65, 243, and 244).

[139] L. Susskind and Y. Zhao, *Switchbacks and the Bridge to Nowhere*, 1408.2823. (Cited on pp. 12, 61, 64, 65, and 243).

[140] L. Susskind, *Computational Complexity and Black Hole Horizons*, *Fortsch. Phys.* **64** (2016) 24–43, [1403.5695]. (Cited on pp. 12, 61, 64, 65, and 243).

[141] D. Stanford and L. Susskind, *Complexity and Shock Wave Geometries*, *Phys. Rev. D* **90** (2014) 126007, [1406.2678]. (Cited on pp. 12, 61, 64, 65, and 243).

[142] F. J. Murray and J. von Neumann, *On Rings of Operators*, *The Annals of Mathematics* **37** (Jan., 1936) 116. (Cited on pp. 12, 243, 288, 289, 291, and 293).

[143] F. J. Murray and J. von Neumann, *On rings of operators. II*, *Transactions of the American Mathematical Society* **41** (1937) 208–248. (Cited on pp. 12, 243, 288, 289, and 291).

[144] J. von Neumann, *On Rings of Operators. III*, *The Annals of Mathematics* **41** (Jan., 1940) 94. (Cited on pp. 12, 243, 288, 289, and 291).

[145] F. J. Murray and J. von Neumann, *On Rings of Operators. IV*, *The Annals of Mathematics* **44** (Oct., 1943) 716. (Cited on pp. 12, 243, 288, 289, and 291).

[146] S. Leutheusser and H. Liu, *Causal connectability between quantum systems and the black hole interior in holographic duality*, *Phys. Rev. D* **108** (2023) 086019, [2110.05497]. (Cited on pp. 12, 245, 289, 290, 297, 298, and 328).

[147] S. Leutheusser and H. Liu, *Subalgebra-subregion duality: emergence of space and time in holography*, 2212.13266. (Cited on pp. 12 and 290).

[148] E. Witten, *Gravity and the crossed product*, *JHEP* **10** (2022) 008, [2112.12828]. (Cited on pp. 12, 245, 289, and 298).

[149] S. W. Hawking and D. N. Page, *Thermodynamics of Black Holes in anti-De Sitter Space*, *Commun. Math. Phys.* **87** (1983) 577. (Cited on pp. 12, 39, 40, 41, 42, and 43).

[150] H. S. M. Coxeter, *Regular Honeycombs in Hyperbolic Space*, *Proceedings of the International Congress of Mathematicians 1954, Amsterdam.* **3** (1956) . (Cited on pp. 12, 83, and 87).

[151] R. Orus, *A Practical Introduction to Tensor Networks: Matrix Product States and Projected Entangled Pair States*, *Annals Phys.* **349** (2014) 117–158, [1306.2164]. (Cited on pp. 14, 71, 72, and 73).

[152] F. Pastawski, B. Yoshida, D. Harlow and J. Preskill, *Holographic quantum error-correcting codes: Toy models for the bulk/boundary correspondence*, *JHEP* **06** (2015) 149, [1503.06237]. (Cited on pp. 14, 75, 218, 225, 234, 238, 243, and 345).

[153] A. Jahn and J. Eisert, *Holographic tensor network models and quantum error correction: a topical review*, *Quantum Sci. Technol.* **6** (2021) 033002, [2102.02619]. (Cited on pp. 14, 71, 72, 73, 74, 75, 76, and 243).

[154] M. B. Plenio and S. Virmani, *An introduction to entanglement measures*, *Quant. Inf. Comput.* **7** (2007) 001–051, [quant-ph/0504163]. (Cited on pp. 14, 47, 51, and 52).

[155] L. Amico, R. Fazio, A. Osterloh and V. Vedral, *Entanglement in many-body systems*, *Rev. Mod. Phys.* **80** (2008) 517–576, [quant-ph/0703044]. (Cited on pp. 14, 47, 51, 53, and 287).

[156] J. Eisert, M. Cramer and M. B. Plenio, *Colloquium: Area laws for the entanglement entropy*, *Rev. Mod. Phys.* **82** (2010) 277–306, [0808.3773]. (Cited on pp. 14, 47, 51, 52, 287, and 288).

[157] P. Basteiro, F. Dusel, J. Erdmenger, D. Herdt, H. Hinrichsen, R. Meyer et al., *Breitenlohner-Freedman Bound on Hyperbolic Tilings*, *Phys. Rev. Lett.* **130** (2023) 091604, [2205.05081]. (Cited on pp. 15, 18, 82, 124, 128, 131, 136, 154, and 351).

[158] P. Basteiro, G. Di Giulio, J. Erdmenger, J. Karl, R. Meyer and Z.-Y. Xian, *Towards Explicit Discrete Holography: Aperiodic Spin Chains from Hyperbolic Tilings*, *SciPost Phys.* **13** (2022) 103, [2205.05693]. (Cited on pp. 15, 18, 82,

115, 117, 158, 163, 165, 168, 169, 171, 186, 198, 199, 200, 202, 217, 218, 220, 222, 230, 231, 232, 235, 237, 238, 348, and 351).

[159] P. Basteiro, R. N. Das, G. Di Giulio and J. Erdmenger, *Aperiodic spin chains at the boundary of hyperbolic tilings*, *SciPost Phys.* **15** (2023) 218, [2212.11292]. (Cited on pp. 15, 18, 82, 95, 115, 117, 158, 165, 186, 189, 191, 192, 194, 196, 197, 198, 205, 212, 213, 215, 216, 217, 348, and 351).

[160] S. Dey, A. Chen, P. Basteiro, A. Fritzsche, M. Greiter, M. Kaminski et al., *Simulating Holographic Conformal Field Theories on Hyperbolic Lattices*, 2404.03062. (Cited on pp. 15, 18, 82, 140, 141, 145, 146, 147, 150, 151, 152, 153, 154, 156, 157, and 351).

[161] P. Basteiro, J. Erdmenger, P. Fries, F. Goth, I. Matthaiakakis and R. Meyer, *Quantum complexity as hydrodynamics*, *Phys. Rev. D* **106** (2022) 065016, [2109.01152]. (Cited on pp. 16, 19, 243, 245, 246, 249, 253, 254, 263, and 351).

[162] S. Banerjee, P. Basteiro, R. N. Das and M. Dorband, *Geometric Quantum Discord Signals Non-Factorization*, *JHEP* **08** (2023) 104, [2305.04952]. (Cited on pp. 16, 19, 244, 280, and 351).

[163] P. Basteiro, G. Di Giulio, J. Erdmenger and Z.-Y. Xian, *Entanglement in Interacting Majorana Chains and Transitions of von Neumann Algebras*, *Phys. Rev. Lett.* **132** (Apr, 2024) 161604, [2401.04764]. (Cited on pp. 16, 19, 245, 298, 348, and 351).

[164] H. Verlinde, *ER = EPR revisited: On the Entropy of an Einstein-Rosen Bridge*, 2003.13117. (Cited on pp. 19, 270, 271, 277, 278, 279, 280, 284, and 287).

[165] M. A. Nielsen and I. L. Chuang, *Quantum Computation and Quantum Information: 10th Anniversary Edition*, Cambridge University Press, 2010, 10.1017/CBO9780511976667. (Cited on pp. 21, 47, 48, 49, 50, 52, 61, and 243).

[166] J. Watrous, *The Theory of Quantum Information*, Cambridge University Press, 2018, 10.1017/9781316848142. (Cited on pp. 21 and 243).

[167] M. M. Wilde, *Quantum Information Theory*, Cambridge University Press, Nov., 2016, 10.1017/9781316809976. (Cited on pp. 21 and 243).

[168] M. Ammon and J. Erdmenger, *Gauge/gravity duality: Foundations and applications*, Cambridge University Press, Cambridge, 2015,

10.1017/CBO9780511846373. (Cited on pp. 22, 25, 27, 30, 31, 32, 33, 34, 36, 37, 78, 125, 150, 212, 217, 224, and 239).

[169] M. Rangamani and T. Takayanagi, *Holographic Entanglement Entropy*, vol. 931, Springer, 2017, 10.1007/978-3-319-52573-0, [1609.01287]. (Cited on pp. 22, 33, 47, 59, 71, 73, 74, and 243).

[170] J. Penedones, *TASI lectures on AdS/CFT*, in *Theoretical Advanced Study Institute in Elementary Particle Physics: New Frontiers in Fields and Strings*, pp. 75–136, 2017, 10.1142/9789813149441˙0002, [1608.04948]. (Cited on p. 22).

[171] B. Chen, B. Czech and Z.-z. Wang, *Quantum information in holographic duality*, *Rept. Prog. Phys.* **85** (2022) 046001, [2108.09188]. (Cited on p. 22).

[172] P. Di Francesco, P. Mathieu and D. Senechal, *Conformal Field Theory*, Graduate Texts in Contemporary Physics, Springer-Verlag, New York, 1997, 10.1007/978-1-4612-2256-9. (Cited on pp. 22, 30, 32, 150, and 160).

[173] J. D. Bekenstein, *Generalized second law of thermodynamics in black hole physics*, *Phys. Rev. D* **9** (1974) 3292–3300. (Cited on p. 23).

[174] J. M. Bardeen, B. Carter and S. W. Hawking, *The Four Laws of Black Hole Mechanics*, *Commun. Math. Phys.* **31** (1973) 161–170. (Cited on pp. 23 and 24).

[175] S. W. Hawking, *Black holes and thermodynamics*, *Phys. Rev. D* **13** (Jan, 1976) 191–197. (Cited on p. 23).

[176] R. Giles and C. B. Thorn, *Lattice approach to string theory*, *Phys. Rev. D* **16** (Jul, 1977) 366–386. (Cited on p. 24).

[177] R. Giles, L. D. McLerran and C. B. Thorn, *String representation for a field theory with internal symmetry*, *Phys. Rev. D* **17** (Apr, 1978) 2058–2073. (Cited on p. 24).

[178] C. B. Thorn, *Substructure of string*, in *Strings 96: Current Trends in String Theory*, 7, 1996, [hep-th/9607204]. (Cited on p. 24).

[179] C. B. Thorn, *Reformulating string theory with the 1/N expansion*, in *The First International A.D. Sakharov Conference on Physics*, The First International A.D. Sakharov Conference on Physics, 5, 1991, [hep-th/9405069]. (Cited on p. 24).

[180] C. B. Thorn, *Calculating the rest tension for a polymer of string bits*, *Phys. Rev. D* **51** (Jan, 1995) 647–664. (Cited on p. 24).

[181] C. Thorn, *Quark confinement in the infinite-momentum frame*, *Phys. Rev. D* **19** (Jan, 1979) 639–651. (Cited on p. 24).

[182] J. W. York, *Role of Conformal Three-Geometry in the Dynamics of Gravitation*, *Phys. Rev. Lett.* **28** (Apr, 1972) 1082–1085. (Cited on p. 25).

[183] G. W. Gibbons and S. W. Hawking, *Action integrals and partition functions in quantum gravity*, *Phys. Rev. D* **15** (May, 1977) 2752–2756. (Cited on pp. 25 and 43).

[184] G. 't Hooft, *A Planar Diagram Theory for Strong Interactions*, *Nucl. Phys. B* **72** (1974) 461. (Cited on pp. 33 and 212).

[185] E. Witten, *Baryons in the 1/n Expansion*, *Nucl. Phys. B* **160** (1979) 57–115. (Cited on p. 33).

[186] N. Seiberg, *Notes on theories with 16 supercharges*, *Nucl. Phys. B Proc. Suppl.* **67** (1998) 158–171, [hep-th/9705117]. (Cited on p. 34).

[187] N. Itzhaki, J. M. Maldacena, J. Sonnenschein and S. Yankielowicz, *Supergravity and the large N limit of theories with sixteen supercharges*, *Phys. Rev. D* **58** (1998) 046004, [hep-th/9802042]. (Cited on p. 34).

[188] N. Seiberg and E. Witten, *The D1 / D5 system and singular CFT*, *JHEP* **04** (1999) 017, [hep-th/9903224]. (Cited on p. 34).

[189] O. Aharony, O. Bergman, D. L. Jafferis and J. Maldacena, *N=6 superconformal Chern-Simons-matter theories, M2-branes and their gravity duals*, *JHEP* **10** (2008) 091, [0806.1218]. (Cited on p. 34).

[190] L. Eberhardt, M. R. Gaberdiel and W. Li, *A holographic dual for string theory on $AdS_3 \times S^3 \times S^3 \times S^1$*, *JHEP* **08** (2017) 111, [1707.02705]. (Cited on p. 34).

[191] L. Eberhardt, M. R. Gaberdiel and R. Gopakumar, *The Worldsheet Dual of the Symmetric Product CFT*, *JHEP* **04** (2019) 103, [1812.01007]. (Cited on p. 34).

[192] L. Eberhardt, M. R. Gaberdiel and R. Gopakumar, *Deriving the AdS_3/CFT_2 correspondence*, *JHEP* **02** (2020) 136, [1911.00378]. (Cited on p. 34).

[193] S. Bhattacharyya, V. E. Hubeny, S. Minwalla and M. Rangamani, *Nonlinear Fluid Dynamics from Gravity*, *JHEP* **02** (2008) 045, [0712.2456]. (Cited on p. 34).

[194] V. E. Hubeny, *The Fluid/Gravity Correspondence: a new perspective on the Membrane Paradigm*, *Class. Quant. Grav.* **28** (2011) 114007, [1011.4948]. (Cited on pp. 34 and 78).

[195] V. E. Hubeny, S. Minwalla and M. Rangamani, *The fluid/gravity correspondence*, in *Theoretical Advanced Study Institute in Elementary Particle Physics: String theory and its Applications: From meV to the Planck Scale*, pp. 348–383, 2012, [1107.5780]. (Cited on p. 34).

[196] P. Breitenlohner and D. Z. Freedman, *Positive Energy in anti-De Sitter Backgrounds and Gauged Extended Supergravity*, *Phys. Lett. B* **115** (1982) 197–201. (Cited on pp. 36, 123, 126, 129, and 130).

[197] P. Breitenlohner and D. Z. Freedman, *Stability in Gauged Extended Supergravity*, *Annals Phys.* **144** (1982) 249. (Cited on pp. 36, 123, 126, 129, and 130).

[198] G. T. Horowitz and D. Marolf, *A New approach to string cosmology*, *JHEP* **07** (1998) 014, [hep-th/9805207]. (Cited on p. 38).

[199] V. Balasubramanian, P. Kraus, A. E. Lawrence and S. P. Trivedi, *Holographic probes of anti-de Sitter space-times*, *Phys. Rev. D* **59** (1999) 104021, [hep-th/9808017]. (Cited on p. 38).

[200] B. G. Carneiro da Cunha, *Inflation and holography in string theory*, *Phys. Rev. D* **65** (2002) 026001, [hep-th/0105219]. (Cited on p. 38).

[201] S. Deser, R. Jackiw and G. 't Hooft, *Three-Dimensional Einstein Gravity: Dynamics of Flat Space*, *Annals Phys.* **152** (1984) 220. (Cited on pp. 38 and 42).

[202] E. Martinec, *Soluble systems in quantum gravity*, *Phys. Rev. D* **30** (Sep, 1984) 1198–1204. (Cited on p. 38).

[203] S. Carlip, *Conformal field theory, (2+1)-dimensional gravity, and the BTZ black hole*, *Class. Quant. Grav.* **22** (2005) R85–R124, [gr-qc/0503022]. (Cited on p. 38).

[204] A. Achucarro and P. K. Townsend, *A Chern-Simons Action for Three-Dimensional anti-De Sitter Supergravity Theories*, *Phys. Lett. B* **180** (1986) 89. (Cited on p. 38).

[205] E. Witten, *(2+1)-Dimensional Gravity as an Exactly Soluble System*, *Nucl. Phys. B* **311** (1988) 46. (Cited on p. 38).

[206] M. Henneaux, W. Merbis and A. Ranjbar, *Asymptotic dynamics of AdS_3 gravity with two asymptotic regions*, *JHEP* **03** (2020) 064, [1912.09465]. (Cited on pp. 38, 42, and 44).

[207] D. Ida, *No black hole theorem in three-dimensional gravity*, *Phys. Rev. Lett.* **85** (2000) 3758–3760, [gr-qc/0005129]. (Cited on p. 38).

[208] M. Bañados, C. Teitelboim and J. Zanelli, *The Black hole in three-dimensional space-time*, *Phys. Rev. Lett.* **69** (1992) 1849–1851, [hep-th/9204099]. (Cited on pp. 38, 43, and 146).

[209] M. Bañados, M. Henneaux, C. Teitelboim and J. Zanelli, *Geometry of the (2+1) black hole*, *Phys. Rev. D* **48** (1993) 1506–1525, [gr-qc/9302012]. (Cited on pp. 38, 41, 43, and 146).

[210] E. Witten, *Anti-de Sitter space, thermal phase transition, and confinement in gauge theories*, *Adv. Theor. Math. Phys.* **2** (1998) 505–532, [hep-th/9803131]. (Cited on p. 41).

[211] S. Carlip, *The (2+1)-Dimensional black hole*, *Class. Quant. Grav.* **12** (1995) 2853–2880, [gr-qc/9506079]. (Cited on pp. 41, 42, and 43).

[212] S. Carlip and C. Teitelboim, *Aspects of black hole quantum mechanics and thermodynamics in 2+1 dimensions*, *Phys. Rev. D* **51** (Jan, 1995) 622–631. (Cited on p. 41).

[213] L. Fidkowski, V. Hubeny, M. Kleban and S. Shenker, *The Black hole singularity in AdS / CFT*, *JHEP* **02** (2004) 014, [hep-th/0306170]. (Cited on pp. 42 and 44).

[214] S. Hyun, G. H. Lee and J. H. Yee, *Hawking radiation from (2+1)-dimensional black hole*, *Phys. Lett. B* **322** (1994) 182–187. (Cited on p. 43).

[215] I. Ichinose and Y. Satoh, *Entropies of scalar fields on three-dimensional black holes*, *Nucl. Phys. B* **447** (1995) 340–372, [hep-th/9412144]. (Cited on p. 43).

[216] S. Carlip and C. Teitelboim, *Aspects of black hole quantum mechanics and thermodynamics in (2+1)-dimensions*, *Phys. Rev. D* **51** (1995) 622–631, [gr-qc/9405070]. (Cited on p. 43).

[217] J. D. Brown, J. Creighton and R. B. Mann, *Temperature, energy and heat capacity of asymptotically anti-de Sitter black holes*, *Phys. Rev. D* **50** (1994) 6394–6403, [gr-qc/9405007]. (Cited on p. 43).

[218] S. Carlip, J. Gegenberg and R. B. Mann, *Black holes in three-dimensional topological gravity*, *Phys. Rev. D* **51** (1995) 6854–6859, [gr-qc/9410021]. (Cited on p. 43).

[219] R. Emparan and I. Sachs, *Quantization of AdS(3) black holes in external fields*, *Phys. Rev. Lett.* **81** (1998) 2408–2411, [hep-th/9806122]. (Cited on p. 43).

[220] S. Holst, *Gott time machines in the anti-de Sitter space*, *Gen. Rel. Grav.* **28** (1996) 387–403, [gr-qc/9501010]. (Cited on p. 43).

[221] S. Aminneborg, I. Bengtsson, S. Holst and P. Peldan, *Making anti-de Sitter black holes*, *Class. Quant. Grav.* **13** (1996) 2707–2714, [gr-qc/9604005]. (Cited on p. 43).

[222] S. Aminneborg, I. Bengtsson, D. Brill, S. Holst and P. Peldan, *Black holes and wormholes in (2+1)-dimensions*, *Class. Quant. Grav.* **15** (1998) 627–644, [gr-qc/9707036]. (Cited on p. 43).

[223] D. Brill, *Black holes and wormholes in (2+1)-dimensions*, *Lect. Notes Phys.* **537** (2000) 143, [gr-qc/9904083]. (Cited on p. 43).

[224] S. Carlip, *Quantum Gravity in 2+1 Dimensions*, Cambridge University Press, July, 1998, 10.1017/cbo9780511564192. (Cited on p. 43).

[225] K. Krasnov, *Holography and Riemann surfaces*, *Adv. Theor. Math. Phys.* **4** (2000) 929–979, [hep-th/0005106]. (Cited on pp. 43 and 44).

[226] K. Skenderis and B. C. van Rees, *Holography and wormholes in 2+1 dimensions*, *Commun. Math. Phys.* **301** (2011) 583–626, [0912.2090]. (Cited on p. 43).

[227] M. Guica and S. F. Ross, *Behind the geon horizon*, *Class. Quant. Grav.* **32** (2015) 055014, [1412.1084]. (Cited on p. 43).

[228] T. Hartman and J. Maldacena, *Time Evolution of Entanglement Entropy from Black Hole Interiors*, *JHEP* **05** (2013) 014, [1303.1080]. (Cited on pp. 45, 61, and 243).

[229] E. Keski-Vakkuri, *Bulk and boundary dynamics in BTZ black holes*, *Phys. Rev. D* **59** (Mar, 1999) 104001. (Cited on pp. 46, 153, and 155).

[230] I. Peschel and V. Eisler, *Reduced density matrices and entanglement entropy in free lattice models*, *Journal of Physics A: Mathematical and Theoretical* **42** (2009) 504003, [0906.1663]. (Cited on pp. 47 and 320).

[231] P. Calabrese, J. Cardy and B. Doyon, *Entanglement entropy in extended quantum systems*, *Journal of Physics A: Mathematical and Theoretical* **42** (Dec., 2009) 500301. (Cited on p. 47).

[232] R. Horodecki, P. Horodecki, M. Horodecki and K. Horodecki, *Quantum entanglement*, *Rev. Mod. Phys.* **81** (2009) 865–942, [quant-ph/0702225]. (Cited on p. 47).

[233] N. Laflorencie, *Quantum entanglement in condensed matter systems*, *Physics Reports* **646** (Aug., 2016) 1–59. (Cited on p. 47).

[234] P. A. M. Dirac, *The Principles of Quantum Mechanics*, The International Series of Monographs on Physics 27, Oxford University Press, 4 ed., 1988. (Cited on p. 48).

[235] J. von Neumann, *Mathematische Grundlagen der Quantenmechanik*, Springer, Berlin, Heidelberg, 2 ed., 1995, 10.1007/978-3-642-61409-5. (Cited on p. 48).

[236] R. F. Werner, *Quantum states with Einstein-Podolsky-Rosen correlations admitting a hidden-variable model*, *Phys. Rev. A* **40** (1989) 4277–4281. (Cited on p. 49).

[237] L. Gurvits, *Classical Deterministic Complexity of Edmonds' Problem and Quantum Entanglement*, in *Proceedings of the thirty-fifth annual ACM symposium on Theory of computing*, STOC '03, (New York, NY, USA), p. 10–19, Association for Computing Machinery, 2003, 10.1145/780542.780545, [quant-ph/0303055]. (Cited on p. 49).

[238] S. Gharibian, *Strong NP-hardness of the quantum separability problem*, *Quant. Inf. Comput.* **10** (2010) 0343–0360, [0810.4507]. (Cited on p. 49).

[239] A. Peres, *Separability Criterion for Density Matrices*, *Phys. Rev. Lett.* **77** (1996) 1413–1415, [quant-ph/9604005]. (Cited on p. 49).

[240] M. Horodecki, P. Horodecki and R. Horodecki, *Separability of mixed states: necessary and sufficient conditions*, *Phys. Lett. A* **223** (1996) 1–8, [quant-ph/9605038]. (Cited on p. 49).

[241] O. Gühne and G. Tóth, *Entanglement detection*, *Phys. Rept.* **474** (2009) 1–75, [0811.2803]. (Cited on p. 49).

[242] E. Schmidt, *Zur Theorie der linearen und nichtlinearen Integralgleichungen: I. Teil: Entwicklung willkürlicher Funktionen nach Systemen vorgeschriebener*, *Mathematische Annalen* **63** (Dec., 1907) 433–476. (Cited on p. 49).

[243] C. D. Meyer and I. Stewart, *Matrix Analysis and Applied Linear Algebra, Second Edition*, Society for Industrial and Applied Mathematics, Jan., 2023, 10.1137/1.9781611977448. (Cited on pp. 49 and 114).

[244] G. Vidal, *Entanglement Monotones*, *J. Mod. Opt.* **47** (2000) 355, [quant-ph/9807077]. (Cited on p. 51).

[245] I. Bengtsson and K. Zyczkowski, *Geometry of Quantum States: An Introduction to Quantum Entanglement*, Cambridge University Press, May, 2006, 10.1017/cbo9780511535048. (Cited on p. 51).

[246] G. Vidal and R. F. Werner, *Computable measure of entanglement*, *Phys. Rev. A* **65** (2002) 032314, [quant-ph/0102117]. (Cited on p. 51).

[247] P. Calabrese, J. Cardy and E. Tonni, *Entanglement negativity in quantum field theory*, *Phys. Rev. Lett.* **109** (2012) 130502, [1206.3092]. (Cited on pp. 51, 56, and 198).

[248] P. Calabrese, J. Cardy and E. Tonni, *Entanglement negativity in extended systems: A field theoretical approach*, *J. Stat. Mech.* **1302** (2013) P02008, [1210.5359]. (Cited on pp. 51 and 56).

[249] M. B. Plenio, *Logarithmic Negativity: A Full Entanglement Monotone That is not Convex*, *Phys. Rev. Lett.* **95** (2005) 090503, [quant-ph/0505071]. (Cited on p. 51).

[250] S. A. Hill and W. K. Wootters, *Entanglement of a Pair of Quantum Bits*, *Phys. Rev. Lett.* **78** (1997) 5022–5025, [quant-ph/9703041]. (Cited on pp. 51 and 270).

[251] W. K. Wootters, *Entanglement of Formation of an Arbitrary State of Two Qubits*, *Phys. Rev. Lett.* **80** (1998) 2245–2248, [quant-ph/9709029]. (Cited on pp. 51 and 270).

[252] V. Vedral, M. B. Plenio, M. A. Rippin and P. L. Knight, *Quantifying Entanglement*, *Phys. Rev. Lett.* **78** (1997) 2275–2279, [quant-ph/9702027]. (Cited on p. 51).

[253] V. Vedral, *The role of relative entropy in quantum information theory*, *Rev. Mod. Phys.* **74** (2002) 197–234, [quant-ph/0102094]. (Cited on p. 51).

[254] C. H. Bennett, D. P. DiVincenzo, J. A. Smolin and W. K. Wootters, *Mixed-state entanglement and quantum error correction*, *Phys. Rev. A* **54** (1996) 3824–3851, [quant-ph/9604024]. (Cited on p. 51).

[255] D. Girolami and G. Adesso, *Interplay between computable measures of entanglement and other quantum correlations*, *Phys. Rev. A* **84** (2011) 052110, [1111.3643]. (Cited on pp. 51 and 271).

[256] W. Zurek, *Einselection and decoherence from an information theory perspective*, *Annalen der Physik* **9** (2000) 855–864, [quant-ph/0011039]. (Cited on pp. 51, 66, and 270).

[257] H. Ollivier and W. H. Zurek, *Quantum Discord: A Measure of the Quantumness of Correlations*, *Phys. Rev. Lett.* **88** (Dec, 2001) 017901, [quant-ph/0105072]. (Cited on pp. 51, 66, 68, 270, 271, and 275).

[258] L. Henderson and V. Vedral, *Classical, quantum and total correlations*, *Journal of physics A: mathematical and general* **34** (2001) 6899, [quant-ph/0105028]. (Cited on pp. 51, 66, 69, and 270).

[259] D. N. Page, *Average entropy of a subsystem*, *Phys. Rev. Lett.* **71** (1993) 1291–1294, [gr-qc/9305007]. (Cited on p. 52).

[260] D. Harlow, *Jerusalem Lectures on Black Holes and Quantum Information*, *Rev. Mod. Phys.* **88** (2016) 015002, [1409.1231]. (Cited on pp. 52 and 243).

[261] M. Srednicki, *Entropy and area*, *Phys. Rev. Lett.* **71** (1993) 666–669, [hep-th/9303048]. (Cited on pp. 52, 55, 288, and 290).

[262] M. B. Hastings, *An area law for one-dimensional quantum systems*, *J. Stat. Mech.* **0708** (2007) P08024, [0705.2024]. (Cited on p. 53).

[263] G. Vidal, J. I. Latorre, E. Rico and A. Kitaev, *Entanglement in Quantum Critical Phenomena*, *Phys. Rev. Lett.* **90** (Jun, 2003) 227902, [quant-ph/0211074]. (Cited on pp. 53, 188, and 288).

[264] A. Kitaev and J. Preskill, *Topological entanglement entropy*, *Phys. Rev. Lett.* **96** (2006) 110404, [hep-th/0510092]. (Cited on pp. 53 and 288).

[265] R. Haag, *Local Quantum Physics*, Springer Berlin Heidelberg, 1996, 10.1007/978-3-642-61458-3. (Cited on pp. 53, 243, 288, 289, and 296).

[266] H. Li and F. Haldane, *Entanglement Spectrum as a Generalization of Entanglement Entropy: Identification of Topological Order in Non-Abelian Fractional Quantum Hall Effect States*, *Phys. Rev. Lett.* **101** (2008) 010504, [0805.0332]. (Cited on p. 54).

[267] F. Pollmann, A. M. Turner, E. Berg and M. Oshikawa, *Entanglement spectrum of a topological phase in one dimension*, *Phys. Rev. B* **81** (2010) 064439, [0910.1811]. (Cited on p. 54).

[268] R. Thomale, A. Sterdyniak, N. Regnault and B. A. Bernevig, *Entanglement Gap and a New Principle of Adiabatic Continuity*, *Phys. Rev. Lett.* **104** (May, 2010) 180502, [0912.0523]. (Cited on p. 54).

[269] T. V. Zache, C. Kokail, B. Sundar and P. Zoller, *Entanglement Spectroscopy and probing the Li-Haldane Conjecture in Topological Quantum Matter*, *Quantum* **6** (2022) 702, [2110.03913]. (Cited on p. 54).

[270] M. Headrick, *Entanglement Renyi entropies in holographic theories*, *Phys. Rev. D* **82** (2010) 126010, [1006.0047]. (Cited on pp. 54, 60, 192, 198, and 243).

[271] L.-Y. Hung, R. C. Myers, M. Smolkin and A. Yale, *Holographic Calculations of Renyi Entropy*, *JHEP* **12** (2011) 047, [1110.1084]. (Cited on pp. 54 and 243).

[272] D. D. Blanco, H. Casini, L.-Y. Hung and R. C. Myers, *Relative Entropy and Holography*, *JHEP* **08** (2013) 060, [1305.3182]. (Cited on pp. 54, 60, and 243).

[273] P. Calabrese and A. Lefevre, *Entanglement spectrum in one-dimensional systems*, *Phys. Rev. A* **78** (2008) 032329, [0806.3059]. (Cited on p. 54).

[274] J. Cardy and E. Tonni, *Entanglement hamiltonians in two-dimensional conformal field theory*, *J. Stat. Mech.* **1612** (2016) 123103, [1608.01283]. (Cited on pp. 54, 55, and 57).

[275] T. Mendes-Santos, G. Giudici, M. Dalmonte and M. A. Rajabpour, *Entanglement Hamiltonian of quantum critical chains and conformal field theories*, *Phys. Rev. B* **100** (2019) 155122, [1906.00471]. (Cited on p. 54).

[276] A. Rényi, *On measures of information and entropy*, *Proceedings of the fourth Berkeley Symposium on Mathematics, Statistics and Probability 1960* **1** (1961) 547–561. (Cited on p. 54).

[277] C. Callan and F. Wilczek, *On geometric entropy*, *Phys. Lett. B* **333** (1994) 55–61, [hep-th/9401072]. (Cited on pp. 55, 56, and 290).

[278] L. Bombelli, R. K. Koul, J. Lee and R. D. Sorkin, *A Quantum Source of Entropy for Black Holes*, *Phys. Rev. D* **34** (1986) 373–383. (Cited on pp. 55, 288, and 290).

[279] K. Ohmori and Y. Tachikawa, *Physics at the entangling surface*, *J. Stat. Mech.* **1504** (2015) P04010, [1406.4167]. (Cited on p. 55).

[280] A. B. Zamolodchikov, *Irreversibility of the Flux of the Renormalization Group in a 2D Field Theory*, *JETP Lett.* **43** (1986) 730–732. (Cited on pp. 56 and 57).

[281] J. Polchinski, *Scale and Conformal Invariance in Quantum Field Theory*, *Nucl. Phys. B* **303** (1988) 226–236. (Cited on pp. 56 and 57).

[282] Y. Nakayama, *Scale invariance vs conformal invariance*, *Phys. Rept.* **569** (2015) 1–93, [1302.0884]. (Cited on p. 56).

[283] P. Calabrese and J. L. Cardy, *Entanglement entropy and quantum field theory: A Non-technical introduction*, *Int. J. Quant. Inf.* **4** (2006) 429, [quant-ph/0505193]. (Cited on p. 56).

[284] J. L. Cardy, O. A. Castro-Alvaredo and B. Doyon, *Form factors of branch-point twist fields in quantum integrable models and entanglement entropy*, *J. Statist. Phys.* **130** (2008) 129–168, [0706.3384]. (Cited on p. 56).

[285] O. A. Castro-Alvaredo and B. Doyon, *Bi-partite entanglement entropy in massive 1+1-dimensional quantum field theories*, *J. Phys. A* **42** (2009) 504006, [0906.2946]. (Cited on p. 56).

[286] G. Vidal, J. I. Latorre, E. Rico and A. Kitaev, *Entanglement in Quantum Critical Phenomena*, *Phys. Rev. Lett.* **90** (Jun, 2003) 227902. (Cited on p. 56).

[287] J. I. Latorre and G. Sierra, *Holographic codes*, 1502.06618. (Cited on pp. 56 and 243).

[288] N. Lashkari, *Relative Entropies in Conformal Field Theory*, *Phys. Rev. Lett.* **113** (2014) 051602, [1404.3216]. (Cited on p. 56).

[289] N. Lashkari, *Modular Hamiltonian for Excited States in Conformal Field Theory*, *Phys. Rev. Lett.* **117** (2016) 041601, [1508.03506]. (Cited on p. 56).

[290] H. Casini, C. D. Fosco and M. Huerta, *Entanglement and alpha entropies for a massive Dirac field in two dimensions*, *J. Stat. Mech.* **0507** (2005) P07007, [cond-mat/0505563]. (Cited on pp. 57, 196, and 198).

[291] H. Casini and M. Huerta, *Reduced density matrix and internal dynamics for multicomponent regions*, *Class. Quant. Grav.* **26** (2009) 185005, [0903.5284]. (Cited on p. 57).

[292] P. Calabrese, J. Cardy and E. Tonni, *Entanglement entropy of two disjoint intervals in conformal field theory*, *J. Stat. Mech.* **0911** (2009) P11001, [0905.2069]. (Cited on pp. 57, 196, and 198).

[293] P. Calabrese, J. Cardy and E. Tonni, *Entanglement entropy of two disjoint intervals in conformal field theory II*, *J. Stat. Mech.* **1101** (2011) P01021, [1011.5482]. (Cited on p. 57).

[294] J. Cardy, *Some results on the mutual information of disjoint regions in higher dimensions*, *J. Phys. A* **46** (2013) 285402, [1304.7985]. (Cited on p. 57).

[295] A. Coser, L. Tagliacozzo and E. Tonni, *On Rényi entropies of disjoint intervals in conformal field theory*, *J. Stat. Mech.* **1401** (2014) P01008, [1309.2189]. (Cited on p. 57).

[296] A. Coser, E. Tonni and P. Calabrese, *Spin structures and entanglement of two disjoint intervals in conformal field theories*, *J. Stat. Mech.* **1605** (2016) 053109, [1511.08328]. (Cited on p. 57).

[297] F. C. Alcaraz, M. I. Berganza and G. Sierra, *Entanglement of low-energy excitations in Conformal Field Theory*, *Phys. Rev. Lett.* **106** (2011) 201601, [1101.2881]. (Cited on p. 57).

[298] M. I. Berganza, F. C. Alcaraz and G. Sierra, *Entanglement of excited states in critical spin chians*, *J. Stat. Mech.* **1201** (2012) P01016, [1109.5673]. (Cited on p. 57).

[299] J. Dubail, J.-M. Stéphan, J. Viti and P. Calabrese, *Conformal field theory for inhomogeneous one-dimensional quantum systems: the example of non-interacting Fermi gases*, *SciPost Physics* **2** (Feb., 2017) , [1606.04401]. (Cited on p. 57).

[300] J. Rodríguez-Laguna, J. Dubail, G. Ramírez, P. Calabrese and G. Sierra, *More on the rainbow chain: entanglement, space-time geometry and thermal states*, *Journal of Physics A: Mathematical and Theoretical* **50** (Mar., 2017) 164001, [1611.08559]. (Cited on p. 57).

[301] S. Murciano, P. Ruggiero and P. Calabrese, *Entanglement and relative entropies for low-lying excited states in inhomogeneous one-dimensional quantum systems*, *Journal of Statistical Mechanics: Theory and Experiment* **2019** (Mar., 2019) 034001, [1810.02287]. (Cited on p. 57).

[302] H. Casini and M. Huerta, *A Finite entanglement entropy and the c-theorem*, *Phys. Lett. B* **600** (2004) 142–150, [hep-th/0405111]. (Cited on p. 57).

[303] H. Casini and M. Huerta, *A c-theorem for the entanglement entropy*, *J. Phys. A* **40** (2007) 7031–7036, [cond-mat/0610375]. (Cited on p. 57).

[304] E. H. Lieb and M. B. Ruskai, *A Fundamental Property of Quantum-Mechanical Entropy*, *Phys. Rev. Lett.* **30** (Mar, 1973) 434–436. (Cited on p. 57).

[305] E. H. Lieb and M. B. Ruskai, *Proof of the strong subadditivity of quantum-mechanical entropy*, *Journal of Mathematical Physics* **14** (Dec., 1973) 1938–1941. (Cited on p. 57).

[306] H. Casini and M. Huerta, *On the RG running of the entanglement entropy of a circle*, *Phys. Rev. D* **85** (2012) 125016, [1202.5650]. (Cited on p. 57).

[307] H. Casini, M. Huerta, R. C. Myers and A. Yale, *Mutual information and the F-theorem*, *JHEP* **10** (2015) 003, [1506.06195]. (Cited on pp. 57 and 243).

[308] H. Casini, E. Testé and G. Torroba, *Markov Property of the Conformal Field Theory Vacuum and the a Theorem*, *Phys. Rev. Lett.* **118** (2017) 261602, [1704.01870]. (Cited on p. 57).

[309] J. J. Bisognano and E. H. Wichmann, *On the duality condition for a Hermitian scalar field*, *Journal of Mathematical Physics* **16** (Apr., 1975) 985–1007. (Cited on p. 57).

[310] J. J. Bisognano and E. H. Wichmann, *On the duality condition for quantum fields*, *Journal of Mathematical Physics* **17** (Mar., 1976) 303–321. (Cited on pp. 57 and 290).

[311] W. G. Unruh, *Notes on black hole evaporation*, *Phys. Rev. D* **14** (1976) 870. (Cited on pp. 57 and 290).

[312] I. Klich, D. Vaman and G. Wong, *Entanglement Hamiltonians for chiral fermions with zero modes*, *Phys. Rev. Lett.* **119** (2017) 120401, [1501.00482]. (Cited on p. 57).

[313] I. Klich, D. Vaman and G. Wong, *Entanglement Hamiltonians and entropy in 1+1D chiral fermion systems*, *Phys. Rev. B* **98** (2018) 035134, [1704.01536]. (Cited on p. 57).

[314] G. Wong, *Gluing together Modular flows with free fermions*, *JHEP* **04** (2019) 045, [1805.10651]. (Cited on p. 57).

[315] D. Blanco, A. Garbarz and G. Pérez-Nadal, *Entanglement of a chiral fermion on the torus*, *JHEP* **09** (2019) 076, [1906.07057]. (Cited on p. 57).

[316] D. Blanco and G. Pérez-Nadal, *Modular Hamiltonian of a chiral fermion on the torus*, *Phys. Rev. D* **100** (2019) 025003, [1905.05210]. (Cited on p. 57).

[317] P. Fries and I. A. Reyes, *Entanglement Spectrum of Chiral Fermions on the Torus*, *Phys. Rev. Lett.* **123** (2019) 211603, [1905.05768]. (Cited on p. 57).

[318] P. D. Hislop and R. Longo, *Modular structure of the local algebras associated with the free massless scalar field theory*, *Communications in Mathematical Physics* **84** (Mar., 1982) 71–85. (Cited on p. 57).

[319] H. Casini, M. Huerta and R. C. Myers, *Towards a derivation of holographic entanglement entropy*, *JHEP* **05** (2011) 036, [1102.0440]. (Cited on pp. 57, 60, and 243).

[320] R. Longo, P. Martinetti and K.-H. Rehren, *Geometric modular action for disjoint intervals and boundary conformal field theory*, *Rev. Math. Phys.* **22** (2010) 331–354, [0912.1106]. (Cited on p. 57).

[321] R. E. Arias, H. Casini, M. Huerta and D. Pontello, *Entropy and modular Hamiltonian for a free chiral scalar in two intervals*, *Phys. Rev. D* **98** (2018) 125008, [1809.00026]. (Cited on p. 57).

[322] M. Mintchev and E. Tonni, *Modular Hamiltonians for the massless Dirac field in the presence of a boundary*, *JHEP* **03** (2021) 204, [2012.00703]. (Cited on p. 57).

[323] M. Mintchev and E. Tonni, *Modular Hamiltonians for the massless Dirac field in the presence of a defect*, *JHEP* **03** (2021) 205, [2012.01366]. (Cited on p. 57).

[324] G. Wong, I. Klich, L. A. Pando Zayas and D. Vaman, *Entanglement Temperature and Entanglement Entropy of Excited States*, *JHEP* **12** (2013) 020, [1305.3291]. (Cited on p. 57).

[325] E. Tonni, J. Rodríguez-Laguna and G. Sierra, *Entanglement hamiltonian and entanglement contour in inhomogeneous 1D critical systems*, *J. Stat. Mech.* **1804** (2018) 043105, [1712.03557]. (Cited on p. 57).

[326] V. Eisler and I. Peschel, *Properties of the entanglement Hamiltonian for finite free-fermion chains*, *Journal of Statistical Mechanics: Theory and Experiment* **2018** (Oct., 2018) 104001, [1805.00078]. (Cited on p. 57).

[327] V. Eisler, E. Tonni and I. Peschel, *On the continuum limit of the entanglement Hamiltonian*, *J. Stat. Mech.* **1907** (2019) 073101, [1902.04474]. (Cited on p. 57).

[328] T. Nishioka, S. Ryu and T. Takayanagi, *Holographic Entanglement Entropy: An Overview*, *J. Phys. A* **42** (2009) 504008, [0905.0932]. (Cited on p. 59).

[329] M. Headrick, *Lectures on entanglement entropy in field theory and holography*, 1907.08126. (Cited on p. 59).

[330] J. D. Brown and M. Henneaux, *Central Charges in the Canonical Realization of Asymptotic Symmetries: An Example from Three-Dimensional Gravity*, *Commun. Math. Phys.* **104** (1986) 207–226. (Cited on p. 59).

[331] V. E. Hubeny, M. Rangamani and T. Takayanagi, *A Covariant holographic entanglement entropy proposal*, *JHEP* **07** (2007) 062, [0705.0016]. (Cited on pp. 60 and 243).

[332] X. Dong, A. Lewkowycz and M. Rangamani, *Deriving covariant holographic entanglement*, *JHEP* **11** (2016) 028, [1607.07506]. (Cited on p. 60).

[333] M. Headrick and T. Takayanagi, *A Holographic proof of the strong subadditivity of entanglement entropy*, *Phys. Rev. D* **76** (2007) 106013, [0704.3719]. (Cited on pp. 60 and 243).

[334] M. Headrick, *General properties of holographic entanglement entropy*, *JHEP* **03** (2014) 085, [1312.6717]. (Cited on p. 60).

[335] M. Headrick, V. E. Hubeny, A. Lawrence and M. Rangamani, *Causality & holographic entanglement entropy*, *JHEP* **12** (2014) 162, [1408.6300]. (Cited on pp. 60 and 243).

[336] A. Lewkowycz and J. Maldacena, *Generalized gravitational entropy*, *JHEP* **08** (2013) 090, [1304.4926]. (Cited on pp. 60 and 243).

[337] T. Faulkner, A. Lewkowycz and J. Maldacena, *Quantum corrections to holographic entanglement entropy*, *JHEP* **11** (2013) 074, [1307.2892]. (Cited on pp. 60 and 243).

[338] T. Hartman, *Entanglement Entropy at Large Central Charge*, (3, 2013) , [1303.6955]. (Cited on pp. 60 and 243).

[339] T. Faulkner, *The Entanglement Renyi Entropies of Disjoint Intervals in AdS/CFT*, (3, 2013) , [1303.7221]. (Cited on pp. 60 and 243).

[340] V. E. Hubeny, H. Maxfield, M. Rangamani and E. Tonni, *Holographic entanglement plateaux*, *JHEP* **08** (2013) 092, [1306.4004]. (Cited on p. 60).

[341] V. Balasubramanian, B. D. Chowdhury, B. Czech and J. de Boer, *Entwinement and the emergence of spacetime*, *JHEP* **01** (2015) 048, [1406.5859]. (Cited on p. 61).

[342] B. Freivogel, R. Jefferson, L. Kabir, B. Mosk and I.-S. Yang, *Casting Shadows on Holographic Reconstruction*, *Phys. Rev. D* **91** (2015) 086013, [1412.5175]. (Cited on p. 61).

[343] J. Erdmenger and M. Gerbershagen, *Entwinement as a possible alternative to complexity*, *JHEP* **03** (2020) 082, [1910.05352]. (Cited on p. 61).

[344] M. Gerbershagen, *Illuminating entanglement shadows of BTZ black holes by a generalized entanglement measure*, *JHEP* **10** (2021) 187, [2105.01097]. (Cited on p. 61).

[345] J. Watrous, *Quantum Computational Complexity*, p. 7174–7201, Springer New York, 2009, 10.1007/978-0-387-30440-3˙428, [0804.3401]. (Cited on p. 61).

[346] S. Aaronson, *The Complexity of Quantum States and Transformations: From Quantum Money to Black Holes*, 1607.05256. (Cited on pp. 61 and 66).

[347] S. Chapman and G. Policastro, *Quantum computational complexity from quantum information to black holes and back*, *Eur. Phys. J. C* **82** (2022) 128, [2110.14672]. (Cited on pp. 61 and 66).

[348] D. P. DiVincenzo, *Two-bit gates are universal for quantum computation*, *Phys. Rev. A* **51** (Feb, 1995) 1015–1022. (Cited on p. 61).

[349] M. A. Nielsen, *A geometric approach to quantum circuit lower bounds*, *Quant. Inf. Comput.* **6** (2006) 213–262, [quant-ph/0502070]. (Cited on pp. 62, 63, 66, and 261).

[350] M. A. Nielsen, M. R. Dowling, M. Gu and A. C. Doherty, *Optimal control, geometry, and quantum computing*, *Phys. Rev. A* **73** (2006) 062323, [quant-ph/0603160]. (Cited on p. 62).

[351] M. R. Dowling and M. A. Nielsen, *The geometry of quantum computation*, *Quant. Inf. Comput.* **8** (2008) 0861–0899, [quant-ph/0701004]. (Cited on pp. 62, 260, and 267).

[352] M. A. Nielsen, M. R. Dowling, M. Gu and A. C. Doherty, *Quantum Computation as Geometry*, *Science* **311** (2006) 1133–1135, [quant-ph/0603161]. (Cited on pp. 62, 63, and 64).

[353] S. A. Rice and M. Zhao, *Optical control of molecular dynamics*, Baker Lecture Series, John Wiley & Sons, Nashville, TN, Feb., 2000. (Cited on p. 62).

[354] H. Rabitz, R. de Vivie-Riedle, M. Motzkus and K. Kompa, *Whither the Future of Controlling Quantum Phenomena?*, *Science* **288** (2000) 824–828. (Cited on p. 62).

[355] R. J. Gordon and S. A. Rice, *Active Control of the Dynamics of Atoms and Molecules*, *Annual Review of Physical Chemistry* **48** (Oct., 1997) 601–641. (Cited on p. 62).

[356] M. Shapiro and P. Brumer, *Optimal Control Theory*, ch. 5, pp. 83–94, John Wiley & Sons, Ltd, 2000, https://doi.org/10.1002/9783527639700.ch5. (Cited on p. 62).

[357] R. Jefferson and R. C. Myers, *Circuit complexity in quantum field theory*, *JHEP* **10** (2017) 107, [1707.08570]. (Cited on pp. 63, 64, and 243).

[358] A. R. Brown, L. Susskind and Y. Zhao, *Quantum Complexity and Negative Curvature*, *Phys. Rev. D* **95** (2017) 045010, [1608.02612]. (Cited on pp. 64, 243, and 266).

[359] A. R. Brown and L. Susskind, *Second law of quantum complexity*, *Phys. Rev. D* **97** (2018) 086015, [1701.01107]. (Cited on pp. 64, 65, 243, 246, 260, 262, and 266).

[360] A. R. Brown and L. Susskind, *Complexity geometry of a single qubit*, *Phys. Rev. D* **100** (2019) 046020, [1903.12621]. (Cited on pp. 64, 243, 259, 260, and 262).

[361] V. Balasubramanian, M. Decross, A. Kar and O. Parrikar, *Quantum Complexity of Time Evolution with Chaotic Hamiltonians*, *JHEP* **01** (2020) 134, [1905.05765]. (Cited on pp. 64, 243, 246, 260, 262, and 267).

[362] R. Auzzi, S. Baiguera, G. B. De Luca, A. Legramandi, G. Nardelli and N. Zenoni, *Geometry of quantum complexity*, *Phys. Rev. D* **103** (2021) 106021, [2011.07601]. (Cited on pp. 64, 243, 246, 260, 262, 266, and 267).

[363] V. Balasubramanian, M. DeCross, A. Kar, Y. C. Li and O. Parrikar, *Complexity growth in integrable and chaotic models*, *JHEP* **07** (2021) 011, [2101.02209]. (Cited on pp. 64, 243, 246, 260, 262, 266, and 267).

[364] S. Chapman, M. P. Heller, H. Marrochio and F. Pastawski, *Toward a Definition of Complexity for Quantum Field Theory States*, *Phys. Rev. Lett.* **120** (2018) 121602, [1707.08582]. (Cited on pp. 64 and 243).

[365] J. M. Magán, *Black holes, complexity and quantum chaos*, *JHEP* **09** (2018) 043, [1805.05839]. (Cited on pp. 64, 243, 249, and 260).

[366] R. Khan, C. Krishnan and S. Sharma, *Circuit Complexity in Fermionic Field Theory*, *Phys. Rev. D* **98** (2018) 126001, [1801.07620]. (Cited on pp. 64 and 243).

[367] L. Hackl and R. C. Myers, *Circuit complexity for free fermions*, *JHEP* **07** (2018) 139, [1803.10638]. (Cited on pp. 64 and 243).

[368] S. Chapman, J. Eisert, L. Hackl, M. P. Heller, R. Jefferson, H. Marrochio et al., *Complexity and entanglement for thermofield double states*, *SciPost Phys.* **6** (2019) 034, [1810.05151]. (Cited on pp. 64 and 243).

[369] J. Erdmenger, M. Gerbershagen and A.-L. Weigel, *Complexity measures from geometric actions on Virasoro and Kac-Moody orbits*, *JHEP* **11** (2020) 003, [2004.03619]. (Cited on pp. 64, 66, 243, and 246).

[370] M. Flory and M. P. Heller, *Conformal field theory complexity from Euler-Arnold equations*, *JHEP* **12** (2020) 091, [2007.11555]. (Cited on pp. 64, 243, and 246).

[371] M. Flory and M. P. Heller, *Geometry of Complexity in Conformal Field Theory*, *Phys. Rev. Res.* **2** (2020) 043438, [2005.02415]. (Cited on pp. 64, 243, and 246).

[372] P. Bocchieri and A. Loinger, *Quantum Recurrence Theorem*, *Phys. Rev.* **107** (Jul, 1957) 337–338. (Cited on p. 64).

[373] J. Haferkamp, P. Faist, N. B. T. Kothakonda, J. Eisert and N. Y. Halpern, *Linear growth of quantum circuit complexity*, *Nature Phys.* **18** (2022) 528–532, [2106.05305]. (Cited on pp. 65 and 243).

[374] D. A. Roberts, D. Stanford and L. Susskind, *Localized shocks*, *JHEP* **03** (2015) 051, [1409.8180]. (Cited on pp. 65 and 243).

[375] S. H. Shenker and D. Stanford, *Multiple Shocks*, *JHEP* **12** (2014) 046, [1312.3296]. (Cited on pp. 65 and 243).

[376] A. R. Brown, D. A. Roberts, L. Susskind, B. Swingle and Y. Zhao, *Holographic Complexity Equals Bulk Action?*, *Phys. Rev. Lett.* **116** (2016) 191301, [1509.07876]. (Cited on pp. 66 and 243).

[377] A. R. Brown, D. A. Roberts, L. Susskind, B. Swingle and Y. Zhao, *Complexity, action, and black holes*, *Phys. Rev. D* **93** (2016) 086006, [1512.04993]. (Cited on pp. 66 and 243).

[378] D. Carmi, R. C. Myers and P. Rath, *Comments on Holographic Complexity*, *JHEP* **03** (2017) 118, [1612.00433]. (Cited on pp. 66 and 243).

[379] J. Couch, W. Fischler and P. H. Nguyen, *Noether charge, black hole volume, and complexity*, *JHEP* **03** (2017) 119, [1610.02038]. (Cited on pp. 66 and 243).

[380] A. Reynolds and S. F. Ross, *Divergences in Holographic Complexity*, *Class. Quant. Grav.* **34** (2017) 105004, [1612.05439]. (Cited on pp. 66 and 243).

[381] S. Chapman, H. Marrochio and R. C. Myers, *Holographic complexity in Vaidya spacetimes. Part I*, *JHEP* **06** (2018) 046, [1804.07410]. (Cited on pp. 66 and 243).

[382] B. Swingle and Y. Wang, *Holographic Complexity of Einstein-Maxwell-Dilaton Gravity*, *JHEP* **09** (2018) 106, [1712.09826]. (Cited on pp. 66 and 243).

[383] Z.-Y. Fan and M. Guo, *On the Noether charge and the gravity duals of quantum complexity*, *JHEP* **08** (2018) 031, [1805.03796]. (Cited on pp. 66 and 243).

[384] M. Alishahiha, A. Faraji Astaneh, A. Naseh and M. H. Vahidinia, *On complexity for F(R) and critical gravity*, *JHEP* **05** (2017) 009, [1702.06796]. (Cited on pp. 66 and 243).

[385] S. Chapman, D. Ge and G. Policastro, *Holographic Complexity for Defects Distinguishes Action from Volume*, *JHEP* **05** (2019) 049, [1811.12549]. (Cited on pp. 66 and 243).

[386] R. Abt, J. Erdmenger, H. Hinrichsen, C. M. Melby-Thompson, R. Meyer, C. Northe et al., *Topological Complexity in AdS_3/CFT_2*, *Fortsch. Phys.* **66** (2018) 1800034, [1710.01327]. (Cited on pp. 66 and 243).

[387] R. Abt, J. Erdmenger, M. Gerbershagen, C. M. Melby-Thompson and C. Northe, *Holographic Subregion Complexity from Kinematic Space*, *JHEP* **01** (2019) 012, [1805.10298]. (Cited on pp. 66 and 243).

[388] J. Erdmenger, M. Flory, M. Gerbershagen, M. P. Heller and A.-L. Weigel, *Exact Gravity Duals for Simple Quantum Circuits*, *SciPost Phys.* **13** (2022) 061, [2112.12158]. (Cited on pp. 66 and 243).

[389] J. Erdmenger, A.-L. Weigel, M. Gerbershagen and M. P. Heller, *From complexity geometry to holographic spacetime*, *Phys. Rev. D* **108** (2023) 106020, [2212.00043]. (Cited on pp. 66 and 243).

[390] A. Belin, R. C. Myers, S.-M. Ruan, G. Sárosi and A. J. Speranza, *Does Complexity Equal Anything?*, *Phys. Rev. Lett.* **128** (2022) 081602, [2111.02429]. (Cited on pp. 66 and 243).

[391] A. Belin, R. C. Myers, S.-M. Ruan, G. Sárosi and A. J. Speranza, *Complexity equals anything II*, *JHEP* **01** (2023) 154, [2210.09647]. (Cited on pp. 66 and 243).

[392] E. Jørstad, R. C. Myers and S.-M. Ruan, *Complexity=anything: singularity probes*, *JHEP* **07** (2023) 223, [2304.05453]. (Cited on pp. 66 and 243).

[393] R. C. Myers and S.-M. Ruan, *Complexity Equals (Almost) Anything*, 2403.17475. (Cited on pp. 66 and 243).

[394] M. Dorband, *Geometric Phases and Factorisation in Quantum Physics and Gravity*, 2023. PhD Thesis, Chair for Theoretical Physics III, Julius-Maximilians-Universität Würzburg. (Cited on pp. 67 and 271).

[395] C. E. Shannon, *A mathematical theory of communication*, *Bell Syst. Tech. J.* **27** (1948) 379–423. (Cited on p. 67).

[396] C. E. Shannon and W. Weaver, *The mathematical theory of communication*, University of Illinois Press, Baltimore, MD, Dec., 1949. (Cited on p. 67).

[397] N. J. Cerf and C. Adami, *Negative Entropy and Information in Quantum Mechanics*, *Phys. Rev. Lett.* **79** (1997) 5194–5197, [quant-ph/9512022]. (Cited on p. 68).

[398] M. Horodecki, J. Oppenheim and A. Winter, *Partial quantum information*, *Nature* **436** (2005) 673–676, [quant-ph/0505062]. (Cited on p. 68).

[399] M. Horodecki, J. Oppenheim and A. Winter, *Quantum State Merging and Negative Information*, *Commun. Math. Phys.* **269** (2007) 107–136, [quant-ph/0512247]. (Cited on p. 68).

[400] N. Li, S. Luo and Z. Zhang, *Quantumness of bipartite states in terms of conditional entropies*, *J. Phys. A: Mathematical and Theoretical* **40** (2007) 11361. (Cited on p. 68).

[401] F. Verstraete, M. Popp and J. I. Cirac, *Entanglement versus Correlations in Spin Systems*, *Phys. Rev. Lett.* **92** (2004) 027901, [quant-ph/0307009]. (Cited on p. 69).

[402] M. Popp, F. Verstraete, M. A. Martin-Delgado and J. I. Cirac, *Localizable entanglement*, *Phys. Rev. A* **71** (2005) 042306, [quant-ph/0411123]. (Cited on p. 69).

[403] C.-J. Lin, W. Ye, Y. Zou, S. Sang and T. H. Hsieh, *Probing sign structure using measurement-induced entanglement*, *Quantum* **7** (2023) 910, [2205.05692]. (Cited on p. 69).

[404] Z. Xi, H. Fan and Y. Li, *One-way unlocalizable quantum discord*, *Phys. Rev. A* **85** (May, 2012) 052102. (Cited on p. 69).

[405] F. Liu, G.-J. Tian, G.-Y. Wen and F. Gao, *General bounds for quantum discord and discord distance*, *Quantum Inf. Proc.* **14** (2015) 1333–1341, [1411.3772]. (Cited on p. 70).

[406] C. C. Rulli and M. S. Sarandy, *Global quantum discord in multipartite systems*, *Phys. Rev. A* **84** (2011) 042109, [1105.2548]. (Cited on p. 70).

[407] J. Eisert, *Entanglement and tensor network states*, in *Autumn School on Correlated Electrons: Emergent Phenomena in Correlated Matter*, 8, 2013, [1308.3318]. (Cited on p. 71).

[408] J. C. Bridgeman and C. T. Chubb, *Hand-waving and Interpretive Dance: An Introductory Course on Tensor Networks*, *J. Phys. A* **50** (2017) 223001, [1603.03039]. (Cited on p. 71).

[409] J. I. Cirac, D. Perez-Garcia, N. Schuch and F. Verstraete, *Matrix product states and projected entangled pair states: Concepts, symmetries, theorems*, *Rev. Mod. Phys.* **93** (2021) 045003, [2011.12127]. (Cited on p. 71).

[410] S. Östlund and S. Rommer, *Thermodynamic Limit of Density Matrix Renormalization*, *Phys. Rev. Lett.* **75** (Nov, 1995) 3537–3540. (Cited on p. 73).

[411] M. Fannes, B. Nachtergaele and R. F. Werner, *Finitely correlated states on quantum spin chains*, *Communications in Mathematical Physics* **144** (Mar., 1992) 443–490. (Cited on p. 73).

[412] A. Klümper, A. Schadschneider and J. Zittartz, *Matrix Product Ground States for One-Dimensional Spin-1 Quantum Antiferromagnets*, *Europhysics Letters (EPL)* **24** (Nov., 1993) 293–297. (Cited on p. 73).

[413] A. Klumper, A. Schadschneider and J. Zittartz, *Equivalence and solution of anisotropic spin-1 models and generalized t-J fermion models in one dimension*, *Journal of Physics A: Mathematical and General* **24** (Aug., 1991) L955–L959. (Cited on p. 73).

[414] D. Perez-Garcia, F. Verstraete, M. M. Wolf and J. I. Cirac, *Matrix product state representations*, *Quant. Inf. Comput.* **7** (2007) 401–430, [quant-ph/0608197]. (Cited on p. 73).

[415] F. Verstraete, V. Murg and J. Cirac, *Matrix product states, projected entangled pair states, and variational renormalization group methods for quantum spin systems*, *Advances in Physics* **57** (Mar., 2008) 143–224. (Cited on p. 73).

[416] F. Verstraete and J. I. Cirac, "Renormalization algorithms for quantum-many body systems in two and higher dimensions." 7, 2004. (Cited on p. 73).

[417] G. Vidal, *Entanglement Renormalization*, *Phys. Rev. Lett.* **99** (2007) 220405, [cond-mat/0512165]. (Cited on pp. 73 and 218).

[418] G. Vidal, *Class of Quantum Many-Body States That Can Be Efficiently Simulated*, *Phys. Rev. Lett.* **101** (2008) 110501, [quant-ph/0610099]. (Cited on p. 73).

[419] G. Vidal, *Entanglement Renormalization: an introduction*, p. 143–166, CRC Press, Nov., 2010, 10.1201/b10273-11, [0912.1651]. (Cited on p. 74).

[420] B. Swingle, *Entanglement Renormalization and Holography*, *Phys. Rev. D* **86** (2012) 065007, [0905.1317]. (Cited on pp. 75, 218, and 243).

[421] C. Beny, *Causal structure of the entanglement renormalization ansatz*, *New J. Phys.* **15** (2013) 023020, [1110.4872]. (Cited on pp. 75 and 243).

[422] S. Singh, *Tensor network state correspondence and holography*, *Phys. Rev. D* **97** (2018) 026012, [1701.04778]. (Cited on pp. 75 and 243).

[423] N. Bao, C. Cao, S. M. Carroll, A. Chatwin-Davies, N. Hunter-Jones, J. Pollack et al., *Consistency conditions for an AdS multiscale entanglement renormalization ansatz correspondence*, *Phys. Rev. D* **91** (2015) 125036, [1504.06632]. (Cited on pp. 75, 221, and 243).

[424] A. Milsted and G. Vidal, *Geometric interpretation of the multi-scale entanglement renormalization ansatz*, 1812.00529. (Cited on pp. 75 and 243).

[425] D. Gottesman, *Stabilizer codes and quantum error correction*, quant-ph/9705052. (Cited on p. 76).

[426] B. M. Terhal, *Quantum error correction for quantum memories*, *Rev. Mod. Phys.* **87** (2015) 307, [1302.3428]. (Cited on p. 76).

[427] S. J. Devitt, W. J. Munro and K. Nemoto, *Quantum error correction for beginners*, *Reports on Progress in Physics* **76** (June, 2013) 076001. (Cited on p. 76).

[428] A. Almheiri, X. Dong and D. Harlow, *Bulk Locality and Quantum Error Correction in AdS/CFT*, *JHEP* **04** (2015) 163, [1411.7041]. (Cited on pp. 76, 225, and 243).

[429] Z. Yang, P. Hayden and X.-L. Qi, *Bidirectional holographic codes and sub-AdS locality*, *JHEP* **01** (2016) 175, [1510.03784]. (Cited on pp. 76 and 243).

[430] P. Hayden, S. Nezami, X.-L. Qi, N. Thomas, M. Walter and Z. Yang, *Holographic duality from random tensor networks*, *JHEP* **11** (2016) 009, [1601.01694]. (Cited on pp. 76, 218, 220, 227, 232, and 243).

[431] X.-L. Qi and Z. Yang, *Space-time random tensor networks and holographic duality*, 1801.05289. (Cited on pp. 76 and 243).

[432] W. Donnelly, B. Michel, D. Marolf and J. Wien, *Living on the Edge: A Toy Model for Holographic Reconstruction of Algebras with Centers*, *JHEP* **04** (2017) 093, [1611.05841]. (Cited on p. 76).

[433] T. J. Osborne and D. E. Stiegemann, *Dynamics for holographic codes*, *JHEP* **04** (2020) 154, [1706.08823]. (Cited on pp. 76, 182, and 342).

[434] R. J. Harris, N. A. McMahon, G. K. Brennen and T. M. Stace, *Calderbank-Shor-Steane holographic quantum error-correcting codes*, *Phys. Rev. A* **98** (2018) 052301, [1806.06472]. (Cited on p. 76).

[435] A. Jahn, M. Gluza, F. Pastawski and J. Eisert, *Holography and criticality in matchgate tensor networks*, *Sci. Adv.* **5** (2019) eaaw0092, [1711.03109]. (Cited on pp. 76, 227, and 237).

[436] T. Kohler and T. Cubitt, *Toy Models of Holographic Duality between local Hamiltonians*, *JHEP* **08** (2019) 017, [1810.08992]. (Cited on pp. 76, 243, and 342).

[437] A. Jahn, Z. Zimborás and J. Eisert, *Central charges of aperiodic holographic tensor network models*, *Phys. Rev. A* **102** (2020) 042407, [1911.03485]. (Cited on pp. 76, 115, 117, 189, 190, 227, 233, 236, 237, 238, 239, and 243).

[438] A. Jahn, M. Gluza, F. Pastawski and J. Eisert, *Majorana dimers and holographic quantum error-correcting codes*, *Phys. Rev. Research.* **1** (2019) 033079, [1905.03268]. (Cited on pp. 76, 218, 227, and 243).

[439] A. Jahn, Z. Zimborás and J. Eisert, *Tensor network models of AdS/qCFT*, *Quantum* **6** (2022) 643, [2004.04173]. (Cited on pp. 76, 115, 117, 218, 227, 228, and 243).

[440] A. Jahn, M. Gluza, C. Verhoeven, S. Singh and J. Eisert, *Boundary theories of critical matchgate tensor networks*, *JHEP* **04** (2022) 111, [2110.02972]. (Cited on pp. 76, 218, and 243).

[441] C. Akers and P. Rath, *Holographic Renyi Entropy from Quantum Error Correction*, *JHEP* **05** (2019) 052, [1811.05171]. (Cited on pp. 76 and 243).

[442] N. Bao, G. Penington, J. Sorce and A. C. Wall, *Holographic Tensor Networks in Full AdS/CFT*, 1902.10157. (Cited on pp. 76 and 243).

[443] E. Gesteau and M. J. Kang, *The infinite-dimensional HaPPY code: entanglement wedge reconstruction and dynamics*, 2005.05971. (Cited on p. 76).

[444] G. Policastro, D. T. Son and A. O. Starinets, *The Shear viscosity of strongly coupled N=4 supersymmetric Yang-Mills plasma*, *Phys. Rev. Lett.* **87** (2001) 081601, [hep-th/0104066]. (Cited on pp. 77 and 78).

[445] P. Kovtun, D. T. Son and A. O. Starinets, *Holography and hydrodynamics: Diffusion on stretched horizons*, *JHEP* **10** (2003) 064, [hep-th/0309213]. (Cited on pp. 77 and 78).

[446] P. Kovtun, D. T. Son and A. O. Starinets, *Viscosity in strongly interacting quantum field theories from black hole physics*, *Phys. Rev. Lett.* **94** (2005) 111601, [hep-th/0405231]. (Cited on pp. 77 and 78).

[447] U. W. Heinz and M. Jacob, *Evidence for a new state of matter: An Assessment of the results from the CERN lead beam program*, nucl-th/0002042. (Cited on pp. 77 and 78).

[448] W. Zhang, H. Yuan, N. Sun, H. Sun and X. Zhang, *Observation of novel topological states in hyperbolic lattices*, *Nature Communications* **13** (2022) . (Cited on pp. 77, 105, 134, and 135).

[449] D. T. Son and A. O. Starinets, *Viscosity, Black Holes, and Quantum Field Theory*, *Ann. Rev. Nucl. Part. Sci.* **57** (2007) 95–118, [0704.0240]. (Cited on p. 78).

[450] B. Muller, *From Quark-Gluon Plasma to the Perfect Liquid*, *Acta Phys. Polon. B* **38** (2007) 3705–3730, [0710.3366]. (Cited on p. 78).

[451] M. Gyulassy and L. McLerran, *New forms of QCD matter discovered at RHIC*, *Nucl. Phys. A* **750** (2005) 30–63, [nucl-th/0405013]. (Cited on p. 78).

[452] PHENIX collaboration, K. Adcox et al., *Formation of dense partonic matter in relativistic nucleus-nucleus collisions at RHIC: Experimental evaluation by the PHENIX collaboration*, *Nucl. Phys. A* **757** (2005) 184–283, [nucl-ex/0410003]. (Cited on p. 78).

[453] PHOBOS collaboration, B. B. Back et al., *The PHOBOS perspective on discoveries at RHIC*, *Nucl. Phys. A* **757** (2005) 28–101, [nucl-ex/0410022]. (Cited on p. 78).

[454] STAR collaboration, J. Adams et al., *Experimental and theoretical challenges in the search for the quark gluon plasma: The STAR Collaboration's critical assessment of the evidence from RHIC collisions*, *Nucl. Phys. A* **757** (2005) 102–183, [nucl-ex/0501009]. (Cited on p. 78).

[455] BRAHMS collaboration, I. Arsene et al., *Quark gluon plasma and color glass condensate at RHIC? The Perspective from the BRAHMS experiment*, *Nucl. Phys. A* **757** (2005) 1–27, [nucl-ex/0410020]. (Cited on p. 78).

[456] A. Dobado, F. J. Llanes-Estrada and J. M. T. Rincon, *The Status of the KSS bound and its possible violations: How perfect can a fluid be?*, *AIP Conf. Proc.* **1031** (2008) 221–231, [0804.2601]. (Cited on p. 78).

[457] A. Buchel and J. T. Liu, *Universality of the shear viscosity in supergravity*, *Phys. Rev. Lett.* **93** (2004) 090602, [hep-th/0311175]. (Cited on p. 78).

[458] A. Buchel, J. T. Liu and A. O. Starinets, *Coupling constant dependence of the shear viscosity in N=4 supersymmetric Yang-Mills theory*, *Nucl. Phys. B* **707** (2005) 56–68, [hep-th/0406264]. (Cited on p. 78).

[459] L. Brekke and P. G. O. Freund, *p-adic numbers in physics*, *Phys. Rept.* **233** (1993) 1–66. (Cited on p. 79).

[460] P. G. O. Freund, *p-adic Strings Then and Now*, 1711.00523. (Cited on p. 79).

[461] I. V. Volovich, *p-ADIC STRING*, *Class. Quant. Grav.* **4** (1987) L83. (Cited on p. 79).

[462] P. G. Freund and E. Witten, *Adelic string amplitudes*, *Physics Letters B* **199** (1987) 191–194. (Cited on p. 79).

[463] S. S. Gubser, J. Knaute, S. Parikh, A. Samberg and P. Witaszczyk, *p-adic AdS/CFT*, *Commun. Math. Phys.* **352** (2017) 1019–1059, [1605.01061]. (Cited on p. 79).

[464] M. Heydeman, M. Marcolli, I. Saberi and B. Stoica, *Tensor networks, p-adic fields, and algebraic curves: arithmetic and the AdS_3/CFT_2 correspondence*, *Adv. Theor. Math. Phys.* **22** (2018) 93–176, [1605.07639]. (Cited on p. 79).

[465] S. S. Gubser, *A p-adic version of AdS/CFT*, *Adv. Theor. Math. Phys.* **21** (2017) 1655–1678, [1705.00373]. (Cited on p. 79).

[466] S. S. Gubser, C. Jepsen and B. Trundy, *Spin in p-adic AdS/CFT*, *J. Phys. A* **52** (2019) 144004, [1811.02538]. (Cited on p. 79).

[467] M. Heydeman, M. Marcolli, S. Parikh and I. Saberi, *Nonarchimedean holographic entropy from networks of perfect tensors*, *Adv. Theor. Math. Phys.* **25** (2021) 591–721, [1812.04057]. (Cited on p. 79).

[468] L.-Y. Hung, W. Li and C. M. Melby-Thompson, *Wilson line networks in p-adic AdS/CFT*, *JHEP* **05** (2019) 118, [1812.06059]. (Cited on p. 79).

[469] L.-Y. Hung, W. Li and C. M. Melby-Thompson, *p-adic CFT is a holographic tensor network*, *JHEP* **04** (2019) 170, [1902.01411]. (Cited on p. 79).

[470] L. Chen, X. Liu and L.-Y. Hung, *Emergent Einstein Equation in p-adic Conformal Field Theory Tensor Networks*, *Phys. Rev. Lett.* **127** (2021) 221602, [2102.12022]. (Cited on p. 79).

[471] L. Chen, X. Liu and L.-Y. Hung, *Bending the Bruhat-Tits tree. Part I. Tensor network and emergent Einstein equations*, *JHEP* **06** (2021) 094, [2102.12023]. (Cited on p. 79).

[472] L. Chen, X. Liu and L.-Y. Hung, *Bending the Bruhat-Tits tree. Part II. The p-adic BTZ black hole and local diffeomorphism on the Bruhat-Tits tree*, *JHEP* **09** (2021) 097, [2102.12024]. (Cited on p. 79).

[473] K. Okunishi and T. Takayanagi, *Statistical mechanics approach to the holographic renormalization group: Bethe lattice Ising model and p-adic AdS/CFT*, *PTEP* **2024** (2024) 013A03, [2310.12601]. (Cited on p. 79).

[474] F. Qu, *P-adic AdS/CFT on subspaces of the Bruhat-Tits tree*, 2402.03730. (Cited on p. 79).

[475] A. Ostrowski, *Über einige Lösungen der Funktionalgleichung* $\psi(x) \cdot \psi(x) = \psi(xy)$, *Acta Mathematica* **41** (1916) 271–284. (Cited on p. 79).

[476] F. Bruhat and J. Tits, *Groupes Réductifs Sur Un Corps Local*, *Publications mathématiques de l'IHÉS* **41** (Dec., 1972) 5–251. (Cited on p. 80).

[477] P. H. Frampton, Y. Okada and M. R. Ubriaco, *On Adelic Formulas for the* P^-*adic String*, *Phys. Lett. B* **213** (1988) 260–262. (Cited on p. 80).

[478] S. S. Gubser, M. Heydeman, C. Jepsen, M. Marcolli, S. Parikh, I. Saberi et al., *Edge length dynamics on graphs with applications to p-adic AdS/CFT*, *JHEP* **06** (2017) 157, [1612.09580]. (Cited on pp. 80 and 346).

[479] Y. Ollivier, *Ricci curvature of Markov chains on metric spaces*, *Journal of Functional Analysis* **256** (Feb., 2009) 810–864. (Cited on p. 80).

[480] Y. Lin, L. Lu and S.-T. Yau, *Ricci curvature of graphs*, *Tohoku Mathematical Journal* **63** (2011) 605 – 627. (Cited on p. 80).

[481] L. N. Vaserstein, *Markovian processes on countable space product describing large systems of automata*, *Probl. Peredachi Inf.* **5** (1969) 64–72. (Cited on p. 80).

[482] E. Gesteau, M. Marcolli and S. Parikh, *Holographic tensor networks from hyperbolic buildings*, *JHEP* **10** (2022) 169, [2202.01788]. (Cited on pp. 80, 81, and 345).

[483] P. Abramenko and K. S. Brown, *Buildings: Theory and Applications*, Springer New York, 2008, 10.1007/978-0-387-78835-7. (Cited on p. 80).

[484] M. Coornaert, T. Delzant and A. Papadopoulos, *Géométrie et théorie des groupes*, Springer Berlin Heidelberg, 1990, 10.1007/bfb0084913. (Cited on p. 80).

[485] A. Thomas, *Lattices in hyperbolic buildings*, p. 345–363, London Mathematical Society Lecture Note Series, Cambridge University Press, 2016. (Cited on p. 80).

[486] M. Gromov, *Hyperbolic Groups*, pp. 75–263, Springer New York, New York, NY, 1987, 10.1007/978-1-4613-9586-7˙3. (Cited on p. 80).

[487] M. Bourdon, *Immeubles hyperboliques, dimension conforme et rigidité de Mostow*, *Geometric and Functional Analysis* **7** (May, 1997) 245–268. (Cited on pp. 81 and 345).

[488] M. Bourdon and H. Pajot, *Poincaré inequalities and quasiconformal structure on the boundary of some hyperbolic buildings*, *Proceedings of the American Mathematical Society* **127** (Apr., 1999) 2315–2324. (Cited on pp. 81 and 345).

[489] R. Diestel, *Graph Theory*, Springer Berlin Heidelberg, 2017, 10.1007/978-3-662-53622-3. (Cited on p. 81).

[490] M. Axenides, E. Floratos and S. Nicolis, *The quantum cat map on the modular discretization of extremal black hole horizons*, *Eur. Phys. J. C* **78** (2018) 412, [1608.07845]. (Cited on p. 81).

[491] M. Axenides, E. Floratos and S. Nicolis, *The arithmetic geometry of AdS_2 and its continuum limit*, *SIGMA* **17** (2021) 004, [1908.06641]. (Cited on p. 81).

[492] M. Axenides, E. G. Floratos and S. Nicolis, *The continuum limit of the modular discretization of AdS_2*, *PoS* **CORFU2021** (2022) 243, [2205.03637]. (Cited on p. 81).

[493] M. Axenides, E. G. Floratos and S. Nicolis, *Modular discretization of the AdS_2/CFT_1 holography*, *JHEP* **02** (2014) 109, [1306.5670]. (Cited on p. 81).

[494] M. Axenides, E. Floratos and S. Nicolis, *Chaotic Information Processing by Extremal Black Holes*, *Int. J. Mod. Phys. D* **24** (2015) 1542012, [1504.00483]. (Cited on p. 81).

[495] M. Axenides, E. Floratos and S. Nicolis, *Arnol'd cat map lattices*, *Phys. Rev. E* **107** (2023) 064206, [2208.03267]. (Cited on p. 81).

[496] M. Axenides, E. Floratos and S. Nicolis, *Exponential mixing of all orders for Arnol'd cat map lattices*, 2401.08521. (Cited on p. 81).

[497] V. I. Arnold and A. Avez, *Ergodic problems of classical mechanics*, The Mathematical physics monograph series, Benjamin, New York, 1968. (Cited on p. 81).

[498] A. Borel, *Groupes Lineaires Algebriques*, *The Annals of Mathematics* **64** (July, 1956) 20. (Cited on p. 82).

[499] T. A. Springer, *Linear Algebraic Groups*, pp. 1–121, Springer Berlin Heidelberg, Berlin, Heidelberg, 1994, 10.1007/978-3-662-03073-8˙1. (Cited on p. 82).

[500] J. Ambjørn, J. Jurkiewicz and R. Loll, *Dynamically triangulating Lorentzian quantum gravity*, *Nucl. Phys. B* **610** (2001) 347–382, [hep-th/0105267]. (Cited on p. 82).

[501] J. Ambjørn, J. Jurkiewicz and R. Loll, *Causal dynamical triangulations and the quest for quantum gravity*, p. 321–337, Cambridge University Press, July, 2012, 10.1017/cbo9780511920998.013, [1004.0352]. (Cited on p. 82).

[502] J. Ambjørn, A. Goerlich, J. Jurkiewicz and R. Loll, *Nonperturbative Quantum Gravity*, *Phys. Rept.* **519** (2012) 127–210, [1203.3591]. (Cited on p. 82).

[503] J. Ambjørn, A. Görlich, J. Jurkiewicz and R. Loll, *Quantum Gravity via Causal Dynamical Triangulations*, pp. 723–741, Springer, 2014, 10.1007/978-3-642-41992-8˙34, [1302.2173]. (Cited on p. 82).

[504] J. Ambjørn and R. Loll, *Causal Dynamical Triangulations: Gateway to Nonperturbative Quantum Gravity*, 2401.09399. (Cited on p. 82).

[505] R. Loll, *Discrete approaches to quantum gravity in four-dimensions*, *Living Rev. Rel.* **1** (1998) 13, [gr-qc/9805049]. (Cited on p. 82).

[506] R. Loll, *Quantum Gravity from Causal Dynamical Triangulations: A Review*, *Class. Quant. Grav.* **37** (2020) 013002, [1905.08669]. (Cited on p. 82).

[507] T. Regge, *GENERAL RELATIVITY WITHOUT COORDINATES*, *Nuovo Cim.* **19** (1961) 558–571. (Cited on p. 82).

[508] J. Brunekreef, R. Loll and A. Görlich, *Simulating CDT quantum gravity*, *Comput. Phys. Commun.* **300** (2024) 109170, [2310.16744]. (Cited on p. 82).

[509] M. Asaduzzaman and S. Catterall, *Scalar fields on fluctuating hyperbolic geometries*, *PoS* **LATTICE2021** (2022) 430, [2112.00927]. (Cited on p. 82).

[510] M. Asaduzzaman and S. Catterall, *Euclidean dynamical triangulations revisited*, *Phys. Rev. D* **107** (2023) 074505, [2207.12642]. (Cited on p. 82).

[511] M. Asaduzzaman, S. Catterall and A. Samlodia, *Fermions, quantum gravity, and holography in two dimensions*, *Phys. Rev. D* **109** (2024) 106010, [2401.15467]. (Cited on p. 82).

[512] R. Penrose, *The Role of Aesthetics in Pure and Applied Mathematical Research*, *Bulletin of the Institute of Mathematics and its Applications* **10** (1974) 266–271. (Cited on pp. 83 and 113).

[513] H. S. M. Coxeter and W. O. J. Moser, *Generators and Relations for Discrete Groups*, Springer Berlin Heidelberg, 1972, 10.1007/978-3-662-21946-1. (Cited on pp. 83, 102, and 103).

[514] A. L. Edmonds, J. H. Ewing and R. S. Kulkarni, *Torsion free subgroups of fuchsian groups and tessellations of surfaces*, *Inventiones Mathematicae* **69** (Oct., 1982) 331–346. (Cited on pp. 83, 96, 101, and 107).

[515] S. Katok, *Fuchsian Groups*, Chicago Lectures in Mathematics, University of Chicago Press, 1992. (Cited on pp. 83, 98, 99, 100, 101, 102, 104, 107, and 108).

[516] F. Sausset and G. Tarjus, *Periodic boundary conditions on the pseudosphere*, *Journal of Physics A: Mathematical and Theoretical* **40** (Oct., 2007) 12873–12899. (Cited on pp. 83 and 101).

[517] I. Boettcher, A. V. Gorshkov, A. J. Kollár, J. Maciejko, S. Rayan and R. Thomale, *Crystallography of hyperbolic lattices*, *Phys. Rev. B* **105** (Mar, 2022) 125118. (Cited on pp. 83, 93, 94, 95, 96, 101, 104, 105, 106, 109, and 134).

[518] J. Maciejko and S. Rayan, *Hyperbolic band theory*, *Science Advances* **7** (2021) eabe9170, [cond-mat/0403635]. (Cited on pp. 83, 105, 106, 107, 109, and 134).

[519] J. Maciejko and S. Rayan, *Automorphic Bloch theorems for hyperbolic lattices*, *Proceedings of the National Academy of Sciences* **119** (2022) e2116869119, [cond-mat/0403635]. (Cited on pp. 83, 105, 106, 109, 110, 111, and 134).

[520] E. Kienzle and S. Rayan, *Hyperbolic band theory through Higgs bundles*, *Adv. Math.* **409** (2022) 108664, [2201.12689]. (Cited on pp. 83 and 110).

[521] K. Ikeda, S. Aoki and Y. Matsuki, *Hyperbolic band theory under magnetic field and Dirac cones on a higher genus surface*, *Journal of Physics: Condensed Matter* **33** (sep, 2021) 485602. (Cited on pp. 83 and 105).

[522] A. Attar and I. Boettcher, *Selberg trace formula in hyperbolic band theory*, *Phys. Rev. E* **106** (Sep, 2022) 034114. (Cited on pp. 83 and 134).

[523] G. Shankar and J. Maciejko, *Hyperbolic lattices and two-dimensional Yang-Mills theory*, 2309.03857. (Cited on pp. 83, 106, 108, 109, 110, 111, 134, and 347).

[524] M. Baake and U. Grimm, *Aperiodic Order*, Cambridge University Press, Aug., 2013, 10.1017/cbo9781139025256. (Cited on pp. 83, 112, and 120).

[525] L. Boyle, M. Dickens and F. Flicker, *Conformal Quasicrystals and Holography*, *Phys. Rev. X* **10** (Jan, 2020) 011009. (Cited on pp. 83, 112, 113, and 228).

[526] N. L. Balazs and A. Voros, *Chaos on the pseudosphere*, *Phys. Rept.* **143** (1986) 109–240. (Cited on pp. 84, 85, 86, and 87).

[527] J. W. Cannon, W. J. Floyd, R. Kenyon and W. R. Parry, *Hyperbolic Geometry*, in *Flavors of Geometry* (S. Levy, ed.), vol. 31, p. 59, MSRI Publications, 1997. (Cited on pp. 84, 85, and 86).

[528] F. Bolyai and J. Bolyai, *Tentamen Juventutem Studiosam in Elementa Matheseos Purae Elementaris Ac Sublimioris Methodo Intuitiva Evidentiaque Huic Propria Introducendi: Cum Appendice Triplici*, Maros V´asa´rhelyini, 1832–1833. (Cited on p. 86).

[529] N. I. Lobachevskiĭ, *Geometrische Untersuchungen zur Theorie der Parallellinien*, Mayer & Müller, 1887, 10.5479/sil.344583.39088005689559. (Cited on p. 86).

[530] R. E. Greene and S. G. Krantz, *Function theory of one complex variable*, Graduate studies in mathematics, American Mathematical Society, Providence, RI, 3 ed., Mar., 2006. (Cited on p. 86).

[531] S. G. Krantz, *Handbook of complex variables*, Birkhauser Boston, Secaucus, NJ, 1999 ed., Oct., 1999. (Cited on p. 86).

[532] W. Magnus, *Noneuclidean Tesselations and Their Groups*, Academic Press, Amsterdam, Boston, 1 ed., 1974. (Cited on p. 87).

[533] H. Coxeter, *Regular Polytopes*, Dover books on advanced mathematics, Dover Publications, 1973. (Cited on p. 87).

[534] H. S. M. Coxeter, *Regular and semi-regular polytopes. I*, *Mathematische Zeitschrift* **46** (Dec., 1940) 380–407. (Cited on p. 87).

[535] H. S. M. Coxeter, *Regular and semi-regular polytopes. II*, *Mathematische Zeitschrift* **188** (Dec., 1985) 559–591. (Cited on p. 87).

[536] H. S. M. Coxeter, *Regular and semi-regular polytopes. III*, *Mathematische Zeitschrift* **200** (Mar., 1988) 3–45. (Cited on p. 87).

[537] L. Schläfli, *Theorie der vielfachen Kontinuität*, pp. 167–387, Springer Basel, Basel, 1950, 10.1007/978-3-0348-4118-4˙13. (Cited on p. 88).

[538] Bonnet, *Mémoire sur la théorie générale des surfaces*, *Journal de l'École Polytechnique* **32** (1848) 1–46. (Cited on pp. 89 and 90).

[539] L. Euler, *Elementa doctrinae solidorum*, *Novi Commentarii Academiae Scientiarum Petropolitanae* **3** (1758) 109–140. (Cited on p. 89).

[540] J. H. Lambert, *Theorie der Parallellinien*, *Leipziger Magazin für reine und angewandte Mathematik* (1786) . (Cited on p. 90).

[541] A. Papadopoulos and G. Théret, *Hyperbolic geometry in the work of Johann Heinrich Lambert*, 1503.01865. (Cited on p. 90).

[542] H. S. M. Coxeter, *The Trigonometry of Hyperbolic Tessellations*, *Canadian Mathematical Bulletin* **40** (1997) 158–168. (Cited on pp. 91 and 93).

[543] H. S. M. Coxeter, *Twelve Geometric Essays*, Southern Illinois University Press, Carbondale, IL, 1968. (Cited on p. 91).

[544] J. Karl, *Entanglement Entropy for Discrete Holography*, 2021. Bachelor's Thesis, Chair for Theoretical Physics III, Julius-Maximilians-Universität Würzburg. (Cited on p. 95).

[545] L. Fuchs and A. Lazarus, *Ueber eine Klasse von Funktionen mehrerer Variablen, welche durch Umkehrung der Integrale von Lösungen der linearen Differentialgleichungen mit rationalen Coeffizienten entstehen*, *J. Reine Angew. Math.* **89** (1880) 151–169. (Cited on p. 98).

[546] W. Dyck, *Über Aufstellung und Untersuchung von Gruppe und Irrationalität regulärer Riemannscher Flächen*, *Mathematische Annalen* **17** (Dec., 1880) 473–509. (Cited on p. 103).

[547] W. Dyck, *Gruppentheoretische Studien*, *Mathematische Annalen* **20** (Mar., 1882) 1–44. (Cited on p. 103).

[548] N. Ashcroft and N. Mermin, *Solid State Physics*, HRW international editions, Holt, Rinehart and Winston, 1976. (Cited on pp. 105 and 106).

[549] A. Chen, Y. Guan, P. M. Lenggenhager, J. Maciejko, I. Boettcher and T. Bzdušek, *Symmetry and topology of hyperbolic Haldane models*, *Phys. Rev. B* **108** (Aug, 2023) 085114. (Cited on pp. 105, 106, 108, and 134).

[550] A. J. Kollár, M. Fitzpatrick, P. Sarnak and A. A. Houck, *Line-Graph Lattices: Euclidean and Non-Euclidean Flat Bands, and Implementations in Circuit Quantum Electrodynamics*, *Comm. Math. Phys.* **376** (Dec, 2019) 1909–1956. (Cited on pp. 105 and 134).

[551] A. Stegmaier, L. K. Upreti, R. Thomale and I. Boettcher, *Universality of Hofstadter Butterflies on Hyperbolic Lattices*, *Phys. Rev. Lett.* **128** (Apr, 2022) 166402. (Cited on pp. 105, 134, and 154).

[552] K. Ikeda, Y. Matsuki and S. Aoki, *Algebra of hyperbolic band theory under magnetic field*, *Can. J. Phys.* **101** (2023) 630–640, [2107.10586]. (Cited on pp. 105 and 134).

[553] T. Bzdusek and J. Maciejko, *Flat bands and band-touching from real-space topology in hyperbolic lattices*, *Phys. Rev. B* **106** (2022) 155146, [2205.11571]. (Cited on pp. 105 and 134).

[554] A. Saa, E. Miranda and F. Rouxinol, *Higher-dimensional Euclidean and non-Euclidean structures in planar circuit quantum electrodynamics*, 2108.08854. (Cited on pp. 105 and 134).

[555] R. Mosseri, R. Vogeler and J. Vidal, *Aharonov-Bohm cages, flat bands, and gap labeling in hyperbolic tilings*, *Phys. Rev. B* **106** (Oct, 2022) 155120. (Cited on pp. 105 and 134).

[556] Q. Pei, H. Yuan, W. Zhang and X. Zhang, *Engineering boundary-dominated topological states in defective hyperbolic lattices*, *Phys. Rev. B* **107** (Apr, 2023) 165145. (Cited on pp. 105 and 134).

[557] S. Yu, X. Piao and N. Park, *Topological Hyperbolic Lattices*, *Phys. Rev. Lett.* **125** (Jul, 2020) 053901, [2003.07002]. (Cited on pp. 105 and 134).

[558] H. Yuan, W. Zhang, Q. Pei and X. Zhang, *Hyperbolic topological flat bands*, *Phys. Rev. B* **109** (Jan, 2024) L041109. (Cited on pp. 105 and 134).

[559] Z.-R. Liu, C.-B. Hua, T. Peng and B. Zhou, *Chern insulator in a hyperbolic lattice*, *Phys. Rev. B* **105** (Jun, 2022) 245301. (Cited on pp. 105 and 134).

[560] D. M. Urwyler, P. M. Lenggenhager, I. Boettcher, R. Thomale, T. Neupert and T. Bzdusek, *Hyperbolic Topological Band Insulators*, *Phys. Rev. Lett.* **129** (Dec, 2022) 246402. (Cited on pp. 105 and 134).

[561] L. Huang, L. He, W. Zhang, H. Zhang, D. Liu, X. Feng et al., *Hyperbolic photonic topological insulators*, *Nat. Commun.* **15** (Feb, 2024) 1647. (Cited on pp. 105 and 135).

[562] Q. Chen, Z. Zhang, H. Qin, A. Bossart, Y. Yang, H. Chen et al., *Anomalous and Chern topological waves in hyperbolic networks*, *Nat. Commun.* **15** (Mar, 2024) 2293. (Cited on pp. 105 and 135).

[563] A. J. Kollár, M. Fitzpatrick and A. A. Houck, *Hyperbolic lattices in circuit quantum electrodynamics*, *Nature* **571** (Jul, 2019) 45–50. (Cited on pp. 105, 134, and 135).

[564] W. Zhang, F. Di, X. Zheng, H. Sun and X. Zhang, *Hyperbolic band topology with non-trivial second Chern numbers*, *Nat. Commun.* **14** (Feb, 2023) 1083. (Cited on pp. 105, 134, and 135).

[565] P. M. Lenggenhager, A. Stegmaier, L. K. Upreti, T. Hofmann, T. Helbig, A. Vollhardt et al., *Simulating hyperbolic space on a circuit board*, *Nature Communications* **13** (July, 2022) , [2109.01148]. (Cited on pp. 105, 134, 135, and 136).

[566] A. Chen, H. Brand, T. Helbig, T. Hofmann, S. Imhof, A. Fritzsche et al., *Hyperbolic matter in electrical circuits with tunable complex phases*, *Nature Commun.* **14** (2023) 622, [2205.05106]. (Cited on pp. 105 and 134).

[567] S. Bundgaard and J. Nielsen, *On normal subgroups with finite index in F-groups*, *Matematisk tidsskrift. B* (1951) 56–58. (Cited on p. 108).

[568] R. H. Fox, *On Fenchel's Conjecture about F-Groups*, *Matematisk Tidsskrift. B* (1952) 61–65. (Cited on p. 108).

[569] J. Mennicke, *Eine Bemerkung Über Fuchssche Gruppen*, *Inventiones Mathematicae* **2** (Aug., 1967) 301–305. (Cited on p. 108).

[570] T. C. Chau, *A Note Concerning Fox's Paper on Fenchel's Conjecture*, *Proceedings of the American Mathematical Society* **88** (1983) 584–586. (Cited on p. 108).

[571] J. Širáň, *Triangle group representations and their applications to graphs and maps*, *Discrete Mathematics* **229** (2001) 341–358. (Cited on p. 108).

[572] R. Hartshorne, *Algebraic Geometry*, Springer New York, 1977, 10.1007/978-1-4757-3849-0. (Cited on p. 108).

[573] M. S. Narasimhan and C. S. Seshadri, *Stable and Unitary Vector Bundles on a Compact Riemann Surface*, *The Annals of Mathematics* **82** (1965) 540–567. (Cited on p. 111).

[574] A. Garcia-Raboso and S. Rayan, *Introduction to Nonabelian Hodge Theory*, in *Calabi-Yau Varieties: Arithmetic, Geometry and Physics*, pp. 131–171, Springer New York, 2015, 10.1007/978-1-4939-2830-9˙5. (Cited on p. 111).

[575] Wikipedia Contributor: Inductiveload, *Penrose Tiling (Rhombi)*, Wikipedia, Feb., 2009. https://de.wikipedia.org/wiki/Datei:Penrose˙Tiling˙(Rhombi).svg, Accessed on 15th May 2024. (Cited on p. 112).

[576] J. M. Luck, *A Classification of Critical Phenomena on Quasi-Crystals and Other Aperiodic Structures*, *Europhysics Letters* **24** (nov, 1993) 359. (Cited on pp. 112, 160, and 163).

[577] M. Senechal, *Quasicrystals and Geometry*, Cambridge University Press, Cambridge, England, Sept., 1996. (Cited on pp. 112 and 346).

[578] C. Janot, *Quasicrystals: A Primer*, Monographs on the Physics and Chemistry of Materials, Clarendon Press, Oxford, England, Oct., 1992. (Cited on p. 112).

[579] A. L. Mackay, *Crystallography and the penrose pattern*, *Physica A: Statistical Mechanics and its Applications* **114** (1982) 609–613. (Cited on p. 112).

[580] D. Shechtman, I. Blech, D. Gratias and J. W. Cahn, *Metallic Phase with Long-Range Orientational Order and No Translational Symmetry*, *Phys. Rev. Lett.* **53** (Nov, 1984) 1951–1953. (Cited on p. 112).

[581] L. Bindi, P. J. Steinhardt, N. Yao and P. J. Lu, *Natural Quasicrystals*, *Science* **324** (June, 2009) 1306–1309. (Cited on p. 112).

[582] L. Bindi, W. Kolb, G. N. Eby, P. D. Asimow, T. C. Wallace and P. J. Steinhardt, *Accidental synthesis of a previously unknown quasicrystal in the first atomic bomb test*, *Proceedings of the National Academy of Sciences* **118** (May, 2021) . (Cited on p. 112).

[583] M. Gardner, *Extraordinary nonperiodic tiling that enriches the theory of tiles*, *Scientific American* **236** (Jan., 1977) 110–221. (Cited on p. 113).

[584] R. Penrose, *Pentaplexity* A Class of Non-Periodic Tilings of the Plane*, *The Mathematical Intelligencer* **2** (Mar., 1979) 32–37. (Cited on p. 113).

[585] D. Smith, J. S. Myers, C. S. Kaplan and C. Goodman-Strauss, *An aperiodic monotile*, 2303.10798. (Cited on p. 113).

[586] D. Smith, J. S. Myers, C. S. Kaplan and C. Goodman-Strauss, *A chiral aperiodic monotile*, 2305.17743. (Cited on p. 113).

[587] B. Klaassen, *Forcing nonperiodic tilings with one tile using a seed*, *European Journal of Combinatorics* **100** (2022) 103454. (Cited on p. 113).

[588] F. Iglói, R. Juhász and Z. Zimborás, *Entanglement entropy of aperiodic quantum spin chains*, *EPL* **79** (2007) 37001, [cond-mat/0701527]. (Cited on pp. 114, 119, 168, 170, 174, 186, 188, 189, 191, and 192).

[589] R. Juhász and Z. Zimborás, *Entanglement entropy in aperiodic singlet phases*, *J. Stat. Mech* **2007** (2007) P04004–P04004, [cond-mat/0703527]. (Cited on pp. 114, 119, 168, 170, 171, 174, 186, 188, 189, 191, 192, 193, and 204).

[590] A. P. Vieira, *Low-Energy Properties of Aperiodic Quantum Spin Chains*, *Phys. Rev. Lett.* **94** (2005) 077201, [cond-mat/0403635]. (Cited on pp. 114, 165, 166, 167, 168, 178, 199, 200, and 204).

[591] A. P. Vieira, *Aperiodic quantum XXZ chains: Renormalization-group results*, *Phys. Rev. B* **71** (Apr, 2005) 134408. (Cited on pp. 114, 163, 165, 166, 167, 168, 172, 173, 176, 199, 200, and 204).

[592] O. Perron, *Zur Theorie der Matrices*, *Mathematische Annalen* **64** (June, 1907) 248–263. (Cited on p. 114).

[593] G. Frobenius, *Über Matrizen aus nicht negativen Elementen*, *Berl. Ber.* **1912** (1912) 456–477. (Cited on p. 114).

[594] G. Arfken, *Mathematical Methods for Physicists*, Elsevier, Orlando, FL, 7th ed., 2013, 10.1016/c2009-0-30629-7. (Cited on p. 115).

[595] J. S. Lomont, *Applications of Finite Groups*, Dover, New York, 1987. (Cited on p. 115).

[596] V. W. de Spinadel, *The metallic means family and multifractal spectra*, *Nonlinear Analysis: Theory, Methods & Applications* **36** (1999) 721–745. (Cited on pp. 119 and 120).

[597] M. Abramowitz and I. A. Stegun, eds., *Handbook of Mathematical Functions: With Formulas, Graphs, and Mathematical Tables*, Dover Books on Mathematics, Dover Publications, Mineola, NY, June, 1965. (Cited on pp. 124, 125, 126, and 336).

[598] I. R. Klebanov and E. Witten, *AdS / CFT correspondence and symmetry breaking*, *Nucl. Phys. B* **556** (1999) 89–114, [hep-th/9905104]. (Cited on p. 125).

[599] D. B. Kaplan, J.-W. Lee, D. T. Son and M. A. Stephanov, *Conformality Lost*, *Phys. Rev. D* **80** (2009) 125005, [0905.4752]. (Cited on p. 125).

[600] L. Mezincescu and P. Townsend, *Stability at a local maximum in higher dimensional anti-deSitter space and applications to supergravity*, *Annals of Physics* **160** (1985) 406–419. (Cited on pp. 129 and 130).

[601] L. Abbott and S. Deser, *Stability of gravity with a cosmological constant*, *Nuclear Physics B* **195** (1982) 76–96. (Cited on p. 129).

[602] N. H. Asmar, *Partial differential equations with Fourier series and boundary value problems*, Courier Dover Publications, Mineola, NY, 1 ed., Sept., 2016. (Cited on p. 133).

[603] K. W. Morton and D. F. Mayers, *Numerical Solution of Partial Differential Equations: An Introduction*, Cambridge University Press, Apr., 2005, 10.1017/cbo9780511812248. (Cited on p. 133).

[604] O. G. Ernst and M. J. Gander, *Why it is Difficult to Solve Helmholtz Problems with Classical Iterative Methods*, p. 325–363, Springer Berlin Heidelberg, Aug., 2011, 10.1007/978-3-642-22061-6˙10. (Cited on p. 133).

[605] Y. Saad, *Iterative Methods for Sparse Linear Systems*, Society for Industrial and Applied Mathematics, Jan., 2003, 10.1137/1.9780898718003. (Cited on p. 133).

[606] Y. Saad and M. H. Schultz, *GMRES: A Generalized Minimal Residual Algorithm for Solving Nonsymmetric Linear Systems*, *SIAM Journal on Scientific and Statistical Computing* **7** (July, 1986) 856–869. (Cited on p. 133).

[607] H. A. van der Vorst, *Bi-CGSTAB: A Fast and Smoothly Converging Variant of Bi-CG for the Solution of Nonsymmetric Linear Systems*, *SIAM Journal on Scientific and Statistical Computing* **13** (Mar., 1992) 631–644. (Cited on p. 133).

[608] M. Schrauth, F. Dusel, Y. Thurn, F. Goth, D. Herdt and J. S. E. Portela, *Hypertiling – a high performance Python library for the generation and visualization of hyperbolic lattices*, 2309.10844. (Cited on pp. 133 and 134).

[609] M. Ruzzene, E. Prodan and C. Prodan, *Dynamics of elastic hyperbolic lattices*, *Extreme Mechanics Letters* **49** (Nov., 2021) 101491. (Cited on p. 134).

[610] M. Asaduzzaman, S. Catterall, J. Hubisz, R. Nelson and J. Unmuth-Yockey, *Holography on tessellations of hyperbolic space*, *Phys. Rev. D* **102** (Aug, 2020) 034511. (Cited on p. 134).

[611] I. Boettcher, P. Bienias, R. Belyansky, A. J. Kollár and A. V. Gorshkov, *Quantum Simulation of Hyperbolic Space with Circuit Quantum Electrodynamics: From Graphs to Geometry*, *Phys. Rev. A* **102** (2020) 032208, [1910.12318]. (Cited on pp. 134, 144, 145, and 154).

[612] R. C. Brower, C. V. Cogburn, A. L. Fitzpatrick, D. Howarth and C.-I. Tan, *Lattice setup for quantum field theory in AdS_2*, *Phys. Rev. D* **103** (2021) 094507, [1912.07606]. (Cited on p. 134).

[613] X. Zhu, J. Guo, N. P. Breuckmann, H. Guo and S. Feng, *Quantum phase transitions of interacting bosons on hyperbolic lattices*, *J. Phys.: Condens. Matter* **33** (June, 2021) 335602. (Cited on p. 134).

[614] P. Bienias, I. Boettcher, R. Belyansky, A. J. Kollar and A. V. Gorshkov, *Circuit Quantum Electrodynamics in Hyperbolic Space: From Photon Bound States to Frustrated Spin Models*, *Phys. Rev. Lett.* **128** (2022) 013601, [2105.06490]. (Cited on p. 134).

[615] R. C. Brower, C. V. Cogburn and E. Owen, *Hyperbolic lattice for scalar field theory in AdS3*, *Phys. Rev. D* **105** (2022) 114503, [2202.03464]. (Cited on pp. 134 and 154).

[616] N. Cheng, F. Serafin, J. McInerney, Z. Rocklin, K. Sun and X. Mao, *Band theory and boundary modes of high-dimensional representations of infinite hyperbolic lattices*, *Phys. Rev. Lett.* **129** (Aug, 2022) 088002. (Cited on p. 134).

[617] N. Gluscevich, A. Samanta, S. Manna and B. Roy, *Dynamic mass generation on two-dimensional electronic hyperbolic lattices*, 2302.04864. (Cited on p. 134).

[618] Z.-R. Liu, C.-B. Hua, T. Peng, R. Chen and B. Zhou, *Higher-order topological insulators in hyperbolic lattices*, *Phys. Rev. B* **107** (Mar, 2023) 125302. (Cited on p. 134).

[619] J. Chen, F. Chen, Y. Yang, L. Yang, Z. Chen, Y. Meng et al., *AdS/CFT Correspondence in Hyperbolic Lattices*, 2305.04862. (Cited on pp. 134, 135, 146, and 147).

[620] Y.-L. Tao and Y. Xu, *Higher-order topological hyperbolic lattices*, *Phys. Rev. B* **107** (May, 2023) 184201. (Cited on p. 134).

[621] N. Gluscevich and B. Roy, *Magnetic catalysis in weakly interacting hyperbolic Dirac materials*, 2305.11174. (Cited on p. 134).

[622] E. Petermann and H. Hinrichsen, *Eigenmodes of the Laplacian on hyperbolic lattices*, *Phys. Rev. D* **109** (2024) 106019, [2306.08248]. (Cited on pp. 134 and 144).

[623] R. Mosseri and J. Vidal, *Density of states of tight-binding models in the hyperbolic plane*, *Phys. Rev. B* **108** (Jul, 2023) 035154. (Cited on p. 134).

[624] J. B. Curtis, P. Narang and V. Galitski, *Absence of Weak Localization on Negative Curvature Surfaces*, 2308.01351. (Cited on p. 134).

[625] A. Chen, J. Maciejko and I. Boettcher, *Anderson localization transition in disordered hyperbolic lattices*, 2310.07978. (Cited on p. 134).

[626] P. M. Lenggenhager, J. Maciejko and T. Bzdusek, *Non-Abelian Hyperbolic Band Theory from Supercells*, *Phys. Rev. Lett.* **131** (Dec, 2023) 226401. (Cited on p. 134).

[627] T. Li, Y. Peng, Y. Wang and H. Hu, *Anderson transition and mobility edges on hyperbolic lattices*, 2312.11857. (Cited on p. 134).

[628] T. Tummuru, A. Chen, P. M. Lenggenhager, T. Neupert, J. Maciejko and T. Bzdušek, *Hyperbolic Non-Abelian Semimetal*, *Phys. Rev. Lett.* **132** (2024) 206601, [2307.09876]. (Cited on p. 134).

[629] T. Kotwal, F. Moseley, A. Stegmaier, S. Imhof, H. Brand, T. Kießling et al., *Active topolectrical circuits*, *Proceedings of the National Academy of Sciences* **118** (2021) e2106411118. (Cited on p. 135).

[630] C. H. Lee, S. Imhof, C. Berger, F. Bayer, J. Brehm, L. W. Molenkamp et al., *Topolectrical Circuits*, *Communications Physics* **1** (Jul, 2018) . (Cited on pp. 135 and 136).

[631] S. Imhof, C. Berger, F. Bayer, J. Brehm, L. W. Molenkamp, T. Kiessling et al., *Topolectrical-circuit realization of topological corner modes*, *Nature Physics* **14** (Sep, 2018) 925–929. (Cited on p. 135).

[632] H. Hohmann, T. Hofmann, T. Helbig, S. Imhof, H. Brand, L. K. Upreti et al., *Observation of cnoidal wave localization in nonlinear topolectric circuits*, *Phys. Rev. Res.* **5** (Mar, 2023) L012041. (Cited on p. 135).

[633] E. Zhao, *Topological circuits of inductors and capacitors*, *Annals of Physics* **399** (Dec, 2018) 289–313. (Cited on p. 135).

[634] T. Ozawa, H. M. Price, A. Amo, N. Goldman, M. Hafezi, L. Lu et al., *Topological photonics*, *Rev. Mod. Phys.* **91** (Mar, 2019) 015006. (Cited on p. 135).

[635] M. Jalali Mehrabad, S. Mittal and M. Hafezi, *Topological photonics: Fundamental concepts, recent developments, and future directions*, *Phys. Rev. A* **108** (Oct, 2023) 040101. (Cited on p. 135).

[636] N. H. Patino, C. Rasmussen and M. Ruzzene, *Hyperbolic Space Spectral Characteristics in a Network of Mechanical Linkages*, 2402.04531. (Cited on p. 135).

[637] K. E. Atkinson, *An Introduction to Numerical Analysis*, John Wiley & Sons, New York, second ed., 1989. (Cited on p. 136).

[638] W. H. Press, S. A. Teukolsky, W. T. Vetterling and B. P. Flannery, *Numerical Recipes 3rd Edition: The Art of Scientific Computing*, Cambridge University Press, 3 ed., 2007. (Cited on p. 136).

[639] A. M. Polyakov, *Quantum Geometry of Bosonic Strings*, *Phys. Lett. B* **103** (1981) 207–210. (Cited on p. 141).

[640] N. Seiberg, *Notes on quantum Liouville theory and quantum gravity*, *Prog. Theor. Phys. Suppl.* **102** (1990) 319–349. (Cited on p. 141).

[641] P. H. Ginsparg and G. W. Moore, *Lectures on 2-D gravity and 2-D string theory*, in *Theoretical Advanced Study Institute (TASI 92): From Black Holes and Strings to Particles*, pp. 277–469, 10, 1993, [hep-th/9304011]. (Cited on pp. 141 and 143).

[642] A. Hamilton, D. N. Kabat, G. Lifschytz and D. A. Lowe, *Local bulk operators in AdS/CFT: A Boundary view of horizons and locality*, *Phys. Rev. D* **73** (2006) 086003, [hep-th/0506118]. (Cited on p. 148).

[643] A. Hamilton, D. N. Kabat, G. Lifschytz and D. A. Lowe, *Holographic representation of local bulk operators*, *Phys. Rev. D* **74** (2006) 066009, [hep-th/0606141]. (Cited on p. 148).

[644] J. Luck, *Critical behaviour of the aperiodic quantum Ising chain in a transverse magnetic field*, *J. Stat. Phys.* **72** (1993) 417–58. (Cited on p. 160).

[645] J. Luck, *Aperiodic structures: Geometry, diffraction spectra, and physical properties*, *Fundamental Problems in Statistical Mechanics* **VIII** (1994) 127–167. (Cited on p. 160).

[646] J. Hermisson, U. Grimm and M. Baake, *Aperiodic Ising quantum chains*, *J. Phys. A* **30** (1997) 7315–7335, [cond-mat/9706106]. (Cited on p. 160).

[647] J. Vidal, D. Mouhanna and T. Giamarchi, *Correlated Fermions in a One-Dimensional Quasiperiodic Potential*, *Phys. Rev. Lett.* **83** (1999) 3908–3911, [cond-mat/9905080]. (Cited on p. 160).

[648] J. Hermisson, *Aperiodic and correlated disorder in XY chains: exact results*, *J. Phys. A* **33** (1999) 57–59, [cond-mat/9808238]. (Cited on pp. 160, 163, 199, and 201).

[649] J. Ziman, *Models of Disorder: The Theoretical Physics of Homogeneously Disordered Systems*, Cambridge University Press, 1979. (Cited on p. 160).

[650] T. Giamarchi, *Disordered Systems*, in *Quantum Physics in One Dimension*, Oxford University Press, 12, 2003, 10.1093/acprof:oso/9780198525004.003.0009. (Cited on p. 160).

[651] F. Iglói and C. Monthus, *Strong disorder RG approach – a short review of recent developments*, *The European Physical Journal B* **91** (Nov., 2018) . (Cited on pp. 160, 163, and 184).

[652] E. Fradkin, *Field Theories of Condensed Matter Physics*, Cambridge University Press, Feb., 2013, 10.1017/cbo9781139015509. (Cited on pp. 160, 199, and 201).

[653] F. D. M. Haldane, *Continuum dynamics of the 1-D Heisenberg antiferromagnetic identification with the O(3) nonlinear sigma model*, *Phys. Lett. A* **93** (1983) 464–468. (Cited on p. 162).

[654] F. D. M. Haldane, *Nonlinear field theory of large spin Heisenberg antiferromagnets. Semiclassically quantized solitons of the one-dimensional easy Axis Neel state*, *Phys. Rev. Lett.* **50** (1983) 1153–1156. (Cited on p. 162).

[655] H. L. Casa Grande, N. Laflorencie, F. Alet and A. P. Vieira, *Analytical and numerical studies of disordered spin-1 Heisenberg chains with aperiodic couplings*, *Phys. Rev. B* **89** (Apr, 2014) 134408. (Cited on pp. 162 and 199).

[656] I. Affleck and J. B. Marston, *Large-n limit of the Heisenberg-Hubbard model: Implications for high-t(c) supconductors*, *Phys. Rev. B* **37** (1987) 3774–3777. (Cited on p. 162).

[657] I. Affleck, *Critical Behavior of SU(n) Quantum Chains and Topological Nonlinear σ Models*, *Nucl. Phys. B* **305** (1988) 582–596. (Cited on p. 162).

[658] J. B. Marston and I. Affleck, *Large-n limit of the Hubbard-Heisenberg model*, *Phys. Rev. B* **39** (1989) 11538–11558. (Cited on p. 162).

[659] N. Read and S. Sachdev, *Some Features of the Phase Diagram of the Square Lattice SU(N) Antiferromagnet*, *Nucl. Phys. B* **316** (1989) 609–640. (Cited on p. 162).

[660] N. Read and S. Sachdev, *Valence-bond and spin-Peierls ground states of low-dimensional quantum antiferromagnets*, *Phys. Rev. Lett.* **62** (1989) 1694–1697. (Cited on p. 162).

[661] Y. Yamashita, N. Shibata and K. Ueda, *SU(4) spin-orbit critical state in one dimension*, *Phys. Rev. B* **58** (1998) 9114–9118, [cond-mat/9804182]. (Cited on p. 162).

[662] Y. Q. Li, M. Ma, D. N. Shi and F. C. Zhang, *SU(4) Theory for Spin Systems with Orbital Degeneracy*, *Phys. Rev. Lett.* **81** (1998) 3527–3530, [cond-mat/9804157]. (Cited on p. 162).

[663] A. V. Gorshkov, M. Hermele, V. Gurarie, C. Xu, P. S. Julienne, J. Ye et al., *Two-orbital S U(N) magnetism with ultracold alkaline-earth atoms*, *Nature Phys.* **6** (2010) 289–295. (Cited on p. 162).

[664] C. Honerkamp and W. Hofstetter, *Ultracold Fermions and the SU(N) Hubbard Model*, *Phys. Rev. Lett.* **92** (2004) 170403, [cond-mat/0309374]. (Cited on p. 162).

[665] R. Gruschinski, G. Nimtz and A. Stahlhofen, *Resonance-like Goos-Hänchen shift induced by nano-metal films*, *Annalen der Physik* **520** (Nov., 2008) 917–921. (Cited on p. 162).

[666] S. Rachel, R. Thomale, M. Führinger, P. Schmitteckert and M. Greiter, *Spinon confinement and the Haldane gap in SU(n) spin chains*, *Phys. Rev. B* **80** (Nov, 2009) 180420. (Cited on p. 162).

[667] A. Weichselbaum, S. Capponi, P. Lecheminant, A. M. Tsvelik and A. M. Läuchli, *Unified phase diagram of antiferromagnetic SU(N) spin ladders*, *Phys. Rev. B* **98** (Aug, 2018) 085104. (Cited on p. 162).

[668] A. Läuchli, F. Mila and K. Penc, *Quadrupolar Phases of the $S = 1$ Bilinear-Biquadratic Heisenberg Model on the Triangular Lattice*, *Phys. Rev. Lett.* **97** (Aug, 2006) 087205. (Cited on p. 162).

[669] P. Corboz, A. M. Läuchli, K. Penc, M. Troyer and F. Mila, *Simultaneous Dimerization and SU(4) Symmetry Breaking of 4-Color Fermions on the Square Lattice*, *Phys. Rev. Lett.* **107** (Nov, 2011) 215301. (Cited on p. 162).

[670] M. Greiter and S. Rachel, *Valence bond solids for* SU(n) *spin chains: Exact models, spinon confinement, and the Haldane gap*, *Phys. Rev. B* **75** (May, 2007) 184441. (Cited on p. 162).

[671] M. Greiter, S. Rachel and D. Schuricht, *Exact results for SU(3) spin chains: Trimer states, valence bond solids, and their parent Hamiltonians*, *Phys. Rev. B* **75** (Feb, 2007) 060401. (Cited on p. 162).

[672] T. Botzung and P. Nataf, *Exact Diagonalization of* SU(N) *Fermi-Hubbard Models*, *Phys. Rev. Lett.* **132** (Apr, 2024) 153001. (Cited on p. 162).

[673] F. Haldane, *Continuum dynamics of the 1-D Heisenberg antiferromagnet: Identification with the O(3) nonlinear sigma model*, *Physics Letters A* **93** (1983) 464–468. (Cited on p. 162).

[674] F. Alet, S. Capponi, H. Nonne, P. Lecheminant and I. P. McCulloch, *Quantum criticality in the SO(5) bilinear-biquadratic Heisenberg chain*, *Phys. Rev. B* **83** (Feb, 2011) 060407. (Cited on p. 162).

[675] S. Chulliparambil, H.-C. Zhang and H.-H. Tu, *Symmetry-protected topological phases, conformal criticalities, and duality in exactly solvable SO(n) spin chains*, *Phys. Rev. B* **108** (Sep, 2023) 094411. (Cited on p. 162).

[676] H. H. Tu, G. M. Zhang and T. Xiang, *Class of exactly solvable SO(n) symmetric spin chains with matrix product ground states*, *Phys. Rev. B* **78** (2008) 094404, [0806.1839]. (Cited on pp. 162, 212, 213, and 215).

[677] C. Wu, J.-p. Hu and S.-c. Zhang, *Exact SO(5) Symmetry in the Spin-*3/2 *Fermionic System*, *Phys. Rev. Lett.* **91** (Oct, 2003) 186402. (Cited on p. 162).

[678] D. Scalapino, S.-C. Zhang and W. Hanke, *SO(5) symmetric ladder*, *Phys. Rev. B* **58** (Jul, 1998) 443–452. (Cited on p. 162).

[679] V. L. Quito, P. L. S. Lopes, J. A. Hoyos and E. Miranda, *Highly symmetric random one-dimensional spin models*, *Phys. Rev. B* **100** (Dec, 2019) 224407. (Cited on pp. 162, 212, 213, 214, and 215).

[680] V. L. Quito, P. L. S. Lopes, J. A. Hoyos and E. Miranda, *Emergent SU(N) symmetry in disordered SO(N) spin chains*, *The European Physical Journal B* **93** (Jan., 2020) . (Cited on p. 162).

[681] S.-k. Ma, C. Dasgupta and C.-k. Hu, *Random Antiferromagnetic Chain*, *Phys. Rev. Lett.* **43** (1979) 1434–1437. (Cited on pp. 163 and 200).

[682] C. Dasgupta and S.-k. Ma, *Low-temperature properties of the random Heisenberg antiferromagnetic chain*, *Phys. Rev. B* **22** (1980) 1305–1319. (Cited on pp. 163 and 200).

[683] A. B. Harris, *Effect of random defects on the critical behaviour of Ising models*, *Journal of Physics C: Solid State Physics* **7** (May, 1974) 1671–1692. (Cited on p. 163).

[684] K. Hida, *New Universality Class in Spin-One-Half Fibonacci Heisenberg Chains*, *Phys. Rev. Lett.* **93** (2004) 037205, [cond-mat/0403602]. (Cited on pp. 168 and 199).

[685] K. Hida, *Real Space Renormalization Group Study of the S=1/2 XXZ Chains with Fibonacci Exchange Modulation*, *Journal of the Physical Society of Japan* **73** (2004) 2296–2304. (Cited on p. 168).

[686] V. Balasubramanian and S. F. Ross, *Holographic particle detection*, *Phys. Rev. D* **61** (2000) 044007, [hep-th/9906226]. (Cited on pp. 172 and 182).

[687] J. Erdmenger and N. Miekley, *Non-local observables at finite temperature in AdS/CFT*, *JHEP* **03** (2018) 034, [1709.07016]. (Cited on p. 182).

[688] G. Refael and J. E. Moore, *Entanglement Entropy of Random Quantum Critical Points in One Dimension*, *Phys. Rev. Lett.* **93** (Dec, 2004) 260602. (Cited on pp. 184, 188, 193, and 216).

[689] R. N. Bhatt and P. A. Lee, *Scaling Studies of Highly Disordered Spin-½ Antiferromagnetic Systems*, *Phys. Rev. Lett.* **48** (Feb, 1982) 344–347. (Cited on p. 184).

[690] D. S. Fisher, *Random antiferromagnetic quantum spin chains*, *Phys. Rev. B* **50** (1994) 3799–3821. (Cited on p. 184).

[691] D. S. Fisher, *Critical behavior of random transverse-field Ising spin chains*, *Phys. Rev. B* **51** (Mar, 1995) 6411–6461. (Cited on p. 184).

[692] Y.-R. Shu, D.-X. Yao, C.-W. Ke, Y.-C. Lin and A. W. Sandvik, *Properties of the random-singlet phase: From the disordered Heisenberg chain to an amorphous valence-bond solid*, *Phys. Rev. B* **94** (Nov, 2016) 174442. (Cited on p. 184).

[693] N. Laflorencie, *Scaling of entanglement entropy in the random singlet phase*, *Phys. Rev. B* **72** (Oct, 2005) 140408. (Cited on p. 188).

[694] I. Peschel, *Entanglement entropy with interface defects*, *Journal of Physics A: Mathematical and General* **38** (May, 2005) 4327–4335. (Cited on p. 189).

[695] J. Zhao, I. Peschel and X. Wang, *Critical entanglement of XXZ Heisenberg chains with defects*, *Phys. Rev. B* **73** (Jan, 2006) 024417. (Cited on p. 189).

[696] K. Sakai and Y. Satoh, *Entanglement through conformal interfaces*, *JHEP* **12** (2008) 001, [0809.4548]. (Cited on p. 189).

[697] V. Eisler and I. Peschel, *On entanglement evolution across defects in critical chains*, *EPL (Europhysics Letters)* **99** (July, 2012) 20001. (Cited on p. 189).

[698] P. Ruggiero, V. Alba and P. Calabrese, *Entanglement negativity in random spin chains*, *Phys. Rev. B* **94** (2016) 035152, [1605.00674]. (Cited on pp. 192, 193, and 194).

[699] S. Furukawa, V. Pasquier and J. Shiraishi, *Mutual Information and Compactification Radius in a c=1 Critical Phase in One Dimension*, *Phys. Rev. Lett.* **102** (2009) 170602, [0809.5113]. (Cited on pp. 196 and 198).

[700] M. Caraglio and F. Gliozzi, *Entanglement Entropy and Twist Fields*, *JHEP* **11** (2008) 076, [0808.4094]. (Cited on pp. 196 and 198).

[701] R. Keown, *An Introduction to Group Representation Theory*, Academic Press, 1975, 10.1016/s0076-5392(08)x6178-8. (Cited on p. 206).

[702] D. Dummit and R. Foote, *Abstract algebra*, John Wiley & Sons, 2004. (Cited on p. 206).

[703] I. Schur, *Neue Begründung der Theorie der Gruppencharaktere*, *Sitzungsberichte der Königlich Preussischen Akademie der Wissenschaften zu Berlin* (1905) 406–432. (Cited on p. 209).

[704] H. Georgi, *Lie Algebras In Particle Physics: from Isospin To Unified Theories*, Frontiers in Physics, Taylor and Francis, 1999, 10.1201/9780429499210. (Cited on pp. 213 and 214).

[705] O. Aharony, S. S. Gubser, J. M. Maldacena, H. Ooguri and Y. Oz, *Large N field theories, string theory and gravity*, *Phys. Rept.* **323** (2000) 183–386, [hep-th/9905111]. (Cited on p. 217).

[706] X.-L. Qi, *Exact holographic mapping and emergent space-time geometry*, 1309.6282. (Cited on p. 218).

[707] B. Czech, L. Lamprou, S. McCandlish and J. Sully, *Tensor Networks from Kinematic Space*, *JHEP* **07** (2016) 100, [1512.01548]. (Cited on p. 218).

[708] A. Bhattacharyya, Z.-S. Gao, L.-Y. Hung and S.-N. Liu, *Exploring the Tensor Networks/AdS Correspondence*, *JHEP* **08** (2016) 086, [1606.00621]. (Cited on p. 218).

[709] G. Evenbly, *Hyperinvariant Tensor Networks and Holography*, *Phys. Rev. Lett.* **119** (2017) 141602, [1704.04229]. (Cited on pp. 218, 227, and 243).

[710] N. Bao, G. Penington, J. Sorce and A. C. Wall, *Beyond Toy Models: Distilling Tensor Networks in Full AdS/CFT*, *JHEP* **11** (2019) 069, [1812.01171]. (Cited on pp. 218 and 243).

[711] Y. Ling, Y. Liu, Z.-Y. Xian and Y. Xiao, *Quantum error correction and entanglement spectrum in tensor networks*, *Phys. Rev. D* **99** (2019) 026008, [1806.05007]. (Cited on pp. 218 and 227).

[712] Y. Ling, Y. Liu, Z.-Y. Xian and Y. Xiao, *Tensor chain and constraints in tensor networks*, *JHEP* **06** (2019) 032, [1807.10247]. (Cited on pp. 218 and 227).

[713] M. Steinberg and J. Prior, *Conformal properties of hyperinvariant tensor networks*, *Sci. Rep.* **12** (2022) 532, [2012.09591]. (Cited on p. 227).

[714] J. de Boer, E. P. Verlinde and H. L. Verlinde, *On the holographic renormalization group*, *JHEP* **08** (2000) 003, [hep-th/9912012]. (Cited on p. 239).

[715] I. Heemskerk and J. Polchinski, *Holographic and Wilsonian Renormalization Groups*, *JHEP* **06** (2011) 031, [1010.1264]. (Cited on p. 239).

[716] P. Hayden, M. Headrick and A. Maloney, *Holographic Mutual Information is Monogamous*, *Phys. Rev. D* **87** (2013) 046003, [1107.2940]. (Cited on p. 243).

[717] A. Allais and E. Tonni, *Holographic evolution of the mutual information*, *JHEP* **01** (2012) 102, [1110.1607]. (Cited on p. 243).

[718] V. Balasubramanian, A. Bernamonti, N. Copland, B. Craps and F. Galli, *Thermalization of mutual and tripartite information in strongly coupled two dimensional conformal field theories*, *Phys. Rev. D* **84** (2011) 105017, [1110.0488]. (Cited on p. 243).

[719] A. C. Wall, *Maximin Surfaces, and the Strong Subadditivity of the Covariant Holographic Entanglement Entropy*, *Class. Quant. Grav.* **31** (2014) 225007, [1211.3494]. (Cited on p. 243).

[720] J. Molina-Vilaplana, *An Operator Product Expansion for the Mutual Information in AdS/CFT*, *Nucl. Phys. B* **888** (2014) 1–16, [1305.1064]. (Cited on p. 243).

[721] N. Bao, S. Nezami, H. Ooguri, B. Stoica, J. Sully and M. Walter, *The Holographic Entropy Cone*, *JHEP* **09** (2015) 130, [1505.07839]. (Cited on p. 243).

[722] N. Bao and I. F. Halpern, *Holographic Inequalities and Entanglement of Purification*, *JHEP* **03** (2018) 006, [1710.07643]. (Cited on p. 243).

[723] N. Bao and I. F. Halpern, *Conditional and Multipartite Entanglements of Purification and Holography*, *Phys. Rev. D* **99** (2019) 046010, [1805.00476]. (Cited on p. 243).

[724] V. E. Hubeny, M. Rangamani and M. Rota, *The holographic entropy arrangement*, *Fortsch. Phys.* **67** (2019) 1900011, [1812.08133]. (Cited on p. 243).

[725] V. E. Hubeny, M. Rangamani and M. Rota, *Holographic entropy relations*, *Fortsch. Phys.* **66** (2018) 1800067, [1808.07871]. (Cited on p. 243).

[726] S. Hernández Cuenca, *Holographic entropy cone for five regions*, *Phys. Rev. D* **100** (2019) 026004, [1903.09148]. (Cited on p. 243).

[727] C. Akers, S. Hernández-Cuenca and P. Rath, *Quantum Extremal Surfaces and the Holographic Entropy Cone*, *JHEP* **11** (2021) 177, [2108.07280]. (Cited on p. 243).

[728] D. L. Jafferis, A. Lewkowycz, J. Maldacena and S. J. Suh, *Relative entropy equals bulk relative entropy*, *JHEP* **06** (2016) 004, [1512.06431]. (Cited on p. 243).

[729] X. Dong, *The Gravity Dual of Renyi Entropy*, *Nature Commun.* **7** (2016) 12472, [1601.06788]. (Cited on pp. 243, 281, and 285).

[730] M. Alishahiha, *Holographic Complexity*, *Phys. Rev. D* **92** (2015) 126009, [1509.06614]. (Cited on p. 243).

[731] S. Chapman, H. Marrochio and R. C. Myers, *Complexity of Formation in Holography*, *JHEP* **01** (2017) 062, [1610.08063]. (Cited on p. 243).

[732] D. Carmi, S. Chapman, H. Marrochio, R. C. Myers and S. Sugishita, *On the Time Dependence of Holographic Complexity*, *JHEP* **11** (2017) 188, [1709.10184]. (Cited on p. 243).

[733] P. Caputa, N. Kundu, M. Miyaji, T. Takayanagi and K. Watanabe, *Liouville Action as Path-Integral Complexity: From Continuous Tensor Networks to AdS/CFT*, *JHEP* **11** (2017) 097, [1706.07056]. (Cited on p. 243).

[734] S. Chapman, H. Marrochio and R. C. Myers, *Holographic complexity in Vaidya spacetimes. Part II*, *JHEP* **06** (2018) 114, [1805.07262]. (Cited on p. 243).

[735] P. Caputa and J. M. Magan, *Quantum Computation as Gravity*, *Phys. Rev. Lett.* **122** (2019) 231302, [1807.04422]. (Cited on pp. 243 and 246).

[736] A. R. Brown, H. Gharibyan, H. W. Lin, L. Susskind, L. Thorlacius and Y. Zhao, *Complexity of Jackiw-Teitelboim gravity*, *Phys. Rev. D* **99** (2019) 046016, [1810.08741]. (Cited on p. 243).

[737] K. Goto, H. Marrochio, R. C. Myers, L. Queimada and B. Yoshida, *Holographic Complexity Equals Which Action?*, *JHEP* **02** (2019) 160, [1901.00014]. (Cited on p. 243).

[738] C. A. Agón, M. Headrick and B. Swingle, *Subsystem Complexity and Holography*, *JHEP* **02** (2019) 145, [1804.01561]. (Cited on p. 243).

[739] E. Caceres, S. Chapman, J. D. Couch, J. P. Hernandez, R. C. Myers and S.-M. Ruan, *Complexity of Mixed States in QFT and Holography*, *JHEP* **03** (2020) 012, [1909.10557]. (Cited on p. 243).

[740] G. Di Giulio and E. Tonni, *Complexity of mixed Gaussian states from Fisher information geometry*, *JHEP* **12** (2020) 101, [2006.00921]. (Cited on p. 243).

[741] S.-K. Jian, B. Swingle and Z.-Y. Xian, *Complexity growth of operators in the SYK model and in JT gravity*, *JHEP* **03** (2021) 014, [2008.12274]. (Cited on p. 243).

[742] N. Chagnet, S. Chapman, J. de Boer and C. Zukowski, *Complexity for Conformal Field Theories in General Dimensions*, *Phys. Rev. Lett.* **128** (2022) 051601, [2103.06920]. (Cited on p. 243).

[743] A. R. Brown, M. H. Freedman, H. W. Lin and L. Susskind, *Universality in long-distance geometry and quantum complexity*, *Nature* **622** (2023) 58–62, [2111.12700]. (Cited on pp. 243, 261, 262, 267, and 268).

[744] M. Rangamani and M. Rota, *Comments on Entanglement Negativity in Holographic Field Theories*, *JHEP* **10** (2014) 060, [1406.6989]. (Cited on p. 243).

[745] P. Chaturvedi, V. Malvimat and G. Sengupta, *Holographic Quantum Entanglement Negativity*, *JHEP* **05** (2018) 172, [1609.06609]. (Cited on p. 243).

[746] J. Kudler-Flam and S. Ryu, *Entanglement negativity and minimal entanglement wedge cross sections in holographic theories*, *Phys. Rev. D* **99** (2019) 106014, [1808.00446]. (Cited on p. 243).

[747] Y. Kusuki, J. Kudler-Flam and S. Ryu, *Derivation of holographic negativity in AdS_3/CFT_2*, *Phys. Rev. Lett.* **123** (2019) 131603, [1907.07824]. (Cited on p. 243).

[748] J. Kumar Basak, D. Basu, V. Malvimat, H. Parihar and G. Sengupta, *Islands for entanglement negativity*, *SciPost Phys.* **12** (2022) 003, [2012.03983]. (Cited on p. 243).

[749] J. Molina-Vilaplana and P. Sodano, *Holographic View on Quantum Correlations and Mutual Information between Disjoint Blocks of a Quantum Critical System*, *JHEP* **10** (2011) 011, [1108.1277]. (Cited on p. 243).

[750] G. Evenbly and G. Vidal, *Tensor Network States and Geometry*, *J. Statist. Phys.* **145** (2011) 891–918. (Cited on p. 243).

[751] X. Dong, D. Harlow and A. C. Wall, *Reconstruction of Bulk Operators within the Entanglement Wedge in Gauge-Gravity Duality*, *Phys. Rev. Lett.* **117** (2016) 021601, [1601.05416]. (Cited on p. 243).

[752] D. Harlow, *The Ryu–Takayanagi Formula from Quantum Error Correction*, *Commun. Math. Phys.* **354** (2017) 865–912, [1607.03901]. (Cited on p. 243).

[753] J. von Neumann, *On Rings of Operators. Reduction Theory*, *Ann. Math.* **50** (1949) 401–485. (Cited on pp. 243 and 289).

[754] M. Takesaki, *Theory of Operator Algebras I-III*, Springer New York, 1979, 10.1007/978-1-4612-6188-9. (Cited on pp. 243, 288, and 323).

[755] E. Verlinde and H. Verlinde, *A Conversation on ER = EPR*, 2212.09389. (Cited on pp. 244 and 269).

[756] S. Leutheusser and H. Liu, *Emergent times in holographic duality*, *Phys. Rev. D* **108** (2023) 086020, [2112.12156]. (Cited on pp. 245, 289, 290, 297, 298, and 328).

[757] E. Witten, *Why Does Quantum Field Theory In Curved Spacetime Make Sense? And What Happens To The Algebra of Observables In The Thermodynamic Limit?*, pp. 241–284, Springer International Publishing, Cham, 2022, 10.1007/978-3-031-17523-7˙11, [2112.11614]. (Cited on pp. 245, 288, 290, 291, 292, 293, 295, 296, and 323).

[758] V. Chandrasekaran, G. Penington and E. Witten, *Large N algebras and generalized entropy*, *JHEP* **04** (9, 2023) 009, [2209.10454]. (Cited on pp. 245, 290, and 298).

[759] V. Chandrasekaran, R. Longo, G. Penington and E. Witten, *An algebra of observables for de Sitter space*, *JHEP* **02** (2023) 082, [2206.10780]. (Cited on pp. 245, 290, and 298).

[760] S. Banerjee, M. Dorband, J. Erdmenger and A.-L. Weigel, *Geometric Phases Characterise Operator Algebras and Missing Information*, *JHEP* **10** (2023) 026, [2306.00055]. (Cited on pp. 245, 271, and 290).

[761] S. E. Aguilar-Gutierrez, E. Bahiru and R. Espíndola, *The centaur-algebra of observables*, *JHEP* **03** (2024) 008, [2307.04233]. (Cited on pp. 245 and 298).

[762] N. Engelhardt and H. Liu, *Algebraic ER=EPR and Complexity Transfer*, 2311.04281. (Cited on pp. 245 and 298).

[763] Q.-F. Wu, *Sectional curvatures distribution of complexity geometry*, *JHEP* **08** (2022) 197, [2108.11621]. (Cited on pp. 246 and 262).

[764] V. Arnold, *Sur la géométrie différentielle des groupes de Lie de dimension infinie et ses applications à l'hydrodynamique des fluides parfaits*, *Annales de l'Institut Fourier* **16** (1966) 319–361. (Cited on pp. 246, 248, and 255).

[765] V. I. Arnold and B. A. Khesin, *Topological Methods in Hydrodynamics*, Springer International Publishing, 2021, 10.1007/978-3-030-74278-2. (Cited on pp. 246, 248, 253, 254, 255, 256, 262, 263, 267, and 268).

[766] W. Pfeifer, *The Lie Algebras su(N)*, Birkhäuser Basel, 2003, 10.1007/978-3-0348-8097-8. (Cited on p. 248).

[767] D. B. Fairlie, P. Fletcher and C. K. Zachos, *Trigonometric Structure Constants for New Infinite Algebras*, *Phys. Lett. B* **218** (1989) 203–206. (Cited on pp. 249, 250, 251, and 254).

[768] D. B. Fairlie and C. K. Zachos, *Infinite Dimensional Algebras, Sine Brackets and SU(Infinity)*, *Phys. Lett. B* **224** (1989) 101–107. (Cited on pp. 249, 250, 251, and 254).

[769] D. B. Fairlie, P. Fletcher and C. K. Zachos, *Infinite Dimensional Algebras and a Trigonometric Basis for the Classical Lie Algebras*, *J. Math. Phys.* **31** (1990) 1088. (Cited on pp. 249, 250, 251, 253, and 254).

[770] J. Patera and H. Zassenhaus, *The Pauli Matrices in n-dimensions and Finest Gradings of Simple Lie Algebras of Type A_{n-1}*, *J. Math. Phys.* **29** (1988) 665. (Cited on pp. 249, 250, 251, and 254).

[771] S. Kobayashi and K. Nomizu, *Foundations of differential geometry, volume 2*, Wiley Classics Library, John Wiley & Sons, Nashville, TN, Feb., 1996. (Cited on pp. 253 and 254).

[772] J. S. Dowker and A. Wolski, *Finite model of two-dimensional ideal hydrodynamics*, *Phys. Rev. A* **46** (Nov, 1992) 6417–6430, [hep-th/9206025]. (Cited on pp. 254 and 258).

[773] A. Fetter and J. Walecka, *Theoretical Mechanics of Particles and Continua*, Dover Books on Physics, Dover Publications, 2003. (Cited on p. 256).

[774] H. Goldstein, C. Poole and J. Safko, *Classical Mechanics*, Addison Wesley, 2002. (Cited on p. 256).

[775] E. V. Moreva, G. A. Maslennikov, S. S. Straupe and S. P. Kulik, *Realization of Four-Level Qudits Using Biphotons*, *Phys. Rev. Lett.* **97** (Jul, 2006) 023602. (Cited on p. 259).

[776] N. Bent, H. Qassim, A. A. Tahir, D. Sych, G. Leuchs, L. L. Sánchez-Soto et al., *Experimental Realization of Quantum Tomography of Photonic Qudits via Symmetric Informationally Complete Positive Operator-Valued Measures*, *Phys. Rev. X* **5** (Oct, 2015) 041006. (Cited on p. 259).

[777] E. Kiktenko, A. Fedorov, A. Strakhov and V. Man'ko, *Single qudit realization of the Deutsch algorithm using superconducting many-level quantum circuits*, *Physics Letters A* **379** (July, 2015) 1409–1413. (Cited on p. 259).

[778] H. Greener and H. Suchowski, *Composite pulses in N-level systems with SU(2) symmetry and their geometrical representation on the Majorana sphere*, *The Journal of Chemical Physics* **148** (Feb., 2018) . (Cited on p. 259).

[779] Y. Wang, Z. Hu, B. C. Sanders and S. Kais, *Qudits and High-Dimensional Quantum Computing*, *Frontiers in Physics* **8** (2020) . (Cited on p. 259).

[780] Y. Dong, Q. Liu, J. Wang, Q. Li, X. Yu, W. Zheng et al., *Simulation of Two-Qubit Gates with a Superconducting Qudit*, *Phys. Status Solidi B* **259** (2022) 2100500. (Cited on p. 259).

[781] Z. Meng, W.-Q. Liu, B.-W. Song, X.-Y. Wang, A.-N. Zhang and Z.-Q. Yin, *Experimental realization of high-dimensional quantum gates with ultrahigh fidelity and efficiency*, *Phys. Rev. A* **109** (Feb, 2024) 022612. (Cited on p. 259).

[782] R. Bishop and R. Crittenden, *Geometry of Manifolds*, American Mathematical Society, Aug., 2001, 10.1090/chel/344. (Cited on pp. 261 and 267).

[783] A. Agrachev, D. Barilari and U. Boscain, *A Comprehensive Introduction to Sub-Riemannian Geometry*, Cambridge Studies in Advanced Mathematics, Cambridge University Press, 2019, 10.1017/9781108677325. (Cited on p. 261).

[784] P. K. Rashevsky, *Any two points of a totally nonholonomic space may be connected by an admissible line*, *Uch. Zap. Ped. Inst. im. Liebknechta, Ser. Phys. Math.* **2** (1938) 83–94. (Cited on p. 261).

[785] W.-L. Chow, *Ueber Systeme von linearen partiellen Differentialgleichungen erster Ordnung*, *Mathematische Annalen* **117-117** (Dec., 1940) 98–105. (Cited on p. 261).

[786] M. Khajeh Salehani and I. Markina, *Controllability on Infinite-Dimensional Manifolds: A Chow–Rashevsky Theorem*, *Acta Applicandae Mathematicae* **134** (Apr., 2014) 229–246. (Cited on p. 262).

[787] A. R. Brown, *A quantum complexity lower bound from differential geometry*, *Nature Phys.* **19** (2023) 401–406, [2112.05724]. (Cited on p. 262).

[788] V. I. Arnold, *Exponential scattering of trajectories and its hydrodynamical applications*, pp. 419–427, Springer Berlin Heidelberg, Berlin, Heidelberg, 2014, 10.1007/978-3-642-31031-7˙40. (Cited on p. 263).

[789] A. M. Lukatskii, *On the curvature of the group of measure-preserving diffeomorphisms of an n-dimensional torus*, *Russian Mathematical Surveys* **36** (Apr., 1981) 179–180. (Cited on pp. 264 and 266).

[790] D. V. Anosov, *Geodesic flows on closed Riemannian manifolds of negative curvature*, *Trudy Mat. Inst. Steklov.* **90** (1967) 209. (Cited on p. 266).

[791] J. Milnor, *Curvatures of left invariant metrics on lie groups*, *Advances in Mathematics* **21** (9, 1976) 293–329. (Cited on p. 266).

[792] G. Misiołek, *Conjugate Points in $\mathcal{D}_\mu(\mathbb{T}^2)$*, *Proceedings of the American Mathematical Society* **124** (1996) 977–982. (Cited on p. 267).

[793] Y. C. Li, *The Poincare Recurrence Problem of Inviscid Incompressible Fluids*, *Asian Journal of Mathematics* **13** (2009) 7–14. (Cited on pp. 269 and 343).

[794] Y. C. Li, *A Recurrence Theorem on the Solutions to the 2D Euler Equation*, *Asian Journal of Mathematics* **13** (2009) 1–6. (Cited on pp. 269 and 343).

[795] J. Dajka, M. Mierzejewski, J. Łuczka, R. Blattmann and P. Hänggi, *Negativity and quantum discord in Davies environments*, *J. Phys. A: Mathematical and Theoretical* **45** (2012) 485306, [1209.1536]. (Cited on pp. 270 and 271).

[796] M. Poxleitner and H. Hinrichsen, *Gaussian continuous-variable isotropic state*, *Phys. Rev. A* **104** (Sep, 2021) 032423. (Cited on p. 271).

[797] Y. Huang, *Computing quantum discord is NP-complete*, *New Journal of Physics* **16** (mar, 2014) 033027. (Cited on p. 271).

[798] B. Dakić, V. Vedral and Č. Brukner, *Necessary and Sufficient Condition for Nonzero Quantum Discord*, *Physical Review Letters* **105** (nov, 2010) . (Cited on p. 271).

[799] A. Bera, T. Das, D. Sadhukhan, S. S. Roy, A. Sen(De) and U. Sen, *Quantum discord and its allies: a review of recent progress*, *Reports on Progress in Physics* **81** (dec, 2017) 024001. (Cited on p. 271).

[800] J. P. Provost and G. Vallee, *Riemannian Structure on Manifolds of Quantum States*, *Commun. Math. Phys.* **76** (1980) 289–301. (Cited on p. 271).

[801] W.-z. Guo, *Correlations in geometric states*, *JHEP* **08** (2020) 125, [2003.03933]. (Cited on pp. 271 and 274).

[802] M. Horodecki and P. Horodecki, *Reduction criterion of separability and limits for a class of distillation protocols*, *Phys. Rev. A* **59** (1999) 4206–4216, [quant-ph/9708015]. (Cited on p. 275).

[803] K. Papadodimas and S. Raju, *Remarks on the necessity and implications of state-dependence in the black hole interior*, *Phys. Rev. D* **93** (2016) 084049, [1503.08825]. (Cited on pp. 278 and 281).

[804] H. Verlinde, *Wormholes in Quantum Mechanics*, 2105.02129. (Cited on pp. 279, 280, 285, 286, and 287).

[805] H. Verlinde, *Deconstructing the Wormhole: Factorization, Entanglement and Decoherence*, 2105.02142. (Cited on pp. 279 and 280).

[806] J. Chakravarty, *Overcounting of interior excitations: A resolution to the bags of gold paradox in AdS*, *JHEP* **02** (2021) 027, [2010.03575]. (Cited on p. 283).

[807] B. Freivogel, D. Nikolakopoulou and A. F. Rotundo, *Wormholes from Averaging over States*, *SciPost Phys.* **14** (2023) 026, [2105.12771]. (Cited on p. 283).

[808] K. Goto, Y. Kusuki, K. Tamaoka and T. Ugajin, *Product of random states and spatial (half-)wormholes*, *JHEP* **10** (2021) 205, [2108.08308]. (Cited on p. 283).

[809] V. Balasubramanian, A. Lawrence, J. M. Magan and M. Sasieta, *Microscopic Origin of the Entropy of Black Holes in General Relativity*, *Phys. Rev. X* **14** (2024) 011024, [2212.02447]. (Cited on pp. 283 and 284).

[810] V. Balasubramanian, A. Lawrence, J. M. Magan and M. Sasieta, *Microscopic Origin of the Entropy of Astrophysical Black Holes*, *Phys. Rev. Lett.* **132** (2024) 141501, [2212.08623]. (Cited on pp. 283 and 284).

[811] F. S. Nogueira, S. Banerjee, M. Dorband, R. Meyer, J. v. d. Brink and J. Erdmenger, *Geometric phases distinguish entangled states in wormhole quantum mechanics*, *Phys. Rev. D* **105** (2022) L081903, [2109.06190]. (Cited on p. 285).

[812] S. Banerjee, M. Dorband, J. Erdmenger, R. Meyer and A.-L. Weigel, *Berry phases, wormholes and factorization in AdS/CFT*, *JHEP* **08** (2022) 162, [2202.11717]. (Cited on p. 285).

[813] W. Cottrell, B. Freivogel, D. M. Hofman and S. F. Lokhande, *How to Build the Thermofield Double State*, *JHEP* **02** (2019) 058, [1811.11528]. (Cited on pp. 285 and 286).

[814] J. M. Deutsch, *Quantum statistical mechanics in a closed system*, *Phys. Rev. A* **43** (1991) 2046. (Cited on p. 286).

[815] M. Srednicki, *Chaos and Quantum Thermalization*, *Phys. Rev. E* **50** (3, 1994) , [cond-mat/9403051]. (Cited on p. 286).

[816] M. Srednicki, *Thermal fluctuations in quantized chaotic systems*, *J. Phys. A* **29** (1996) L75–L79, [chao-dyn/9511001]. (Cited on p. 286).

[817] J. M. Deutsch, *Eigenstate thermalization hypothesis*, *Rept. Prog. Phys.* **81** (2018) 082001. (Cited on p. 286).

[818] J.-M. Souriau, *Quantification géométrique*, *Commun. Math. Phys.* **1** (1966) 374–398. (Cited on p. 286).

[819] J.-M. Souriau, *Quantification géométrique. Applications*, *Annales de l'institut Henri Poincaré. Section A, Physique Théorique* **6** (1967) 311–341. (Cited on p. 286).

[820] B. Kostant, *Quantization and unitary representations*, in *Lectures in Modern Analysis and Applications III* (C. T. Taam, ed.), (Berlin, Heidelberg), pp. 87–280, Springer Berlin Heidelberg, 1970, 10.1007/BFb0079068. (Cited on p. 286).

[821] A. Osterloh, L. Amico, G. Falci and R. Fazio, *Scaling of entanglement close to a quantum phase transition*, *Nature* **416** (2002) 608–610. (Cited on p. 287).

[822] T. J. Osborne and M. A. Nielsen, *Entanglement, quantum phase transitions, and density matrix renormalization*, *Quantum Information Processing* **1** (2002) 45–53. (Cited on p. 287).

[823] T. J. Osborne and M. A. Nielsen, *Entanglement in a simple quantum phase transition*, *Phys. Rev. A* **66** (2002) 032110, [quant-ph/0202162]. (Cited on p. 287).

[824] V. Eisler and I. Peschel, *Reduced density matrices and entanglement entropy in free lattice models*, *J. Phys. A* **42** (2009) 504003, [0906.1663]. (Cited on p. 287).

[825] J. H. Bardarson, F. Pollmann and J. E. Moore, *Unbounded Growth of Entanglement in Models of Many-Body Localization*, *Phys. Rev. Lett.* **109** (Jul, 2012) 017202. (Cited on p. 288).

[826] M. Serbyn, Z. Papić and D. A. Abanin, *Universal Slow Growth of Entanglement in Interacting Strongly Disordered Systems*, *Phys. Rev. Lett.* **110** (Jun, 2013) 260601. (Cited on p. 288).

[827] M. Levin and X.-G. Wen, *Detecting Topological Order in a Ground State Wave Function*, *Phys. Rev. Lett.* **96** (Mar, 2006) 110405. (Cited on p. 288).

[828] R. Haag, N. M. Hugenholtz and M. Winnink, *On the Equilibrium states in quantum statistical mechanics*, *Commun. Math. Phys.* **5** (1967) 215–236. (Cited on pp. 288, 289, and 323).

[829] H. Araki, *Mathematical Theory of Quantum Fields*, International series of monographs on physics, Oxford University Press, 10, 1999, 10.1093/oso/9780198517733.001.0001. (Cited on pp. 288 and 289).

[830] E. Witten, *APS Medal for Exceptional Achievement in Research: Invited article on entanglement properties of quantum field theory*, *Rev. Mod. Phys.* **90** (2018) 045003, [1803.04993]. (Cited on pp. 288, 290, 291, 292, 296, 323, 324, 325, 326, and 328).

[831] J. Sorce, *Notes on the type classification of von Neumann algebras*, *Rev. Math. Phys.* **36** (2024) 2430002, [2302.01958]. (Cited on pp. 288, 290, 291, 292, and 293).

[832] H. Araki and E. J. Woods, *A classification of factors*, *Publications of the Research Institute for Mathematical Sciences* **4** (1968) 51–130. (Cited on pp. 288, 293, 297, 323, 324, 325, and 328).

[833] R. T. Powers, *Representations of Uniformly Hyperfinite Algebras and Their Associated von Neumann Rings*, *The Annals of Mathematics* **86** (July, 1967) 138. (Cited on pp. 288, 293, 297, 323, 324, 325, and 328).

[834] M. Takesaki, *Tomita's Theory of Modular Hilbert Algebras and its Applications*, Lecture Notes in Mathematics, Springer-Verlag, 1970, 10.1007/bfb0065832. (Cited on p. 288).

[835] J. von Neumann, *Zur Algebra der Funktionaloperationen und Theorie der normalen Operatoren*, *Math. Ann.* **102** (1930) 370–427. (Cited on pp. 289, 291, and 295).

[836] H. Araki and E. J. Woods, *Representations of the Canonical Commutation Relations Describing a Nonrelativistic Infinite Free Bose Gas*, *Journal of Mathematical Physics* **4** (05, 1963) 637–662. (Cited on p. 289).

[837] H. Araki, *A Lattice of Von Neumann Algebras Associated with the Quantum Theory of a Free Bose Field*, *Journal of Mathematical Physics* **4** (11, 1963) 1343–1362. (Cited on p. 289).

[838] R. Haag, *Local Quantum Physics: Fields, Particles, Algebras*, Springer Science & Business Media, 1992, 10.1007/978-3-642-97306-2. (Cited on p. 289).

[839] H. Halvorson and M. Muger, *Algebraic Quantum Field Theory*, pp. 731–864, North-Holland, Amsterdam, 2007, 10.1016/B978-044451560-5/50011-7, [math-ph/0602036]. (Cited on p. 289).

[840] C. J. Fewster, *A Generally Covariant Measurement Scheme for Quantum Field Theory in Curved Spacetimes*, p. 253–268, Springer International Publishing, 2020, 10.1007/978-3-030-38941-3˙11, [1904.06944]. (Cited on p. 289).

[841] H. Reeh and S. Schlieder, *Bemerkungen zur Unitäräquivalenz von Lorentzinvarianten Feldern*, *Nuovo Cim.* **22** (1961) 1051–1068. (Cited on pp. 289 and 292).

[842] M. McGuigan, *Finite black hole entropy and string theory*, *Phys. Rev. D* **50** (1994) 5225–5231, [hep-th/9406201]. (Cited on p. 290).

[843] L. Susskind and J. Uglum, *Black hole entropy in canonical quantum gravity and superstring theory*, *Phys. Rev. D* **50** (1994) 2700–2711, [hep-th/9401070]. (Cited on p. 290).

[844] A. S. Wightman and L. Gårding, *Fields as Operator-valued Distributions in Relativistic Quantum Theory*, *Arkiv f. Fysik, Kungl. Svenska Vetenskapsak.* **28** (1964) 129–189. (Cited on p. 290).

[845] K. Osterwalder and R. Schrader, *Axioms for Euclidean Green's functions*, *Communications in Mathematical Physics* **31** (June, 1973) 83–112. (Cited on p. 290).

[846] R. Haag and D. Kastler, *An Algebraic Approach to Quantum Field Theory*, *Journal of Mathematical Physics* **5** (07, 1964) 848–861. (Cited on p. 290).

[847] T. Senthil, *Symmetry-Protected Topological Phases of Quantum Matter*, *Annual Review of Condensed Matter Physics* **6** (2015) 299–324. (Cited on p. 290).

[848] Y. Ogata, *A classification of pure states on quantum spin chains satisfying the split property with on-site finite group symmetries*, *Transactions of the American Mathematical Society, Series B* **8** (Feb., 2021) 39–65. (Cited on p. 290).

[849] C. Bourne and Y. Ogata, *The classification of symmetry protected topological phases of one-dimensional fermion systems*, *Forum of Mathematics, Sigma* **9** (2021) e25. (Cited on p. 290).

[850] T. Faulkner and M. Li, *Asymptotically isometric codes for holography*, 2211.12439. (Cited on p. 290).

[851] K. Furuya, N. Lashkari, M. Moosa and S. Ouseph, *Information loss, mixing and emergent type III_1 factors*, *JHEP* **08** (2023) 111, [2305.16028]. (Cited on p. 290).

[852] E. Gesteau, *Emergent spacetime and the ergodic hierarchy*, 2310.13733. (Cited on pp. 290 and 298).

[853] E. Gesteau, *Large N von Neumann algebras and the renormalization of Newton's constant*, 2302.01938. (Cited on pp. 290 and 298).

[854] G. Penington and E. Witten, *Algebras and States in JT Gravity*, 2301.07257. (Cited on pp. 290 and 298).

[855] D. K. Kolchmeyer, *von Neumann algebras in JT gravity*, *JHEP* **06** (2023) 067, [2303.04701]. (Cited on pp. 290 and 298).

[856] K. Jensen, J. Sorce and A. J. Speranza, *Generalized entropy for general subregions in quantum gravity*, *JHEP* **12** (2023) 020, [2306.01837]. (Cited on pp. 290 and 298).

[857] E. Witten, *A background-independent algebra in quantum gravity*, *JHEP* **03** (2024) 077, [2308.03663]. (Cited on pp. 290 and 298).

[858] E. Gesteau and L. Santilli, *Explicit large N von Neumann algebras from matrix models*, 2402.10262. (Cited on pp. 290, 291, 298, and 344).

[859] J. von Neumann, *On infinite direct products*, *Compositio Mathematica* **6** (1939) 1–77. (Cited on pp. 291, 293, 323, 324, 325, and 328).

[860] I. Gelfand and M. Naimark, *On the imbedding of normed rings into the ring of operators in Hilbert spaces*, *Recueil Mathématique [Mat. Sbornik] N.S.* **12(54)** (1943) 192–217. (Cited on p. 292).

[861] I. E. Segal, *Irreducible Representations of Operator Algebras*, *Bull. Am. Math. Soc.* **53** (1947) 73–88. (Cited on p. 292).

[862] A. Strohmaier, R. Verch and M. Wollenberg, *Microlocal analysis of quantum fields on curved space-times: Analytic wavefront sets and Reeh-Schlieder theorems*, *J. Math. Phys.* **43** (2002) 5514–5530, [math-ph/0202003]. (Cited on p. 292).

[863] K. Sanders, *On the Reeh-Schlieder Property in Curved Spacetime*, *Commun. Math. Phys.* **288** (2009) 271–285, [0801.4676]. (Cited on p. 292).

[864] C. Gérard and M. Wrochna, *Analytic Hadamard States, Calderón Projectors and Wick Rotation Near Analytic Cauchy Surfaces*, *Commun. Math. Phys.* **366** (2019) 29–65, [1706.08942]. (Cited on p. 292).

[865] I. A. Morrison, *Boundary-to-bulk maps for AdS causal wedges and the Reeh-Schlieder property in holography*, *JHEP* **05** (2014) 53, [1403.3426]. (Cited on p. 292).

[866] M. Takesaki, *Duality for crossed products and the structure of von Neumann algebras of type III*, *Acta Math.* **131** (1973) 249–310. (Cited on pp. 293 and 298).

[867] A. Connes, *Une classification des facteurs de type III*, *Annales scientifiques de l'École Normale Supérieure* **4e série, 6** (1973) 133–252. (Cited on pp. 293, 296, and 298).

[868] A. Connes, *Classification of Injective Factors Cases II_1, II_∞, III_λ, $\lambda \neq 1$*, *Annals of Mathematics* **104** (1976) 73–115. (Cited on p. 293).

[869] W. Driessler, *On the Type of Local Algebras in Quantum Field Theory*, *Commun. Math. Phys.* **53** (1977) 295. (Cited on p. 293).

[870] J. Yngvason, *The Role of type III factors in quantum field theory*, *Rept. Math. Phys.* **55** (2005) 135–147, [math-ph/0411058]. (Cited on p. 293).

[871] H. Araki, *Type of von Neumann Algebra Associated with Free Field*, *Prog. Theor. Phys.* **32** (1964) 956–965. (Cited on p. 296).

[872] R. Longo, *Algebraic and modular structure of von Neumann algebras of Physics*, in *Operator algebras and applications, Part 2 (Kingston, Ont., 1980)*, vol. 38 of *Proc. Symp. Pure Math.*, pp. 551–566, Amer. Math. Soc., Providence, R.I., 1982, 10.1090/pspum/038.2/679537. (Cited on p. 296).

[873] K. Fredenhagen, *On the Modular Structure of Local Algebras of Observables*, *Commun. Math. Phys.* **97** (1985) 79–89. (Cited on p. 296).

[874] G. Festuccia and H. Liu, *Excursions beyond the horizon: Black hole singularities in Yang-Mills theories. I.*, *JHEP* **04** (2006) 044, [hep-th/0506202]. (Cited on p. 298).

[875] G. Festuccia and H. Liu, *The Arrow of time, black holes, and quantum mixing of large N Yang-Mills theories*, *JHEP* **12** (2007) 027, [hep-th/0611098]. (Cited on p. 298).

[876] S. Ali Ahmad and R. Jefferson, *Crossed product algebras and generalized entropy for subregions*, *SciPost Phys. Core* **7** (2024) 020, [2306.07323]. (Cited on p. 298).

[877] J. Kudler-Flam, S. Leutheusser and G. Satishchandran, *Generalized Black Hole Entropy is von Neumann Entropy*, 2309.15897. (Cited on p. 298).

[878] J. Xu, *Von Neumann Algebras in Double-Scaled SYK*, 2403.09021. (Cited on p. 298).

[879] H. Tang, *Entanglement entropy in type II_1 von Neumann algebra: examples in Double-Scaled SYK*, 2404.02449. (Cited on p. 298).

[880] D. Pérez-García, L. Santilli and M. Tierz, *Hawking-Page transition on a spin chain*, 2401.13963. (Cited on p. 298).

[881] D. J. Gross and A. Neveu, *Dynamical symmetry breaking in asymptotically free field theories*, *Phys. Rev. D* **10** (Nov, 1974) 3235–3253. (Cited on p. 299).

[882] P. Saad, S. H. Shenker and D. Stanford, *A semiclassical ramp in SYK and in gravity*, (6, 2018) , [1806.06840]. (Cited on p. 299).

[883] A. Altland and B. D. Simons, *Condensed Matter Field Theory*, Cambridge University Press, March, 2010, 10.1017/cbo9780511789984. (Cited on p. 301).

[884] J. Maldacena and D. Stanford, *Remarks on the Sachdev-Ye-Kitaev model*, *Phys. Rev. D* **94** (2016) 106002, [1604.07818]. (Cited on pp. 305 and 348).

[885] S. Sachdev, *Quantum phase transitions*, *Physics World* **12** (apr, 1999) 33. (Cited on p. 315).

[886] I. Peschel, *Calculation of reduced density matrices from correlation functions*, *J. Phys. A* **36** (2003) L205. (Cited on pp. 318 and 319).

[887] G. C. Wick, *The Evaluation of the Collision Matrix*, *Phys. Rev.* **80** (Oct, 1950) 268–272. (Cited on p. 319).

[888] L. Niermann and T. J. Osborne, *Holographic networks for (1+1)-dimensional de Sitter space-time*, *Phys. Rev. D* **105** (2022) 125009, [2102.09223]. (Cited on p. 342).

[889] L. Masanes, *Discrete holography in dual-unitary circuits*, 2301.02825. (Cited on p. 342).

[890] P. Basteiro, J. Elfert, J. Erdmenger and H. Hinrichsen, *Fractional Klein–Gordon equation on AdS_{2+1}*, *J. Phys. A* **55** (2022) 364002, [2201.10870]. (Cited on pp. 344 and 351).

[891] K. B. Oldham and P. Howlett, *The fractional calculus*, Mathematics in Science and Engineering, Elsevier Science & Technology, May, 2014. (Cited on p. 344).

[892] R. Hilfer, *Applications of Fractional Calculus in Physics*, WORLD SCIENTIFIC, Mar., 2000, 10.1142/3779. (Cited on p. 344).

[893] F. B. Tatom, *The Relationship between Fractional Calculus and Fractals*, *Fractals* **03** (Mar., 1995) 217–229. (Cited on p. 344).

[894] A. Carpinteri, *Fractional Calculus Applied to Fractal Media and Nonlocal Continua*, p. 689–728, Springer Netherlands, 2021, 10.1007/978-94-024-2026-5˙12. (Cited on p. 344).

[895] A. Szameit and S. Nolte, *Discrete optics in femtosecond-laser-written photonic structures*, *Journal of Physics B: Atomic, Molecular and Optical Physics* **43** (July, 2010) 163001. (Cited on p. 344).

[896] C. Koke, C. Noh and D. G. Angelakis, *Dirac equation in 2-dimensional curved spacetime, particle creation, and coupled waveguide arrays*, *Annals Phys.* **374** (2016) 162–178, [1607.04821]. (Cited on p. 345).

[897] C. Koke, C. Noh and D. G. Angelakis, *Dirac equation on a square waveguide lattice with site-dependent coupling strengths and the gravitational Aharonov-Bohm effect*, *Phys. Rev. A* **102** (2020) 013514, [1909.12543]. (Cited on p. 345).

[898] F. Gahler and J. Rhyner, *Equivalence of the generalised grid and projection methods for the construction of quasiperiodic tilings*, *Journal of Physics A: Mathematical and General* **19** (Feb., 1986) 267–277. (Cited on p. 346).

[899] N. de Bruijn, *Quasicrystals and their Fourier transform*, *Indagationes Mathematicae (Proceedings)* **89** (June, 1986) 123–152. (Cited on p. 346).

[900] A. A. Migdal, *Recursion Equations in Gauge Theories*, *Sov. Phys. JETP* **42** (1975) 413. (Cited on p. 347).

[901] E. Witten, *On quantum gauge theories in two-dimensions*, *Commun. Math. Phys.* **141** (1991) 153–209. (Cited on p. 347).

[902] S. Sachdev and J. Ye, *Gapless spin-fluid ground state in a random quantum Heisenberg magnet*, *Phys. Rev. Lett.* **70** (May, 1993) 3339–3342. (Cited on p. 347).

[903] A. Kitaev, *A simple model of quantum holography*, 2015. Talks at KITP, April 7 and May 27. (Cited on p. 347).

[904] R. Jackiw, *Lower Dimensional Gravity*, *Nucl. Phys. B* **252** (1985) 343–356. (Cited on p. 348).

[905] C. Teitelboim, *Gravitation and Hamiltonian Structure in Two Space-Time Dimensions*, *Phys. Lett. B* **126** (1983) 41–45. (Cited on p. 348).

[906] J. Maldacena and X.-L. Qi, *Eternal traversable wormhole*, 1804.00491. (Cited on p. 348).

[907] P. Basteiro, G. Di Giulio, J. Erdmenger, R. Meyer and Z.-Y. Xian, "in preparation." 2024. (Cited on p. 348).